James E. Martin

Physics for Radiation Protection

Related Titles

Turner, J. E., Downing, D. J., Bogard, J. S.

Statistical Methods in Radiation Physics

2012
ISBN: 978-3-527-41107-8

Turner, J. E.

Atoms, Radiation, and Radiation Protection

2007
ISBN: 978-3-527-40606-7

Knoll, G. F.

Radiation Detection and Measurement

2000
ISBN: 978-0-471-07338-3

Bevelacqua, J. J.

Basic Health Physics

Problems and Solutions

1999
ISBN: 978-0-471-29711-6

Bevelacqua, J. J.

Contemporary Health Physics

Problems and Solutions

1995
ISBN: 978-0-471-01801-8

Attix, F. H.

Introduction to Radiological Physics and Radiation Dosimetry

1986
ISBN: 978-0-471-01146-0

James E. Martin

Physics for Radiation Protection

Third Completely Updated Edition

WILEY

WILEY-VCH Verlag GmbH & Co. KGaA

The Author

James E. Martin
2604 Bedford Road
Ann Arbour MI 48104
USA

Library of Congress Card No.:
applied for

British Library Cataloguing-in-Publication Data
A catalogue record for this book is available from the British Library.

Bibliographic information published by the Deutsche Nationalbibliothek
The Deutsche Nationalbibliothek lists this publication in the Deutsche Nationalbibliografie; detailed bibliographic data are available on the Internet at <http://dnb.d-nb.de>.

Cover Design Adam-Design, Weinheim
Typesetting Kühn & Weyh, Satz und Medien, Freiburg
Printing and Binding Markono Print Media Pte Ltd, Singapore

Print ISBN: 978-3-527-41176-4
ePDF ISBN: 978-3-527-66709-3
ePub ISBN: 978-3-527-66708-6
mobi ISBN: 978-3-527-66707-9
oBook ISBN: 978-3-527-66706-2

To the memory of

Frank A. and Virginia E. Martin
and JoAnn Martin Burkhart.

Contents

Physics for Radiation Protection, Third Edition. James E. Martin

Preface

This book is the outcome of teaching radiation physics to students beginning a course of study in radiation protection, or health physics. This 3rd edition attempts as the first two did to provide in one place a comprehensive treatise of the major physics concepts required of radiation protection professionals. Numerous real-world examples and practice problems are provided to demonstrate concepts and hone skills, and even though its limited uses are thoroughly developed and explained, some familiarity with calculus would be helpful in grasping some of the subjects.

The materials in this compendium can be used in a variety of ways, both for instruction and reference. The first two chapters describe the atom as an energy system, and as such they may be of most use for those with minimal science background. Chapter 3 addresses the special condition of radioactive transformation (or disintegration) of atoms with excess energy, regardless of how acquired. Chapters 4 and 5 describe activation and fission processes and the amount of energy gained or lost due to atom changes; these define many of the sources that are addressed in radiation protection. Chapter 6 develops natural sources of radiation and radioactive materials primarily as reference material; however, the sections on radioactive dating and radon could be used as supplemental, though specialized, material to Chapter 3.

The interaction of radiation with matter and the resulting deposition of energy is covered in Chapter 7 along with the corollary subjects of radiation exposure and dose. Radiation shielding, also related to interaction processes, is described in Chapter 8 for various source geometries. Chapters 9 and 10, on internal radiation dose and environmental dispersion of radioactive materials, are also fundamental for understanding how such materials produce radiation dose inside the body and how they become available for intakes by humans. These are followed by specialty chapters on nuclear criticality (Chapter 11); radiation detection and measurement (Chapter 12); applied statistics (Chapter 13); and finally (Chapter 14) neutron sources and interactions. A course in radiation physics would likely include the material in Chapters 3, 4, 5, 7, and 8 with selections from the other chapters, all or in part, to develop needed background and to address specialty areas of interest to instructor and student. In anticipation of such uses, attempts have been made

Physics for Radiation Protection, Third Edition. James E. Martin

to provide comprehensive and current coverage of the material in each chapter and relevant data sets.

Health physics problems require resource data. To this end, decay schemes and associated radiation emissions are included for about 100 of the most common radionuclides encountered in radiation protection. These are developed in the detail needed for health physics uses and cross referenced to standard compendiums for straightforward use when these more in-depth listings need to be consulted. Resources are also provided on activation cross sections, fission yields, fission-product chains, photon absorption coefficients, nuclear masses, and abbreviated excerpts of the Chart of the Nuclides. These are current from the National Nuclear Data Center at Brookhaven National Laboratory; the Center and its staff are a national resource.

The units used in radiation protection have evolved over the hundred years or so that encompass the field. They continue to do so with a fairly recent, but not entirely accepted, emphasis on System Internationale (SI) Units while U.S. standards and regulations have continued to use conventional units. To the degree possible, this book uses fundamental quantities such as eV, transformations, time, distance, and the numbers of atoms or emitted particles and radiations to describe nuclear processes, primarily because they are basic to concepts being described but partially to avoid conflict between SI units and conventional ones. Both sets of units are defined as they apply to radiation protection, but in general the more fundamental parameters are used. For the specific units of radiation protection such as exposure, absorbed dose, dose equivalent, and activity, text material and examples are generally presented in conventional units because the field is very much an applied one; however, the respective SI unit is also included where feasible. By doing so, it is believed presentations are clearer and relevant to the current conditions, but it is recognized that this quandary is likely to continue.

This endeavor has been possible because of the many contributions of my research associates and students whose feedback shaped the teacher on the extent and depth of the physics materials necessary to function as a professional health physicist. I am particularly indebted to Chul Lee who began this process with me with skill and patience and to Rachael Nelson who provided invaluable help in capping off this 3rd edition. I hope it helps all who undertake study in this exciting field to appreciate how physics underpins it.

In an undertaking of this scope, it is inevitable that undetected mistakes creep in and remain despite the best efforts of preparers and editors; thus, reports (jemartin@umich.edu) of errors found would be appreciated.

James E. Martin, Ph.D., CHP
Associate Professor (emeritus) of
Radiological Health
The University of Michigan, 2012

1
Structure of Atoms

"I have discovered something very interesting."

W. C. Roentgen (Nov. 8, 1895)

The fifty years following Roentgen's discovery of x-rays saw remarkable changes in physics that literally changed the world forever, culminating in a host of new products from nuclear fission. Discovery of the electron (1897) and radioactivity (1898) focused attention on the makeup of atoms and their structure as did other discoveries. For example, in 1900, Planck introduced the concept that the emission (or absorption) of electromagnetic radiation occurs only in a discrete amount where the energy is proportional to the frequency, ν, of the radiation, or

$$E = h\nu$$

where h is a constant (Planck's constant) of nature; its value is

$$h = 6.1260693 \times 10^{-34} \text{ J s or } 4.13566743 \times 10^{-15} \text{ eV s}$$

Planck presumed that he had merely found an ad hoc solution for blackbody radiation, but in fact he had discovered a basic law of nature: any physical system capable of emitting or absorbing electromagnetic radiation is limited to a discrete set of possible energy values or levels; energies intermediate between them simply do not occur. Planck's theory was revolutionary because it states that the emission and absorption of radiation must be discontinuous processes, i.e. only as a transition from one particular energy state to another where the energy difference is an integral multiple of $h\nu$. This revolutionary theory extends over 22 orders of magnitude from very long wavelength radiation such as radio waves up to and including high energy gamma rays. It includes the energy states of particles in atoms and greatly influences their structure.

Einstein (in 1905) used Planck's discrete emissions (or quanta) to explain why light of a certain frequency (wavelength) causes the emission of electrons from the surface of various metals (the photoelectric effect). Light photons clearly have no rest mass, but behaving like a particle, a photon can hit a bound electron and "knock" it out of the atom.

Physics for Radiation Protection, Third Edition. James E. Martin

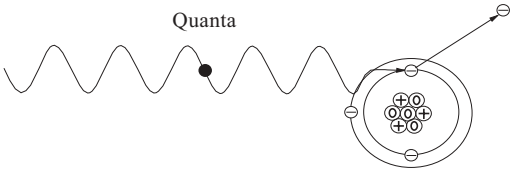

The kinetic energy of the ejected electrons is KE = $h\nu - \phi$.

Example 1–1. Light with a wavelength of 5893 Å produces electrons from a potassium surface that are stopped by 0.36 volts. Determine: a) the maximum energy of the photoelectron, and b) the work function.

Solution. a) The maximum energy KE_{max} of the ejected photoelectrons is equal to the stopping potential of 0.36 eV.

b) the work function is the energy of the incident photon minus the energy given to the ejected electron, or

$$\phi = [4.13566743 \times 10^{-15} \text{ eV s}) \ (3 \times 10^{8} \text{ m/s}) \ / \ 5.893 \times 10^{-10} \text{ m}] - 0.36 \text{ eV}$$
$$= 1.7454 \text{ eV}.$$

A. H. Compton used a similar approach to explain x-ray scattering as interactions between "particle-like" photons and loosely bound (or "free") electrons of carbon (now known as the Compton effect). Energy and momentum are conserved and the calculated wavelength changes agreed with experimental observations.

1.1 Atom Constituents

Atoms consist of protons and neutrons (discovered in 1932 by Chadwick) bound together to form a nucleus which is surrounded by electrons that counterbalance each proton in the nucleus to form an electrically neutral atom. Its components are: a) *protons* which have a reference mass of about 1.0 and an electrical charge of +1; b) *electrons* which have a mass about 1/1840 of the proton and a (–1) electrical charge; and c) *neutrons* which are electrically neutral and slightly heavier than the proton. The number of protons (or Z) establishes the identity of the atom and its mass number (A) is the sum of protons and neutrons (or N) in its nucleus. Electrons do not, and, according to the uncertainty principle, cannot exist in the nucleus, although they can be manufactured and ejected during radioactive transformation. Modern theory has shown that protons and neutrons are made up of quarks, leptons, and bosons (recently discovered), but these are not necessary for understanding atoms or how they produce radiant energy.

Four forces of nature determine the array of atom constituents. The *electromagnetic force* between charged particles is attractive if the charges (q_1 and q_2) are of opposite signs (i.e. positive or negative); if of the same sign, the force F will be

repulsive and quite strong for the small distances between protons in the nucleus of an atom. This repulsion is overcome by the *nuclear force* (or strong force) which is about 100 times stronger; it only exists in the nucleus and only between protons and neutrons (there is no center point towards which nucleons are attracted). The weak force (relatively speaking) has been shown to be a form of the electromagnetic force; it influences radioactive transformation; and the gravitational force, though present, is negligible in atoms.

The nucleus of an atom containing Z protons is essentially a charged particle (with charge Ze) that attracts an equal number of electrons that orbit the nucleus some distance away. Thomson theorized that each negatively charged electron was offset by a positively charged proton and that these were arrayed somewhat like a plum pudding to form an electrically neutral atom. This model proved unsatisfactory for explaining the large-angle scattering of alpha particles by gold foils as observed by Rutherford and Geiger-Marsden. Such large deflections were due the electromagnetic force between a positively charged nucleus (Ze) at the center of the atom and that of the alpha particle ($2e$).

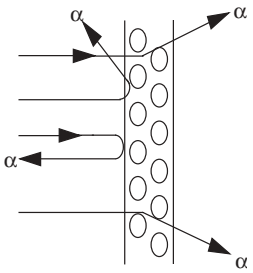

The force for such deflections is inversely proportional to the distance r between them, or

$$F = k\frac{q_1 q_2}{r^2} = k\frac{(2e)(Ze)}{r^2},$$

which yields a value of r of about 10^{-15} m which Rutherford proposed as the radius of a small positively-charged nucleus surrounded by electrons in orbits about 10^{-10} m in size. This model had a fatal flaw: according to classical physics the electrons would experience acceleration, v^2/r, causing them to continuously emit radiation and to quickly (in about 10^{-8} s) spiral into the nucleus.

In 1913, Niels Bohr explained Rutherford's conundrum by simply declaring (postulate I) that atoms are stable and that an electron in its orbit does not radiate energy, but only does so when it experiences one of Planck's quantum changes to an orbit of lower potential energy (postulate III) with the emission of a photon of energy

$$h\nu = E_2 - E_1$$

And, that the allowed stationary states for orbiting electrons (postulate II) are those for which the orbital angular momentum, L, is an integral multiple of $h/2\pi$, or:

$$L = n\frac{h}{2\pi}$$

where $n = 1, 2, 3, 4, \ldots$, represents the principal quantum number for discrete, quantized energy states. Since $L = mvr$, the calculated radius of the first (or when $n = 1$) electron orbit for hydrogen (the simplest atom) was found to be 0.529×10^{-8} cm, which agreed with experiment. Postulate III is apparently based on Planck's quantum hypothesis, but postulate II appeared to be arbitrary even though it worked , at least for hydrogen. It would only be explained by de Broglie's hypothesis some 13 years later (see below).

Bohr assumed that electrons orbiting a nucleus moved in circular orbits under the influence of two force fields: the coulomb attraction (a centripetal force) provided by the positively charged nucleus and the centrifugal force of each electron in orbital motion at a radius, r_n, and velocity, v_n. These forces are equal and opposite each other, or:

$$\frac{mv_n^2}{r_n} = k\frac{q_1 q_2}{r_n^2}$$

where r_n can be calculated from postulate II. And, since q_1 and q_2 are unity for hydrogen

$$r_n = \frac{(nh)^2}{(2p)2kmq^2} = n^2 r_1$$

where $n = 1, 2, 3, 4, \ldots$ and r_1 is the radius of the first orbit of the electron in the hydrogen atom, the so-called Bohr orbit. And since the quantum hypothesis limits values of n to integral values, the electron can only be in those orbits which are given by:

$$r_n = r_1, 4r_1, 9r_1, 16r_1, \ldots$$

These relationships can be used to calculate the total energy E_n of an electron in the nth orbit where the sum of its kinetic and potential energy is

$$E_n = \frac{mv_n^2}{2} + \left(-\frac{ke^2}{r_n}\right)$$

$$E_n = -\frac{1}{n^2}\frac{(2\pi)^2 k^2 q^4 m}{2h^2} = -\frac{1}{n^2} \times 13.58 \text{ eV}$$

which is the binding energy of the electron in hydrogen and is in perfect agreement with the measured value of the energy required to ionize hydrogen. For other values of n, the allowed energy levels of hydrogen are:

$$E_n = -\frac{E_1}{4}, -\frac{E_1}{9}, -\frac{E_1}{16}, \ldots$$

where $E_1 = -13.58$ eV. These predicted energy levels can be used to calculate the possible emissions (or absorption) of electromagnetic radiation and their wavelengths for hydrogen. When Bohr did so for $n = 3$ he obtained the series of wavelengths measured by Balmer, and since the theory holds for $n = 3$, Bohr postulated that it should also hold for other values of n, and the corresponding wavelengths were soon found providing dramatic proof of the theory.

In 1926, Louis de Broglie postulated that if Einstein's and Compton's assignment of particle properties to waves was correct, why shouldn't the converse be true; i.e., that particles have wave properties such that an electron (or a car for that matter) has a wavelength,associated with its motion, or

$$\lambda = \frac{h}{p} = \frac{h}{mv}$$

and that as a wave it has momentum, p, with the value:

$$p = \frac{h}{\lambda}$$

This simple but far-reaching concept was later proved by Davisson and Germer who observed diffraction (a wave phenomenon) of electrons (clearly particles) from a nickel crystal. De Broglie's wave/particle behavior of electrons also opened the door to description of the dynamics of particles by wave mechanics, perhaps the most revolutionary development in physics since Einstein's special theory of relativity.

Simple though it appears, de Broglie's hypothesis has consequences as significant as Einstein's equivalence of mass and energy ($E = mc^2$) which are related to each other through c^2, a large constant of proportionality; in de Broglie's equations, the wavelength,and the momentum p of a particle are related to each other through Planck's constant, a very small one.

1.2
Structure, Identity, and Stability of Atoms

The identity of an atom is determined by the number and array of protons and neutrons in its nucleus. An atom with one proton is defined as hydrogen; it has one orbital electron for electrical neutrality. Deuterium (or hydrogen-2) also con-

tains one proton and one electron but also a neutron and is quite stable; tritium (hydrogen-3) with one proton and one electron has a second neutron which causes it to be unstable, or radioactive. These three are isotopes of hydrogen.

Two protons cannot be joined to form an atom because the repulsive electromagnetic force between them is so great that it even overcomes the strongly attractive nuclear force. If, however, a neutron is present, the distribution of forces is such that a stable nucleus is formed and two electrons will then join up to balance the two plus (+) charges of the protons to create a stable, electrically neutral atom of helium so defined because it has two protons. Its mass number (A) is 3 (2 protons plus 1 neutron) and is written as helium-3 or ^{3}He. Because neutrons provide a cozy effect, yet another neutron can be added to obtain ^{4}He which still has two electrons to balance the two positive charges. This atom is the predominant form (or isotope) of helium on earth, and it is very stable (this same atom, minus the two orbital electrons, is ejected from some radioactive atoms as an alpha particle, i.e., a charged helium nucleus). Helium-5 (^{5}He) cannot be formed because the extra neutron creates a very unstable atom that breaks apart very fast (in 10^{-21} s or so). But, for many atoms an extra neutron(s) is easily accommodated to yield one or more isotopes of the same element, and for some elements adding an extra neutron (or proton) to a nucleus only destabilizes it; i.e., it will often exist as an unstable, or radioactive, atom. Such is the case for hydrogen-3 (^{3}H, or tritium) and carbon-14 (^{14}C). Elements are often identified by name and mass number, e.g., hydrogen-3 (^{3}H) or carbon-14 (^{14}C).

Three protons can be assembled with three neutrons to form lithium-6 (^{6}Li) or with four neutrons, lithium-7 (^{7}Li). Since lithium contains three protons, it must also have three orbital electrons, but because the first orbit can only hold two electrons (there is an important reason for this which is explained by quantum theory) the third electron occupies another orbit further away.

1.3 Chart of the Nuclides

As shown in Figure 1-1, a plot of the number of protons versus the number of neutrons increases steadily for heavier atoms because extra neutrons are necessary to distribute the nuclear force and moderate the repulsive electrostatic force between protons. The heaviest element in nature is ^{238}U with 92 protons and 146 neutrons; it is radioactive, but very long-lived. The heaviest stable element in nature is ^{209}Bi with 83 protons and 126 neutrons. Lead with 82 protons is much more common in nature than bismuth and for a long time was thought to be the heaviest of the stable elements; it is also the stable endpoint of the radioactive transformation of uranium and thorium, two primordial naturally occurring radioactive elements (see Chapter 6).

The *chart of the nuclides* contains basic information on each element, how many isotopes it has (atoms on the horizontal lines) and which ones are stable (shaded) or unstable (unshaded). A good example of such information is shown in

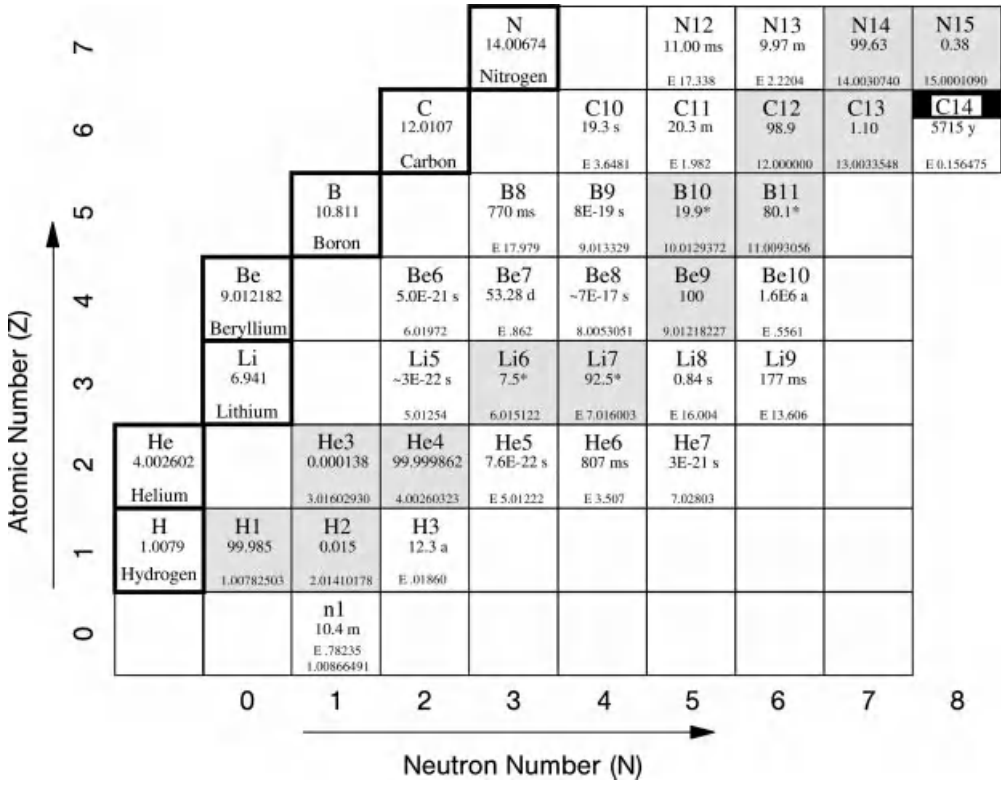

Fig. 1-1 Part of the chart of the nuclides.
(*Nuclides and Isotopes*, 16th Edition, KAPL, Inc, 2002.)

Figure 1-2 for four isotopes of carbon (actually there are 8 measured isotopes of carbon but these 4 are the most important). They are all carbon because each contains 6 protons, but each has a different number of neutrons, hence they are distinct isotopes with different weights. ^{12}C and ^{13}C are shaded and thus are stable, as are the two shaded blocks for boron (5 protons) and nitrogen (7 protons) also shown in Figure 1-2. The nuclides in the unshaded blocks (e.g., ^{11}C and ^{14}C) are unstable simply because they don't have the right array of protons and neutrons to be stable (we will use these properties later to discuss radioactive transformation). The dark band at the top of the block for ^{14}C denotes that it is a naturally-occurring radioactive isotope, a convention used for several other such radionuclides. The block to the far left contains information on naturally abundant carbon: it contains the chemical symbol, C, the name of the element, and the atomic weight of natural carbon, or 12.0107 grams/mole, weighted according to the percent abundance of the two naturally occurring stable isotopes. The shaded blocks contain the atom percent abundance of ^{12}C and ^{13}C in natural carbon at 98.90 and 1.10 atom percent, respectively; these are listed just below the chemical symbol. Similar information is provided for all of the elements in the chart of the nuclides.

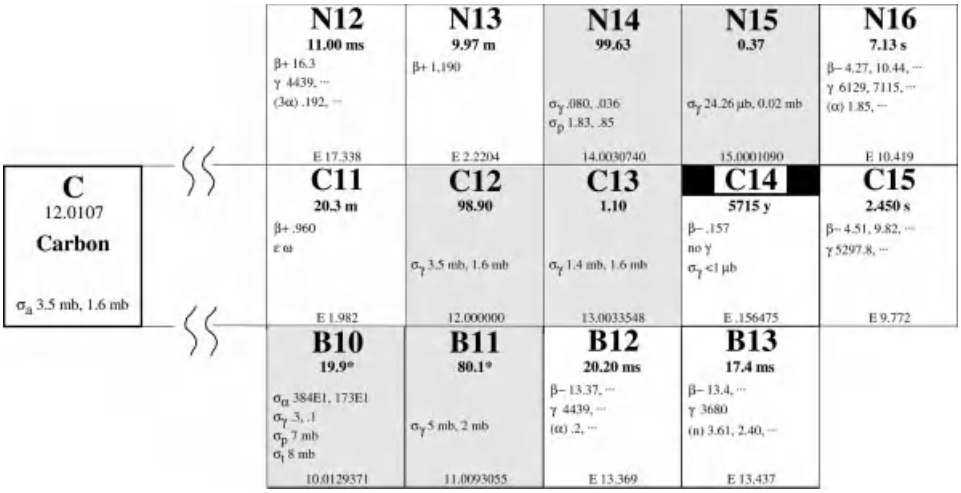

Fig. 1-2 Excerpt from the chart of the nuclides for the two stable isotopes of carbon ($Z = 6$) and its two primary radioactive isotopes, in relation to primary isotopes of nitrogen ($Z = 7$) and boron ($Z = 5$). (Adapted from KAPL, 2002.)

1.4 Nuclear Models

The array of protons and neutrons in each element is unique because nature forces these constituents toward the lowest potential energy possible; when they attain it they are stable, and until they do they have excess energy and are thus unstable, or radioactive; e.g. tritium or carbon-14. Descriptions of the dynamics and changes in energy states of nuclear constituents often use a shell model; however, descriptions of fission and other phenomena are best done with a liquid drop model. The exact form of the nuclear force in the nucleus is not yet known nor the structure of potential energy states of its constituents, but a shell model corresponds nicely with the emission of gamma rays from excited nuclei. These emissions are similar to those that occur when orbital electrons change to one of lower potential energy.

The nucleus exhibits periodicities that suggest energy shells not unlike those observed for electron shells. Atoms that have 2, 8, 20, 28, 50, and 82 neutrons or protons and 126 neutrons are particularly stable. These values of N and Z are called magic numbers, and elements with them have many more stable isotopes than their immediate neighbors. For example, Sn ($Z = 50$) has 10 stable isotopes, while In ($Z = 49$) and Sb ($Z = 51$) each have only 2. Similarly, for $N = 20$, there are 5 stable isotones (differing elements with the same N number), while for $N = 19$, there is none, and for $N = 21$, there is only one. The same pattern holds for other magic numbers.

A *nebular model of the atom*, as shown in Figure 1-3, provides an overall description of the atom. In it the electrons are spread as waves of probability over the whole volume of the atom, a direct consequence of de Broglie's discovery of the wave characteristics of electrons and other particles. Electrons are distributed around a nucleus in energy states that are an equal number of de Broglie wavelengths, or $n\lambda$, where n, the principal quantum number, corresponds to energy shells, K, L, M, etc. for $n = 1, 2, 3, \ldots$; changes between electron states are quantized with discrete energies. The outer radius of the nebular cloud of electrons is about 10^{-10} m which is some 4 to 5 orders of magnitude greater than the nuclear radius at about one femtometer (10^{-15} m), commonly called one fermi in honor of the great Italian physicist and nuclear navigator, Enrico Fermi. The radius of the nucleus is proportional to $A^{1/3}$ or

$$r = r_o A^{1/3}$$

where A is the atomic mass number of the atom in question and the constant r_o has an average value of about 1.3×10^{-15} m, or 1.3 fermi.

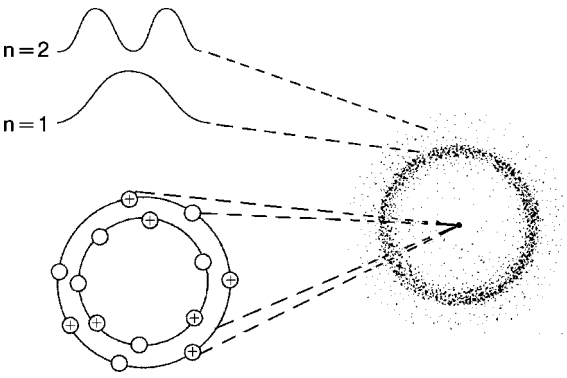

Fig. 1–3 Very simplified model of a nebular atom consisting of an array of protons and neutrons with shell-like states within a nucleus surrounded by a cloud of electrons with three dimensional wave patterns and also with shell-like energy states.

Problems – Chapter 1

1–1. How many neutrons and how many protons are there in: a) ^{14}C, b) ^{27}Al, c) ^{133}Xe, and d) ^{209}Bi?
1–2. Calculate the radius of the nucleus of ^{27}Al in meters and fermis.
1–3. When light of wavelength 3132 Å falls on a caesium surface, a photoelectron is emitted for which the stopping potential is 1.98 volts. Calculate the maximum energy of the photoelectron, the work function, and the threshold frequency.

1–4. The work function of potassium is 2.20 eV. What should be the wavelength of the incident electromagnetic radiation so that the photoelectrons emitted from potassium will have a maximum kinetic energy of 4 eV? Also calculate the threshold frequency.

1–5. Calculate the de Broglie wavelength associated with the following:

a) an electron with a kinetic energy of 1 eV

b) an electron with a kinetic energy of 510 keV

c) a thermal neutron (2200 m/s)

d) a 1500 kg automobile at a speed of 100 km/h.

1–6. Calculate the de Broglie wavelength associated with: a) a proton with 15 MeV of kinetic energy, and b) a neutron of the same energy.

2
Atoms and Energy

"$E = mc^2$" A. Einstein (1905)

Atoms contain enormous amounts of energy distributed among the energy states of its constituent parts. A decrease in the potential energy state of one or more of the constituents will cause the emission of energy either as a particle or a photon, or both. For example, an electron "free" of the nucleus will experience a decrease in potential energy as it goes from the surface (the "free" state) to level 2, or on down to level 1.

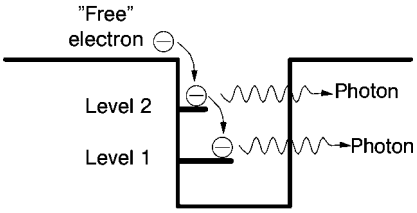

The levels represent negative energy states because it would take work to return the electrons to an unbound (or "free") state. The atom with bound electrons has been determined to be slightly lighter, and the loss of mass exactly matches the energy of the emitted photon(s). These concepts also apply to protons and neutrons which are bound in the nucleus at different energy levels, or

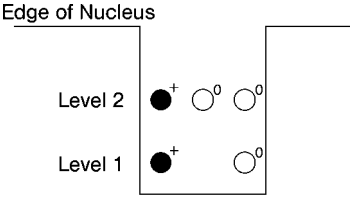

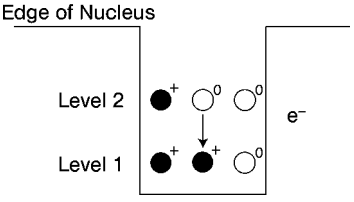

Physics for Radiation Protection, Third Edition. James E. Martin

Rearranging the neutrons and protons to lower potential energy states yields energy in the form of an ejected particle (energy = mass), or pure electromagnetic radiation, or both. Conversely, absorption of energy by an atom yields an increase in the potential energy of one or more of its constituents. Processes which change the array of particles in the nucleus are fundamental to radioactive transformation (see Chapter 3).

2.1 Atom Measures

Many radiation protection problems require knowledge of the number of atoms (Avogadro's number) in an amount (mass) of an element; the mass of each atom and its component particles; and the energy (in electron volts) associated with mass changes in and between atoms. Appendix A contains these and other key parameters related to atoms and radiation physics.

Avogadro's number, N_A, is the number of atoms or molecules in a mole of any substance and is a constant, independent of the nature of the substance. When Avogadro stated the concept in 1811 he had no knowledge of its magnitude only that the number was very large. Its modern value is:

$$N_A = 6.0221367 \times 10^{23} \text{ atoms per mole}$$

Example 2–1. Calculate the number of atoms of ^{13}C in 0.1 gram of natural carbon.
Solution. From Figure 1–2, the atomic weight of carbon is 12.0107 g and the atom percent abundance of ^{13}C is 1.10%. Thus

$$\text{Number of atoms of } {}^{13}\text{C} = \frac{0.1 \text{ g} \times N_A \text{ atoms/mole}}{12.0107 \text{ g/mole}} \times 0.011$$

$$= 5.5154 \times 10^{19} \text{ atoms}$$

The *atomic mass unit*, or to be precise the unified mass unit, u, is used to express the masses of atom constituents as well as atoms themselves (since the sum of protons and neutrons in individual atoms is the mass number, one of these must be a "mass unit"). The u is defined as one-twelfth the mass of the neutral ^{12}C atom, which weighs exactly 12.000000 g. All other elements and their isotopes are assigned weights relative to ^{12}C. The atomic mass unit was originally defined relative to oxygen-16 at 16.000000 grams per mole but carbon-12 has proved to be a better reference nuclide, and since 1962, atomic masses have been based on the unified mass scale referenced to carbon-12.

The mass of a single atom of ^{12}C can be obtained from the mass of one mole of ^{12}C which contains Avogadro's number of atoms as follows:

$$m(^{12}\mathrm{C}) = \frac{12.000000\ \mathrm{g/mole}}{6.0221367 \times 10^{23}\ \mathrm{atoms/mole}} = 1.9926482 \times 10^{-23}\ \mathrm{g/atom}$$

This mass is shared by 6 protons and 6 neutrons; thus, the average mass of each of the 12 building blocks of the carbon-12 atom, including the paired electrons, can be calculated by distributing the mass of one atom of carbon-12 over the 12 nucleons. This quantity, or u, has the value:

$$\mathrm{u} = 1.9926482 \times 10^{-23}\ \mathrm{g}/12 = 1.66053886 \times 10^{-24}\ \mathrm{g}$$

which is close to the actual mass of the proton (actually $1.6726231 \times 10^{-24}$ g) or the neutron (actually $1.6749286 \times 10^{-24}$ g). In unified mass units, the mass of the proton is 1.00727647 u and that of the neutron is 1.008664923 u. Each of these values is so close to unity that the mass number of an isotope is thus a close approximation of its atomic weight. Measured masses of elements are given in unified mass units, u, and these are listed at the bottom of their respective blocks (e.g., ^{12}C and ^{13}C in Figure 1–2) in the chart of the nuclides. Masses of atoms have been determined to six or more decimal places, and since energy changes in nuclear processes represent mass changes, accurate masses (as listed in Appendix B) are very useful for calculations of energies of nuclear events, e.g. radioactive transformation.

The *electron volt* (eV) is defined as the increase in kinetic energy of a particle with one unit of electric charge (e.g., an electron) when it is accelerated through a potential difference of one volt, or

$$\begin{aligned} 1\ \mathrm{eV} &= (q)\ (\Delta \mathrm{V}) = (1.60217653 \times 10^{-19}\ \mathrm{C})\ (1\ \mathrm{V}) \\ &= 1.60217653 \times 10^{-19}\ \text{Volt Coloumb} \\ &= 1.60217653 \times 10^{-19}\ \mathrm{J} \\ &= 1.60217653 \times 10^{-12}\ \mathrm{erg} \end{aligned}$$

This relationship, $1\ \mathrm{eV} = 1.60217653 \times 10^{-19}\ \mathrm{J} = 1.60217653 \times 10^{-12}$ erg, is used frequently in calculations of the amount of energy deposited in a medium. In absolute terms, the eV is not very much energy, thus the energy of atomic changes is commonly expressed in keV (10^3 eV) and MeV (10^6 eV). For example, a one MeV beta particle has essentially received a jolt of one million volts.

Example 2–2. An x-ray tube accelerates electrons from a cathode into a tungsten target anode to produce x-rays. If the electric potential across the tube is 90 kilovolts, what will be the energy of the electrons when they hit the target in eV, joules, ergs?

Solution. E = 90,000 eV, or in joules is

$$E = 90{,}000\ \mathrm{eV} \times 1.60217653 \times 10^{-19}\ \mathrm{J/eV} = 1.442 \times 10^{-14}\ \mathrm{J}$$

and in ergs

$$E = 1.442 \times 10^{-14}\ \text{J} \times 10^{7}\ \text{erg/J} = 1.442 \times 10^{-7}\ \text{erg}.$$

2.2 Energy Concepts for Atoms

The energy associated with atoms is governed by Einstein's special theory of relativity which states that mass and energy are one and the same. He also showed that the mass m of a body varies with its speed, v, according to

$$m = \frac{m_o}{\sqrt{1 - (v^2/c^2)}}$$

where m_o is the rest mass and c is the velocity of light in a vacuum, which is a constant. The net force on a body is, according to Newton's second law, a function of its momentum , or

$$F = \frac{d(mv)}{dt}$$

which, if mass can be assumed to remain constant, reduces to

$$F = m\frac{dv}{dt} = ma$$

which is the classical relationship used to calculate the force on objects at low speeds (less than 10% of the speed of light). For atoms, however, many particles in and associated with atoms move at high speeds; thus, Newton's second law must be stated in terms of the relativistic mass, or

$$F = \frac{d(mv)}{dt} = \frac{d}{dt}\left(\frac{m_o v}{\sqrt{1 - (v^2/c^2)}}\right)$$

In relativistic mechanics, as is classical mechanics, the kinetic energy, KE, of a body is equal to the work done by a force over a distance ds:

$$\text{KE} = \int F\, ds$$

Using $ds = vdt$ and the relativistic generalization of Newton's second law,

$$\mathrm{KE} = \int_0^s \frac{d(mv)}{dt} \cdot v\, dt = \int_0^{mv} v\, d(mv)$$

If the term in the parenthesis is differentiated, and the integration performed,

$$\mathrm{KE} = \frac{m_o c^2}{\sqrt{1 - v^2/c^2}} - m_o c^2 = (m - m_o)\, c^2$$

thus, the kinetic energy (KE) gained by a moving particle occurs from the mass increase due to its motion; it is also the difference between the total energy, mc^2, of the particle and its rest energy, $m_o c^2$. Thus, mass and energy are equivalent, or

$$E = mc^2 = \mathrm{KE} + m_o c^2$$

Thus, even when a body is at rest it still has an energy content given by $E_o = m_o c^2$, so that in principle the potential energy inherent in the mass of an object can be completely converted into kinetic energy. Atomic and nuclear processes routinely convert mass to energy and vice versa, thus nuclear processes that yield or consume energy can be conveniently described by the mass changes that occur. Such measurements are among the most accurate in science.

Although Einstein's concepts are fundamental to atomic phenomena, they are even more remarkable because when he stated them in 1905 no model of the atom existed. He had deduced the theory in search of the basic laws of nature that govern the dynamics and motion of objects. Einstein's discoveries encompass Newton's laws for the dynamics of macro-world objects but more importantly also apply to micro-world objects where velocities approach the speed of light; Newton's laws break down at these speeds, but Einstein's relationships do not. Einstein believed that the forces of nature were interconnected and he sought, without success, a unified field theory for it.

2.2.1 Mass-energy

Energy changes in nuclear processes are readily determined by the mass changes that occur. The energy equivalent of one unified mass unit, u, is

$$E = m_o c^2 = 1.660539 \times 10^{-27}\ \mathrm{kg/u}\ (2.99792458 \times 10^8\ \mathrm{m/s})^2 / 1.6021892\ \mathrm{J/MeV}$$
$$= 931.494\ \mathrm{MeV/u}$$

And, for an electron mass:

$$E = m_o c^2 = 9.1093826 \times 10^{-31}\ \mathrm{kg}\ (2.99792458 \times 10^8\ \mathrm{m/s})^2 / 1.6021892\ \mathrm{J/MeV}$$
$$= 0.511\ \mathrm{MeV}$$

Various nuclear processes occur in which an electron mass is converted to 0.511 MeV photons or vice versa. For example, a photon with $E = h\nu > 1.022$ MeV can, in the vicinity of a charged body (a nucleus or an electron), vanish yielding two electron masses (a process called pair production) and kinetic energy. This net kinetic energy (KE = $h\nu$ – 1.022 MeV) is shared by the particles thus produced. And in similar fashion, the amount of energy potentially available from the complete annihilation of 1 g of matter is:

$$E = 1 \text{ g } (2.99792458 \times 10^{10} \text{ cm/s})^2 = 8.988 \times 10^{20} \text{ g} \cdot \text{cm}^2/\text{s}^2$$

or 8.988×10^{13} J, which is about 25 million kilowatt · hours, an enormous amount of energy. Both fission and fusion cause atoms to become more tightly bound (see below) with significant changes in mass that is converted to energy.

2.2.2 Binding Energy of Nuclei

The potential energy states of the particles that make up an atom are less than when they exist separately; i.e., if two masses, m_1 and m_2, are brought together to form an atom of mass M, it will hold together only if:

$$M < m_1 + m_2$$

The energy released in binding the two masses is called the binding energy, E_b, or

$$E_b = (m_1 + m_2 - M)\ c^2 = \Delta m c^2$$

E_b is also the energy that must be supplied to break M into separate masses; it is calculated by finding the mass difference between the mass of the assembled atom and that of its individual particles. For example, deuterium, ^{2}H, with a rest mass of 2.01410178 u contains a proton (m = 1.00727647 u), one electron (m = 0.00054858 u), and one neutron (m = 1.008664904 u). These constituents total 2.01648996 u which exceeds the measured mass of deuterium by 0.00238818 u; therefore the binding energy holding the deuterium atom together is

$$E_b = 0.00238818 \text{ u} \times 931.5 \text{ MeV/u} = 2.2246 \text{ MeV}$$

which is released as photon energy as the constituents become bound to form deuterium. This calculation could also be written as a nuclear reaction

$$^1_1\text{H} + ^1_0\text{n} \rightarrow ^2_1\text{H} + \gamma + Q$$

where $Q = 2.2246$ MeV. The binding energy of the orbital electron is implicitly ignored in this example; however, it is only 13.6 eV which is negligible compared to 2.2246 MeV.

The *Q-value* represents the amount of energy that is gained when atoms change their bound states or that must be supplied to break them apart in a particular way. For example, in order to break ^{2}H into a proton and a neutron, an energy equal to 2.2246 MeV (the *Q*-value) would need to be added to the ^{2}H atom, usually as a photon, i.e.

$$^2_1\mathrm{H} + Q \rightarrow {}^1_1\mathrm{H} + {}^1_0\mathrm{n}$$

If the photon energy is greater than 2.2246 MeV the excess energy will exist as kinetic energy shared by the proton and the neutron. For tritium, the constituent masses are:

mass of 1 proton	= 1.00727647 u
mass of 2 neutrons	= 2 × 1.00866491 u
mass of electron	= 0.0005485799 u
Total	= 3.025155 u

which is larger than the measured mass of 3.016049 u (see Appendix B) for ^{3}H by 0.0091061 u; thus, and the total binding energy of tritium is

$$E_b = 0.009106 \text{ u} \times 931.5 \text{ MeV/u} = 8.48 \text{ MeV}$$

and the average binding energy for each of its three nucleons is 2.83 MeV per nucleon.

The *binding energy per nucleon* (E_b/A) can be calculated for each of the elements (from masses listed in Appendix B), and when plotted (Figure 2-1) shows several significant features:

- The elements in the middle part of the curve are the most tightly bound, the highest being ^{62}Ni at 8.7945 MeV/nucleon and ^{58}Fe at 8.7921 MeV/nucleon;
- Certain nuclei, ^{4}He, ^{12}C, ^{16}O, ^{28}Si, and ^{32}S, are extra stable because their masses are multiples of the mass of helium ($A = 4$), with the exception of ^{8}Be, which breaks up very rapidly (10^{-16} s or so) into two atoms of ^{4}He;
- Fission of a heavy nucleus like ^{235}U and ^{239}Pu produces two lighter atoms (or products) with nucleons that are more tightly bound with a net energy release; and
- Fusion of light elements (e.g. ^{2}H and ^{3}H to produce helium) yields an atom that is more tightly bound causing a large release of energy.

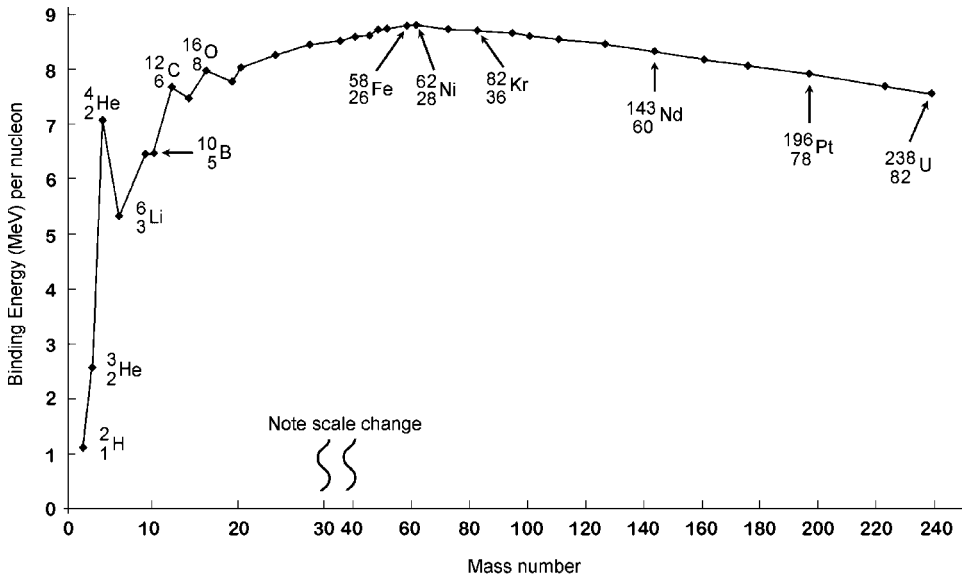

Fig. 2-1 Curve of binding energy per nucleon versus atomic mass number (plotted from data in Appendix B).

2.3 Summary

Einstein's theory of special relativity is applicable to atom systems where particles undergo interchangeable mass/energy processes. These processes yield "radiation" which can be characterized as the emission of energy in the form of particles or electromagnetic energy proportional to the change in mass that occurs as atom constituents change potential energy states. The mass values are very exact as is the calculated energy change (or *Q*-value). Binding energy is one important result of such calculations; it denotes the amount of energy given off as constituents come together to form an atom, or alternatively, the energy required to disengage them.

Other Suggested Sources

Chart of the nuclides, in *Nuclides and Isotopes*, 16th Edition, 2002. Available at: www.ChartOfTheNuclides.com.

National Nuclear Data Center, Brookhaven National Laboratory, Upton, Long Island, NY 11973. Data resources are accessible through the internet at www.nndc.bnl.gov.

Problems – Chapter 2

2–1. What is the energy, in electron volts, of a quantum of wavelength $\lambda = 5500$ Å?
2–2. A one gram target of natural lithium is to be put into an accelerator for bombardment of ^{6}Li to produce ^{3}H. Use the information in Figure 1-1 to calculate the number of atoms of ^{6}Li in the target.
2–3. If one were to base the atomic mass scale on ^{16}O at 16.000000 atomic mass units (amu), calculate the mass of the ^{16}O atom and the mass of one amu. Why is its mass on the ^{12}C scale different from 16.000000?
2–4. Calculate the number of atoms in one gram of natural hydrogen.
2–5. Hydrogen is a diatomic molecule, or H_2. Calculate the mass of one molecule of H_2.
2–6. Electrons in an x-ray tube are accelerated through a potential difference of 3000 volts. What is the minimum wavelength of the x-rays produced in a target?
2–7. A linear accelerator is operated at 700 kilovolts to accelerate protons. What energy will the protons have when they exit the accelerator in: a) eV, and b) joules. If deuterium ions are accelerated what will be the corresponding energy?
2–8. Calculate the velocity required to double the mass of a particle.
2–9. Use the masses in Appendix B to calculate the total binding energy and the binding energy per nucleon of: a) beryllium-7, b) iron-56, c) nickel-62, and d) uranium-238.

3
Radioactive Transformation

"Don't call it transmutation...they'll have our heads off as alchemists."
Ernest Rutherford (1902)

Much of what has been learned about atomic and nuclear physics is based on this remarkable property by which certain nuclei transform themselves spontaneously from one value of Z and N to another. Discovery of the emissions of alpha and beta particles established that atoms are not indivisible, but are made up of more fundamental particles. Use of the emitted particles as projectiles to transform nuclei led eventually to some of the greatest discoveries in physics.

The process of radioactive transformation was recognized by Rutherford as transmutation of one element to another. It is also quite common to use the term radioactive decay, but transformation is a more accurate description of what actually happens; decay suggests a process of disappearance when what actually happens is an atom with excess energy transforms itself to another atom that is either stable or one with more favorable conditions to proceed on to stability.

3.1
Processes of Radioactive Transformation

Atoms undergo radioactive transformation because constituents in the nucleus are not arrayed in the lowest potential energy states possible; therefore, a rearrangement of the nucleus occurs in such a way that this excess energy is emitted and the nucleus is transformed to an atom of a new element. The transformation of a nucleus may involve the emission of alpha particles, negatrons, positrons, electromagnetic radiation in the form of x-rays or gamma rays, and, to a lesser extent, neutrons, protons, and fission fragments. Such transformations are spontaneous, and the Q-values are positive; if the array of nuclear constituents is in the lowest potential energy states possible, the transformation yields a stable atom; if not, another transformation must occur.

Perhaps the best way to relate the dynamics of radioactive transformations is to consider unstable, or radioactive nuclei relative to those that are stable in nature. Figure 3-1 shows a plot of the number of protons (Z) and the number of neutrons (N, or $A - Z$) in all stable nuclei. This plot uses the same axes as the *chart of the*

Physics for Radiation Protection, Third Edition. James E. Martin

nuclides. Stable nuclei are shown as black squares on this plot extending from $Z = 1$ for hydrogen up to $Z = 83$ for ^{209}Bi. Also shown in Figure 3-1 are very long-lived ^{238}U and ^{232}Th which are quite prevalent in nature even though they are radioactive. These nuclides and their transformation products exist well above the end of the "line" of stable nuclei. Also shown is ^{239}Pu, a very important artificial radionuclide produced in nuclear reactors; it is above uranium (or transuranic). These long-lived radionuclides produce long chains of radioactive products before they become stable.

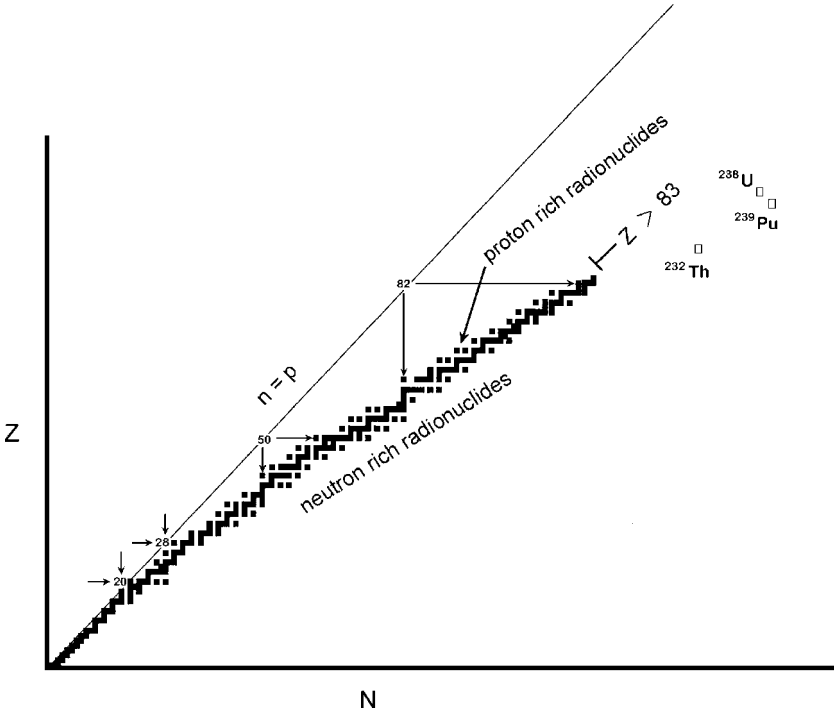

Fig. 3-1 Line of stable nuclides on the chart of the nuclides relative to neutron-rich (below the line), proton-rich (above the line), and long-lived heavy ($Z > 83$) nuclei.

Although the plot of the stable nuclei is called the line of stability, it is not a line but more a zigzag array with some gaps. For light nuclei, the neutron and proton numbers are roughly equal. However, for heavy nuclei, the coulomb repulsion between the protons is substantial and extra neutrons are needed to supply additional binding energy to hold the nucleus together. Thus, all heavy stable nuclei have more neutrons than protons. Interestingly, there are no stable nuclei with $A = 5$ or $A = 8$. A nucleus with $A = 5$, such as ^{5}He or ^{5}Li, will quickly (in 10^{-21} s or so) disintegrate into an alpha particle and a neutron or proton. A nucleus with $A = 8$, such as ^{8}Be, will quickly break apart into two alpha particles or two helium nuclei. The helium nucleus, $^{4}_{2}He^{2+}$, is particularly stable with a binding energy

per nucleon of 7.07 MeV; the energetics of existing separately as two helium nuclei is more favorable than being joined as ^{8}Be.

Regardless of their origin, radioactive nuclides surround the "zigzag" line of stable nuclei. These can be grouped into three major categories that will determine how they must undergo transformation to become stable:

- neutron-rich nuclei, which lie below the zigzag line of stable elements
- proton-rich nuclei, which are above the line
- heavy nuclei with $Z > 83$.

The basic energy changes represented by these groupings comprise several transformation modes of importance to health physics for they govern how a particular nuclide undergoes transformation and the form of the emitted energy. The characteristics of these emissions in turn establish how much energy is available for potential absorption in a medium to produce biological change(s) and how they may be detected. We examine first the energetics of these transformations, followed by the mathematical laws describing the rate of radioactive transformation.

3.1.1 Transformation of Neutron-rich Radioactive Nuclei

Neutron-rich nuclei fall below the line of stable nuclei as shown in Figure 3-2 for ^{14}C, an activation product produced by an (n,p) reaction with stable nitrogen thus reducing the proton number from 7 to 6 and increasing the neutron number from 7 to 8. For neutron-rich nuclei to become stable, they need to reduce the number of neutrons in order to become one of the stable nuclides which are diagonally up and to the left on the chart of the nuclides. In simplest terms, this requires a reduction of one negative charge (or addition of a positive one) in the nucleus. Since these nuclei have excess energy (mass), the transformation can occur if the nucleus emits a negatively charged electron (or beta particle). This results in an increase in the charge on the nucleus and a slight reduction of mass (equal to the electron mass and the mass equivalence of emitted energy) and has the effect of conversion of a neutron to a proton. The negatively charged electron is emitted with high energy. The mass change is small; the only requirement is to reduce the ratio of neutrons to protons.

The transformation of ^{14}C (see Figure 3-2) by beta particle emission can be shown by a reaction equation as follows:

$$^{14}_{6}\mathrm{C} \rightarrow ^{14}_{7}\mathrm{N} + ^{0}_{-1}\mathrm{e} + \bar{\nu} + Q$$

The Q-value for this transformation is 0.156 MeV and is positive, which it must be for the transformation to be spontaneous. This energy is distributed between the recoiling product nucleus (negligible) and the ejected electron, which has most of

it. When ^{14}C undergoes transformation to ^{14}N, the atomic number Z increases by 1, the neutron number N decreases by 1, and the mass number A remains the same. The transition should be thought of as a total nuclear change producing a decrease in the neutron number (or an increase in the proton number); this change is shown in Figure 3-2 as a shift upward and to the left on the chart of the nuclides to stable ^{14}N.

Radioactive transformations are typically displayed in decay schemes, which are a diagram of energy (vertical axis) versus Z (horizontal axis). Because the net result is an increase in atomic number and a decrease in total energy, transformation by beta particle (β^-) emission is shown by an arrow down and to the right on a plot of energy versus Z, also shown in Figure 3-2.

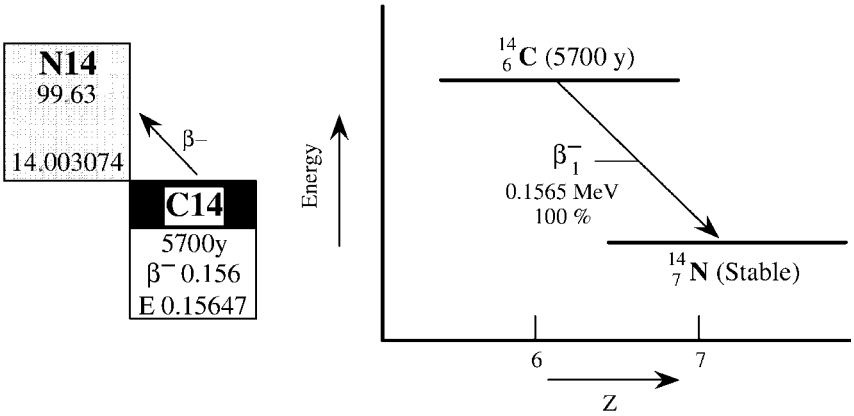

Fig. 3-2 Position of ^{14}C relative to its transformation product, ^{14}N, on the chart of the nuclides and its decay scheme.

Somewhat more complex transformations of neutron-rich radionuclides are shown in Figure 3-3 for ^{60}Co and ^{137}Cs along with their positions on the chart of the nuclides. These neutron-rich nuclei fall below the line of stability; some are fission products (e.g., ^{137}Cs), but they may also be the product of nuclear interactions (e.g., ^{60}Co, an activation product) which result in an increase in the N number. Both of these radionuclides undergo transformation by the emission of two beta particles with different probabilities, and gamma emission follows one of the routes to relieve the excitation energy that remains because the shell configuration of the neutrons in the nucleus has not achieved the lowest potential energy states possible via the beta emission.

Decay schemes for simplicity do not typically show the vertical and horizontal axes, but it is understood that the transformation product is depicted below the radioactive nuclide (i.e., with less energy) and that the direction of the arrow indicates the change in atomic number Z. For similar reasons, gamma emission (Figure 3-3) is indicated by a vertical line (no change in Z) often with a wave motion.

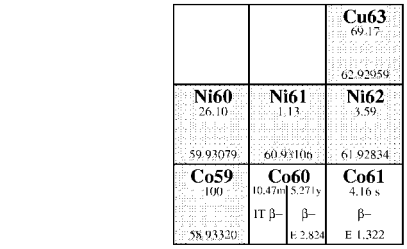

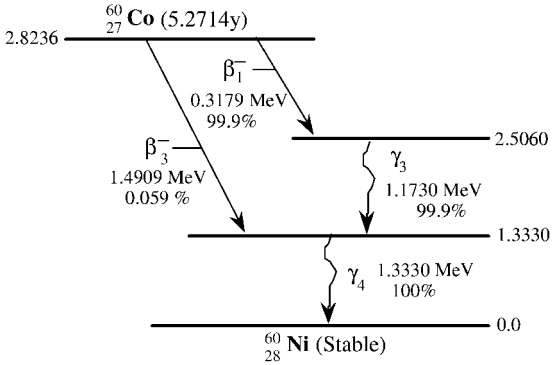

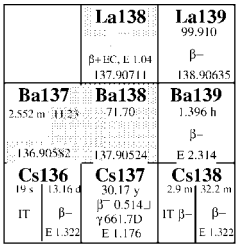

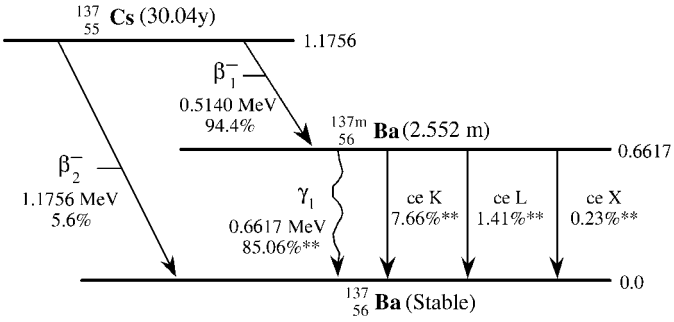

** Percent transformation of the ^{137}Cs parent

Fig. 3-3 Artificial radionuclides of neutron-rich ^{60}Co and ^{137}Cs relative to stable nuclides and their transition by β^- emission (note that the excerpt from the chart of the nuclides lists a gamma ray energy for ^{137}Cs of 661.7D indicating that it is delayed, which occurs through ^{137m}Ba).

Unlike alpha particles, which are monoenergetic from a given source, beta particles are emitted with a range of energies ranging from just above 0 MeV to the maximum energy (denoted as $E_{\beta,\max}$) available from the mass change for the particular radioactive nuclide. These energies form a continuous spectrum, as illustrated in Figure 3-4 for ^{14}C.

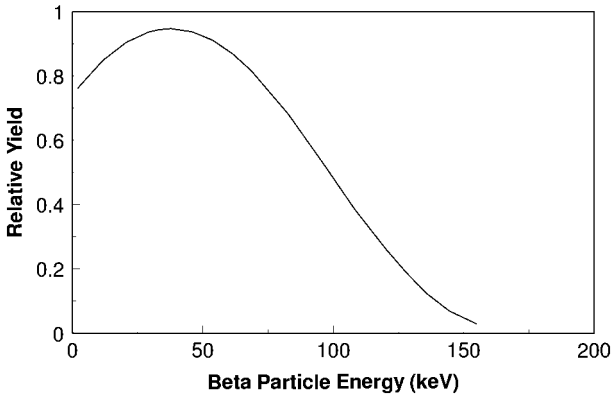

Fig. 3-4 Continuous spectrum of beta particle emission from ^{14}C.

When it was first observed that beta particles are emitted with a spectrum of energies, it was most perplexing to physicists, since conservation of energy requires that all beta transformations from a given source undergo the same energy change since the mass change is constant. For example, in the transformation of ^{14}C to ^{14}N, the energy of the nucleus decreases by 0.156 MeV because of the decrease in mass that occurs during the transformation. Some of the emitted beta particles have the maximum energy, $E_{\beta,\max}$, but most do not, being emitted at some smaller value with no observable reason since the "missing" energy is not detectable. The "missing" energy posed an enigma to physicists: is the well-established law of conservation of energy wrong, is Einstein's mass–energy relation wrong, or is there a way to explain the missing energy? The suggestion was made by Pauli and further developed by Fermi in 1934 that the emission of a beta particle is accompanied by the simultaneous emission of another particle, a neutrino (Fermi's "little one") with no charge and essentially no mass, that would carry off the rest of the energy. The neutrino (actually an antineutrino, $\bar{\nu}$, from ^{14}C transformation to conserve spin) does possess momentum and energy; however, it is so evasive that its existence was not confirmed until 1956 when Reines and Cowan obtained direct evidence for it using an extremely high beta field from a nuclear reactor and an ingenious experiment as described later in this chapter.

Radioactive transformation is a process that involves the whole atom which is demonstrated by the transformation of ^{187}Re to ^{187}Os by negative beta particle emission; i.e., the entire atom must "participate." The Q-value for $^{187}Re \rightarrow {}^{187}Os + \beta^-$ is 2.64 keV; however, the binding energy of atomic electrons in Os is 15.3 keV greater than in Re. This means that a Re nucleus weighs less than an Os nucleus

plus an electron by 12.7 keV (15.3 – 2.6 keV) and the ^{187}Re nucleus alone cannot supply the mass/energy to yield ^{187}Os. The entire ^{187}Re atom must supply the energy for the transformation from ^{187}Re to ^{187}Os by an adjustment of all of the constituent particles and energy states; this circumstance influences the very long half-life of 4.3×10^{10} y of this primordial radionuclide.

3.1.2
Double Beta ($\beta\beta$) Transformation

A very rare transformation of neutron-rich radionuclides is $\beta\beta$ transformation, in which two negatively charged beta particles are emitted in cascade. Double beta transformation can occur in cases where only one beta transformation would be energetically impossible. For example, ^{128}Te to ^{128}I would require a Q-value of –1.26 MeV which cannot occur spontaneously, but $\beta\beta$ transformation from ^{128}Te to ^{128}Xe has a Q-value of 0.87 MeV, and is therefore energetically possible.

Since two beta particles must be emitted for $\beta\beta$ transformation to occur, it would be expected to be highly improbable and the half-life would be very long. A classic example of $\beta\beta$ transformation is ^{130}Te to ^{130}Xe associated with the primordial radionuclide ^{130}Te which has a half-life of 2.5×10^{21} y (see the chart of the nuclides). The long half-life for $\beta\beta$ transformation of ^{130}Te was determined by mass spectroscopy. The method was based on observing an excess abundance of Xe (relative to its abundance in atmospheric Xe) in a tellurium-bearing rock. If the rock is T years old and short compared to the $\beta\beta$ half-life of ^{130}Te, the number of Xe atoms from $\beta\beta$ transformation is

$$N(\mathrm{Xe}) = N(\mathrm{Te})(1 - e^{-\lambda t}) \cong N(\mathrm{Te})\lambda(\mathrm{Te})$$

thus the half-life of ^{130}Te is

$$T_{1/2}(\mathrm{Te}) = \ln 2 \frac{N(\mathrm{Te})}{N(\mathrm{Xe})}$$

The number of Te and Xe atoms measured by the mass spectrometer can be used directly to determine the $\beta\beta$ half-life for $^{130}\mathrm{Te} \rightarrow {}^{130}\mathrm{Xe}$, which is 2.5×10^{21} y. Similarly, the $\beta\beta$ half-life for $^{82}\mathrm{Se} \rightarrow {}^{82}\mathrm{Kr}$ has been measured at 1.4×10^{20} y.

The long half-lives of $\beta\beta$ transformation preclude direct detection since a mole of a sample would produce just a few transformations per year, and this rate would be virtually impossible to distinguish from natural radioactivity or cosmic rays.

3.1.3
Transformation of Proton-rich Nuclei

Proton-rich nuclei have charge and mass such that they are above the line of stable nuclei, i.e., they are unstable due to an excess of protons. These nuclei are typically produced by interactions of protons or deuterons with stable target mate-

rials, thereby increasing the number of protons in the target nuclei. Such interactions commonly occur with cyclotrons, linear accelerators, or other particle accelerators, and there are numerous (p,n) reactions that occur in nuclear reactors that produce them. Proton-rich nuclei achieve stability by a total nuclear change in which a positively charged electron mass, or positron, is emitted or an orbital electron is captured by the unstable nucleus. Both processes transform the atom to one with a lower Z value.

Some of the common proton-rich radionuclides, ^{11}C, ^{13}N, ^{18}F, and ^{22}Na, are shown in Figure 3-5 as they appear on the chart of the nuclides relative to stable nuclei. These nuclei will transform themselves to the stable elements ^{11}B, ^{13}C, ^{18}O, and ^{22}Ne, respectively, which are immediately down and to the right (i.e., on the diagonal) on the chart. The mass number does not change in these transitions, only the ratio Z/N.

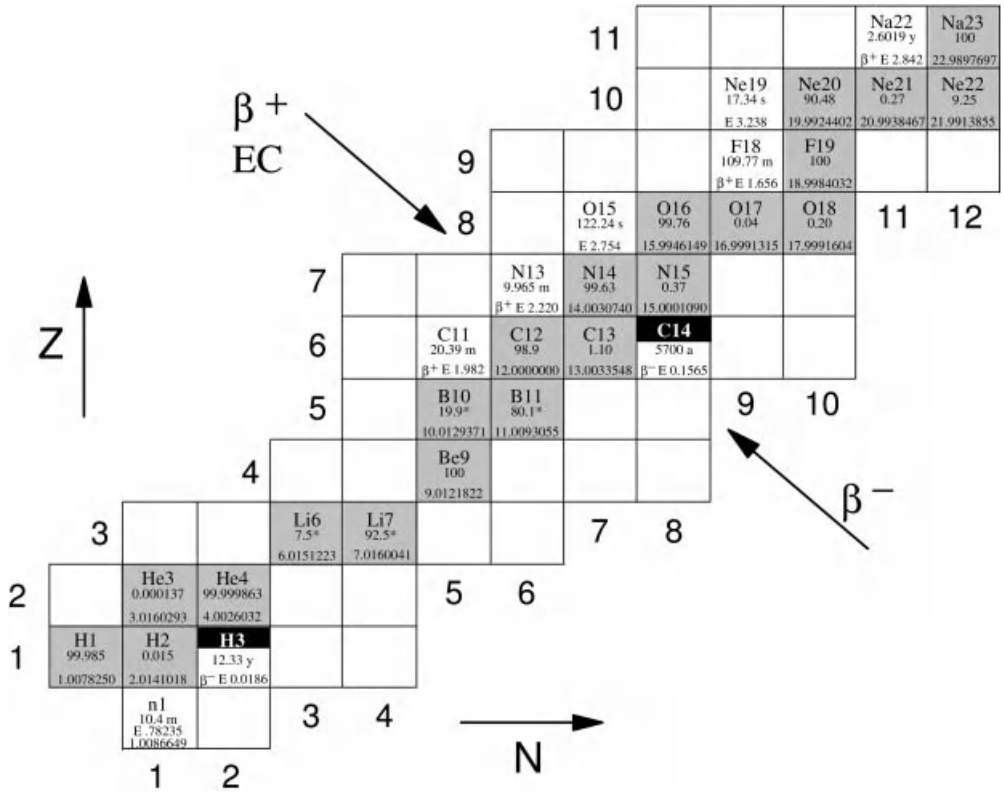

Fig. 3-5 Proton-rich radionuclides ^{11}C, ^{13}N, ^{18}F, and ^{22}Na relative to stable nuclei and neutron-rich ^{3}H and ^{14}C and the radioactive free neutron.

3.1.4 Positron Emission

Radioactive transformation by positron emission is often described as a proton being converted to a neutron and a positively charged electron, which is not quite correct because the proton cannot supply the mass necessary to produce a neutron (which is heavier than the proton) plus the electron mass and the associated kinetic energy carried by the positron. Rather, the process occurs as a total change in the nucleus where the protons and neutrons rearrange themselves to become more tightly bound, thus supplying the energy needed to yield a neutron and create a positron, and the kinetic energy given to it when it is emitted.

Two examples of radioactive transformation of proton-rich nuclides by positron emission are ^{18}F and ^{22}Na (as shown in Figure 3-6). These transformations are represented by the following nuclear reactions:

$$^{18}_{9}\mathrm{F} \xrightarrow{\beta^+} {}^{18}_{8}\mathrm{O} + {}^{0}_{1}\mathrm{e} + \nu + Q + \text{orbital electron}$$

$$^{22}_{11}\mathrm{Na} \xrightarrow{\beta^+} {}^{22}_{10}\mathrm{Ne} + {}^{0}_{1}\mathrm{e} + \nu + Q + \text{orbital electron}$$

It is particularly important to note that two electron masses are necessary on the product side to balance these reaction equations. One electron mass is the emitted positron; the other occurs because of the reduced charge on the ^{18}O or ^{22}Ne product nucleus. Therefore, for a nucleus to undergo transformation by positron emission, it must have enough excess mass to be able to supply these two electron masses over and above the mass of the product nucleus. In simpler terms, if the radioactive proton-rich nucleus is not two electron masses (i.e., 1.022 MeV) heavier than the product nucleus, transformation by positron emission cannot occur. When positron emission is possible, the positron is emitted with a maximum energy $E_{\beta,\max}$ that is equal to the Q-value of the transition minus 1.022 MeV that is consumed in producing two electron masses. Since the available energy is shared between the positron and a neutrino, a spectrum of energies is produced.

The spectrum of positron energies is skewed to the right because the coulomb force field of the positively charged nucleus gives the positively charged electron an added "kick" as it leaves the nucleus. Figure 3-7 shows the different shaped spectra for β^- emission and β^+ emission from radioactive transformation of ^{64}Cu. The average β^+ and β^- energy is about $(1/3)E_{\max}$; however, the true average energy requires a weighted sum of the energies across the spectrum, and these are tabulated in the listings of positron emitting nuclides included in Appendix D.

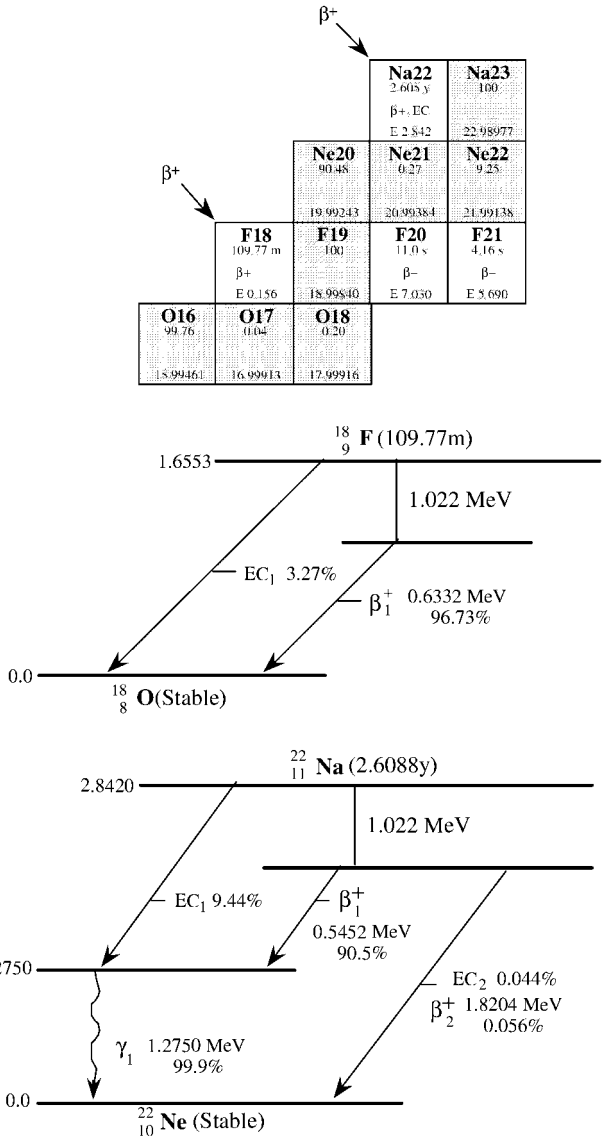

Fig. 3-6 Proton-rich ^{18}F and ^{22}Na relative to stable nuclei and their transformation by β^+ emission (E_{avg} = 0.2498 and 0.2155, respectively), electron capture, and gamma-ray emission.

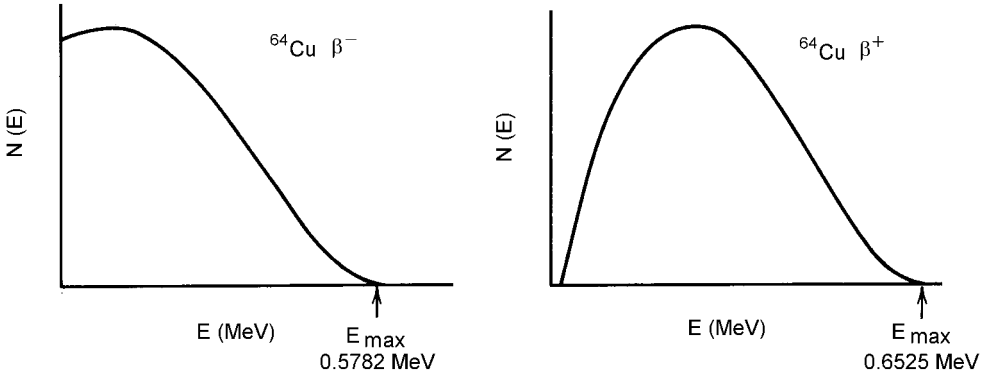

Fig. 3-7 Comparison of β^- and β^+ energy spectrum from ^{64}Cu transformation showing the effect of the positively charged nucleus on spectral shape.

Annihilation radiation always accompanies positron emission because the emitted positively charged electrons are antimatter, which will interact with and be annihilated by negative electrons that are so freely distributed throughout matter. Annihilation of the positron with a negatron results in the complete conversion of the two electron masses into pure energy which almost always occurs as the simultaneous emission of two 0.511 MeV photons by the reaction

$$e^+ + e^- \rightarrow h\nu_1 + h\nu_2$$

This interaction is shown in Figure 3-8. The positron and negatron come together for a fleeting moment to form positronium which consists of the two electron masses with unique spin, charge neutralization, and energetics before the complete conversion of the electrons to pure energy. The 0.511 MeV photons produced are emitted back-to-back or 180° from each other; they are commonly called gamma rays, but they do not originate from the nucleus and it is more accurate to refer to them as annihilation photons or just 0.511 MeV photons.

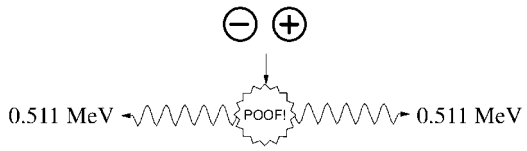

Fig. 3-8 Annihilation of a positron and a negatron, which converts the electron masses to electromagnetic radiation.

3.1.5 Average Energy of Negatron and Positron Emitters

A general relationship for the average kinetic energy of the β^- particles emitted in radioactive transformation is

$$E_{\beta^-,\text{avg}} = \frac{1}{3} E_{\beta^-,\text{max}} \left(1 - \frac{\sqrt{Z}}{50}\right)\left(1 + \frac{\sqrt{E_{\beta^-,\text{max}}}}{4}\right)$$

where $E_{\beta^-,\text{avg}}$ and $E_{\beta^-,\text{max}}$ are in MeV. A reasonable rule of thumb for $E_{\beta^-,\text{avg}}$ is $\frac{1}{3}E_{\beta^-,\text{max}}$.

The general relationship for the average kinetic energy for the β^+ particles emitted by positron emitters is

$$E_{\beta^+,\text{avg}} = \frac{1}{3} E_{\beta^+,\text{max}} \left(1 + \frac{\sqrt{E_{\beta^+,\text{max}}}}{4}\right)$$

where $E_{\beta^+,\text{avg}}$ and $E_{\beta^+,\text{max}}$ are in MeV. Although the β^+ energy spectrum has a different shape from the β^- spectrum, a reasonable rule of thumb for $E_{\beta^+,\text{avg}}$ is also $\frac{1}{3}E_{\beta^+,\text{max}}$.

The best values of $E_{\beta^-,\text{avg}}$ and $E_{\beta^+,\text{avg}}$ are weighted averages based on the beta spectrum for each radionuclide that emits beta particles or positrons. These weighted values are all incorporated into the tables of radiation emissions listed in Appendix D.

Example 3-1. Determine the average beta energy for negatron emission of ^{64}Cu which by a Q-value calculation has a maximum beta energy of 0.5787 MeV. How does this compare with the $\frac{1}{3}E_{\beta^-,\text{max}}$ rule of thumb calculation?
Solution.

$$E_{\beta^-,\text{avg}} = \frac{1}{3}(0.5787)\left(1 - \frac{\sqrt{29}}{50}\right)\left(1 + \frac{\sqrt{0.5787}}{4}\right) = 0.2049 \text{ MeV}$$

By rule of thumb:

$$E_{\beta^-,\text{avg}} = \frac{0.5787}{3} = 0.1929 \text{ MeV}$$

which is roughly 94.2% of the more careful calculation; the accepted value based on spectrum weighting (Appendix D) is 0.1902 MeV.

Copper-64 also emits a positron with $E_{\beta^+,\text{max}}$ of 0.6531 MeV. Its average energy, $E_{\beta^+,\text{avg}}$, is 0.2335 MeV by the detailed calculation and 0.2177 MeV by the rule of thumb determination; both are considerably lower (83.9% and 78.3%, respectively) than the value of 0.2782 MeV listed in Appendix D. These examples are

adequate for most radiation protection considerations, but the more exact values listed in Appendix D and the NNDC database are perhaps more appropriate for beta dose determinations.

3.1.6 Electron Capture (EC)

The decay scheme for ^{22}Na discussed above shows that only 90% of the transformations of ^{22}Na occur by positron emission. The remaining 10% is by electron capture, which is a competing mechanism by which proton-rich nuclei reduce the number of protons. Electron capture competes with positron emission only when positron emission is energetically possible as in ^{22}Na; when sufficient energy is not available for positron emission, the number of protons in proton-rich nuclei can only be reduced by capture of an orbital electron. Since both positron emission and electron capture reduce the number of protons to achieve stability, they compete with each other, but only if both can occur.

Electron capture transformation occurs because the wave motion of orbital electrons can bring them close enough to the unstable nucleus such that capture of the electron results in the reduction of the number of protons in the nucleus (as illustrated in Figure 3-9).

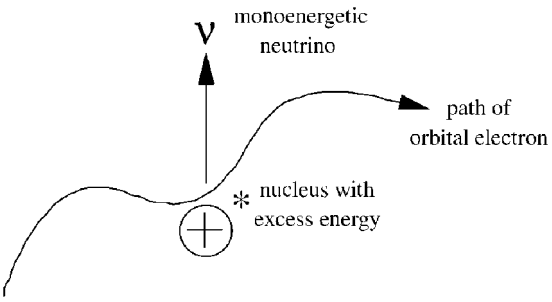

Fig. 3-9 Capture of an orbital electron in electron capture transformation of proton-rich radionuclides to reduce the nuclear charge. The de Broglie wave pattern of the orbiting electrons causes them to come close to or pass through the nucleus allowing capture to occur.

Typical reactions for electron capture are represented by the transformation of ^{59}Ni and ^{55}Fe, neither of which have sufficient excess mass to supply two electron masses (i.e., $Q < 1.022$ MeV); thus, electron capture is the only means by which such nuclei can undergo transformation to more stable products by the following reactions:

$$^{59}_{28}\mathrm{Ni} + {}^{0}_{-1}\mathrm{e} \rightarrow {}^{59}_{27}\mathrm{Co} + \nu + Q$$

$$^{55}_{26}\mathrm{Fe} + {}^{0}_{-1}\mathrm{e} \rightarrow {}^{55}_{25}\mathrm{Mn} + \nu + Q$$

The accompanying decay schemes for these transitions are shown in Figure 3-10.

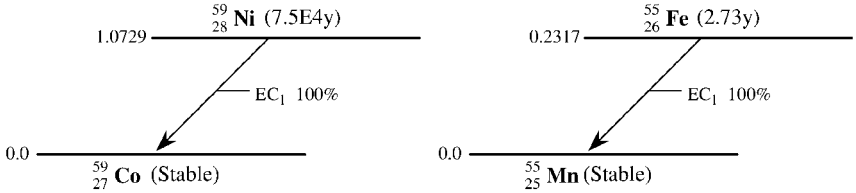

Fig. 3-10 Decay scheme of ^{55}Fe and ^{59}Ni. Each is followed by emission of characteristic x-rays (as shown in Figure 3-11 for $^{55}_{26}\text{Fe} \rightarrow ^{55}_{25}\text{Mn}$).

Since K-shell electrons are closest to the nucleus to begin with, most electron capture events (of the order of 90%) involve K capture; however, it is probable for L-shell electrons to come close enough for capture and some 10% of the captured electrons are L-shell electrons. M-shell electrons can also be captured, but with much lower (about 1%) probability.

In electron capture transformations, Z decreases by 1, N increases by 1, and A, the mass number, remains the same. However, the capture of an electron from the K, L, or M shell leaves a vacancy that is immediately filled by electrons from higher energy levels. This process is accompanied by the emission of x-rays characteristic of the product nuclide. For example, as shown in Figure 3-11, radioactive transformation of ^{55}Fe by electron capture results in the emission of x-rays that are due to energy changes between the electron shells of ^{55}Mn, the transformed atom, and hence the emitted x-rays are characteristic of Mn. The energy of the characteristic x-rays emitted by ^{55}Mn is about 5.9 keV. Therefore, the only way electron capture transformations produce energy emission or deposition (radiation dose) is by these very weak x-rays or Auger electrons associated with them (see Chapter 4). They also represent the only practical means for detecting these radioactive nuclides.

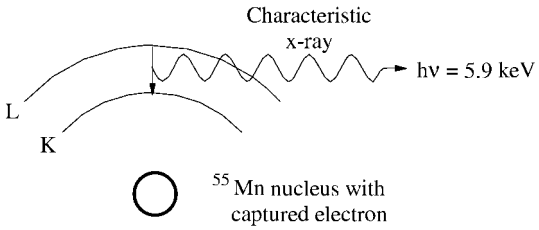

Fig. 3-11 Emission of a 5.9 keV characteristic x-ray by filling the K-shell electron vacancy from the L shell in an atom of ^{55}Mn, the product of K-shell electron capture transformation of a nucleus of ^{55}Fe.

Electron capture transformation is accompanied by emission of a monoenergetic neutrino in contrast to the spectrum of neutrino energies in β^- and β^+ trans-

formations. Electron capture is also referred to as a form of beta transformation because an electron is involved and the mass number of the transforming nucleus does not change, only the ratio of protons to neutrons. The energy of the monoenergetic neutrino is just the *Q*-value for the transformation minus any excitation energy that may be emitted in the form of gamma rays to relieve excitation energy retained by the transformed nucleus.

Example 3-2. What is the energy of the neutrino emitted in electron capture transformation of ^{22}Na to ^{22}Ne?
Solution. From Figure 3-6, electron capture of ^{22}Na is followed by emission of a 1.28 MeV gamma photon. The *Q*-value of the reaction is 2.84 MeV, thus

$$E_{\text{neutrino}} = 2.84 - 1.28 = 1.56 \text{ MeV}$$

3.1.7 Radioactive Transformation of Heavy Nuclei by Alpha Particle Emission

A number of unstable nuclei exist above $Z = 83$ (bismuth). These nuclei include the long-lived naturally occurring ^{238}U, ^{235}U, and ^{232}Th and their transformation products, and they also include artificially produced transuranic radionuclides such as ^{239}Pu, ^{241}Am, etc. ^{238}U and ^{232}Th are so long lived that they still exist after the formation of the solar system some 4 to 14 billion years ago. For them to achieve stability, they must convert themselves to one of the stable isotopes of lead (^{206}Pb for ^{238}U or ^{208}Pb for ^{232}Th), each of which is considerably lighter than the parent; ^{238}U atoms must lose 32 mass units including 10 protons ($Z = 92$ to $Z = 82$) and 22 neutrons, and ^{232}Th must lose 24 mass units, or 8 protons ($Z = 90$ to $Z = 82$) and 16 neutrons. The most efficient way for these nuclides to reduce both mass and charge is through the emission of several $^{4}He^{2+}$ nuclei (or alpha particles), each of which will reduce the proton and neutron numbers by 2 and the mass number by 4. Reduction of *A*, *Z*, and *N* for these heavy nuclides yields a long chain of transformation products (called series decay) before a stable end product is reached, as shown in Figure 3-12 for series transformation of ^{235}U (the stable end product is ^{207}Pb). A hypothetical dashed "line of stability" is shown as an extrapolation from the stable nuclei below to indicate how the path of transformation crosses back and forth before a stable configuration of *N* and *Z* is found at stable ^{207}Pb. The intermediate alpha emissions yield unstable nuclei, and some of these emit beta particles if the neutron to proton ratio is "too high." A zigzag path of transformation prevents the transformation to nuclei that are too far from the projected line of stability (no actual line of stability exists above bismuth).

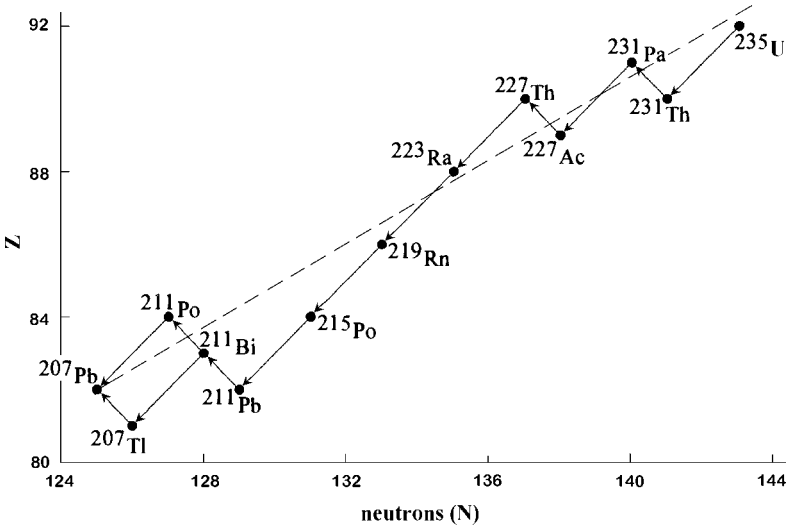

Fig. 3-12 Change in proton number (*Z*) versus neutron number (*N*) for the uranium-235 series relative to an extrapolated "line of stability."

The alpha particle is a helium nucleus, i.e., a helium atom stripped of its electrons, and it consists of two protons and two neutrons. It is, on the nuclear scale, a relatively large particle. In order for a nucleus to release such a large particle, the nucleus itself must be relatively large. Alpha particles resulting from a specific nuclear transformation are monoenergetic, and they have large energies, generally above about 4 MeV. A typical example is ^{226}Ra which has a *Q*-value of 4.87 MeV:

$$^{226}_{88}\mathrm{Ra} \rightarrow ^{222}_{86}\mathrm{Rn} + ^{4}_{2}\mathrm{He} + 4.87\mathrm{MeV}$$

where both *Z* and *N* of the transforming atom decrease by 2 while the mass number *A* decreases by 4. Although the total energy change for the reaction is 4.87 MeV, the energy of the emitted alpha particle is only 4.78 MeV. The difference of 0.09 MeV is the energy of recoil imparted to the newly formed radon nucleus. As shown in Figure 3-13, the parent nucleus is essentially at rest before the alpha particle is emitted, and the mass of the emitted alpha particle is large enough that the product nucleus undergoes recoil in order to conserve momentum.

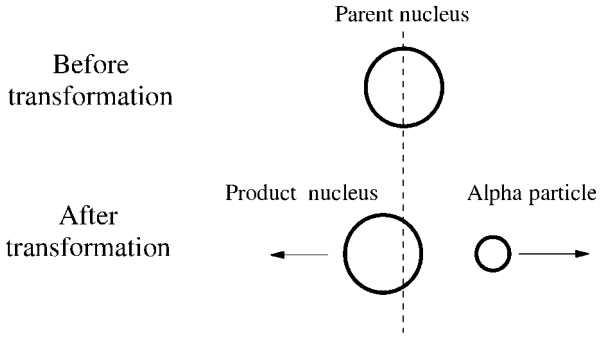

Fig. 3-13 Parent nucleus at rest before and after transformation. The emitted alpha particle and the product nucleus recoil in opposite directions to conserve linear momentum.

Calculation of the *Q*-value for alpha particle emission yields the total disintegration energy, which is shared between the emitted alpha particle and the recoiling product nucleus. The kinetic energy of the ejected alpha particle will be equal to the *Q*-value of the reaction minus the recoil energy imparted to the product nucleus. For ^{226}Ra the *Q*-value is

$$\begin{aligned} Q &= \text{mass of } {}^{226}\text{Ra} - (\text{mass of } {}^{222}\text{Rn} + \text{mass of } {}^{4}\text{He}) \\ &= 226.025406 \text{ u} - (222.017574 + 4.002603) \text{ u} \\ &= 0.005227 \text{ u} \times 931.5 \text{ MeV/u} = 4.87 \text{ MeV} \end{aligned}$$

The *Q*-value energy is shared between the product nucleus and the alpha particle, both of which can be considered nonrelativistically in terms of their velocity and mass, or

$$Q = \frac{1}{2}(Mv_{\mathrm{p}})^2 + \frac{1}{2}(mv_a)^2$$

since energy is conserved. Momentum is also conserved such that $Mv_{\mathrm{p}} = mv_a$ and the kinetic energy E_a imparted to the alpha particle is

$$E_a = \frac{Q}{1 + (m_a/M)}$$

where m_a and M are the masses (approximated by the mass numbers) of the alpha particle and the recoiling product nucleus, respectively.

Example 3-3. Calculate the kinetic energy of the alpha particle emitted when ^{226}Ra is transformed directly to the ground state of ^{222}Rn. What is the recoil energy of the ^{222}Rn product nucleus?
Solution. The *Q*-value of the transformation reaction is 4.87 MeV; thus

$$E_a = \frac{4.87\,\text{MeV}}{1 + (4/222)} = 4.78\,\text{MeV}$$

and the recoil energy is

$$E_R = 4.87\ \text{MeV} - 4.78\ \text{MeV} = 0.09\ \text{MeV}$$

Alpha particle transformation is shown schematically in the decay scheme (or the *E*–*Z* diagram) as a decrease in energy due to the ejected mass and a decrease in the atomic number by two units. Figure 3-14 shows the transformation of ^{226}Ra to ^{222}Rn, and the change in position of the transforming nucleus and the product nucleus on the chart of the nuclides.

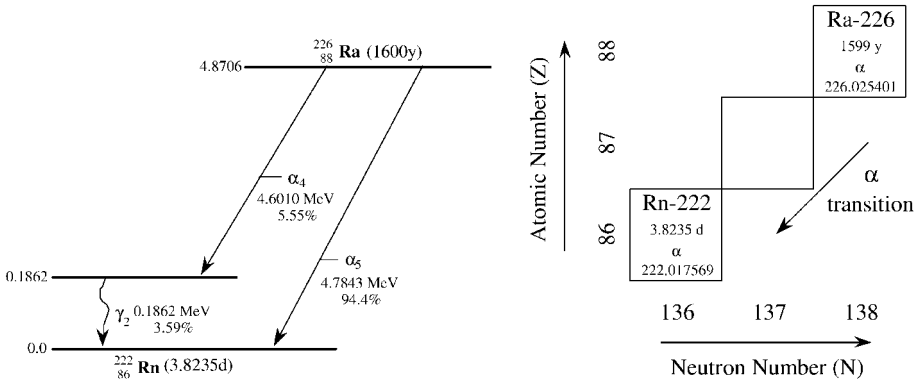

Fig. 3-14 Decay scheme of ^{226}Ra plotted as a change in *E* and *Z* and its transition to ^{222}Rn on the chart of the nuclides.

The decay scheme shows two alpha particles of different energies from the radioactive transition of ^{226}Ra. The first (4.78 MeV) occurs in 94% of the transformations and leads directly to the ground state of ^{222}Rn; the other (4.59 MeV) occurs 6% of the time and leaves the product nucleus in an excited state. The excited nucleus reaches the ground state by emitting a gamma ray of 0.186 MeV with a yield of 3.59% (internal conversion accounts for the other 2.1% by this route). The existence of these two different alpha particle energies and the gamma ray demonstrates the existence of discrete nuclear energy states. The alpha particles for a given transition are monoenergetic, i.e., they all have the same energy.

3.1.8 Theory of Alpha Particle Transformation

Alpha particle transformation cannot be explained by classical physics because the alpha particle does not have enough energy to penetrate the large potential energy barrier of heavy nuclei like radium, etc. This potential energy barrier can be as much as 30–40 MeV, whereas most emitted alpha particles have energies

well below 10 MeV. When considered as a wave mechanical phenomenon, however, the de Broglie wavelength of an alpha particle in the nucleus has a probability of existing beyond the barrier, and in fact does so. An alpha particle confined to the nucleus can be thought of as two protons and two neutrons coming together to temporarily make up the particle. An alpha particle of 4–5 MeV will have a velocity such that it will bounce back and forth within the potential well of the nucleus some 10^{22} times per second. This large number of attacks on the potential barrier of the nucleus combined with the de Broglie wavelength (Figure 3-15) eventually leads to the alpha particle "tunneling through" the barrier.

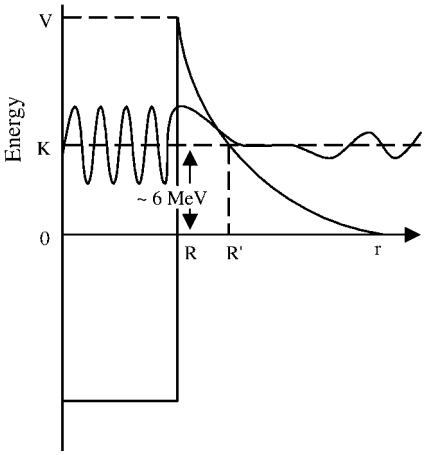

Fig. 3-15 Barrier penetration of a heavy nucleus by an alpha particle.

The probability of emission (tunneling) increases with alpha particle energy, as shown in Figure 3-16 which is a plot of the half-lives of various alpha emitters versus the energies of the emitted alpha particles. Clearly, the higher the alpha particle energy, the shorter the half-life indicating that the probability of transformation is markedly higher. This can be explained by the "thickness" of the potential energy barrier in Figure 3-15. The higher energy particles interact with the thinner part of the barrier and have a greater likelihood of tunneling through whereas the lower energy ones interact the thicker part of the potential barrier and are less likely to penetrate. From Figure 3-16 it is startling that a twofold change in alpha energy results in a change in half-life of 10^{22}. This effect, which is quite uniform over typical alpha particle energies, is characterized as the Geiger–Nuttall rule after the scientists who first deduced the relationship. It is often plotted as the logarithm of the disintegration constant, λ, or of the half-life, each of which shows an approximate straight-line relationship.

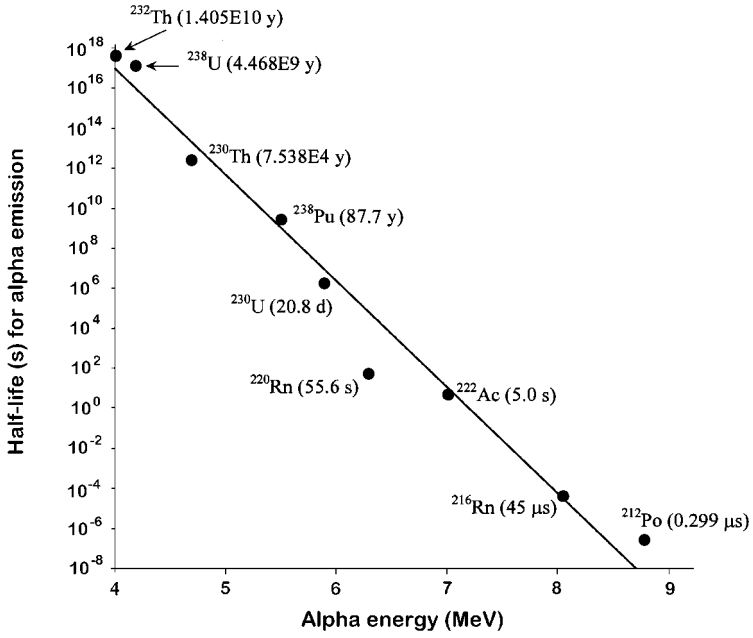

Fig. 3-16 Geiger–Nuttall relationship between probability of alpha particle emission, i.e., half-life, and kinetic energy of the emitted alpha particle. A twofold change in alpha particle energy changes the half-life by a factor of 10^{22}.

3.1.9
Transuranic (TRU) Radionuclides

Transuranic elements, which exist above $Z = 92$, also emit a large number of alpha and beta particles to reduce mass and charge as they undergo transformation to a stable isotope of bismuth or lead. They represent a special group of heavy elements all of which are radioactive and are produced primarily by bombarding ^{238}U with neutrons. Transformation of TRUs typically joins one of the naturally radioactive series in the process of achieving a path to stability. Selected TRUs are shown in Figure 3-17. All of these are well above the end of the curve of stable nuclei and are above uranium in the chart, hence the name TRU nuclides. The arrows in Figure 3-17 provide a general path of the formation of some of the major TRU nuclides by neutron activation and beta transformation from ^{238}U to produce ^{239}Pu and further neutron activation of ^{239}Pu to yield increasingly heavier TRUs, many of which undergo radioactive transformation by alpha particle emission. For example, ^{240}Pu (half-life of 6564 years) emits two alpha particles with energies of 5.17 MeV and 5.12 MeV, as shown in Figure 3-18.

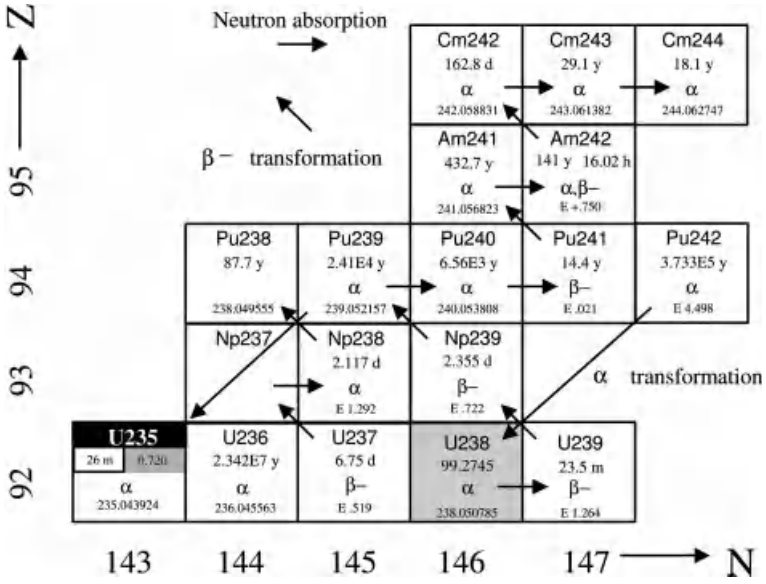

Fig. 3-17 Transuranic (TRU) radionuclides relative to naturally occurring uranium with arrows showing routes of production via neutron absorption and/or beta transformation.

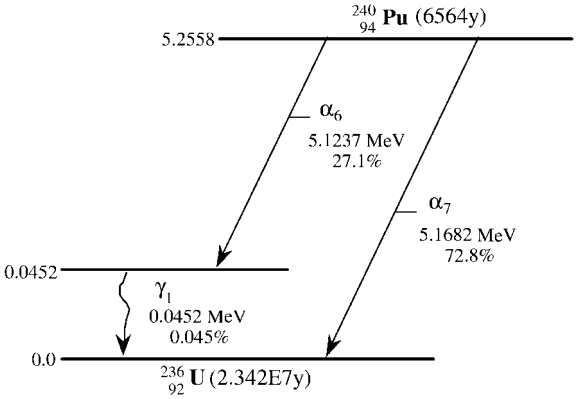

Fig. 3-18 Radioactive transformation of ^{240}Pu to ^{236}U by alpha particle emission.

3.1.10 Gamma Emission

Radioactive transformation is a chaotic process and often leaves the transforming nucleus in an excited state in which the protons and neutrons in the shells of the nucleus are not in the most tightly bound state possible. This excitation energy

will be emitted as electromagnetic radiation as the protons and neutrons in the nucleus rearrange themselves to the desired lowest energy state. The shell model of the nucleus suggests discrete energy states for neutrons and protons; it is this difference between energy states that is emitted as a gamma photon when rearrangement takes place. Thus, the emitted gamma ray is characteristic of that particular nucleus.

Gamma emission, as important as it is in radiation protection, occurs only after radioactive transformation has occurred by alpha particle emission, negatron emission, positron emission, or electron capture, all of which change the unstable atom to another atom. It is incorrect to refer to this process as gamma decay because gamma rays are produced only to relieve excitation energy, i.e., the atom is still the same atom after the gamma ray is emitted. The decay schemes in Figure 3-3 for ^{60}Co and ^{137}Cs illustrate how gamma emission occurs to relieve excited states after the emission of a negatively charged beta particle.

3.1.11 Internal Transition (Metastable or Isomeric States)

Most excited states in atoms are relieved in less than 10^{-9} s or so by gamma emission; however, some excited states may exist long enough to be readily measurable, and in these cases the entire process of radioactive transformation may be thought of as two separate events. Such a delayed release of excitation energy represents a metastable (or isomeric state); when radioactive transformation is interrupted by a metastable state, it is known as internal transition.

Figure 3-19 illustrates the radioactive transformation of ^{99}Mo, with about 15% of the beta transitions omitted for clarity; the beta transitions shown yield a metastable state of ^{99m}Tc at an energy level of 0.1405 MeV above the ground state of ^{99}Tc. The metastable state, ^{99m}Tc, is delayed considerably with a 6-hour half-life, and it is relieved by the emission of gamma radiation (or internal transition) to the ground state of ^{99}Tc. The only change that occurs in ^{99m}Tc (i.e., the excited ^{99}Tc nucleus) is the relief of the excitation energy, and although the gamma emission rate of ^{99m}Tc is often stated in curies or becquerels, this is not strictly correct because these units define the quantity of a radionuclide undergoing radioactive transformation to another element, which ^{99m}Tc does not do because it only emits excitation energy.

The production of ^{99m}Tc by ^{99}Mo has found widespread use in nuclear medicine because a ^{99}Mo source with its 66-hour half-life can be fabricated into a generator of ^{99m}Tc, which provides a relatively pure source of 140 keV gamma rays without the confounding effects of beta particles. The ^{99m}Tc can be extracted periodically by eluting an ion-exchange column with saline solution. This selectively strips the ^{99m}Tc; however, some ^{99}Mo may also be eluted. The gamma emission rate of the eluted ^{99m}Tc is directly dependent on the activity of the ^{99}Mo parent, the fraction (82.84%) of beta particle transformations that produce the metastable state of Tc, and the period of ingrowth that occurs between elutions. These relative activities represent series transformation (see below).

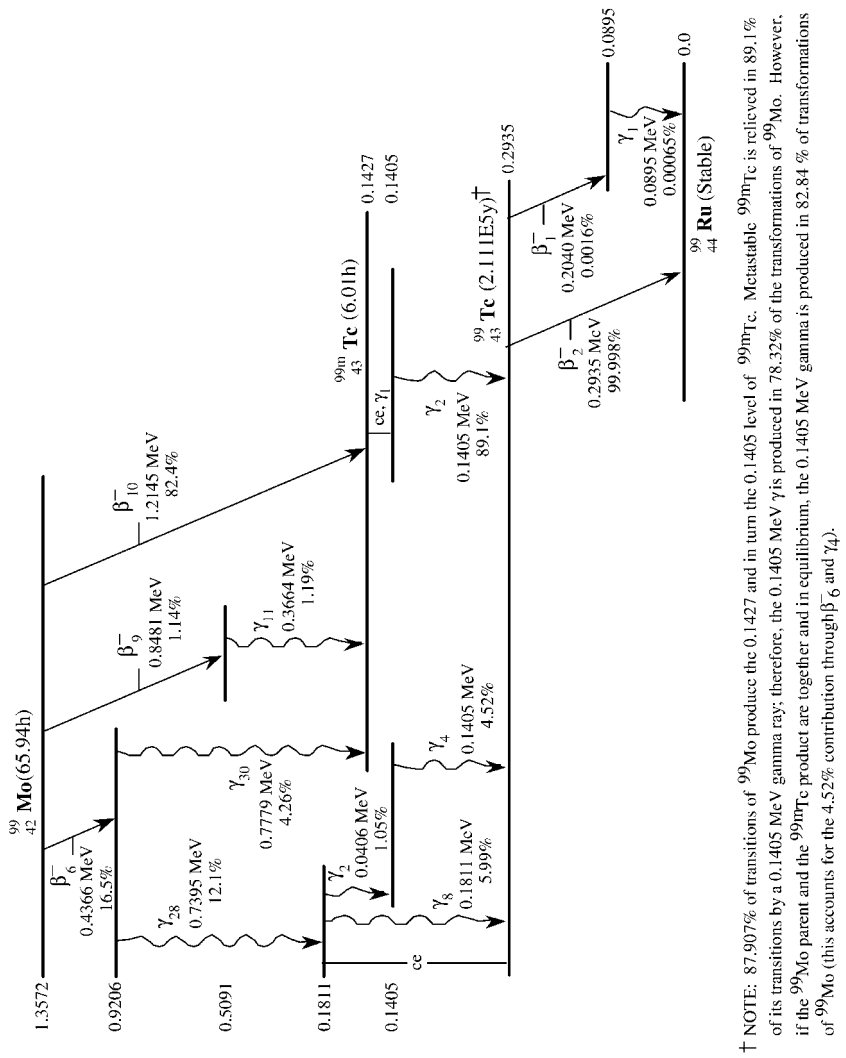

Fig. 3-19 Decay scheme of ^{99}Mo through ^{99m}Tc to ^{99}Tc. The gamma-ray yields are for isomeric transition of ^{99m}Tc and thus total 100%; however, the emission rate of 0.1405 MeV gamma rays is only 82.84 per 100 transformations of ^{99}Mo. The ^{99}Tc end product is effectively stable.

3.1.12
Internal Conversion

Many nuclei are left in an excited state following radioactive transformation. This excitation energy is usually relieved by the emission of a gamma ray, but the wave

motion of the orbital electrons can bring them close enough to the nucleus such that the excitation energy can be transferred directly to one of the orbital electrons, ejecting it from the atom; i.e., they are internally converted to an ejected electron to relieve the excitation energy remaining in the nucleus. The kinetic energy of the conversion electron is discrete; it is the difference between that available for emission as a gamma photon minus the binding energy of the electron in the particular shell from which it is converted (i.e., from a bound electron to an ejected electron with kinetic energy). This process competes with gamma emission to relieve the excitation energy left in the nucleus after a transformation occurs by particle emission or electron capture. Since internal conversion occurs when an orbital electron and an excited nucleus meet, it is more prevalent for metastable nuclides in which the nucleus retains the excitation energy for a longer period, but it can occur with any excited nucleus that could emit gamma radiation, just with lower (often negligible) probability. The process of internal conversion is shown schematically in Figure 3-20.

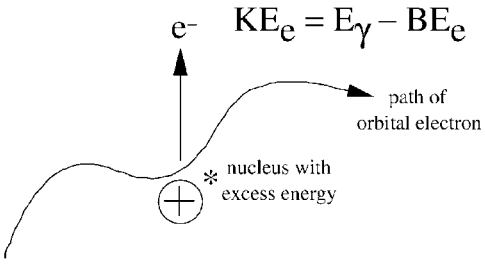

Fig. 3-20 Relief of excitation energy by internal conversion. The excitation energy of the nucleus is transferred directly to an orbital electron, which due to its wave motion can exist close to or in the nucleus where it can "pick up" the energy and be ejected. The kinetic energy of the internally converted electron is equal to that available for gamma emission minus the orbital binding energy of the ejected electron.

Energetically, the process of internal conversion can be thought of as similar to an internal photoelectric effect, except that the photon does not appear, only the energy. The gamma photon is not emitted because the excitation energy in the nucleus is transferred directly to the orbital electron. The kinetic energy of the ejected electron is the energy available for gamma emission minus the binding energy of the electron in its particular orbit; thus, it is similar to the work function energy that must be overcome when photons undergo photoelectric interactions with bound orbital electrons in target atoms. Conversion of K-shell electrons is most probable because the K electrons spend more time close to the nucleus than do any of those of the outer orbitals, but internal conversions can occur for L, M, and, on rare occasions, the more distant orbital electrons. In contrast to beta emission, the electron is not created in the transformation process, and no neutrinos are involved. For this reason internal conversion rates can be altered slightly by changing the chemical environment of the atom, thus changing somewhat the atomic orbits. It is not a two-step process: a photon is not emitted to knock loose

an orbiting electron as in the photoelectric effect; the probability of such an event would be negligible.

A common example of internal conversion occurs in the transformation of ^{137}Cs through ^{137m}Ba, as shown in Figure 3-21. When ^{137}Cs atoms undergo transformation, 94.4% go to an excited state of ^{137}Ba, indicated as ^{137m}Ba, with a metastable half-life of 2.55 minutes. The excited nuclei of ^{137m}Ba then emit gamma rays in 90.1% of emissions, 8.11% by internal conversion of K-shell electrons (α_K = 0.0811), and 1.72% by electron conversion from other shells; i.e., for each 100 transformations of ^{137}Cs, 85.1 gamma photons, 7.66 internally converted electrons from the K shell, and 1.64 electrons from other shells will occur through relief of the excitation energy retained in ^{137m}Ba.

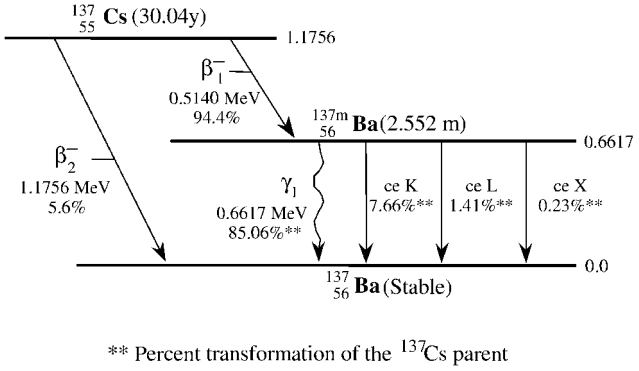

Fig. 3-21 Gamma emission and internal conversion of ^{137m}Ba in the radioactive transformation of ^{137}Cs through ^{137m}Ba to ^{137}Ba.

Conversion electrons are emitted monoenergetically because all of the energy states involved in internal conversion have definite values. The excitation energy left in a transformed nucleus is discrete as is the electron binding energy associated with each shell; therefore, electrons emitted due to internal conversion are expected to have discrete energies. Beta spectra of beta/gamma emitting radionuclides will have the usual energy distribution but will also show the internally converted electrons as lines superimposed on the beta continuum. Figure 3-22 shows beta spectra of ^{137}Cs and ^{203}Hg with internal conversion electrons appearing as discrete lines associated with the electron shells from which they are ejected. The internal conversion electrons from ^{137}Cs appear as a sharp peak at 0.624 MeV and above the 0.514 MeV endpoint energy of ^{137}Cs because the internally converted electrons have a kinetic energy of 0.662 MeV (the gamma excitation energy) minus the orbital binding energy of 0.038 MeV, or 0.624 MeV, which happens to be larger than $E_{\beta^-,\max}$ of ^{137}Cs beta particles. This sharp peak of internally converted electrons makes ^{137}Cs a useful source for energy calibration of a beta spectrometer.

The energy peaks of internal conversion electrons in beta spectra vary considerably. As shown in Figure 3-22, the peaks of internally converted electrons of ^{203}Hg

are superimposed on the spectrum of beta particles and serve to extend it somewhat. Also notable is the combined peak for converted L- and M-shell electrons. These electron spectra indicate that a beta source that also emits gamma rays has a number of individual and discrete components. Furthermore, characteristic x-rays follow internal conversion to fill electron shell vacancies; thus, gamma spectra from a radioactive source in which internal conversion is prominent can also contain peaks due to these x-rays, usually in the low-energy range.

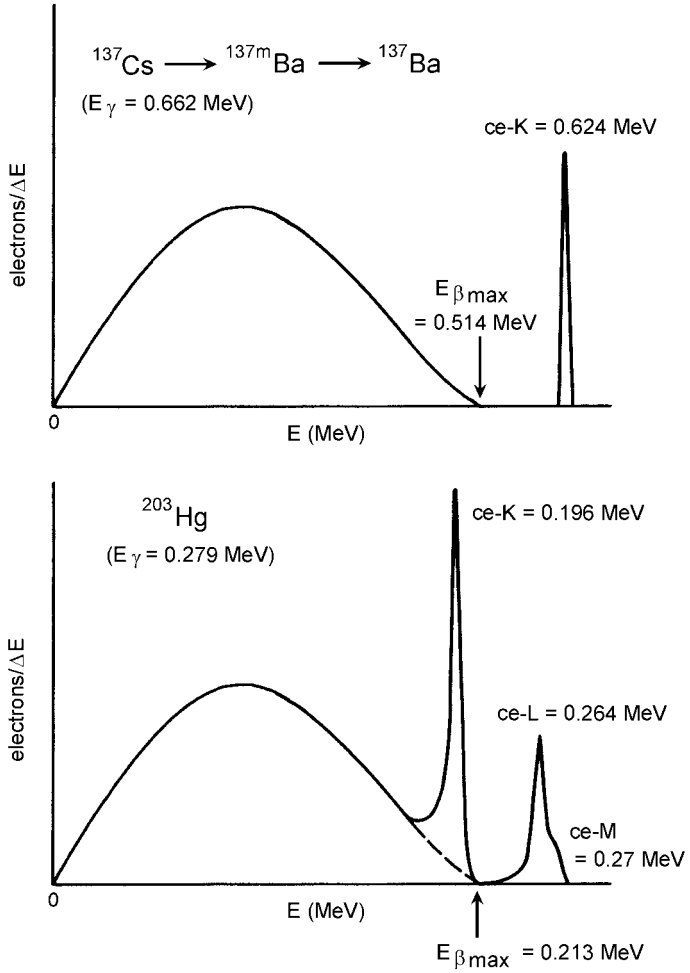

Fig. 3-22 Internal conversion electron emission superimposed upon continuous beta spectra of ^{137}Cs and ^{203}Hg illustrating the effect of the available excitation energy in the transformed nucleus on the position of the discrete energy peaks.

Conversion electrons are labeled according to the electronic shell from which they come: K, L, M, and so on. These are designated in the listings of radiations (see for example Figure 3-21 for ^{137}Cs) and Appendix D as ce-K, ce-L, etc. Some listings also include the substructure corresponding to the individual electrons in the shell, e.g., L_I, L_{II}, L_{III}.

Since internal conversion *competes* with gamma emission, an internal conversion coefficient, α, has been defined as the fraction of de-excitation that occurs by internal conversion. This fraction is listed in some decay tables, and can be used to compute the number of gamma emissions that actually occur versus those that could occur, or likewise the number of internally converted electrons. The coefficient is denoted α_K, α_L, α_M, etc., where the subscripts designate the electron shell from which the conversion electron originates. More recent compilations (see Appendix D) do not list the conversion coefficient but instead list the fraction of such electrons per transformation and the fractional emission of the competing gamma ray(s).

Internal conversion coefficients have a number of interesting features. First, they increase as Z^3, and so the conversion process is more important for heavy nuclei than for light nuclei. For example, α_K for the 1.27 MeV transition in $^{22}_{10}$Ne has a value of 6.8×10^{-6} and that for the 1.22 MeV transition in $^{187}_{74}$W has a value of 2.5×10^{-3}; thus, the ratio of converted electrons is very nearly equal to $(10/74)^3$, as expected. The conversion coefficient also decreases rapidly with increasing transition energy, and for higher atomic shells ($n > 1$) it decreases as $1/n^3$ such that for a given transition the ratio $\alpha_K/\alpha_L \approx 8$.

Example 3-4. What are the energies of internally converted electrons when ^{203}Hg undergoes transformation to ^{203}Tl, in which the residual excitation energies are emitted as a single gamma ray of energy 279.190 keV or by internal conversion from the K, L, or M_I shells?

Solution. Binding energies of electrons in Tl are (from Appendix C)

$E_b(K) = 85.529$ keV
$E_b(L_I) = 15.347$ keV
$E_b(L_{II}) = 14.698$ keV
$E_b(L_{III}) = 12.657$ keV
$E_b(M_I) = 3.704$ keV

Consequently, the conversion electrons emitted from the excited nuclei of ^{203}Tl after β^- transformation of ^{203}Hg will have the following energies:

ce-K = 279.190 – 85.529 keV = 193.661 keV
ce-L_I = 279.190 – 15.347 keV = 263.843 keV
ce-L_{II} = 279.190 – 14.698 keV = 264.492 keV
ce-L_{III} = 279.190 – 12.657 keV = 266.533 keV
ce-M_I = 279.190 – 3.704 keV = 275.486 keV

and so on for higher energy shells. The designations for these conversion electrons (ce-K, etc.) are the same as those listed in Appendix D.

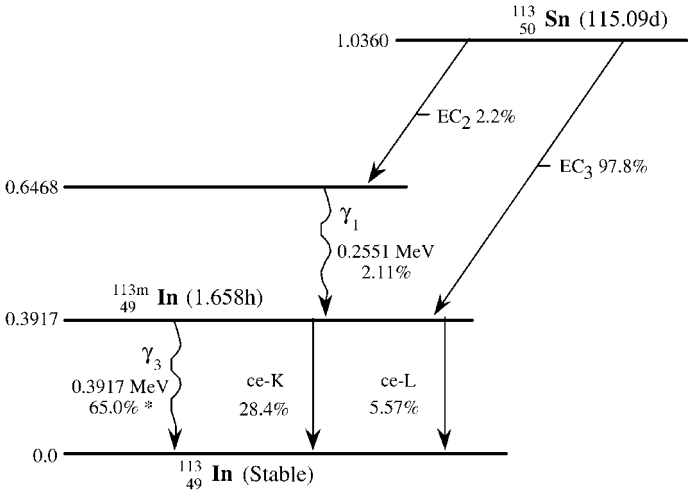

* Gamma yield per transformation of ^{113}Sn is 65%; the independent gamma yield for ^{113m}In alone is 64.2%.

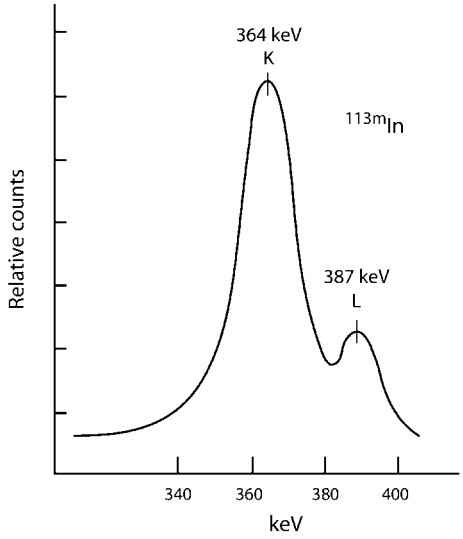

Fig. 3-23 Transformation of ^{113}Sn to ^{113}In by electron capture (EC) through metastable ^{133m}In, and the spectrum of conversion electrons ejected from the K and L shells of ^{113m}In.

The transformation of ^{113}Sn through ^{113m}In ($T_{1/2}$ = 1.66 h) to ^{113}In is another example of internal conversion. The metastable atoms of ^{113m}In have a half-life of 1.66 h and thus can exist in an excited state for a relatively long time during which orbital electrons passing by can receive the excitation energy. In this case, 98% of the electron capture transformations of ^{113}Sn go to the 392 keV excitation state of ^{113m}In. The energy of the internally converted electrons will be 392 keV minus

27.93 keV, the binding energy of the K-shell electron, or 4.25 keV for the L-shell electron. Figure 3-23 shows the discrete energies of the K-shell and L-shell converted electrons at 364 and 388 keV and their relative yields. Indium characteristic x-rays are also emitted as the vacant electron shells are filled.

Example 3-5. What will be the kinetic energy of internally converted electrons from the K and L shells of ^{113}In due to radioactive transformation of ^{113}Sn through ^{113m}In to ^{113}In?
Solution. The binding energies of K- and L-shell electrons in ^{113}In are 27.93 and 4.25 keV, respectively. Since ^{113m}In has excitation energy of 392 keV above the ground state of ^{113}In, it can be relieved either by gamma emission or internal conversion. The energy of K-shell converted electrons is therefore

$$KE_{eK} = (392 - 27.93)\ \text{keV} = 364\ \text{keV}$$

and that of the L-shell conversion is

$$KE_{eL} = (392 - 4.25)\ \text{keV} = 388\ \text{keV}$$

3.1.13 Multiple Modes of Radioactive Transformation

Some nuclei, e.g., ^{64}Cu (Figure 3-24), are so configured that they can undergo transformation by β^+, β^-, or electron capture, without a change in the mass number. As shown in Figure 3-24, the position of ^{64}Cu on the chart of the nuclides is such that it could, if energetics allow, transform to Zn or Ni. The test of whether any given radionuclide can undergo a given type of transformation is whether sufficient energy is available for the transformation, which is determined first by whether a positive Q-value exists, and second if it meets the conditions that must be satisfied for the respective transformation to occur (Example 3-6).

Example 3-6. Determine whether ^{64}Cu can undergo radioactive transformation by β^-, β^+, and electron capture processes.
Solution. The reactions are

$$^{64}_{29}\text{Cu} \rightarrow {}^{64}_{30}\text{Zn} + \beta^- + \bar{\nu} + Q$$

$$^{64}_{29}\text{Cu} \rightarrow {}^{64}_{29}\text{Ni} + \beta^+ + \nu + Q$$

$$^{64}_{29}\text{Cu} + {}^{0}_{-1}\text{e} \rightarrow {}^{64}_{29}\text{Ni} + \nu + Q$$

and the atomic masses of the three isotopes are

$$^{64}_{29}\text{Cu}(63.929768\text{u}),\ {}^{64}_{29}\text{Ni}(63.9297698\text{u}),\ {}^{64}_{30}\text{Zn}(63.929147\text{u})$$

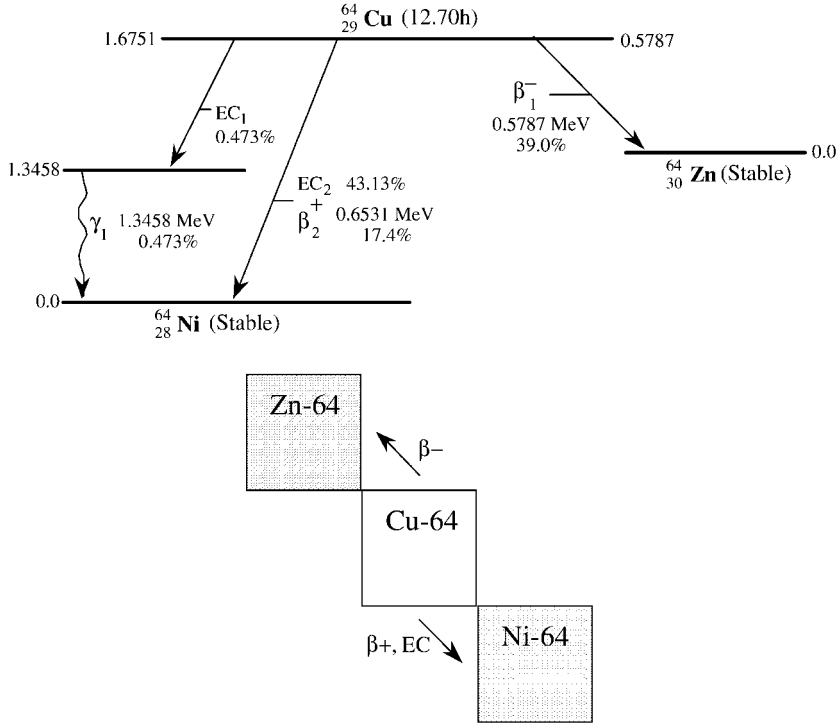

Fig. 3-24 Decay scheme of ^{64}Cu for β^- transformation to ^{64}Zn and β^+ and electron capture transformation to ^{64}Ni.

For transformation by negative beta particle emission, the Q-value need only be positive, which is determined from the nuclide masses:

$$Q(\beta^-) = 63.929768 - 63.929147 \text{ u} = (0.000621 \text{ u})(931.5 \text{ MeV/u}) = 0.58 \text{ MeV}$$

therefore, β^- transformation can occur.

For transformation by positron emission or β^+, the Q-value must be positive *and* larger than the energy equivalent of two electron masses (1.022 MeV), or

$$Q(\beta^+) = 63.929768 - 63.927970 \text{ u} = 0.001798 \text{ u}$$
$$= (0.0001798 \text{ u})(931.5 \text{ MeV/u}) = 1.675 \text{ MeV}$$

which is greater than 1.022 MeV by 0.655 MeV, and thus transformation by positron emission can occur.

For electron capture transformation to occur the Q-value for $^{64}_{29}\text{Cu} \rightarrow ^{64}_{29}\text{Ni}$ need only be positive, which it is; therefore, it too can occur (whether it actually does occur is a random probabilistic process since it competes with β^+ transformation). It is possible, therefore, for $^{64}_{29}$Cu to undergo radioactive transformation by all three processes: 39% by β^- to stable ^{64}Zn; 19% by β^+ to stable ^{64}Ni; and ~40% by EC to stable ^{64}Ni.

3.1.14
Transformation by Delayed Neutron Emission

A few nuclides, usually fission products, emit neutrons, and these emissions can be very important to reactor physics. This process does not change the element, but it does produce a transformation of the atom to a different isotope of the same element; for example, the radioactive transformation of ^{87}Br, a fission product, produces ^{87m}Kr by β^- emission in 70% of its transformations, which in turn emits gamma radiation or a 0.3 MeV neutron to stable ^{86}Kr, as shown in Figure 3-25. The neutron emission of ^{87m}Kr is delayed entirely by the 56 s half-life of the ^{87}Br parent; therefore, these delayed neutrons can be considered as having a 56 s half-life in nuclear reactor physics and criticality control procedures.

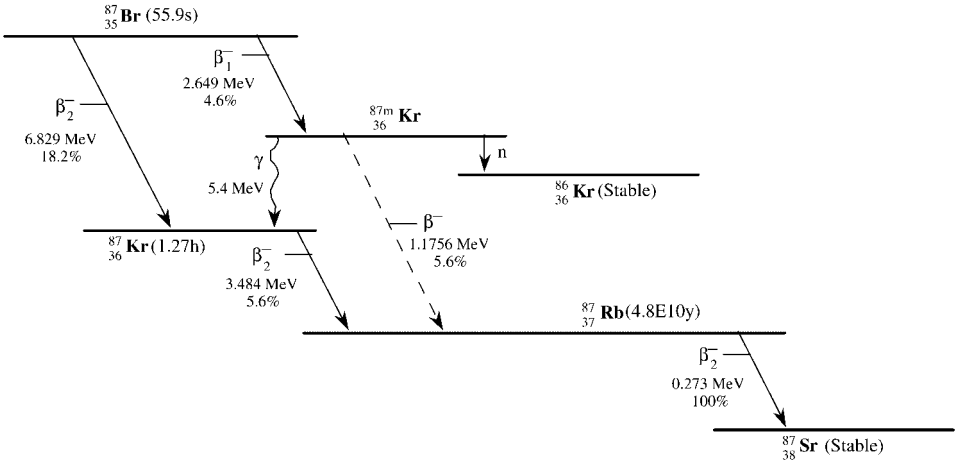

Fig. 3-25 Decay scheme of ^{87}Br and its products, including neutron emission from ^{87m}Kr.

3.1.15
Transformation by Spontaneous Fission

Another means of neutron emission is spontaneous fission in which a heavy nucleus has so much excess energy that it splits on its own, i.e., it undergoes transformation without the addition of energy or a bombarding particle. The process yields the usual two fission fragments and 2 to 4 neutrons depending on the distribution probability of each fission. Radioactive transformation by emission of an alpha or beta particle may compete with spontaneous fission. For example, ^{252}Cf emits an alpha particle in about 97% of its transformations and neutrons in 2.97%, as shown in Figure 3-26. The neutron yield is 2.3×10^{12} neutrons/s per gram of ^{252}Cf, or 4.3×10^{9} neutrons/s per curie of ^{252}Cf. Although the spontaneous fission half-life is 87 years, the overall half-life of ^{252}Cf is 2.638 years because alpha transformation to ^{248}Cm is more probable than spontaneous fission.

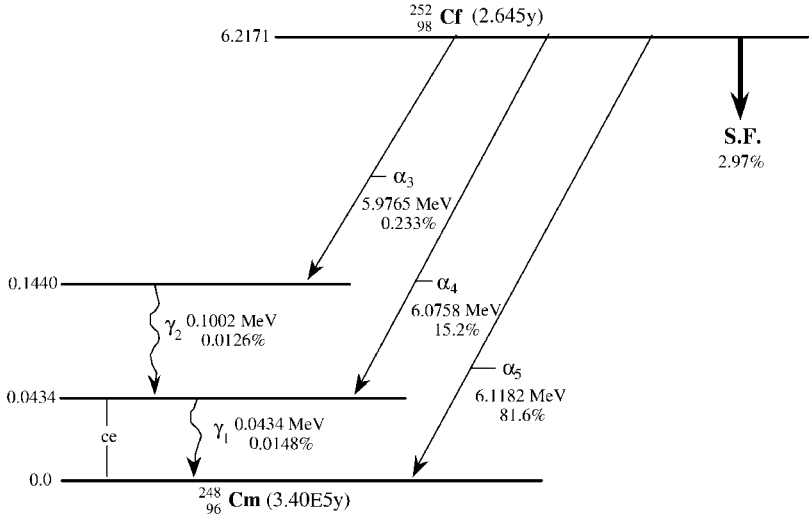

Fig. 3-26 Decay scheme of ^{252}Cf showing spontaneous fission in competition with alpha transition.

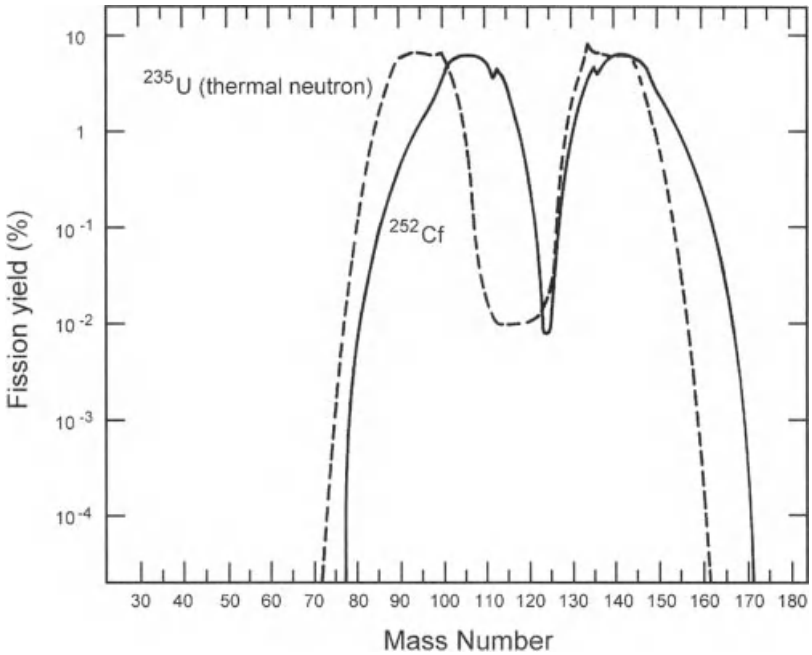

Fig. 3-27 Mass number distribution of ^{252}Cf spontaneous fission fragments compared to thermal neutron fission of ^{235}U.

The distribution of fission fragments from ^{252}Cf fission is shown in Figure 3-27 compared to that from ^{235}U fission. The fission product yield from spontaneous fission of ^{252}Cf is quite different from thermal neutron fission of ^{235}U, being somewhat skewed for lighter fragments and containing a few products of slightly heavier mass.

Other examples of nuclides that undergo spontaneous fission are ^{256}Fm ($T_{1/2}$ = 1.30 h) and ^{254}Cf ($T_{1/2}$ = 60.5 d). Isotopes of plutonium, uranium, thorium, and protactinium also experience spontaneous fission as do many other heavy nuclei. Most of these are not useful as neutron sources, but ^{252}Cf is commonly produced to provide a source of neutrons with a spectrum of energies representative of those of fission.

3.1.16 Proton Emission

A few radionuclides far above the "line of stability" are so proton-rich that they may emit protons as they undergo radioactive transformation. These are rare and of little, if any, interest in radiation protection, but physically can occur because of so much excess mass. An example is $^{73}_{36}$Kr which undergoes transformation by positron emission, 0.7% of which yields an excitation state of $^{73m}_{35}$Br which is relieved by proton emission to $^{72}_{34}$Se. The decay scheme is shown in Figure 3-28 with two end products: $^{72}_{34}$Se due to protons emitted from $^{73m}_{35}$Br, or $^{73}_{35}$Br when positrons are emitted. For proton emission the mass number decreases by one unit; for positron emission it remains the same. Another example is ^{59}Zn, and there are others, although all are only of academic interest in radiation protection.

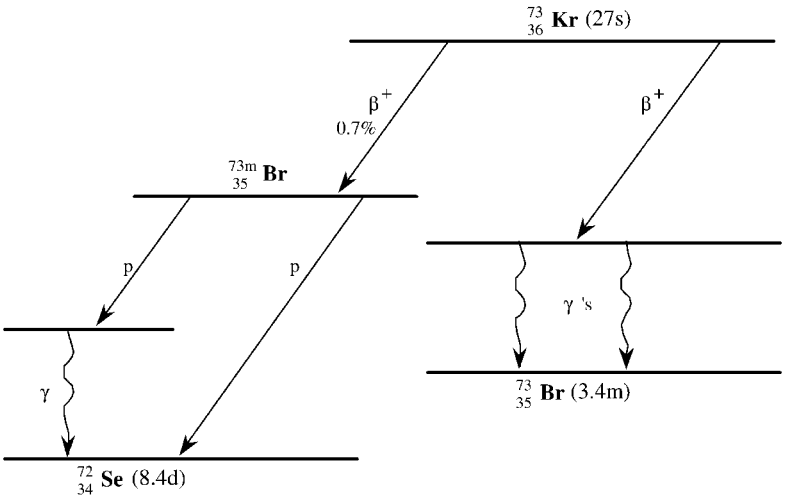

Fig. 3-28 Proton emission in the radioactive transformation of ^{73}Kr in which 0.7% of β^+ transitions are to the metastable state of ^{73m}Br which is relieved by emission of protons to ^{72}Se (greatly simplified).

3.2 Decay Schemes

The probability that a radionuclide will undergo transformation by a particular route is constant, and it is possible to predict, on the average, the percentage of transformations that will occur by any given mode. Several compilations of the various modes of radioactive transformation have been made with varying degrees of completeness. The chart of the nuclides provides very basic information on whether an isotope is radioactive and if so the primary modes of radioactive transformation, the total transition energy, and the predominant energies of the emitted "radiations." Examples of these for ^{11}C, ^{13}N, and ^{14}C are shown in Figure 3-29. Each is denoted as radioactive by having no shading; the half-life is provided just below the isotopic symbol; the principal (but not necessarily all) mode(s) of transformations and the energies are shown just below the half-life; and the disintegration energy in MeV is listed at the bottom of each block. The emitted energies for particles are listed in MeV; however, gamma energies are listed in keV presumably because gamma spectroscopy uses this convention.

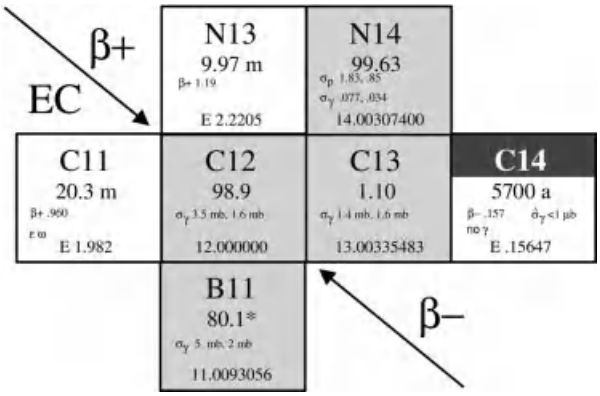

Fig. 3-29 Excerpt from the chart of the nuclides showing basic transformation modes with principal energies, half-lives, and disintegration energies of ^{11}C, ^{13}N, and ^{14}C. Also shown are stable isotopes and their percent abundances, activation cross-sections, and rest masses (u).

The most complete information on radioactive transformation is displayed in diagrams such as those for ^{51}Cr and ^{131}I shown in Figures 3-30 and 3-31. Such representations, which are commonly called decay schemes, provide a visual display of the modes of transformation and the principal radiations involved, but much more detailed information on the frequency and energy of emitted particles and related electromagnetic energy is necessary, and it is useful to provide these data in a detailed listing. Figures 3-30 and 3-31 contain such listings for ^{51}Cr and ^{131}I; these listings and diagrams are typical of those provided in Appendix D for many of the common radionuclides of interest to radiation protection.

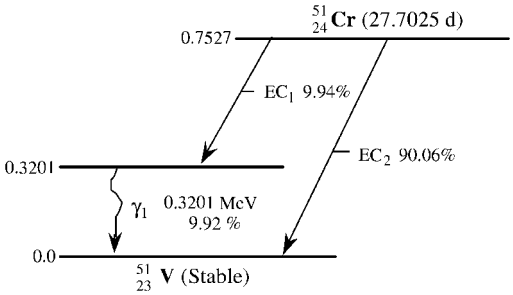

^{50}Cr(n,γ) FEB-2001

Radiation	Y_i (%)	E_i (MeV)
γ_1	9.92	0.3201
ce-K, γ_1	0.0167	0.3146
ce-L, γ_1	0.0016	0.3195[a]
ce-M, γ_1	2.58E-04	0.3200[a]
Kα_1 X-ray	13.4	0.0050
Kα_2 X-ray	6.8	0.0049
Kβ X-ray	2.69	0.0054*
L X-ray	0.337	0.0005*
Auger-K	66.3	0.0044*

* Average Energy
[a] Maximum Energy For Subshell

Fig. 3-30 Decay scheme of ^{51}Cr and a listing of principal radiations emitted.

Two other compilations on radioactive transformation data are those published by the Medical Internal Radiation Dosimetry (MIRD) Committee of the Society of Nuclear Medicine and Report Number 38 of the International Commission on Radiological Protection (ICRP-38). Both of these data sets were compiled for internal dosimetry calculations and contain all the radiation information necessary for such calculations. They are available from the National Nuclear Data Center (NNDC), which is operated for the US Department of Energy by Brookhaven National Laboratory and is an invaluable national resource for such data. The ICRP-38 report lists just about all the radionuclides; however, even though it is very comprehensive, it is quite old (published in 1978). The MIRD compilation (published in 1989) is more recent but lists only those radionuclides of interest to nuclear medicine. The decay schemes and listed data in Appendix D were compiled with the same designators used by MIRD, ICRP-38, and NNDC, though somewhat simplified for radiation protection needs. The abbreviations used in the

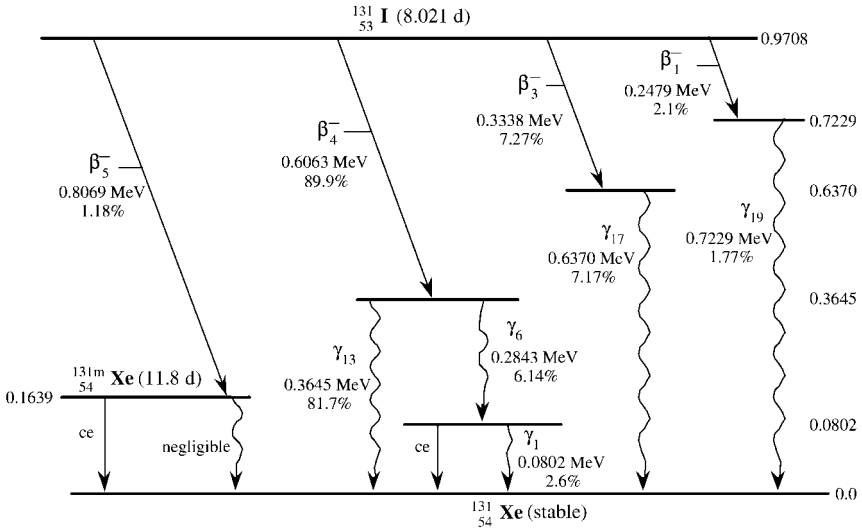

FP 14-DEC-94

Radiation	Y_i (%)	E_i (MeV)
β^-_1	2.10	0.0694*
β^-_3	7.27	0.0966*
β^-_4	89.9	0.1916*
β^-_5	1.18	0.8069*
γ_1	2.62	0.0802
ce-K, γ_1	3.54	0.0456
ce-L, γ_1	0.464	0.0747[a]
γ_6	6.14	0.2843
ce-K, γ_6	0.252	0.2497
γ_{13}	81.7	0.3645
ce-K, γ_{13}	1.55	0.3299
ce-L, γ_{13}	0.246	0.3590[a]
ce-M+, γ_{13}	0.051	0.3633[a]
γ_{17}	7.17	0.6370
γ_{19}	1.77	0.7229
Kα_1 X-ray	2.56	0.0298
Kα_2 X-ray	1.38	0.0295

* Average Energy
[a] Maximum Energy For Subshell
^{131m}Xe product, yield 1.18%; ^{131}Xe yield 98.8%

Fig. 3-31 Decay scheme of ^{131}I and a listing of major radiations emitted and their yield.

decay scheme tables are described in Appendix D. Also shown in Figures 3-30 and 3-31 and in Appendix D are the mode of production of the radioisotope (upper left of the table of radiation) and the date the data were compiled (at the upper right). Data for other radionuclides can be obtained from the MIRD and ICRP-38 reports, or if up-to-date information is desired, from the NNDC.

Iodine-131 is an example of a nuclide having an especially complex decay scheme, as shown in Figure 3-31. Four distinct beta particle transitions occur (plus others of lesser yield) and each has its own particular yield and transformation energy, referred to as the disintegration energy. The most important of these transitions is beta particle emission in 89.9% of transformations with a maximum beta energy of 0.61 MeV followed by immediate gamma emission through two routes including the prominent gamma ray energy of 0.364 MeV. This 0.364 MeV gamma ray, which occurs for 81.7% of the transformations of ^{131}I, is often used to quantitate sources of ^{131}I. Several other gamma ray energies also appear from other beta transitions.

3.3
Rate of Radioactive Transformation

The rate of transformation of radioactive atoms is not affected by natural processes such as burning, freezing, solidifying, dilution, or making chemical compounds with them. The presence or absence of oxygen or other substances has no effect; thus, radioactive substances can be used as energy sources in outer space or in other hostile environments. One small exception is a chemical change which increases the electron density near the nucleus which in turn can have a small influence on the probability of electron capture or internal conversion, both of which are related to the likelihood of interaction with orbital electrons. The effect has been observed to increase the half-life of electron capture transformation of $^{7}BeF_2$ by 0.08% as compared with ^{7}Be metal. The half-life of photon emission from $^{99m}Tc_2S_7$ has been observed to be 0.27% greater than in the pertechnetate form because of chemical alteration of the electron density and the corresponding effect on the probability of internal conversion. Other metastable nuclei also exhibit this small effect in half-life; however, the effect is of minimal consequence in most radiation protection circumstances.

Radioactive transformation requires definition of three important concepts: (a) activity, or transformation rate, (b) a unit to describe the rate of transformation, and (c) a mathematical law that allows calculation of the amount and rate of radioactive transformation over time.

3.3.1 Activity

Up to this point, radioactive transformation has been discussed in terms of those features of atoms that cause energy emission to occur, the particles and radiations that are emitted, and the processes that cause them to do so. The types of particles and radiations emitted and their energy are of utmost importance for radiation protection because they determine how much is available to produce various radiation effects. Equally important to these concepts is the rate of radioactive transformation or the activity of a radioactive source. Regardless of which mode of transformation occurs (β^-, β^+, γ, EC, etc.) radioactive atoms of a given species have a constant probability of transformation, designated by the disintegration constant λ; therefore, the activity of a source containing N atoms is defined as

$$\text{Activity} \equiv \lambda N$$

The number of radioactive atoms N is determined from the mass of the radioactive isotope by Avogadro's number (see Chapter 1); and the disintegration constant λ has been determined experimentally for each radionuclide as the fraction of the number of atoms in a radionuclide that will undergo transformation in a given amount of time, usually per second, minute, hour, etc.

3.3.2 Units of Radioactive Transformation

Activity, or intensity of radioactive emission, is the number of atoms that undergo transformation to new atoms per unit time. For many years the standard unit of radioactivity has been the curie (Ci), first defined as the emission rate of 1 g of radium (assumed to be 3.7×10^{10} transformations per second) at the request of Marie Curie, the discoverer of radium, to honor her husband, Pierre. As measurements of the activity of a gram of radium became more precise, this definition led to a standard that, unfortunately, varied. This variability, which is unacceptable for a standard unit, was eliminated by defining the curie as that *quantity* of *any* radioactive material that produces 3.7×10^{10} transformations per second (t/s):

$$\text{Transformation rate per curie} = 3.7 \times 10^{10} \text{ t/s}$$

Unfortunately, the curie is a very large unit for most samples and sources commonly encountered in radiation protection. Consequently, activity is often stated in terms of decimal fractions of a curie, especially for laboratory or environmental samples. The millicurie (mCi), which is one-thousandth of a curie, and the microcurie (μCi) (equal to one-millionth of a curie) correspond to amounts of radioactive materials that produce 3.7×10^7 (37 million) and 3.7×10^4 (37,000) t/s, respectively. Environmental levels of radioactivity are often reported in nanocuries (1 nCi = 37 t/s) or picocuries (1 pCi = 0.037 t/s, or 2.22 t/min). Despite its familiar-

ity to radiation physicists, the curie is a somewhat inconvenient unit because of the necessity to state most measured decay rates in μCi, nCi, or even pCi. The rutherford (Rd), defined as 10^6 disintegrations per second, was used for a time to provide a smaller decimalized unit, but it is rarely used and not specified by international units.

International units have been defined by the Système International (SI) which attempts to use basic quantities (kg, m, s, etc.) and decile and decimal multiples of each. It has defined the becquerel (Bq) in honor of Henri Becquerel, the discoverer of radioactivity, as that quantity of any radioactive material that produces one transformation per second:

$$\text{Transformation rate per Bq} = 1 \text{ t/s}$$

The SI unit for radioactivity suffers from being small compared to most radioactive sources measured by radiation physicists, which in turn requires the use of a different set of prefixes, i.e., kBq, MBq, GBq, etc., for kilobecquerel (10^3 t/s), megabecquerel (10^6 t/s), gigabecquerel (10^9 t/s), etc., respectively.

Neither the curie nor the becquerel are easy to use despite the tradition of paying respect to great and able scientists or the SI goal of pure units. Nonetheless, both are used with appropriate prefixes and it is necessary for radiation protection to adapt. It is perhaps useful to reflect that both units are just surrogates for listing the number of emissions that occur per unit of time and when used with the energy for each emission an energy deposition rate or the total energy deposition can be determined for use in measurement of radiation and/or determination of its effects. In this context, the number of transformations per second (t/s) or disintegrations per minute (d/m) are useful starting points; therefore, the most practical expressions and uses of activity may be to convert Ci and Bq to t/s or d/m whenever they are encountered. The becquerel, which has units of t/s, may offer some advantages in this respect, but the curie, the conventional unit for activity, is still widely used. These considerations are illustrated in Example 3-7.

Example 3-7. A radioactive source with an activity of 0.2 μCi is used to determine the counting efficiency of a radiation detector. (a) If the response of the detector is 66,600 counts per minute (c/m), what is the detector efficiency? (b) What is the efficiency if the source activity is 20 kBq?

Solution. The 0.2 μCi source produces an emission rate of

$$A = 0.2 \text{ μCi} \times 2.22 \times 10^6 \text{ d/m μCi} = 4.44 \times 10^5 \text{ d/m}$$

$$\text{Counting efficiency} = \frac{\text{counts/min}}{\text{activity}}$$

$$= \frac{66,600 \text{ c/m}}{4.44 \times 10^5 \text{ d/m}} = 0.15 \text{ or } 15\%$$

(b) The 20 kBq source produces an emission rate of

$$A = 20\ \text{kBq} \times 10^3\ \text{Bq/kBq} \times 1\ \text{t/s Bq} = 2 \times 10^4\ \text{t/s}$$

$$\text{Counting efficiency} = \frac{\text{counts/min}}{\text{activity}}$$

$$= \frac{66,600\ \text{c/m}}{2 \times 10^4\ \text{t/s} \times 60\ \text{s/m}} = 5.55 \times 10^{-2}\ \text{or}\ 5.55\%$$

3.3.3 Mathematics of Radioactive Transformation

The activity of a radioactive source is proportional to the number of radioactive atoms present; therefore, it can be written mathematically as a differential change in N in a differential unit of time as

$$\text{Activity} = -\frac{dN}{dt} = \lambda N$$

where the constant of proportionality λ is the disintegration constant and $-dN/dt$ is the rate of decrease of the number, N, of radioactive atoms at any time t. Rearranging the equation gives an expression that can be integrated directly between the limits N_0 at $t = 0$ and $N(t)$, the number of atoms for any other time t:

$$\int_{N_0}^{N(t)} \frac{dN}{N} = -\lambda \int_0^t dt$$

Integration and evaluation of the limits yields

$$\ln N(t) - \ln N_0 = -\lambda t$$

or

$$\ln N(t) = -\lambda t + \ln N_0$$

which is an equation of a straight line with slope of $-\lambda$ and a y-intercept of $\ln(N_0)$. By applying the law of logarithms, this can also be written as

$$\ln\left(\frac{N(t)}{N_0}\right) = -\lambda t$$

and since the logarithm of a number is the exponent to which the base (in this case e) is raised to obtain the number, the above expression is literally

$$\frac{N(t)}{N_0} = e^{-\lambda t}$$

or

$$N(t) = N_0 e^{-\lambda t}$$

If both sides are multiplied by λ,

$$\lambda N(t) = \lambda N_0 e^{-\lambda t}$$

and recalling that activity = λN, then

$$A(t) = A_0 e^{-\lambda t}$$

In other words, the activity $A(t)$ at some time t of a source of radioactive atoms, all of the same species with a disintegration constant λ, is equal to the initial activity A_0 multiplied by the exponential $e^{-\lambda t}$, where e is the base of the natural logarithm. If the activity $A(t)$ is plotted against time, the exponential curve in Figure 3-32a is obtained. A plot of the natural logarithm of the activity with time yields the straight line shown in Figure 3-32b. Neither curve goes to zero except when t is infinite.

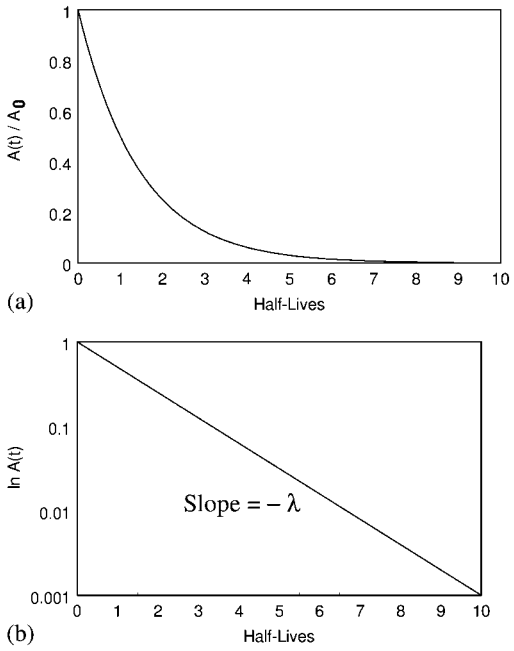

Fig. 3-32 Radioactive transformation versus the number of elapsed half-lives plotted (a) as a linear function and (b) as the natural logarithm of activity.

3.3.4 Half-Life

The half-life (or half-period) of a radioactive substance is used to describe the exponential behavior of radioactive transformation since it is more meaningful than the disintegration constant with reciprocal units of time. The half-life is the amount of time it takes for half of the atoms in a radioactive source to undergo transformation; this special value of time, $T_{1/2}$, is calculated as the value of t that corresponds to $A(t)/A_0 = 1/2$ (or $N(t)/N_0$ if one prefers) as follows:

$$\frac{A(t)}{A_0} = \frac{1}{2} = e^{-\lambda T_{1/2}}$$

which can be solved by taking the natural logarithm of both sides, or

$$\ln 1 - \ln 2 = -\lambda T_{1/2}$$

such that

$$T_{1/2} = \frac{\ln 2}{\lambda}$$

The disintegration constant λ, which is required for calculating activity, follows directly from this relationship as

$$\lambda = \frac{\ln 2}{T_{1/2}}$$

The disintegration constant λ has units of reciprocal time (s^{-1}, min^{-1}, h^{-1}, y^{-1}) and is a value much less than 1.0. Consequently, it is also not a familiar quantity; thus, radioactive isotopes are characterized in terms of their half-life instead of λ, which makes communication about radioactive transformation much easier. Half-life, which is given in amounts of time, is easier to relate to, but one needs to be mindful that the process is still exponential. It does not matter how much activity you start with nor when you start the clock, only that you know how much you have, i.e., A_0, when you start the clock; after one half-life, you will have only half the activity. Then you must start again and so on; i.e., the decrease is exponential.

Since λ is derived from the known half-life of a radioactive substance, the expression $\lambda = \ln(2)/T_{1/2}$ can be used in the general relationship for activity to provide an equation for straightforward calculations of activity with time, or

$$A(t) = A_0 e^{-(\ln 2/T_{1/2})t}$$

The exponential nature of radioactive transformation must be kept in mind when dealing with radioactive sources. As shown in Figure 3-32b, the activity of a source

will diminish to 1% ($A/A_0 = 0.01$) after about 6.7 half-lives and to 0.1% ($A/A_0 = 0.001$) after 10 half-lives. Although these are good rules of thumb for most sources, some activity will, because of exponential removal, remain after these periods. The common practice of assuming a source has decayed away after 10 half-lives should be used with caution because in fact it has only diminished to $0.001A_0$, which may or may not be of significance.

3.3.5 Mean Life

The mean life of each atom in a radioactive source can be useful for determining the total number of emissions of radiation from the source. The mean life is the average time it takes each atom to transmute, recognizing that some will transmute right away, some will last an infinite time, and others will have lifetimes in between. The mean life can be deduced from the relationship between N_0, dN, dt, and λ.

As shown in Figure 3-33, the number of atoms in a source will decrease exponentially with time which will affect the average time each persists. The area under the curve will have units of atom·seconds if t is in seconds, though other units of t could also be used.

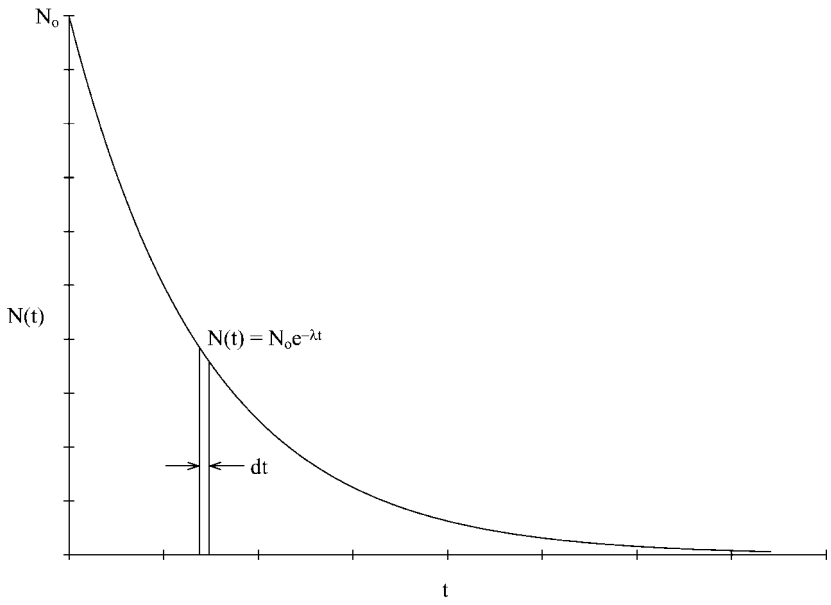

Fig. 3-33 Mean life τ of a radioactive substance is obtained by determining a value τN_0 that equals the total area under the curve, or the sum of the differential areas $N(t)dt$ from $t = 0$ to $t = \infty$.

The area under the curve is obtained by integrating each differential unit of area, which has a width of dt and a height of $N(t) = N_0 e^{-\lambda t}$, from $t = 0$ to $t = \infty$:

$$\text{Area} = \int_0^t N(t)dt = \int_0^\infty N_0 e^{-\lambda t} dt = N_0/\lambda$$

which has units of atom·seconds. If each of the initial atoms N_0 in the source has a mean life of τ, then the quantity $N_0\tau$ will represent the same total area so that

$$N_0\tau = \frac{N_0}{\lambda}$$

The mean life of the atoms in a particular radioisotope is therefore

$$\tau = \frac{1}{\lambda}$$

where λ is actually the fraction of the total number of atoms of the given radioelement disintegrating in unit time. The expression for mean life can also be simplified in terms of the half-life of the substance:

$$\tau = \frac{T_{1/2}}{\ln 2} = 1.4427\, T_{1/2}$$

which states that the mean life of each of the atoms in a radionuclide is about 44.3% longer than the half-life. Any given atom may disintegrate immediately or it may last forever; it is impossible to tell in advance when a given atom will do so, but each atom will, on average, exist for a time τ. On the other hand, for a large number of radioactive atoms of the same type, a definite fraction λ will decay in unit time. Radiation physicists are, therefore, somewhat like insurance companies that cannot foretell the fate of any individual, but by the laws of statistics they can accurately predict the life expectancy of a given set and respond accordingly. Mean life has a practical use in dosimetry because it provides an average time that can be assigned to all of the atoms in a source that may deposit energy in a medium. Although the mean life of atoms is analogous to the average life expectancy of persons, a given radioactive atom might never transform and atoms do not age.

3.3.6 Effective Half-life

Other processes may serve to reduce radioactivity in a source separate and distinct from that due to atom transformations. For example, if a radioactive material is located in a physiological system in which it is removed by biological processes it may be necessary to account for both in assessing the number of atoms that transform over some period of time. To do so, an effective removal constant which is obtained by adding the biological rate constant λ_b and other removal constants λ_i

(with similar units, of course) to the radioactivity constant. The effective removal constant for a biological system is

$$\lambda_{\text{eff}} = \lambda_{\text{r}} + \lambda_{\text{b}} + \text{other removal constants}$$

The amount of radioactivity in an organ of the body is often described by an effective removal constant λ_{eff} when biological removal is a factor. An effective half-life can be derived from the effective removal constant as

$$\frac{\ln 2}{T_{\text{eff}}} = \frac{\ln 2}{T_{\text{r}}} + \frac{\ln 2}{T_{\text{b}}}$$

where T_{eff}, T_{r}, and T_{b} are the effective, radioactive, and biological half-lives, respectively. Solving for T_{eff} yields

$$T_{\text{eff}} = \frac{T_{\text{r}} T_{\text{b}}}{T_{\text{r}} + T_{\text{b}}}$$

Example 3-8. Determine the effective removal constant and the effective half-life of iodine-131 ($T_{1/2}$ = 8.02 d) in the human thyroid if it is removed with a biological half-life of 120 days.
Solution.

$$\lambda_{\text{eff}} = \lambda_{\text{r}} + \lambda_{\text{b}} = \frac{\ln 2}{8.02\,\text{d}} + \frac{\ln 2}{120\,\text{d}} = 0.092\ \text{d}^{-1}$$

$$T_{\text{eff}} = \frac{8.02\,\text{d} \times 120\,\text{d}}{8.02\,\text{d} + 120\,\text{d}} = 7.52\text{d}$$

The effective removal constant could also be obtained from the effective half-life when it is known, and vice versa.

3.4 Radioactivity Calculations

Many useful calculations can be made for radioactive substances using the relationships just derived, for example:

- What activity does a given mass of a radioactive substance have, or vice versa?
- From a set of activity measurements made at different times, what is the half-life and disintegration constant of a substance?
- How radioactive will a substance be at some time t in the future?
- If the current activity is known, what is the activity at some previous time, such as when the source was shipped or stored?
- How long will it take for a source to diminish to a given level, perhaps one that will no longer be of concern?

These calculations can be made with some basic starting information, and the equation for activity $A(t)$ and its decrease with time:

$$A(t) = A_0 e^{-(\ln 2/T_{1/2})t}$$

which relates A and t in terms of A_0 and the half-life $T_{1/2}$. Calculations with this relationship are mathematically precise but familiarity with exponential relationships is necessary; these are now relatively straightforward with scientific calculators which have a natural logarithm function (i.e., a key labeled ln(x), ln x, or ln).

Since the half-life is a fundamental part of this exponential relationship, the change in the activity of a radioactive source can be calculated by just dividing the initial activity by 2 a sufficient number of times to account for the half-lives elapsed. Mathematically, this is given as

$$A(t) = \frac{A_0}{2^n}$$

where n is the number of half-lives that have elapsed during time t. If n is an integer, the activity after an elapsed time is calculated by simply dividing A_0 by 2 n times. If n is not an integer, then it is necessary to solve the relationship by other means, one of which is a ratio, $A(t)/A_0$, versus the number of half-lives that have elapsed. Figure 3-34 shows such a plot that is generally applicable, subject of course to the uncertainty in reading such curves. The use of such a curve is demonstrated in Examples 3–9 and 3–10.

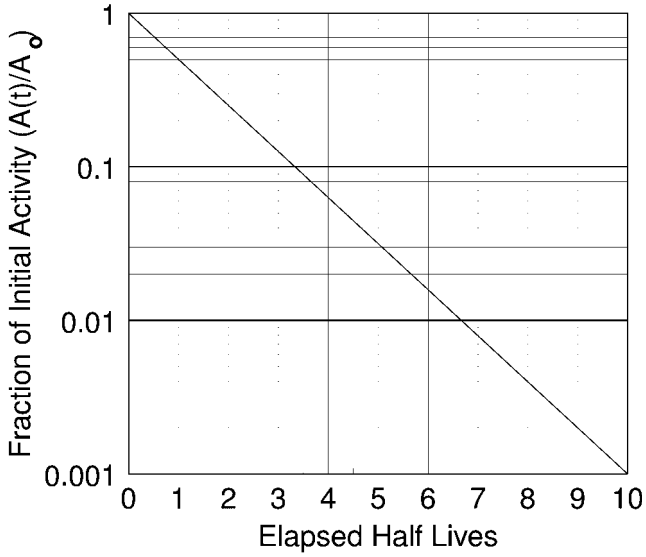

Fig. 3-34 Semilog plot of the fraction of activity, $A(t)/A_0$, remaining versus the number of elapsed half-lives.

Example 3-9. If a reactor part contains 1000 curies of cobalt-60 (half-life = 5.27 y), how much will exist in 40 years?
Solution. Figure 3-34 can be used. The number of elapsed half-lives in 40 years is 7.59. The fractional activity from Figure 3-34 is approximately 0.0052, and the activity at 40 years is

$$A(40\text{ y}) = 1000\text{ Ci} \times 0.0052 = 5.2\text{ Ci}$$

Example 3-10. Assume that a source of ^{137}Cs ($T_{1/2}$ = 30.07 y) can be safely managed if it contains less than 0.01 Ci. How long would it take for a source containing 5 Ci of ^{137}Cs to reach this value?
Solution. First we determine what fraction 0.01 Ci is of the original 5 Ci, i.e., $A(t)/A_0 = 0.002$. From Figure 3-34, the number of elapsed half-lives that corresponds to 0.002 is 8.97. The time required for 5.0 Ci to diminish to 0.01 Ci is 8.97 × 30.07 y = 269.7 y.

Example 3-11. A waste shipment contains 800 Ci of iodine-125 ($T_{1/2}$ = 60 d). How much will be left (a) in a year (b) in 11 months?
Solution. (a) Since a year is 12 months, the elapsed time will be 6 half-lives. Dividing 800 by 2 six times yields

$$A(1\text{y}) = \frac{800\text{ Ci}}{2^6} = 12.5\text{ Ci}$$

(b) At 11 months, or 5.5 half-lives, the activity can be obtained directly by solving the general expression for activity with time:

$$A(11\text{ months}) = 800e^{[-(\ln 2)/2]\times 11} = 17.68\text{ Ci}$$

The activity at 11 months can also be solved in terms of half-lives. Since 5.5 half-lives would have elapsed the activity is between 25 Ci (5 half-lives) and 12.5 Ci for 6 half lives (note that it is not halfway between because radioactive transformation is exponential). The solution for 5.5 half-lives can be represented as

$$A(11\,\text{months}) = \frac{800\text{ Ci}}{2^{5.5}}$$

which can be solved by one of at least four methods:

1. Solving $2^{5.5}$ by y^x and completing the arithmetic, the activity A is

$$A = \frac{800\text{ Ci}}{45.2548} = 17.68\text{ Ci}$$

2. By taking the natural logarithm of both sides and finding the corresponding natural antilogarithm:

$\ln(A) = \ln(800) - 5.5\ln(2) = 2.8723$

$A = e^{2.8723} = 17.68\,\text{Ci}$

3. By taking $\log_{10}$ of both sides and finding the corresponding antilog_{10}:

$\log(A) = \log(800) - 5.5\log(2) = 1.247425$

$A = 10^{1.247425} = 17.68\,\text{Ci}$

4. Using the graph in Figure 3-34 to determine the ratio $A(t)/A_0$ at 5.5 half-lives as

$$\frac{A(t)}{A_0} = 0.022$$

from which $A(t)$ is calculated to be 17.68 Ci. (Note: the accuracy of this method is limited by the accuracy in reading the graph.)

3.4.1 Half-life Determination

The half-life of an unknown radioactive substance can be determined by taking a series of activity measurements over several time intervals and plotting the data. If the data are plotted as $\ln A(t)$ versus t and a straight line is obtained, it can be reasonably certain that the source contains only one radioisotope. The slope of the straight line provides the disintegration constant, and once the disintegration constant is known, the half-life can be determined directly.

Example 3-12. What is the half-life of a sample of ^{55}Cr which has activity at 5 min intervals of 19.2, 7.13, 2.65, 0.99, and 0.27 t/s?
Solution. The general relationship between activity and time can be expressed as

$$\ln A(t) = -\lambda t + \ln A$$

which is a straight line with slope of $-\lambda$ where $\ln A_0$ is the y-intercept. Figure 3-35 shows a plot of a least squares fit of the data in Table 3-1. (Note that is necessary to take the natural logarithm of each activity rate.) From the curve in Figure 3-35, the slope $-\lambda$ is $-0.197\ \text{min}^{-1}$, and $\lambda = 0.197\ \text{min}^{-1}$; therefore,

$$T_{1/2} = \frac{\ln 2}{0.197\,\text{min}^{-1}} = 3.52\ \text{min}$$

Table 3-1 Data for Example 3-12.

t (min)	ln *A*(*t*)
0	2.95
5	21.96
10	0.98
15	–0.01
20	–1.31

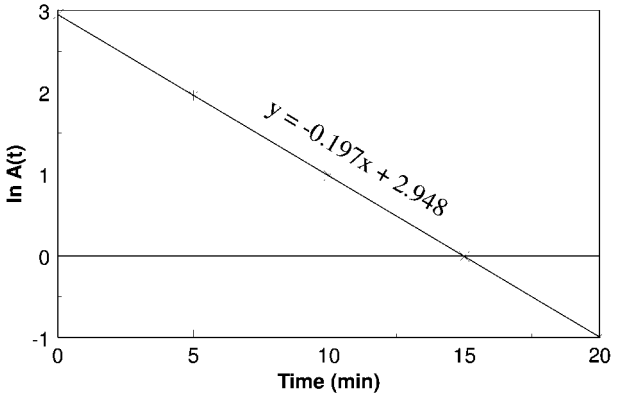

Fig. 3-35 Linear least squares fit of ln *A*(*t*) versus time for a sample of ^{55}Cr.

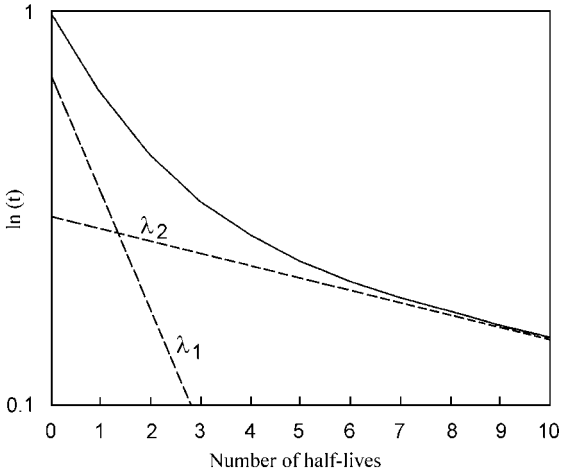

Fig. 3-36 Plot of ln *A*(*t*) as a function of time for two radionuclides with two different half-lives.

The technique used in Example 3-12 is also applicable to a source that contains more than one radionuclide with different half-lives. This can be readily determined by plotting ln $A(t)$ of a series of activity measurements with time as shown in Figure 3-36 for two radionuclides. If only one radionuclide were present, the semilog plot would be a straight line; however, when two or more are present, the line will be curved as in Figure 3-36. The straight-line portion at the right-hand end represents the longer-lived component, and thus can be extrapolated back to time zero and subtracted from the total curve to yield a second straight line. The slopes of these two lines establish the disintegration constants, λ_1 and λ_2, from which the half-life of each can be calculated for possible identification of the two radionuclides in the source.

3.5 Activity–mass Relationships

The activity of a radioisotope is directly related to the number of atoms, or

$$\text{Activity} = \lambda N$$

and since N is determined from the mass m of the sample by Avogadro's number, mass can be used directly as a surrogate for activity, or

$$m(t) = m_0 e^{-\lambda t}$$

Example 3-13. If a sample of ^{24}Na ($T_{1/2}$ = 15 h) originally contains 48 g, how many hours will be required to reduce the ^{24}Na concentration in this sample to 9 g?
Solution. Since activity = λN, and N is determined from the mass of the radioelement, the activity of ^{24}Na is directly proportional to its mass. Therefore,

$$9\ \text{g} = (48\text{g}) \times e^{-(\ln 2/T_{1/2})t}$$

$$\ln\left(\frac{9\ \text{g}}{48\ \text{g}}\right) = -\frac{\ln 2}{15\ \text{h}}t \qquad t = 36.2\ \text{h}$$

3.5.1 Specific Activity

The basic equation for the radioactivity of a substance is

$$A(t) = \lambda N = \frac{\ln 2}{T_{1/2}} N$$

Since the number N of radioactive atoms in a radioactive element and its half-life $T_{1/2}$ are specific for each and every isotope of a radioactive element, the activity per

unit mass of a pure radionuclide is a constant that is defined as the specific activity of the element. The specific activity of a radioelement is obtained by determining the number of atoms in a unit mass (e.g., 1 g) of the element, multiplying by the disintegration constant λ to obtain its transformation rate, and then expressing the transformation rate in activity units (Ci, Bq, etc.) per unit mass, as shown in Example 3-14.

Example 3-14. What is the specific activity of 1 g of ^{226}Ra if the radioactive half-life is 1600 y?
Solution. The number of atoms per gram of ^{226}Ra is

$$N = \frac{1\text{g} \times 6.02214 \times 10^{23}\text{atoms/mol}}{226\,\text{g/mol}} = 2.665 \times 10^{21}\ \text{atoms/g}$$

The disintegration constant λ is

$$\lambda = \frac{\ln 2}{T_{1/2}} = \frac{\ln 2}{1600\,\text{y} \times 3.1557 \times 10^{7}\,\text{s/y}} = 1.373 \times 10^{-11}\text{s}^{-1}$$

and the activity A is

$$\text{A} = \lambda N = 1.373 \times 10^{-11}\ \text{s}^{-1} \times 2.665 \times 10^{21}\ \text{atoms/g} = 3.66 \times 10^{10}\ \text{t/s g}$$

This value is slightly less than the current official definition of the curie (3.700×10^{10} t/s) primarily because the half-life measurement has become more precise.

The specific activity (SpA) of pure radioelements is often given in units of Ci/g. A general expression of specific activity in Ci/g for radioelements of atomic mass A (g/mol) where half-life is given in seconds is

$$\text{SpA(Ci/g)} = \frac{1.12824 \times 10^{13}\text{s Ci/mol}}{T_{1/2}\,(\text{s}) \times A\,(\text{g/mol})}$$

Example 3-15. Calculate the specific activity of ^{131}I, which has a half-life of 8.0207 d.
Solution.

$$\text{SpA(Ci/g)} = \frac{1.12824 \times 10^{13}\ \text{s Ci/mol}}{T_{1/2}\,(\text{s}) \times A\,(\text{g/mol})} = \frac{1.12824 \times 10^{13}\text{s Ci/mol}}{(8.0207\,\text{d}) \times (86,400\,\text{s/d}) \times (131\,\text{g/mol})}$$
$$= 1.243 \times 10^{5}\text{Ci/g}$$

Table 3-2 lists values of specific activity for several radionuclides that were calculated with half-lives from the National Nuclear Data Center. Integer mass numbers were used rather than actual masses, except for ^{3}H where the exact mass was used. It is very important to note that specific activities for the radionuclides listed in Table 3-2 are for pure samples of the radioisotope, although it is recognized that no radioactive substance is completely pure since transformations produce new atoms, which generally remain in the source.

Table 3-2 Specific activity of selected pure radionuclides.

Radionuclide	$T_{1/2}$	SpA (Ci/g)	Radionuclide	$T_{1/2}$	SpA (Ci/g)
Hydrogen-3	12.3 y	9.64×10^{3}	Ruthenium-106	373.59 d	3.30×10^{3}
Carbon-14	5730 y	4.46	Cadmium-109	462.0 d	2.59×10^{3}
Nitrogen-16	7.13 s	9.89×10^{10}	Iodine-123	13.27 h	1.92×10^{6}
Sodium-22	2.6088 y	6.23×10^{3}	Iodine-125	59.402 d	1.76×10^{4}
Sodium-24	14.959 h	8.73×10^{6}	Iodine-131	8.0207 d	1.24×10^{5}
Phosphorus-32	14.26 d	2.86×10^{5}	Barium-133	10.52 y	262.00
Sulfur-35	87.51 d	4.27×10^{4}	Cesium-134	2.0648 y	1.29×10^{3}
Chlorine-36	3.01×10^{5} y	3.30×10^{-2}	Cesium-137	30.07 y	86.90
Argon-41	109.43 m	4.19×10^{7}	Barium-140	12.752 d	7.32×10^{4}
Potassium-42	12.36 h	6.04×10^{6}	Lanthanum-140	40.22 h	5.57×10^{5}
Calcium-45	162.61 d	1.79×10^{4}	Cerium-141	32.5 d	2.85×10^{4}
Chromium-51	27.704 d	9.25×10^{4}	Cerium-144	284.9 d	3.18×10^{3}
Manganese-54	312.12 d	7.76×10^{3}	Praseodymium-144	17.28 m	7.56×10^{7}
Iron-55	2.73 y	2.39×10^{3}	Promethium-147	2.6234 y	928.00
Manganese-56	2.5785 h	2.17×10^{7}	Europium-152	13.542 y	174.00
Cobalt-57	271.79 d	8.44×10^{3}	Tantalum-182	114.43 d	6.27×10^{3}
Iron-59	44.503 d	4.98×10^{4}	Iridium-192	73.831 d	9.21×10^{3}
Nickel-59	7.6×10^{4} y	7.99×10^{-2}	Gold-198	2.69517 d	2.45×10^{5}
Cobalt-60	5.2714 y	1.13×10^{3}	Mercury-203	46.612 d	1.38×10^{4}
Nickel-63	100.1 y	56.80	Thallium-204	3.78 y	4.64×10^{2}
Copper-64	12.7 h	3.86×10^{6}	Thallium-208	3.053 m	2.96×10^{8}
Zinc-65	244.26 d	8.23×10^{3}	Polonium-210	138.4 d	4.49×10^{3}
Gallium-72	14.1 h	3.09×10^{6}	Polonium-214	164 μs	3.13×10^{14}
Arsenic-76	1.0778 d	1.60×10^{6}	Radium-226	1600 y	0.99
Bromine-82	35.3 h	1.08×10^{6}	Thorium-232	1.41×10^{10} y	1.10×10^{-7}
Rubidium-86	18.631 d	8.16×10^{4}	Uranim-233	1.592×10^{5} y	9.64×10^{-3}
Strontium-89	50.53 d	2.91×10^{4}	Uranium-235	7.0×10^{8} y	2.16×10^{-6}
Strontium-90	28.74 y	138.00	Uranium-238	4.468×10^{9} y	3.36×10^{-7}
Yttrium-90	64.1 h	5.44×10^{5}	Plutonium-239	24,110 y	6.21×10^{-2}
Molybdenum-99	65.94 h	4.80×10^{5}	Plutonium-241	14.35 y	103.00
Technetium-99m	6.01 h	5.27×10^{6}	Americium-241	432.2 y	3.43

It is common practice to measure a source containing a radioactive substance after weighing it and to report the measured value in units of activity/gram and to refer to this value as its "specific activity." However, this use of the term is not consistent with the definition of specific activity, which refers to a pure sample. It is more appropriate to refer to measured values of activity per unit mass in a non-pure sample as having a concentration of so many Bq or Ci per gram of a sample or source, otherwise the impression may be given that the sample is pure when in fact it is a mixture.

3.6 Radioactive Series Transformation

The radioactive transformation of many radionuclides often yields a product that is also radioactive. The radioactive product in turn undergoes transformation to produce yet another radioactive product and so on until stability is achieved (see, for example, Figure 3-12 for $^{238}U \rightarrow {}^{206}Pb$). Occasionally, the product radionuclide may be more important for radiation protection considerations. For example, ^{222}Rn, the product of the radioactive transformation of ^{226}Ra, can migrate while its parent (^{226}Ra) remains fixed in soil. The transformation of ^{90}Sr produces ^{90}Y which is also radioactive, and since it has a much higher beta energy than the ^{90}Sr parent, it is a larger contributor to radiation dose than ^{90}Sr itself. Because of its higher energy, ^{90}Y is also used to measure ^{90}Sr indirectly.

3.6.1 Series Decay Calculations

The number of atoms of each member of a radioactive series at any time t can be obtained by solving a system of differential equations which relates each product N_1, N_2, N_3,..., N_i with corresponding disintegration constants λ_1, λ_2, λ_3,..., λ_i. Each series begins with a parent nuclide N_1, which has a rate of transformation

$$\frac{dN_1}{dt} = -\lambda_1 N_1$$

The second nuclide in a radionuclide series will be produced at a rate of $\lambda_1 N_1$ due to the transformation of N_1, but as soon as atoms of N_2 exist, they too can undergo transformation if they are radioactive; thus, the rate of change of atoms of N_2 is the rate of production minus the rate of removal of N_2 atoms, or

$$\frac{dN_2}{dt} = \lambda_1 N_1 - \lambda_2 N_2$$

Similarly, for atoms of N_3 which are produced by transformation of N_2 atoms and subject to removal as a function of the disintegration constant λ_3,

$$\frac{dN_3}{dt} = \lambda_2 N_2 - \lambda_3 N_3$$

and so on up to the *i*th member of the series:

$$\frac{dN_i}{dt} = \lambda_{i-1} N_{i-1} - \lambda_i N_i$$

If the end product is stable, the atoms of the stable end product appear at the rate of the last radioactive precursor, and of course are not removed since they are stable.

It is useful to solve this system of equations for the first four members of a radioactive series in order to demonstrate their direct applicability to radon and its progeny in a later section. The number of atoms of N_1 is

$$N_1(t) = N_1^0 e^{-\lambda_1 t}$$

where $N_1{}^0$ is the number of atoms of parent at $t = 0$. This expression for N_1 can be inserted into the equation for dN_2/dt to give

$$\frac{dN_2}{dt} = \lambda_1 N_1^0 e^{-\lambda_1 t} - \lambda_2 N_2$$

or, collecting terms

$$\frac{dN_2}{dt} + \lambda_2 N_2 = \lambda_1 N_1^0 e^{-\lambda_1 t}$$

This type of equation can be converted into one that can be integrated directly by multiplying through by an appropriate integrating factor, which for this form is always an exponential with an exponent that is equal to the constant in the second term multiplied by the variable in the denominator of the derivative, or in this case $e^{\lambda_2 t}$:

$$e^{\lambda_2 t}\frac{dN_2}{dt} + e^{\lambda_2 t}\lambda_2 N_2 = \lambda_1 N_1^0 e^{(\lambda_2 - \lambda_1)t}$$

Multiplying through by $e^{\lambda_2 t}$ converts the left side of the equation to the time derivative of $N_2 e^{\lambda_2 t}$, which can be demonstrated by differentiating the expression. It also yields an exponential expression multiplied by a constant on the right side, or

$$\frac{d}{dt}(N_2 e^{\lambda_2 t}) = \lambda_1 N_1^0 e^{(\lambda_2 - \lambda_1)t}$$

which can be integrated directly to give

$$N_2 e^{\lambda_2 t} = \frac{\lambda_1}{\lambda_2 - \lambda_1} N_1^0 e^{(\lambda_2 - \lambda_1)t} + C$$

where C, the constant of integration, is determined by stating the condition that when $t = 0$, $N_2 = 0$; thus

$$C = \frac{\lambda_1}{\lambda_2 - \lambda_1} N_1^0$$

Therefore, the solution for N_2 as a function of time is

$$N_2(t) = \frac{\lambda_1}{\lambda_2 - \lambda_1} N_1^0 (e^{-\lambda_1 t} - e^{-\lambda_2 t})$$

The number of atoms of the third kind is found by inserting this expression for N_2 into the equation for the rate of change of N_3, which as before is the rate of production of N_3 by transformation of atoms of N_2 (or $\lambda_2 N_2$) minus the rate of removal of N_3 by radioactive transformation (or $\lambda_3 N_3$):

$$\frac{dN_3}{dt} = \lambda_2 N_2 - \lambda_3 N_3$$

After the integration is performed and the constant of integration is evaluated, the equation for the number of atoms of N_3 with time is

$$N_3(t) = \lambda_1 \lambda_2 N_1^0 \left[\frac{e^{-\lambda_1 t}}{(\lambda_2 - \lambda_1)(\lambda_3 - \lambda_1)} + \frac{e^{-\lambda_2 t}}{(\lambda_1 - \lambda_2)(\lambda_3 - \lambda_2)} + \frac{e^{-\lambda_3 t}}{(\lambda_1 - \lambda_3)(\lambda_2 - \lambda_3)} \right]$$

In a similar fashion, for the number of atoms of the fourth kind, the expression for $N_3(t)$ is inserted into the equation for dN_4/dt, which is integrated to obtain the number of atoms of N_4 with time:

$$N_4(t) = \lambda_1 \lambda_2 \lambda_3 N_1^0 \left[\frac{e^{-\lambda_1 t}}{(\lambda_2 - \lambda_1)(\lambda_3 - \lambda_1)(\lambda_4 - \lambda_1)} + \frac{e^{-\lambda_2 t}}{(\lambda_1 - \lambda_2)(\lambda_3 - \lambda_2)(\lambda_4 - \lambda_2)} \right.$$
$$\left. + \frac{e^{-\lambda_3 t}}{(\lambda_1 - \lambda_3)(\lambda_2 - \lambda_3)(\lambda_4 - \lambda_3)} + \frac{e^{-\lambda_4 t}}{(\lambda_1 - \lambda_4)(\lambda_2 - \lambda_4)(\lambda_3 - \lambda_4)} \right]$$

These equations yield the number of atoms of each of the first four members of a radioactive series that begins with a pure radioactive parent, i.e., there are no transformation products at $t = 0$.

A radioactive series typically ends at a stable nuclide or one with a very large half-life such that it is not unreasonable to terminate the production of radioactive atoms. In this case, the disintegration constant λ_i for the end product will be zero,

or at least very small. For example, if the third element in a series is stable (i.e., $\lambda_3 = 0$), then the number of atoms of N_3 will be

$$N_3(t) = N_1^0\left(1 - \frac{\lambda_2}{\lambda_2 - \lambda_1}e^{-\lambda_1 t} - \frac{\lambda_1}{\lambda_1 - \lambda_2}e^{-\lambda_2 t}\right)$$

3.6.2 Recursive Kinetics: the Bateman Equations

The solutions for the numbers of atoms in the first four members of a radioactive series yields a recursion of similar terms, which has been generalized into a series of expressions known as the Bateman equations. If it is assumed, as Bateman did, that at $t = 0$ only the parent substance is present then the number of atoms of any member of the chain at a subsequent time t is given by

$$N_n(t) = C_1 e^{-\lambda_1 t} + C_2 e^{-\lambda_2 t} + C_3 e^{-\lambda_3 t} + \ldots + C_n e^{-\lambda_n t}$$

where

$$C_1 = \frac{\lambda_1\lambda_2 \ldots \lambda_{n-1}}{(\lambda_2 - \lambda_1)(\lambda_3 - \lambda_1)\ldots(\lambda_n - \lambda_1)}N_1^0$$

$$C_2 = \frac{\lambda_1\lambda_2 \ldots \lambda_{n-1}}{(\lambda_1 - \lambda_2)(\lambda_3 - \lambda_2)\ldots(\lambda_n - \lambda_2)}N_1^0$$

$$\vdots$$

$$C_n = \frac{\lambda_1\lambda_2 \ldots \lambda_{n-1}}{(\lambda_1 - \lambda_n)(\lambda_2 - \lambda_n)\ldots(\lambda_{n-1} - \lambda_n)}N_1^0$$

The constants also require the condition that if the value $(\lambda_n - \lambda_n)$ appears, it be set equal to 1.0, otherwise the denominator would be zero and the constant (and the number of atoms) would be infinite.

These relationships can be further simplified using product notation in the following general expression, which holds for any member of the series:

$$N_i(t) = N_1^0 \prod_{i=1}^{n-1}\lambda_i \sum_{i=1}^{n}\frac{e^{-\lambda_1 t}}{\prod_{i=1}^{n}(\lambda_n - \lambda_i)}$$

again with the provision that $(\lambda_n - \lambda_n) = 1.0$. It is left to the reader to become familiar with the use of this expression by using it to write down the equations for the number of atoms for the first four members of a radioactive series as developed above. The product expression applies to any member of a radioactive series that begins with a pure parent. It can be readily programmed for computer solutions, but most radioactive series calculations as a practical matter rarely extend past the fourth member of the series. Radon progeny calculations (see Chapter 6) are one of the most important and can be calculated as a subseries of four transformation products.

3.7 Radioactive Equilibrium

The relative activities of a radioactive parent and its radioactive product (commonly referred to as the daughter) can be determined from the equation for the number of atoms for the second member of a series by multiplying both sides by λ_2, with the following result:

$$A_2(t) = \frac{\lambda_2}{\lambda_2 - \lambda_1} A_1^0 (e^{-\lambda_1 t} - e^{-\lambda_2 t})$$

Calculations with this equation can be made somewhat simpler by use of the identity

$$\frac{\lambda_2}{\lambda_2 - \lambda_1} = \frac{T_1}{T_1 - T_2}$$

Thus

$$A_2(t) = \frac{T_1}{T_1 - T_2} A_1^0 (e^{-\lambda_1 t} - e^{-\lambda_2 t})$$

The *time of maximum activity* of $A_0(t)$ can be determined exactly for all cases by differentiating the equation for $A_2(t)$, setting it equal to zero, and solving for t_m as follows:

$$\frac{d(A_2)}{dt} = -\lambda_1 e^{-\lambda_1 t_m} + \lambda_2 e^{-\lambda_2 t_m} = 0$$

or

$$t_m = \frac{\ln(\lambda_2/\lambda_1)}{\lambda_2 - \lambda_1}$$

where λ_1 and λ_2 must be expressed in the same units. The value of t_m can also be expressed in terms of half-lives as

$$t_m = 1.4427 \frac{T_1 T_2}{T_1 - T_2} \ln \frac{T_1}{T_2}$$

The time of maximum activity occurs at the same time that the activities of the parent and daughter are equal (see Figure 3-37) if, and only if, the parent has only one radioactive product. As a general rule of thumb t_m occurs in 7–10 half-lives for a long-lived parent and a relatively short-lived product; however, the best practice is to calculate it. Once the time of maximum activity is known it can, in turn, be used in the equation for activity of the second species to determine the maximum amount of activity of the product.

Example 3-16. If 10 kBq of ^{132}Te ($T_{1/2}$ = 3.2 d = 76.8 h) is used as a generator of ^{132}I ($T_{1/2}$ = 2.28 h), what will be the maximum activity of ^{132}I that will grow into the source and when will it occur?

Solution. First determine the time of maximum activity, t_m:

$$t_m = 1.4427 \frac{76.8 \times 2.28}{76.8 - 2.28} \times \ln \frac{76.8\,\text{h}}{2.28\,\text{h}} = 11.92\text{h}$$

And since the maximum activity of the product occurs at t_m = 11.92 h, then

$$A_2(11.92\text{h}) = \frac{T_1}{T_1 - T_2} A_1^0 \left[e^{[-(\ln 2)/T_1]/T_m} - e^{[-(\ln 2)/T_2]T_m} \right]$$

$$A_2(11.92\text{h}) = \frac{76.8}{76.8 - 2.28} \times 10\,\text{kBq} \times \left[e^{[-(\ln 2)/76.8] \times 11.92} - e^{[-(\ln 2)/2.28] \times 11.92} \right]$$
$$= 8.98\ \text{kBq}$$

Therefore, at t_m = 11.92 h, the activity of ^{132}I in the source will have a transformation rate of 8980 t/s.

3.7.1 Secular Equilibrium

If the period of observation (or calculation) is such that the activity of the parent nuclide remains essentially unchanged, then the activity of the radioactive product (commonly referred to as the radioactive daughter) in the equation for the second member of a radioactive series can be simplified as follows:

$$A(t) = A_1^0 (1 - e^{-\lambda_2 t})$$

It should be noted that this is accurate only if the parent is much longer lived than the product. When this condition is satisfied, the product activity will grow to a level that is essentially identical to that of the parent, as shown in Figure 3-37, and the activities of the parent and the product show no appreciable change during many half-lives of the product. This condition is called *secular equilibrium*. The build-up of ^{90}Y from the transformation of ^{90}Sr is a good example of secular equilibrium as is the ingrowth of ^{222}Rn from the transformation of ^{226}Ra. In both instances the activity of the product will increase until it is the same as that of the parent (i.e., it is in equilibrium with the parent); the activity of the product reaches a value of 99% of the parent activity after about 6.7 half-lives of the product nuclide and is effectively in equilibrium with the parent at this and subsequent times.

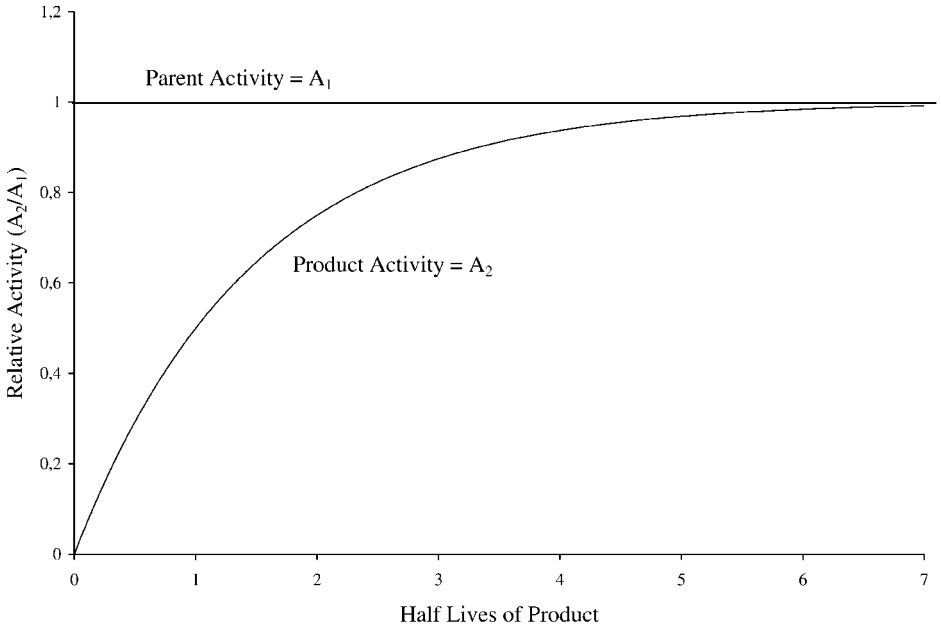

Fig. 3-37 Example of secular equilibrium in which the parent activity remains essentially unchanged while the short-lived product (activity = 0 at $t = 0$) activity builds up to 99% of the parent activity in about 6.7 half-lives.

The simplified equation for secular equilibrium is very convenient and easy to use, but it is necessary to ensure that the conditions for its appropriate use are met. If any uncertainty exists, then the general solution for the second member of a series will always give the correct result for a radioactive parent undergoing transformation to a radioactive product.

Example 3-17. ^{90}Sr ($T_{1/2}$ = 28.78 y) is separated from a radioactive waste sample and measured as containing 2 μCi of ^{90}Sr. If measured again 10 days later, how much ^{90}Y ($T_{1/2}$ = 2.67 d) will be in the sample?
Solution. This is a clear case of secular equilibrium, therefore

$$A(t) = A_1^0(1 - e^{-\lambda_2 t})$$

or

$$A(t) = 2\,\mu\text{Ci} \times (1 - e^{[-(\ln 2)/2.67\text{d}] \times 10\text{d}}) = 1.85\,\mu\text{Ci}\,^{90}\text{Y}$$

3.7.2 Transient Equilibrium

A condition called transient equilibrium results between a radioactive parent and a radioactive product if the parent is longer-lived than the product ($\lambda_1 < \lambda_2$), but the half-life of the parent is such that its activity diminishes appreciably during the period of consideration. If no product activity exists at $t = 0$, the activity of the product is given by

$$A_2(t) = \frac{T_1}{T_1 - T_2} A_1^0 (e^{-\lambda_1 t} - e^{-\lambda_2 t})$$

For values of t above 6.7 half-lives or so, $e^{-\lambda_2 t}$ becomes negligible compared with $e^{-\lambda_1 t}$ and the activity of the product is essentially

$$A_2(t) = \frac{T_1}{T_1 - T_2} A_1^0 e^{-\lambda_1 t}$$

Thus, the product eventually diminishes with the same half-life as the parent. When this condition exists, the two nuclides are said to be in transient equilibrium, and the product activity is greater than that of the parent by the factor $T_1/(T_1 - T_2)$. And since $A_1^0 e^{-\lambda_1 t}$ is just the activity of the parent at time t, the product activity can be obtained easily by determining the parent activity $A_1(t)$ at time t and multiplying it by $T_1/(T_1 - T_2)$ *if* it is known that transient equilibrium has been established. This is done by determining that the ingrowth time has exceeded the time when the product activity has reached its maximum value (see preceding section on time of maximum activity).

An example of transient equilibrium is shown graphically in Figure 3-38 for ^{132}Te ($T_{1/2}$ = 76.8 h) undergoing transformation to ^{132}I ($T_{1/2}$ = 2.28 h). Transient equilibrium is achieved just after, but not before, the activity of the product nuclide ^{132}I crosses over the activity curve for ^{132}Te. Once transient equilibrium is established, the product activity can be obtained by simply multiplying the existing parent activity by the ratio $T_1/(T_1 - T_2)$.

When the parent has a shorter half-life than the product ($\lambda_1 > \lambda_2$), no state of equilibrium is attained. If the parent and product are separated initially, then as the parent undergoes transformation the number of product atoms will increase, pass through a maximum, and the product activity will eventually be a function of its own unique half-life.

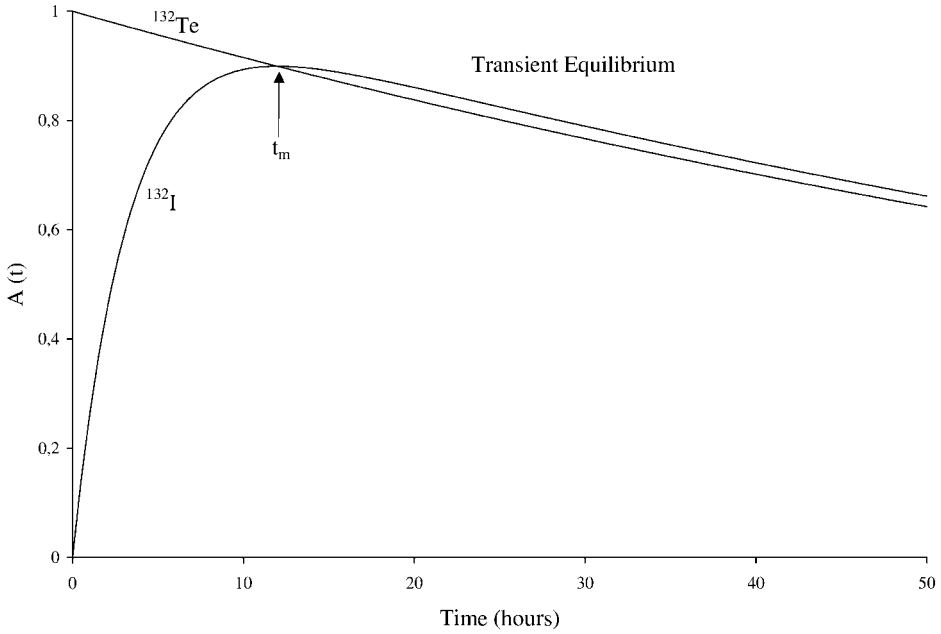

Fig. 3-38 Activity of ^{132}I produced from initially pure ^{132}Te undergoing radioactive transformation to ^{132}I, showing the establishment of transient equilibrium.

3.7.3 Radionuclide Generators

Various radionuclide generators are fabricated to produce relatively short-lived radionuclides from a long-lived parent; for example:

$$^{99}\text{Mo} \rightarrow ^{99m}\text{Tc} \rightarrow ^{99m}\text{Tc}$$
$$(66\text{h}) \rightarrow (6\text{h}) \rightarrow (> 10^5\text{y})$$

$$^{113}\text{Sn} \rightarrow ^{113m}\text{In} \rightarrow ^{113}\text{In}$$
$$(115\text{d}) \rightarrow (1.67\text{h}) \rightarrow (\text{stable})$$

$$^{67}\text{Ge} \rightarrow ^{68}\text{Ga} \rightarrow ^{68}\text{Zn}$$
$$(275\text{d}) \rightarrow (1.1\text{h}) \rightarrow (\text{stable})$$

The transformation rate of the parent radionuclide determines the activity of the product radionuclide, which is produced continuously such that a state of equilibrium often occurs. Once equilibrium has been achieved between the parent and daughter radioactivities, it can be disturbed only by chemical separation (referred to as milking) of the two radionuclides which will be followed by regrowth of the

product radioactivity as new atoms are produced by transformation of the parent. For example, the ^{99m}Tc activity in a ^{99}Mo–^{99m}Tc generator will achieve a state of transient equilibrium with ^{99}Mo, and the activity of ^{99m}Tc in the generator at any given time is governed by the 66 h half-life of ^{99}Mo rather than the 6 h half-life of ^{99m}Tc. In transient equilibrium the activities of the two radionuclides maintain a constant ratio with time even though the half-lives of the two radionuclides are quite different. Once ^{99m}Tc is removed (eluted) from the generator its activity is, of course, governed by its 6 h half-life. Transient equilibrium is re-established in about 7 half-lives of the product, although at a new level due to the decrease in activity of the parent. In practical terms, a fresh supply of the product radionuclide is available in about 2–4 half-lives; however, the generator can be remilked sooner, and the extracted activity determined by the parent source strength and the ingrowth period. The growth and removal of the product activity in a generator can be predicted exactly using the radioactive series transformation equations.

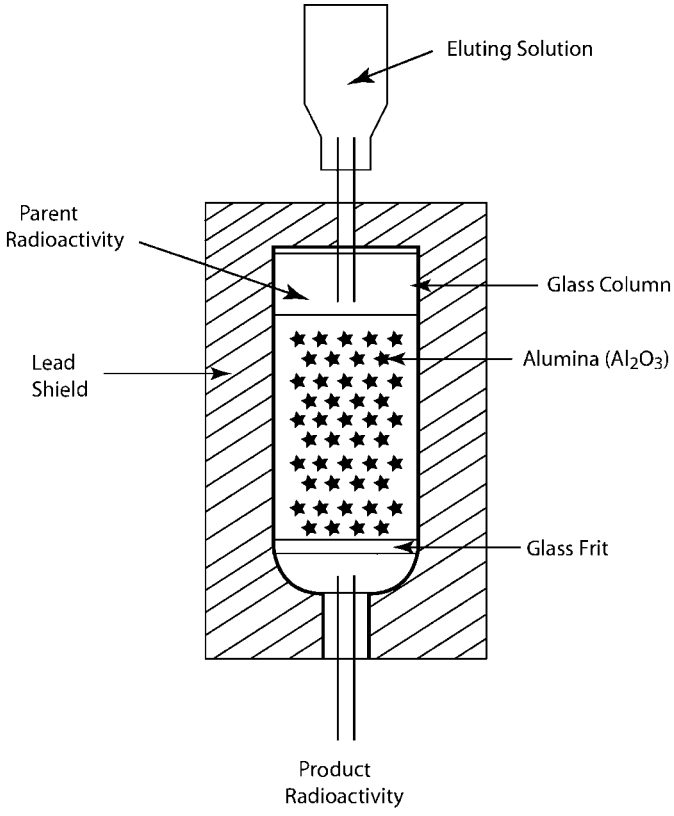

Fig. 3-39 Schematic of a typical radionuclide generator.

In a typical ^{99}Mo–^{99m}Tc generator, ^{99}Mo in the form of sodium molybdate is absorbed onto alumina, and when eluted with 0.9% sodium chloride solution (or

saline) technetium is extracted as sodium pertechnetate (Na $^{99m}TcO_4$). A typical generator consists of a glass column filled with a suitable exchange material such as alumina (Al_2O_3) held in place with a porous glass disk and enclosed in a lead shield (Figure 3-39). The parent radionuclide is firmly absorbed on the top of the alumina and the product is also retained in the matrix until it is separated (eluted or milked) from the parent radionuclide by a solution that preferentially leaches the product radionuclide without removing the parent. The ^{99}Mo used in the generator can be produced by neutron activation of ^{98}Mo or by nuclear fission of ^{235}U, which yields a carrier-free product with very high activity; the activity for neutron activation of ^{98}Mo is generally much lower.

Transformation branching affects the relative activity of a radionuclide in a series. For example, the decay scheme for ^{99}Mo–^{99m}Tc indicates (as shown in Figure 3-19) that the ^{99m}Tc product is produced in only 82.84% of the transformations, and it is necessary to account for this branching fraction in calculations of the activity of ^{99m}Tc produced from ^{99}Mo; i.e.,

$$A(^{99m}\mathrm{Tc}) = (0.8284)\frac{T_1}{T_1 - T_2}A^0(^{99}\mathrm{Mo})(e^{-\lambda_1 t} - e^{-\lambda_2 t})$$

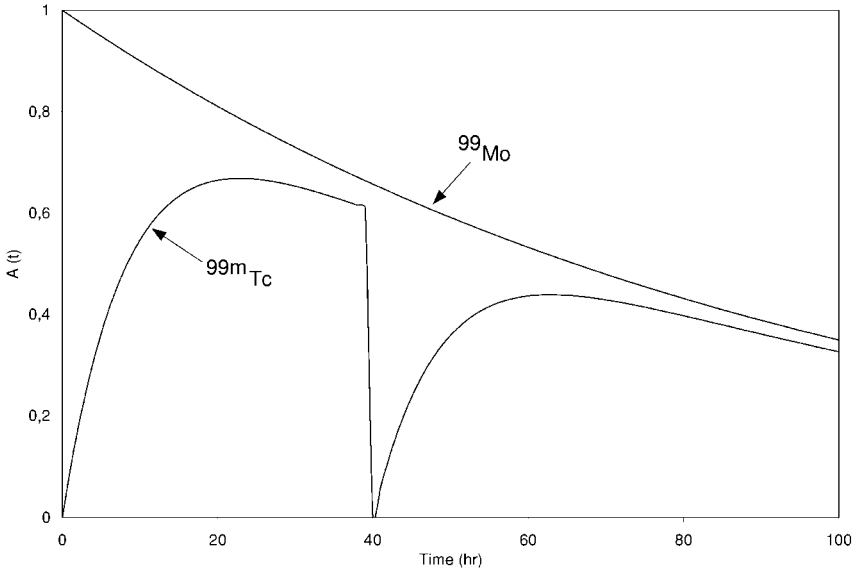

Fig. 3-40 Transient equilibrium for branched radioactive transformation of ^{99}Mo to ^{99m}Tc.

where T_1 and T_2 are in the same units, $A^0(^{99}Mo)$ is the activity of ^{99}Mo at any initial time t_0, and t is the elapsed time measured from t_0. This relationship is plotted in Figure 3-40 for the ingrowth of ^{99m}Tc (in gamma transitions) for several extractions of ^{99m}Tc produced in the generator. The gamma transition rate of ^{99m}Tc that grows into the generator never reaches the parent activity (as it does for ^{132}I in Figure 3-38) because only 82.84% of ^{99}Mo transformations produce ^{99m}Tc, and

thus the recovery curve does not rise above the parent even though a state of transient equilibrium is established.

3.8
Total Number of Transformations (Uses of τ and λ_{Eff})

Many circumstances in radiation dosimetry or measurement require knowledge of the total number of transformations that occur over a time interval. If the time interval is short and the activity remains essentially constant over the interval, the number of transformations is just activity multiplied by time, and fortunately many situations can be so represented (a count taken over a few minutes, a detector reading, a dose rate measurement, etc.). In other situations, the activity will change significantly over the time of interest and determination of the number of transformations must account for the change. One such circumstance is clearance of a radioactive substance that has been deposited in a biological tissue (e.g., a human organ) and removal is not only by radioactive transformation but biological processes as well, i.e., with an effective half-life. If an initial activity A_0 is deposited in a biological system it will vary with time as shown in Figure 3-41.

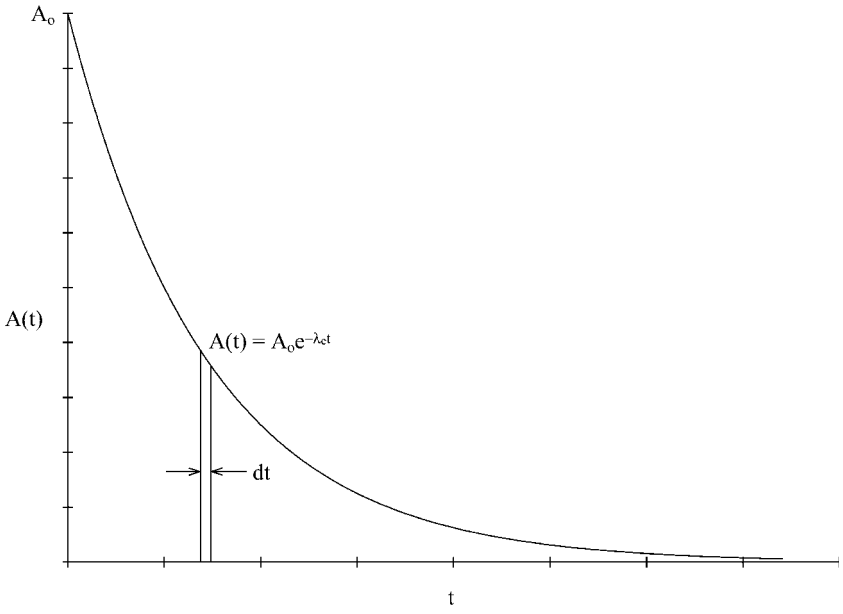

Fig. 3-41 Variation of activity in a system due to multiple removal processes where λ_e accounts for both biological, λ_b, and radiological, λ_r, removal processes.

The number of transformations that occur over a given time interval from $t = 0$ to t is obtained by determining the area under the curve. The area will have units

of activity·seconds (or other time units if preferred) and can be obtained by integration of each of the differential units of area $A(t)dt$ recognizing that both are variables, or

$$\text{Area(activity} \cdot \text{seconds)} = \int_0^t A(t)dt = \int_0^t A_o e^{-\lambda_e t} dt$$
$$= \frac{A_0}{\lambda_e}(1 - e^{-\lambda_e t}) = 1.4427 T_e A_0 (1 - e^{-\lambda_e t})$$

which yields the total number of transformations that occur in a time t because activity has units of transformations per unit time and T_e is in units of time. And if $t \to \infty$, which it effectively does in 7–10 effective half-lives, then the total number of transformations is

$$\text{Area(activity} \cdot \text{seconds)} = \frac{A_0}{\lambda_e} = 1.4427 T_e A_0$$

Example 3-18. For a radiopharmaceutical containing ^{32}P ($T_{1/2}$ = 14.3 d) with an activity of 10^4 d/m that is deposited in the liver of a person from which it clears with a biological half-life of 18 d, (a) how many transformations will occur in 7 days and (b) how many total transformations will occur?
Solution. First, determine the effective half-life and the effective removal constant:

$$T_e = \frac{14.3 \times 18}{14.3 + 18} = 7.97\text{d} = 1.15 \times 10^4 \text{ min}$$

(a) The number of transformations occurring in 7 d is

$$\text{Transformations} = 1.4427 \times 1.15 \times 10^4 \text{ m} \times 10^4 \text{ t/m} \times [1 - e^{[-(\ln 2)/7.97\text{d}] \times 7\text{d}}]$$
$$= 7.55 \times 10^7 \text{ transformations}$$

(b) The total number of transformations as $t \to \infty$ is

$$\text{Transformations} = 1.4427 \times 1.15 \times 10^4 \text{ m} \times 10^4 \text{ t/m} = 1.66 \times 10^8 \text{ transformations}$$

The results of Example 3-18 can be used to determine the amount of energy deposited in the tissue by assigning an energy to each transformation and determining the fraction of each energy unit that is absorbed. For ^{32}P in the liver, the average energy per transformation is 0.695 MeV (see Appendix D) and the absorbed fraction is 1.0; therefore, the total energy deposited is

$$E_{dep} = 1.66 \times 10^8 \text{ t} \times 0.695 \text{ MeV/t} = 1.154 \times 10^8 \text{ MeV} = 1.85 \times 10^2 \text{ erg}$$

which can be converted to radiation absorbed dose by dividing by the tissue mass (see Chapter 7).

3.9
Discovery of the Neutrino

The discovery of the neutrino was accomplished by Reins and Cowan some 20 years after its existence was first postulated. They used the intense radiation field from a high-powered nuclear reactor at the Savannah River Site to determine whether the inverse of β^- transformation occurred in a tank containing 1400 L of proton-rich triethylbenzene, as shown schematically in Figure 3-42. The theoretical reaction being tested was for the inverse of proton transformation in which the large flux of postulated antineutrinos would produce positrons and neutrons in a proton-rich solution, or

$$\bar{\nu} + {}^{1}_{1}\mathrm{p} + 1800\ \mathrm{keV} \rightarrow {}^{0}_{1}\beta^{+} + {}^{1}_{0}\mathrm{n}$$

which is the inverse of β^- transformation. Antineutrino absorption by a proton should produce a positron and a neutron, and the reaction would require a Q-value of 780 keV plus the energy of two electron masses for a total of 1800 keV.

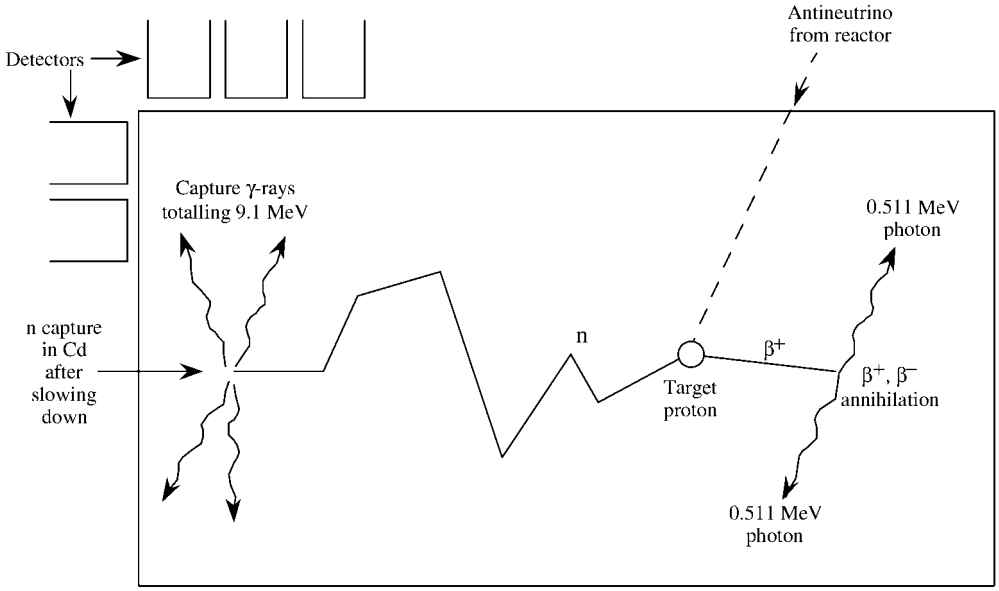

Fig. 3-42 Tank of liquid scintillating triethylbenzene used to detect the neutrino by inducing antineutrino capture by protons yielding a prompt signal (interactions of the positron produced in the interaction and its annihilation) and a delayed signal when the neutron produced by the reaction is captured in cadmium. The two signals were detected some 30 μs apart by scintillation detectors surrounding the tank.

Coincidences between positrons and neutrons in the liquid scintillator were used as the primary means of detecting the reactions. If antineutrino reactions occurred with protons, both a positron and a neutron would be produced. The postulated positron would quickly ionize the medium and then annihilate with an available electron, and the neutron would slow down and be captured yielding a capture gamma ray; therefore, $CdCl_2$ was dissolved in the scintillator to enhance their detection. Detectors surrounding the tank of liquid scintillator would produce two signals: a *prompt* signal from the ionization produced by absorption of the emitted positron and the two 0.511 MeV annihilation photons in the scintillator, and a *delayed* signal produced by 9.1 MeV gamma rays emitted when the neutron was captured in cadmium, which due to the slowing down time of the neutron should occur in about 30 μs. Reines and Cowan measured 36 ± 4 events associated with the reactor being on and calculated the cross-section for neutrino capture to be $(11 \pm 2.6) \times 10^{-44}$ cm^2, thus confirming its existence.

Acknowledgments

This chapter was compiled with the able and patient assistance of Arthur Ray Morton III, MS, major, US Army, and Chul Lee, MS, both graduates of the University of Michigan Radiological Health Program.

Other Suggested Sources

Evans, R. D. **1955**, *The Atomic Nucleus*, McGraw Hill, New York.
General Electric **1996**, Chart of the nuclides, in *Nuclides and Isotopes*, 15th edn, General Electric Company, San Jose, CA.
ICRP **1978**, *Radionuclide Transformations – Energy and Intensity of Emissions*, Report 38, Pergamon Press.
Krane, K. S. **1988**, *Introductory Nuclear Physics*, Wiley, New York.
MIRD **1989**, *Radionuclide Data and Decay Schemes*, Society of Nuclear Medicine, New York.
National Nuclear Data Center, Brookhaven National Laboratory, Upton, NY. Accessible at: www.nndc.bnl.gov
Reines, F., Cowan, C. L. **1953**, Detection of the free neutrino, *Phys. Rev.* 92, 8301.
Robson, J. M. **1951**, The radioactive decay of the neutron, *Phys. Rev.* 83, 349–358.

Problems – Chapter 3

3–1. It is noted that a sample of ^{134}La with a half-life of 6.5 min has an activity of 4 Ci. What was its activity an hour ago?
3–2. Determine by Q-value analysis whether ^{65}Zn can undergo radioactive transformation by β^+, EC, or β^- transition.
3–3. A sample of material decays from 10 to 1 Ci in 6 h. What is the half-life?
3–4. An isotope of fission is ^{151}Sm, with a half-life of 90 y. How long will it take 0.05 g to decay to 0.01 g?
3–5. How many days will it take to reduce 4 Ci of ^{210}Po ($T_{1/2}$ = 138 d) to 1 Ci? How many grams of ^{210}Po does it take to produce 4 Ci of activity?
3–6. What is the initial activity of 40 g of ^{227}Th ($T_{1/2}$ = 18.72 d)? How many grams will be in the sample two years later?
3–7. In August 1911 Marie Curie prepared an international standard of activity containing 21.99 mg of $RaCl_2$. Calculate the original activity of the solution, and its activity as of August 1996 using constants from the chart of the nuclides.
3–8. Calculate the specific activity of ^{210}Pb ($T_{1/2}$ = 22.3 y). What activity/gram does a pure sample of ^{210}Pb have after it has aged 3 y?
3–9. A reference person weighs 70 kg and contains, among other elements, 18% carbon (65 billion atoms of ^{14}C per gram of C) and 0.2% potassium. How many microcuries of ^{14}C and of ^{40}K will be present in such a person?
3–10. What must be the activity of radiosodium (^{24}Na) compound when it is shipped from Oak Ridge National Laboratory so that upon arrival at a hospital 24 h later its activity will be 100 mCi?
3–11. An amount of 750 mg of ^{226}Ra is used as a source of radon which is pumped off and sealed into tiny seeds or needles. How many millicuries of radon will be available at each pumping if this is done at weekly intervals? How much time will be required to accumulate 700 mCi of the gas?
3–12. An assay of an equilibrium ore mixture shows an atom ratio for ^{235}U/^{231}Pa of 3.04×10^6. Calculate the half-life of ^{235}U from the assay data and the known half-life of ^{231}Pa (3.28×10^4 y).
3–13. Regulations permit use of ^{3}H in luminous aircraft safety devices up to 4 Ci. How many grams of ^{3}H could be used in such a device? What change in luminosity would occur after 8 y of use?
3–14. What is the energy of neutrino(s) from electron capture transformation of ^{55}Fe? What energy distribution do these neutrinos have?
3–15. Artificially produced ^{47}Ca ($T_{1/2}$ = 4.54 d) is a useful tracer in studies of calcium metabolism, but its assay is complicated by the presence of its radioactive product ^{47}Sc ($T_{1/2}$ = 3.35 d). Assume an assay based on beta particle counting with equal counting efficiencies for the two nuclides, and calculate the data for and plot a correction curve that can be used to determine ^{47}Ca from a total beta count.
3–16. What mass of ^{3}H will be needed to replace 0.08 Ci of ^{210}Po in a luminous instrument dial if each is equally effective in producing scintillations? How much ^{3}H would be needed for equal luminosity of ^{210}Po one year after fabrication?

3–17. A source of radioactivity was measured to have 40, 14, 5.5, 2, and 0.6 d/m at 8 min intervals. Use a plot of the data to determine the half-life of the radionuclide in the source.

3–18. A mixed source was measured to produce the following activity levels at 3 min intervals: 60, 21, 8, 1, and 0.3 d/m. What are the half-lives of the radionuclides in the source?

3–19. An amount of 10 mCi of ^{90}Sr is separated from a fission product mixture and allowed to set for ^{90}Y to grow in. What is the activity of ^{90}Y at (a) 20 h and (b) 600 h?

3–20. What is the maximum activity of ^{90}Y that will ever be present in the sample in Problem 3–19 and at approximately what time after separation does it occur?

3–21. If ^{140}Ba ($T_{1/2}$ = 12.75 d) is freshly separated from a fission product mixture and found to contain 200 mCi: (a) what is the activity of ^{140}La ($T_{1/2}$ = 1.678 d) that will grow into the sample in 12 h? (b) What is the maximum activity of ^{140}La that will ever be present in the sample and when will it occur?

3–22. Derive from first principles the equation for the third member of a radioactive series that begins with a radioactive parent containing $N_1{}^0$ atoms.

3–23. The steel compression ring for the piston of an automobile engine has a mass of 30 g. The ring is irradiated with neutrons until it has an activity of 10 μCi of ^{59}Fe ($T_{1/2}$ = 44.529 d). The ring is installed in an engine and removed 30 d later. If the crankcase oil has an average activity due to ^{59}Fe of 0.126 d/m per cm^3, how much iron was worn off the piston ring? (Assume that the total volume of the crankcase oil is 4.732 L.)

3–24. The mass of the human thyroid is about 20 g and it clears iodine deposited in it with a biological half-life of 80 d. If 2 μCi of ^{131}I ($T_{1/2}$ = 8.02 d) is present in a person's thyroid, (a) how many transformations will occur in a period of 6 d? (b) How many will occur over a period of 1 y, or effectively infinite time? (c) If the principal beta of $E_{\beta,\max}$ = 0.605 MeV and $E_{\beta,\text{avg}}$ = 0.192 MeV occurs in 89.9% of transformations, how much energy will be deposited per gram of thyroid tissue?

4
Interactions

"When the intervals, passages, connections, weights, impulses, collisions, movement, order and position of the atoms interchange, so also must the things formed from them change."
Lucretius (ca. 100 BC)

Much of what is known about atoms and radiation from them was learned by aiming subatomic particles at various target materials. The discovery of cathode rays provided a source of projectiles that led to the discovery of x-rays and subsequently radioactivity. Scattering of alpha particles emitted from radioactive substances gave the first clues and insight that the positive charges of atoms are coalesced into a very small nucleus. Interactions of alpha particles, protons, deuterons, neutrons, and light nuclei with various target nuclei have produced many new products including transmutation and/or fission of heavy elements and fusion of light atoms.

4.1
Production of X-rays

Roentgen was able to describe most of the known characteristics of x-rays after his monumental discovery by conducting several experiments; however, it was not possible to explain how x-rays were produced until the concepts of atoms, particles, and quanta were understood. It is now known that x-ray production occurs, as shown in Figure 4-1, when a negatively charged electron of kinetic energy eV enters the force field of the positively charged nucleus of a target atom. This force field, which is strongest for high-Z materials like tungsten, deflects and accelerates the electron, which causes the emission of electromagnetic radiation as it is bent near the nucleus. This is consistent with classical electromagnetic theory because the electron is not bound. Because radiation is emitted and energy is lost in the process, the electron must slow down, so that when it escapes the force field of the nucleus it has less energy. Overall, the electron experiences a net deceleration, and its energy after being decelerated is $eV - hv$ where hv appears as electromagnetic radiation. Roentgen named these radiations x-rays to characterize their unknown status. This process of radiation being produced by an overall net deceleration of the electrons is called *Bremsstrahlung*, a German word meaning *braking radiation*.

Physics for Radiation Protection, Third Edition. James E. Martin

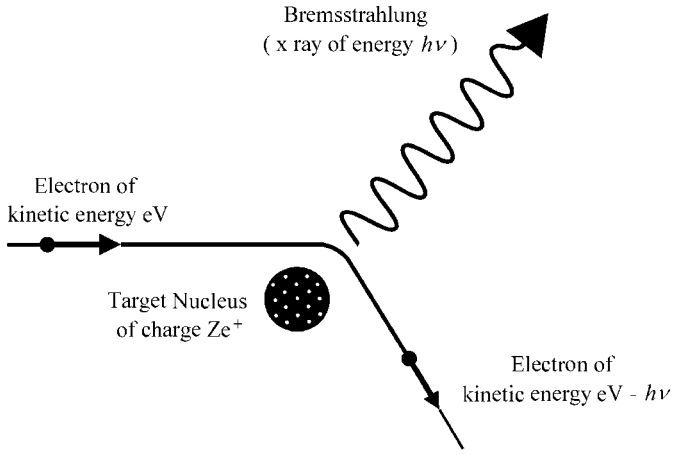

Fig. 4-1 Production of x-rays in which accelerated electrons emit bremsstrahlung.

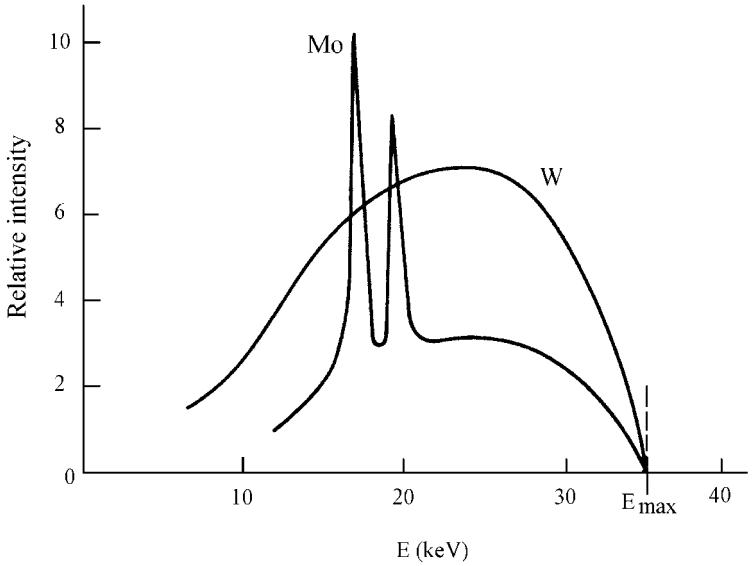

Fig. 4-2 X-ray spectra of intensity $I(\nu)$ versus electron energy E for tungsten (W) and molybdenum (Mo) targets, each of which is operated at 35 kV.

X-ray production is a probablistic process because any given electron may take any path past a target nucleus including one in which all of its energy is lost. Bremsstrahlung photons are thus emitted at all energies up to the accelerating energy eV and in all directions, including absorbtion in the target. As shown in Figure 4-2 for tungsten (W) and molybdenum (Mo), x-ray spectra have a continuous distribution of energies up to the maximum energy E_{max} of the incoming elec-

tron. The value of E_{max} does not depend on the target material, but is directly proportional to the maximum voltage. About 98% of the kinetic energy of the accelerated electrons is lost as heat because most of the impinging electrons expend their energy in ionizing target atoms. Other aspects of the production and uses of x-rays are described in Chapter 15.

4.2 Characteristic X-rays

Figure 4-2 shows discrete lines superimposed on the continuous x-ray spectrum for a molybdenum target because the 35 keV electrons can overcome the 20 keV binding energy of inner shell electrons in the molybdenum target. However, this does not occur for the tungsten target spectrum because the inner shell electrons of tungsten are tightly bound at 69.5 keV. The vacancy created by a dislodged orbital electron can be filled by an outer shell (or free) electron changing its energy state, or, as Bohr described it, jumping to a lower potential energy state with the emission of electromagnetic radiation; the emitted energy is just the difference between the binding energy of the shell being filled and that of the shell from whence it came. And since the electrons in each element have unique energy states, these emissions of electromagnetic radiation are "characteristic" of the element, hence the term "characteristic x-rays" (see Figure 4-3). They uniquely identify each element.

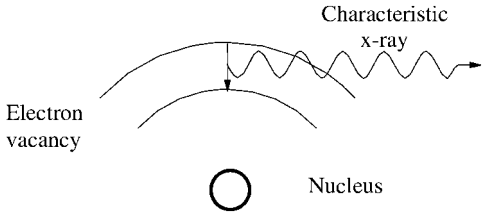

Fig. 4-3 Emission of a characteristic x-ray due to a higher energy electron giving up energy to fill a particular shell vacancy.

If an electron vacancy exists in the K shell, the characteristic x-rays that are emitted in the process of filling this vacancy are known as K-shell x-rays, or simply K x-rays. Although the filling electrons can come from the L, M, N, etc., shells, characteristic x-rays are known by the shell that is filled. Further, the K x-ray that originates from the L shell is known as the K_{α} x-ray; if the transition is from the L_{III} subshell it is a $K_{\alpha 1}$ x-ray, and if from the L_{II} subshell a $K_{\alpha 2}$ x-ray. A transition from the L_I subshell is forbidden by the laws of quantum mechanics. In a similar fashion those from M, N, and O shells and subshells are known as K_{β}, K_{γ}, K_{δ} and so forth with appropriate numerical designations for the originating subshells. Figure 4-4 illustrates these transitions in molybdenum, including the energies of the L subshells.

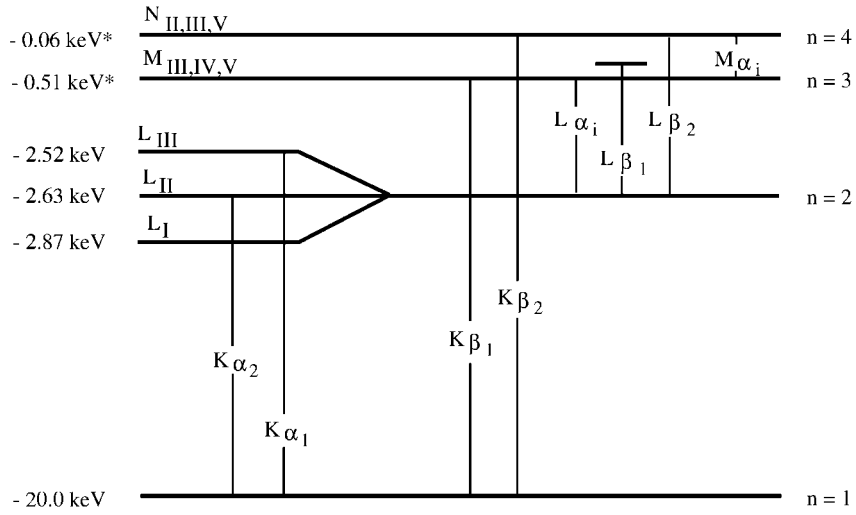

* Maximum energy for the shell; for subshell energy levels see Appendices C and D.

Fig. 4-4 Emission of characteristic x-rays from a molybdenum target due to electron vacancies in various shells followed by a higher energy electron giving up energy to fill a particular shell vacancy.

L x-rays are produced when the bombarding electrons knock loose an electron from the L shell and electrons from higher levels drop down to fill these L-shell vacancies. The lowest-energy x-ray of the L series is known as L_a, and the other L x-rays are labeled in order of increasing energy, which corresponds to being filled by electrons from higher energy orbits as shown in Figure 4-4. Characteristic x-rays for M, N, etc., shells are designated by this same pattern. Interactions in the higher-energy shells occurs with lower probability than for K-shell x-rays because target-atom electrons in outer shells are spread out over a larger volume, thus presenting a smaller target to incoming electrons.

A wide array of characteristic x-rays can be observed for a given element due to the subshells within the major shells. For example, the K_a x-ray could originate from any one of the subshells of the $n = 2$ level, as shown on the left-hand side of Figure 4-4. The energies of these different transitions will be slightly different, and emissions associated with each are possible. The energy differences are very small for most shells, but worth noting for the K and L shells especially for the higher Z elements. Listings of emitted radiations associated with radioactive transformations denote these as K_{a1}, K_{a2}, L_{a1}, L_{a2}, etc. (see Chapter 3 and Appendix D).

Example 4-1. From the data in Figure 4-4, compute the energy of $K_{\alpha 1}$, $K_{\alpha 2}$, K_{β}, K_{γ}, and L_{α} characteristic x-rays.

Solution. The emitted x-rays occur because electrons change energy states to fill shell vacancies. Each characteristic x-ray energy is the difference in potential energy the electron has before and after the transition. For K x-rays:

$$K_{\alpha 1} = -2.52 - (-20.0) = 17.48 \text{ keV}$$
$$K_{\alpha 2} = -2.63 - (-20.0) = 17.37 \text{ keV}$$
$$K_{\beta} = -0.50 - (-20.0) = 19.50 \text{ keV}$$
$$K_{\gamma} = -0.06 - (-20.0) \cong 20.00 \text{ keV}$$

For L-shell vacancies, it is presumed that the lowest energy subshell is filled from the lowest energy M shell, or

$$L_{\alpha} = -0.51 - (-2.87) = 2.36 \text{ keV}$$

Other permutations are also possible, which would produce a large array of discrete characteristic x-rays, all of which can be resolved with modern x-ray spectrometers.

4.2.1 X-rays and Atomic Structure

Study of characteristic x-rays led to fundamental information on atomic structure. Moseley's analyses of K x-rays proved that the periodic table should be ordered by increasing Z instead of by mass and that certain elements were out of order and others were not yet discovered. The relative positions of the K_{α} and K_{β} lines in Moseley's original photographic images are shown in Figure 4-5 for elements from calcium to copper; the images clearly show that the wavelengths decrease in a regular way as the atomic number increases. The gap between the calcium and titanium lines represents the positions of the lines of scandium, which occurs between those two elements in the periodic system.

Before Moseley's work the periodic table was ordered according to increasing mass, which placed certain elements in the wrong group (e.g., cobalt and nickel or iodine and tellurium). Moseley found that when the elements were ordered according to Z the chemical properties corresponded to the proper group. He also found gaps corresponding to yet undiscovered elements. For example, the radioactive element technetium ($Z = 43$) does not exist in nature and was not known at the time, but was later discovered based on his work.

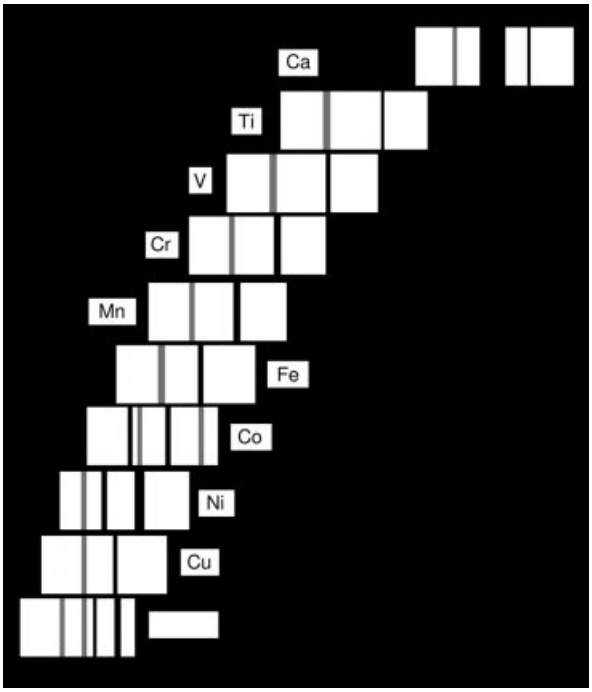

Fig. 4-5 Moseley's photographs of K_α and K_β x-ray lines for various light elements.

4.2.2 Auger Electrons

A characteristic x-ray photon is produced any time an electron vacancy is filled by a higher-energy electron. Many of these characteristic x-rays are emitted from the atom, but many do not exit the atom because of a phenomenon called the Auger effect. When this occurs the x-ray interacts with an electron from a shell farther out, thus ejecting it from the atom. These are known as Auger electrons.

The Auger effect is similar to an "inner photoelectric effect" as shown schematically in Figure 4-6. First a K-shell vacancy occurs, which can be filled by any higher-energy electron but most likely from the L shell with the energy released as a characteristic x-ray. If, instead of leaving the atom, the x-ray interacts with a second L-shell electron, it is ejected from the atom and the L shell loses two electrons. These are then replaced by electrons from the M shell or farther out, sometimes producing a cascade of Auger electrons. The probability of such nonradiative processes, which compete with x-ray emission, has been found to decrease with increasing nuclear charge, as shown in Figure 4-7 where the fraction of total emissions that occur by Auger electrons is denoted by $1 - \eta$. In light atoms with low Z, the ejection of Auger electrons far outweighs characteristic x-ray emissions (Figure 4-7), but is the reverse for high-Z atoms.

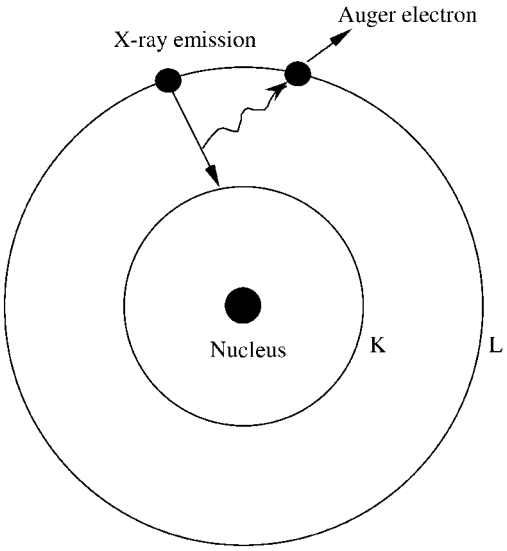

Fig. 4-6 Auger electron emission (right) competes with emission by characteristic x-rays (left).

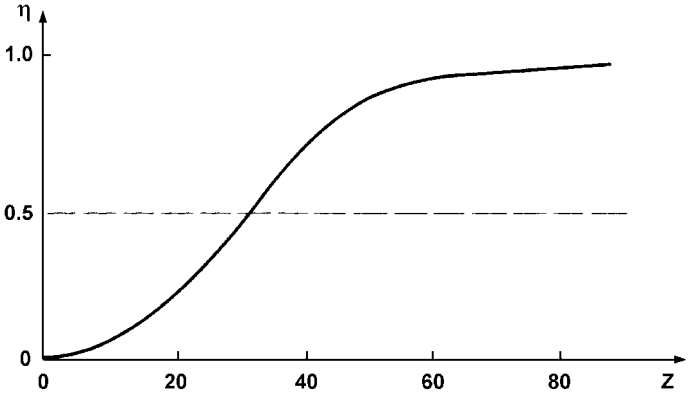

Fig. 4-7 Ratio η of characteristic x-ray emission to Auger electron production as a function of the atomic number Z.

The kinetic energy of an ejected Auger electron is equal to the energy hv of the characteristic x-ray (if it were to be emitted) minus the binding energy of the ejected electron in its respective shell, or

$$KE_{auger} = hv - BE_e$$

Example 4-2. Silver is bombarded with 59.1 keV K_α radiation from tungsten. If the binding energies of the K- and L-shell electrons in Ag are 25.4 and 3.34 keV,

respectively, what are the energies of (a) electrons ejected from the K and L shells by direct ionization and (b) Auger electrons ejected from the L shell by the K_α and K_β x-rays?

Solution. (a) The energy of photoelectrons from the L shell of Ag is

$$59.1 - 3.34 = 55.76 \text{ keV}$$

and from the K shell,

$$59.1 - 25.4 = 33.7 \text{ keV}$$

(b) The energy of Auger electrons ejected from the L shell by K_β x-rays is

$$24.9 - 3.34 = 21.56 \text{ keV}$$

and by K_α x-rays

$$22.1 - 3.34 = 18.76 \text{ keV}$$

4.3 Nuclear Interactions

Nuclear interactions are those that involve a bombarding particle and a target nucleus (in x-ray production the electron is not absorbed by the nucleus). Projectiles used in nuclear interactions can be alpha particles (α), protons (p), deuterons (d), neutrons (n), or light nuclei such as tritium (^{3}H) or helium (^{3}He). Interaction of a projectile with a target atom (the reactants) yields first a compound nucleus which then breaks up to produce the final products:

$$X + x \rightarrow [\text{compound nucleus}] \rightarrow Y + y$$

where X is the target nucleus, x is the bombarding particle or projectile, Y is the product nucleus, and y is the emitted product (either a particle, a nucleus, or a photon). Such reactions are also shown in condensed form as

Target (projectile, emission) product

The total charge (total Z) and the total number of nucleons (total A) are the same before and after the reaction, and momentum and energy must be conserved.

Three categories of interactions can occur as illustrated in Figure 4-8: (a) scattering, in which the projectile bounces off the target nucleus with a transfer of some of its energy; (b) pickup and stripping reactions in which a high-energy projectile either collects (picks up) or loses (strips) nucleons from a target atom, and

(c) absorption of the projectile into the target nucleus to form a new (or excited) atom that then undergoes change. Each type of interaction will produce recoil of the nucleus and deceleration (or stopping) of the particle, which alters its momentum and energy.

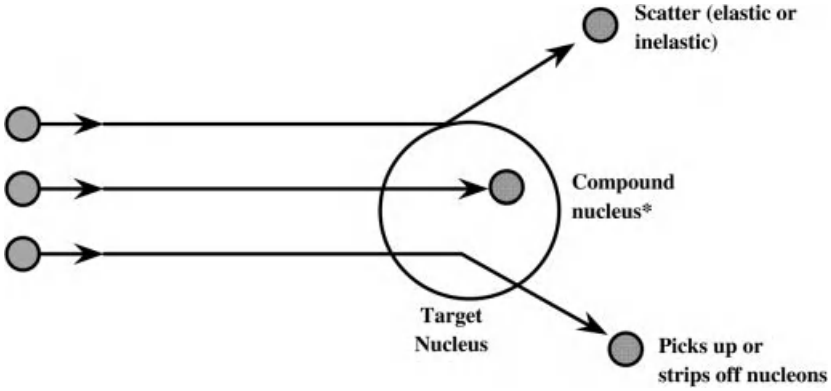

Fig. 4-8 Nuclear interactions in which a bombarding particle is scattered by the target nucleus, absorbed to form a compound nucleus with excess energy, or picks up or strips nucleons.

Scattering reactions produce a decrease in the energy of the projectile by elastic or inelastic scattering. If the residual nucleus is left in its lowest or ground state, the scattering is elastic; if left in an excited state, the scattering is called inelastic.

Pickup and stripping reactions usually occur when the projectile has high energy, and in such reactions the nucleon enters or leaves a definite "shell" of the target nucleus without disturbing the other nucleons in the target. Rutherford's (α, p) reaction with nitrogen may be thought of as a stripping reaction.

Absorption reactions occur when the incident projectile is fully absorbed into a target atom to form a new compound nucleus which lives for a very short time in an excited state and then breaks up. The new nucleus only exists for 10^{-16} s or so; thus, it cannot be observed directly, but this is much longer than the 10^{-21} seconds required for a projectile to traverse the nucleus. It is therefore assumed that the compound nucleus does not "remember" how it was formed, and consequently it can break up any number of ways depending only on the excitation energy available. The formation and breakup of ^{64}Zn is one example:

$$
\begin{aligned}
^{63}\mathrm{Cu} + {}^{1}_{1}\mathrm{H} &\rightarrow \\
{}^{64}\mathrm{Zn}* &\rightarrow {}^{62}\mathrm{Cu} + \mathrm{n} + \mathrm{p} \\
^{60}\mathrm{Ni} + {}^{4}_{2}\mathrm{He} &\rightarrow \\
&\rightarrow {}^{63}\mathrm{Zn} + \mathrm{n} \\
&\rightarrow {}^{62}\mathrm{Zn} + 2\mathrm{n}
\end{aligned}
$$

The relative probabilities of forming any of the three interaction products from the compound nucleus ^{64}Zn* are essentially identical, even though the initial par-

ticles are different. Bombardment of lithium with protons is another example (see below) of multiple ways the compound nucleus can break up, yielding different products.

4.3.1 Cross-Section

The charge, mass, and energy of a bombarding particle (or projectile) determine its interaction probability with a target atom, which is assumed to be at rest. Their mass and charge also affect the likelihood of interaction. A particle(s) from the compound nucleus also has mass, charge, and kinetic energy which also influence the probability of any given interaction. These effects are collectively described by the "cross-section" of the interaction, denoted as σ_i where i refers to the product of the interaction. There is no guarantee that a particular bombarding projectile will interact with a target nucleus to bring about a given reaction; thus, σ only provides a measure of the probability that it will occur. The cross-section is dependent on the target material and features of the incident "particle," which may in fact be a photon. These include the energy, charge, mass, and de Broglie wavelength of the projectile, as shown schematically in Figure 4-9, and the vibrational frequency, the spin, and the energy states of nucleons in the target atom. These cannot be predicted directly by nuclear theory; thus, cross-sections for any given arrangement of projectile and target are usually determined by measuring the number of projectiles per unit area (i.e., the flux) before and after they impinge on a target containing N atoms. As shown in Figure 4-10, the reduction in the flux of projectile after passing through the target is a direct measure of the number of interactions that occur in the target; it is a function of ϕ and the interaction probability σN of the target atoms:

$$-\frac{d\varphi}{dx} = \sigma N \varphi$$

which can be integrated to yield

$$\phi(x) = \phi_0 e^{-\sigma N x}$$

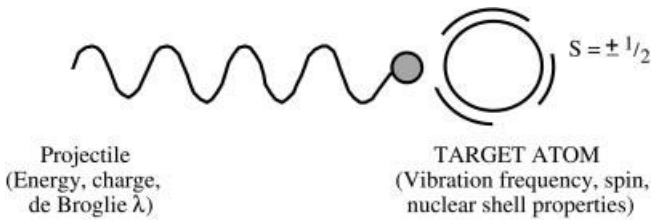

Fig. 4-9 Parameters related to interactions of particles with target nuclei.

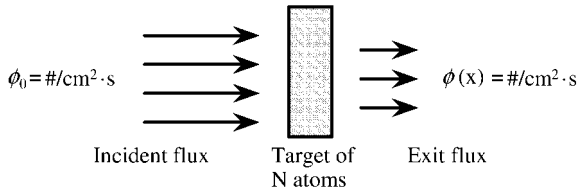

Fig. 4-10 Incident flux ϕ_0 of projectiles on a target containing N atoms/cm^3 is reduced to $\phi(x)$ after traversing a thickness x (cm).

The units of σ will be in terms of apparent area (m^2 or cm^2) per target atom. Although the cross-section has the dimensions of area, it is not the physical area presented by the nucleus to the incoming particle but is better described as the sum total of those nuclear properties that determine whether a reaction is favorable or not. When such measurements and calculations were first made for a series of elements, the researchers were surprised that the calculated values of σ were as large as observed. Apparently, one of them exclaimed that it was "as big as a barn," and the name stuck. One barn, or b, is

$$1\text{ b} = 10^{-24}\text{ cm}^2 \text{ or } 10^{-28}\text{ m}^2$$

which is of the order of the square of a nuclear radius. Cross-sections vary with the energy of the bombarding particle, the target nucleus, and the type of interaction.

Example 4-3. A flux of 10^6 neutrons/s in a circular beam of 1 cm radius is incident on a foil of aluminum (density = 2.7 g/cm^3) that was measured in several places with a micrometer to average 0.5 cm thickness. After passing through the foil the beam contained 9.93×10^5 neutrons/s. Calculate the cross-section σ_γ.
Solution. The number of atoms/cm^3 in the foil is

$$\frac{(2.7\text{ g/cm}^3)(6.022 \times 10^{23}\text{ atoms/mol})}{26.982\text{ g/mol}} = 6.026 \times 10^{22}\text{ atoms/cm}^3$$

$$\ln \frac{\varphi(x)}{\varphi_0} = -\sigma_\gamma N x = \sigma_\gamma \times 6.026 \times 10^{22}\text{ atoms/cm}^2 \times 0.5\text{ cm}$$

$$\ln \frac{9.93 \times 10^5}{10^6} = -3.013 \times 10^{22}\sigma_\gamma$$

and $\sigma_\gamma = 0.233 \times 10^{-24}$ cm^2 or 0.233 b

Cross-sections are highly dependent on incident particle energy and target material as shown in Figure 4-11 for neutrons on cadmium and boron. Such plots show a general fall-off of σ with increasing neutron energy, i.e., a $1/v$ dependence of σ on neutron speed, and often contain resonance energies where the cross-sec-

tion is very high. The National Nuclear Data Center at Brookhaven National Laboratory (nndc@bnl.gov) is the authoritative source for similar information on cross-section data for a host of nuclear interactions, including protons, deuterons, alpha particles, and other projectiles, as well as neutrons.

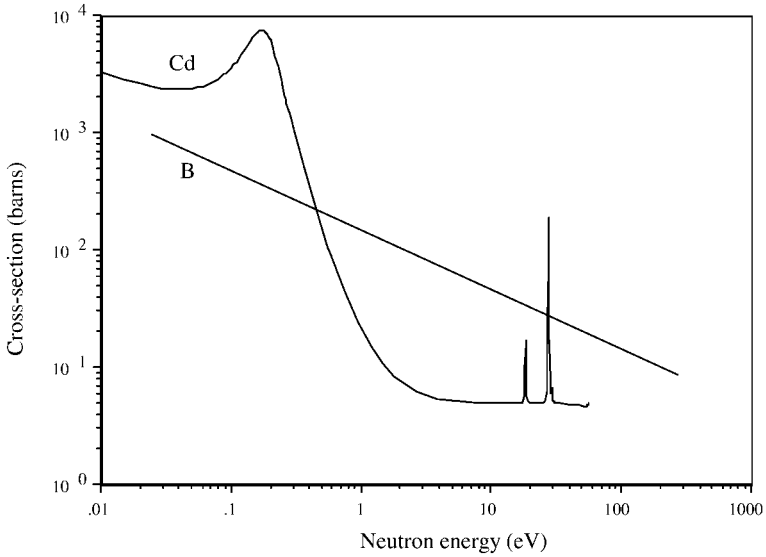

Fig. 4-11 Neutron absorption cross-sections versus energy for cadmium and boron.

4.3.2 *Q*-values for Nuclear Reactions

The energy balance, or *Q*-value, of a reaction is a function of the mass change (since mass is proportional to energy) that occurs between a particle and a target and the resulting products:

$$Q = (M_X + m_x)c^2 - (M_Y + m_y)c^2$$

where m_x, M_X, m_y, and M_Y represent the masses of the incident particle, target nucleus, product particle, and product nucleus, respectively. Thus, the *Q*-value is easily calculated by subtracting the masses of the products from the masses of the reactants. If the *Q*-value is positive, the kinetic energy of the products is greater than that of the reactants and the reaction is "exoergic," i.e., energy is gained at the expense of the mass of the reactants. If the *Q*-value is negative, the reactions are "endoergic" and energy must be supplied for the reaction to occur.

The amount of energy actually needed to bring about an endoergic reaction is somewhat greater than the *Q*-value. When the incident particle collides with the target nucleus, conservation of momentum requires that the fraction

$m_x/(m_x + M_X)$ of the kinetic energy of the incident particle must be retained by the products as kinetic energy; thus, only the fraction $M_X/(m_x + M_X)$ of the energy of the incident particle is available for the reaction. The threshold energy E_{th}, which is somewhat larger than the Q-value, is the kinetic energy the incident particle must have for the reaction to be energetically possible; it is given by

$$E_{th} = -Q\left[\frac{M_X + m_x}{M_X}\right]$$

Example 4-4. Calculate the Q-value for the ^{14}N (α,p) O^{17} reaction and the threshold energy.

Solution. The atomic masses from Appendix B are:

Mass of reactants

- 14.003074 u for ^{14}N
- 4.002603 u for ^{4}He

Mass of products

- 16.999131 u for ^{17}O
- 1.007826 u for ^{1}H

The mass difference is –0.001280 u, which has an energy equivalent of Q = –1.19 MeV; thus, the reaction is endoergic (i.e., energy must be supplied). The threshold energy E_{th} that the bombarding alpha particle must have for the reaction to occur is

$$E_{th} = -(-1.19 \text{ MeV})\left(\frac{14.003074 + 4.002603}{14.003074}\right) = 1.53 \text{ MeV}$$

which can be supplied by almost any natural source of alpha particles. Although this example uses exact mass values, calculations of E_{th} using integer mass numbers yield sufficiently accurate values.

Q-value calculations are done with the masses of the neutral atoms rather than the masses of the bombarding and ejected particles. The number of electrons required for a nuclear reaction equation balances when the masses of the neutral atoms are used because the number of electrons is the same on both sides of the equation. It is necessary, however, to examine the balance equation for a given reaction to confirm that this is in fact the case. Two reactions involving radioactive transformation illustrate these factors:

$$^{14}_{6}C \rightarrow {}^{14}_{7}N + {}^{0}_{-1}e + Q$$

$$^{22}_{11}Na \rightarrow {}^{22}_{10}Ne + {}^{0}_{+1}e + \text{orbital electron} + Q$$

The first reaction yields a positive Q-value (as all radioactive transformations must) of 0.156 MeV which is obtained by simply subtracting the ^{14}N mass from that of ^{14}C. It may appear that the beta particle (electron) mass was left out, but it is in fact included because the mass of neutral ^{14}N includes 7 electrons, one more

than the parent ^{14}C. By using the masses of the neutral isotopes, we have effectively "waited" until the product ^{14}N picks up an additional orbital electron to balance the net increase of one proton in the nucleus due to the beta particle transformation of ^{14}C; i.e., the electron mass is included as though the beta particle stopped and attached itself to the ionized ^{14}N product. The binding energy of the electron in ^{14}N is in fact not accounted for but this is very small compared to the other energies involved.

This convenient circumstance does not occur, however, in the second reaction in which a positron is emitted. The proton number decreases by one unit, which requires that an electron drift off from the product atom. Using the neutral masses of the parent and product nuclei to calculate the *Q*-value leaves two electron masses unaccounted for (the orbital electron that drifts off and the emitted positron); thus, it is necessary to add these in order to obtain a correct *Q*-value (see Chapter 5).

4.4 Alpha Particle Interactions

Rutherford's experiments on the scattering of alpha particles led him to put the nucleus at the center of the atom. He obtained an equally startling result from bombarding nitrogen with alpha particles, which showed that nitrogen could be transmuted into oxygen accompanied by a stream of emitted protons. He very cleverly did so by placing a moveable source of radium C′, which emits 7.69 MeV alpha particles, inside a box that could be filled with different gases. A zinc sulfide screen was placed just outside the box to detect scintillations that occurred. When the box was filled with oxygen or carbon dioxide at atmospheric pressure, no scintillations were seen on the screen with the source 7 cm or more away, which is the range of the alpha particles in these gases. However, when the box was filled with nitrogen, scintillations were observed on the screen when the source of the alpha particles was as much as 40 cm away. Since the alpha particles could not penetrate 40 cm of air, Rutherford concluded that the scintillations were caused by particles ejected from the nitrogen nuclei by the impact of the alpha particles. Measurement of the magnetic deflection of the emitted particles confirmed that they were, in fact, protons. This very famous nuclear interaction, which was the first demonstration of the transmutation of elements, is

$$^{14}_{7}\mathrm{N} + {}^{4}_{2}\mathrm{He} \rightarrow \left[{}^{18}_{9}\mathrm{F}\right] \rightarrow {}^{17}_{8}\mathrm{O} + {}^{1}_{1}\mathrm{H}$$

or in abbreviated form ^{14}N (α,p) ^{17}O. The probability of such disintegration is very small; one million alpha particles are required to produce one interaction. When Rutherford first observed it, he was uncertain whether the alpha particle and the nitrogen nucleus had combined to form a new compound nucleus or whether a proton had just been knocked out of the nitrogen nucleus. Blackett performed a classic experiment, the results of which are shown schematically in Figure 4-12;

his photograph (one of only 8 from 20,000 cloud chamber photographs and over 400,000 alpha tracks) shows that the only tracks observed from the collision were those of the incident alpha particle, an expelled proton, and a recoil nucleus. The alpha particle had vanished; atoms had been transmuted, and Blackett received a Nobel prize in 1948 for providing the experimental proof of this fundamental precept.

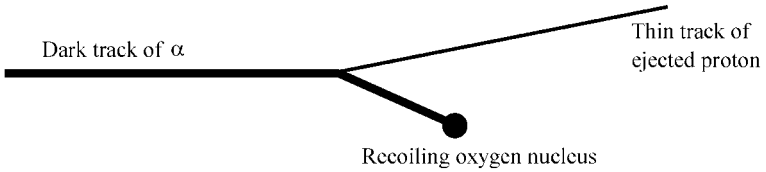

Fig. 4-12 Schematic of P. M. S. Blackett's classic photograph showing the thick alpha track before it "vanishes" (absorbed), the thin track of the proton, and the heavy track of the recoiling product nucleus.

Rutherford and his colleagues observed alpha particle transmutation for all of the light elements from boron to potassium, except carbon and oxygen. Some of these are

$$^{10}_{5}\mathrm{B} + {}^{4}_{2}\mathrm{He} \rightarrow \left[{}^{14}_{7}\mathrm{N}\right] \rightarrow {}^{13}_{6}\mathrm{C} + {}^{1}_{1}\mathrm{H}$$

$$^{23}_{11}\mathrm{Na} + {}^{4}_{2}\mathrm{He} \rightarrow \left[{}^{27}_{13}\mathrm{Al}\right] \rightarrow {}^{26}_{12}\mathrm{Mg} + {}^{1}_{1}\mathrm{H}$$

$$^{27}_{13}\mathrm{Al} + {}^{4}_{2}\mathrm{He} \rightarrow \left[{}^{31}_{15}\mathrm{P}\right] \rightarrow {}^{30}_{14}\mathrm{Si} + {}^{1}_{1}\mathrm{H}$$

$$^{32}_{16}\mathrm{S} + {}^{4}_{2}\mathrm{He} \rightarrow \left[{}^{36}_{18}\mathrm{Ar}\right] \rightarrow {}^{35}_{17}\mathrm{Cl} + {}^{1}_{1}\mathrm{H}$$

$$^{39}_{19}\mathrm{K} + {}^{4}_{2}\mathrm{He} \rightarrow \left[{}^{43}_{21}\mathrm{Se}\right] \rightarrow {}^{42}_{20}\mathrm{Ca} + {}^{1}_{1}\mathrm{H}$$

The ejected protons from some of these interactions were found to have more energy than the bombarding alpha particles. This extra energy was acquired by rearrangement of the potential energy states of constituents in the bombarded nucleus, an important result in understanding atoms and how they acquire and emit energy due to the associated mass changes.

4.4.1 Alpha–Neutron Reactions

The neutron was discovered (1932) due to an (α, n) reaction with beryllium; it is of extraordinary importance because it provided a comprehensive structure of the atom (see Chapter 3). Several researchers observed a very penetrating radiation that was first assumed to be high-energy gamma radiation, which would have re-

quired formation of ^{13}C with a Q-value of about 50 MeV, which was highly questionable. Rutherford and Chadwick had long suspected the existence of a neutral particle, and Chadwick turned his attention to these strange emissions from bombarding beryllium with alpha particles. The Joliet-Curies had provided an important piece of the puzzle by showing that the emissions produced a stream of protons when directed at paraffin, a hydrogenous material. Chadwick assumed that a neutral particle with mass near that of the proton was emitted and that elastic collisions had occurred with the hydrogen nuclei in the paraffin. From the momenta observed, he showed that this was the correct hypothesis and that the emitted radiation was in fact a neutral particle (the neutron) with a mass very nearly equal to that of the proton and that the correct nuclear reaction was

$$^{9}_{4}\mathrm{Be} + {}^{4}_{2}\mathrm{He} \rightarrow \left[{}^{13}_{6}\mathrm{C}\right] \rightarrow {}^{12}_{6}\mathrm{C} + {}^{1}_{0}\mathrm{n}$$

where $^{1}_{0}n$ is the symbol for the neutron. Neutrons were highly penetrating because they had no charge and thus were not repelled by positively charged nuclei. This discovery was so important that Chadwick was awarded a Nobel prize just two years later.

Once it was known that neutrons existed and were produced by alpha particle interactions, other reactions were soon discovered. Some important ones are

$$^{7}_{3}\mathrm{Li} + {}^{4}_{2}\mathrm{He} \rightarrow \left[{}^{11}_{5}\mathrm{B}\right] \rightarrow {}^{10}_{5}\mathrm{B} + {}^{1}_{0}\mathrm{n}$$

$$^{14}_{7}\mathrm{N} + {}^{4}_{2}\mathrm{He} \rightarrow \left[{}^{18}_{9}\mathrm{F}\right] \rightarrow {}^{17}_{9}\mathrm{F} + {}^{1}_{0}\mathrm{n}$$

$$^{23}_{11}\mathrm{Na} + {}^{4}_{2}\mathrm{He} \rightarrow \left[{}^{27}_{13}\mathrm{Al}\right] \rightarrow {}^{26}_{13}\mathrm{Al} + {}^{1}_{0}\mathrm{n}$$

$$^{27}_{13}\mathrm{Al} + {}^{4}_{2}\mathrm{He} \rightarrow \left[{}^{31}_{15}\mathrm{P}\right] \rightarrow {}^{30}_{15}\mathrm{P} + {}^{1}_{0}\mathrm{n}$$

The reactions of alpha particles with ^{14}N, ^{23}Na, and ^{27}Al may, in accordance with the theory of a compound nucleus, also emit a proton. The (α, p) reaction with aluminum was found by the Joliet-Curies to be radioactive, which was the first observation of artificial radioactivity and gained them a Nobel prize in 1935.

4.5 Transmutation by Protons and Deuterons

Although alpha particles can be used to produce a number of useful interactions, they are limited to light-element targets because the coulombic repulsion between their +2 charge and the high Z of heavy elements is just too great to overcome. The range of possible interactions can be extended somewhat by using long-range alpha particles of 10–12 MeV from short-lived alpha emitters, but these are very difficult to produce and are very short lived.

Protons and deuterons with a single positive charge are more useful for nuclear interactions, but since no natural sources exist, such reactions only became available with the development of the Cockcroft and Walton linear accelerator and the cyclotron (see Figure 4-14), which was developed somewhat later.

Cockcroft and Walton used a voltage multiplier to accelerate protons to energies of 0.l–0.7 MeV, which though miniscule by today's standards, led to major contributions to nuclear physics. Bombardment of lithium with protons produced two alpha particles with equal energies according to the reaction

$$^{7}_{3}\mathrm{Li} + {}^{1}_{1}\mathrm{H} \rightarrow \left[{}^{8}_{4}\mathrm{Be}\right] \rightarrow {}^{4}_{2}\mathrm{He} + {}^{4}_{2}\mathrm{He}$$

The calculated *Q*-value is 17.32 MeV, and the measured value (from the energies of the incident protons and the emergent alpha particles) was found to be 17.33 MeV. This experiment thus demonstrated a genuine release of energy from the lithium atom at the expense of its mass, and was the first quantitative proof of Einstein's mass–energy relationship.

A modern linear accelerator, as shown in Figure 4-13, introduces hydrogen ions (protons, deuterons, tritons) at the beginning of a series of drift tubes, and these are accelerated by applying an alternating voltage across the gaps between each tube. The accelerated particles enter each successive drift tube where they travel just far enough to be in phase to receive another "kick" as they enter the next gap. The length of the drift tubes increases along the particle path because the accelerated particles are traveling faster and faster as they proceed down the line.

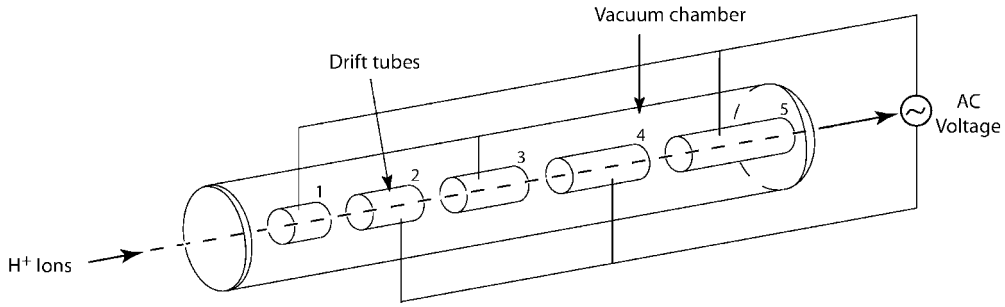

Fig. 4-13 Schematic of a linear accelerator for protons and deuterons.

Cyclotrons are used to accelerate protons and deuterons and occasionally tritium (tritons) and helium atoms. These ionized atoms are introduced into a source region as shown in Figure 4-14 where they are "kicked" towards the negatively charged pole by an alternating electric field placed across the gap. The accelerated particle passes through a slit into an evacuated zone called a "dee" because of its shape. A strong magnetic field across the dee and perpendicular to the path of the particle deflects it into a circular path bringing it back to the gap on the other side. During this passage, the electric field is reversed by the alternating voltage, and when the particle re-enters the gap it receives another "kick" before it

passes into the other dee where it is deflected once again back to the gap where by now the electric field has once again been reversed. This series of field reversals at the gap provides a series of "kicks" which continuously increases the velocity (and energy) of the particle at each pass through the gap. The ever-increasing circular path is convenient because it allows the particle to travel greater and greater distances in just the time required for the alternating field to switch. When the desired energy is reached, another magnetic field is used to draw off the accelerated particles and direct them to the target.

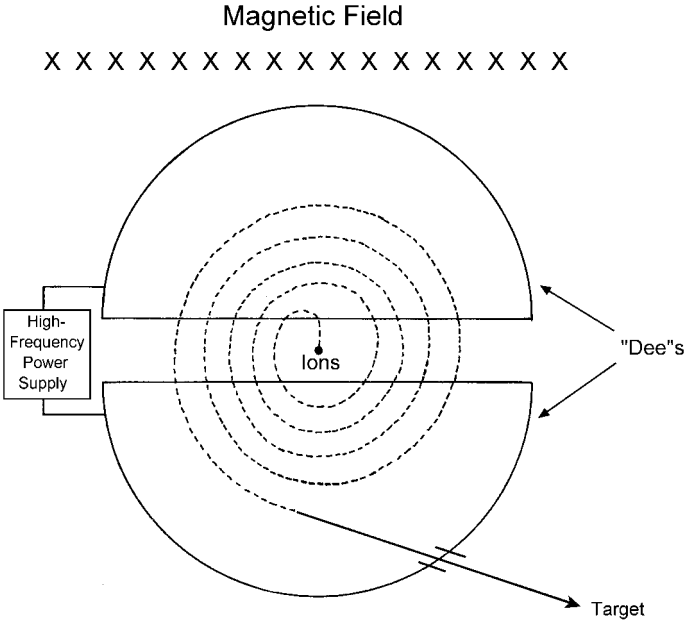

Fig. 4-14 Schematic of a cyclotron with the magnetic field directed into the plane of the page. Ions introduced into the gap are accelerated numerous times by the alternating voltage causing them to travel in increasingly larger circles in the "dee" space before being deflected toward a target.

Accelerator beams are commonly characterized in terms of current, typically in amperes or fractions thereof. For example, a 1 μA(10^{-6} C/s) beam current of protons (charge = 1.6022×10^{-19} C/proton) represents 6.24×10^{12} protons (see Example 4-5).

4.5.1 Proton–Alpha Particle (p,α) Reactions

Irradiation of various target materials with protons yields alpha particles; some of these are

$$^{6}_{3}\mathrm{Li} + {}^{1}_{1}\mathrm{H} \rightarrow \left[{}^{7}_{4}\mathrm{Be}\right] \rightarrow {}^{3}_{2}\mathrm{He} + {}^{4}_{2}\mathrm{He}$$

$$^{9}_{4}\mathrm{Be} + {}^{1}_{1}\mathrm{H} \rightarrow \left[{}^{10}_{5}\mathrm{B}\right] \rightarrow {}^{6}_{3}\mathrm{Li} + {}^{4}_{2}\mathrm{He}$$

$$^{11}_{5}\mathrm{B} + {}^{1}_{1}\mathrm{H} \rightarrow \left[{}^{12}_{6}\mathrm{C}\right] \rightarrow {}^{8}_{4}\mathrm{Be} + {}^{4}_{2}\mathrm{He}$$

$$^{19}_{9}\mathrm{F} + {}^{1}_{1}\mathrm{H} \rightarrow \left[{}^{20}_{10}\mathrm{Ne}\right] \rightarrow {}^{16}_{8}\mathrm{O} + {}^{4}_{2}\mathrm{He}$$

$$^{27}_{13}\mathrm{Al} + {}^{1}_{1}\mathrm{H} \rightarrow \left[{}^{28}_{14}\mathrm{Si}\right] \rightarrow {}^{24}_{12}\mathrm{Mg} + {}^{4}_{2}\mathrm{He}$$

Proton bombardment of ^{11}B yields $^{8}_{4}$Be, which is highly unstable and immediately breaks up into two alpha particles, yielding three alpha particles overall.

4.5.2
Proton–Neutron (p,n) Reactions

Protons can be used to produce neutrons in certain target elements through interactions that are mostly endoergic. The effect of these transmutations is to increase the charge on the target nucleus by one unit, moving it above the line of stability on the chart of the nuclides with no change in the mass number. Such reactions are usually endoergic because mass changes are negative. Some examples are

$$^{11}_{5}\mathrm{B} + {}^{1}_{1}\mathrm{H} \rightarrow \left[{}^{12}_{6}\mathrm{C}\right] \rightarrow {}^{11}_{6}\mathrm{C} + {}^{1}_{0}\mathrm{n}$$

$$^{18}_{8}\mathrm{O} + {}^{1}_{1}\mathrm{H} \rightarrow \left[{}^{19}_{9}\mathrm{F}\right] \rightarrow {}^{18}_{9}\mathrm{F} + {}^{1}_{0}\mathrm{n}$$

$$^{58}_{28}\mathrm{Ni} + {}^{1}_{1}\mathrm{H} \rightarrow \left[{}^{59}_{29}\mathrm{Cu}\right] \rightarrow {}^{58}_{29}\mathrm{Cu} + {}^{1}_{0}\mathrm{n}$$

$$^{65}_{29}\mathrm{Cu} + {}^{1}_{1}\mathrm{H} \rightarrow \left[{}^{66}_{30}\mathrm{Zn}\right] \rightarrow {}^{65}_{30}\mathrm{Zn} + {}^{1}_{0}\mathrm{n}$$

Protons can thus also be used to produce neutrons by (p,n) reactions. For example the Q-value of the (p,n) for ^{65}Cu is –2.13 MeV and the threshold energy is –2.16 MeV. Protons incident on foils of ^{56}Fe, as shown in Example 4-5, also yield neutrons by the ^{56}Fe(p,n) ^{56}Co reaction.

Example 4-5. The (p,n) reaction with iron has a cross-section of 0.6 b. How many neutrons/s would be produced by a 3.0 μA proton beam incident on an iron foil of 1 cm^2 and 1.0 μm thick?
Solution. The reaction is

$$^{56}\mathrm{Fe} + {}^{1}_{1}\mathrm{H} \rightarrow [{}^{57}\mathrm{Co}] \rightarrow {}^{56}\mathrm{Co} + {}^{1}_{0}\mathrm{n}$$

The number of nuclei in the target (density = 7.9 g/cm^3) is

$$N = \frac{(1.0 \times 10^{-4}\ \mathrm{cm}^3)(7.99\ \mathrm{g/cm}^3)(6.022 \times 10^{23}\ \mathrm{atoms/mol}}{56\ \mathrm{g/mol}}$$

$$= 8.5 \times 10^{18}\ \text{atoms of } {}^{56}\mathrm{Fe}$$

The flux of protons per second in the incident beam of 3 μA (3×10^{-6} C/s) is

$$\varphi_{\mathrm{p}} = \frac{3.0 \times 10^{-6}\mathrm{C/s}}{(1.602 \times 10^{-19}\mathrm{C/proton})(1\mathrm{cm}^2)}$$

$$= 1.87 \times 10^{13}\ \text{protons/cm}^2\ \text{s}$$

And the number of neutrons produced per second is

$$\phi_{\mathrm{n}} = (8.5 \times 10^{18}\ \text{atoms})(0.6 \times 10^{-24}\ \text{cm}^2\text{/atom})(1.87 \times 10^{13}\ \text{protons/cm}^2\ \text{s})$$

$$= 9.6 \times 10^{7}\ \text{neutrons/cm}^2\ \text{s}$$

4.5.3
Proton–Gamma (p,γ) Reactions

Some proton interactions produce an excited state of the target nucleus which is relieved by emission of a gamma photon. Examples of (p, γ) reactions are

$${}^{7}_{3}\mathrm{Li} + {}^{1}_{1}\mathrm{H} \rightarrow \left[{}^{8}_{4}\mathrm{Be}\right] \rightarrow {}^{8}_{4}\mathrm{Be} + \gamma$$

$${}^{12}_{6}\mathrm{C} + {}^{1}_{1}\mathrm{H} \rightarrow \left[{}^{13}_{7}\mathrm{N}\right] \rightarrow {}^{13}_{7}\mathrm{N} + \gamma$$

$${}^{19}_{9}\mathrm{F} + {}^{1}_{1}\mathrm{H} \rightarrow \left[{}^{20}_{10}\mathrm{Ne}\right] \rightarrow {}^{20}_{10}\mathrm{Ne} + \gamma$$

$${}^{27}_{13}\mathrm{Al} + {}^{1}_{1}\mathrm{H} \rightarrow \left[{}^{28}_{14}\mathrm{Si}\right] \rightarrow {}^{28}_{14}\mathrm{Si} + \gamma$$

Proton–gamma interactions with lithium are particularly important because they yield photons with an energy of 17.2 MeV, which is far more energetic than those from naturally radioactive substances. These high-energy photons can thus be used to produce nuclear interactions by a process called photodisintegration.

4.5.4
Proton–Deuteron Reactions

Proton interactions may also produce deuterons, for example:

$${}^{9}_{4}\mathrm{Be} + {}^{1}_{1}\mathrm{H} \rightarrow \left[{}^{10}_{5}\mathrm{B}\right] \rightarrow {}^{8}_{4}\mathrm{Be} + {}^{2}_{1}\mathrm{H}$$

$${}^{7}_{3}\mathrm{Li} + {}^{1}_{1}\mathrm{H} \rightarrow \left[{}^{8}_{4}\mathrm{Be}\right] \rightarrow {}^{6}_{3}\mathrm{Li} + {}^{2}_{1}\mathrm{H}$$

The (p,d) reaction with lithium is yet another example of the random breakup of a compound nucleus of beryllium, which in this case yields a deuteron. As noted previously, absorption of a proton can also result in the emission of an alpha particle or a photon. Each product is possible from the highly unstable ^{8}Be nucleus that is formed, affected to a degree by the projectile energy and conditions of the irradiation.

4.5.5
Deuteron–Alpha (d,α) Reactions

Deuterons, which like protons also have the advantage of a single positive charge, can also be used as bombarding particles by accelerating them up to energies of several MeV, typically in a cyclotron (see Figure 4-14). One of the first reactions was with ^{6}Li, which constitutes 7.5% of natural lithium, or

$$^{6}_{3}\mathrm{Li} + {}^{2}_{1}\mathrm{H} \rightarrow \left[{}^{8}_{4}\mathrm{Be}\right] \rightarrow {}^{4}_{2}\mathrm{He} + {}^{4}_{2}\mathrm{He}$$

Other examples of (d,α) reactions are

$$^{16}_{8}\mathrm{O} + {}^{2}_{1}\mathrm{H} \rightarrow \left[{}^{18}_{9}\mathrm{F}\right] \rightarrow {}^{14}_{7}\mathrm{N} + {}^{4}_{2}\mathrm{He}$$

$$^{27}_{13}\mathrm{Al} + {}^{2}_{1}\mathrm{H} \rightarrow \left[{}^{29}_{14}\mathrm{Si}\right] \rightarrow {}^{25}_{12}\mathrm{Mg} + {}^{4}_{2}\mathrm{He}$$

$$^{20}_{10}\mathrm{Ne} + {}^{2}_{1}\mathrm{H} \rightarrow \left[{}^{22}_{11}\mathrm{Na}\right] \rightarrow {}^{18}_{9}\mathrm{F} + {}^{4}_{2}\mathrm{He}$$

The latter reaction produces ^{18}F, which is radioactive with a 110 min half-life and is widely used in nuclear medicine (see below). These reactions are usually exoergic, i.e., they have positive Q-values.

4.5.6
Deuteron–Proton (d,p) and Deuteron–Neutron (d,n) Reactions

Depending on the energies, it is possible for deuterons to produce protons, just as protons produce deuterons. Examples of (d,p) reactions are

$$^{12}_{6}\mathrm{C} + {}^{2}_{1}\mathrm{H} \rightarrow \left[{}^{14}_{7}\mathrm{N}\right] \rightarrow {}^{13}_{6}\mathrm{C} + {}^{1}_{1}\mathrm{H}$$

$$^{23}_{11}\mathrm{Na} + {}^{2}_{1}\mathrm{H} \rightarrow \left[{}^{25}_{12}\mathrm{Mg}\right] \rightarrow {}^{24}_{11}\mathrm{Na} + {}^{1}_{1}\mathrm{H}$$

$$^{31}_{15}\mathrm{P} + {}^{2}_{1}\mathrm{H} \rightarrow \left[{}^{33}_{16}\mathrm{S}\right] \rightarrow {}^{32}_{15}\mathrm{P} + {}^{1}_{1}\mathrm{H}$$

These transformations increase the mass of the nucleus by one unit, leaving the charge unchanged. The reactions are usually exoergic.

Deuteron bombardment can also yield neutrons as in the following (d,n) reactions:

$$^{7}_{3}\mathrm{Li} + {}^{2}_{1}\mathrm{H} \rightarrow \left[{}^{9}_{4}\mathrm{Be}\right] \rightarrow {}^{8}_{4}\mathrm{Be} + {}^{1}_{0}\mathrm{n}$$

$$^{9}_{4}\mathrm{Be} + {}^{2}_{1}\mathrm{H} \rightarrow \left[{}^{11}_{5}\mathrm{B}\right] \rightarrow {}^{10}_{5}\mathrm{B} + {}^{1}_{0}\mathrm{n}$$

$$^{12}_{6}\mathrm{C} + {}^{2}_{1}\mathrm{H} \rightarrow \left[{}^{14}_{7}\mathrm{N}\right] \rightarrow {}^{13}_{7}\mathrm{N} + {}^{1}_{0}\mathrm{n}$$

$$^{14}_{7}\mathrm{N} + {}^{2}_{1}\mathrm{H} \rightarrow \left[{}^{16}_{8}\mathrm{O}\right] \rightarrow {}^{15}_{8}\mathrm{O} + {}^{1}_{0}\mathrm{n}$$

An interesting reaction occurs when frozen D_2O ("heavy water") is bombarded with deuterons, in effect fusing deuterium by accelerator processes. Both the (d,p) and the (d,n) reactions have been observed because the "excited" compound nucleus (^{4}He) can break up in two ways:

$$^{2}_{1}\mathrm{H} + {}^{2}_{1}\mathrm{H} \rightarrow \left[{}^{4}_{2}\mathrm{He}\right] \rightarrow {}^{3}_{1}\mathrm{H} + {}^{1}_{1}\mathrm{H}$$

$$^{2}_{1}\mathrm{H} + {}^{2}_{1}\mathrm{H} \rightarrow \left[{}^{4}_{2}\mathrm{He}\right] \rightarrow {}^{3}_{2}\mathrm{He} + {}^{1}_{0}\mathrm{n}$$

The first (d,p) reaction produces tritium with the release of a proton and 4.03 MeV of energy; the cross-section for the tritium reaction as a function of deuteron energy is shown in Figure 4-15. Tritium is unstable and has a half-life of about 12.3 years. The second reaction produces helium and a neutron and 3.27 MeV of energy; helium-3 is stable and is found in nature.

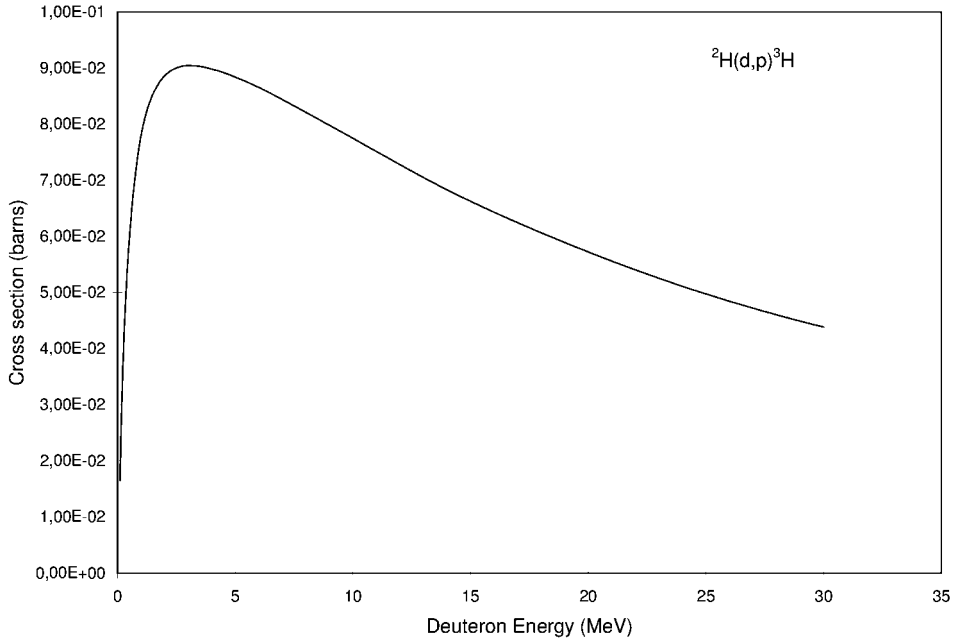

Fig. 4-15 Cross-section versus deuteron energy for (d,p) production of ^{3}H from ^{2}H.

Acceleration of deuterons on targets of deuterium (a D-D neutron generator) and/or tritium (the D-T generator) both yield neutrons. The cross-sections for these reactions are shown in Figures 4-16 and 4-17, respectively. Other typical (d,n) targets are ^{7}Li, ^{9}Be, ^{12}C, and ^{14}N, or protons could be used (see Example 4-5) These sources yield fast neutrons which can be used as produced, moderated to intermediate energies, or moderated to thermal energies.

A recently discovered device for neutron production uses a pyroelectric crystal of lithium tantalate, which generates a strong electric field when heated or cooled. A lithium tantalate crystal about 1.25 inches in diameter and 0.5 inches long is enclosed in a cylinder and surrounded with deuterium gas. When warmed to 50 °F it produces a charge that creates a field of 1000 V on a tungsten-tipped electrode that ionizes the deuterium gas and accelerates the ions into a deuterium target. This DD process can produce some 1000 neutrons/s; use of a tritium target would increase the yield substantially, perhaps as high as 10^{6} neutrons/s.

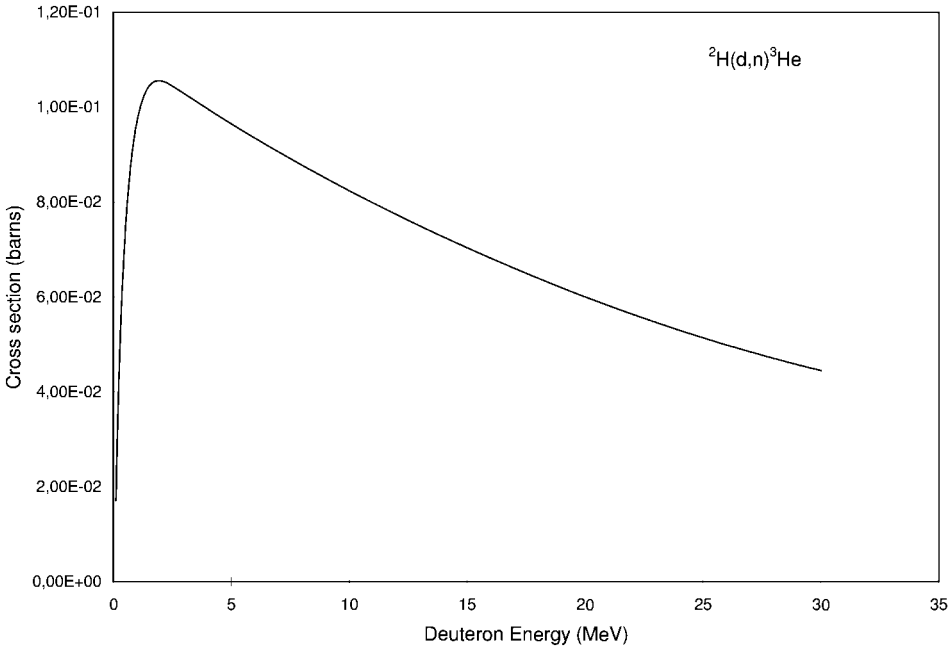

Fig. 4-16 Cross-section versus deuteron energy for producing neutrons and ^{3}He by (d,n) reactions with ^{2}H target atoms.

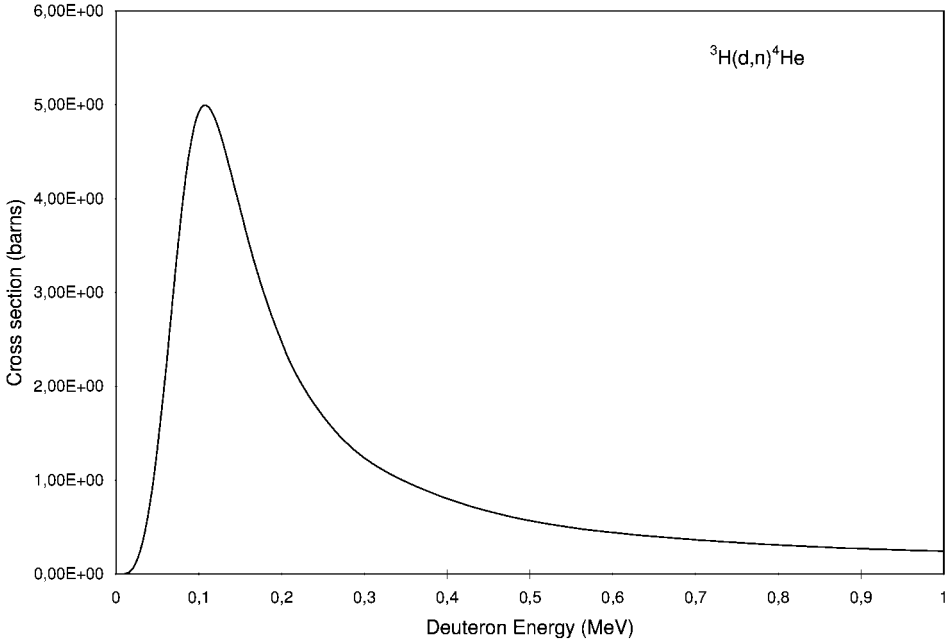

Fig. 4-17 Cross-section versus deuteron energy for producing neutrons and ^{4}He by (d,n) reactions with ^{3}H target atoms.

4.6
Neutron Interactions

Neutrons have proved to be especially effective in producing nuclear transformations because, with no electric charge, they are more likely to penetrate nuclei than are protons, deuterons, or alpha particles. Nuclear reactors provide copious quantities of neutrons; other important sources are alpha emitters mixed with beryllium and/or deuterium; energetic gamma sources or x-rays on deuterium or beryllium to create photodisintegration neutron sources; spontaneous fission nuclides such as ^{252}Cf; and (d,n) reactions produced in accelerators.

4.6.1
Radiative Capture (n,γ) Reactions

The most common neutron interaction is radiative capture in which the mass number of an element is increased by one unit due to the addition of a neutron. The excitation energy induced by the extra neutron is relieved by gamma radiation, and Q-values are always positive. The element remains the same since Z does not change, but the product of the reaction, which is often radioactive, is shifted to the right of the line of stable nuclides on the chart of the nuclides since Z does not change.

Numerous (n,γ) reactions are possible with slow neutrons, beginning with hydrogen to produce deuterium:

$$^{1}_{1}\mathrm{H} + ^{1}_{0}\mathrm{n} \rightarrow [^{2}_{1}\mathrm{H}] \rightarrow ^{2}_{1}\mathrm{H} + \gamma$$

which in turn can be bombarded with slow neutrons to produce tritium:

$$^{2}_{1}\mathrm{H} + ^{1}_{0}\mathrm{n} \rightarrow [^{3}_{1}\mathrm{H}] \rightarrow ^{3}_{1}\mathrm{H} + \gamma$$

Even though the (n, γ) reaction with deuterium has a very small cross-section, all light-water cooled nuclear reactors will have tritium in the coolant due to these two reactions.

Other typical (n, γ) reactions, which are quite probable with thermal neutrons, are

$$^{59}_{27}\mathrm{Co} + ^{1}_{0}\mathrm{n} \rightarrow [^{60}_{27}\mathrm{Co}] \rightarrow ^{60}_{27}\mathrm{Co} + \gamma$$

$$^{27}_{13}\mathrm{Al} + ^{1}_{0}\mathrm{n} \rightarrow [^{28}_{13}\mathrm{Al}] \rightarrow ^{28}_{13}\mathrm{Al} + \gamma$$

$$^{115}_{49}\mathrm{In} + ^{1}_{0}\mathrm{n} \rightarrow [^{116}_{49}\mathrm{In}] \rightarrow ^{116}_{49}\mathrm{In} + \gamma$$

$$^{202}_{80}\mathrm{Hg} + ^{1}_{0}\mathrm{n} \rightarrow [^{203}_{80}\mathrm{Hg}] \rightarrow ^{203}_{80}\mathrm{Hg} + \gamma$$

The products of these and similar reactions are commonly radioactive. Targets made of such materials can be important sources of artificial radionuclides, e.g., ^{60}Co, ^{99}Mo, ^{116}In, ^{203}Hg, etc.

4.6.2 Charged Particle Emission (CPE)

Charged particle emission (CPE) reactions are those in which the compound nucleus that is formed breaks up by the emission of a charged particle such as a proton (n,p) or alpha particle (n,α). Such reactions usually require energetic neutrons to expel a particle from a nucleus. Cross-sections versus energy for some reactions are provided in Appendix F for several target materials. The chart of the nuclides also contains various cross-sections, including CPE reactions. Whereas radiative capture (n,γ) cross-sections are designated on the chart by σ_{γ}, CPE cross-sections are designated as σ_{p}, σ_{α}, etc., where the subscript denotes the emitted particle, and if fissionable by σ_{f}. In most charged particle reactions, the product radionuclide is a new element, and therefore it can be chemically separated yielding a carrier-free source.

Neutron–alpha (n, α) reactions can occur with various elements. Examples of such (n,α) reactions are

$$^{6}_{3}\mathrm{Li} + ^{1}_{0}\mathrm{n} \rightarrow [^{7}_{3}\mathrm{Li}] \rightarrow ^{3}_{1}\mathrm{H} + ^{4}_{2}\mathrm{He}$$

$$^{10}_{5}\mathrm{B} + ^{1}_{0}\mathrm{n} \rightarrow [^{11}_{5}\mathrm{B}] \rightarrow ^{7}_{3}\mathrm{Li} + ^{4}_{2}\mathrm{He}$$

$$^{27}_{13}\mathrm{Al} + ^{1}_{0}\mathrm{n} \rightarrow [^{28}_{13}\mathrm{Al}] \rightarrow ^{24}_{11}\mathrm{Na} + ^{4}_{2}\mathrm{He}$$

The first two reactions have a relatively high cross-section, and both are often used to detect neutrons. In one method, an ionization chamber is lined with boron, usually BF_3, which provides efficient capture of neutrons. The liberated alpha particle produces significant ionization, which can be collected and amplified to produce an electronic signal allowing detection.

Another important (n,*a*) reaction is with ^{6}Li, which yields tritium which allows ^{6}Li (7.5% of natural lithium) to be used as source material for fusion-type nuclear weapons.

4.6.3
Neutron–Proton (n,p) Reactions

When a proton in the nucleus is replaced by a neutron the mass number is not changed, but the charge is decreased by one unit and the atom is moved below the line of stability on the chart of the nuclides. Such (n,p) reactions are rare with low-energy neutrons because the expulsion of a charged particle usually requires a considerable amount of energy; however, one important (n,p) reaction that occurs with low-energy neutrons is

$$^{14}_{7}\mathrm{N} + {}^{1}_{0}\mathrm{n} \rightarrow \left[{}^{15}_{7}\mathrm{N}\right] \rightarrow {}^{14}_{6}\mathrm{C} + {}^{1}_{1}\mathrm{H}$$

This reaction yields ^{14}C, an important long-lived radionuclide that exists in natural media as described in Chapter 6. Other examples of (n,p) reactions are

$$^{27}_{13}\mathrm{Al} + {}^{1}_{0}\mathrm{n} \rightarrow \left[{}^{28}_{13}\mathrm{Al}\right] \rightarrow {}^{27}_{12}\mathrm{Mg} + {}^{1}_{1}\mathrm{H}$$

$$^{64}_{30}\mathrm{Zn} + {}^{1}_{0}\mathrm{n} \rightarrow \left[{}^{65}_{30}\mathrm{Zn}\right] \rightarrow {}^{64}_{29}\mathrm{Cu} + {}^{1}_{1}\mathrm{H}$$

$$^{39}_{19}\mathrm{K} + {}^{1}_{0}\mathrm{n} \rightarrow \left[{}^{40}_{19}\mathrm{K}\right] \rightarrow {}^{39}_{18}\mathrm{Ar} + {}^{1}_{1}\mathrm{H}$$

These latter three reactions require energetic neutrons. Activation of ^{39}K to produce ^{39}Ar can be used in the potassium–argon dating method.

4.6.4
Neutron–Neutron (n,2n) Reactions

Sometimes when a high-energy neutron is captured, two or more neutrons are emitted. The mass change in the (n,2n) reaction is always negative; thus, the *Q*-value is negative and fast neutrons are needed for these reactions. Very high-energy neutrons can produce reactions in which 3 or 4 or more neutrons are emitted. The (n,2n) reaction leaves the charge of the nucleus unchanged and the product is an isotope of the target nucleus with a mass number one unit smaller. Examples of this reaction are

$$^{7}_{3}\mathrm{Li} + {}^{1}_{0}\mathrm{n} \rightarrow \left[{}^{8}_{3}\mathrm{Li}\right] \rightarrow {}^{6}_{3}\mathrm{Li} + {}^{1}_{0}\mathrm{n} + {}^{1}_{0}\mathrm{n}$$

$$^{27}_{13}\mathrm{Al} + {}^{1}_{0}\mathrm{n} \rightarrow \left[{}^{28}_{13}\mathrm{Al}\right] \rightarrow {}^{26}_{13}\mathrm{Al} + {}^{1}_{0}\mathrm{n} + {}^{1}_{0}\mathrm{n}$$

$$^{238}_{92}\mathrm{U} + {}^{1}_{0}\mathrm{n} \rightarrow \left[{}^{239}_{92}\mathrm{U}\right] \rightarrow {}^{237}_{92}\mathrm{U} + {}^{1}_{0}\mathrm{n} + {}^{1}_{0}\mathrm{n}$$

The first reaction is significant for design of thermonuclear weapons that use lithium deuteride because it provides significant neutron multiplication that induces fission in natural uranium as well as production of ^{6}Li which readily absorbs neutrons to yield tritium, an additional fusion fuel. In the latter reaction, ^{237}U is radioactive and undergoes transformation to ^{237}Np, which is long lived and of significance in radioactive wastes. It is also a target material for neutron activation by an (n,γ) reaction to ^{238}Np which soon transforms to ^{238}Pu, a useful radioisotope for remote power systems.

4.7 Activation Product Calculations

Activation product formation is shown schematically in Figure 4-18 for a flux of ϕ neutrons/cm^2 s incident upon a thin target containing $N_1{}^0$ atoms. It is assumed that the target thickness is such that the flux of neutrons remains essentially the same as it passes through. When these conditions occur, absorption reactions will produce new atoms of N_2 at a rate

$$\text{Production of } N_2 = \phi\sigma N_1{}^0$$

where ϕ is the flux, σ is the absorption cross-section in barns for projectiles (commonly neutrons) of a given energy, and $N_1{}^0$ is the number of target atoms. As soon as atoms of N_2 are formed they can be removed by radioactive transformation and/or activation to a new product:

$$\text{Removal of } N_2 = \lambda_2 N_2 + \phi\sigma_2 N_2$$

If activation of N_2 can be ignored, which is usually (but not always) the case, the rate of removal of N_2 atoms is due only to radioactive transformation, and for thin foils containing $N_1{}^0$ atoms, the rate of change of new atoms of N_2 with time is the rate of production minus the rate of removal:

$$\frac{dN_2}{dt} = \varphi\sigma_1 N_1^0 - \lambda_2 N_2$$

which can be solved by multiplying through by the integrating factor $e^{\lambda_2 t}$ and performing the integration to obtain

$$N_2(t) = \frac{\varphi\sigma_1 N_1^0}{\lambda_2}(1 - e^{-\lambda_2 t})$$

or in terms of activity

$$A_2(t) = \lambda_2 N_2 = \varphi\sigma_1 N_1^0(1 - e^{-\lambda_2 t})$$

If the half-life of the product radionuclide is more than 10 times the irradiation time, the above equation can be reduced to a simpler form by expanding the exponential term in a series to yield

$$A(t) = \phi\sigma_1 N_1{}^0(\lambda t)$$

with an error of less than 3%. Because of the factor $(1 - e^{-\lambda t})$, irradiation of a target for one half-life or more yields a substantial fraction of the saturation amount of the desired radionuclide.

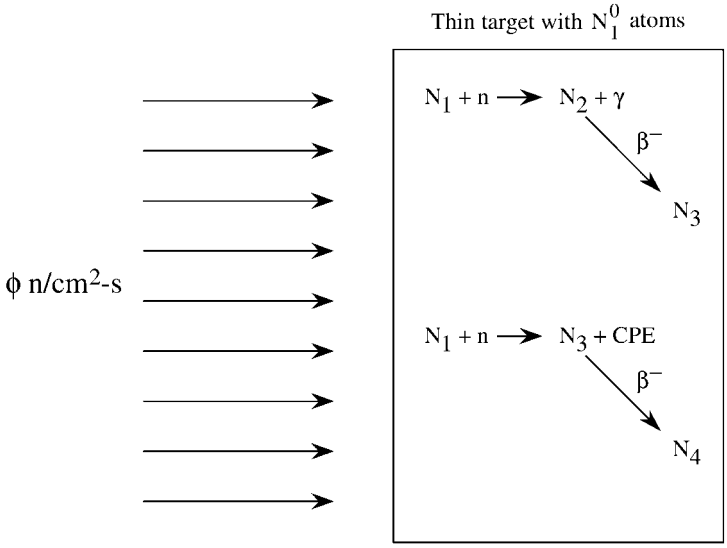

Fig. 4-18 Schematic of neutron irradiation of a thin (greatly amplified) target material to produce new atoms of a radioactive product.

These equations assume insignificant burn up of target atoms and no significant alteration of the projectile flux over the target, both of which are conservative but realistic assumptions when thin foils are used for target materials.

Depletion of target atoms is of little concern for short irradiation of most materials because the number of target atoms can be presumed to remain constant. However, several products such as cobalt have long half-lives and it may require several years to produce them, which can significantly deplete the number of tar-

get atoms available. In order to account for target depletion, N_1 is treated as a variable, such that

$$N_1(t) = N_1^0 e^{-\varphi\sigma_1 t}$$

where $N_1(t)$ is the number of target atoms after an irradiation time t, $N_1{}^0$ is the initial number of target atoms, and $\phi\sigma_1$ in the exponential term is the depletion constant. The rate of change of atoms of the product N_2 is, as before,

$$\frac{dN_2}{dt} = \varphi\sigma_1 N_1(t) - \lambda_2 N_2$$

but since $N_1(t)$ is treated as a variable,

$$\frac{dN_2}{dt} = \varphi\sigma_1 N_1^0 e^{-\varphi\sigma_1 t} - \lambda_2 N_2$$

which when solved yields

$$N_2 = \frac{\varphi\sigma_1 N_1^0}{\lambda_2 - \varphi\sigma_1}(e^{-\varphi\sigma_1 t} - e^{-\lambda_2 t})$$

Target depletion and product activation may both be significant in special circumstances. In this case, a similar approach can be used to obtain the number of product atoms with time:

$$\frac{dN_2}{dt} = \varphi\sigma_1 N_1(t) - \lambda_2 N_2 - \varphi\sigma_2 N_2$$

which has the solution

$$N_2 = \frac{\varphi\sigma_1 N_1^0}{\lambda_2 + \varphi\sigma_2 - \varphi\sigma_1}(e^{-\varphi\sigma_1 t} - e^{-(\lambda_2 + \varphi\sigma_2)t})$$

Activation product calculations thus require several parameters: the number of atoms in the target material, the particle flux in the area where irradiation occurs, the activation cross-section σ_1 for the primary reaction, the disintegration constant λ_2 of the product, and, if applicable, the activation cross-section σ_2 of the product.

4.7.1 Neutron Activation Product Calculations

Cross-sections for thermal neutron interactions are listed in the chart of the nuclides for most isotopes of stable elements and for many radioactive isotopes that may be formed and/or depleted by neutron irradiation. The chart also lists

the activation cross-section for the first resonance interval above thermal energy, but does not state at what energy the resonance occurs. For example, four values of σ_γ are provided for neutron activation of ^{59}Co to ^{60m}Co and ^{60}Co in the chart of the nuclides as shown in Figure 4-19: (21 + 16), (39 + 35). The first two values in

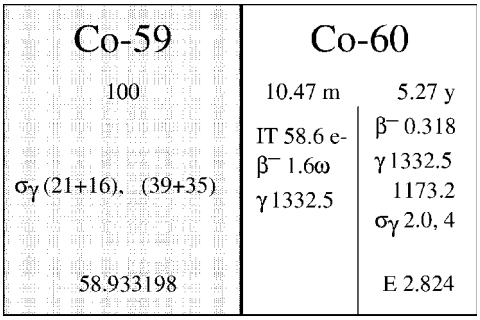

Fig. 4-19 Excerpt from the chart of the nuclides showing the thermal neutron radiative cross-section σ_γ for ^{59}Co to produce the activation products ^{60m}Co and ^{60}Co and σ_γ for the first resonance interval for higher energy neutrons as well as radioactive properties of ^{60m}Co and ^{60}Co.

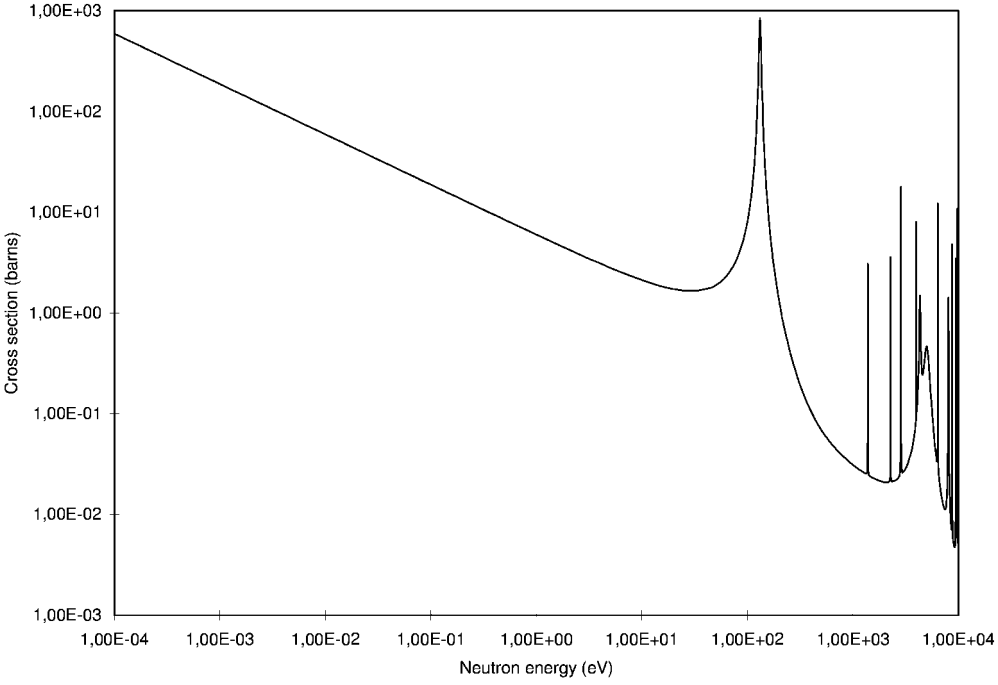

Fig. 4-20 Neutron activation cross-section versus energy for ^{59}Co.

parentheses indicate (a) that ^{60m}Co is formed from thermal neutron irradiation with a cross-section of 21 b, and (b) that ^{60}Co is formed directly (i.e., in its ground state) with 16 b. The second set of values has the same designation except for the important distinction that these are the metastable and ground state cross-sections at the first resonance energy above thermal neutron energies. The neutron energy at which the first resonance interval occurs is not given; it is obtained by consulting a plot of σ versus neutron energy for cobalt. As shown in Figure 4-20 these cross-sections occur at a neutron energy of 132 eV.

Figures 4-21 and 4-22 contain excerpts from the chart of nuclides for several important elements that are the source of activation products. Such information can be used to calculate activation product inventories, as shown in Example 4-6.

Example 4-6. A thin foil of 0.1 g of tungsten is placed in a neutron flux of 10^{12} neutrons/cm^2 s. What is the activity of ^{187}W (a) after 24 h and (b) at saturation?
Solution. (a) The reaction equation to produce ^{187}W is

$$^{186}\mathrm{W} + {}^{1}_{0}\mathrm{n} \rightarrow [^{187}\mathrm{W}] \rightarrow {}^{187}\mathrm{W} + \gamma + Q$$

Thus only the ^{186}W portion of the foil yields ^{187}W, and from the excerpt of the chart of the nuclides in Figure 4-22 the atom percent of ^{186}W in natural tungsten is 28.426%. The number of ^{186}W atoms in the foil is

$$N_1^0 = \frac{0.1\mathrm{g} \times 6.022 \times 10^{23}\mathrm{atoms/mol}}{183.85\,\mathrm{g/mol}} \times 0.28426 = 9.31 \times 10^{19}\mathrm{atoms}$$

and the activation cross-section σ_γ = 37.8 b (also from the chart of the nuclides). The activity at 24 h is

$$A(24\mathrm{h}) = \varphi\sigma N_1(1 - e^{[-(\ln 2)/23.9\mathrm{h}] \times 24\mathrm{h}})$$

$$= 10^{12}\ \mathrm{neutrons/cm^2\ s} \times 37.8 \times 10^{-24}\ \mathrm{cm^2} \times 9.31 \times 10^{19}(1 - 0.5)$$

$$= 1.77 \times 10^9\ \mathrm{d/s} = 47.8\ \mathrm{mCi}$$

(b) At saturation the exponential term will approach zero (at about 10 half-lives or 240 h), and the saturation activity is

$$A_{\mathrm{sat}} = \phi\sigma N_1{}^0 = 3.54 \times 10^9\ \mathrm{d/s} = 95.7\ \mathrm{mCi}$$

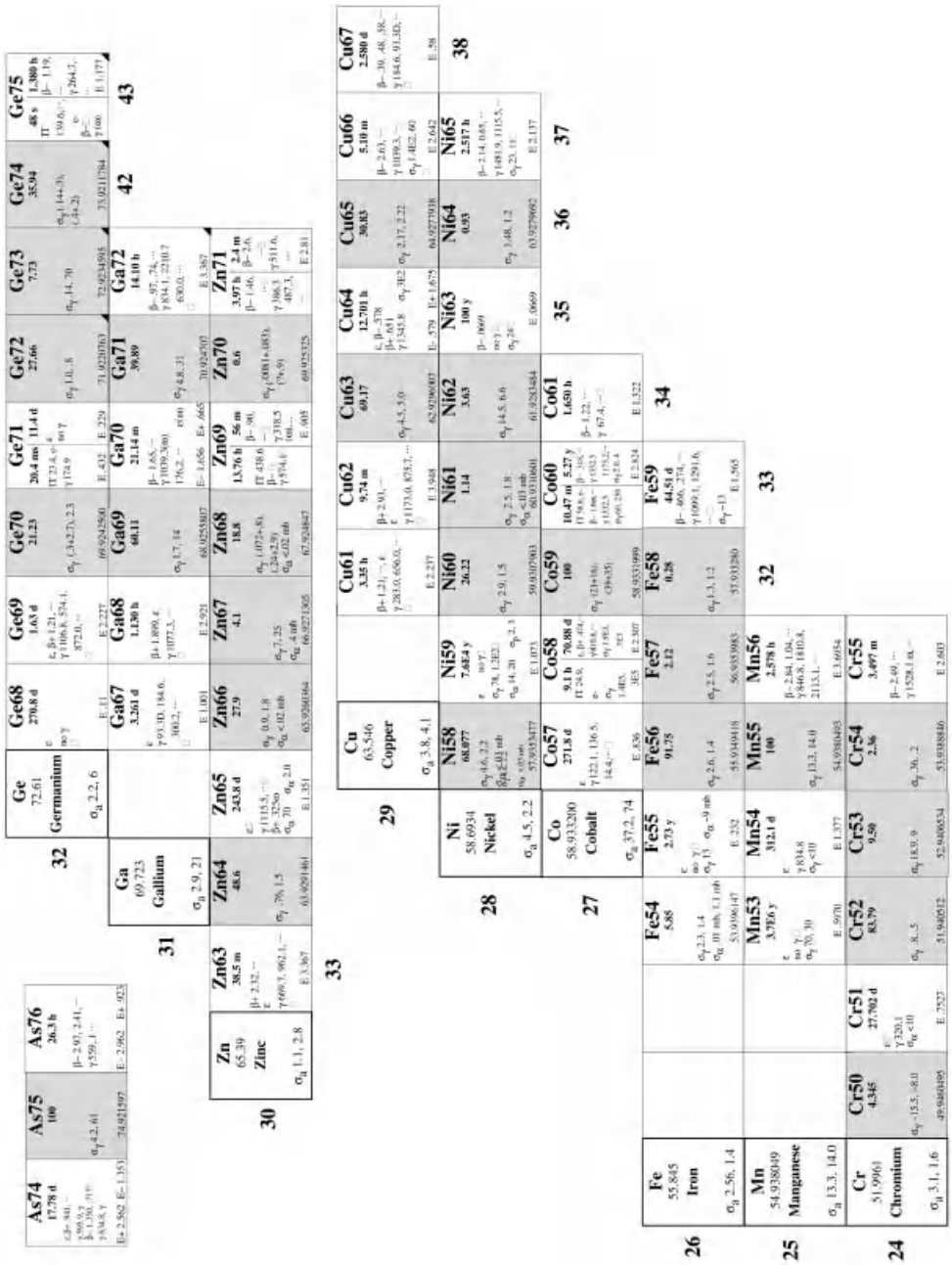

Fig. 4-21 Excerpt from the chart of the nuclides of light elements (Z = 24 to 32) that form activation products when irradiated with neutrons.

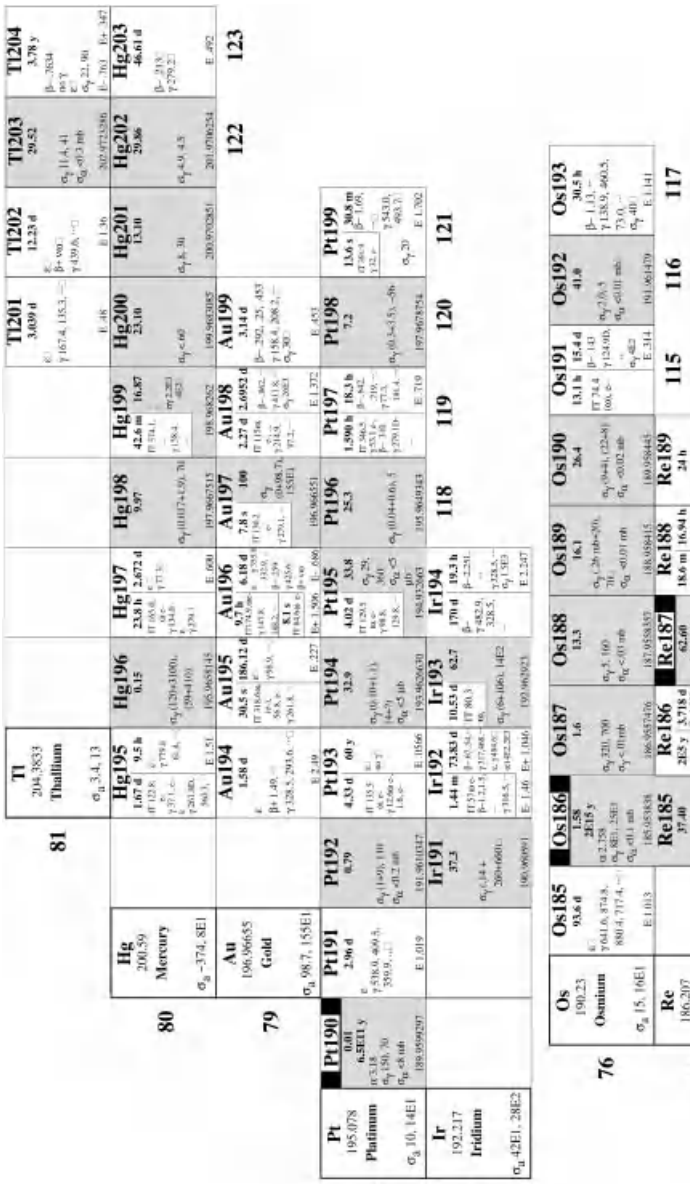

Fig. 4-22 Excerpt from the chart of the nuclides of heavy elements ($Z = 73$ to 81) that form activation products when irradiated with neutrons.

4.7.2
Charged Particles Calculations

Cross-sections for charged particle reactions are typically in the millibarn range and much less available. Some data are available from the National Nuclear Data Center, and other data by Xiaoping et al. are provided in Figure 4-23 for deuteron irradiations.

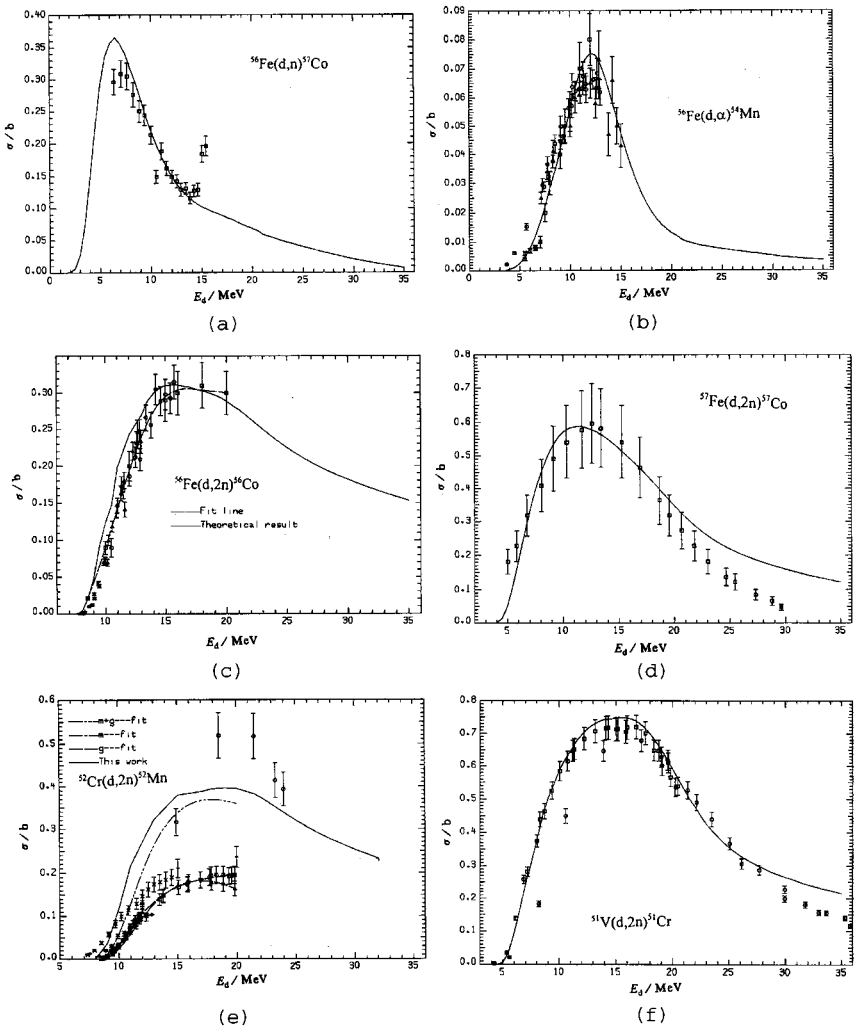

Fig. 4-23 Cross-section versus deuteron energy for: (a) (d,n) production of ^{57}Co from ^{56}Fe; (b) (d,α) production of ^{54}Mn from ^{56}Fe; (c) (d,2n) production of ^{56}Co from ^{56}Fe; (d) (d,2n) production of ^{57}Co from ^{57}Fe; (e) (d,2n) production of ^{52}Mn from ^{52}Cr; and (f) (d,2n) production of ^{51}Cr from ^{51}V.

Particle beams from accelerators are often given in terms of "beam current," usually in micro- or milliamperes. The beam current can, in turn, be converted into the number of particles per second and used to determine the production of various products, as illustrated in Example 4-7.

Example 4-7. A 2 μA beam of 15 MeV deuterons with an area of 1 cm^2 is focused on an iron wall 0.2 cm thick. What activity of ^{56}Co will be induced in the wall if the beam strikes the wall for 10 min?
Solution. The reaction for producing ^{56}Co is

$$^{56}_{26}\mathrm{Fe} + {}^{2}_{1}\mathrm{H} \rightarrow [{}^{58}_{27}\mathrm{Co}*] \rightarrow {}^{56}_{27}\mathrm{Co} + 2{}^{1}_{0}\mathrm{n} + Q$$

And the number of ^{56}Fe atoms (91.72 atom % of iron) in the beam is

$$\mathrm{Atoms}({}^{56}\mathrm{Fe}) = \frac{0.2\mathrm{cm}^3 \times 7.9\mathrm{g/cm}^3 \times 6.022 \times 10^{23}\mathrm{atoms/mol} \times 0.9172}{55.847\mathrm{g/mol}}$$

$$= 1.563 \times 10^{22} \text{ atoms of } {}^{56}\mathrm{Fe}$$

The number of deuterons striking the 1 cm^2 area of the wall, or the flux ϕ is

$$\frac{2 \times 10^{-6}\mathrm{A} \times 1\mathrm{C/s\ A}}{1.6022 \times 10^{-19}\mathrm{C/d}} = 1.25 \times 10^{13}\mathrm{d/cm}^2\ \mathrm{s}$$

From Figure 4-23c, the ^{56}Fe (d,2n) cross-section is about 0.3 b; thus, the production rate of atoms of ^{56}Co, ignoring radioactive transformation of the product, is

$$\begin{aligned} N_\mathrm{i} &= \phi\sigma N \\ &= 1.25 \times 10^{13}\ \mathrm{d/cm^2\ s} \times 0.3 \times 10^{-24}\ \mathrm{cm^2/atom} \times 1.563 \times 10^{22}\ \mathrm{atoms} \\ &= 5.86 \times 10^{10}\ \mathrm{atoms/s} \end{aligned}$$

or, for a 10 min (600 s) irradiation time

$$N_\mathrm{i} = 3.52 \times 10^{13} \text{ atoms of } {}^{56}\mathrm{Co}$$

And since the half-life of ^{56}Co is 77.3 d, the activity induced in the irradiated steel is

$$A_\mathrm{i} = \lambda N_\mathrm{i} = \frac{\ln 2}{T_{1/2}} N_\mathrm{i} = 3.65 \times 10^{6}\ \mathrm{t/s}$$

4.8 Medical Isotope Reactions

Several (n,γ) reactions produce radionuclides used in nuclear medicine. Examples are

$$^{50}_{24}\mathrm{Cr} + {}^{1}_{0}\mathrm{n} \rightarrow [^{51}_{24}\mathrm{Cr}] \rightarrow {}^{51}_{24}\mathrm{Cr} + \gamma$$

$$^{98}_{42}\mathrm{Mo} + {}^{1}_{0}\mathrm{n} \rightarrow [^{99}_{42}\mathrm{Mo}] \rightarrow {}^{99}_{42}\mathrm{Mo} + \gamma$$

$$^{132}_{54}\mathrm{Xe} + {}^{1}_{0}\mathrm{n} \rightarrow [^{133}_{54}\mathrm{Xe}] \rightarrow {}^{133}_{54}\mathrm{Xe} + \gamma$$

Chromium-51 is used for labeling red blood cells and spleen scanning; ^{99}Mo is the source of ^{99m}Tc, the most commonly used radionuclide in nuclear medicine; and ^{133}Xe is used for lung ventilation studies.

Medical isotopes can also be produced by accelerating protons, deuterons, ^{3}He, and ^{4}He nuclei toward targets. A certain threshold energy is required (generally 5–30 MeV) for these reactions in order to overcome the repulsive coulomb forces of target nuclei. Common reactions are

$$^{16}_{8}\mathrm{O} + {}^{3}_{2}\mathrm{He} \rightarrow [^{19}_{10}\mathrm{Ne}] \rightarrow {}^{18}_{9}\mathrm{F} + {}^{1}_{1}\mathrm{H}$$

$$^{68}_{30}\mathrm{Zn} + {}^{1}_{1}\mathrm{H} \rightarrow [^{69}_{31}\mathrm{Ga}] \rightarrow {}^{67}_{31}\mathrm{Ga} + 2\mathrm{n}$$

Fluorine-18 is used for labeling radiopharmaceuticals for positron emission tomography (PET) imaging, and ^{67}Ga is widely used for soft tumor and occult abscess detection.

A radionuclide of interest may be formed indirectly from radioactive transformation of the product of a nuclear reaction. Two examples of these indirect methods are production of ^{123}I by positron emission of ^{123}Xe and ^{201}Tl by electron capture by ^{201}Pb

$$^{122}_{52}\mathrm{Te} + {}^{4}_{2}\mathrm{He} \rightarrow [^{126}_{54}\mathrm{Xe}] \rightarrow {}^{123}_{54}\mathrm{Xe} + 3\mathrm{n}$$

$$^{123}_{54}\mathrm{Xe} \rightarrow {}^{123}_{53}\mathrm{I} + {}^{0}_{1}\mathrm{e}^{+}$$

$$^{203}_{81}\mathrm{Tl} + {}^{1}_{1}\mathrm{H} \rightarrow [^{204}_{82}\mathrm{Pb}] \rightarrow {}^{201}_{82}\mathrm{Pb} + 3\mathrm{n}$$

$$^{201}_{82}\mathrm{Pb} + {}^{0}_{-1}\mathrm{e} \rightarrow {}^{201}_{81}\mathrm{Tl}$$

Iodine-123 ($T_{1/2}$ = 13 h) shows promise for replacing ^{131}I in many diagnostic studies which would produce lower patient doses, and ^{201}Tl ($T_{1/2}$ = 3.04 d), where transforms by electron capture and gamma emission, is useful in heart imaging studies.

Positron-emitting radionuclides, which can be used to diagnose various medical conditions by tagging them onto pharmaceuticals, are readily produced in cyclo-

trons because protons and deuterons increase the proton number of many target materials. Since many of the light-element positron emitters are short lived, they need to be produced near where they will be used. Positron emitters produce annihilation radiation, and the differential absorption patterns of these photons can provide important medical information using PET. Two common PET nuclides are ^{11}C and ^{18}F, which are produced by the reactions

$$^{14}_{7}\mathrm{N} + {}^{1}_{1}\mathrm{H} \rightarrow [{}^{15}_{8}\mathrm{O}^{*}] \rightarrow {}^{11}_{6}\mathrm{C} + {}^{4}_{2}\mathrm{He} + Q$$

$$^{18}_{8}\mathrm{O} + {}^{1}_{1}\mathrm{H} \rightarrow [{}^{19}_{9}\mathrm{F}^{*}] \rightarrow {}^{18}_{9}\mathrm{F} + {}^{1}_{0}\mathrm{n} + Q$$

The cross-sections for these reactions are shown in Figures 4-24 and 4-25. Fluorine-18 is also produced by

$$^{20}_{10}\mathrm{Ne} + {}^{2}_{1}\mathrm{H} \rightarrow [{}^{22}_{11}\mathrm{Na}^{*}] \rightarrow {}^{18}_{9}\mathrm{F} + {}^{4}_{2}\mathrm{He} + Q$$

and ^{13}N by the reaction

$$^{16}_{8}\mathrm{O} + {}^{1}_{1}\mathrm{H} \rightarrow [{}^{17}_{9}\mathrm{F}^{*}] \rightarrow {}^{13}_{7}\mathrm{N} + {}^{4}_{2}\mathrm{He} + Q$$

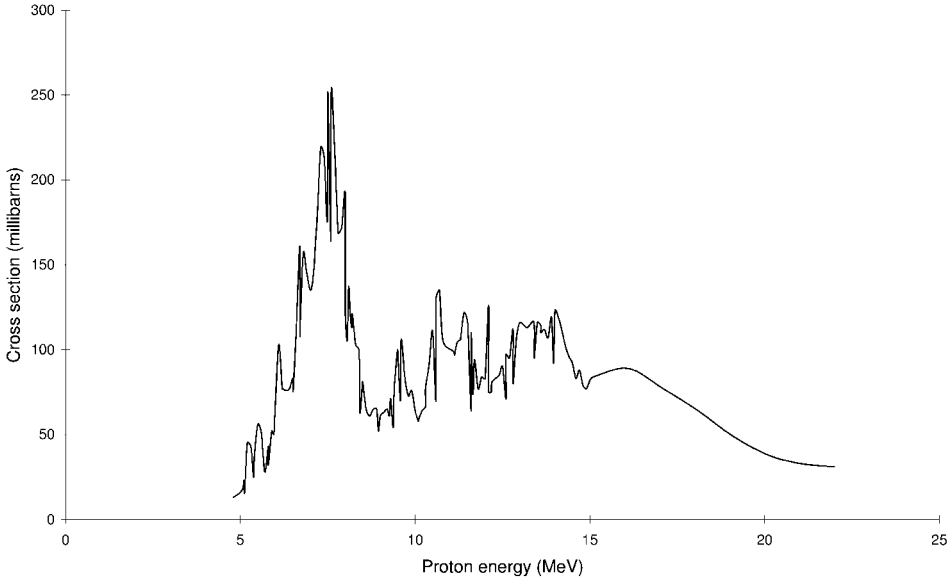

Fig. 4-24 Cross-section versus proton energy for (p, α) production of ^{11}C from ^{14}N.

Each of these reactions require projectiles in the MeV range and the reaction cross-sections are smaller than neutron interactions. As shown in Figure 4-24, the ^{14}N (p,α) ^{11}C reaction has several resonance peaks and the energy of the proton beam is an important factor in determining the yield of ^{11}C in a given target.

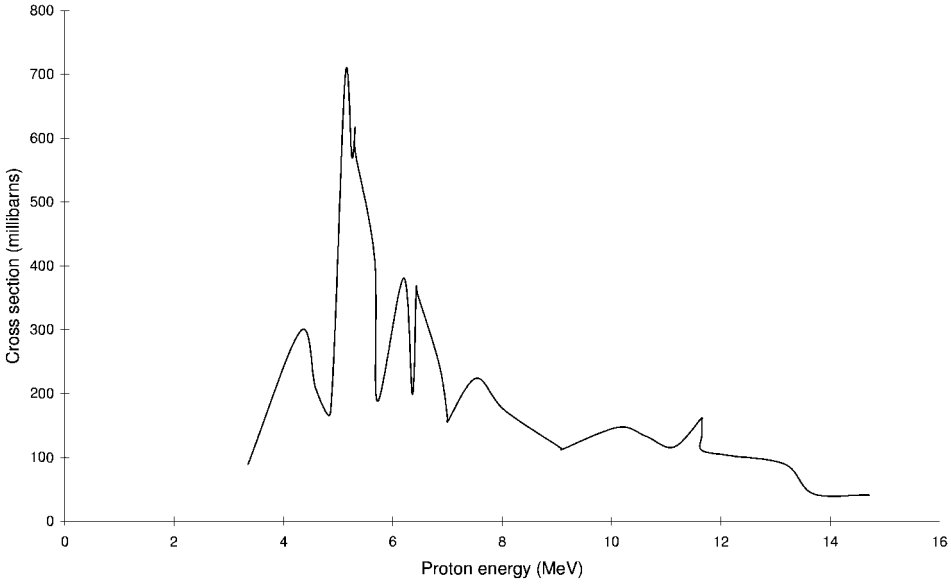

Fig. 4-25 Cross-section versus proton energy for (p,n) production of ^{18}F from ^{18}O.

4.9 Transuranium Elements

In 1934 Fermi bombarded uranium with neutrons to make and identify new elements with nuclear charge greater than 92, or transuranic (TRU) elements. Fermi undoubtedly was one of the first to fission uranium but did not recognize it because in his focus on TRU production, he had covered the uranium target with foil, thus preventing the detection of the resulting fission fragments. Neutron capture in ^{238}U yields

$$^{238}_{92}\mathrm{U} + {}^{1}_{0}\mathrm{n} \rightarrow \left[{}^{239}_{92}\mathrm{U}\right] \rightarrow {}^{239}_{92}\mathrm{U} + \gamma$$

The ^{239}U product undergoes radioactive transformation by beta particle emission to produce ^{239}Np, which does not exist in nature. Radioactive transformation of ^{239}Np by beta particle emission forms an isotope of another new element with $Z = 94$: ^{239}Pu. Plutonium-239 ($T_{1/2}$ = 24,110 y) is an important nuclide because it can be fissioned in nuclear reactors and nuclear weapons.

Soon after the discovery of ^{239}Np, two other isotopes were made by the following reactions:

$$^{238}_{92}\mathrm{U} + {}^{2}_{1}\mathrm{H} \rightarrow [{}^{240}_{93}\mathrm{Np}] \rightarrow {}^{238}_{93}\mathrm{Np} + {}^{1}_{0}\mathrm{n} + {}^{1}_{0}\mathrm{n}$$

$$^{238}_{92}\mathrm{U} + {}^{1}_{0}\mathrm{n} \rightarrow {}^{237}_{92}\mathrm{U} + {}^{1}_{0}\mathrm{n} + {}^{1}_{0}\mathrm{n}$$

The ^{238}Np product in the first reaction is transformed by beta particle emission (half-life of 2.0 d) to ^{238}Pu ($T_{1/2}$ = 87.7 y), which is an alpha emitter that is used in thermoelectric generators, primarily for space missions. The ^{237}U produced in the second (n,2n) reaction undergoes radioactive transformation with a half-life of 6.8 d to ^{237}Np, which is the head of the neptunium series (see Chapter 6). It has a half-life of 2.14 × l0^6 y and is the longest-lived of the known TRU nuclides.

The production of TRU elements generally starts with neutron bombardment of uranium, plutonium, americium, curium, etc., to first build mass, then waiting for radioactive transformation to yield the desired target for further neutron bombardment to gradually reach the desired combination of Z and A. Sometimes it is necessary to use high-energy neutrons to obtain the desired product by (n,2n) or (n,3n) or greater reactions. Figure 4-26 shows the interrelationships of some of these paths of formation for some of the important TRU elements.

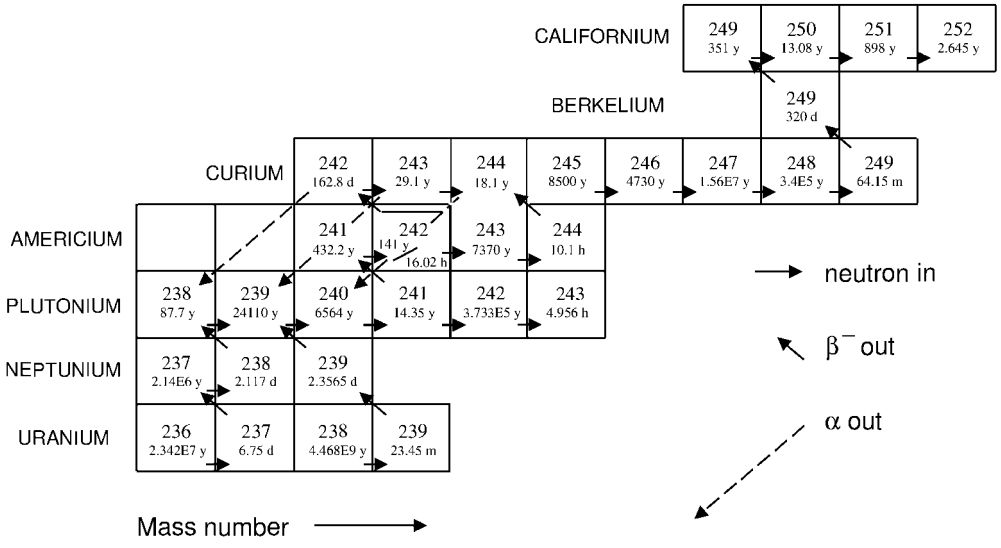

Fig. 4-26 Transuranium element production by a combination of neutron interactions to build mass followed by radioactive transformation to new products which may also be activated by neutrons to produce even heavier elements.

4.10 Photon Interactions

High-energy photons, through a process called photodisintegration, can also be used to transform nuclei. Since the photon has no mass, it can supply only its kinetic energy, which must be at least as great as the binding energy of a neutron or proton in order to eject them from a target nucleus. Photodisintegration reactions are, therefore, endoergic, and with the exception of deuterium and beryllium, the threshold energies are of the order of 8–10 MeV or more.

Photodisintegration is practical for deuterium in which the binding energy between the neutron and proton is only 2.225 MeV by the reaction

$$^{2}_{1}\mathrm{H} + \gamma \rightarrow [^{2}_{1}\mathrm{H}*] \rightarrow ^{1}_{1}\mathrm{H} + ^{1}_{0}\mathrm{n}$$

Photodisintegration of deuterium is the inverse of the (n,γ) reaction with hydrogen.

Beryllium, which has a loosely bound neutron, has a Q-value of –1.67 MeV and is relatively easy to use with a source of high-energy photons to produce neutrons by the reaction

$$^{9}_{4}\mathrm{Be} + \gamma \rightarrow [^{9}_{4}\mathrm{Be}*] \rightarrow ^{8}_{4}\mathrm{Be} + ^{1}_{0}\mathrm{n}$$

The Q-value of this reaction is –1.67 MeV which can be supplied by several high-energy gamma sources. Fermi and his colleagues extracted radon from a sizeable radium source and used the gamma rays from the radon transformation products to generate neutrons from beryllium. The (p,a) reaction with Li yields 17.2 MeV gamma rays which can be used to produce photoneutrons, as in the (γ,n) reaction with ^{31}P:

$$^{31}_{15}\mathrm{P} + \gamma \rightarrow [^{31}_{15}\mathrm{P}] \rightarrow ^{30}_{15}\mathrm{P} + ^{1}_{0}\mathrm{n}$$

The (γ,p) reaction requires still higher energies, which can be obtained from a betatron.

4.10.1 Activation by Photons

High-energy photons can be used to activate various materials, usually by (γ,n), (γ,p), and (γ,2n) reactions. These are threshold reactions with high Q-values, and high-energy photons (well in excess of 7 MeV) are required to induce them. Production of these high-energy photons requires high-energy acceleration of electrons to produce bremsstrahlung, which can be problematical since high energies are required and photon yields are low. Such sources are known as synchrotron light sources and they are quite expensive, which limits their use for photonuclear activation.

Brey and colleagues at Idaho State University have used photonuclear activation for the analysis of ^{129}I ($T_{1/2} = 1.57 \times 10^7$ y) by a (γ,n) reaction:

$$^{129}_{53}\mathrm{I} + {}^{0}_{0}\gamma \rightarrow [^{129}_{53}\mathrm{I}*] \rightarrow {}^{128}_{53}\mathrm{I} + {}^{1}_{0}\mathrm{n} + Q$$

The ^{128}I product has a 25 min half-life, which allows use of a much smaller number, relatively speaking, of ^{129}I atoms for measurement than would be required for radioactivity measurement of the much longer lived ^{129}I atoms. A beam of 30 μA on a thick tungsten target produces about 10^{13} γ/cm^2 s, which yields sufficient activity of ^{128}I for measurement after a 2 h irradiation.

Photonuclear cross-sections are quite small, usually in the millibarn range. As shown in Figure 4-27 for a target of ^{129}I, the (γ,n) cross-section for most materials is zero below a threshold energy but then rises smoothly through a peak, known as the "giant resonance," and then decreases. For ^{129}I, the cross-section peaks at about 280 mb for 18 MeV photons.

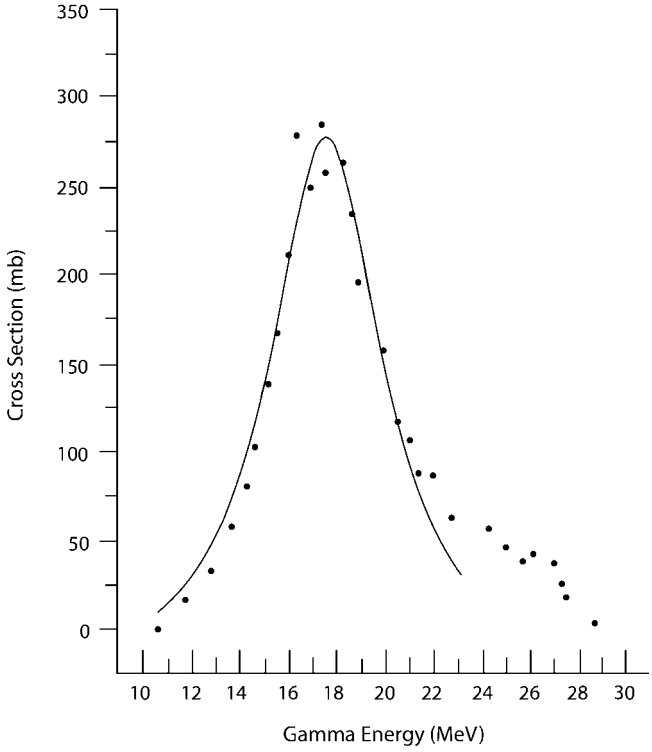

Fig. 4-27 Photonuclear cross-section versus energy for (γ,n) reaction in ^{129}I, adjusted from the well-established photonuclear cross-section spectrum for ^{127}I. (Adapted from Brey et al. (1998), with permission.)

The calculated number of product atoms N_p is, as for other types of activation products, directly determined by the photon flux ϕ_γ, the photonuclear cross-section σ_γ at the photon energy, the number of target atoms per cm^2, N, and the irradiation time:

$$\text{Productatoms} = \frac{\varphi_\gamma \sigma_\gamma N}{\lambda_p}(1 - e^{-\lambda_p t})$$

where λ_p is the disintegration constant of the radioactive product.

Example 4-8. A synchrotron accelerator is used as a "light source" to produce 18 MeV bremsstrahlung peaked in the forward direction at a flux of 10^{13} γ/cm^2 s. If a sample that contains 0.1 Bq of ^{129}I is irradiated uniformly in the beam for 2 h, what activity of ^{128}I will exist upon removal?
Solution. The number of atoms of ^{129}I in the sample is

$$0.1 \text{ t/s} = \lambda N$$

therefore, the number of ^{129}I target atoms is

$$N = \frac{0.1\text{t/s}}{\ln 2} \times 1.57 \times 10^7 \text{y} \times 3.15576 \times 10^7 \text{s/y}$$

$$= 7.148 \times \text{x } 10^{13} \text{ atoms}$$

From Figure 4-27, σ_γ at 18 MeV is 280 mb (0.28 b) and the number of product atoms after 2 h is

$$N = \frac{7.148 \times 10^{13} \times 0.28\text{b} \times 10^{-24}\text{cm}^2/\text{atom} \times 10^{13}\gamma/\text{cm}^2 \text{ s}}{4.62 \times 10^{-4}\text{s}^{-1}}(1 - e^{-(\ln 2/25) \times 120\,\text{m}})$$

$$= 4.176 \times 10^5 \text{ atoms}$$

The activity of ^{128}I is

$$A = \lambda N$$

$$= \frac{\ln 2}{25\,\text{m} \times 60\,\text{s/m}} \times 4.176 \times 10^5 \text{ atoms}$$

$$= 193 \text{ t/s}$$

which can be readily measured by detection of the 0.443 MeV gamma emitted by ^{128}I.

4.11
Fission and Fusion Reactions

4.11.1
Fission

Fission occurs when the nucleus of a fissionable material such as ^{235}U or ^{239}Pu absorbs a neutron and splits into two fragments that are both smaller and more tightly bound than the fissioning nucleus. The products of this reaction, in addition to the two fission fragments, are two or three neutrons plus a considerable quantity of energy. Fission reactions are therefore exoergic, and because of this can be a source of energy. Since excess neutrons are emitted, these reactions are also sources of neutrons. A typical fission reaction with each of these components is

$$^{235}_{92}\mathrm{U} + {}^{1}_{0}\mathrm{n} \rightarrow [^{236}\mathrm{U}^{*}] \rightarrow {}^{144}\mathrm{Nd} + {}^{90}\mathrm{Zr} + 2\mathrm{n} + Q$$

The Q-value of this reaction is +205.4 MeV. Numerous other reactions are possible since the uranium nucleus can split any number of ways after absorbing a neutron.

The discovery of fission occurred due to the efforts of several researchers, including Enrico Fermi, to produce transuranic elements by irradiating uranium with neutrons and other particles. Products were indeed found, and many were radioactive, but the products were varied with many different half-lives. These physicists did chemical separations to better understand the interaction processes and found unexpected barium-like radioactive products in the precipitates; however, the presence of these products was attributed to their rudimentary chemistry techniques. When Hahn, an expert chemist, and Strassmann showed that the products of neutron irradiation of uranium indeed contained radioactive barium, Hahn's former assistant Lise Meittner and her nephew Otto Frisch decided to apply Bohr's recent liquid drop model of the nucleus to the results: and there it was! Uranium had split into lighter fragments, one of which was an isotope of barium, which subsequently transformed to lanthanum. They termed it nuclear fission because it resembled division of cells (called fission) in biology. As soon as this insight was announced, physicists all over the world used ion chambers to observe the high rates of ionization produced by the fission fragments. If Fermi had not wrapped his uranium target in foil, this foremost physicist would also have been the discoveror of fission, a phenomenon to which he contributed so much.

The discovery of nuclear fission not only changed physics, but has also changed the world. Fissioning of the ^{235}U nucleus yields neutrons, numerous radioactive fission products, and enormous amounts of energy. These concepts, their use in recovering the energy of nuclear fission, and the dynamics of producing radioactive fission products are discussed in detail in Chapter 5.

4.11.2 Fusion

Fusion reactions occur when light elements are brought together to form a heavier element in which the nucleons are more tightly bound. Such reactions, when they can be made to occur, are exoergic, yielding considerable amounts of energy because the products move up the curve of binding energy per nucleon for light elements (see Figure 1-3).

Fusion reactions are the source of the sun's tremendous energy generation and the enormous energy release in thermonuclear weapons (or hydrogen bombs). Isotopes of hydrogen are fused in the following typical reactions:

$$^1_1\mathrm{H} + {}^1_1\mathrm{H} \rightarrow {}^2_1\mathrm{H} + \mathrm{e}^+$$

$$^1_1\mathrm{H} + {}^2_1\mathrm{H} \rightarrow {}^3_2\mathrm{He}$$

$$^3_2\mathrm{He} + {}^3_2\mathrm{He} \rightarrow {}^4_2\mathrm{He} + 2{}^1_1\mathrm{H}$$

These reactions, which are shown here as reactions between whole elements, actually occur between bare nuclei in the sun. Electrons are present to maintain electrical neutrality, but because of the sun's intense temperature, they are stripped away and do not participate in the reactions. Once a deuteron is created, it can fuse with another proton to make a nucleus of ^{3}He, and two ^{3}He nuclei fuse to form an alpha particle and two protons, which can participate in other reactions. The net result of these reactions is the fusing of four protons to produce an alpha particle, two positrons which annihilate, and 26.7 MeV of energy. This cycle of reactions is known as the proton–proton cycle. The sun burns 5.3×10^{16} kg/d of its hydrogen into alpha particles thereby transforming about 3.7×10^{14} kg of its mass into energy every day.

Fusion reactions are called thermonuclear reactions because high temperatures are required to overcome the coloumbic repulsion between the nuclei being fused, i.e., "thermo" for the heat required and "nuclear" for the interactions that occur. In order for a pair of deuterons, or a deuteron and a triton, to come close enough together to fuse, their centers must be separated by not more than about 10^{-14} m. At this separation, the potential energy is

$$\mathrm{PE} = \frac{1}{4\pi e_0}\frac{e^2}{r} = \frac{(8.987 \times 10^9 \mathrm{N/C^2})(1.602 \times 10^{-19}\mathrm{C})^2}{10^{-14}\mathrm{m}}$$

$$= 2.3 \times 10^{-14}\ \mathrm{J} = 144\ \mathrm{keV}$$

shared between the two; therefore, each hydrogen nucleus (deuteron or triton) would need at least 72 keV of kinetic energy to come close enough to fuse. The Boltzmann distribution of the kinetic energy of molecules of a gas is

$$\overline{E} = \frac{3}{2}kT$$

where the Boltzmann constant $k = 1.38 \times 10^{-23}$ J/K and T is the absolute temperature. Therefore, for a hydrogen nucleus to have $\overline{E}$ of 72 keV (or 1.15×10^{-14} J),

$$T = 5.6 \times 10^{8}\ \text{K}$$

The actual temperature required is not quite this extreme because some nuclei have considerably more kinetic energy than the average and not all the nuclei need to surmount the potential energy barrier to interact. In practice, thermonuclear reactions proceed at temperatures of about a tenth of this value or 6×10^7 K. A fission bomb can provide this temperature.

The fusing of protons to form deuterons in the proton–proton cycle takes place on a very long timescale, which effectively controls the rate of energy generation in the sun. For hotter stars, which the sun will one day inevitably become, the sequence of reactions will be dominated by the carbon cycle, which is comprised of the following reactions:

$$^{12}\text{C} + {}^{1}\text{H} \rightarrow {}^{13}\text{N} + \gamma$$

$$^{13}\text{N} \rightarrow {}^{13}\text{C} + \text{e}^{+}$$

$$^{13}\text{C} + {}^{1}\text{H} \rightarrow {}^{14}\text{N} + \gamma$$

$$^{14}\text{N} + {}^{1}\text{H} \rightarrow {}^{15}\text{O} + \gamma$$

$$^{15}\text{O} \rightarrow {}^{15}\text{N} + \text{e}^{+}$$

$$^{15}\text{N} + {}^{1}\text{H} \rightarrow {}^{12}\text{C} + {}^{4}\text{He}$$

These reactions require more thermal energy to overcome the repulsion between carbon and hydrogen nuclei, or about 2×10^7 K. Since the sun's interior temperature is about 1.5×10^7 K, a long period of time must elapse during which sufficient helium is produced by burning hydrogen. When all of the hydrogen has been converted to helium, the sun will contract and heat up which will create conditions whereby helium nuclei can fuse into ^{12}C. The presence of carbon, which is neither produced nor consumed, permits this sequence of reactions to take place at a much greater rate than the reactions in the proton–proton cycle. The net process is still the fusion of four protons to produce a helium nucleus with the release of 26.7 MeV of energy.

The primordial matter produced when the universe was formed consisted of about 75% hydrogen and 25% helium; all of the other chemical elements were formed by nuclear reactions in the interiors of stars. At about 10^8 K three ^{4}He nuclei are converted into ^{12}C by the two-step process

$$^{4}\mathrm{He} + {}^{4}\mathrm{He} \rightarrow {}^{8}\mathrm{Be}$$

$$^{8}\mathrm{Be} + {}^{4}\mathrm{He} \rightarrow {}^{12}\mathrm{C}$$

The first reaction is endothermic with a Q-value of 92 keV. The ^{8}Be nucleus is unstable and quickly (in about 10^{-16} s) transforms back into two alpha particles. Even so, at 10^{8} K there will be a small concentration of ^{8}Be which because of a particularly large cross-section allows fusion with ^{4}He to form ^{12}C and 7.3 MeV of energy before the breakup of ^{8}Be can occur. Once ^{12}C is formed, it can successively fuse with other alpha particles to make even heavier elements. For example:

$$^{12}\mathrm{C} + {}^{4}\mathrm{He} \rightarrow {}^{16}\mathrm{O}$$

$$^{16}\mathrm{O} + {}^{4}\mathrm{He} \rightarrow {}^{20}\mathrm{Ne}$$

$$^{20}\mathrm{Ne} + {}^{4}\mathrm{He} \rightarrow {}^{24}\mathrm{Mg}$$

Each of these reactions is exothermic. At still higher temperatures (10^{9} K), fusion of carbon and oxygen atoms can occur to produce still heavier products:

$$^{12}\mathrm{C} + {}^{12}\mathrm{C} \rightarrow {}^{20}\mathrm{Ne} + {}^{4}\mathrm{He}$$

$$^{16}\mathrm{O} + {}^{16}\mathrm{O} \rightarrow {}^{28}\mathrm{Si} + {}^{4}\mathrm{He}$$

Such processes will continue with the buildup of elements until ^{56}Fe is reached (see Figure 1-3); beyond this point no further energy can be gained by fusion.

Nitrogen is almost as abundant in nature as carbon and oxygen, which are the two most abundant elements, presumably because they are products of fusion processes involving hydrogen and helium. The likely reactions that yield nitrogen are

$$^{12}\mathrm{C} + {}^{1}\mathrm{H} \rightarrow {}^{13}\mathrm{N} + \gamma$$

$$^{13}\mathrm{N} \rightarrow {}^{13}\mathrm{C} + \mathrm{e}^{+} + \nu$$

$$^{13}\mathrm{C} + {}^{1}\mathrm{H} \rightarrow {}^{14}\mathrm{N} + \gamma$$

and

$$^{16}\mathrm{O} + {}^{1}\mathrm{H} \rightarrow {}^{17}\mathrm{F} + \gamma$$

$$^{17}\mathrm{F} \rightarrow {}^{17}\mathrm{O} + \mathrm{e}^{+}$$

$$^{17}\mathrm{O} + {}^{1}\mathrm{H} \rightarrow {}^{14}\mathrm{N} + {}^{4}\mathrm{He}$$

The stable isotopes ^{13}C and ^{17}O are found in natural carbon and oxygen with abundances of 1.1% and 0.04%, which confirms that reactions of this sort can indeed take place.

Formation of elements beyond ^{56}Fe requires the presence of neutrons which become abundant after fusion yields atoms with an excess of neutrons such as ^{13}C, ^{17}O, etc. Neutron captures in ^{56}Fe begin a sequence of mass building and radioactive transformation to build heavier and heavier elements:

$$^{56}Fe + n \rightarrow {}^{57}Fe + n \rightarrow {}^{58}Fe + n \rightarrow {}^{59}Fe$$

and since ^{59}Fe is radioactive, it transforms to ^{59}Co which can absorb neutrons to become ^{60}Ni, and so on.

Thermonuclear weapons release energy by fusion reactions. Lithium deuteride ($^{6}Li^{2}H$) made of ^{6}Li and deuterium is a solid at normal temperature and makes an excellent fuel. The deuterons are held close together in this formulation, which enhances the DD reaction, and neutron irradiation of ^{6}Li "manufactures" tritium to stoke the DT reaction. The related reactions are

$$^{2}_{1}H + {}^{2}_{1}H \rightarrow {}^{3}_{1}H + p \qquad \text{(energy release = 4.0 MeV)}$$

$$^{2}_{1}H + {}^{2}_{1}H \rightarrow {}^{3}_{2}He + n \qquad \text{(energy release = 3.3 MeV)}$$

$$^{3}_{1}H + {}^{3}_{1}H \rightarrow {}^{4}_{2}He + n + n \qquad \text{(energy release = 11.27 MeV)}$$

$$^{2}_{1}H + {}^{3}_{1}H \rightarrow {}^{4}_{2}He + n \qquad \text{(energy release = 17.6 MeV)}$$

$$^{6}_{3}Li + n \rightarrow {}^{3}_{1}H + {}^{4}_{2}He \qquad \text{(energy release = 4.9 MeV)}$$

$$^{3}_{2}He + {}^{2}_{1}H \rightarrow {}^{4}_{2}He + {}^{1}_{1}H \qquad \text{(energy release = 18.35 MeV)}$$

These interlocked reactions use both tritons and neutrons, which are not initially present in the fuel. The first two reactions fuse deuterium to produce energy, and tritium from the first reaction participates in TT and DT fusion (shown in the third and fourth reactions). The neutrons produced interact with ^{6}Li according to the fifth reaction to supply additional tritium for DT fusion. The fifth reaction is not in itself a thermonuclear reaction since the neutron has no potential energy barrier to overcome to reach the ^{6}Li nucleus, and is, in fact, a fission reaction, although fission is usually associated with the heavy elements. The neutrons from DD and DT fusion are used to induce more tritium, neutrons, and fission-energy releases in fissionable materials. These reactions have been used by weapons designers to produce very efficient highly classified thermonuclear weapons.

The DT reaction yields 14 MeV neutrons which can induce fission in ^{238}U which is often fabricated into weapons to increase the yield substantially. The fissioning of ^{238}U yields several lower energy neutrons that can stimulate the production of ^{3}H in ^{6}Li thus adding more fuel and neutrons. This sequence of fission–fusion–

fission–fusion can be used to multiply the yield of a fission weapon 1000 times with cheap and readily available ^{6}Li, ^{2}H, and natural uranium. The products of fission cause radioactive fallout when detonated in the open atmosphere; fusion produces "clean" but very powerful weapons.

4.12 Summary

Much of what is known about atoms and radiation from them was learned by aiming subatomic particles at various target materials. The discovery of cathode rays provided a source of projectiles that led to the discovery of x-rays, which is now recognized as a special interaction between an accelerated electron and an atom in the target material of an x-ray tube that causes the emission of radiation known as bremsstrahlung with energies up to that of the accelerated electrons. Electrons that impinge on the target may also dislodge orbital electrons, and when the electron vacancy is filled by an outer shell electron, discrete-energy x-rays, known as characteristic x-rays, are also emitted. Characteristic x-rays that are emitted in the process of filling a K-shell vacancy are known as K-shell x-rays, or simply K x-rays, and similarly for other shell vacancies, as L, M, etc., x-rays. Moseley's detailed analysis of K_{α} x-rays established that the periodic table should be ordered by increasing Z instead of by mass; determined that certain elements were out of order; and identified gaps which guided the discovery of the "missing" elements.

Nuclear interactions are those that involve absorption of a bombarding particle by the nucleus of a target material (in x-ray production the electron is not absorbed by the nucleus). Absorption of the projectiles produces first a compound nucleus which then breaks up to yield the final products; these changes are characterized by the Q-value, or the energy balance between the products of the reaction and the interacting particle and the target atom (the reactants). If the Q-value is positive, the reaction is exoergic, i.e., energy is gained at the expense of the mass of the reactants. If the Q-value is negative, the reaction is endoergic and energy must be supplied for the reaction to occur.

The likelihood of an interaction between a bombarding particle and a nucleus is described by the concept of cross-section. The cross-section denotes the "target size" or apparent area presented to the bombarding particle; it is not specifically an area but a measure of the probability that an interaction will occur. The cross-section for a specific interaction is dependent on the energy, charge, mass, and de Broglie wavelength of the projectile, and the vibrational frequency, the spin, and the energy states of nucleons in the target atom. These cannot be predicted directly by nuclear theory; thus, cross-sections for any given arrangement of projectile and target are usually determined experimentally.

Neutrons have proved to be especially effective in producing nuclear transformations because they have no electric charge and are not repelled by the positively charged nuclei of target atoms. Consequently, they are more likely to penetrate nuclei than are protons, deuterons, or alpha particles, and many different reac-

tions have been produced. The most common neutron interaction is an (n,γ) or radiative capture reaction in which the mass number of the target element is increased by one unit and the excitation energy induced by the extra neutron is relieved by emission of gamma radiation.

Protons, deuterons, tritons (^{3}H), and helium nuclei can be accelerated in cyclotrons and linear accelerators and used to produce various products. A certain threshold energy is required (generally 5–30 MeV) for these reactions in order to overcome the repulsive coulomb forces of target nuclei. Cross-sections for charged particles are typically much lower than those for neutrons, typically in the millibarn range.

Nuclear reactions can also be used to induce fission and fusion of nuclei. Fission occurs when the nucleus of a fissionable material such as ^{235}U or ^{239}Pu absorbs a neutron and splits into two fragments that are both smaller and more tightly bound than the fissioning nucleus. The products of this reaction, in addition to the two fission fragments, are two or three neutrons plus a considerable quantity of energy. Fusion reactions occur when light elements are brought together to form a heavier element in which the nucleons are much more tightly bound. Such reactions, when they can be made to occur, are exoergic, and yield considerable amounts of energy.

Other Suggested Sources

Brey, R., Harmon, F., Wells, D., Tonchev, A. **1998**, *The Possibility of Photon Activation Analysis of Radionuclides at Environmental-Levels*, Department of Physics, Idaho State University, Pocatello, ID.

General Electric **1996**, Chart of the nuclides, in *Nuclides and Isotopes*, 15th edn, General Electric Company, San Jose, CA.

National Nuclear Data Center, Brookhaven National Laboratory, Upton, NY. Data resources available at: www.nndc.bnl.gov

Xiaoping, X., Yinlu, H., Youxiang, Z. **1999**, Evaluation and calculation of nuclear data for deuteron-induced reaction on ^{51}V, ^{52}Cr, ^{56}Fe, and ^{57}Fe, *Health Physics*, 76 (1).

Problems – Chapter 4

4–1. Complete the following reactions by writing them in equation form to show the balance of atomic and mass numbers and the compound nucleus: ^{7}Li (p,α); ^{9}Be (d,p); ^{9}Be (p, α); ^{11}B (d, α); ^{12}C (d,n); ^{14}N (α,p); ^{15}N (p, α); ^{16}O (d,n).

4–2. Calculate from the masses listed in Appendix B: (a) the *Q*-value for each of the reactions of Problem 4-1, and determine which reactions are exoergic and which are endoergic; and (b) the *Q*-value and threshold energy for the reaction in Example 4-5.

4–3. The reactions ^{9}Be (p,n) ^{9}B, ^{13}C (p,n) ^{13}N, and ^{18}O (p,n) ^{18}F have threshold energies of 2.059, 3.236, and 2.590 MeV, respectively. What are the *Q*-values for the reactions?

4–4. Calculate, from the atomic masses in Appendix B, the threshold energies for the reactions ^{11}B (p,n) ^{11}C, ^{18}O (p,n) ^{18}F, and ^{23}Na (p,n) ^{23}Mg.

4–5. If ^{12}C is bombarded with neutrons, protons, deuterons, and alpha particles, each having kinetic energy of 10.00 MeV, what would be the excitation energy of each compound nucleus if it is assumed that the recoil energy of the compound nucleus can be neglected?

4–6. With the mass data in Appendix B, calculate the binding energy of the "last neutron" in each of the following sets of isotopes: (a) ^{11}C, ^{12}C, ^{13}C and (b) ^{13}N, ^{14}N, ^{15}N.

4–7. With the mass data in Appendix B, calculate the binding energy of the "last proton" in ^{11}C, ^{12}C, ^{13}C.

4–8. What causes the binding energy for those reactions in Problems 4-6 and 4-7 to be particularly small, i.e., smaller than 5 MeV?

4–9. An (n,γ) reaction in ^{113}Cd using thermal neutrons (E = 0.025 eV) produces ^{114}Cd. What energy does the emitted photon have?

4–10. Find the energy of the gamma ray emitted in the (α,γ) reaction with ^{7}Li assuming the alpha particle energy is negligible.

4–11. Find the *Q*-value (and therefore the energy released) from the masses in Appendix B for the fission reaction

$$^{235}_{92}\mathrm{U} + {}^{1}_{0}\mathrm{n} \rightarrow [^{236}_{92}\mathrm{U}^{*}] \rightarrow {}^{93}_{40}\mathrm{Zr} + {}^{141}_{58}\mathrm{Ce} + {}^{1}_{0}\mathrm{n} + {}^{1}_{0}\mathrm{n} + 6\,{}^{0}_{-1}\beta^{-}$$

4–12. Find the kinetic energy of the emitted neutron in the (d, triton) fusion reaction. (Hint: the recoil energies must be accounted for.)

4–13. Under the proper conditions two alpha particles can combine to produce a proton and a nucleus of ^{7}Li. (a) Write the equation for this reaction. (b) What minimum kinetic energy must one of the alpha particles have to make the reaction proceed if the other alpha particle is at rest?

4–14. Thermal neutrons (0.025 eV) produce an (n,α) reaction with ^{6}Li in natural lithium. Calculate the kinetic energy of the ejected alpha particle.

4–15. Two reactions that occur in the upper atmosphere due to the effects of cosmic "rays" are $^{14}_{7}$N (n,p) _ and $^{14}_{7}$N (n,_) $^{12}_{6}$C. (a) Complete the nuclear reaction equation for each and calculate the *Q*-value of each. (b) Is the nuclide formed in each case stable or radioactive?

4–16. Radioactive transformation is a special kind of exoergic reaction. Carbon-14 emits an electron (beta particle) to transform to ^{14}N. From the *Q*-value, determine the maximum energy available to the ejected electron (beta particle).

4–17. Calculate the maximum activity (d/s), assuming no source depletion, that could be induced in a copper foil of 100 mg exposed to a thermal neutron flux of 10^{12} neutrons/cm^2 s. (Note: natural copper consists of 69.1% ^{63}Cu and 30.9% ^{65}Cu.)

4-18. For the conditions of Problem 4-1, determine the activity (Ci) that would exist for ^{64}Cu 26 h after irradiation.
4-19. Derive the equation for activation of a product accounting for source depletion (ignore activation of the product nucleus).
4-20. A 20 g sample of cobalt is irradiated in a power reactor with a flux of 10^{14} neutrons/cm^2 s for 6 y. Calculate (a) the activity of ^{60m}Co immediately upon removal from the reactor and (b) the activity of ^{60}Co 50 h after removal. (Assume no source depletion.)
4-21. Repeat Problem 4-20b assuming source depletion. Explain the change.
4-22. A sample of dirt (or CRUD) is irradiated for 4 h in a beam tube of 10^{12} neutrons/cm^2 s. By counting the ^{56}Mn product it is determined that the disintegration rate is 10,000 d/m. How much manganese is in the sample?
4-23. Measurement of ^{129}I can be done by neutron activation. Describe the nuclear reaction for the technique and recommend an irradiation time to optimize the sensitivity of the procedure using a constant thermal neutron flux.
4-24. An amount of 10 g of HgO is irradiated uniformly in a research reactor at a flux of 10^{12} neutrons/cm^2 s for ten days to produce ^{203}Hg and ^{197}Hg. How much activity of each will be in the sample upon removal from the reactor?
4-25. A target of iridium metal is irradiated for one year to produce ^{192}Ir; however, the product also has a relatively important activation cross-section. Determine (a) an equation for the product activity that accounts for activation of the product and (b) the activity per mg that will be present upon removal from a neutron flux of 10^{14} neutrons/cm^2 s (ignore the production of ^{192m}Ir).
4-26. An amount of 10 g of thallium is irradiated uniformly in a research reactor at a flux of 10^{12} neutrons/cm^2 s for five years to produce ^{204}Tl. How much activity will be in the sample upon removal from the reactor?
4-27. A cyclotron is used to produce 16 MeV protons which are directed at a transparent capsule containing 10 g of nitrogen. If the target is irradiated uniformly with a flux of 10^{10} protons/cm^2 s for 50 min, what is the activity of ^{11}C produced?
4-28. A 1 g sample of common salt, NaCl, is irradiated in a reactor for 30 days at 10^{14} neutrons/cm^2 s. What would be the total activity (in Ci) of each species upon removal from the reactor?

5
Nuclear Fission and its Products

"The Italian navigator has landed in the new world; the natives are very friendly."
December 2, 1942

Many radiation protection considerations deal with the products of fission. A number of materials undergo fission, but the most important ones are ^{235}U, ^{238}U, and ^{239}Pu. Fission occurs when a fissionable atom absorbs a neutron as shown schematically in Figure 5-1.

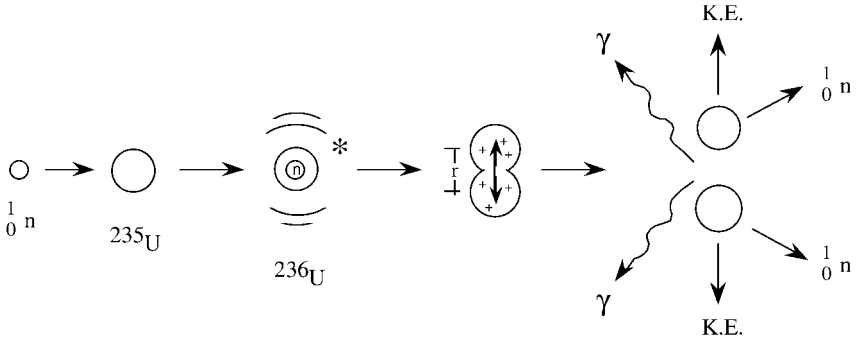

Fig. 5-1 An absorbed neutron in uranium produces an elongated nucleus due to added excitation energy. If the centers of the "halves" reach a separation distance, *r*, fission is likely to occur, which it does 85% of the time in ^{235}U; if not, the nucleus returns to its original shape and the excitation energy is emitted as a gamma photon, which occurs 15% of the time for ^{235}U to yield an atom of ^{236}U.

The liquid drop model developed by Bohr and Wheeler can be used to explain fission. Absorption of a neutron by a heavy nucleus like uranium adds excitation energy that causes it to oscillate, producing an elongation of the nucleus much like that observed in a drop of liquid. If, as shown in Figure 5-1, the elongation causes the asymmetrical "halves" of the dumbbell-shaped drop to separate by a distance *r*, then repulsive forces exerted by the positive charges in each will cause the two parts to separate, or fission.

The energy associated with the critical distance *r* represents a barrier energy E_b that must be overcome for separation to occur. For a neutron added to ^{235}U and

Physics for Radiation Protection, Third Edition. James E. Martin

^{239}Pu, E_b is 5.2 and 4.8 MeV, respectively; for ^{238}U it is 5.7 MeV. Absorption of a thermal neutron in ^{235}U adds 6.55 MeV of excitation energy (see Example 5-1); in ^{239}Pu, 6.4 MeV; and in ^{238}U, only 4.8 MeV. Consequently, ^{235}U and ^{239}Pu fission readily when they absorb thermal neutrons. In contrast, ^{238}U can only fission if the incoming neutron has at least 1.3 MeV of kinetic energy. The amount of excitation energy added by absorbing a neutron is just the Q-value of the reaction, as shown in Example 5-1 when ^{235}U absorbs a thermal neutron.

Example 5-1. Calculate the amount of excitation energy added to a nucleus of ^{235}U by a thermal neutron.
Solution. The excitation energy is just the Q-value of the reaction, or

$$Q = 235.043924\ \text{u} + 1.008665\ \text{u} - 236.045563\ \text{u}$$
$$= 0.007026\ \text{u} \times (931.5\ \text{MeV/u}) = 6.55\ \text{MeV}$$

As shown in Example 5-1, adding a neutron to ^{235}U yields an excited nucleus of ^{236}U which is 6.55 MeV above the ground state of the ^{236}U nucleus. This excitation energy must be relieved; this can occur by emission of a gamma photon, or since the added energy is more than the barrier energy (5.2 MeV) by fission. These are competing processes, but fission is much more likely and occurs 85% of the time. The fissioning nucleus yields energy, high-speed neutrons, prompt gamma rays, and highly charged fission fragments, or fission products as they are more commonly called. All of these components are released almost instantaneously at the moment of fission.

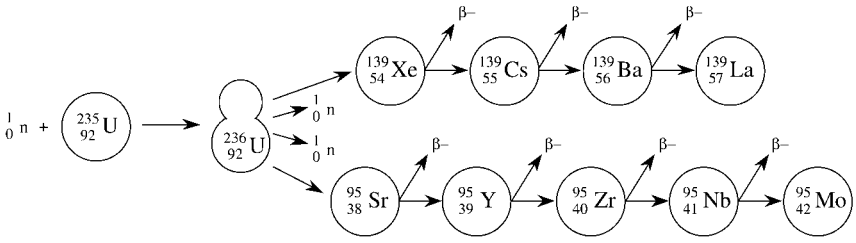

Fig. 5-2 Uranium-235 fission and the series of transformations by beta emission of the fission products to stable end products when mass numbers 95 and 139 are produced.

Uranium, plutonium, and other heavy nuclei are very neutron rich because extra neutrons help to distribute the nuclear force and counteract the repulsive forces exerted by the large number of protons in the nucleus. This excess ratio of neutrons to protons carries over to the fission products. Hence each product that is formed will be extremely neutron rich and will appear quite far from the line of stability. Consequently, these products are very unstable and several beta particles must be emitted to lower the neutron number (and increase the proton number) so that the fission product nucleus can become stable. Several gamma rays are

also emitted during the series of beta particle transformations. Two typical mass chains of the series of radionuclide transformations that occur to yield a stable end product are shown in Figure 5-2. The stable end product eventually formed from each series of transformations will have the same mass number as the product initially formed.

5.1 Fission Energy

The reaction for fissioning ^{235}U into two products plus two neutrons and energy is

$$^{235}_{92}\mathrm{U} + {}^{1}_{0}\mathrm{n} \rightarrow [{}^{236}_{92}\mathrm{U}^*] \rightarrow \mathrm{X} + \mathrm{Y} + 2{}^{1}_{0}\mathrm{n} + \gamma + Q$$

where X and Y are the fission products of the reaction. The ^{235}U nucleus can split in a great many ways, and so it is impossible to say in any given fission reaction just exactly what the fission products will be. One typical split is shown in Figure 5-2 in which the stable end products are ^{95}Mo and ^{139}La. This reaction can be written as

$$^{235}_{92}\mathrm{U} + {}^{1}_{0}\mathrm{n} \rightarrow [{}^{236}_{92}\mathrm{U}^*] \rightarrow {}^{95}_{42}\mathrm{Mo} + {}^{139}_{57}\mathrm{La} + 2{}^{1}_{0}\mathrm{n} + Q$$

And the energy liberated in the reaction is simply the Q-value. The mass difference is 0.21526 u, calculated as follows:

Masses before fission		*Masses after fission*	
^{235}U	235.043923 u	^{95}Mo	94.905841 u
1 n	1.008665 u	^{139}La	138.906348 u
Total	236.052588 u	2 n	2.017330 u
		7 β^-	0.003840 u
		Total	235.837331 u

The energy released per fission is

$$E_{\mathrm{rel}} = 0.21526\ \mathrm{u} \times 931.5\ \mathrm{MeV/u} = 200.5\ \mathrm{MeV}$$

Although this calculation was made for one particular fission of an atom of ^{235}U, it may be regarded as typical. Each fission produces its own distinct mass chain with a slightly different Q-value; however, 200 MeV of energy is released on average for each atom of ^{235}U fissioned. Most (85% or so) of this energy (see Table 5-1) appears as kinetic energy of the fission fragments, and this immediately manifests itself as heat as these heavy, highly charged fission fragments are absorbed in the fuel matrix (the fission product nuclei are ejected with so much energy that they tend to leave their orbital electrons behind; therefore, they are highly charged

particles with about 20–22 units of positive charge which causes them to be absorbed in a few micrometers, producing considerable amounts of heat in the fuel). Part of the remaining energy is released instantaneously by gamma rays and fission neutrons; the rest is released gradually by radioactive transformation of the fission products as they emit beta particles, neutrinos, and gamma rays. The energy values of each of these processes are summarized in Table 5-1.

Table 5-1 Emitted and recoverable energies for fission of ^{235}U.

Form	Emitted energy (MeV)	Recoverable energy (MeV)
Fission fragments	168	168
Fission neutrons	5	5
Fission product decay		
Beta rays	8	8
Gamma rays	7	7
Neutrinos	12	–
Prompt gamma rays	7	7
Capture gamma rays in ^{235}U and ^{238}U	–	3–12[a]
Total	207	198–207

a Not associated with fission.

Prompt gamma rays are emitted from the fissioning nucleus at the instant of fission to relieve some of the excess energy in the highly excited compound nucleus. Their number and energy vary but the average energy is about 7 MeV. They are referred to as prompt gamma rays to distinguish them from the delayed gamma rays emitted by the radioactive fission products, which are usually emitted with energies quite a bit less than those of the prompt gamma rays.

Capture gamma rays are also emitted when neutrons are absorbed in ^{235}U and ^{238}U without producing fission (about 15% of the time in ^{235}U). Even though the capture gamma rays are due to (n,γ) activation of ^{235}U to ^{236}U and not fission, they contribute to the energy that is released and recovered in fission reactors.

Table 5-1 indicates that not all of the energy released in fission can be recovered as heat. The energies of the fission products, the fission product beta particles and gamma rays, the prompt and delayed neutrons, the capture gamma rays, and the prompt gamma rays are usually absorbed and recovered, especially in nuclear reactors. The neutrinos emitted in beta transformations of the radioactive fission products constitute about 12 MeV per fission; however, these escape completely and their energy is irrevocably lost.

It can be shown that complete fission of 1 g of ^{235}U yields about 1 MW of thermal energy which probably contributed to the irresistible temptation for pioneering physicists to produce and collect this abundant source of energy. The modern world has chosen to do this by building nuclear reactors to release fission energy at a controlled rate, and also in nuclear weapons that seek to have large instantaneous releases of fission energy at an uncontrolled but predictable rate.

The release of fission energy is governed by a fundamental set of physical principles that eventually dictate the design and performance of nuclear reactors and other critical assemblies. Radiation protection for these circumstances must also recognize these same principles in the various applications of nuclear fission, applications that range from sustained and controlled chain reactions in nuclear reactors for nuclear research and electricity production to nuclear criticalities for various purposes including nuclear weapons. Radioactive fission products and activation products are byproducts of these reactions, and these represent a number of radiation protection issues for workers, the public, and the environment; nuclear power reactors are particularly challenging because they are designed to operate for 30–40 years.

Fission energy is determined by the fission rate, and reactor thermal power, in watts, is an important parameter for calculating fission product inventories in reactor fuel. Since 1 W is 1 J/s, and each fission yields about 200 MeV, 1 W of reactor power corresponds to a fission rate of

$$\text{Fission rate} = \frac{1\,\text{J/s W}}{(1.6022 \times 10^{-13}\,\text{J/MeV})(200\,\text{MeV/fission})}$$

$$= 3.12 \times 10^{10}\ \text{fissions/s per watt}$$

and, for 1 MW of thermal energy

$$1\ \text{MW} = 3.12 \times 10^{16}\ \text{fissions/s}$$

A common unit of energy production is the megawatt day, which is directly related to the number of fissions that occurred:

$$1\ \text{MW d} = 3.12 \times 10^{16}\ \text{fissions/s MW} \times 86{,}400\ \text{s/d} = 2.696 \times 10^{21}\ \text{fissions}$$

5.2 Physics of Sustained Nuclear Fission

Release of the large quantities of energy available from fissioning uranium (or other fissile materials) depends on sustaining fission reactions once they are begun. This requires careful management of the neutrons released when fission occurs. Fission of ^{235}U yields, on average, 2.44 neutrons per fission, which can be

induced to produce other fissions if certain conditions exist. Achieving and sustaining a controlled chain reaction is governed by the data shown in Figures 5-3 to 5-5 and Table 5-2.

Table 5-2 Neutron cross-sections in ^{235}U and ^{238}U.

Cross-section	^{235}U (b)	^{238}U (b)
σ_f (thermal)	584	0
σ_f (fast)	~1.1	~0.55
σ_γ (thermal)	107	0.05
σ_s (elastic)	9.0	4.55
σ_s (inelastic)		2.10

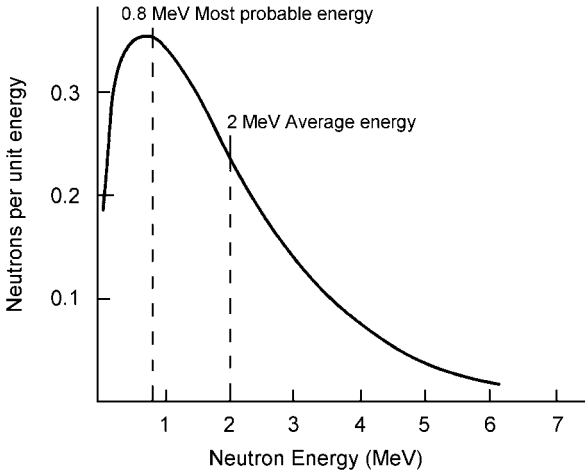

Fig. 5-3 Spectrum of neutron energies released in uranium fission.

As shown in Figure 5-3, most of the neutrons produced in fission have energies of 1–2 MeV, ranging up to about 5 MeV. Therefore, most of the neutrons available for fissioning other ^{235}U atoms are fast neutrons, and these have a fairly low fission cross-section (~1 b). Modern fission reactors incorporate features to slow them down to take advantage of the very high fission cross-section for thermal neutrons in ^{235}U (584 b) as shown in Figure 5-4. Figure 5-4 also shows that fission in ^{238}U, the most abundant isotope of natural uranium at 99.3%, occurs *only* with neutrons above 1.4 MeV, and is effectively a threshold phenomenon with a very low fission cross-section of just 0.55 b. As shown in Table 5-2, a fast neutron striking ^{238}U is more likely to be scattered than absorbed because of significantly higher elastic and inelastic scattering cross-sections (4.55 and 2.1 b versus 0.55 b for

fission); thus, a neutron born fast with enough energy (>1.4 MeV) to induce fission in ^{238}U is much more likely to be scattered than absorbed to produce fission, and only one such interaction will reduce its energy below the fission threshold. Also, once a neutron in uranium is slowed down below the fission threshold of 1.4 MeV it is very likely to be absorbed at an intermediate energy because of the prominent and very high resonance absorption cross-sections in ^{238}U (see Figure 5-5) and lost before it can induce fission in the less abundant (0.72%) but highly fissionable (σ_f = 584 b) ^{235}U. Because of these factors a nuclear chain reaction cannot occur in even a large block of natural uranium. There are enough ^{235}U atoms in natural uranium to sustain a chain reaction if the neutrons can be slowed to thermal energies without losing them by absorption in ^{238}U. In order to have a sustained nuclear chain reaction in natural uranium it is essential to get the neutrons outside of the uranium matrix so they can be slowed down in a good moderator without losing them due to resonance capture in ^{238}U.

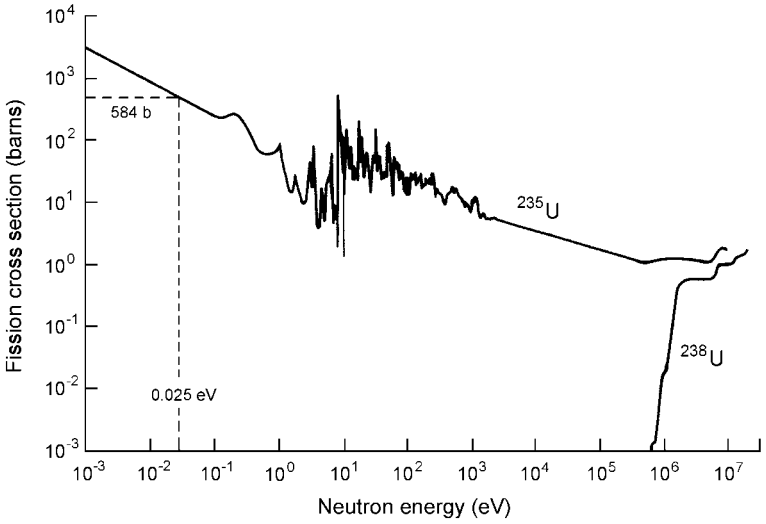

Fig. 5-4 Neutron fission cross-sections for ^{235}U and ^{238}U showing fast fission effect of ^{238}U and thermal fission effect for ^{235}U.

Neutrons of any energy (see Figure 5-4) can cause fission in ^{235}U and resonance is not a problem because it simply enhances σ_f since it is larger than σ_a at resonance energies (this is also true for fissionable ^{239}Pu which is produced by neutron absorption in ^{238}U). If neutrons are moderated to thermal energies with minimal losses the high probability of fission in ^{235}U makes it possible to use natural uranium even though the amount of ^{235}U is small. This is accomplished in a very clever way by surrounding small clusters of natural uranium with a low-Z moderator to slow neutrons down outside the uranium where resonance capture cannot occur. Fermi did so by placing lumps of uranium in a graphite pile, and

the CANDU (Canadian deuterium–uranium) reactor accomplishes the same effect with small-diameter uranium rods surrounded by a deuterium oxide (heavy water) moderator. Ordinary water captures too many neutrons for it to be used as a moderator in a reactor fueled with natural uranium even though H_2O is very effective in slowing neutrons to thermal energies. If H_2O is used it is necessary to enrich the amount of ^{235}U in uranium, but even with enrichment, it is still necessary to surround the uranium fuel with a moderator to slow neutrons to thermal energies.

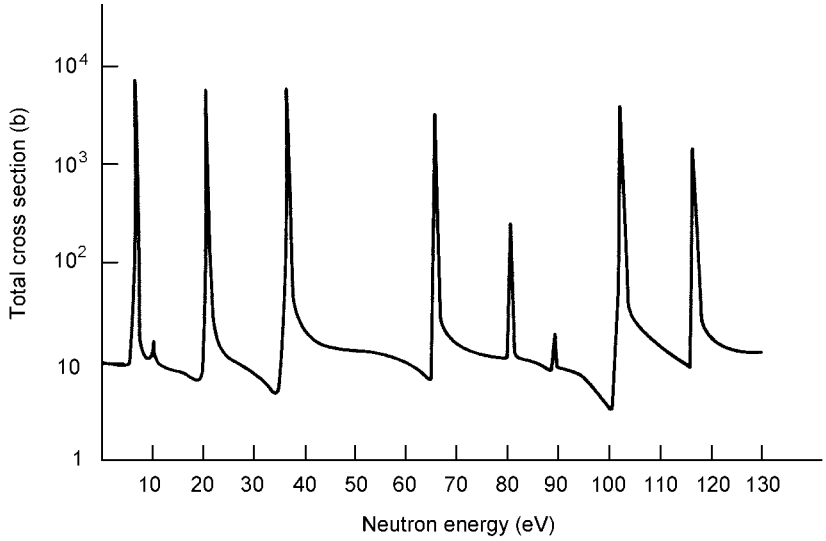

Fig. 5-5 Resonance capture of neutrons in ^{238}U.

The physical design of a nuclear reactor is governed by those factors that influence interactions of neutrons with the fissionable material. Figure 5-6 illustrates the effects of the major scattering and absorption interactions on a population of 100 neutrons for uranium rods interspersed in a moderator material. Figure 5-6 shows the fate of 100 neutrons born fast in one fuel element (at the left) and the average effects of absorption, leakage, and control rods in determining that the right number of neutrons are thermalized in the moderator before they enter the next fuel element (on the right) where they yield a new generation of 101 neutrons, the number required to sustain the chain reaction.

It is first necessary to have a *critical mass* of fissionable material to sustain the fission chain reaction. This is the smallest mass in which fission will continue once started, i.e., where at least one neutron will be absorbed to produce fission from one generation to another. This mass is a function of the configuration involved and is dependent on the leakage fraction and the likelihood of capture without producing fission. The 100 neutrons born in a fuel element will be fast neutrons, and two or so will fission ^{238}U by the fast fission effect (ε) to increase

the number to about 104; however, about 5 of these will be lost due to leakage, characterized as the fast leakage effect ($L_f = 0.95$). A fast neutron that remains in the uranium fuel matrix is much more likely to undergo a scattering interaction with ^{238}U than fission it since the fission cross-section is lower. A scattering reaction will reduce its energy below the fission threshold where resonance capture is very likely. Elastic scattering (4.55 b) has little effect on fast neutrons; however, inelastic scattering (σ = 2.1 b) reduces the neutron energy below the 1.4 MeV threshold in just one collision. The probability of a neutron reaching thermal energy without capture in the abundant ^{238}U atoms is referred to as the resonance escape probability, p; i.e., it escapes resonance capture. A typical value of p is 0.9. Although the neutron number is momentarily increased to 104 by the fast fission effect ε, the fast leakage effect L_f and the resonance escape probability p combine to reduce the number of neutrons that enter the moderator to about 89.

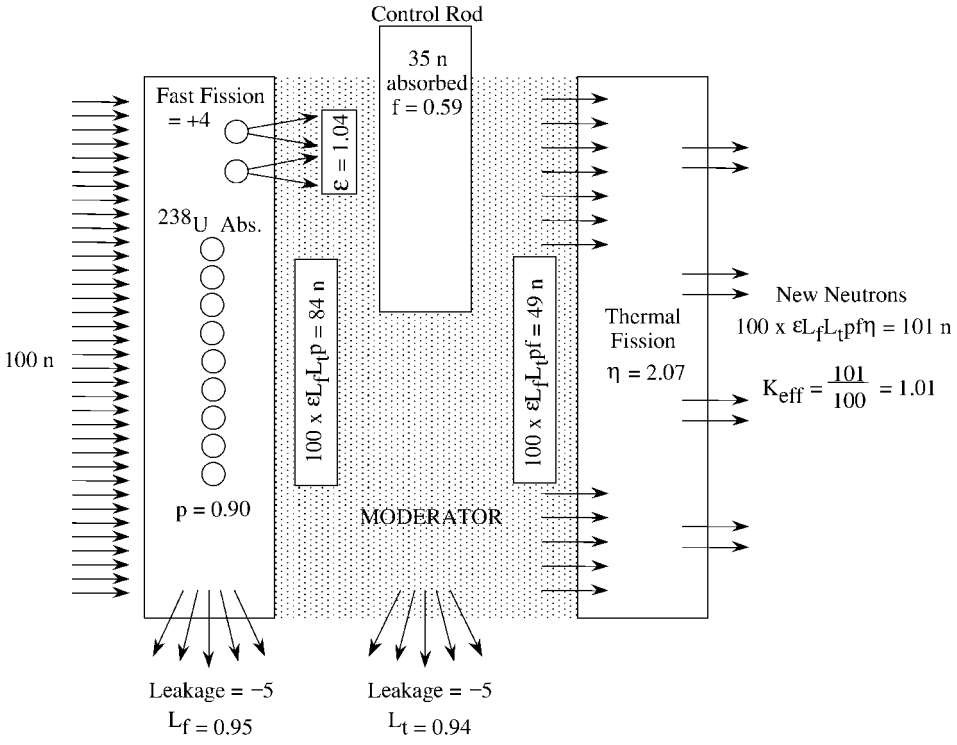

Fig. 5-6 Fate of 100 neutrons born fast in one fuel element (on the left) and average effects of absorption, leakage, and control rods in ensuring that the right number of neutrons (49) are thermalized in the moderator before they enter the next fuel element (at the right) to fission enough atoms to yield a new generation of 101 neutrons, thus sustaining the chain reaction. The six factors are multiplied as $\varepsilon L_f L_t pf\eta$, which is known as the six-factor formula; for a large system, leakage can be ignored and the four-factor formula $\varepsilon pf\eta$ determines the neutron population.

The 89 neutrons that enter the moderator are slowed down to thermal energies; in doing so another 5 or so are lost due to the thermal leakage effect (L_t), and the population of neutrons is reduced to about 84. At this point it is necessary to look ahead. The chain reaction will continue if more than 100 neutrons are available after the next generation of fission; therefore, about 49 are needed to cause thermal fission in the ^{235}U in the adjacent fuel element. Control rods are used to reduce the number to 49 by soaking up about 35 of the available neutrons. About 85% of the remaining 49 neutrons can be relied on to cause fission yielding on average 2.44 neutrons per fission with a thermal utilization factor η of 2.07 ($2.44 \times 0.85 = 2.07$); therefore, the 49 neutrons remaining will produce 101 new neutrons after they fission atoms of ^{235}U in the adjacent fuel rod. This number is the result of multiplying 100 initial neutrons by the six factors just considered:

$$\varepsilon L_f L_t p f \eta \times (100 \text{ neutrons}) = 101 \text{ neutrons}$$

The multiple $\varepsilon L_f L_t p f \eta$ is commonly referred to as the "six-factor formula." If systems are large and leakage of both fast and thermal neutrons is minimal then the factors L_f and L_t are essentially 1.0, and the number of neutrons is given by $\varepsilon p f \eta$, commonly called the "four-factor formula":

$$\varepsilon p f \eta \times 100 \text{ neutrons} = 101 \text{ neutrons}$$

These factors can combine to sustain a chain reaction in natural uranium only if a moderator is used that does not absorb neutrons; if light water is used both as moderator and coolant it is necessary to increase the number of ^{235}U atoms by enrichment to overcome absorption losses.

5.3 Neutron Economy and Reactivity

The various factors illustrated in Figure 5-6 are multiplicative. The six-factor formula accounts for both fast and thermal neutron leakage; the four-factor formula is appropriate when neutron leakage can be considered minimal. In either case, the value of the multiplication formula yields the number of neutrons in a given generation, and the change in the number of neutrons from one generation to the next is defined as the effective reactivity, k_{eff}:

$$k_{eff} = \frac{\text{neutrons in next generation}}{\text{neutrons in first generation}}$$

The chain reaction will be sustained as long as k_{eff} is greater than 1.00, which in turn is determined by the combined effect of the net positive or negative amount of reactivity provided by each parameter.

More than 99% of the neutrons in a reactor are released at the instant of fission. They are called "prompt" neutrons. Others are emitted by radioactive fission fragments as "delayed" neutrons with half-lives ranging between 0.2 and 56 s. They account for 0.65% of the total for ^{235}U (but only 0.21% for ^{239}Pu). Delayed neutrons in an otherwise critical reactor contribute reactivity of 0.0065, which is often rounded to 0.007. These are dominated by 55 s ^{87}Br and 22 s ^{127}I, both of which are fission products. Without these delayed neutrons reactors would be very difficult to control because the necessary adjustments in reactor reactivity cannot be made in the lifetimes (about 10^{-3} s) of the prompt neutrons. A reactor with reactivity above 1.007 is said to be prompt critical, i.e., it does not need to wait for the delayed neutrons to run; between 1.00 and 1.007 it is delayed critical and easily controlled because the delayed neutrons appear to sustain criticality at a much slower rate.

The amount by which k_{eff} exceeds 1.000 is termed the excess reactivity, Δk. If there are n neutrons in the core in one generation, there will then be $n\Delta k$ additional neutrons in the next generation. The growth of neutrons with time is

$$n(t) = n_0 e^{t/T}$$

where T is the reactor period. This is the time required to increase reactor power by e times, i.e., by a factor of 2.718. The reactor period is calculated as

$$T = L/\Delta k$$

where L is the average lifetime of the neutrons released in fission. For prompt neutrons, $L = 0.001$ s; for delayed neutrons it is about 0.082 s.

Example 5-2. If the excess reactivity in a reactor increases by 0.005, what would be the increase in reactor power in 1 s?

Solution. The prompt neutrons would cause the reactor to have a period of $T = 0.001/0.005 = 0.2$ s, and in 1 s the power level (neutron flux) would increase by e^5 or a factor of 150! Thus, control adjustments would need to be made within a fraction of a second which is virtually impossible. The delayed neutrons, however, have an effective lifetime of 0.082 s, and for the same amount of excess reactivity (0.005) the reactor period would be $0.082/0.005 = 17$ s which provides sufficient time to adjust control rods to the desired reactivity level. Clearly, the delayed neutrons are vital for controlling nuclear reactors.

When excess reactivity exceeds 0.0065, the reactor is said to be "prompt critical" and the chain reaction is sustained by the prompt neutrons regardless of any contribution from the delayed neutrons. This causes the reactor period to be very short (as seen in the above example), a condition that must always be avoided. A prompt critical condition led to the explosion of the Chernobyl reactor, and was brought about because it had a net positive reactivity coefficient (since redesigned and made negative by reducing the amount of graphite moderator).

Excess reactivity is commonly expressed in dollars and cents where \$1 is exactly the amount of reactivity required to make the reactor prompt critical (This requires a Δk of 0.0065 for ^{235}U-fueled reactors, which is, of course, the delayed neutron fraction; for a ^{239}Pu-fueled reactor, \$1 of excess reactivity would correspond to a Δk of 0.0021). Thus if a control rod movement inserts \$0.10 of reactivity into a reactor running with $k_{\text{eff}} = 1.0000$, the reactor is one-tenth of the way to becoming prompt critical, which corresponds to $\Delta k = 0.0065/10$ or 0.00065 in a reactor fueled with ^{235}U.

5.4 Nuclear Power Reactors

Electricity is generated when a conductor is passed through a magnetic field, which is usually done by rotating it between the poles of a stationary magnet. The electromotive forces associated with cutting through the magnetic field lines cause the electrons in the conducting wire to flow as a current and to create a potential drop, or voltage. A rotational force is required to move the conductor (actually multiple conductors in a generator) through the magnetic field. This rotational force can be provided by causing a high-pressure gas, usually steam, to expand against the blades of a turbine connected in turn to a shaft that rotates the conductors. In essence, electrical energy is just converted mechanical energy, which in turn is produced from heat when steam is used to induce the energy. These interconnected systems constitute a turbogenerator – it is a key component of all electric power plants regardless of the energy source used to turn it.

A typical turbogenerator driven by superheated high-pressure steam is shown in Figure 5-7. A turbine may have high- and low-pressure stages, and the energy expended in turning the turbine is directly proportional to the pressure drop across it. To enhance this effect a vacuum is induced on the low-pressure side of the turbine such that the largest pressure drop possible occurs. The vacuum on the low-pressure side of the turbine is maintained by a steam-jet air ejector that entrains any gases present, including those that are radioactive, and exhausts them from the steam system.

Energy transfer is also a function of temperature drop; therefore, a condenser is provided to lower the exit temperature of the steam. A coolant loop through the condenser removes residual heat energy from the spent steam thus condensing it back to water, which is then pumped back to the heat source.

The turbogenerator/air ejector/condenser system shown in Figure 5-7 is typical of modern power plants regardless of whether the heat energy is provided by fossil fuels or nuclear fuels. Nuclear reactors of various designs can be and are used to produce the heat energy supplied to the turbogenerator system. The major designs are light water-cooled pressurized water reactors (PWR) and boiling water reactors (BWR); heavy water reactors; liquid metal fast breeder reactors (LMFBR); and high-temperature gas-cooled reactors (HTGR). Each design has particular features as listed in Table 5-3.

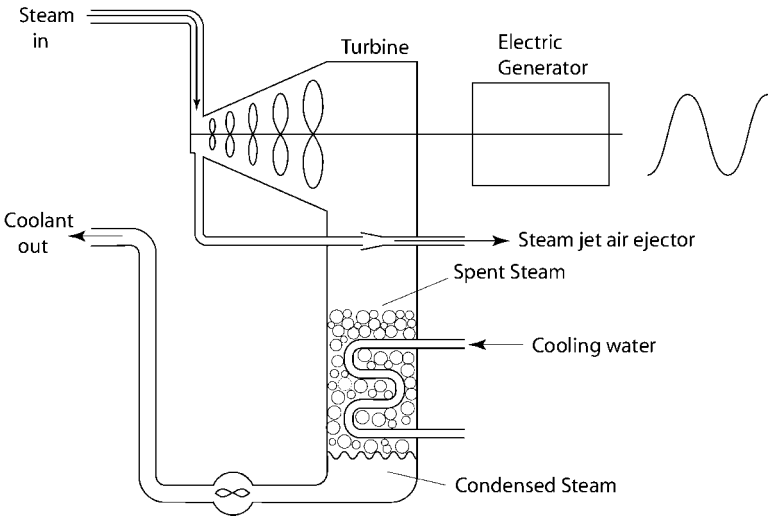

Fig. 5-7 Schematic of a turbogenerator.

Table 5-3 General parameters for different reactor types.

	BWR	PWR	CANDU	HTGR	LMFBR
Fuel	3–4% UO_2	3–4% UO_2	Natural U	HEU[a]	HEU[a]
Moderator	H_2O	H_2O	D_2O	Graphite	None
Coolant	H_2O	H_2O	D_2O	He, CO_2	Na
Inlet temp. (°C)	260	290	266	405	~300
Outlet temp. (°C)	290	325	310	775	500
Pressure (psig)	1100	2200	1500	100–400	~atm
Efficiency (%)	33	32–33	29	~40	~40

a Highly enriched uranium.

5.4.1 Reactor Design: Basic Systems

Nuclear reactors contain a number of basic components as shown in Figure 5-8. Fission energy is released as heat energy in the core of the reactor which contains the fuel, the control rods, the moderator, and a coolant. This dynamic system is enclosed in a vessel with various components and subsystems to enhance fissioning in the fuel, to control its rate, to extract heat energy, and provide protection of materials and persons.

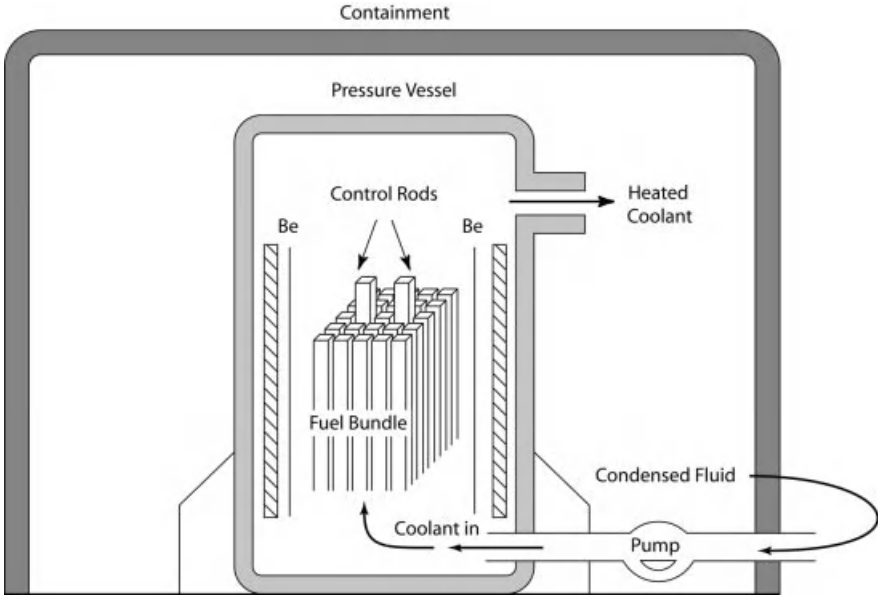

Fig. 5-8 Schematic of major components of a nuclear reactor.

Coolant is required to remove the heat produced by fission and to maintain the fuel well below its melting point. The heat extracted into the coolant is used to produce steam either directly or through a heat exchanger. Coolant is typically water but can be a gas, a liquid metal, or in rare cases another good heat transfer material.

Fuel for light water reactors is UO_2 fabricated into ceramic pellets which have good stability and heat transfer characteristics. These pellets are loaded into zirconium alloy (zircalloy) tubes to make a fuel rod. A typical 1000 MWe plant contains about 50,000 such rods. The rods are thin to promote heat transfer and to minimize effects on neutron flux. The large number of rods and the thin walls of each almost guarantees that some imperfections will exist through which volatile fission products can pass into the circulating coolant stream.

Moderators are usually heavy water, light water, or graphite, and are used to moderate neutrons to thermal energies. A water moderator can also serve to cool the fuel and extract the heat produced. If light water is used the fuel is enriched to 3–4% to overcome neutron absorption by hydrogen in the water. The properties of typical moderators are shown in Table 5-4.

A *reflector* made of a light metal such as beryllium ($Z = 4$) is provided next to the core to reflect neutrons back into the core where they can cause fission. The relatively light atoms in the reflector also help moderate the neutrons. Ordinary water is also a good reflector, and light water-cooled reactors consider the effect of this feature on the neutron population.

Table 5-4 Slowing down properties of moderators.

Moderator	Slowing power (cm^{-1})	Moderating ratio[a]
H_2O	1.28	58
D_2O	0.18	21,000
He (STP)	10^{-5}	45
Beryllium	0.16	130
Graphite	0.065	200

a Moderating ratio is a combination of the minimum number of collisions required to slow neutrons to thermal energies and their loss due to absorption.

Adapted from J. R. Lamarsh **1983**. *Introduction to Nuclear Engineering*, 2nd edn, Addison Wesley, Reading, MA. With permission.

Control rods are movable pieces of cadmium or boron which are used to absorb and stabilize the neutron population. Withdrawing these rods increases the multiplication factor and hence the power level; insertion decreases it.

A *pressure vessel* encloses the entire fission reaction and must be strong enough to withstand the stresses of pressure and heat. A *thermal shield* is provided to absorb radiation and reduce embrittlement of the vessel. A *biological shield* is placed outside the pressure vessel to reduce radiation exposure levels.

A *containment structure* encloses the entire reactor system to prevent potential releases of radioactivity to the environment, especially during incidents when fission products may escape. This may include a primary containment around the steam supply system and a secondary containment associated with the reactor building.

5.5 Light Water Reactors (LWRs)

5.5.1 Pressurized Water Reactor (PWR)

The PWR was one of the first reactors designed to produce power, originally for use in submarines. As indicated in Figure 5-9, water enters the pressure vessel at a temperature of about 290 °C, flows down around the outside of the core where it helps to reflect neutrons back into the core, passes upward through the core where it is heated, and then exits from the vessel with a temperature of about 325 °C. This primary coolant water is maintained at a high pressure (2200 psi) so it will not boil. Any decrease in the coolant volume and the subsequent drop in pressure could vaporize some of the primary coolant, which in turn could lead to fuel damage. PWRs have four coolant pumps, one for each coolant loop, but only one pressurizer for the entire system.

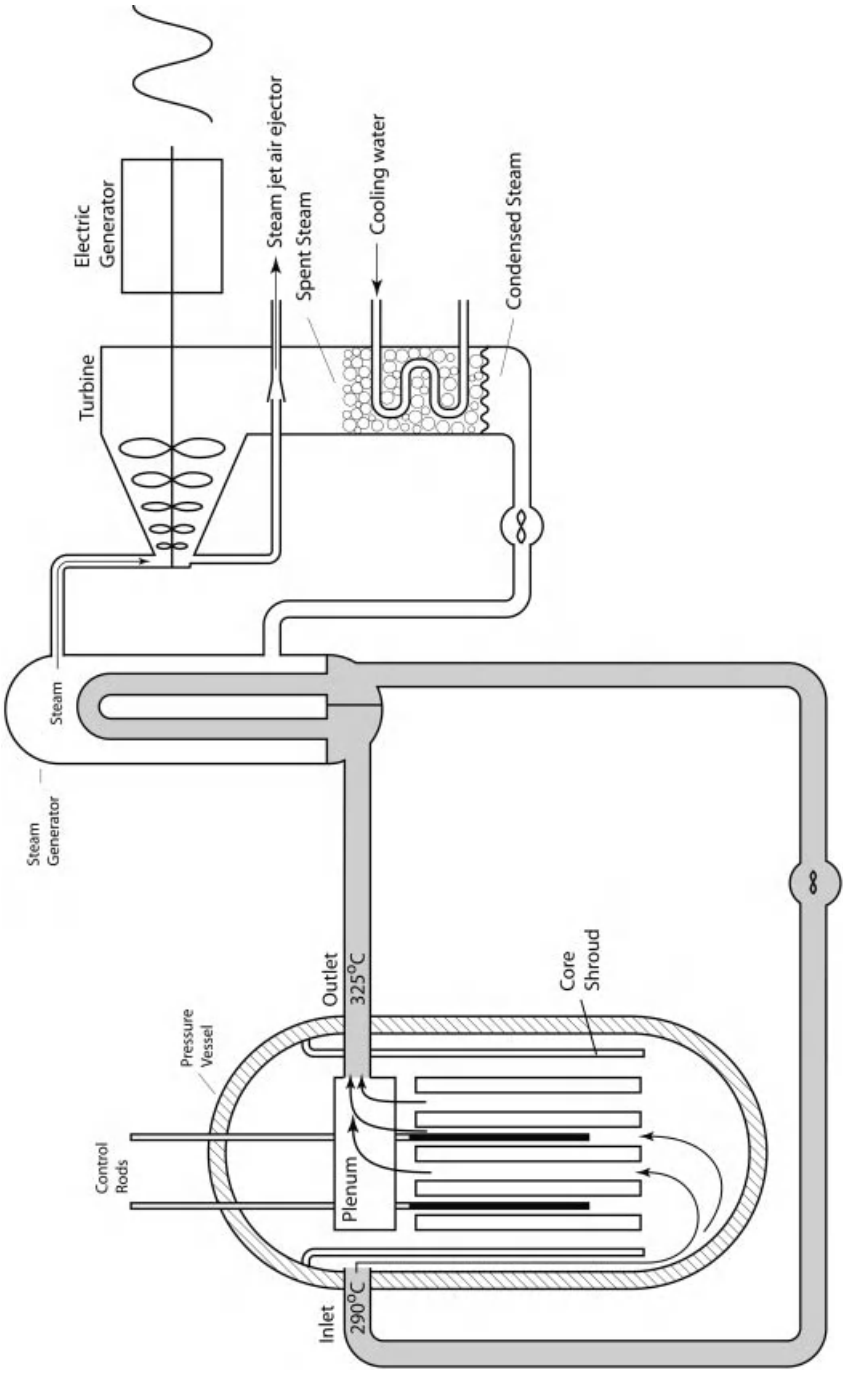

Fig. 5-9 Schematic of a pressurized water reactor.

Since the primary coolant is not allowed to boil, steam for the turbines must be produced in a secondary circuit containing steam generators (also shown in Figure 5-9). The heated coolant water from the reactor enters the steam generator at the bottom and passes upward and then downward through several thousand tubes each in the shape of an inverted U. The outer surfaces of these tubes are in contact with lower-pressure and cooler feed water which extracts heat, boils, and produces steam that is routed to the turbine. The spent steam is condensed and pumped back to the steam generators to complete the secondary circuit.

Where the size of the reactor is an important consideration, as it is in a submarine, the fuel is enriched to over 90% in ^{235}U (often called highly enriched uranium, or HEU) which makes it possible to have a smaller core and pressure vessel. HEU is expensive, however, and for stationary power plants where size is less of an issue, the fuel is only slightly enriched (from 2 to 4%) uranium dioxide, UO_2, which is a black ceramic material with a high melting point of approximately 2800 °C. The UO_2 is in the form of small cylindrical pellets, about 1 cm in diameter and 2 cm long, which are loaded into sealed tubes, usually made of zircalloy. Each tube is about 4 m long and designed to contain the fission products, especially fission product gases, that are released from the pellets during reactor operation. In this context, the fuel tubes are also known as the fuel cladding. Fuel of this type is nominally capable of delivering about 30,000 MW d per metric ton of heavy metal (mostly uranium) before it is replaced, typically after about three years.

The fuel rods are loaded into fuel assemblies and kept apart by various spacers to prevent contact between them. Otherwise, they may overheat and cause fission products to be released. Some of the fuel pellets in the rods may contract slightly at operating temperatures and create void spaces within the fuel tubes. In order to prevent fuel ruptures because of the high pressure of the moderator–coolant the fuel tubes are pressurized with helium. Fission product gases also build up pressure in the tubes, which can be as much as 14 MPa by the time they are replaced.

Control of the PWR is accomplished by the use of control rods, which normally enter the core from the top (see Figure 5-9), and by dissolving a neutron-absorbing chemical shim (usually boric acid) into the coolant water to reduce the multiplication factor. The chemical shim concentration is continually adjusted over the life of a given core to optimize the reactivity balance.

5.5.2 Boiling Water Reactor (BWR)

The BWR uses light water for both coolant and moderator. The water boils within the reactor which produces steam that is routed directly to the turbines, as shown in Figure 5-10. This direct cycle design can be a major advantage because it eliminates the need for a separate heat transfer loop. Since the BWR is a direct cycle plant more heat is absorbed to produce steam than in a PWR in which the heat is extracted as sensible heat, which only changes the temperature of the fluid; therefore, less water is required to extract heat from a BWR for a given power output.

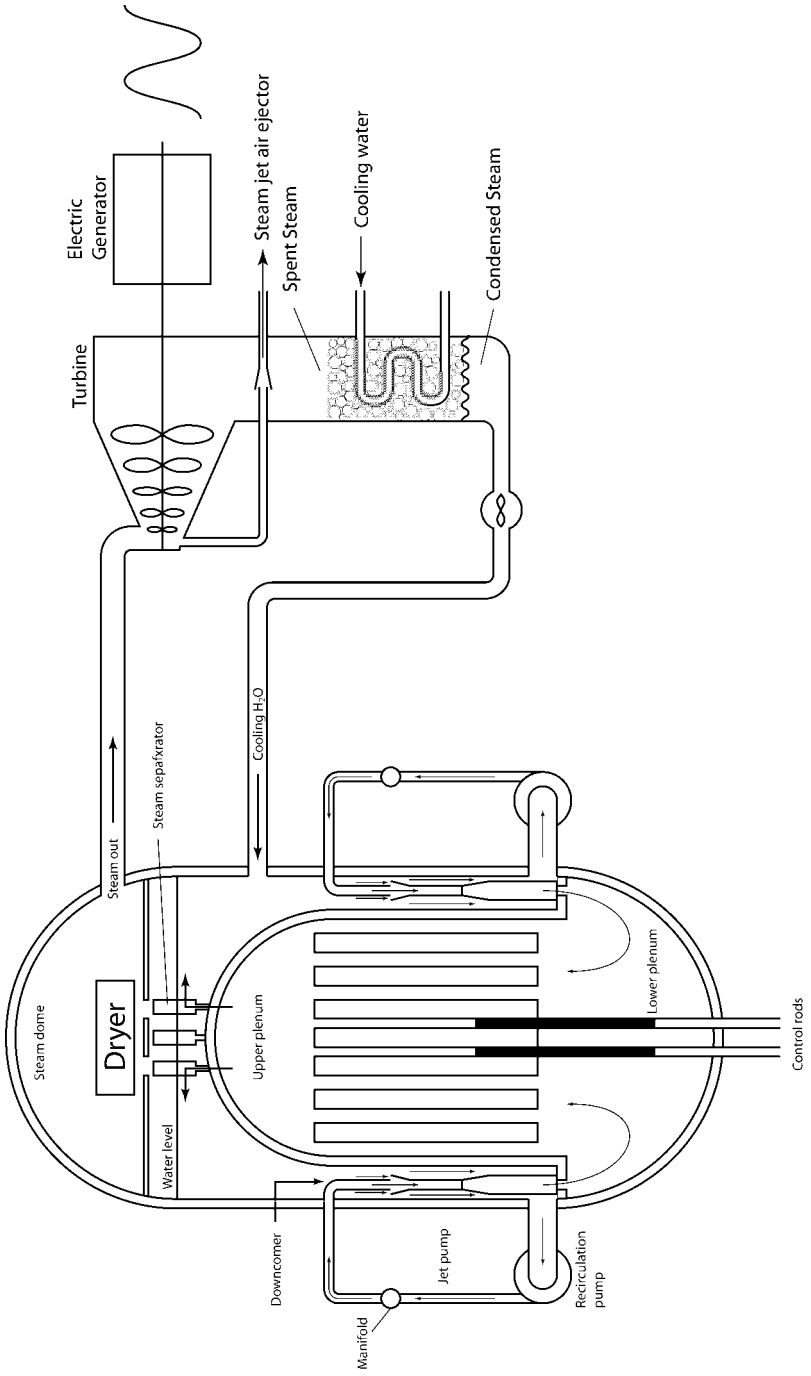

Fig. 5-10 Schematic of a boiling water reactor.

However, the water becomes radioactive in passing through the reactor core which requires shielding of the steam piping, the turbines, the condenser, reheaters, pumps, pipings, etc. The radioactivity entrained in the steam contains radioactive isotopes of xenon, krypton, iodine, and other halogens in addition to disassociated oxygen and hydrogen. These gases will be exhausted by the steam jet air ejector after they pass through the turbine and must be held for decay before release to the environment.

Cooling water in a BWR enters a chamber at the bottom and flows upward through the core. Voids are produced as the water boils, and by the time it reaches the top of the core the coolant is a mixture of steam and liquid water. Uneven formation and behavior of the steam bubbles could make control difficult; however, the boiling is stable if done at high pressures. The turbine requires only steam so the steam–water mixture passes through stream separators and dryers located at the top of the reactor vessel. Residual water from the separators and dryers is mixed with feed water returning from the condenser and is routed back into the core.

Water entering the reactor passes through an annular region between the core shroud and the reactor vessel, known as the downcomer. Pumps withdraw water near the bottom of the downcomer and pump it at high pressure through a pipe manifold to 18 to 24 jet pumps, depending upon the reactor power level. The jet pumps are located within the downcomer, as indicated in Figure 5-10. Water emerges from the nozzle of the jet pumps at high speed which entrains water by suction flow and forces it into the lower plenum of the reactor where it again passes up through the core.

A typical BWR produces saturated steam at about 290 °C and 7 MPa and has an overall efficiency of 33–34%. The pressure in a BWR is approximately half that in a PWR so that thinner pressure vessels can be used, but because the power density (W/cm^3) is smaller, the pressure vessel must be made larger which tends to equalize the costs for each.

The fuel in a BWR is slightly enriched UO_2 pellets in sealed tubes, and the core configuration is similar to that of a PWR. However, BWR control rods are always placed at the bottom (in a PWR they are at the top). Since steam voids exist in the coolant at the upper portion of the core, the value of k_{eff} for a given control rod movement will be higher in the lower part of the core.

5.5.3
Inherent Safety Features of LWRs

Power reactors in the USA are designed such that if k_{eff} is increased to slightly greater than 1.00 and then left alone, the power level does not continue to rise, but instead levels out at some equilibrium value. The power rise creates effects that cause k_{eff} for the core to be held in check as a kind of "internal brake" on the reactor. This "negative reactivity" coefficient is due to the combined effect of changes in three quantities: moderator temperature, steam void fraction, and fuel temperature.

Moderator temperature increases affect reactivity in three major ways. First, a reduction in moderator density results in fewer hydrogen nuclei per unit volume to thermalize neutrons so they travel farther during their lifetime and more are lost due to leakage, so reducing k_{eff}. Second, the decrease in coolant density reduces the number of neutrons lost to absorption by hydrogen and oxygen creating a positive reactivity effect; i.e., k_{eff} increases as does reactor power from this effect. Third, the reduction in moderator density results in neutrons having a higher average energy which in turn increases their absorption in the ^{238}U resonances because they spend more time in the resonance energy range causing a decrease in k_{eff} due to decrease in the resonance escape probability. US reactors are designed such that the negative effects of an increase in temperature outweigh the positive effects; therefore, the overall effect of an increase in moderator temperature is to introduce negative reactivity, and control rods need to be moved to overcome these negative temperature effects.

A slightly positive moderator temperature coefficient may also exist for large PWRs that use chemical shim control (boric acid dissolved in the coolant to supplement the control rods). This effect occurs because an increase in moderator temperature decreases moderator density and effectively removes chemical shim from the core. The effect, if it exists, is most pronounced early in the life of the core, but as the reactor operates, the chemical shim is burned up, and the coefficient becomes more negative. This positive temperature coefficient is small, and PWRs are overall quite stable. In reactor designs that allow temperature increases to produce a net positive effect, k_{eff} would continue to increase with temperature increases and the reactor would be very difficult to control. The Chernobyl reactor that exploded in April 1986 had a positive moderator temperature coefficient which accelerated a change in power level to a runaway condition. (This effect was especially pronounced at low power, which was the condition established for an experimental test, as discussed in Chapter 11.)

Steam voids affect reactivity by reducing the density of the moderator which tends to increase resonance absorption of neutrons by ^{238}U since neutrons are not slowed down. An increase in resonance absorption produces a negative reactivity effect, which tends to shut the reactor down. Steam voids also reduce neutron absorption by hydrogen and oxygen, which is a positive effect, but this is offset by the reduction in moderator density, and the overall effect of steam voids on reactivity is negative. The effect of steam voids in BWRs is pronounced because they can represent 30% or more of the total moderator volume, and at the top of the core can be as high as 70% (these effects are less in a PWR because the reactor pressure prevents boiling). Reactor power can be increased by simply adding cold water to the core to reduce the number of voids; therefore, feedwater valves and pressure control devices offer very effective supplementary means for controlling a reactor.

Fuel temperature increases cause a broadening and flattening of the resonance absorption cross-section resonance in ^{238}U. This is a Doppler effect which causes a neutron "see" a larger target over a wider range of energies, resulting in more resonance capture and a reduction in k_{eff}. The Doppler coefficient is particularly

important because it is a prompt effect that occurs in the fuel itself and immediately follows an increase in reactor power. In contrast, moderator temperature effects and steam void effects are delayed because it takes longer for the heat liberated in fission to be conducted out of the UO_2 and the fuel rods to change the moderator temperature. Consequently, the moderator temperature and void coefficients will be delayed for several seconds should a sudden change in power occur. The fuel temperature coefficient changes instantly, and is the primary mechanism for stopping the effects of fast transients.

5.5.4
Decay Heat in Power Reactors

A reactor can be shut down by interrupting the generation of neutrons; however, as shown in Table 5-2, a significant fraction of the energy released in a nuclear reactor is due to the beta particles and gamma radiation emitted as the highly radioactive fission products undergo radioactive transformation. This energy release occurs after fission, and because the various fission products persist well after reactor shutdown, it is still necessary to continue core cooling even after the fission reaction is safely stopped. For a 3300 MWt reactor (about 1000 MWe), about 200 MWt (or about 7% of the total) is represented by radioactive decay heat at the instant of shutdown. Although the latent heat due to fission product radioactivity falls off rapidly, as shown in Figure 5-11, it is large enough that continued cooling of the reactor core is required for several hours after reactor shutdown to prevent fuel damage.

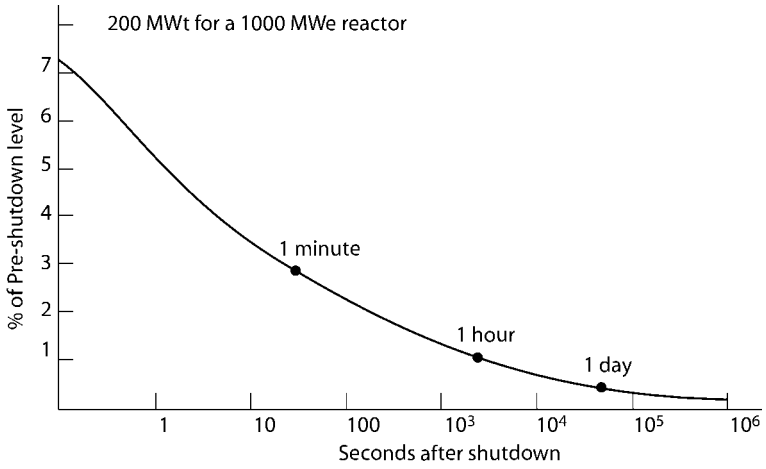

Fig. 5-11 Decay heat in a 1000 MWe power reactor after shutdown.

The accidents at Three Mile Island (TMI) and Fukushima Japan occurred due to loss of the ability to remove the delayed heat. TMI had operated at 2700 MWt for about three months (see Chapter 11) at a coolant temperature of 600 °F and a sys-

tem pressure of 2200 psi. A pressure relief value stuck open which caused the operators to misinterpret a number of circumstances, and they mistakenly shut down the primary coolant pumps. Fukushima also lost core cooling, and the fission products in the fuel continued to produce heat which caused the fuel to overheat and melt releasing fission products to the primary system and the containment. Systems at TMI were designed to contain such an event and releases to the environment were minimal; however, Fukushima systems were overwhelmed.

5.5.5 Uranium Enrichment

Ordinary light water, H_2O, has desirable features for use in reactors. First, it has good heat transfer and is plentiful so that it can be easily replaced if leakage or evaporation occurs. Second, it is very effective in slowing down neutrons, but this good feature is offset by a high capture cross-section for neutrons making it unsuitable as the coolant/moderator for reactors fueled with natural uranium.

Light water can be used as a coolant/moderator if the amount of ^{235}U in the fuel is enriched to about 3–4%. The USA could readily have chosen this option because it had developed gaseous diffusion plants during World War II. The Canadian reactor industry chose not to develop enrichment technology but rather to develop the technology to produce heavy water so that natural uranium could be used as reactor fuel. Since most nuclear utilities in the USA have chosen reactors moderated and cooled by light water, enrichment technology is an important adjunct of the nuclear fuel cycle.

Enrichment technology in the USA uses gaseous diffusion in which uranium hexaflouride (UF_6) gas is pumped through a porous nickel diffusion barrier as shown in Figure 5-12. About 1700 such stages are required to increase the amount of ^{235}U in uranium to 3–5%. Since uranium is not a gas, enrichment of uranium by gaseous diffusion requires its conversion to UF_6 which is easily vaporized if held at an appropriate temperature. UF_6 is a stable compound but is highly reactive with water and corrosive to most common metals. As a consequence, any surface in contact with it must be fabricated from nickel or austenitic stainless steel, and the entire system must be leak tight. Despite these requirements, UF_6 is the only compound of uranium sufficiently volatile to be used in the gaseous diffusion process.

Fortunately, natural fluorine consists of only one isotope, ^{19}F, so that the diffusion rates of UF_6 are due only to the difference in weights of the uranium isotopes. However, the molecular weights of $^{235}UF_6$ and $^{238}UF_6$ are very nearly equal and little separation of the ^{235}U and ^{238}U occurs in passing through a barrier; thus, a sequence of stages is required in which the outputs of each stage become the inputs for two adjoining stages. The gas must be compressed at each stage which produces compression heating which then must be cooled; the requirements for pumping and cooling UF_6 through hundreds of stages make diffusion plants enormous consumers of electricity.

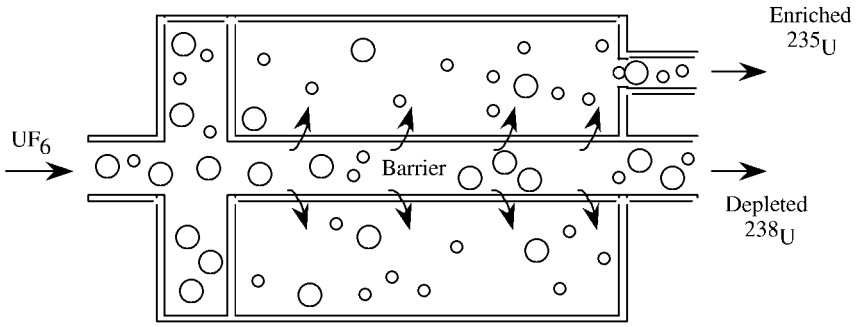

Fig. 5-12 Uranium enrichment process.

5.6
Heavy Water Reactors (HWRs)

An alternative to using ordinary water (H_2O) as the moderator and coolant in a thermal reactor is to choose D_2O, or "heavy" water, for one or both of these purposes. Because heavy water absorbs much fewer neutrons than ordinary water, heavy water-moderated reactors do not require enriched uranium fuel but can be designed to use natural uranium (0.72% ^{235}U). Neutrons must travel farther in heavy water to reach thermal energies so that the separation distance between fuel bundles is greater than in LWRs. This increased separation distance has been used to advantage in the Canadian deuterium–uranium (CANDU) reactor which uses a series of individually cooled fuel channels one bundle thick with the fuel bathed in D_2O moderator. The use of fuel channels allows a CANDU reactor to be refueled on-line without shutting the reactor down.

A typical CANDU reactor and coolant system is shown schematically in Figure 5-13. It has many similarities to a PWR (see Figure 5-9) except that the primary coolant is usually heavy water (each channel could be cooled with light water as long as the moderator between the fuel channels is heavy water; the Japanese Fugen reactor is designed this way). Coolant from a primary pump passes through a distribution header to the individual tubes, goes once through the reactor, through another header to the steam generator, through the U-tube steam generator, and finally back to the primary coolant pump. The heavy water coolant in each fuel tube is maintained at a pressure of about 1500 psi (10 MPa) and in passing through the pressure tubes reaches a temperature of 310 °C (590 °F), which is below the boiling point at that pressure. It is this characteristic that makes a CANDU reactor very similar to a PWR, at least in terms of how the primary coolant is managed.

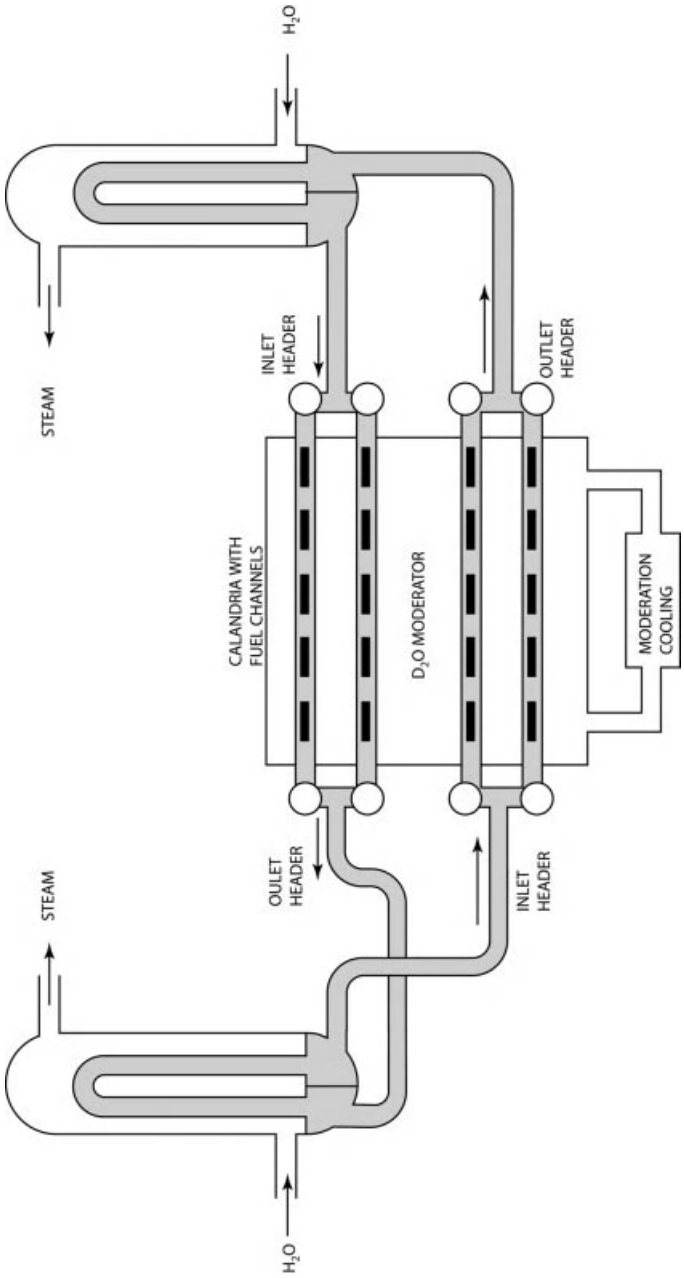

Fig. 5-13 Major components of a CANDU heavy water reactor. Heavy water flows through zircalloy fuel channels immersed in a calandria of heavy water moderator where it is heated under pressure before flowing through a header to steam generators for extraction of the heat energy to produce steam in the light water secondary coolant system.

The secondary coolant is light water which is converted to steam in the steam generators, routed to a turbine, and then condensed and returned to the steam generators as feedwater. There are four steam generators and pumps, a single pressurizer, and pumps that induce a flow rate through the pressurized tubes, which is about 60 million pounds per hour for a 600 MWe CANDU. The overall electrical efficiency of a CANDU system is about 29%, which is significantly lower than that of most LWR commercial nuclear power plants.

Figure 5-13 shows only four of the fuel channels; however, a typical CANDU has hundreds of channels, containing some 4500 fuel bundles arranged end to end. Each fuel bundle is made up of 37 zircalloy-clad fuel pins containing 0.72% $^{235}UO_2$, as shown in Figure 5-14. The fuel channels, which are made of zircalloy and are pressurized, pass horizontally through a lattice of tubes placed in a large calandria containing the heavy water moderator which is maintained near atmospheric pressure; therefore, a large pressure vessel is not required. The calandria is a stainless steel cylinder about 25 feet (7.6 m) in diameter and 25 feet (7.6 m) long with walls that are about 1 in (2.5 cm) thick and end pieces that are about 2 in (5 cm) thick. The moderator picks up some of the reactor heat since it envelopes the pressure tubes where fission occurs. This heat is removed by two pumps and two heat exchangers such that the moderator temperature is about 70 °C (160 °F) when the reactor is running. Representative values of these various parameters are listed in Table 5-3.

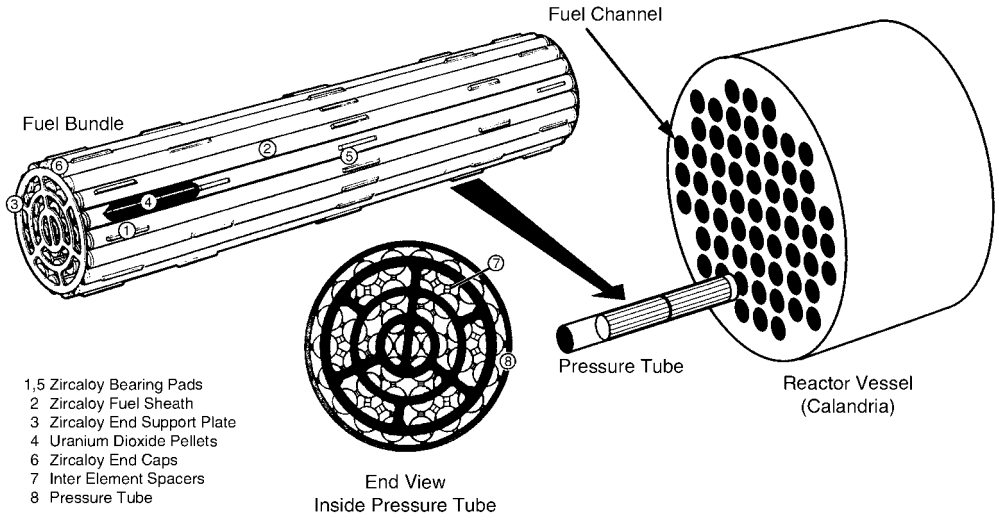

Fig. 5-14 CANDU fuel bundle. (Courtesy of Ontario Hydro.)

Heavy water reactors have two significant advantages over LWRs: very few neutrons are lost due to absorption in the moderator, and the design permits on-line refueling. The heavy water moderator is very efficient since less than 0.1 of the 2.44 neutrons produced per fission are lost to absorption in D_2O versus 0.3 for

H_2O. This efficiency allows burnup of ^{235}U in natural uranium fuel (originally 0.72%) down to about 0.25%. When the fuel is removed from the reactor the ratio of fissile material produced to fissile material destroyed is 0.75 to 0.80. This factor is called the conversion ratio, and since a significant amount of new fissile material is produced, CANDUs are often called converter reactors. The fissile content of the discharged fuel is about 0.5%, about half of which is fissile plutonium; therefore, if the plutonium produced were recycled the overall amount of uranium used could be reduced by about half. Use of natural uranium reduces fuel costs; however, the reactor requires a million pounds of very expensive heavy water, which tends to offset these savings.

Reactivity control in a heavy water reactor is achieved by several systems, including light water zone absorbers, solid control rods, and neutron poisons added to the moderator. Routine on-line control is accomplished by the zone absorbers, which consist of compartments in the core into which light water, a neutron absorber, can be introduced. Cadmium control rods can be dropped under gravity for quick power reduction, but long-term reactivity control and startup reactivity control are usually provided by mixing neutron-absorbing compounds of boron and gadolinium into the moderator. Power distribution across the core can be effectively controlled by the refueling sequence, since each pressure tube can be serviced individually and optimal distributions of fuel can be made.

Continuous refueling can reduce outage times, but its main advantage is in fuel management since refueling can take place as needed and the maximum energy may be extracted from each fuel bundle. Refueling also serves as a reactivity control, increasing the fissile content precisely when and where it is required in the core. On the average, about 15 bundles are replaced per day of operation. Relatively little neutron absorber is necessary during reactor operation because there are no large swings in fissile content or fission product poisons during the fuel cycle. This leads to a higher conversion ratio and, under some conditions, to significantly improved use of the uranium resource.

Since heavy water is expensive (about $100/kg), the reactor building contains systems for the collection, purification, and upgrading of heavy water. A moderator cleanup system uses filters and ion exchange resins to control impurities including adjustments for boron and gadolinium neutron poisons. Two shutdown cooling systems, each consisting of a pump and heat exchanger, are also provided to remove decay heat during reactor shutdown because the primary pumps are isolated along with the steam generators.

5.6.1 HWR Safety Systems

Under abnormal conditions, HWRs can be shut down by gravity drop of the shutdown control rods. Earlier CANDUs were designed to dump the moderator out of the calandria into a large tank to stop the chain reaction, which is a very effective procedure because the reactor cannot run unless the neutrons are slowed down. This capability is no longer used in CANDUs because it is burdensome to replace

the moderator in an optimal condition, and fast injection of gadolinium into the moderator has proved to be just as effective and reliable.

An emergency core cooling system is provided for controlling loss-of-coolant accidents. Should a reactor coolant system rupture, valves close to isolate the intact system, and light water from a storage tank (dousing tank) built into the roof of the containment system is injected into the ruptured system. Heat is initially rejected through the steam generators. As the dousing tank is emptied, water is recovered from the bottom of the reactor building, passed through a heat exchanger, and reinjected into the ruptured system. The moderator in the calandria provides some independent heat capacity, and the moderator heat exchangers remove this heat.

Since CANDU HWRs have many pressure tubes, gross failure of the pressure vessel is highly unlikely. Even if one of the headers is ruptured, the other independent coolant loop would presumably still be intact and it and the moderator could carry off enough heat to prevent gross melting. Consequently, CANDU HWRs are inherently safe designs; however, as a precaution, a prestressed concrete containment structure is provided and operated at negative pressure. A spray system and air coolers are also provided to reduce the building pressure from a loss-of-coolant incident.

It is perhaps significant and reflective of the CANDU design that no major accidents have occurred with CANDU reactors. Since D_2O is used as coolant/moderator considerable amounts of tritium are produced and require management during operation and water handling, and precautions against its environmental release are required. Routine releases of radioactive fission and activation products to the environment are, like their US counterparts, minimal to nonexistent.

5.7 Breeder Reactors

All reactors that contain natural uranium can be thought of as converter reactors because neutron absorption in ^{238}U produces ^{239}Pu, another fissile material. Practically all of the fuel in a light water reactor is ^{238}U, and the conversion of ^{238}U to ^{239}Pu takes place as a matter of normal operation. Plutonium, being a different element, can be chemically separated from the uranium, but this is generally limited to production reactors. After ^{239}Pu has been formed in a reactor, it may absorb a neutron and undergo fission or be transformed into ^{240}Pu. The ^{240}Pu, which is not fissile, may in turn capture another neutron to produce ^{241}Pu, which is fissile. Finally, the ^{241}Pu may undergo fission or be transformed into ^{242}Pu. Thus a reactor contains, in decreasing amounts, the isotopes ^{239}Pu, ^{240}Pu, ^{241}Pu, and ^{242}Pu depending upon the burnup of the fuel (see Figure 5-15).

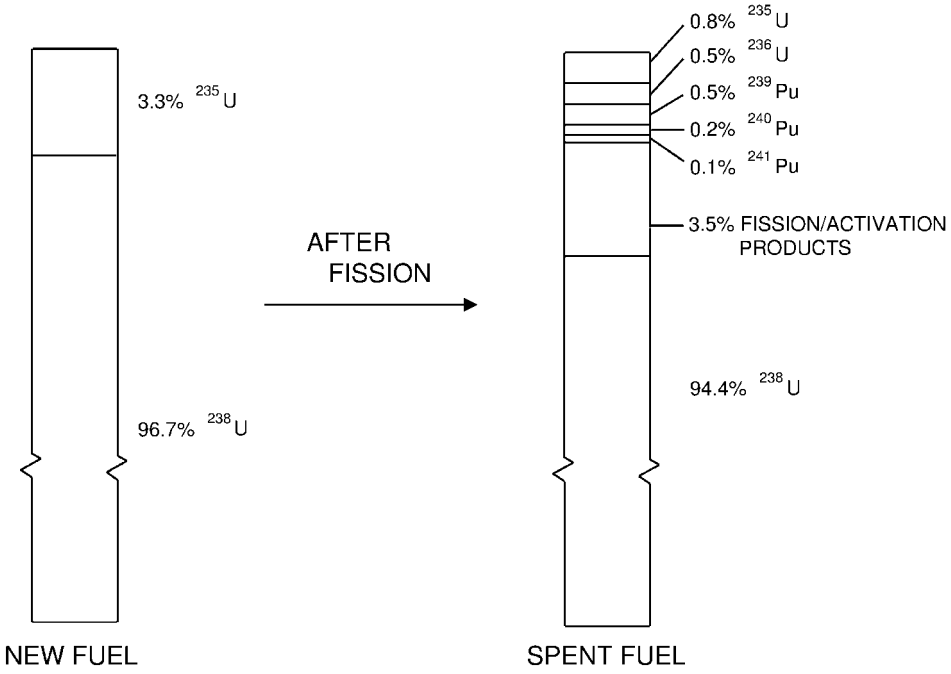

Fig. 5-15 Typical composition (in percent) of ^{235}U and ^{238}U in new fuel and typical composition (in percent) of fission and activation products and ^{236}U from neutron absorption in ^{235}U and plutonium isotopes from neutron absorption in ^{238}U (fuel burnup of 33,000 MW d/MT).

Light water-cooled and moderated reactors strive to minimize the production of ^{239}Pu and other fissile materials because it robs the system of neutrons which need to be made up by enrichment of ^{235}U in the fuel. The phenomenon can, however, be used to advantage to create a "breeder" reactor, one that produces more fissionable material than it consumes. To do so, it is necessary to maintain a population of fast neutrons to enhance resonance capture of neutrons in ^{238}U (see Figure 5-4) to produce (or breed) more atoms of ^{239}Pu. The major design feature of such reactors is to prevent neutrons from slowing down appreciably, and hence they are called "fast" reactors. For these reasons the coolant must not only provide effective heat removal but must also have minimal moderating properties. A gas can be used or a liquid metal such as sodium, and both designs have been developed for breeder reactors. Each has advantages and disadvantages, but the sodium-cooled liquid metal fast breeder reactor has received the most attention; it is based on the reaction

$$^{238}\mathrm{U}(\mathrm{n},\gamma)^{239}\mathrm{U} \underset{23.5\mathrm{m}}{\overset{\beta^-}{\rightarrow}} {}^{239}\mathrm{Np} \underset{2.35\mathrm{d}}{\overset{\beta^-}{\rightarrow}} {}^{239}\mathrm{Pu}$$

It is more difficult to design a reactor that will breed more fissionable material than it consumes than to design one that merely converts ^{238}U to ^{239}Pu because η must be greater than 2.00; i.e., one fission neutron must be absorbed to keep the chain reaction going, and more than one neutron must be absorbed in fertile material to produce a new fissile atom. In actual fact, η must be substantially greater than 2.00 because some neutrons inevitably are absorbed by nonfuel atoms or lost by leakage. The value of η is 2.07 for ^{235}U and 2.14 for ^{239}Pu if neutron energies can be kept above about 100 keV, and it is possible to breed fissile material with these fuels if the bulk of the fissions are induced by fast neutrons. If, however, neutrons are in the thermal energy range, ^{233}U, which has a value of η of 2.3, is the only fuel that can be used for a thermal breeder reactor. ^{233}U is produced by the reaction

$$^{232}\mathrm{Th}(n,\gamma)^{233}\mathrm{Th} \xrightarrow[22.3\mathrm{m}]{\beta^-} {}^{233}\mathrm{Pa} \xrightarrow[27.0\mathrm{d}]{\beta^-} {}^{233}\mathrm{U}$$

Naturally occurring thorium is entirely ^{232}Th, which is not fissionable; therefore, it is used as a target material in a reactor to produce ^{233}U which in turn can be chemically separated from thorium because it is a different element. Production of ^{233}U also occurs readily with fast neutrons.

An experimental breeder reactor was built at Los Alamos in 1946, and its potential impact on future energy supplies was immediately recognized. It was a small plutonium-fueled, mercury-cooled device that operated at a power level of 25 kW. This was followed in 1951 by the Experimental Breeder Reactor-I (EBR-I) and EBR-II a few years later, both located in Idaho. The EBR-I was cooled with a mixture of sodium and potassium (NaK); a secondary loop and a turbine generator were provided and it produced 200 kW of electricity, the world's first nuclear-generated electricity. The EBR-II was designed to recycle fuel, which was successfully demonstrated, but it too has been discontinued.

5.7.1 Liquid Metal Fast Breeder Reactor (LMFBR)

The LMFBR uses uranium–plutonium fuel and has a blanket of natural or depleted uranium, which absorbs neutrons to produce ^{239}Pu. Sodium is used as a coolant and is excellent for this purpose because it has an atomic weight of 23 and does not appreciably slow down neutrons by elastic scattering, although it does moderate neutrons to some extent by inelastic scattering. It is also an excellent heat transfer agent, allowing the LMFBR to be operated at high power density. Sodium is not corrosive so it does not degrade structural materials, and its high boiling point (882 °C at 1 atm) allows high-temperature operation at essentially atmospheric pressure which eliminates the need for a heavy pressure vessel. Steam from a LMFBR plant is delivered superheated to the turbines at about 500 °C and between 16 and 18 MPa. The overall plant efficiency is in the region of 40%.

Sodium also has some undesirable characteristics. It solidifies at room temperature; thus, the entire coolant system must be kept above 98 °C at all times. Sodium reacts violently with water and catches fire when it comes in contact with air; therefore, a cover gas of nitrogen and/or argon is maintained in empty regions above the sodium to reduce the likelihood of fires. Sodium also absorbs neutrons to form 15 h ^{24}Na which emits high-energy gamma rays. Two sodium loops are used to mitigate these potential effects: a primary reactor loop contains the radioactive sodium, and an intermediate sodium loop containing nonradioactive sodium extracts the heat from the primary loop through an intermediate heat exchanger. A third loop containing ordinary water and a steam generator extracts the heat from the secondary loop, producing very hot steam that is routed to a conventional turbogenerator. Since the sodium in the primary loop is radioactive, heavy shielding is provided. The sodium in the secondary loops is not radioactive and neither is the water or steam, so these loops are not shielded. Because of these characteristics, LMFBRs are designed with very tight systems, and they emit far less radiation to the environment than comparable LWRs.

There are two principal LMFBR designs: the loop-type and the pool-type LMFBR. Loop-type LMFBRs generally incorporate the features shown in Figure 5-16. The core and blanket are enclosed in a reactor vessel, not unlike that of an LWR, except that the vessel need not withstand high pressure. The intermediate heat exchanger and all other components of the heat transfer system are located external to the reactor vessel; therefore, those portions of the primary loop outside the reactor vessel must be shielded. A typical 1000 MWe LMFBR plant has three or four primary loops, each of which is connected to a separate intermediate and water–steam loop, and since these separate systems are external to the reactor vessel, inspection, maintenance, and repairs are straightforward. Substantial amounts of shielding are required around the primary loops, which makes these plants rather large and heavily built.

In the pool-type LMFBR, all of these components are immersed in hot, radioactive, and opaque sodium. Pool-type reactor vessels are located at least partially underground, so that only the uppermost portion of the vessel requires heavy shielding. No radioactivity leaves the reactor vessel, so no other component of the plant must be shielded; therefore, one can walk into the reactor room and even across the top of the reactor while it is operating without receiving a significant radiation dose.

Fission heat is extracted by the liquid sodium as it passes upward around each fuel assembly which contain stainless steel fuel pins 6 or 7 mm in diameter that are separated from each other by spacers. The fuel pins contain pellets of a mixture of oxides of plutonium (PuO_2) and uranium (UO_2) with an equivalent enrichment (the percent of the fuel that is plutonium) of 15 and 35%, respectively. The pins in the blanket, which contain only natural or depleted UO_2, are larger in diameter (about 1.5 cm) because they require less cooling than the fuel pins. The fuel and blanket pins can be more tightly packed than in LWRs or HWRs because of the excellent heat transfer properties of sodium.

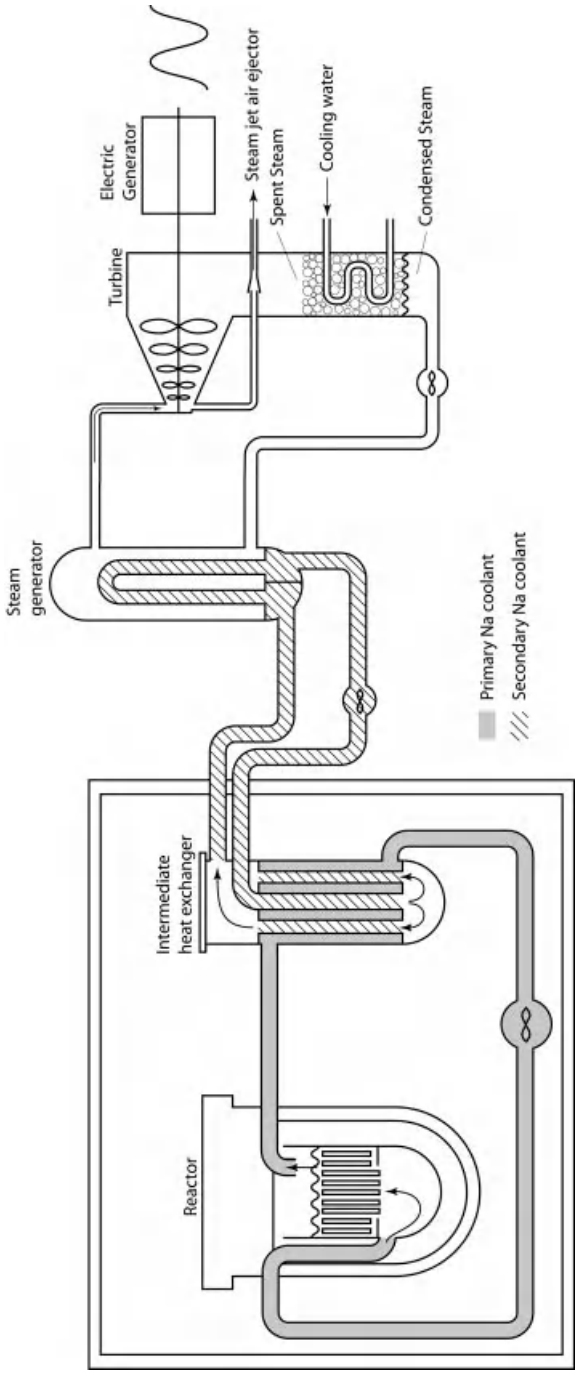

Fig. 5-16 Schematic of a loop-type liquid metal fast breeder reactor.

Modern LMFBRs operate with uranium–plutonium oxide fuel; however, there is considerable interest in uranium–plutonium carbide fuel because with only one atom of carbon per uranium atom it produces less moderation of neutrons than UO_2 that contains two atoms of oxygen. The spectrum of neutrons in a carbide-fueled LMFBR would contain neutrons of somewhat higher energies than an oxide-fueled LMFBR, and as shown in Table 5-5 a higher breeding ratio is possible because η increases with neutron energy.

Table 5-5 Breeding ratios for LMFBRs with oxide or carbide fuel.

	U–^{239}Pu fuel	**Th–^{233}U fuel**
Oxide	1.277	1.041
Carbide	1.421	1.044

The control rods for LMFBRs usually contain boron carbide, although other materials have also been used. At one time it was thought that LMFBRs would be more difficult to control than most thermal reactors, because the fission neutrons do not spend as much time slowing down before inducing further fissions. However, years of operating experience have shown that fast reactors, in fact, are highly stable and easily controlled.

5.8 Gas-cooled Reactors

Carbon, usually in the form of high-purity graphite, is another good moderator because it absorbs few neutrons. With an atomic mass of 12, more collisions are required in graphite than water to slow down neutrons, but like D_2O it has a better "moderator ratio" than light water (see Table 5-4) which allows natural uranium to be used as fuel. The coolant in a carbon-moderated reactor is usually a gas such as air, helium, or carbon dioxide, but water can be used if it is confined to tubes containing the fuel bundles.

A number of carbon dioxide-cooled graphite-moderated reactors have been operated in the UK for electricity production. A 330 MWe high-temperature gas-cooled reactor was built in the USA, but is now shut down, and the larger commercial versions of the design were withdrawn from the market in 1976. A "pebble bed," graphite-moderated gas-cooled reactor is being developed in Germany.

5.8.1
High-temperature Gas Reactor (HTGR)

The HTGR design is shown schematically in Figure 5-17. The reactor is designed to use helium as the coolant since it absorbs essentially no neutrons and can be operated at high temperatures to produce electricity at an efficiency of about 40%, which is unusually high for nuclear power plants. Steam is produced in the HTGR by heating ordinary water through a heat exchanger similar to those used in PWRs, or the HTGR can be operated in a direct cycle with a gas turbine to further improve plant efficiency.

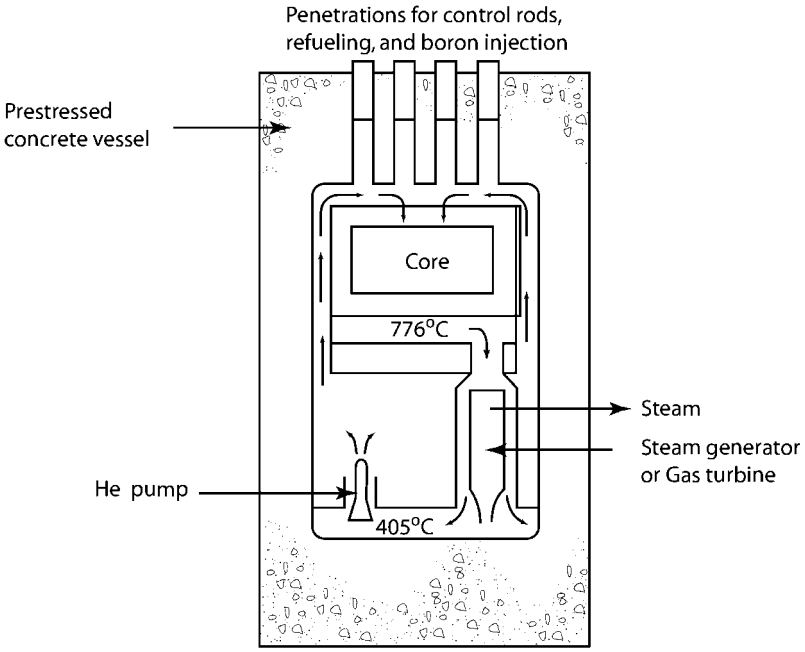

Fig. 5-17 Schematic of a high-temperature gas reactor.

The core of the HTGR does not use metal fuel rods but consists of stacked carbon blocks that enclose small uranium–thorium fuel regions. The fuel/moderator system is also quite distinct since it consists of uranium and thorium pellets fabricated inside carbon moderator blocks. The fuel pellets contain 93% ^{235}U and are coated with pyrolytic carbons and silicon carbide, and the fertile pellets (^{232}Th) are coated with carbon to moderate neutrons to thermal energies so they will be absorbed in thorium to produce fissile ^{233}U. The silicon carbide, because it does not burn, aids in separating the two particle types at reprocessing, which is performed by burning away the carbon. All the fuel elements have holes through which the coolant flows. Refueling occurs around a central stack, which has two vertical control rod penetrations, and six adjacent stacks, which do not have fuel

rod channels. The central stack also has a safety channel designed for rapid injection of boron carbide balls to provide quick shutdown.

The helium coolant in the HTGR is pumped at a pressure of 700 psi (5 MPa) downward through the core where it exits with a temperature of about 776 °C (1430 °F), and is routed to a steam generator. The "cooled" helium exiting the steam generators is purified by filtration, adsorption, and a hydrogen getter to remove particulates and contaminant gases, and is pumped back into the core. Two purification systems are provided; one operates while the other is shut down for decay and regeneration. Regeneration of the purification system produces radioactive gases which are separated and returned to the reactor; it also produces a stable component, which is released to the atmosphere. Liquid wastes are produced only from decontamination operations, and the principal solid wastes are the tritium-contaminated getters from the helium purification systems.

The core, the entire primary coolant system, and other components of the nuclear steam supply system are contained in a prestressed concrete reactor vessel (PCRV) which is a unique feature of the HTGR. The reactor vessel has penetrations for refueling, control rods, and steam pipes. Removal plugs are provided for servicing of steam generators, helium circulators, etc.

Inherent safety features for the HTGR are numerous and substantially different from those of water-cooled reactors. The core provides a massive heat sink and the HTGR fuel particles, with their ceramic coatings, can survive without coolant flow for as much as an hour (decay heat will melt LWR fuel in a minute or so if cooling is lost). The structural strength of the core is provided by the graphite, and this strength increases with temperature. A complete loss of helium cooling is extremely improbable because there are several primary cooling loops, which are largely independent; however, just in case, auxiliary cooling loops are provided to handle the decay heat. Furthermore, helium is always a gas and is nonreactive; therefore, metal–water reactions which could produce explosive hydrogen gas are eliminated.

5.9
Reactor Radioactivity

Reactors are sources of many radioactive materials, many of which exist in offgas systems, effluents, or in waste materials. Large amounts of radioactive fission products and activation products are produced because of the large population of neutrons. These products accumulate in some reactor systems where they can cause radiation exposures of workers, and some of the products are released during routine operations, incidents, or in the form of radioactive wastes. Releases to the environment can, of course, produce radiation exposures of the public depending on various pathways.

Release of radioactivity during routine operations is a complex process governed by reactor type, power level and operating history, fuel performance and overall system cleanliness, and the particular waste processing and cleanup systems

used. The direct cycle design of the BWR introduces any entrained radionuclides into the various cleanup systems whereas these same materials would remain in the primary coolant of the PWR and would be released primarily through steam generator leaks. These features are reflected in the capacities and designs of auxiliary systems for the two reactor types. The general patterns of environmental releases for BWRs and PWRs and the influence of the various elements of each design are shown schematically in Figure 5-18.

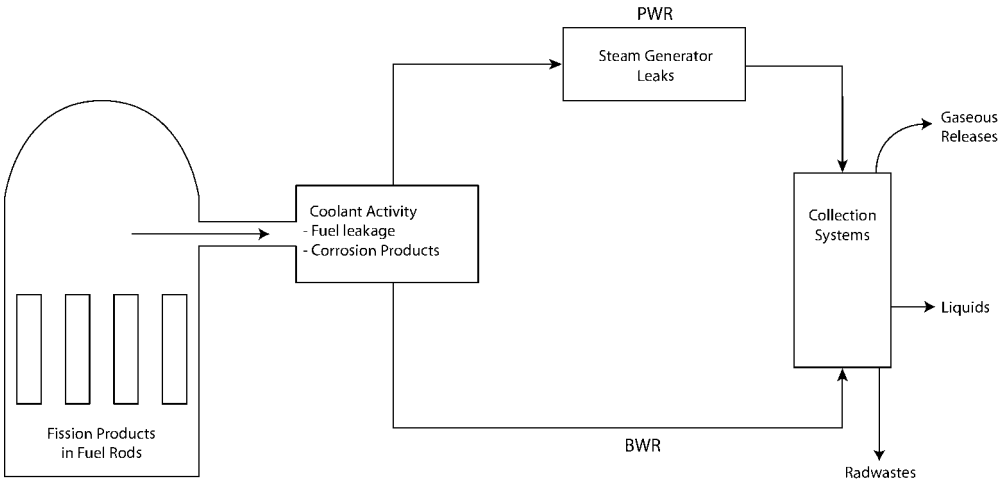

Fig. 5-18 Environmental release pathways for radioactive fission and activation products produced in pressurized water and boiling water reactors.

5.9.1 Fuel Cladding

The fuel in light water reactors is the first and perhaps the most important barrier to release of fission products. Enriched UO_2 is fabricated into ceramic pellets that have good stability and heat transfer characteristics. These ceramic pellets are loaded into fuel rods of zircalloy tubing which are welded at each end, as shown in Figure 5-19. As fissioning proceeds, gaseous and volatile fission products migrate slowly through the ceramic fuel matrix into the gap between the pellets and the zircalloy tube walls. As more and more atoms of these products are produced, the gap activity builds up and generates considerable pressure which may drive radioactive atoms through any imperfections in the zircalloy cladding. The rods are thin to promote heat transfer and minimize effects on neutron flux, and because of this and the large number some imperfections are to be expected that may result in leakage of volatile fission products into the passing coolant. Fuel manufacture is subjected to intense quality control to minimize such leakage.

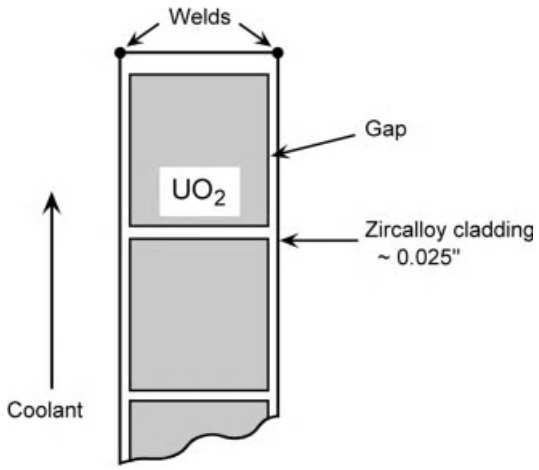

Fig. 5-19 UO_2 fuel pellet in zircalloy cladding.

Fuel cladding is the major barrier to eventual release of fission products. Zircalloy cladding thickness is quite thin at 0.024–0.034 in (0.61–0.81 mm) and receives considerable stress especially from gaseous products. Most reactors have cleanup systems designed to tolerate releases of 0.25–1% of the volatile and gaseous radioactivity into the coolant from such flaws. If fuel flaws exceed these design considerations, it is necessary to reduce power or refuel to deal with the fission products that may be circulating in the reactor or perhaps released in various effluents. This performance specification provides a good starting place for estimating fission product release.

5.9.2 Radioactive Products of Fission

Thermal neutron fission of ^{235}U yields over 60 primary fission products with mass numbers from 72 to 160. Being neutron rich, these products undergo radioactive transformation by emission of negatively charged beta particles, and several such transformations can occur for each atom formed before a product of fission reaches a stable end product. As shown in Figure 5-20, an excerpt from the chart of the nuclides for mass numbers 94, 95, 139, and 140, the products of fission are formed far from the line of their stable endpoints and several beta transformations are necessary for them to become stable. The fission product sequences in Figure 5-20 represent chains that can be represented by the reactions

$$^{235}_{92}\mathrm{U} + {}^{1}_{0}\mathrm{n} \rightarrow [{}^{236}_{92}\mathrm{U}^{*}] \rightarrow {}^{94}_{40}\mathrm{Zr} + {}^{140}_{58}\mathrm{Ce} + 2{}^{1}_{0}\mathrm{n} + 6{}^{0}_{-1}\beta^{-} + Q$$

and

$$^{235}_{92}\mathrm{U} + {}^{1}_{0}\mathrm{n} \rightarrow [{}^{236}_{92}\mathrm{U}^{*}] \rightarrow {}^{95}_{42}\mathrm{Mo} + {}^{139}_{57}\mathrm{La} + 2{}^{1}_{0}\mathrm{n} + 7{}^{0}_{-1}\beta^{-} + Q$$

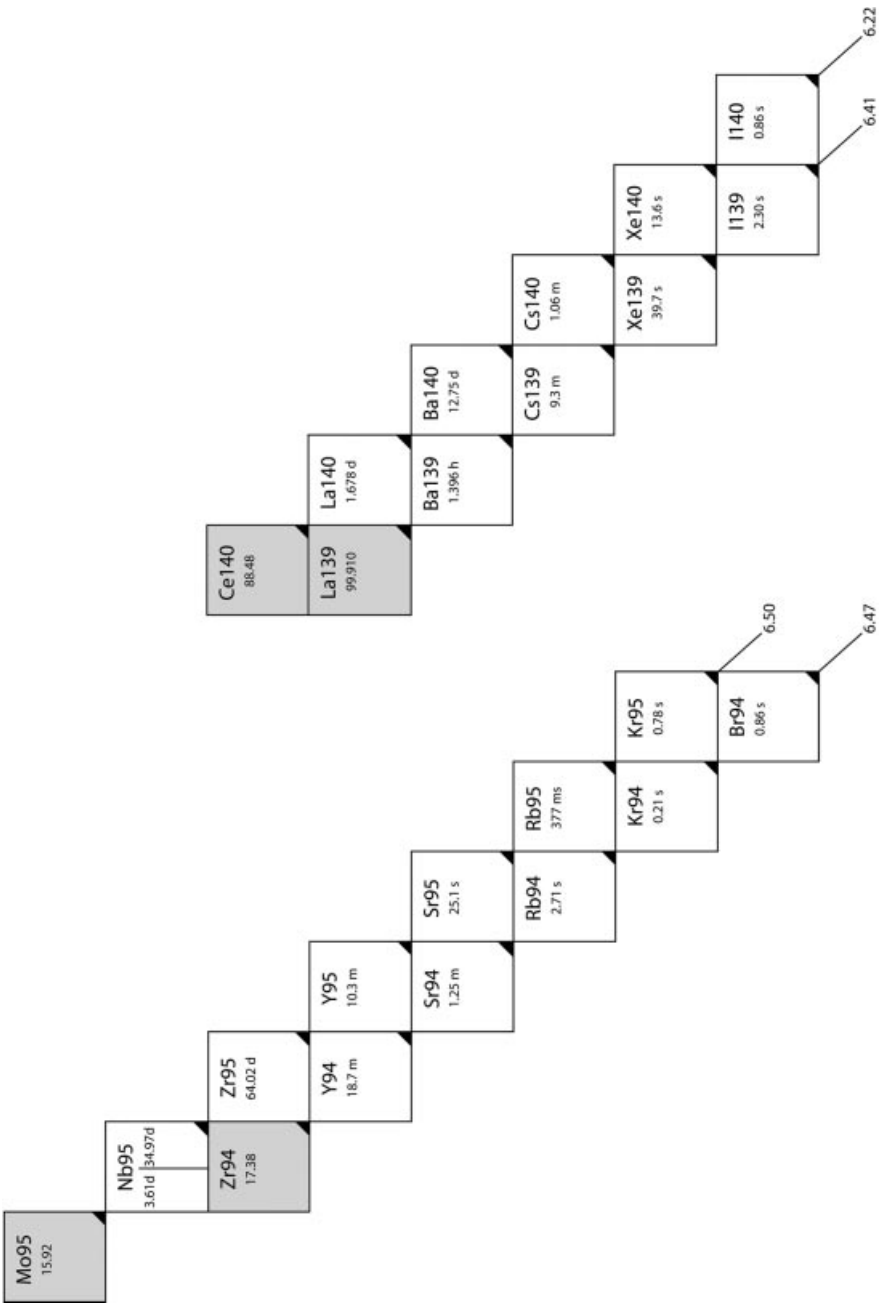

Fig. 5-20 Excerpt from the chart of the nuclides for formation of fission products with masses 94, 95, 139, and 140 through a series of elements that transform by negative beta particle emission. Percent cumulative fission yields for the stable endpoints of the mass chain are shown by the numbers at each diagonal (e.g., 6.47% for mass number 94).

The total fission product yields for each of the stable end products are shown at the beginning of each diagonal and represent the sum of the independent fission yields of each element in the fission product chain. Since there are some 88 fission product chains and since each has numerous beta transformations, there are well over 1200 different products formed from fission of ^{235}U, ^{239}Pu, and other fissionable elements.

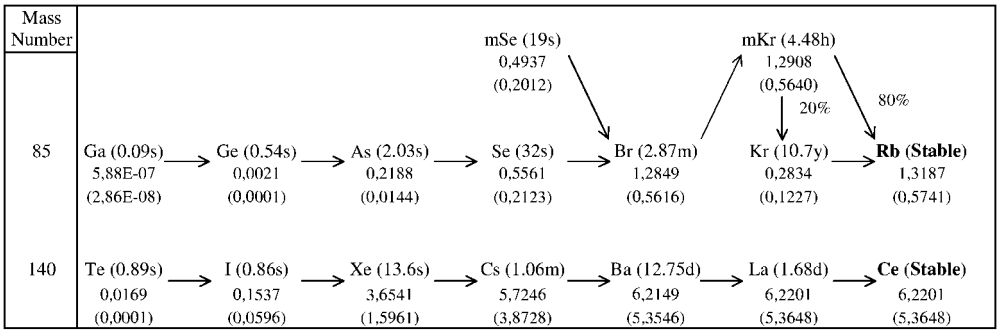

Fig. 5-21 Fission product chains for masses 85 and 140.

The mass number for any given fission product chain remains the same even though the element changes, as shown in Figure 5-21 for mass numbers 85 and 140. The formation of ^{85}Kr, which is perhaps of most importance in the chain for mass number 85, is typical of many of the important fission product radionuclides encountered in radiation protection in that it is not formed directly, but is the product of several precursors. A similar situation exists for mass number 140 for which ^{140}Ba and ^{140}La are of most interest. Most fission products of interest to radiation protection are the products of precursor radionuclides that are formed directly with their own independent fission yield or are the transformation products of such products (^{90}Sr, ^{131}I, ^{137}Cs, etc.).

The fission yield of a given mass number is expressed as a percentage of the fissions that occur as shown in Figure 5-22 for ^{235}U and ^{239}Pu. Figure 5-22 also shows that most fission is asymmetrical and that the masses of the major fission products fall into two broad groups, a "light" group, dominated by mass numbers from 80 to 110, and a "heavy" group, with mass numbers from 130 to 150. The most likely mass numbers produced in fission are products with mass numbers of 95 and 134, which occur with a percentage yield of about 6.5% and 7.87%, respectively. The highest fission yield is for mass number 134 at 7.87%.

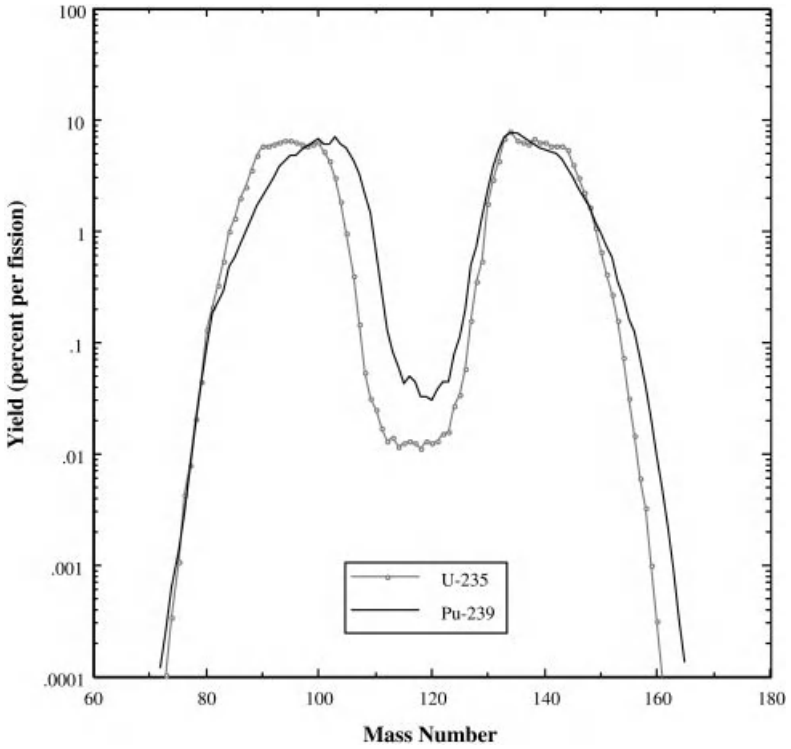

Fig. 5-22 Total fission product yields for each fission product mass number due to thermal fission of ^{235}U and ^{239}Pu.

The mass number for any given fission product chain remains the same even though the element changes, as shown in Figure 5-21 for mass numbers 85 and 140. The formation of ^{85}Kr, which is perhaps of most importance in the chain for mass number 85, is typical of many of the important fission product radionuclides encountered in radiation protection in that it is not formed directly, but is the product of several precursors. A similar situation exists for mass number 140 for which ^{140}Ba and ^{140}La are of most interest. Most fission products of interest to radiation protection are the products of precursor radionuclides that are formed directly with their own independent fission yield or are the transformation products of such products (^{90}Sr, ^{131}I, ^{137}Cs, etc.).

The fission yield data in Figure 5-20 are total yields for each mass number but no information is gained on how a given fission product is formed nor its independent or cumulative yield. Such information is, however, provided in a detailed fission product mass chain as shown in Figure 5-21 for mass numbers 85 and 140. Similar data are provided in Appendix C for all the fission product chains produced by thermal fission of ^{235}U and ^{239}Pu (cumulative fission yields shown in parentheses). Such information is quite useful for determining fission product inventories.

The fission yields for each element in a mass chain are given in cumulative percent yield. It is important to note that each yield value (given in %) may contain a portion due to formation by its own independent yield, a value that can be obtained by subtracting the cumulative yield of the most immediate precursor. If precursors are short lived, as is often the case, the cumulative yield data for the isotope of interest can be used directly in calculations of fission product inventories, but if they are not, it is necessary to consider the independent formation of the element of interest and any precursors that are important in its formation, and to then account for their buildup and removal by radioactive transformation or other processes (see Example 5-3).

5.9.3 Production of Individual Fission Products

The number of atoms of any given fission product, N_i, formed from fission of fissionable nuclei (^{235}U, ^{239}Pu, ^{233}U, etc.) can be readily determined from the total number of fissions (or fission rate) and the fission yield, Y_i, of the particular product:

$$N_i = \text{number of fissions} \times Y_i$$

where Y_i is the fractional yield of atoms of species i that are formed. Tabulations of Y_i account for the fact that two new atoms are formed from each atom that fissions, i.e., the total of all possible modes of fission is 200% (fission of 100 ^{235}U atoms yields 200 fission products). Since Y_i is usually listed as a percentage, it is necessary to convert it to a fractional value when calculating the number of fission product atoms. It is also necessary to account for removal of atoms of N_i by radioactive transformation or activation in determining the inventory of atoms of N_i at any given time.

The rate of change of the number of atoms of fission product, N_i, in a nuclear reactor of power level P (in MWt) is

$$\frac{dN_i}{dt} = (\text{amount produced}) - (\text{amount removed})$$

$$= 3.12 \times 10^{16}\ \text{fissions/s MW} \times P\ (\text{MW}) \times Y_i - \lambda_i N_i - \sigma_i \phi N_i$$

For the case where $\sigma_i \approx 0$, and assuming $N_i = 0$ at $t = 0$, the number of atoms N_i at any time t after operation begins for a sustained power level P (in MWt) is

$$N_i(t) = \frac{3.12 \times 10^{16} P Y_i}{\lambda_i}(1 - e^{-\lambda_i t})\text{atoms}$$

and since activity $= \lambda_i N_i$, the activity (or transformation rate) of fission product i is

$$A_i(t) = 3.12 \times 10^{16} P Y_i (1 - e^{-\lambda_i t})\text{t/s}$$

or

$$A_i(t) = 8.43 \times 10^5 PY_i(1 - e^{-\lambda_i t})\text{Ci}$$

where $A_i(t)$ = activity of fission product i at t; P = power level in MWt; Y_i = fractional yield of fission product i; λ_i = disintegration constant of fission product i; and t = time after reactor startup (operating time).

Example 5-3. Calculate the number of curies of ^{131}I in a 3000 MWt reactor fueled with ^{235}U at 8 days after startup.
Solution. From Appendix C, the cumulative fission yield of ^{131}I is 0.029 (2.9%). By assuming that all precursors have reached equilibrium with ^{131}I, the activity of ^{131}I at 8 days is

$$\text{A} = (^{131}\text{I})\ 8.43 \times 10^5 \times 3000 \times 0.029(1 - e^{-(\ln 2/8\,\text{d}) \times 8\,\text{d}}) = 3.67 \times 10^7\ \text{Ci}$$

As shown in Example 5-3, it is relatively straightforward to determine the amount of a fission product if it can be assumed that all the precursors are short compared to the reactor operating time. When this is the case the cumulative fission yield for the nuclide of interest can be used; however, this is not always the case, as illustrated for ^{140}La in the chain for mass number 140. Lanthanum-140 ($T_{1/2}$ = 40.28 h) is produced solely by ingrowth due to radioactive transformation of ^{140}Ba ($T_{1/2}$ = 12.76 d) which has a cumulative fission yield of 6.3%. In most cases, the short-lived precursors of ^{140}Ba can be ignored and the ^{140}Ba inventory calculated from the cumulative fission yield; however, the formation of ^{140}La must consider not only its formation from ^{140}Ba but also its removal by radioactive transformation. The general case for formation of N_2 from the transformation of N_1 which is also being formed and removed with time is

$$\frac{dN_2}{dt} = \lambda_1 N_1 - \lambda_2 N_2$$

and since N_1 atoms are produced at a rate of

$$\frac{3.12 \times 10^{16} PY_i}{\lambda_i}(1 - e^{-\lambda_1 t})$$

then

$$\frac{dN_2}{dt} + \lambda_2 N_2 = 3.12 \times 10^{16} PY_i(1 - e^{-\lambda_1 t})$$

which can be converted to a form for direct integration by the integrating factor $e^{\lambda_2 t}$, and solved to yield

$$N_2 = \frac{3.12 \times 10^{16} PY_i}{\lambda_2}(1 - e^{-\lambda_2 t}) + \frac{3.12 \times 10^{16} PY_i}{\lambda_2 - \lambda_1}(e^{-\lambda_2 t} - e^{-\lambda_1 t})$$

An almost exact solution for fission product formation from a relatively long-lived fission product parent is to assume that the product and all of its precursor radionuclides are in equilibrium such that the production of the product is at a steady state. In this case, the activity of the shorter-lived product will be the same as the activity of the parent while both are in the reactor and the reactor is still running. If both are removed from the reactor at the same time (e.g., in a waste product or spent fuel), the number of product atoms at a time t_r after removal is

$$N_2 = \frac{N_1^0}{\lambda_2}(e^{-\lambda_1 t_r} - e^{-\lambda_2 t_r}) + N_2^0 e^{-\lambda_2 t_r}$$

where $N_1{}^0 = 3.12 \times 10^{16} PY_i/\lambda$ (the saturation value of the number of atoms of N_i) and $N_2{}^0$ are stated at the time of shutdown. The activity corresponding to atoms of N_2 is obtained by multiplying by λ_2.

5.9.4 Fission Products in Spent Fuel

Most nuclear power plants manage the fuel such that it lasts about three years and produces from 25,000 to 35,000 MW d of energy per ton of fuel. This is referred to as fuel burnup. Other reactors can have shorter or longer burnup periods and different burnup values, and future research is expected to develop fuels with burnups well above 50,000 MW d per ton of fuel.

Since the total energy produced is directly related to the number of fissions that occurred, there is a direct relationship between fuel burnup and the inventory of radionuclides in the fuel elements. Since 1 MW d of energy corresponds to 2.7×10^{21} fissions, the activity of relatively long-lived products in fuel can be readily determined when the burnup is known, as shown in Example 5-4.

Example 5-4. A fuel element is removed from a university research reactor when it reaches a burnup of 10 MW d. Determine the inventory of ^{90}Sr in such a fuel element if it has been in the reactor for about 1 y by (a) fuel burnup and (b) average power level.

Solution. (a) At 10 MW d of burnup, 2.7×10^{22} fissions will have occurred. The approximate number of atoms of ^{90}Sr (ignoring all precursors) can be determined based on the number of fissions since the 1 y period of operation is small compared to the half life of ^{90}Sr ($T_{1/2} = 28.79$ y); i.e., the removal of ^{90}Sr atoms during the year is relatively small. On this basis, then

$$\text{Atoms of } {}^{90}\text{Sr} = 2.7 \times 10^{22} \text{ fissions} \times 0.058 \text{ atoms } {}^{90}\text{Sr/fission}$$
$$= 1.57 \times 10^{21} \text{ atoms}$$

$$\text{Activity} = \lambda N = (\ln 2/28.79 \text{ y} \times 3.1558 \times 10^7 \text{ s/y}) \times 1.57 \times 10^{21} \text{ atoms}$$
$$= 1.197 \times 10^{12} \text{ d/s} = 32.35 \text{ Ci}$$

(b) The effect of both buildup and radioactive removal on the ^{90}Sr activity can be considered by determining the average power level over the 1 y period and calculating the activity in the usual way based on power level. In this case the average power level would be 10 MW d/365 d = 0.0274 MW and the activity of ^{90}Sr is

$$A(^{90}\text{Sr}) = 8.43 \times 10^5 P Y_i (1 - e^{-\lambda_1 t})$$

$$= 8.43 \times 10^5 (0.0274)(0.058)(1 - e^{-(\ln 2 \times 1)/28.19}) = 31.87 \text{ Ci}$$

which is essentially the same as in (a) because radioactive transformation of long-lived ^{90}Sr is minor over the period of operation.

For shorter-lived fission products in which removal by radioactive transformation is significant, it is necessary to determine the average power level over the period of fuel burnup (as shown in part (b) of Example 5-4) to calculate the fission product inventory. This approach is somewhat more exact even for fission products with half-lives considerably longer than the burnup time, but the approximation is more straightforward for most long-lived products ($T_{1/2}$ > 10 y or so) and provides satisfactory accuracy for most circumstances (see Problems 5–9 and 5–10).

5.9.5 Fission Product Poisons

Some of the fission fragments produced in fission and their progeny have substantial neutron absorption cross-sections, which can have a significant effect on the multiplication factor k_{eff}. Xenon-135 ($\sigma_a = 2.6 \times 10^6$ b) and samarium-149 ($\sigma_a = 4.0 \times 10^4$ b) have fission yields and cross-sections large enough to decrease the thermal utilization factor f. Both change with power level since their formation is a direct function of the fission rate, and it is necessary to adjust control rods and chemical shim to compensate for the negative reactivity effects induced by their ingrowth and burnup as fissioning proceeds.

Xenon-135 is the most important fission product poison. It is formed directly as a fission product and also by decay of its ^{135}I precursor (Y_i = 6.28%). As shown in Appendix C for mass chain 135, ^{135}Xe is formed as follows:

^{135}Sn	→	^{135}Sb	→	^{135}Te	→	^{135}I	→	^{135}Xe	→	^{135}Cs	→	^{135}Ba
0.0006		0.1458		3.3395		6.2823		6.5390		6.5395		6.5395

where the numbers below each nuclide represents its cumulative fission yield. The inventory of ^{135}Xe is affected by radioactive transformation of ^{135}I which produces it, its own transformation which removes it, and removal by neutron absorption due to its very large cross-section which results in burnup. For all practical purposes it can be assumed that all of the ^{135}I present is formed directly by fission even though it is produced by short-lived ^{135}Te and its precursors. Since the iodine half-life is 6.57 h, xenon and iodine will have exceeded 99% of their

final equilibrium values in 46 h or about 2 d. After shutdown, xenon continues to be produced in the reactor by the transformation of ^{135}I to ^{135}Xe, and since it too is radioactive with a half-life of 9.1 h, it in turn is removed by its own radioactive transformation. After about 2 d of steady-state reactor operation, the amount of iodine (and xenon) present in the reactor is in equilibrium; however, after reactor shutdown, ^{135}Xe will be produced more rapidly than it is removed and the amount will peak about 7 h after shutdown and then decrease due to iodine transformation, as shown in Figure 5-23. Some 18 h after shutdown, xenon will have peaked and returned to the starting equilibrium level, and by about 72 h essentially all of the ^{135}Xe atoms will have transformed to provide a clean core free of ^{135}Xe poisons.

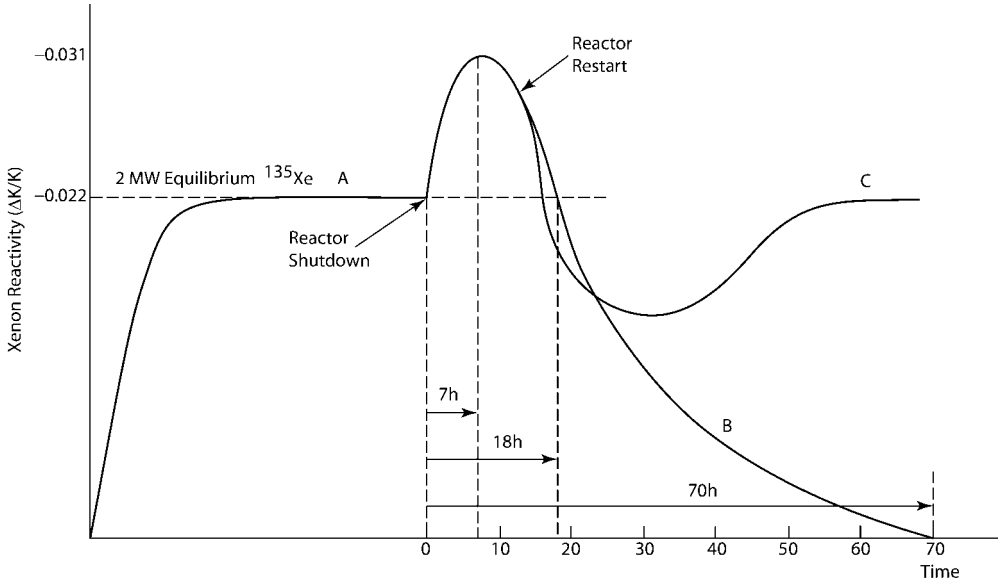

Fig. 5-23 Effect of ^{135}Xe on reactor reactivity for steady-state operation (curve A), after shutdown (curve B), and shutdown followed by restart (curve C). The ^{135}Xe at steady state introduces negative reactivity of $\Delta k/k = -0.022$, which becomes even more negative due to ingrowth by radioactive transformation reaching a maximum ($\Delta k/k = -0.031$) 7 h later at which point removal by radioactive transformation overcomes its production decreasing it to zero if the reactor remains shut down for a period of about 70 h (curve B). If the reactor is restarted before the ^{135}Xe decays, the population of neutrons further accelerates the removal of ^{135}Xe by neutron activation; however, new ^{135}Xe is produced by fission and the negative reactivity eventually returns to an equilibrium condition ($\Delta k/k = -0.022$) some 48 h later.

If sufficient excess core reactivity is available to overcome the negative reactivity induced by xenon buildup following a shutdown, the reactor can be restarted. Returning the power level reestablishes the full neutron flux and any xenon present is first depleted rapidly by neutron capture, and its associated negative reactiv-

ity will drop rapidly as shown by curve C in Figure 5-23. The return to power also results in fissions which produce new atoms of iodine and xenon which balances the removal of xenon by transformation and burnout, and equilibrium will be reestablished. If the power level were to be returned to a value different from the pre-shutdown level, a different equilibrium level would eventually be established, but at essentially the same time (i.e., 46 h) due to the ingrowth of 6.7 h ^{135}I.

Samarium-149 also affects reactor reactivity in a similar way because of its large cross-section. It is a stable nuclide produced by radioactive transformation of ^{149}Pm, which is formed in the fission process by the decay of ^{149}Nd. Samarium-149 is stable, but it is depleted by burnout. Because the half-life of ^{149}Nd is short in comparison to that of ^{149}Pm, the two are treated as if ^{149}Pm were formed directly from fission with a fission yield of 1.082%. The half-life of ^{149}Pm (2.212 d) is the controlling time constant; therefore, promethium and samarium will reach equilibrium in about 16 d.

Increases and decreases in reactor power represent transient conditions as illustrated in Figure 5-24. If reactor power is increased, the samarium concentration will decrease initially due to higher burnout, but ^{149}Pm production will eventually bring the samarium concentration back up to its equilibrium value. If power is decreased, burnout decreases, production of promethium continues, and the samarium concentration increases due to replenishment by radioactive transformation of new atoms of promethium produced by fission. A power decrease eventually decreases the concentration of promethium due to the lower neutron flux, and the samarium concentration reaches an equilibrium value. In both cases, the transient time is approximately 16 days.

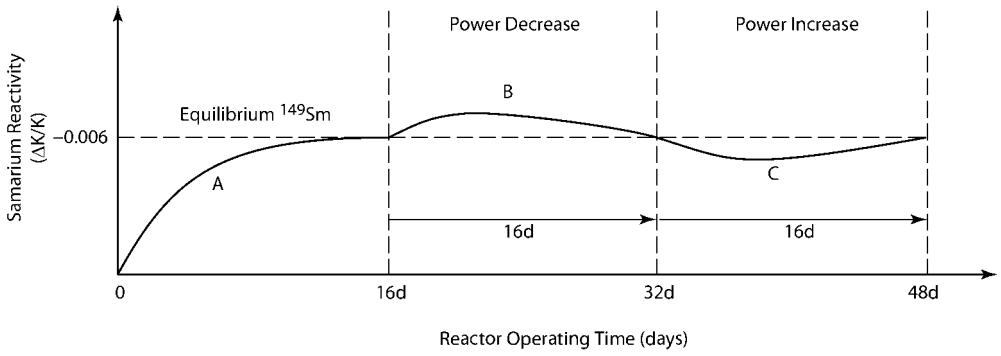

Fig. 5-24 Effect of stable ^{149}Sm, a product of fission, on reactor reactivity. An equilibrium condition of negative reactivity ($\Delta k/k = 0.006$) is achieved in about 16 days (curve A). If the power level is decreased, $\Delta k/k$ becomes even more negative due to ingrowth of ^{149}Sm from the decay of ^{149}Pm (curve B), which returns to equilibrium some 16 days later. If the power level is increased back to its original level (curve C), ^{149}Sm is at first decreased due to neutron absorption, but the increased fission rate produces more ^{149}Pm and ^{149}Sm and the negative reactivity coefficient returns to the equilibrium value ($\Delta k/k = -0.006$).

5.10
Radioactivity in Reactors

Fission and activation reactions in reactors produce numerous new products as the fissile material is consumed and neutrons are absorbed. As shown in Figure 5-15, fuel that initially contains 3.3% ^{235}U and 96.7% ^{238}U will, after about 3 y in the reactor, still contain mostly ^{238}U, but substantial amounts of fission and activation products and isotopes of plutonium. These "spent fuel" rods or any byproducts of processing them constitute high-level wastes.

There are over 1200 individual fission products produced in fission; however, the major ones fall into two groups with mass numbers of 78–99 and 123–143 or so. The features of key fission products in these groupings are shown in Figures 5-25 and 5-26 excerpted from the chart of the nuclides.

5.10.1
Activation Products in Nuclear Reactors

Important sources of activation products in reactors are structural components containing cobalt, manganese, chromium, and other elements used to harden steel, and natural constituents and coolant additives (e.g., boron and lithium compounds) for controlling water chemistry of the plant. Likewise, if air contacts the flux of neutrons in a reactor, ^{40}Ar will be converted by an (n,γ) reaction to

$$^{40}_{18}\mathrm{Ar} + {}^{1}_{0}\mathrm{n} \rightarrow [{}^{41}_{18}\mathrm{Ar}] \rightarrow {}^{41}_{18}\mathrm{Ar} + \gamma$$

Cobalt, which is added to steel to give it desired tensile properties, is often a troublesome byproduct of reactor operation as is the iron in steel. Cobalt-60 is produced from stable ^{59}Co by the (n,γ) reaction

$$^{59}\mathrm{Co} + {}^{1}_{0}\mathrm{n} \rightarrow [{}^{60}\mathrm{Co}^{*}] \rightarrow {}^{60}\mathrm{Co} + \gamma + Q$$

Other (n,γ) activation products produced in nuclear reactors yield ^{51}Cr, ^{54}Mn, ^{56}Mn, ^{55}Fe, ^{59}Fe, ^{58}Co, ^{60}Co, ^{95}Zr, ^{97}Zr, ^{65}Zn, and ^{95}Nb produced by neutron activation of corrosion products as they circulate through the various systems. Corrosion products, as well as long-lived fission products, tend to collect in piping bends, joints, and other low points creating significant "hot spots" (high radiation sources); contamination occurs if they leak out of the systems.

Water itself contains oxygen and hydrogen, both of which can be activated. Oxygen-16 (99.8% of naturally occurring oxygen) can be activated to form radioactive nitrogen (N) by the following reactions:

$$^{16}_{8}\mathrm{O} + {}^{1}_{0}\mathrm{n} \rightarrow [{}^{16}_{8}\mathrm{O}^{*}] \rightarrow {}^{16}_{7}\mathrm{N} + {}^{1}_{1}\mathrm{p}$$

$$^{16}_{8}\mathrm{O} + {}^{1}_{1}\mathrm{p} \rightarrow [{}^{17}_{9}\mathrm{F}^{*}] \rightarrow {}^{13}_{7}\mathrm{N} + {}^{4}_{2}\mathrm{He}$$

Fig. 5-25 Features of fission products with mass number 78–99 as shown on the chart of the nuclides.

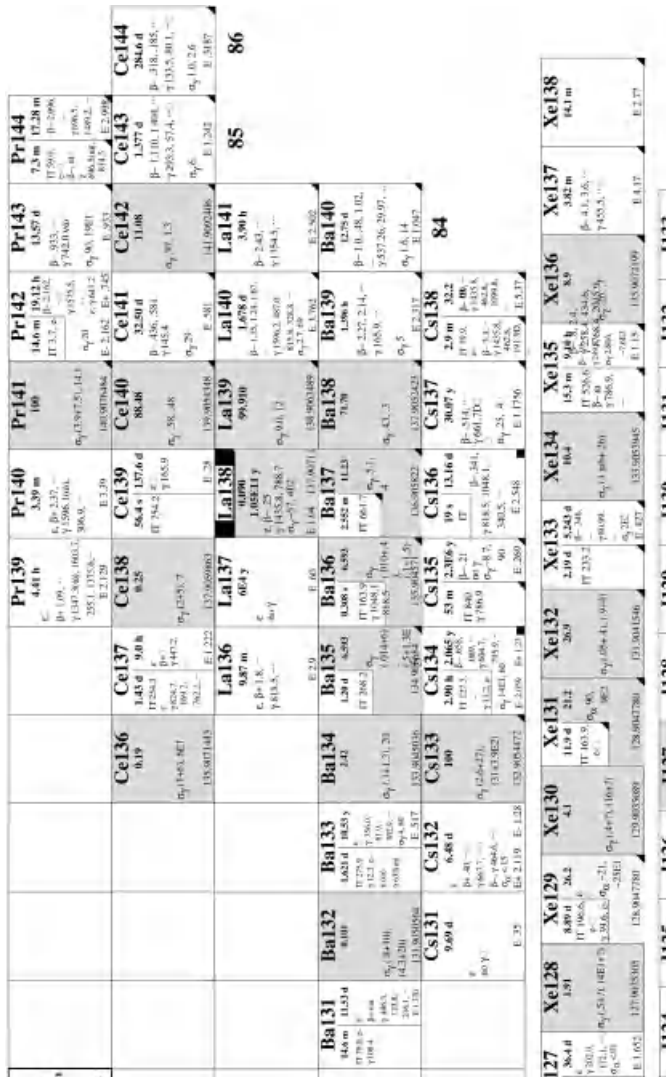

Fig. 5-26 Features of fission products with mass number 123–143 as shown on the chart of the nuclides.

After formation, the nitrogen atoms usually combine with oxygen and hydrogen in the coolant to form ions or compounds such as NO_2^-, NO_3^-, NH_4^+, NO, NO_2, and N_2. Nitrogen-16 has a relatively large formation rate and emits extremely high-energy gamma rays (6.13 and 7.12 MeV); therefore, it represents a major contributor to radiation levels near primary system piping containing either water or steam. Fortunately, the half-life of ^{16}N is only 7.l s so that it is no problem once the activation process terminates (i.e., after the reactor is shut down). Nitrogen-13 has a 9.97 min half-life and undergoes radioactive transformation by positron emission, which in itself represents little concern; however, positron annihilation photons can contribute to gamma exposure fields.

During normal operation of BWRs ^{16}N is the major contributor to the radiation levels around the turbine equipment since it travels in steam to the turbine. In a PWR the coolant is contained in a primary loop and the nitrogen activity is confined to the reactor water. The contribution to plant radiation levels from ^{13}N is completely masked by the predominance of ^{16}N, and in PWR systems it has no practical significance at all. However, in BWR systems the half-life of ^{13}N (9.97 min) is long enough for some of it to be discharged to the environment in gaseous releases to the atmosphere, and it can also be detected in steam leaks.

Fluorine-18 is produced by proton interaction with ^{18}O, which makes up about 0.2% of natural oxygen, by the following reaction:

$$^{18}_{8}\mathrm{O} + {}^{1}_{1}\mathrm{p} \rightarrow [{}^{19}_{9}\mathrm{F}] \rightarrow + {}^{18}_{9}\mathrm{F} + {}^{1}_{0}\mathrm{n} + Q$$

Flourine-18 is radioactive and undergoes transformation by positron emission. Sometimes the ^{18}F and ^{13}N are confused since they both emit positrons which ultimately yield 0.511 MeV annihilation photons.

5.10.2 Tritium Production in Reactors

Tritium (^3H), with maximum and average beta energies of 0.0186 MeV and 0.006 MeV, can be produced in nuclear reactors in large quantities primarily by activation of boron or lithium, both of which have been used as additives to reactor coolant systems to control plant conditions. The reactions, which are different for thermal (n_{th}) and fast (n_f) neutrons, are

$$^{10}_{5}\mathrm{B} + {}^{1}_{0}\mathrm{n}_{\mathrm{th}} \rightarrow {}^{7}_{3}\mathrm{Li} + {}^{4}_{2}\mathrm{He}$$

$$^{10}_{5}\mathrm{B} + {}^{1}_{0}\mathrm{n}_{\mathrm{f}} \rightarrow ({}^{7}_{3}\mathrm{Li})^* + {}^{4}_{2}\mathrm{He}$$

where the excited lithium nucleus further breaks up to yield ^3H by the reaction

$$({}^{7}_{3}\mathrm{Li})^* \rightarrow {}^{3}_{1}\mathrm{H} + {}^{4}_{2}\mathrm{He}$$

Boron becomes a source of tritium in reactors because it is often injected into the coolant of PWRs in concentrations up to 4000 ppm to provide a chemical shim for control of reactivity; therefore, PWRs that add boron to coolant produce more tritium than BWRs which do not require it.

Lithium hydroxide is often used to control the pH of reactor coolant. Fast neutron reactions with ^{7}Li and thermal neutron reactions with ^{6}Li form tritium by the reactions

$$^{7}_{3}\mathrm{Li} + {}^{1}_{0}\mathrm{n_f} \rightarrow {}^{3}_{1}\mathrm{H} + {}^{4}_{2}\mathrm{He} + {}^{1}_{0}\mathrm{n}$$

$$^{6}_{3}\mathrm{Li} + {}^{1}_{0}\mathrm{n_{th}} \rightarrow {}^{3}_{1}\mathrm{H} + {}^{4}_{2}\mathrm{He}$$

Natural lithium contains 92.5% ^{7}Li and 7.5% ^{6}Li; however, it is the presence of ^{6}Li in the reactor coolant that constitutes the most significant source of ^{3}H because of its high thermal neutron cross-section. Tritium production in PWRs can be reduced considerably by use of ^{7}LiH, which is generally available.

Ternary fission of ^{235}U, in which three products are produced, also produces tritium, for example:

$$^{235}_{92}\mathrm{U} + {}^{1}_{0}\mathrm{n_{th}} \rightarrow {}^{140}_{54}\mathrm{Xe} + {}^{91}_{37}\mathrm{Rb} + {}^{3}_{1}\mathrm{H} + 2{}^{1}_{0}\mathrm{n} + Q$$

The ternary fission yield for tritium production is 1.25×10^{-4}%, i.e., 1.25 atoms of tritium are produced for every million fissions. However, over 99% of ternary tritium is retained within the fuel rods. Ternary fission also produces ^{14}C, but at a lower yield and it too remains in the fuel rods.

5.10.3
Low-level Radioactive Waste

Even with good fuel performance, some radioactive materials will be present in various parts of a nuclear reactor that must be removed as wastes. Although the sources, amounts, and types vary from plant to plant, most radioactive wastes contain fission and activation products that escaped the fuel matrix or were entrained in coolant and removed. These are characterized as low-level radioactive wastes, and for reactors generally fall into one of the following categories:

- *Condensate filter sludges and resins*, which are used to clean up condensate from the turbine before it is returned to the reactor. Deep-bed or powdered resins are typically used, including precoat filter/demineralizers used in many plants.
- *Filter sludges and resins* and associated prefilters used to clean up reactor water. Clean-up demineralizer resins are used in BWRs and in the primary coolant letdown system in PWRs; both can become very radioactive.
- *Evaporator concentrates (or bottoms)* remaining from the distillation of liquids in both BWR and PWR plants. In BWRs, most

such liquids are produced during regeneration of demineralizer used to clean up condensate and various waste streams. In PWRs, evaporator concentrates are produced from primary equipment drain sumps, radwaste sumps, and liquids from regeneration of demineralizer resins.
- *Resins and filters* used to cleanse water in the fuel storage pool and various other liquids before they are evaporated.
- *Crud*, which is a scale/deposit on surfaces of vessels, pipes, and equipment. Crud builds up radioactivity some of which may break off and reach a waste processing system. Crud is normally not discharged from the plant, but these deposits can be important in maintenance and decommissioning.
- *Trash*, which includes paper used on floors, plastic bags and sheeting, disposable shoe covers, and contaminated clothing.
- *Scrap*, which consists of structural materials, piping, small valves, and various other components from maintenance and plant modifications.

5.11 Summary

The principal fissionable materials are ^{235}U, ^{238}U, and ^{239}Pu. Absorption of a neutron by a fissionable nucleus produces a dumbbell-shaped deformation in which repulsive forces exerted by the positive charges in each of the two "halves" can cause the two parts to separate, or fission. The excitation energy added by the neutron can also be relieved by emission of a gamma photon, but fission, which occurs 85% of the time, is more likely. Radioactive fission products and activation products are byproducts of these reactions, and these represent a number of radiation protection issues for workers, the public, and the environment.

Uranium, plutonium, and other fissionable nuclei are very neutron rich because extra neutrons help to distribute the nuclear force and counteract the repulsive forces exerted by the large number of protons in the nucleus. This excess ratio of neutrons to protons carries over to the fission products. Hence each product that is formed will also be extremely neutron rich and very unstable, and several beta particles and gamma rays are emitted to decrease the neutron number (and increase the proton number) in order for the fission product to become stable.

Each fission produces its own distinct mass chain with a slightly different Q-value; however, about 200 MeV of energy is released per fission and most (85% or so) of this energy appears as heat as the heavy, highly charged fission fragments are absorbed in the fuel matrix. Part of the remaining energy is released instantaneously by gamma rays and fission neutrons, and the rest is released gradually by radioactive transformation of the fission products as they emit beta particles, neutrinos, and gamma rays. Thermal neutron fission of ^{235}U yields over

88 primary fission products with mass numbers from 72 to 160 and well over 1200 different fission products. Inventories of these products can be calculated from the fission rate (or reactor power) and the fission yield of the product.

The release of fission energy is governed by a fundamental set of physical principles which eventually dictate the design and performance of nuclear reactors and other critical assemblies. Radiation protection for these circumstances must also recognize these same principles. The central feature of a nuclear reactor is the core, which contains the fuel, the control rods, the moderator, and a coolant; it is enclosed in a vessel with various components and subsystems to enhance fissioning in the fuel, to control its rate, to extract heat energy, and provide protection of materials and persons.

The two principal reactor designs used in the USA and many other countries are the PWR and the BWR. The primary coolant water in a PWR is maintained at a high pressure (2200 psi) so it will not boil; therefore, steam for the turbines must be produced in a secondary circuit containing steam generators. The heated coolant water from the reactor enters the steam generator at the bottom and passes upward and then downward through several thousand tubes each in the shape of an inverted U. The outer surfaces of these tubes are in contact with lower-pressure and cooler feed water which extracts heat, boils, and produces steam that is routed to the turbine. The spent steam is condensed and pumped back to the steam generators to complete the secondary circuit.

The BWR uses light water for both coolant and moderator, and the water is allowed to boil to produce steam that is routed directly to the turbines. This direct cycle design can be a major advantage because it eliminates the need for a separate heat transfer loop. However, the water becomes radioactive in passing through the reactor core, which requires shielding of the steam piping, the turbines, the condenser, reheaters, pumps, pipings, etc.

Ordinary light water, H_2O, has desirable features for use in reactors. It has good heat transfer and is plentiful so that it can be easily replaced if leakage or evaporation occurs. It is also very effective in slowing down neutrons, but this good feature is offset by a high capture cross-section for neutrons making it unsuitable as the coolant/moderator unless the fuel is enriched to about 3–4% ^{235}U. Alternatively, D_2O, or heavy water, which absorbs very few neutrons, can be used as the moderator and coolant allowing the use of natural uranium (0.72% ^{235}U) as fuel.

Reactors are sources of many radioactive materials, many of which exist in off-gas systems, effluents, or in waste materials to cause radiation exposures of workers, or to be released during routine operations, incidents, or in wastes.

Acknowledgments

This chapter was compiled with major help from Chul Lee M.S. and Ihab R. Kamel M.S., Ph.D. Dr. Kamel complied the table of fission product chains and yields from recent data graciously provided by Dr. Tal England who made it available before it was published.

Other Suggested Sources

England, T. R., Rider, B. F. **1994**, Evaluation and compilation of fission product yields, Report LA-UR-94-3106 (ENDF-349), Los Alamos National Laboratory.
Lamarsh, J. R. **1983**, *Introduction to Nuclear Engineering*, 2nd edn, Addison Wesley, Reading, MA.

Problems – Chapter 5

5–1. In 1000 atoms of present-day natural uranium, 993 are ^{238}U and 7 are ^{235}U. (a) What would have been the percentage of ^{235}U in natural uranium 2 billion years ago? (b) Could a natural reactor have existed 2 billion years ago? Why?
5–2. A nuclear reactor of 1000 MWe and a generation efficiency of 32% starts up and runs for 1 d. (a) What is the inventory of ^{133m}Xe and ^{133}Xe in the core? (b) How long would it have to run to reach an equilibrium level of ^{133}Xe and what would be the inventory at equilibrium?
5–3. A nuclear reactor operates for 3 y at a power level of 1000 MWe (3300 MWt) after which all the fuel is removed (a problem core) and processed soon after releasing all of the noble gases. How many curies of ^{85}Kr would be released to the world's atmosphere?
5–4. A nuclear reactor of 1000 MWe and a generation efficiency of 32% starts up and runs for 10 d. (a) What is the inventory of ^{140}Ba in the core? (b) How long would it have to run to reach an equilibrium level of ^{140}Ba and what would be the inventory at equilibrium? (c) At 10 d after startup, what would be the inventory of ^{140}La?
5–5. Estimate the ^{14}C inventory in a 1000 MWe PWR after 350 d of operation if the coolant volume is 80,000 gal and the coolant contains dissolved air of 50 ppm in the primary coolant. If this is released continuously as CO_2 with other stack gases, estimate the dilution needed to reduce the ^{14}C concentration to 10^{-6} $\mu Ci/cm^3$.
5–6. A nuclear criticality incident occurred instantaneously in a tank containing enriched uranyl/nitrate and water when a mixer was turned on. It was determined that 10^{20} fissions occurred. (a) What would be the activity (in Ci) of ^{138}Xe 10 s after the incident? (b) What would be the activity of ^{138}Xe 1 h later (use exact solution)?
5–7. A 100 KT nuclear fission device is exploded underground in Nevada. All the iodines produced vent immediately. What would be the inventory of ^{131}I released (i.e., produced)?
5–8. Estimate the ^{85}Kr content in a reactor core containing 100 tons of UO_2 after 2 y of operation at a burnup of 33,000 MW d/metric ton (assume 3% enrichment and no leakage of ^{85}Kr from the fuel).
5–9. High-level radioactive waste standards for spent nuclear fuel are based on inventories of various radionuclides. (a) What is the inventory of ^{137}Cs in 1000 metric tons of spent fuel based on a burnup of 33,000 MW d per ton over 3 y? (b)

What would be the ^{137}Cs inventory based on an average power level for the 3 y period?

5–10. What is the inventory of ^{99}Tc for the fuel in Problem 5-9? Show whether it is necessary to use average power level in this calculation, and explain why.

5–11. Find the energy difference between ^{235}U + n and ^{236}U, which can be regarded as the "excitation energy" of a compound nucleus of ^{236}U, and repeat for ^{238}U + n and ^{239}U. Use these data to explain why ^{235}U will fission with very low-energy neutrons, while fission of ^{238}U requires fast neutrons of 1–2 MeV of energy. From a similar calculation, predict whether ^{239}Pu requires low- or high-energy neutrons to fission.

5–12. Carbon-14 is produced in a pool reactor by an (n,p) reaction with nitrogen which is dissolved in the pool water. If the water in and surrounding the reactor core contains 2 g of nitrogen and the neutron flux is 10^{13} neutrons/cm^2 s, how much ^{14}C is produced each year?

6
Naturally Occurring Radiation and Radioactivity

"The majority of a person's environmental radiation dose is due to the natural radiation background ..."

Floyd L. Galpin (1999)

The natural radiation environment consists of cosmic rays and naturally radioactive materials. Some of the materials are cosmogenic, others are primordial, and others exist naturally because of the radioactive transformation of substances produced by these processes. Their radiological significance is closely linked to their physical behavior and how they change with time.

6.1
Discovery and Interpretation

Henri Becquerel set out to find the source of the Roentgen's rays, believing they were due to fluorescence. He placed a fluorescent crystal of potassium uranyl sulfate, on a photographic plate and exposed it to sunlight. An image of the crystal appeared on the photographic plate, clearly penetrating the wrapping. At almost the same time, Silvanus Thompson in London exposed several fluorescent compounds on thin sheets of aluminum atop sealed photographic plates and noted that only a uranium compound produced a silhouette of the crystals on the developed photographic plate. On February 24, 1986 Becquerel reported his finding; Thompson's much broader observations were made on February 26. Even though Thompson's results were the more definitive, Becquerel, who published first, is credited with the discovery. It was the persistence of the Curies and the seminal work of Rutherford and Soddy that established the science and importance of substances with, to use Becquerel's phrase, "radiation activitié."

The work of the Curies is quite remarkable when contrasted to the times, in particular that of Marie who observed that the intensity of radiation from unprocessed uranium ore was greater than from purified uranium salts; thus something else in the ore must be producing it. To find it, she processed a ton of pitchblende ore from which most of the uranium had been removed and discovered in

Physics for Radiation Protection, Third Edition. James E. Martin

two different precipitates the element polonium, and a second element with even more activity that she named radium.

The Curies claimed that radioactivity is "an atomic property of substances; however, models of the atoms were not available to develop the necessary understanding of the process.

Rutherford, in studies of the ionization of air by thorium, he concluded that it produced a substance he called emanation (now known as ^{220}Rn, or thoron) that migrated away from the source. Frederick Soddy quickly demonstrated that the emanation was unchanged by heating and it condensed at low temperatures. It was clearly a gas, and since it could pass unaffected through a series of solutions and metals, it was also a noble gas – a unique element quite distinct from thorium. And if the emanation was a noble gas, it could not have been present in the original thorium sample, i.e. thorium was spontaneously producing a noble gas, a different element, by transmutation of atoms.

Rutherford and Soddy performed chemical separations on thorium nitrate and uranium and discovered a substance (^{224}Ra), they called thorium X (ThX). Most of the original radioactivity ended up in the precipitate containing ThX and UX, and as expected, they gradually recovered their activity. More importantly, they noted that the activity of the precipitates decreased exponentially, while the activity of the purified thorium and uranium recovered at precisely the same rate! Figure 6-1 contains the classic and historical plots of their data for uranium and the UX precipitate and ThX and its ThX precipitate. These results, together with the evidence that their samples were also producing a noble gas, clearly established that radioactivity, despite Rutherford's reluctance was a phenomenon of transmutation. The atom could no longer be considered permanent.

The shapes of the curves in Figure 6-1 show that activity diminishes exponentially related to the total number of atoms present by a constant which Rutherford and Soddy called the *radioactive constant* of the element (now commonly referred to as the disintegration or decay constant λ, which is a definite and specific property of a given radioelement). Its value depends only on the nature of the species, is independent of the physical or chemical conditions of the atoms, and the exponential equations represent very accurately the rates of transformations for radioelements for values of λ ranging over 24 orders of magnitude.

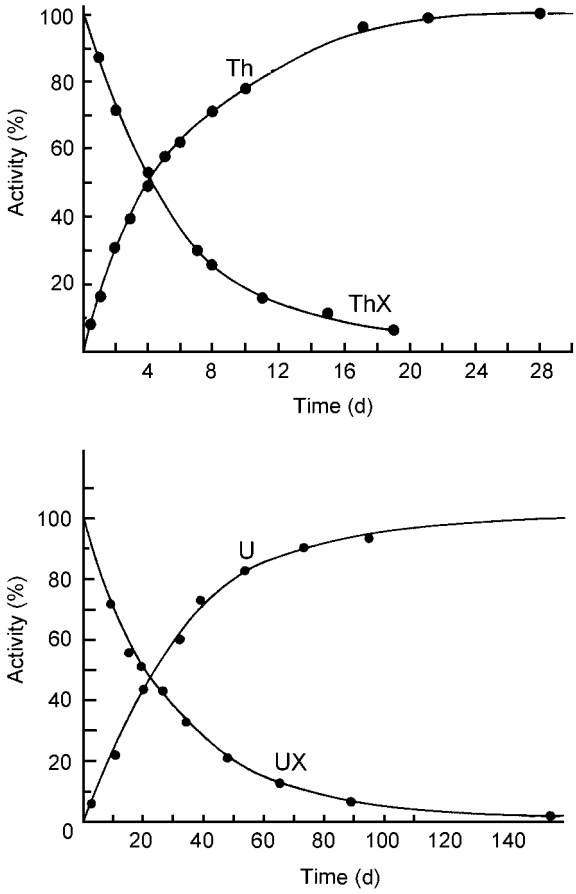

Fig. 6-1 Recovery of uranium activity after separation and loss of UX (^{234}Th; $T_{1/2}$ = 24.1 d).

6.2 Background Radiation

Creatures on the earth are continually exposed to external radiation from cosmic rays and a number of naturally occurring radionuclides that produce external gamma radiation or can be incorporated into the body to produce internal radiation doses. These sources, of course, vary widely depending on location and the surrounding environment. Average values of exposure data from the various sources of natural radiation are listed in Table 6-1.

Table 6-1. Average effective dose equivalent rates from various sources of natural background radiation in the USA.

Source	Dose equivalent rate (mrem/y)
Cosmic radiation	27
Cosmogenic nuclides	1
External terrestrial	28
Nuclides in body	39

Source: adapted from NCRP (1987).

The doses in Table 6-1 do not include radon and its products though it is common to do so. Published estimates of total actual background exposure that are of the order of 300 mrem/y usually include an average for the uncertain radon product lung dose adjusted to a whole body effective dose so it can be added to the other common sources which expose the whole body. Although it is proper to recognize radon exposure, it should be done warily.

6.3 Cosmic Radiation

The earth is bombarded continuously by radiation originating from the sun, and from sources within and beyond the galaxy. This cosmic radiation slams into the earth's upper atmosphere which provides an effective shield for beings below. Cosmic rays consist of high-energy atomic nuclei, some 87% of which are protons. About 11% are alpha particles, approximately 1% are heavier atoms which decrease in importance with increasing atomic number, and the remaining 1% are electrons. These "rays" have very high energies, some as high as 10^{14} MeV but most are in the range 10 MeV to 100 GeV.

Cosmic rays are extraterrestrial radiations. They consist of "galactic" particles that originate outside the solar system and "solar" particles emitted by the sun. As they strike the atmosphere they produce cascades of nuclear interactions that yield many secondary particles which are very important in production of cosmogenic radionuclides. The distribution of cosmic ray components and energy spectra is shown in Figure 6-2. Galactic cosmic radiation produces various spallation reactions in the upper atmosphere which yield secondary neutrons and protons. Many pions are also produced and their subsequent disintegration results in electrons, photons, neutrons, and muons. Muon disintegrations, in turn, lead to secondary electrons, as do coulombic scattering interactions of charged particles in the atmosphere. As shown in Figure 6-3, the number and mix of these particles varies with altitude as does the resulting tissue absorbed dose rate.

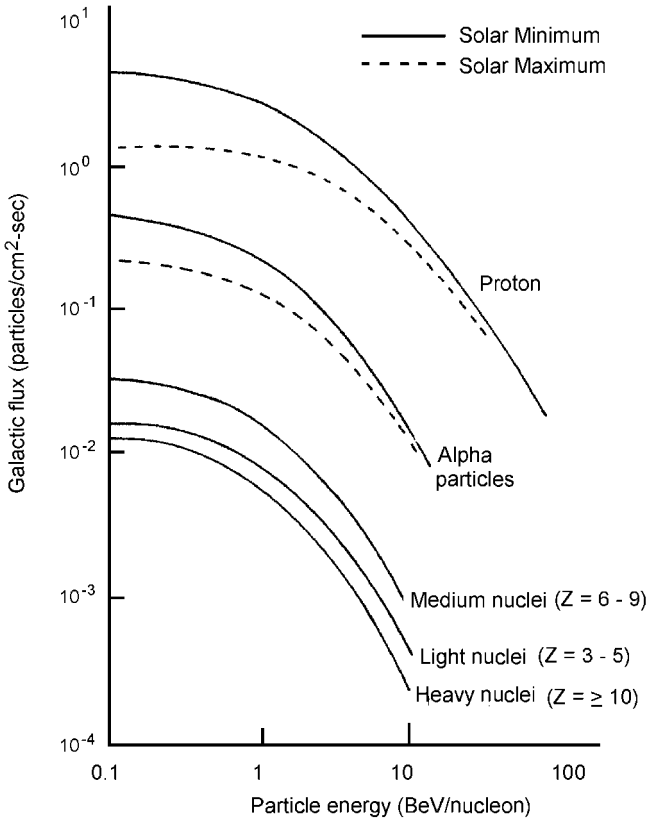

Fig. 6-2 Various components of galactic cosmic radiation and their energies. (Adapted from NCRP (1987). With permission.)

Radiation dose rates at the earth's surface due to cosmic radiation are largely caused by muons and electrons, and both vary with elevation and with latitude. The atmospheric shield is a column of air that weighs 1033 g/cm^2 at sea level; the effectiveness of this shield is related to the atmospheric thickness or depth in units of g/cm^2 of overlying air. Consequently, the total dose rate from cosmic rays will increase with altitude as the thickness of the atmosphere decreases, as shown in Figure 6-3. At geomagnetic latitude 55° N, for example, the absorbed dose rate in tissue approximately doubles with each 2.75 km (9000 ft) increase in altitude, up to about 10 km (33,000 ft). The neutron component of the dose equivalent rate increases more rapidly with altitude than does the directly ionizing component and dominates at altitudes above about 8 km (UN 1988).

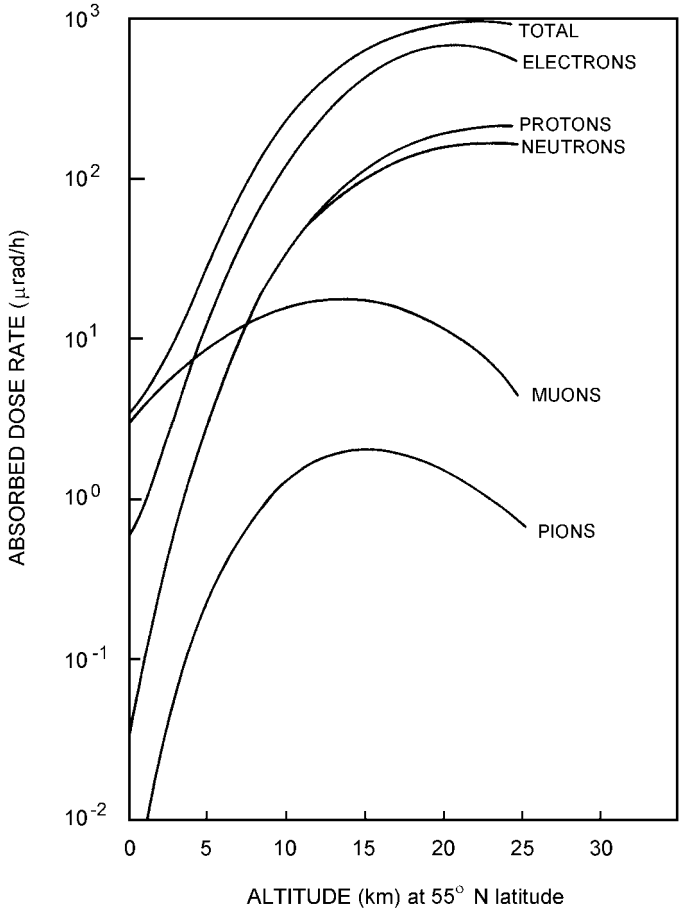

Fig. 6-3 Absorbed dose rates from various components of cosmic radiation at solar minimum at 5 cm depth in a 30 cm slab of tissue. (To convert to μGy/h, divide by 100.)

Cosmic rays of solar origin are mainly hydrogen and helium nuclei of relatively low energy (about 1 keV), but solar flares can generate particles of several GeV. Their energies contribute little to radiation doses at the surface of the earth; however, they perturb the earth's magnetic field which in turn deflects galactic cosmic rays that might otherwise reach the earth's atmosphere and the surface. Maximum solar flare activity leads to decreases in dose rates and vice versa. Consequently, at any given location, cosmic ray doses may vary in time by a factor of about three. At sea level they can vary with geomagnetic latitude by as much as a factor of 8, being greatest at the poles and least at the equator. The global average cosmic ray dose equivalent rate at sea level is about 24 mrem (240 μSv) per year for the directly ionizing component and 2 mrem (20 μSv) per year for the neutron component. The annual tissue dose rate from cosmic rays increases with altitude,

as shown in Figure 6-4, which contains data averaged over geomagnetic latitudes between 43° and 55° and over two periods of solar activity.

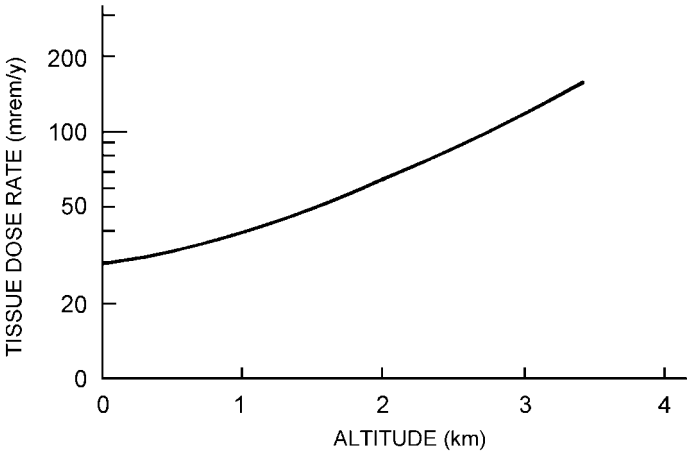

Fig. 6-4 Long-term average outdoor total dose equivalent rate (charged particles plus neutrons) due to cosmic radiation at 5 cm depth in a 30 cm thick slab of tissue. (To convert to mSv/y, divide by 100.)

6.4 Cosmogenic Radionuclides

Several radionuclides of cosmogenic origin are produced when high-energy protons (87% of cosmic radiation) interact with constituents of the atmosphere. Showers of secondary particles, principally neutrons, from such interactions yield a number of such radionuclides, in particular ^{3}H, ^{7}Be, ^{14}C, and ^{22}Na (see Table 6-2) which are produced at relatively uniform rates. The high-energy (ca. MeV) secondary neutrons that produce these interactions originate in the atmosphere from cosmic ray interactions, rather than coming from outer space. Free neutrons are radioactive with a life of only about 12 min; thus, they do not last long enough to travel from outer space. Their concentration in the atmosphere rises with altitude to a maximum around 40,000 ft and then decreases.

Cosmic ray interactions can also occur with constituents of the sea or the earth, but atmospheric interactions dominate. The total neutron flux density at sea level is only about 30 neutrons/cm^2 h of which only 8 are thermal neutrons; therefore, production of radioactive materials by neutron capture in the earth's crust or the sea is minor. An important exception is the production of long-lived ^{36}Cl (NCRP 1975) by neutron activation of ^{35}Cl in the earth's crust.

Table 6-2. Global distribution of cosmogenic radionuclides.

	^{3}H	^{7}Be	^{14}C	^{22}Na
Global inventory (pBq)	1300	37	8500	0.4
Distribution (%)				
stratosphere	6.8	60	0.3	25
troposphere	0.4	11	1.6	1.7
land surface	27	8	4	21
mixed ocean layer	35	20	2.2	44
deep ocean	30	0.2	92	8
ocean sediments	–	–	0.4	–

Oxygen in the atmosphere is essentially transparent to neutrons, but (n,p) interactions with ^{14}N to form ^{14}C are very probable. Neutron interactions with ^{14}N yield ^{14}C 99% of the time and tritium through (n,t) reactions 1% of the time. Carbon-14 from $^{14}N(n,p)^{14}C$ reactions exists in the atmosphere as CO_2, but the main reservoir is the ocean. It has a half-life of 5730 y and undergoes radioactive transformation back to ^{14}N by beta particle emission with a maximum energy of 157 keV (average energy of 49.5 keV). The natural atomic ratio of ^{14}C to stable carbon is 1.2×10^{-12} (corresponding to 0.226 Bq ^{14}C per gram of carbon (NCRP 1975). For carbon weight fractions of 0.23, 0.089, 0.41, and 0.25 in the soft tissues, gonads, red marrow, and skeleton, annual average absorbed doses in those tissues are, respectively, 1.3, 0.5, 2.3, and 1.4 mrem.

Tritium is produced mainly from $^{14}N(n,t)^{12}C$ and $^{16}O(n,t)^{14}N$ reactions in the atmosphere and exists in nature almost exclusively as HTO but, in foods, may be partially incorporated into organic compounds. Tritium has a half-life of 12.3 y and, upon transformation, releases beta particles with maximum energy of 18.6 keV (average energy 5.7 keV). The average concentration of cosmogenic tritium in environmental waters is 100–600 Bq/m^3 (3–16 pCi/L) based on a seven-compartment model (NCRP 1975). If it is assumed that ^{3}H exists in the body, which contains 10% hydrogen, at the same concentration as surface water (i.e., 400 Bq/m^3 or 12 pCi/L) the average annual absorbed dose in the body is 1.2 μrem (0.012 μSv).

Except as augmented by human-made sources, ^{14}C and ^{3}H have existed for eons in the biosphere in equilibrium, i.e., the rate of production by neutron interactions is equal to the subsequent removal by radioactive transformation. The cosmogenic content of ^{14}C in the environment has been diluted in the past century or so by combustion of fossil fuels which has caused the emission of CO_2 not containing ^{14}C. In contrast, atmospheric nuclear weapons tests and other human activities have added to the natural inventories of ^{3}H and ^{14}C, and these nuclides

no longer exist in natural equilibria in the environment. However, they are now returning to natural levels since atmospheric nuclear testing stopped for the most part in 1962.

Beryllium-7, with a half-life of 53.4 d, and ^{10}Be ($T_{1/2} = 1.6 \times 10^6$ y) to a lesser extent, are also produced by cosmic ray interactions with nitrogen and oxygen in the atmosphere. Beryllium-7 undergoes radioactive transformation by electron capture to ^{7}Li with 10.4% of the captures resulting in the emission of a 478 keV gamma ray, which makes its quantitation relatively straightforward. Also, being a naturally occurring radionuclide, it is often observed in gamma ray spectra of environmental samples. Environmental concentrations in temperate regions are about 3000 Bq/m^3 in surface air and 700 Bq/m^3 in rainwater (UN 1988). Atmospheric concentrations of ^{7}Be are noticeably influenced by seasonal changes in the troposphere as shown in Figure 6-5 and by latitude as shown in Figure 6-6. Average annual absorbed doses in the adult are 1.2 mrem to the walls of the lower large intestine, 0.12 mrem to the red marrow, and 0.57 mrem to the gonads.

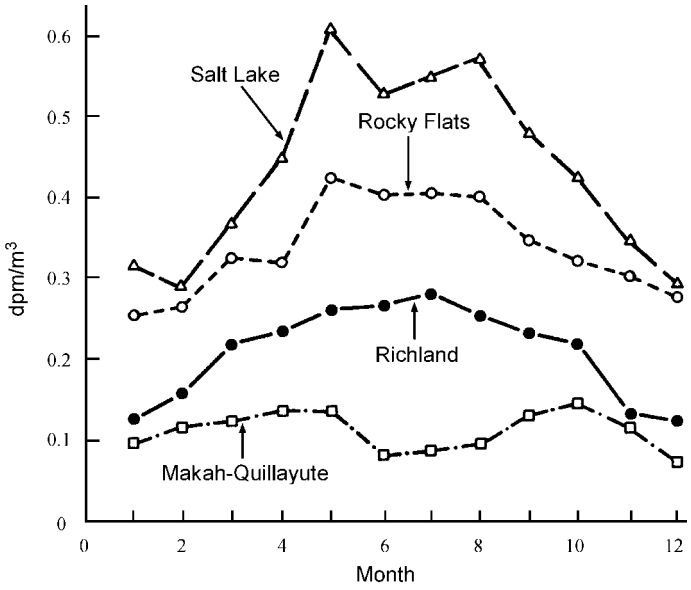

Fig. 6-5 Variation of atmospheric ^{7}Be concentrations at Makah-Quillayute, WA (48° N), Richland, WA (46° N), Salt Lake City, UT (41° N), and Rocky Flats, CO (40° N).

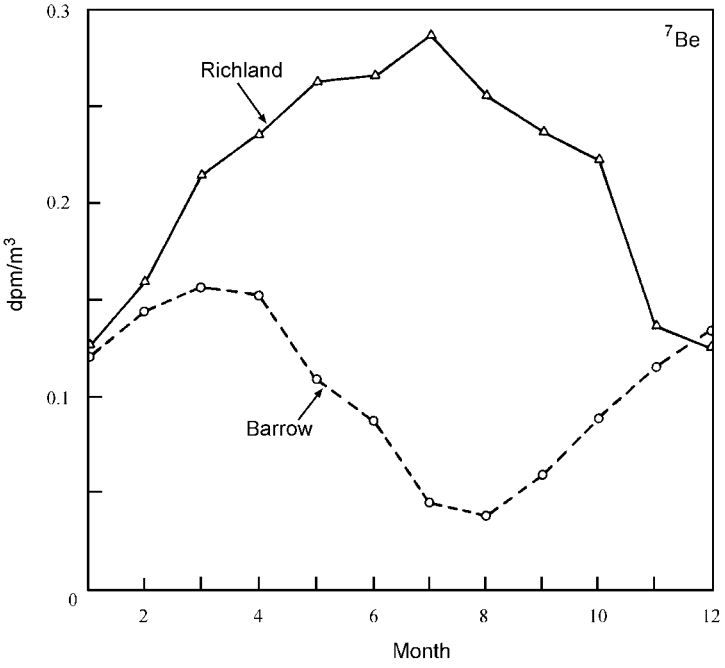

Fig. 6-6 Variation of atmospheric ^{7}Be concentration by month and latitude. Richland, WA, is at 46° N and Barrow, AK, at 70° N latitude.

Sodium-22 is produced by spallation interactions between atmospheric argon and high-energy secondary neutrons from cosmic rays. It has a half-life of 2.60 y, and is transformed by positron emission (90%) and electron capture (10%) to ^{22}Ne. The positron has a maximum energy of 546 keV (average energy 216 keV), and essentially all transformations are accompanied by emission of a 1.28 MeV gamma ray from the excited ^{22}Ne product. A large fraction of ^{22}Na remains in the stratosphere where it is produced but nearly half the natural inventory is in the mixed layer of the ocean (Table 6-2). Annual average absorbed doses to the adult are about 1 mrad to the soft tissues, 2.2 mrad to red marrow, and 2.7 mrad to bone surfaces.

A whole host of other radionuclides (^{26}Al, ^{35}Cl, ^{38}Cl, ^{39}Cl, ^{31}Si, ^{32}Si, ^{32}P, ^{35}S, ^{38}Mg, ^{24}Na, etc.) are produced by spallation reactions with atmospheric ^{40}Ar including ^{39}Ar ($T_{1/2}$ = 269 y) and ^{37}Ar ($T_{1/2}$ = 35 d). Since the energies of cosmic ray particles are so high, they can cause an argon nucleus to break up in many different ways to yield these diverse products. Although these spallation products are detectable in environmental media to varying degrees, most are of minimal consequence in radiation protection.

Finally, neutrons of thermal energies interact with ^{80}Kr to produce ^{81}Kr ($T_{1/2}$ = 2.1×10^5 y) and with ^{84}Kr to produce ^{85}Kr ($T_{1/2}$ = 10.7 y), both in relatively small amounts. The quantities of cosmogenic ^{81}Kr and ^{85}K produced by these interactions are of little interest in radiation protection.

6.5
Naturally Radioacitve Series

Many of the naturally occurring radioactive elements are members of one of four long chains, or radioactive series, stretching through the last part of the chart of the nuclides. These series are named the uranium (^{238}U), actinium (^{235}U), thorium (^{232}Th), and neptunium (^{237}Np) series according to the radionuclides that serve as progenitor (or parent) of all the series products. With the exception of neptunium, each of the parent radionuclides is primordial in origin because they are so long lived that they still exist some 4.5 billion years after the solar system was formed.

The members of each of the three naturally radioactive series and the neptunium series are listed in Tables 6-3 to 6-6 along with the principal emissions, the half-life, and the maximum energy and frequency of occurrence of emitted particles and electromagnetic radiations. Each table contains a diagram of the progression of the series including information on branching ratios that occur. Only the modern symbols are shown despite the historical significance of the earlier designations; however, the names of many of the nuclides are derived from their historical names: radium, radon (radium emanation), thorium (named after the god Thor), etc.

Primordial sources of ^{237}Np no longer exist because its half-life is only 2.1 million years. Table 6-6, which contains the nuclides of the ^{237}Np series, is shown as starting with the radioactive transformation of ^{241}Pu to ^{241}Am, the two parent radionuclides produced in nuclear reactors that are now common sources of ^{237}Np. Were it not for large-scale uses of nuclear fission, ^{237}Np and its series products would be insignificant.

There are notable similarities in radioactive transformations in the radioactive series, and also some striking differences. The uranium, thorium, and actinium series each have an intermediate gaseous isotope of radon and each ends in a stable isotope of lead. The neptunium series has no gaseous product and its stable end product is ^{209}Bi instead of an isotope of lead. Other common factors exist, especially in the sequences of transformation, as follows:

^{238}U---*α-β-β-α-α-α-α-β-β-α-β-β-α*--^{206}Pb $\quad \Delta Z = 10,\ \Delta A = 32$

^{232}Th--*α-β-βα-α-α-α-β-β-α*----------^{208}Pb $\quad \Delta Z = 8,\ \Delta A = 24$

^{235}U---*α-β-α-β-α-α-α-α-β-α-β*----------^{207}Pb $\quad \Delta Z = 10,\ \Delta A = 28$

^{237}Np--*α-β-α-α-β-α-α-α-β-α-β*----------^{209}Bi $\quad \Delta Z = 10,\ \Delta A = 28$

Table 6-3. The ^{238}U series and radiations of yield Y_i greater than 1% (x-rays, conversion electrons, and auger electrons are not listed).

		α		β⁻		γ	
Nuclide	**Half-life**	***E* (MeV)**	***Y*$_i$ (%)**	***E* (MeV)[a]**	***Y*$_i$ (%)**	***E* (keV)**	***Y*$_i$ (%)**
^{238}U	4.468×10^9 y	4.15	21				
α		4.2	79				
^{234}Th	24.10 d			0.08	2.9	63.3	4.8
				0.1	7.6	92.4	2.8
β⁻				0.1	19.2	92.8	2.8
				0.2	70.3		
^{234m}Pa[b]	1.17 m			2.27	98.2	766	0.3
IT						1,001	0.84
^{234}Pa	6.75 h			22 β⁻s		1,313	18
				E_{avg} = 0.224		1,527	5.97
β⁻				E_{max} = 1.26			
^{234}U	2.457×10^5 y	4.72	28.4				
α		4.78	71.4				
^{230}Th	7.538×10^4 y	4.62	23.4				
α		4.69	76.3				
^{226}Ra	1600 y	4.6	5.55			186.2	3.6
α		4.79	94.5				
^{222}Rn	3.8235 d	5.49	99.9			510	0.08
α							
^{218}Po[b]	3.11 m	6	100.0				
α							
^{214}Pb	26.8 m			0.19	2.35	53.2	1.11
				0.68	46.0	242	7.5
β⁻				0.74	40.5	295.2	18.5
				1.03	9.3	351.9	35.8
^{214}Bi[b]	19.9 m			0.79	1.45	609.3	44.8
				0.83	2.74	768.4	4.8
				1.16	4.14	934.1	3.03
				1.26	2.9	1,120.3	14.8
				1.26	1.66	1,238.1	5.86
β⁻				1.28	1.38	1,377.7	3.92
				1.38	1.59	1,408.9	2.8
				1.43	8.26	1,729.6	2.88
				1.51	16.9	1,764.5	15.4
				1.55	17.5	2,204.2	4.86
				1.73	3.05	2,447.9	1.5
				1.9	7.18	Nine other γs	
				3.27	19.9		
^{214}Po	164.3 μs	7.69	99.99				
α							
^{210}Pb	22.3 y			0.02	84	46.5	4.25
				0.06	16		
β⁻							
^{210}Bi[b]	5.013 d			1.16	100	1,764.5	15.4
β⁻							
^{210}Po	138.376 d	5.3	100.0				
α							
^{206}Pb	(Stable)						

a Maximum beta energy.

b Branching occurs in 0.13% of ^{234m}Pa to ^{234}Pa by IT; 0.02% of ^{218}Po to ^{218}At by β^-; 0.02% of ^{214}Bi to ^{210}Tl by α; 0.00013% of ^{210}Bi to ^{206}Tl by α.

Source: NNDC (1995).

Table 6-4. The ^{235}U series and radiations of yield Y_i greater than 1% (x-rays, conversion electrons, and auger electrons are not listed).

		α		β⁻		γ	
Nuclide	**Half-life**	***E* (MeV)**	***Y*** $_i$ **(%)**	***E* (MeV)[a]**	***Y*** $_i$ **(%)**	***E* (keV)**	***Y*** $_i$ **(%)**
^{235}U	703.8×10^6 y	4.2–4.32	11			143.8	11
		4.37	17			163.3	5.1
α		4.4	55			185.7	57.2
		4.5–4.6	10.9			205.3	5
^{231}Th	25.52 h			0.21	12.8	25.6	14.5
				0.29	12	84.2	6.6
β^-				0.31	35		
^{231}Pa	3.276×10^4 y	4.95	22.8			27.4	10.3
		5.01	25.4			283.7	1.7
α		5.03	20			300.1	2.5
		5.06	11			330.1	1.4
^{227}Ac	21.773 y	4.94	0.55	0.02	10		
		4.95	0.66	0.03	35		
β^- 98.62%				0.04	54		
α 1.38% ^{227}Th	18.72 d	5.76	20.4			50	8
		5.98	23.5			236	12.3
		6.04	24.2			300	2.3
α						304	1.2
						330	2.7
^{223}Fr	21.8 m			0.91	10.1	50	36
				1.07	16	79.7	9.1
β^-				1.09	67	234.9	3
^{223}Ra	11.435 d	5.43	2.27			144	3.2
		5.54	9.2			154	5.6
α		5.61	25.7			269	13.7
		5.72	52.6			324	3.9
		5.75	9.2			338	2.8
^{219}Rn	3.96 s	6.43	7.5			271	10.8
		6.55	12.9			401.8	6.4
α		6.82	79.4				
^{215}Po[b]	1.781 ms	7.39	100				
α							
^{211}Pb	36.1 m			0.97	1.5	405	3.8
				1.38	91.3	427	1.8
β^-						832	3.5
^{211}Bi	2.14 m	6.28	16.2	0.58	0.28	351	12.9
		6.62	83.5				
α 99.7%	β^- 0.276%						
^{207}Tl	4.77 m			1.43	99.7	898	0.26
β^-							
^{207}Pb	(Stable)						
^{211}Po	0.516 s	7.45	98.9				
α							

a Maximum beta energy

b ^{215}Po has minor branching (0.00023%) by β^- emission to ^{215}At followed by α emission.

Source: NNDC (1995).

Table 6-5. The ^{232}Th series and radiations of yield Y_i greater than 1% (x-rays, conversion electrons, and auger electrons are not listed).

		α		β⁻		γ	
Nuclide	**Half-life**	***E* (MeV)**	***Y*$_i$ (%)**	***E* (MeV)[a]**	***Y*$_i$ (%)**	***E* (keV)**	***Y*$_i$ (%)**
^{232}Th	14.05×10^{9} y	3.95	22.1				
α		4.01	77.8				
^{228}Ra	5.75 y			0.02	40		
β⁻				0.04	60		
^{228}Ac[b]	6.15 h			0.45	2.6	209.3	3.88
				0.5	4.18	270.2	3.43
				0.61	8.1	328	2.95
β⁻				0.97	3.54	338.3	11.3
				1.02	5.6	463	4.44
				1.12	3	794.9	4.34
				1.17	31	835.7	1.68
				1.75	11.6	911.2	26.6
				2.08	10	964.8	5.11
						969.9	16.2
						1,588	3.3
^{228}Th	1.9131 y	5.34	28.2			84.4	1.27
α		5.42	71.1				
^{224}Ra	3.62 d	5.45	5.06			241	3.97
α		5.69	94.9				
^{220}Rn	55.6 s	6.29	99.9				
α							
^{216}Po	0.145 s	6.78	100				
α							
^{212}Pb	10.64 h			0.16	5.17	238.6	43.3
				0.34	82.5	300.1	3.28
β⁻				0.57	12.3		
^{212}Bi	60.55 m	6.05	25.13	0.63	1.87	727.3	6.58
		6.09	9.75	0.74	1.43	785.4	1.1
α 35.9%	β⁻ 64.1%			1.52	4.36	1,621	1.49
				2.25	55.5		
^{212}Po	0.299 μs	8.79	100				
^{208}Tl	3.053 m			1.03	3.1	277.4	6.3
				1.29	24.5	510.8	22.6
				1.52	21.8	583.2	84.5
β⁻	α			1.8	48.7	763.1	1.8
						860.6	12.4
						2,615	99.2
^{208}Pb	(Stable)						

a Maximum beta energy.
b Only gammas with yield greater than 2% listed.
Source: NNDC (1995).

Table 6-6. The ^{237}Np series and ^{241}Pu and ^{241}Am precursors, including radiations of yield Y_i greater than 1% (x-rays, conversion electrons, and auger electrons are not listed).

		α		β⁻		γ	
Nuclide	**Half-life**	***E* (MeV)**	***Y*$_i$ (%)**	***E* (MeV)[a]**	***Y*$_i$ (%)**	***E* (keV)**	***Y*$_i$ (%)**
^{241}Pu	14.35 y	4.85	0.0003	0.021	~100	149	0.0002
α		4.9	0.002				
^{241}Am	432.2 y	5.44	13			26.3	2.4
		5.49	84.5			59.5	35.9
α						26.3	2.4
^{237}Np[b]	2.14×10^6 y	4.64	6.18			29.4	15
		4.766	8			86.5	12.4
α		4.771	25				
		4.79	47				
^{233}Pa	26.976 d			0.16	27.7	300	6.62
				0.17	16.4	312	38.6
β⁻				0.23	40	341	4.47
				0.26	17		
^{233}U	1.592×10^5 y	4.78	13.2			42.4	0.09
α		4.82	84.4			97	0.3
^{229}Th	7340 y	4.82	9.3			31.5	1.19
		4.84	5			86.4	2.57
		4.85	56.2			137	1.18
α		4.9	10.2			156	1.19
		4.97	5.97			194	4.41
		4.98	3.17			211	2.8
		5.05	6.6				
^{225}Ra	14.9 d			0.33	69.5	40	30
β⁻				0.37	30.5		
^{225}Ac	10.0 d	5.73	8			99.6	0.62
		5.79	18.1			157	0.36
α		5.83	50.7			188	0.54
^{221}Fr	4.9 m	6.13	15.1			219	11.6
α		6.34	83.4			411	0.14
^{217}At	0.0323 s	7.07	~100			259	0.06
α							
^{213}Bi	45.59 m	5.87	1.94	0.98	31	293	0.43
β⁻		5.55	0.15	1.42	65.9	440	26.1
^{213}Po	4.2 μs	8.38	~100				
α							
^{209}Pb	3.253 h			0.644	100		
β⁻							
^{209}Bi	(Stable)						

a Maximum beta energy.
b Beginning of ^{237}Np series.
Source: NNDC (1995).

The long-lived parent of each series undergoes transformation by alpha particle emission, which is followed by one or more beta transitions. Near the middle of each series there is a sequence of 3 to 5 alpha emissions, which are followed by one or two beta transformations; and there is at least one more alpha emission before stability is reached. Figure 6-7 illustrates these similarities graphically for the ^{232}Th and ^{238}U series using the same sequences found in the chart of the nuclides. These patterns produce a zigzag path back and forth across a stability "line" (there are no stable nuclides above ^{209}Bi; thus, such a "line" is only theoretical) extrapolated from the zigzag line of stable nuclides below ^{208}Pb or ^{209}Bi.

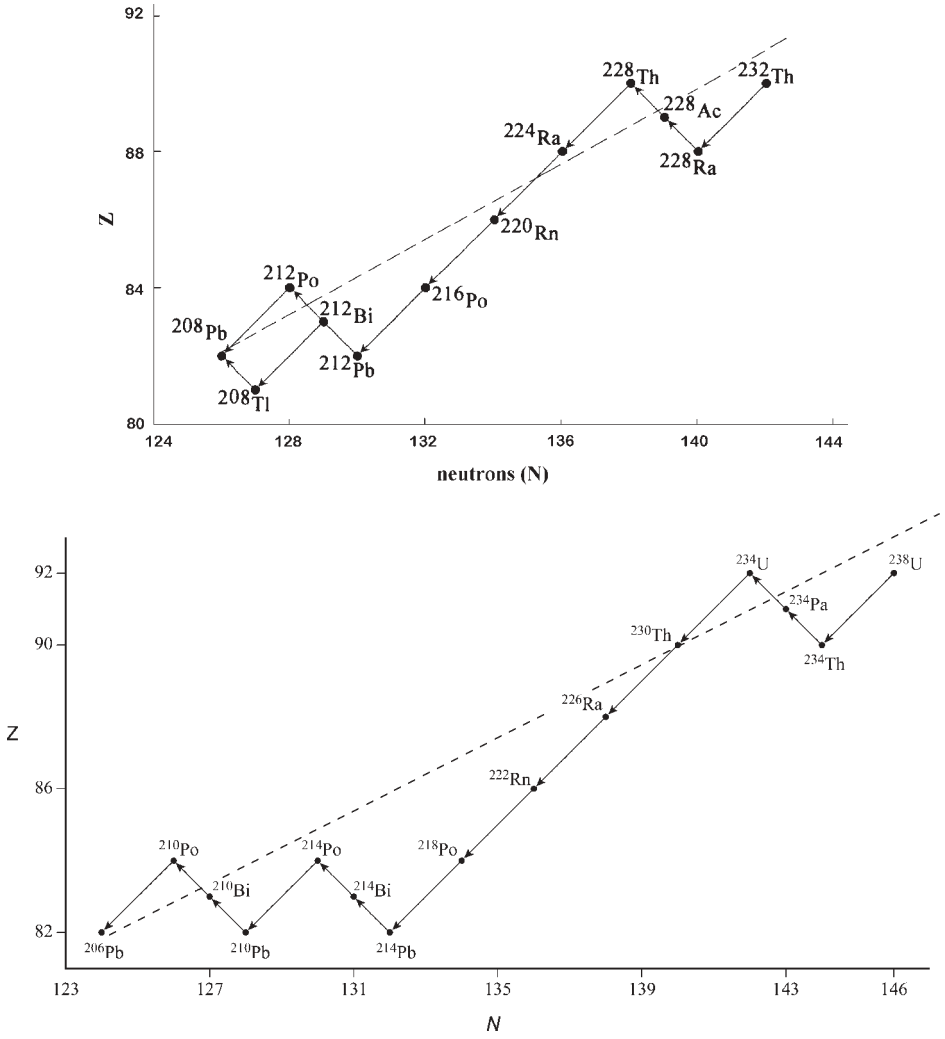

Fig. 6-7 Comparative series transformation of ^{232}Th and ^{238}U relative to an extrapolated line of stability.

The zigzag patterns in the ^{238}U series shown in Figure 6-7 suggest some explanation for the types of transformation that occur. In the ^{238}U series the first alpha particle emission produces a product that is quite a bit less stable, and apparently farther away from the line. Beta emissions from ^{234}Th and ^{234}Pa bring the product nuclei back across the stability line, apparently in search of a stable endpoint. The resulting product is once again well away from the line of stability, and a sequence of five alpha particle emissions occurs from ^{234}U to ^{214}Pb again producing product nuclei that move steadily away from the line. This departure is reflected in the half-life sequence in the ^{238}U series: 2.5×10^5 y, 8×10^4 y, 1.6×10^3 y, 3.82 d, and 3.11 min. Beta particle emissions then occur to bring the nuclei back across the stability line, followed by alpha emission to the stable end product of ^{206}Pb. Somewhat similar sequences are observed in the other series (see Figure 6-7).

In practical terms, the uranium series contains several subseries in addition to ^{238}U itself. The more important ones are ^{230}Th, ^{226}Ra, ^{222}Rn, and ^{210}Pb and their subsequent products. Thorium-230 is strongly depleted from its precursors in sea water and enhanced in bottom sediments; thus, it can also be used to date such sediments. It has also been found in raffinates from uranium processing, and as such represents a separated source that produces ^{226}Ra and ^{222}Rn and their products. Radium-226 is often found separated from its precursors, and is rarely found in sufficient concentrations to precipitate in the presence of anions for which it has a strong affinity, particularly sulfate, although ^{226}Ra "hot spots" remain where uranium deposits have contacted sulfuric acid from natural oxidation of ferrous sulfide. Once released into natural waters, ^{226}Ra and other radium isotopes are mobile until scavenged or coprecipitated, e.g., the cement-like calcium carbonate "sinters" around some hot springs. Radium can also be separated from its precursors by precipitation and recrystallization as either the chloride or the bromide. When freshly prepared, and free of its decay products, ^{226}Ra produces minimal gamma radiation (a 0.19 MeV gamma ray is emitted in 6% of ^{226}Ra transformations). However, as ^{222}Rn and its succeeding products achieve equilibrium, the gamma intensity increases substantially.

Radon-222 is also a subseries when separated from ^{226}Ra as it often is because it is a noble gas and the only gaseous member of the ^{238}U series. It is produced from ^{226}Ra and grows into any radium source in a few days. Since it is a noble gas it can migrate away from ^{226}Ra and its other long-lived parents or be readily separated from them and when it becomes separated it is a subseries. Radon-222 can be removed from radium sources, and because of its high intrinsic specific activity can be concentrated into tubes and needles for implantation in malignant tissues for treatment of disease. For similar reasons, ^{222}Rn was obtained from ^{226}Ra generators by early researchers to be mixed with beryllium to produce neutrons. Radon-222 has a half-life of 3.82 d and its principal transformation products are ^{218}Po, ^{214}Pb, ^{214}Bi, and ^{214}Po, which have half-lives ranging from 26.8 min to 164 μs. The gamma rays of ^{214}Bi have the highest yield and are the most energetic of the uranium series which make this subseries important with respect to external radiation.

Lead-210, a long-lived radon transformation product, heads the final subseries of ^{238}U. Lead-210 itself and its ^{210}Bi and ^{210}Po products can be observed in significant concentrations in the atmosphere. The stable end product of this subseries, and the end of the ^{238}U series, is ^{206}Pb.

The thorium series may also be considered in three subseries: ^{232}Th itself, ^{228}Ra, and ^{220}Rn. Thorium-232 is the least mobile of the series radionuclides. It exists naturally in the tetravalent state as a very stable oxide or in relatively inert silicate minerals, and it is strongly adsorbed on silicates. The subseries headed by ^{228}Ra yields ^{228}Ac, ^{228}Th, and ^{224}Ra, which are generally in radioactive equilibrium. The third subseries is headed by ^{220}Rn (thorium emanation, or thoron) which has a 56 s half-life and which quickly forms transformation products down to stable ^{208}Pb, the longest lived of which is 10.6 h ^{212}Pb. Although generally less important than ^{222}Rn in the uranium series, ^{220}Rn and its products can occasionally present radiation exposure situations if high concentrations of ^{228}Ra exist. An important product of ^{220}Rn (and ^{228}Ra itself because of the short half-life of ^{220}Rn) is ^{208}Tl, which emits 2.62 MeV gamma rays that can produce significant gamma exposures from residues of thorium recovery.

6.5.1
Neptunium Series Radionuclides

Primordial sources of ^{237}Np ($T_{1/2} = 2.14 \times 10^6$ y) have long since decayed away; however, once produced it can be a challenge to provide long-term management as a waste product. Two important precursors of ^{237}Np are ^{241}Pu and ^{241}Am, both of which are fairly abundant because ^{241}Pu is produced by neutron activation of ^{239}Pu through ^{240}Pu in nuclear reactors. Plutonium-241 is transformed by beta particle emission to ^{241}Am which emits alpha particles to become ^{237}Np. Americium-241 is used in smoke detectors, and if disposed in landfills can accumulate a source of ^{237}Np and its series products.

6.6
Singly Occurring Primordial Radionuclides

Naturally occurring primordial radioactive nuclides exist that are not members of any of the four series. Most of the major ones are listed in Table 6-7. Each of these nonseries nuclides has an extremely long half-life and a correspondingly low specific activity which makes detection and identification of the emitted radiations very difficult. Some nuclides, now thought to be stable, may be added in the future because of detectable radioactivity. Bismuth-209, now considered to be stable and the endpoint of the neptunium series, has been on and off this list; it is currently believed to be stable ($T_{1/2} > 10^{18}$ y). So has ^{192}Pt, which is also now considered stable.

Table 6-7. Naturally occurring primordial radionuclides.

Nuclide	Abundance (%)	$T_{1/2}$ (y)	Emission(s)	Q (MeV)
^{40}K	0.0117	1.27×10^{9}	β^-, EC, γ	1.505, 1.311
^{50}V	0.25	1.4×10^{17}	β^-, EC, γ	2.208
^{87}Rb	27.83	4.9×10^{10}	β^-	0.283
^{113}Cd	12.22	9.3×10^{15}	β^-	0.316
^{115}In	95.7	4.4×10^{14}	β^-	0.495
^{123}Te	0.91	$>1.3 \times 10^{13}$	EC	0.052
^{130}Te	33.87	1.25×10^{20}	$\beta^-\beta^-$	0.42
^{138}La	0.09	1.05×10^{11}	EC, β^-, γ	1.737, 1.044
^{142}Ce	11.13	5.0×10^{16}	α	?
^{144}Nd	23.8	2.1×10^{15}	α	1.905
^{147}Sm	15	1.06×10^{11}	α	2.31
^{152}Gd	0.2	1.08×10^{14}	α	2.205
^{174}Hf	0.162	2.0×10^{15}	α	2.496
^{176}Lu	2.59	3.8×10^{10}	β^-, γ	1.192
^{180}Ta	0.012	$>1.2 \times 10^{15}$	EC, β^+, γ	0.853, 0.708
^{186}Os	1.58	2.0×10^{15}	α	2.822
^{187}Re	62.6	4.4×10^{10}	β^-	0.00264
^{190}Pt	0.01	6.5×10^{11}	α	3.249

Source: NNDC (1995).

There is no obvious pattern to the distribution of the long-lived, nonseries radioactive nuclei. Some of the half-lives are surprisingly long in view of the energies available in the transitions. The double-beta transformation of ^{130}Te to ^{130}Xe is unique and has been used in connection with the properties of the neutrino. All of the half-lives listed in Table 6-7 are compatible with the formation of the elements at about the time of the Big Bang some 4.5 billion years ago.

The primordial radionuclides of ^{40}K and ^{87}Rb are of particular interest to radiation protection because of their presence in environmental media and their contribution to human exposure. Potassium-40 contributes about 40% of the exposure humans receive from natural radiation. It is present in natural potassium with an isotopic abundance of 0.0117% and has a half-life of 1.28×10^9 y. It undergoes radioactive transformation both by electron capture (10.67 %) and beta particle emission (89.23 %). The beta particle has a maximum energy of 1.312 MeV (aver-

age energy 0.51 MeV). Electron capture is followed by emission of a 1461 keV gamma ray in 10.7% of the transformations of ^{40}K, conversion electrons (0.3% of ^{40}K transformations), and the usual low-energy Auger electrons and characteristic x-rays. The average elemental concentration of potassium in reference man is 2% which produces annual doses of 14 mrem to bone surfaces, 17 mrem on average to soft tissue, and 27 mrem to red marrow (UN 1988). It also contributes in a major way to external exposure due to an average soil concentration of 12 pCi/g. This concentration results in an annual whole-body dose equivalent due to external gamma radiation of 12 mrem (UN 1988).

Rubidium-87 has a half-life of 4.8×10^{10} y and emits beta particles of maximum energy of 292 keV (average energy ~79 keV). Its natural isotopic abundance is 27.84% and the mass concentrations in reference man range from 6 ppm in the thyroid to 20 ppm in the testes (ICRP 1975). It contributes an annual dose to body tissues of 1.4 mrem to bone surface cells (UN 1988) and an annual effective dose equivalent of about 0.6 mrem.

6.7 Radioactive Ores and Byproducts

Many ores are processed for their mineral content which enhances either the concentration of the radioactive elements in process residues or increases their environmental mobility; these processes result in materials that are no longer purely "natural." The presence of uranium and/or thorium, ^{40}K, and other naturally radioactive materials in natural ores or feedstocks is often the result of the same geochemical conditions that concentrated the main mineral-bearing ores (e.g., uranium in bauxite and phosphate ore) or that led to separation of decay products like radium into groundwater. Radium in groundwater has been observed to concentrate onto water treatment filters or pipes and equipment used in oil and gas recovery. These technologically enhanced sources of naturally occurring radioactive material represent radiation sources that can pose generally low-level radiation exposures of the public, or in some localized areas exposures significantly above the natural background.

Various sites contain residues of naturally occurring radionuclides, principally the series products of ^{238}U and ^{232}Th. For example, processing of uranium-rich ores for the uranium required for the Manhattan Project in World War II created residues containing thorium, radium, and other transformation products of uranium. These and related issues enjoy a special category in radiation protection called NORM (naturally occurring radioactive material) and technologically enhanced NORM, or TENORM. A similar categorization is NARM (naturally occurring and accelerator-produced radioactive material), which captures those materials not regulated under the Atomic Energy Act of 1954, as amended.

Enhanced levels of NORM may be difficult to discern because natural concentrations of ^{226}Ra, ^{40}K, and ^{232}Th and its products vary widely, especially in minerals and extracts, as shown in Table 6-8.

Table 6-8. Radiological constituents of selected minerals and extracts.

Mineral	Nuclide(s)	Concentration (pCi/g)
Aluminum ore	U	6.76
Bauxitic lime, soil	Th	0.8–3.5
Bauxitic lime, soil	Ra	3–10
Tailings	Ra	20–30
Iron	U + products	Varies
	Th + products	Varies
Molybdenum	U + products	Varies
Tailings	U + products	Varies
Monazite	Th + products	4–8%
	U + products	150–500
Natural gas		
USA	^{222}Rn	0.1–500 pCi/L
Canada	^{222}Rn	0.01–1500 pCi/L
Scale	^{210}Pb	3–1500
Oil		
Brines	^{226}Ra	3–3000
Sludges	^{226}Ra	30–2000
Scales	^{226}Ra	300–100,000
Phosphate ore	U + products	3,000-100,000
	Th + products	400–4000
	^{226}Ra	15–100
Potash	Th + products	Varies
	^{40}K	Varies
Rare earths	U + products	Varies
	Th + products	Varies
Vanadium	U + products	Varies
Zirconium	U	~100
	Th	~15
	Ra	100–200

Source: NCRP (1993).

6.7.1 Resource Recovery

Resource recovery of metals and oil and gas has produced huge inventories of NORM radionuclides that are discarded because they are not of value or interest to the recovery industry. For example, vanadium mining in Colorado produced residues that contained uranium; these residues (or tailings) were later reprocessed for uranium producing the usual uranium tailings with elevated concentrations of ^{230}Th and ^{226}Ra and their transformation products. Similar circumstances exist to varying degrees for aluminum, iron, zironium, and other metals.

Removing a mineral from ore can concentrate the residual radioactivity especially if the ore is rich, i.e., it contains a high fraction of the metal of interest. This process of concentration is called beneficiation. For example, bauxite is rich in aluminum, and its removal yields a residue in which uranium and radium originally present in the ore can be concentrated to 10–20 pCi of ^{226}Ra per gram in the residues, or "red mud," so called because its iron content (also concentrated) has a red hue. Similarly, processing phosphate rock in furnaces to extract elemental phosphorous produces a vitrified waste called slag which contains 10–60 pCi/g of ^{226}Ra. Slag has been commonly used as an aggregate in making roads, streets, pavements, residential structures, and buildings. Such uses of high bulk materials from ore processes raise risk/benefit tradeoffs of the values of such uses and whether exposure conditions exist that warrant attention. High volumes and relatively low, but enhanced, concentrations make such decisions challenging. For example, radium-contaminated soil from radium recovery in Montclair, NJ, and Denver, CO, caused higher than normal direct gamma radiation exposure levels. The use of elemental phosphorus slag to construct streets, roads, and parking lots in Soda Springs and Pocatello, ID, has doubled the natural background radiation levels in some areas. In Mississippi and Louisiana, the use of pipes contaminated with radium scale in playgrounds and welding classes has resulted in some radiation exposures to students.

6.7.2 Uranium Ores

Prior to Becquerel's discovery, uranium had been mined for use as a coloring agent in the glass industry. Most of the material used in this way came from the Joachistimal mines in Czechoslovakia, which was also the source of pitchblende, a brown-black ore which contains as much as 60–70% uranium as the oxide U_3O_8, commonly called yellowcake because of its golden color when purified. The US form is primarily yellow carnotite (hydrated potassium uranium vanadate) which was first processed for vanadium, then later to recover uranium when it became valuable.

The principal radioactive products associated with uranium residues are the tailings from milling the ores to extract uranium oxide. These tailings contain ^{230}Th and ^{226}Ra in concentrations directly related to the richness of uranium in the orig-

inal ores. Radon gas is continually produced by ^{226}Ra in the tailings, which requires that they be managed to preclude radon problems as well as ^{226}Ra exposures. Some milling processes contain a large fraction of ^{230}Th; for example, raffinate streams, which contained much of the ^{230}Th, were sluiced to separate areas for storage and/or further processing. These ^{230}Th residues represent minor radiation problems in themselves since ^{230}Th is a pure alpha emitter, but its radioactive transformation produces ^{226}Ra which will slowly grow in to create a future source of external gamma radiation and radon gas. Modern management of uranium tailings is done under regulations that require stabilization for up to 1000 years in such a way that emissions of radon and its products are controlled. Older abandoned mill sites are being remediated to achieve the same requirements.

6.7.3 Water Treatment Sludge

Most water treatment wastes are believed to contain ^{226}Ra in concentrations comparable to those in typical soils. However, some water supply systems, primarily those relying on groundwater sources, may generate sludge with higher ^{226}Ra levels especially if the process equipment is effective in removing naturally occurring radionuclides from the water. A typical drinking water source contains about 8 pCi/L of ^{226}Ra which yields an average ^{226}Ra concentration of about 16 pCi/g in sludge after processing. About 700 water utilities in the USA generate and dispose of 300,000 metric tons (MT) of sludge, spent resin, and charcoal beds in landfills and lagoons, or by application to agricultural fields.

6.7.4 Phosphate Industry Wastes

Phosphate deposits occurred by geochemical processes in ancient seas that were also effective in depositing uranium; thus, some phosphate deposits, principally in Florida (see Figure 6-8), contain significant amounts of uranium and its radioactive progeny. Uranium in phosphate ores found in the USA ranges in concentration from 20 to 300 ppm (or about 7 to 100 pCi/g), while thorium occurs at essentially ambient background concentrations, between 1 and 5 ppm (or about 0.1 and 0.6 pCi/g).

Phosphate rock is processed to produce phosphoric acid and elemental phosphorus. Some 5 million MT of phosphate rock is used each year to produce fertilizer which contain 8 pCi/g of ^{226}Ra; thus 20 years of repeated fertilizer applications would increase the soil concentration by about 0.002 pCi/g above a natural soil concentration of 0.1–3 pCi/g. About 86% of the uranium and 70% of the thorium originally present in the ore are found in the phosphoric acid because the process used to extract phosphorous also entrains these elements.

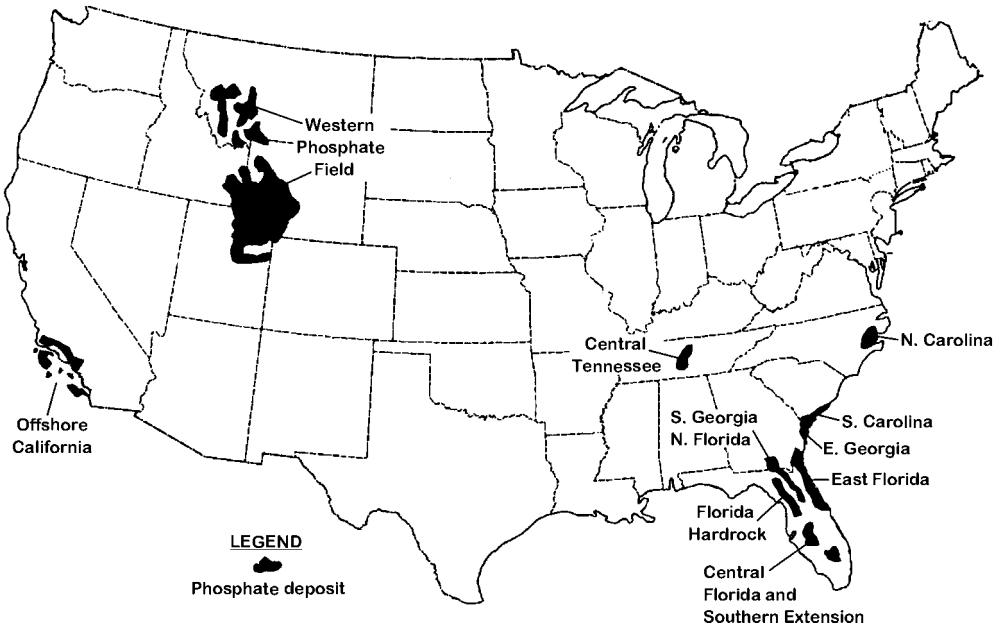

Fig. 6-8 Major uraniferous phosphate deposits in the USA.

Phosphogypsum is the principal waste byproduct generated from the production of phosphoric acid. It is stored in waste piles called stacks and contains about 80% of the ^{226}Ra originally present in the phosphate rock. A huge inventory of phosphogypsum totaling some 8 billion MT now exists, which is being increased at rate of about 40 million MT per year. Phosphogypsum stacks are huge, ranging from 2 to 300 hectares (750 acres) in area and from 3 to 60 m high. They are typically covered with water in ponds, beaches, and ditches. Sixty-three large stacks and three relatively smaller ones exist, mostly in Florida. Phosphogypsum could be used in wall board or applied as a soil conditioner but such use is very small because it contains radium which most consumers would expect to be removed.

6.7.5 Elemental Phosphorus

About 10% of mined phosphate ore goes into production of elemental phosphorus which is used in the production of high-grade phosphoric acid, phosphate-based detergents, and organic chemicals used in cleaners, foods, baking powder, dentifrice, animal feed, etc. There are only eight elemental phosphorus plants in the USA, and these are located in Florida, Idaho, Montana, and Tennessee; only three are active: two in Idaho, and one in Montana. Production of elemental phosphorus has declined from a peak of 4 million MT in 1979 to 310,000 MT in 1988, a trend that is expected to continue due to rising energy costs and decreasing demand.

Slag is the principal waste byproduct of elemental phosphorus, and ferrophosphorus is also a byproduct. Because of furnace temperatures, the slag is a glassy-like material which seals the radionuclides in a vitrified matrix which reduces their leachability. Some 90% of phosphate rock ore processed into elemental phosphorus ends up in slag, and large inventories (some 200 million to 400 million MT) of slag are stored at operating and closed elemental phosphorus plants. Some of this inventory has, until recently, been used in road building, paving of airport runways and streets, and backfill which may cause exposure to the public due to external gamma radiation (radon emanation is minimal because of the glassy matrix of slag).

6.7.6 Manhattan Project Wastes

During World War II a major effort, called the Manhattan Project, required considerable amounts of uranium to develop an atomic bomb. The African Metals Co. provided over 1200 tons of pitchblende from the Belgian Congo to the US Government in the early 1940s. This material contained as much as 65% uranium, and was processed at a number of nongovernment owned sites in the 1940s, and to some extent into the 1950s and 1960s. As a result, many private properties, including former laboratories, processing facilities, and waste disposal facilities, contain residues of naturally radioactive materials from storage, sampling, assaying, processing, and metal machining. Over 2 million cubic yards of soil and soil-like material that contain various concentrations of ^{238}U, ^{234}U, ^{230}Th, ^{226}Ra, ^{232}Th, and ^{228}Ra and their associated transformation products remain at these sites. In some cases, contaminated material from these properties spread to surrounding properties, including many residential properties, through erosion and runoff or improper management. Most of the radioactivity concentrations are less than 50 pCi/g; however, some materials contain thousands of pCi/g of ^{226}Ra or ^{230}Th.

The major radionuclides in Manhattan Project residues are ^{230}Th and ^{226}Ra since the parent ores were processed to remove uranium which was scarce and very valuable for development of nuclear weapons. It is fortunate that African Metals Co. also required the USA to remove most of the ^{226}Ra which was considered valuable at the time; it is equally unfortunate that the ^{226}Ra materials (labeled K-65) were poorly handled after African Metals Co. decided it no longer wanted them. Thorium-230 transforms into ^{226}Ra which has a 1600 y half-life; thus, if the ^{226}Ra has been removed (as it was in the Manhattan Project) the residues pose little exposure because ^{226}Ra and its gamma-emitting transformation products are absent and ^{230}Th by itself does not produce significant gamma radiation. However, after several hundred years ^{226}Ra and its radioactive products will grow back in.

The Belgian Congo pitchblende also contained significant amounts of ^{235}U and its transformation products even though the abundance of ^{235}U in natural uranium is only 0.72%. The richness of the ores accounts for two other interesting

circumstances associated with the process residues. Whereas ^{222}Rn is effectively a subseries in the ^{238}U series, ^{219}Rn, its counterpart in the actinium (^{235}U) series, is rarely observed in nature because the concentration of ^{235}U in most ores is so low and the half-life of ^{219}Rn is so short (3.96 s). However, ^{219}Rn is noticeably present in the process residues left over from the Belgian Congo ores, although it is not a health threat due to its short half-life.

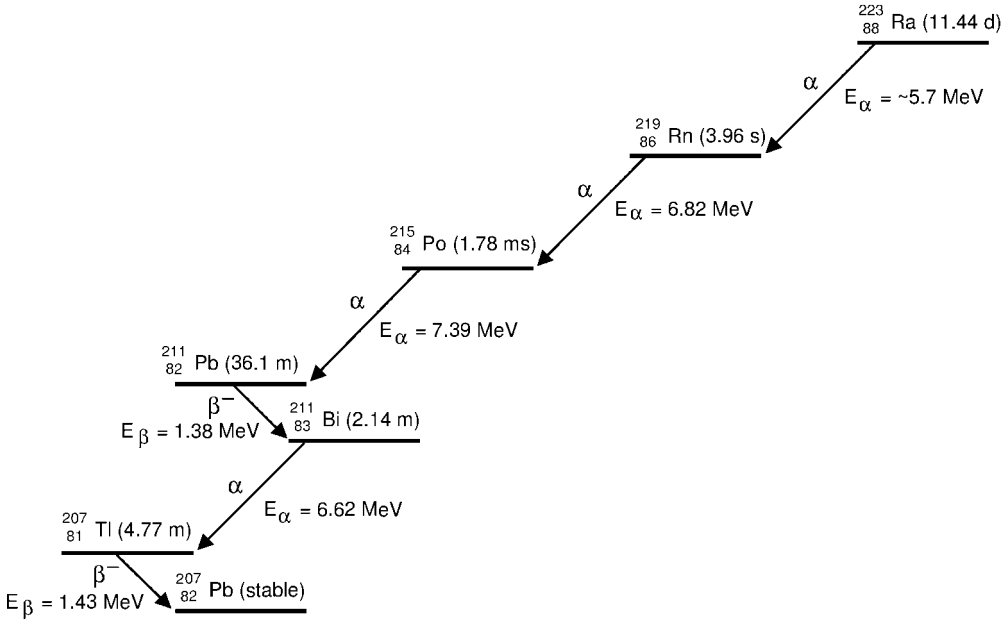

Fig. 6-9 Radioactive transformation of ^{223}Ra to stable ^{207}Pb, a subseries of the actinide (^{235}U) series.

In a similar way, ^{227}Ac, a transformation product in the actinium series, is also present in significant concentrations due to the large amounts of ^{235}U in the rich ores. This nuclide can be separated and used in interesting ways. Since it is fairly long lived ($T_{1/2}$ = 21.773 y), ^{227}Ac was used for a period as the alpha emitter of choice to be mixed with beryllium to produce neutron initiators for nuclear weapons. It has recently found application as a generator of ^{223}Ra ($T_{1/2}$ = 11.435 d) which can be tagged onto a monoclonal antibody or injected as a colloid into a tumor site. Purified ^{227}Ac is captured on a resin column and the ^{223}Ra product which grows in after a few weeks is in turn eluted off for processing. As such, ^{223}Ra and its subsequent alpha-emitting transformation products, which rapidly reach radioactive equilibrium, can deliver a whopping radiation dose to cancer cells. Figure 6-9 shows schematically that each transformation of ^{223}Ra can yield about 28 MeV of deposited energy if it can be assumed that ^{219}Rn does not diffuse away from the cancer site.

Although ^{227}Ac exists as a subseries of the ^{235}U series, it is perhaps more practical to produce it by an (n,γ) reaction with ^{226}Ra in reactors rather than by separating it from K-65 or other actinium ore residues. Such production requires high neutron fluxes which are available in large reactors, and neutron activation to ^{227}Ac may be a useful way to convert considerable amounts of ^{226}Ra to more useful products; ^{226}Ra itself is now problematic since earlier uses of the material have been replaced by artificially produced radionuclides.

6.7.7 Thorium Ores

Thorium ores have been processed since about 1900 to recover rare earth elements and thorium, a soft silvery metal used in specialized applications such as welding electrodes, gas lantern mantles, ultraviolet photoelectric cells, and in certain glasses and glazes. Thorium-232 is also a "fertile" material that can be transmuted by neutron irradiation into ^{233}U, a fissionable material.

Thorium-232 is a naturally occurring radionuclide, which heads the thorium series of radioactive transformation products (see Table 6-4). Concentrations of 1 pCi/g are typical of natural soils and minerals, but some areas of the world contain significant thorium; for example, Monazite sands in Brazil and India contain 4–8% thorium.

Thorium extraction does not appear to have been as thorough as that for uranium, or perhaps not as much care was exercised because sources are more available. And, of course, processing for rare earths would not preferentially remove the thorium which would become a waste byproduct. Regardless, residues from processing monazite and other thorium-rich ores may still contain significant amounts of ^{232}Th, and huge inventories of these residual materials exist. Thorium-232 emits alpha particles to become ^{228}Ra ($T_{1/2}$ = 5.75 y) which will exist in secular equilibrium with ^{232}Th some 40 y after ^{232}Th is purified. Radium-228 has a number of short-lived, gamma-emitting decay products; thus, even if radium is removed in processing ^{232}Th will produce an external gamma flux after a few decades. Concentrations of 5 pCi/g of ^{232}Th in equilibrium with its transformation products and spread over a large area with no soil cover will produce an estimated exposure of 15 mrem/y to an average person standing on the area.

Residues that contain significant concentrations of ^{232}Th represent long-term radiological source terms because each of the transformation products will achieve equilibrium in about 40 y and will continue indefinitely because they are driven by the ^{232}Th parent with a half-life of 10 billion years. The series transformation products emit significant gamma radiation primarily from ^{208}Tl at 2.6 MeV (see Table 6-4). If, however, ^{232}Th were removed then the remaining products would constitute a subseries headed by ^{228}Ra ($T_{1/2}$ = 5.75 y) and through series decay would be effectively eliminated in about 40 y.

Whereas radon exposures can be significant for uranium wastes if elevated ^{226}Ra concentrations exist in soil and a structure is present, ^{220}Rn (thoron) in the ^{232}Th series is of minor significance because it has such a short (56 s) half-life. In general, concentrations of thoron are quite low and generally undetectable.

6.8 Radioactivity Dating

6.8.1 Carbon Dating

Carbon dating of objects that were previously alive depends on an assumption that cosmic ray production of ^{14}C and its natural distribution has remained constant throughout the time interval being considered. In general, this assumption is valid with the exception of the past 150 years or so in which the ^{14}C pool has been perturbed by the burning of fossil fuels and the atmospheric testing of nuclear weapons.

Cosmic ray interactions in the atmosphere produce copious quantities of neutrons with MeV energies. Oxygen in the atmosphere is essentially transparent to these neutrons, but they interact readily with ^{14}N to form ^{14}C through (n,p) interactions about 99% of the time and tritium in the remaining 1% by (n,t) reactions. It is well established that the neutrons that produce these interactions are secondary products of cosmic ray interactions in the atmosphere for two reasons. First, since free neutrons are radioactive with a life of only about 12 min, they would not last long enough to have come from outer space; second, because their concentration rises up to an altitude of about 40,000 ft and then decreases.

Atmospheric ^{14}C exists primarily as $^{14}CO_2$ which diffuses throughout the atmosphere and comes into equilibrium with the carbonate pool of the earth; thus, it will be acquired by any living organism that metabolizes carbon. While alive, the organisms will contain carbon in a constant $^{14}C/^{12}C$ ratio, which, before the advent of atmospheric testing of nuclear devices, was about 15.3 d/m per gram of carbon. When an organism (e.g., a plant or animal) dies, ^{14}C incorporation ceases and the ^{14}C activity per gram of carbon will then decrease with a half-life of 5700 y; thus, measurement of the activity per gram can be used to fix the time of death. Organic materials can be dated by ^{14}C measurements to about 50,000 y because of the half-life of ^{14}C and the concentration of carbon in materials of interest.

The accuracy of radiocarbon dating is influenced by human activity, principally the fossil fuel effect (or Suess effect) and ^{14}C production by nuclear weapon tests. Since about 1850, the combustion of coal and oil has released large quantities of ^{14}C-free CO_2 since coal and oil are millions of years old and the ^{14}C in these hydrocarbons has long since decayed away. Injecting this "old" carbon into the atmosphere dilutes the radiocarbon activity of recently grown samples by about 2% compared to samples prior to 1850. Early dating laboratories used recently grown samples as a standard of ^{14}C activity before the importance of the Suess effect was recognized, and dates based on such recent samples are too young by 100–200 years. New standards prepared by the US National Institute of Standards and Technology (NIST) and Heidelberg University should remove these inaccuracies. Offsetting somewhat the fossil fuel effect since 1954 has been the production of ^{14}C by hydrogen bomb explosions. The radioactivity of plants grown since that time has risen to a little under 1% higher than in the pre-bomb era.

Since ^{14}C is heavier than ^{12}C, it is concentrated somewhat higher in ocean carbonate in the exchange reaction between the atmosphere and the ocean. The ^{14}C concentration in terrestrial plant life resulting from the photosynthesis of atmospheric carbon dioxide is lower, and modern wood should be about 4% lower in ^{14}C than air. Marine plants, however, are less affected than wood because they are fed by bicarbonate already enriched in ^{14}C relative to atmospheric $^{14}CO_2$. Also modern carbonate is enriched in ^{14}C, and there is a calculated 5% ^{14}C excess in the shells of marine organisms compared with wood. This 5% enrichment means that the date for shell would be 400 years older relative to modern wood.

6.8.2
Dating by Primordial Radionuclides

For ages ranging in millions of years, several methods have been developed that are based upon the radioactive transformation of elements occurring naturally in the earth's crust at its formation. Of these, the most useful are

^{238}U ($T_{1/2}$ = 4.47 billion years) to ^{206}Pb

^{232}Th ($T_{1/2}$ = 14.0 billion years) to ^{208}Pb

^{230}Th ($T_{1/2}$ = 80,000 years) to ^{226}Ra

^{87}Rb ($T_{1/2}$ = 48 billion years) to ^{87}Sr

^{40}K ($T_{1/2}$ = 1.28 billion years) to ^{40}Ar

The age of a rock sample can be determined by measuring the relative amounts of the primordial "parent" radionuclide and its related transformation product, usually by means of a mass spectrometer. For example, the greater the amount of ^{206}Pb relative to ^{238}U in a sample, the greater is the age of that sample. This was one of the earliest applications of radioactive dating because the complete transformation of ^{238}U is equivalent to

$$^{238}U \rightarrow {}^{206}Pb + 8\alpha + 6\beta + \gamma\text{'s}$$

The longest intermediate half-life is 75,380 y ^{230}Th; however, after a few million years, the holdup at this point will be negligible compared to the amount of ^{206}Pb that has been formed. If one can be sure that no ^{206}Pb was formed by other processes, an assay for the two nuclides in question will serve to determine the time at which the ^{238}U was incorporated into the mineral. Times determined by this method agree well with those obtained from purely geological considerations. An assay for ^{4}He may also be used when there is some doubt as to the radiogenic purity of the ^{206}Pb; however, helium can diffuse out of porous structures and caution is in order when age determinations are based on ^{4}He gas analyses.

6.8.3 Potassium–Argon Dating

Radioactive dating can also be done with ^{40}Ar, a radioactive transformation product of ^{40}K, a primordial radionuclide, which undergoes radioactive transformation by two competing decay modes:

$$^{40}K \rightarrow {}^{40}Ca + \beta^- + \bar{\nu}$$

$$^{40}K + e^- \rightarrow {}^{40}Ar + \gamma$$

Eighty-nine percent of the transformations of ^{40}K are by beta emission, and 11% produce ^{40}Ar by electron capture. Both of the product elements are found in nature with well-established abundances. If radiogenic ^{40}Ar is present, measurement with a mass spectrometer will show an abnormal $^{39}Ar/^{40}Ar$ ratio and the excess ^{40}Ar can be attributed to transformation of ^{40}K.

This method has been used successfully to date samples up to about 2 million years old. Volcanic ash beds interlayered with fossils are ideal sources because they can be stratigraphically defined. The potassium-bearing mineral laid down by molten lava would contain no ^{40}Ar since, as a gas, it would have boiled away. After the lava layer cooled, however, all ^{40}Ar atoms produced by ^{40}K transformation would be entrapped in the matrix. The number of ^{40}Ar atoms locked therein is a direct measure of the time required to produce them.

Use of the potassium–argon method relies on the ratio of ^{40}K atoms to ^{40}Ar atoms. The ^{40}Ar atoms can be distinguished from other isotopes of argon whereas ^{40}Ca atoms are nearly impossible to distinguish from naturally occurring ^{40}Ca atoms. The method is a two-step process. First, it is necessary to remove surface-layer ^{40}Ar atoms that may have been entrained from the air since only the ^{40}Ar atoms within the sample are wanted. These are removed by heating the sample in a vacuum furnace at about 750 °F for 12–48 h. After the surface-layer Ar is removed, the sample is heated to about 2200 °F to melt the rock and release the entrapped ^{40}Ar atoms from inside the rock matrix. These are absorbed on porous charcoal cooled to –40 °F and their number is determined by mass spectrometry or neutron activation analysis. The mass spectrometer uses a magnetic field to separate the lighter and heavier argon atoms into separate circular paths and aims them at an electronic target where they are registered. A separate sample of the rock is analyzed for the gamma emission rate to quantify ^{40}K and the relative amounts of each are used to date the sample.

The potassium–argon technique requires separate analyses of potassium in a sample and the entrapped argon. A modification of the technique, called argon–argon dating, is to place the sample in a flux of fast neutrons to produce ^{39}Ar by (n,p) interactions with ^{39}K in natural potassium at 93.3% abundance. The rock sample is then heated, the argon collected, and a mass spectrogram ratio of $^{39}Ar/^{40}Ar$ obtained. After suitable correction for irradiation time, depletion of ^{40}Ar to ^{41}Ar by neutron activation, and fractional transformation of ^{40}K by electron cap-

ture to ^{40}Ar, the age of the sample is directly related to the argon ratio. The method can be used to test various layers of rock by differential heating, and has the advantage that experimental errors cancel out in determining the $^{39}Ar/^{40}Ar$ ratio, which can be precisely done with mass spectroscopy.

6.8.4 Ionium (^{230}Th) Method

The ionium, or ^{230}Th ($T_{1/2}$ = 75,380 y), method can be used to date some deep ocean sediments. Ionium is continually formed in seawater and in rocks by the radioactive transformation of uranium (see Table 6-8). The chemistry of the ocean causes ^{230}Th to be preferentially deposited in sediments where its radioactivity decreases according to its own half-life rather than the half-life of uranium which remains in the seawater. The transformation product of ^{230}Th is ^{226}Ra ($T_{1/2}$ = 1600 y); thus, measuring the radium concentration, which can be done with gamma spectroscopy, yields the amount of ^{230}Th. The ionium method can only be used alone if the sediment has been deposited in an undisturbed condition and is of uniform mineralogical composition over its thickness; however, this restriction can be overcome by measuring the activity of ^{231}Pa, a transformation product of ^{235}U, which is also deposited preferentially along with ionium from seawater. Since its half-life is only 38,800 y, the ratio of the activities of ^{231}Pa and ^{230}Th is a measure of the age of the sediment, independent of the rate of deposition.

6.8.5 Lead-210 Dating

Lead-210, with a half-life of 22.6 y, can be used to date recent sediments that have remained relatively stable, for example in lakes and estuaries. Lead-210 is the end product of the relatively short-lived ^{222}Rn decay series. Radon-222 ($T_{1/2}$ = 3.82 d) is fairly uniformly dispersed within the atmosphere from decay of uranium and radium in soils and minerals, and produces a relatively steady ubiquitous fallout of long-lived ^{210}Pb, which is transferred from the atmosphere to the lithosphere in about a month. If the buildup of sediment layers can be assumed to be uniform and steady, a not unreasonable assumption, the activity of ^{210}Pb will decrease with depth in sediments, allowing the age of a given sediment layer to be estimated. This dating method is based on the assumption that there is a uniform flux of ^{210}Pb to the sediments and that the sediments are not disturbed after deposition occurs. Further, core samples need to be collected carefully to prevent commingling of sediment layers, and if significant amounts of ^{228}Ra exist in the sediment the samples need to be corrected for the *in situ* formation of ^{210}Pb from its transformation.

6.9 Radon and its Progeny

Radon is a radioactive transformation product of ^{238}U, ^{235}U, and ^{232}Th, and it exists in various concentrations in all soils and minerals. Radon-220, or thoron from the ^{232}Th series, and ^{219}Rn from ^{235}U have very short half-lives (55.6 μs and 3.96 s, respectively), and they are of minor significance compared to ^{222}Rn in the ^{238}U series. Uranium has a half-life of 4.5 billion years and its intermediate transformation products, ^{230}Th and ^{226}Ra, the immediate parent of ^{222}Rn, have half-lives of 75,380 and 1600 y, respectively. In natural soils, ^{230}Th and ^{226}Ra are in radioactive equilibrium with uranium, thus a perpetual source of radon exists naturally even though its half-life is only 3.82 d. Even if ^{230}Th and ^{226}Ra are separated from uranium, each, especially ^{230}Th, will still represent a long-term source of radon.

Whereas uranium and its intermediate products are solids and remain in the soils and rocks where they originate, ^{222}Rn is a radioactive noble gas which migrates through soil to zones of low pressure such as homes. Its 3.82 d half-life is long enough for it to diffuse into and build up in homes unless they are constructed in ways that preclude entry of radon gas, or provisions are made to remove the radon. Once radon accumulates in a home it will undergo radioactive transformation; however, the resulting transformation products are no longer gases but are solid particles, which, due to an electrostatic charge, become attached to dust particles that are inhaled by occupants, or the particles can be inhaled directly. Because they are electrically charged, the particles readily deposit in the lung, and since they have half-lives of the order of minutes or seconds their transformation energy is almost certain to be deposited in lung tissue. Radon transformation products (commonly called daughters) emit alpha particles with energies ranging from 6 to 7.69 MeV, and because alpha particles (as helium nuclei) are massive and highly charged, this energy is delivered in a huge jolt to the cellular structure of the surface of the bronchi and the lung, which damages and kills these cells. The body can tolerate and replace killed cells, but damaged lung tissue cells can replicate, and cellular defects may eventually lead to lung cancer.

Unlike many pollutants that are controlled by standards, lung cancer has been observed directly in humans exposed to radon. Over 300 years ago, before radioactivity was known to science, it was common for feldspar miners in Germany and Czechoslovakia to contract and die from a mysterious disease – it is now known that this mysterious disease was lung cancer caused by the short-lived alpha-emitting transformation products of radon continuously emanating from the uranium in the rocks. Similarly, in the USA and Canada there is a direct epidemiological association between uranium miner exposure to radon and lung cancer, evidence so compelling that vigorous controls have been used to reduce the concentrations of radon and its transformation products in uranium mines.

6.9.1
Radon Subseries

The radioactive transformation of radon and its radioactive products is a practical example of series decay. As shown in Figure 6-10, ^{222}Rn undergoes transformation by alpha particle emission to produce ^{218}Po (RaA), which in turn emits 6.0 MeV alpha particles with a half-life of 3.11 min to ^{214}Pb (RaB). Beta particle emissions from RaB (^{214}Pb, $T_{1/2}$ = 26.8 min) and ^{214}Bi (RaC, $T_{1/2}$ = 19.9 min) produce ^{214}Po (RaC′) which quickly ($T_{1/2}$ = 164 μs) produces the end product ^{210}Pb (RaD) by emission of 7.69 MeV alpha particles. The alpha transformation of RaC′ is effectively an isomeric alpha transformation of RaC because it occurs so quickly after RaC′ is formed. The end product ^{210}Pb (RaD) is effectively stable with a half-life of 22.3 y and is treated as such in most calculations of radon and its progeny. Properties of this important segment of the uranium series are shown in simplified form in Figure 6-10 and Table 6-9.

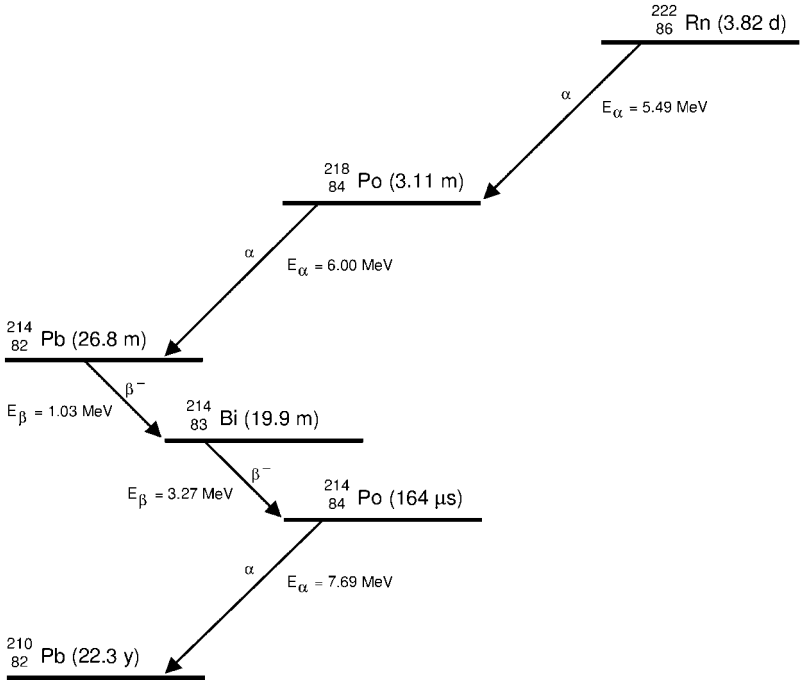

Fig. 6-10 Radioactive series transformation of ^{222}Rn to long-lived ^{210}Pb (minor branching of ^{218}Po to ^{218}At and ^{214}Bi to ^{210}Th not included).

Table 6-9. Radon and its radioactive products.

Name	Isotope	Radiation	Half-life	Atoms in 100 pCi
Radon	^{222}Rn	α	3.82 d	1,770,000
Radium A	^{218}Po	α	3.11 min	996
Radium B	^{214}Pb	β, γ	26.8 min	8583
Radium C	^{214}Bi	β, γ	19.9 min	6374
Radium C′	^{214}Po	α	164 μs	0.0008
Radium D	^{210}Pb	β	22.3 y	3.7×10^9

The Bateman equations for series transformation can be used to determine the activity and the number of atoms of each of the products of radon through ^{214}Po (RaC′). Since RaC′ is so short lived, its activity will be exactly the same as RaC so that the determination of the amounts of the primary energy-emitting products as a function of time and radon concentration only involves equations for the first four members of a radioactive series, starting with ^{222}Rn. The activity of each of the transformation products for time, t, in minutes is the following.

For Rn:

$$A_{\text{Rn}} = A_1^0 \tag{6-1}$$

For RaA (A_2):

$$A_2(t) = A_1^0(1 - e^{-t/4.49}) \tag{6-2}$$

For RaB (A_3):

$$A_3(t) = A_1^0(1 + 0.1313e^{-t/4.49} - 1.1313e^{-t/38.66}) \tag{6-3}$$

For RaC (A_4):

$$A_4(t) = A_1^0(1 - 0.0243e^{-t/4.49} - 4.394e^{-t/38.66} + 3.4183e^{-t/28.71}) \tag{6-4}$$

For RaC′ (A_5):

$$A_5 = A_4(t) \tag{6-5}$$

Figure 6-11 shows a plot of the *activity* of each radon transformation product obtained from these equations. The activity of each product approaches equilibrium with the ^{222}Rn activity when t is about 3 h or more.

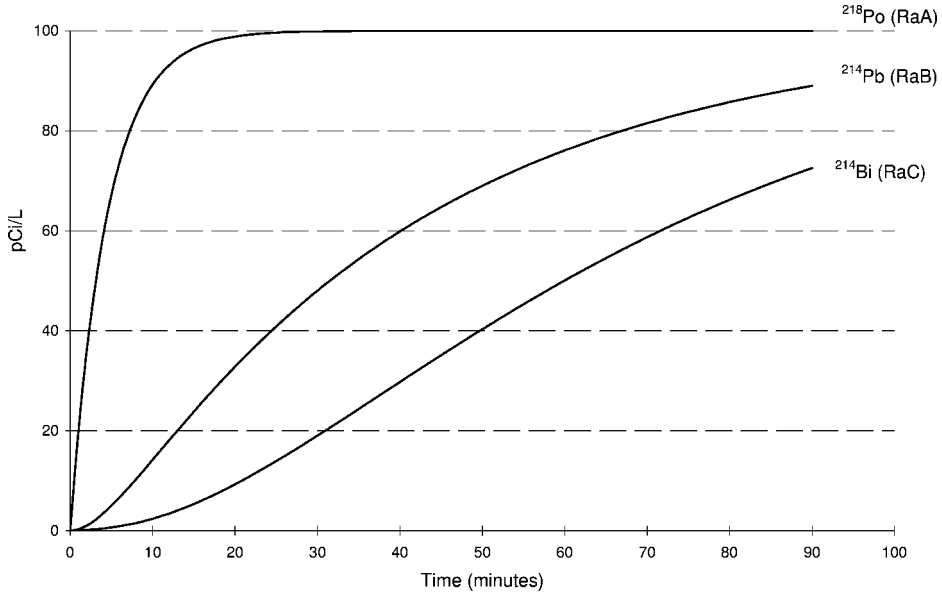

Fig. 6-11 Ingrowth of activity of ^{222}Rn transformation products from 100 pCi.

An amount of 100 pCi of ^{222}Rn in 1 L of standard air contains 1.77×10^6 atoms ($N_1{}^0$) which will remain essentially unchanged over a period of 3 h or so, the period of interest for ^{222}Rn calculations. When the numerical values of the half-lives of Rn, RaA, RaB, and RaC are substituted into the Bateman equations, the number of atoms of each of the products at any time t is obtained by dividing the activity by λ for each product; thus the number of atoms of Rn ($N_{\mathrm{Rn}} = N_1{}^0$) is

$$N_{\mathrm{Rn}} = N_1{}^0 \tag{6-6}$$

The number of atoms of RaA, $N_2(t)$, is

$$N_2(t) = N_1^0(5.657 \times 10^{-4} e^{-t/7936} - 5.657 \times 10^{-4} e^{-t/4.49}) \tag{6-7}$$

and of RaB, $N_3(t)$, is

$$N_3(t) = N_1^0(4.875 \times 10^{-3} e^{-t/7936} + 6.4 \times 10^{-4} e^{-t/4.49} - 5.547 \times 10^{-3} e^{-t/38.66}) \tag{6-8}$$

and of RaC, $N_4(t)$, is

$$\begin{aligned} N_4(t) = N_1^0(&3.6176 \times 10^{-3} e^{-t/7936} - 8.81 \times 10^{-5} e^{-t/4.49} \\ &-1.59 \times 10^{-2} e^{-t/38.66} + 1.237 \times 10^{-2} e^{-t/28.71}) \end{aligned} \tag{6-9}$$

Since RaC′ can be thought of as an alpha-isomeric state of RaC ($N_4(t)$), the number of atoms that produce RaC′ emissions, $N_5(t)$, will be the same as $N_4(t)$:

$$N_5(t) = N_4(t) \tag{6-10}$$

6.9.2 Working Level for Radon Progeny

The "working level" (WL) has been defined to deal with the special conditions of exposure to radon and its decay products. It was first defined for exposure of uranium miners as 100 pCi of ^{222}Rn in 1 L of standard air in equilibrium with its transformation products RaA, RaB, RaC, and RaC′; however, this condition rarely exists in working environments or in homes. Since radiation exposure of the human lung is caused by deposition of alpha particle energy from the radioactive transformation of the particulate atoms of RaA, RaB, RaC, and RaC′ inhaled into and deposited in the lung, and not ^{222}Rn itself, the WL is defined as "any combination of the short-lived decay products of radon (RaA, RaB, RaC, and RaC′) in 1 L of air that will result in the ultimate emission by them of 1.3×10^5 MeV of alpha ray energy (to lung tissue)."

Radon is not deposited in the lung because it is an inert gas, and since it does not interact with lung tissue it is quickly exhaled. Beta particle emissions and gamma rays emitted by RaB and RaC make a negligible contribution to the amount of energy deposited in the lung when compared to the alpha particles emitted by RaA and RaC′.

Calculation of the WL requires first a determination of the number of atoms of each of the radon transformation products and the ultimate alpha energy each of the product atoms will produce as it undergoes radioactive series transformation to the end product ^{210}Pb. The number of atoms of each is directly related to the "age" of the radon in the air being considered. For 100 pCi of ^{222}Rn in equilibrium with its transformation products, the ultimate alpha energy emitted by the number of atoms at equilibrium will be 1.3×10^5 MeV, as shown in Table 6-10.

Table 6-10. Determination of ultimate alpha energy due to a concentration of 100 pCi of radon in equilibrium with its four principal decay products, or one working level (WL).

Nuclide	MeV/t	$T_{1/2}$	Atoms in 100 pCi	α energy per atom (MeV)	Total energy (MeV/100 pCi)	Fraction of total α energy
^{222}Rn	5.5	3.82 d	1.77×10^6	Excluded	None	None
^{218}Po (RaA)	6	3.11 min	996	13.69	1.36×10^4	0.11
^{214}Pb (RaB)	0[a]	26.8 min	8583	7.69	6.60×10^4	0.51
^{214}Bi (RaC)	0[a]	19.9 min	6374	7.69	4.90×10^4	0.38
^{214}Po (RaC′)	7.69	164 μs	0.0008	7.69	0	0
					Total: 1.3×10^5	

a β and γ emissions excluded in WL because of minimal energy deposition in the lung.

The data in Table 6-10 (for 100 pCi of ^{222}Rn in equilibrium with its progeny) show that each atom of RaA can deliver not only its own characteristic 6.00 MeV energy but also the 7.69 MeV alpha emission from RaC′ since each RaA atom will transition through RaB and RaC and eventually into RaC′ as well (see Figure 6-10). Hence the "ultimate" or "potential" alpha energy associated with each atom of RaA is 6.00 + 7.69 = 13.69 MeV. Likewise, every atom of RaB and RaC, even though they are beta emitters, will undergo transformation to RaC′ which will emit 7.69 MeV of alpha energy when it rapidly undergoes radioactive transformation.

Table 6-10 also shows that RaA, in equilibrium with ^{222}Rn, contributes only about 11% of the ultimate or "potential" alpha energy, and that RaB contributes about 51% because in equilibrium with 100 pCi of ^{222}Rn it constitutes the largest number of atoms (because it has the longest half-life) that will eventually produce 7.69 MeV alpha emissions through RaC′ transformations. Analogously, the atoms in 100 pCi of RaC, the other beta and gamma emitter, supply 38% of the ultimate alpha energy through RaC′. RaC′ produces ^{210}Pb ($T_{1/2}$ = 22.3 y) which is unlikely to remain in the lung, thus the alpha energy of its subsequent transformation product ^{210}Po (RaF) is excluded.

Radioactive equilibrium between ^{222}Rn and its short-lived transformation products takes well over an hour, and in a practical sense such equilibrium rarely exists. Consequently, determination of the working level cannot rely on determination of the ^{222}Rn concentration alone. Since the particulate progeny of radon determine the working level, it is necessary always to determine the number of atoms of these products, which in turn is directly determined by the amount of ^{222}Rn present and the time period over which ingrowth occurs, or in effect the age of the radon/progeny mixture. The number of atoms of each product can be calculated from Equations (6-7)–(6-10) or they can be determined from the curves in

Figure 6-12, which shows a plot of the number of atoms of RaA, RaB, and RaC at any given time from a pure source of 100 pCi of radon.

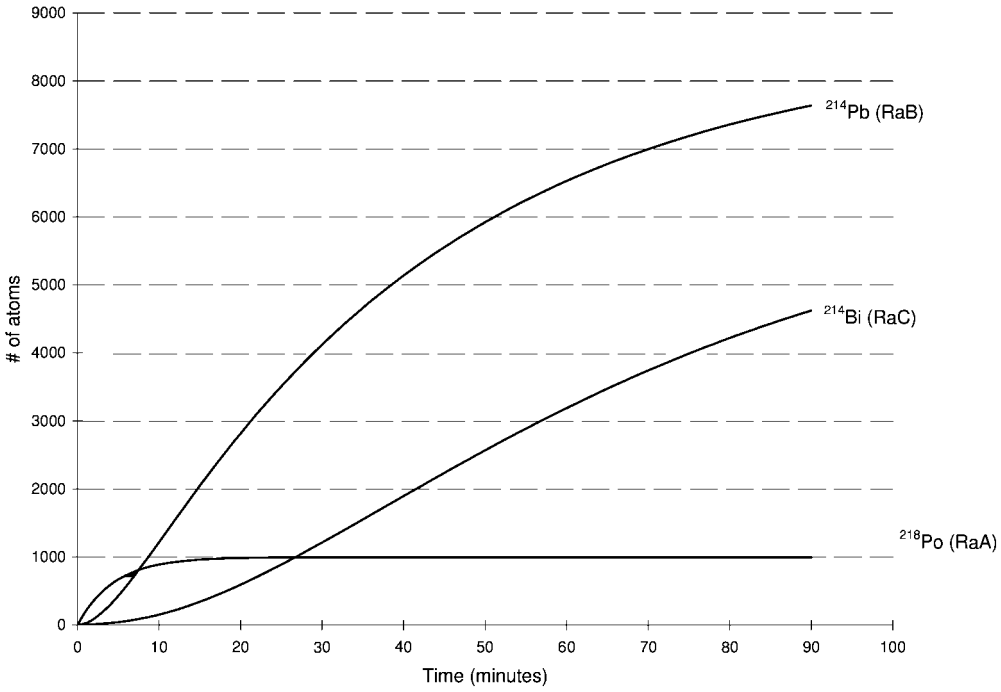

Fig. 6-12 Graphical representation of the number of atoms of RaA, RaB, RaC, and RaC′ activity in a radon source, the activity of which does not change appreciably over the period of observation.

As shown in Figure 6-13, it takes 40–60 min to achieve 0.5–0.7 of the equilibrium value of 1.0 WL. During the first few minutes the WL is due almost entirely to the rapid but limited ingrowth of RaA. Between 4 and 20 min the increase in the WL is approximately linear and is due primarily to the ingrowth of RaB. The contribution from RaC is delayed considerably due to the 26.8 min and 19.9 min half-lives of RaB and RaC; thus, the RaB contribution becomes significant only after the radon source is more than 15 min old and the RaC contribution only after about 40 min. Clearly, the age of the air has a significant effect on the WL; thus, it is desirable to breathe young air. This can be achieved by passing the air through an efficient filter shortly before it is to be inhaled or by using ventilation to mix in fresh air free of radon and its products.

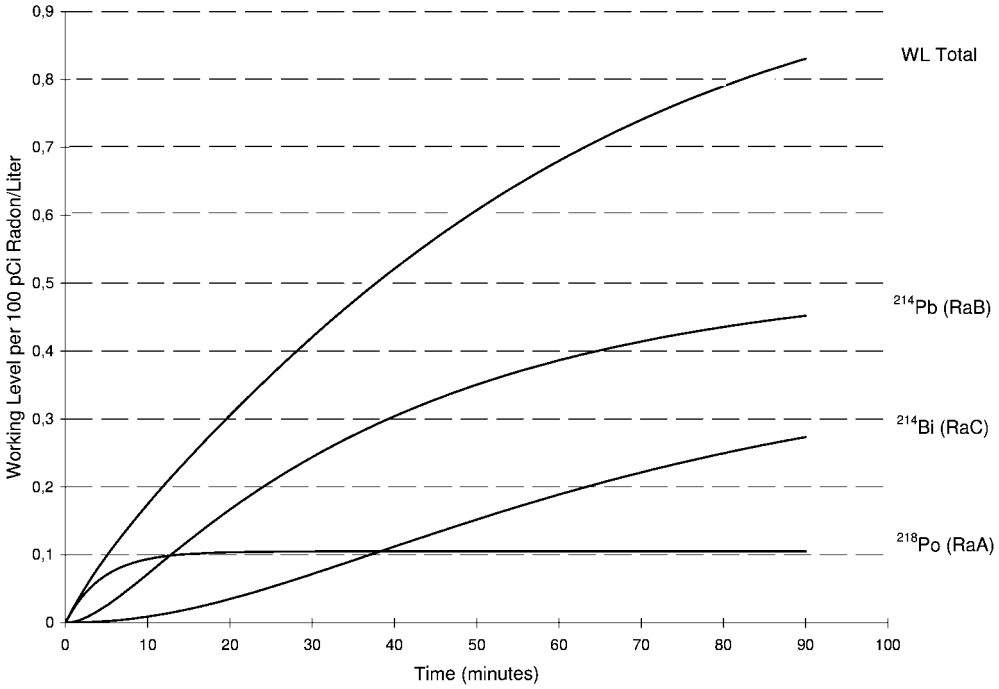

Fig. 6-13 Contribution of each of the transformation products of ^{222}Rn to the working level.

Example 6-1. Determine the WL for air containing 100 pCi/L of radon 10 min after filtration.

Solution. Following the example for defining the WL, the number of atoms present after 10 min of ingrowth are calculated by Equations (6-7)–(6-10) or alternatively read from the curves in Figure 6-12. Tabulated answers are as follows:

Nuclide	Atoms in 100 pCi	α energy per atom (MeV)	α energy (MeV/100 pCi)
^{222}Rn	1.77×10^6	Excluded	None
^{218}Po (RaA)	876	13.69	1.2×10^4
^{214}Pb (RaB)	1219	7.69	9.4×10^3
^{214}Bi (RaC)	114	7.69	8.8×10^2
^{214}Po (RaC′)	~0	7.69	0
			Total: 2.23×10^4

The working level is

$$\text{WL} = \frac{2.23 \times 10^4 \text{ MeV}}{1.3 \times 10^5 \, \alpha \text{ MeV/WL}} = 0.17 \text{ WL}$$

Although the WL unit has shortcomings, it is the most practical single parameter for describing the effect of radon and its transformation products. Since the WL is based on radon, it is, like the roentgen (for x-rays), a unit of exposure, not radiation dose. Controls are based on limiting exposure of people by keeping airborne levels of radon and its products below a specified number of WLs.

The *working-level month (WLM)* is used to describe cumulative radon exposure. The average number of exposure hours in a month is 173 (40 × 52/12 = 173); thus, a WLM would be exposure to 1 WL for 1 month. The WLM is calculated by multiplying the exposure in WL by the number of hours of exposure and dividing by 173 h/month. For example, exposure to 1 WL for 173 h = 1 WLM; similarly, exposure to 10 WL for 173 h would be 1730 WL h, or 10 WLM.

Example 6-2. A person is exposed to air containing radon and transformation products which is determined ultimately to emit 10^5 MeV of alpha energy per liter of air. If a person is exposed to this atmosphere for 1000 h, what is the cumulative exposure in WLM?
Solution.

$$\frac{10^5 \text{ MeV}}{1.3 \times 10^5 \text{ MeV/WL}} = 0.77 \text{ WL}$$

$$\frac{0.77 \text{ WL} \times 1000 \text{ h}}{173 \text{ h/month}} = 4.45 \text{ WLM}$$

6.9.3 Measurement of Radon

The two principal measurement methods for radon are (a) collecting the particles of the transformation products and determining the WL directly, or (b) absorbing the radon, a noble gas, on an adsorbent and measuring it to determine its concentration in air. Since both the radon concentration and the WL are related, each can be inferred from the other if certain parameters (e.g., fraction of equilibrium) are known or assumed.

Working environments such as mines or uranium mills are usually characterized by a WL measurement, which is made by collecting a short-term (5–10 min) particulate sample on a filter paper and measuring the alpha disintegration rate. Home environments are usually sampled over a period of several days (2–7) by adsorbing radon onto activated charcoal. This is then measured by counting the

gamma emission rate from RaC (^{214}Bi), which is the same as the radon transformation rate when secular equilibrium exists. The first method (work place) requires a particulate air sampler and a field method for measurement; the second method (residences) uses passive adsorption and a laboratory technique.

Particulate sampling for radon involves a field method that can be summarized as follows:

1. Collect a 5–10 min air sample at a flow rate of 10 ft^3/min or greater, and record the liters (L) of air sampled.
2. Measure the alpha activity (in d/m) on the filter 40–90 min later and adjust it by dividing by the appropriate correction factor (CF) from Figure 6-14 to obtain MeV of alpha energy per sample.
3. Calculate the WL as

$$\text{WL} = \frac{\alpha\,\text{d/m (measured)}}{\text{volume (L)} \times \text{CF(d/m per L per WL)}}$$

This method is often referred to as the Kusnetz method after the person who devised and published the correction factors in 1956. The Kuznetz method is illustrated in Example 6-3.

Example 6-3. A particulate air sample was collected for 5 min at 2 ft^3/min in a tent erected over an excavation site at an old uranium processing site. The filter was measured 50 min later with a portable ZnS alpha scintillation detector and found to contain alpha activity of 10,000 d/m. The air filter is assumed to have 100% collection efficiency and no self-absorption of the emitted alpha particles. (a) What was the WL for the tent atmosphere? (b) If a worker worked inside the tent 40 h per week for 25 weeks, what would be the accumulated exposure?

Solution.

(a) The WL in the tent is based on the activity per liter of air:

$$\text{Volume (L)} = 5\ \text{min} \times 2\ \text{ft}^3/\text{min} \times 28.32\ \text{L/ft}^3 = 283.2\ \text{L}$$

From Figure 6-14, the Kusnetz correction factor at 50 min after sample collection is 129 (d/m)/(L WL), and

$$\text{WL} = \frac{10,000\,\text{d/m}}{283.2\,\text{L} \times 129\,\text{(d/m)/(L WL)}} = 0.274\,\text{WL}$$

which is just below the recommended exposure guide for uranium miners.

(b) The accumulated exposure in WLM for the worker in the tent is

$$\text{WLM} = \frac{0.274\,\text{WL} \times 25\,\text{weeks} \times 40\,\text{h/week}}{173\,\text{WL h/WLM}} = 1.58\,\text{WLM}$$

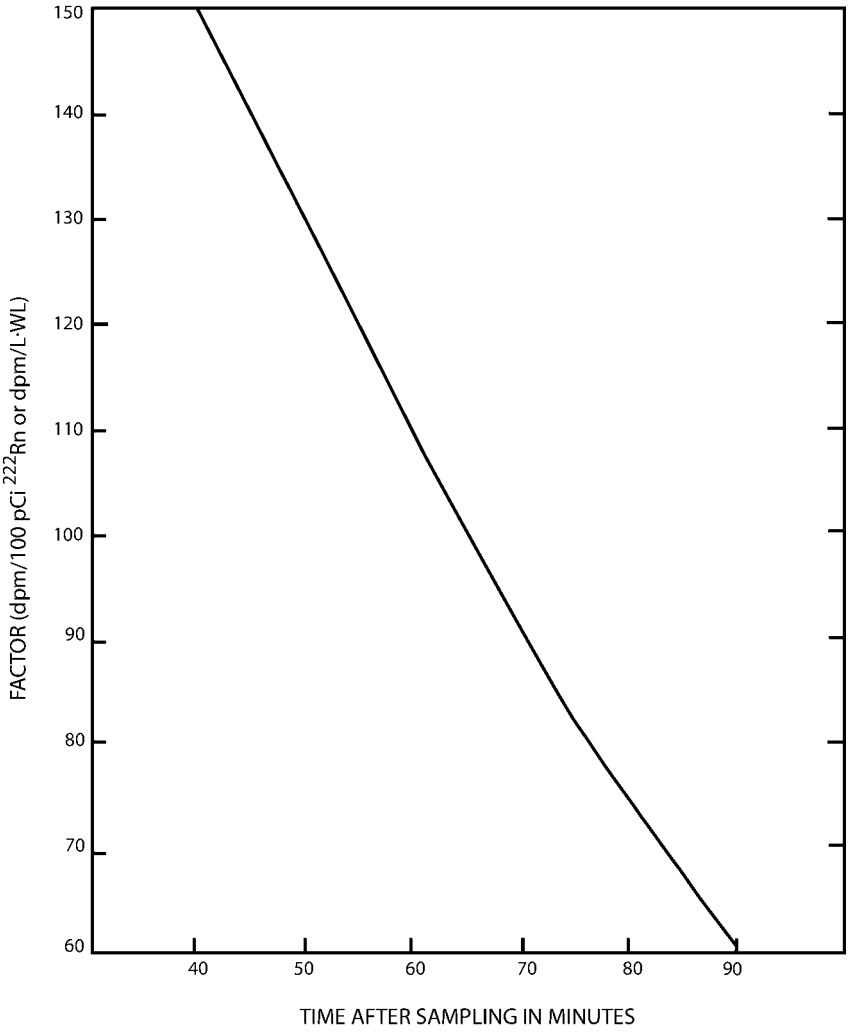

Fig. 6-14 Factors of d/m per 100 pCi of ^{222}Rn (or (d/m)/(L WL)) for times after collection of alpha-emitting particulate progeny of radon.

The *radon absorption method* uses activated charcoal to absorb radon directly from the air. Since this procedure is passive (i.e., no air sampler is used to force air through the charcoal) it requires a standard sampler, usually a small canister that contains about 75 g of charcoal, which is calibrated in a known radon atmosphere. The absorption of radon on the charcoal of the reference canister occurs at a constant rate and is a function of the exposure time; thus, the activity of the absorbed radon is directly proportional to the concentration of radon (pCi/L) in the air surrounding the canister and the exposure period, as given in the following relationship for a 75 g canister (USEPA 1987):

$$\text{Absorption } ((\text{d/m})\ \text{L/pCi min}) = 35.8511 \times 10^{-3} - (5.1353 \times 10^{-5} \times t)$$

where t is exposure time in hours.

The absorbed radon is determined by counting ^{214}Bi (RaC) gamma rays to determine the ^{214}Bi disintegration rate, and since ^{222}Rn and ^{214}Bi are in equilibrium after 90 min or so, their activities are the same. This activity is then decay-corrected back to the midpoint of the sampling period and reported as pCi of radon per liter of air.

Example 6-4. A 75 g charcoal canister was exposed in the author's home for 189 h (11,340 min) with doors and windows closed. A 10 min count taken 40 h later yielded a net gamma count rate of 119.3 counts per minute of ^{214}Bi (RaC) gamma rays after subtraction of background, and the detector efficiency for ^{214}Bi was 26.2%. What was the radon concentration (pCi/L)?

Solution. Since the radon transformation products were in equilibrium, the measured activity of ^{214}Bi and ^{222}Rn is

$$\frac{119.3\,\text{c/m}}{0.262\,(\text{c/m})(\text{d/m})} = 455.34\,\text{d/m}$$

Since ^{222}Rn is the parent of ^{214}Bi, both of which would be in equilibrium on the charcoal, the activity rate of ^{222}Rn is also 455.34 d/m. The activity of ^{222}Rn at the midpoint of the sample collection period is a good value of the average ^{222}Rn concentration in the home; therefore, this value should be decay-corrected back to the midpoint which occurred 5.85 d before the measurement. The ^{222}Rn activity at the midpoint of the sampling period is

$$455.34\text{d/m} = A_0 e^{-(\ln 2/3.82\text{d})(5.85\text{d})}$$

$A_0 = 1254$ d/m

The absorbed radon on the canister is

$$\text{Absorbed radon} = 35.85 \times 10^{-3} - 5.1353 \times 10^{-5} \times 189\ \text{h} = 0.0261\ (\text{d/m})\ \text{L/pCi min}$$

The average radon concentration over the sampling period is

$$\text{Rn (pCi/L)} = \frac{1254\,\text{d/m}}{11,340\,\text{min} \times 0.0261(\text{d/m})\ \text{L/pCi min}} = 4.23\,\text{pCi/L}$$

The working level (WL) can be calculated from the measured radon concentration if the degree of radioactive equilibrium between radon and its transformation products is known. For a residence, this equilibrium fraction is about 50% due to the number of air changes that occur; for energy-efficient homes it can be as high as 75–80%, and for some older homes it could be as low as 20–30%. The working level can be defined in terms of the equilibrium fraction as

$$\text{WL} = \frac{\text{Rn (pCi/L)}}{100\,\text{pCi/L WL}} \times F$$

where F is the fractional equilibrium between radon and its alpha-emitting transformation products.

Example 6-5. The recommended action level guideline for a residence is 4 pCi of radon per liter of air. (a) If the fractional equilibrium between ^{222}Rn and its particulate, alpha-emitting transformation products is assumed to be 50%, what is the corresponding WL? (b) If 70% occupancy of the residence is assumed, what is the cumulative WLM associated with this exposure level in 1 y?
Solution. (a)

$$\text{WL} = \frac{4\,\text{pCi/L}}{100\,\text{pCi/L WL}} \times 0.5 = 0.02\,\text{WL}$$

(b) At 70% occupancy, the annual exposure period is

$$E\,(\text{h}) = 365\ \text{d/y} \times 24\ \text{h/d} \times 0.7 = 6132\ \text{h}$$

$$\text{Total exposure} = \frac{6132\,\text{h} \times 0.02\,\text{WL}}{173\,\text{WL h/WLM}} = 0.71\,\text{WLM}$$

6.10 Summary

Natural radiation and radioactivity represent a continuous exposure of beings on the earth and produce a natural background that must be considered in every measurement of a radiation level or the radioactivity in a sample or source. The natural radiation environment consists of cosmic rays and naturally radioactive materials that are cosmogenic, primordial, or the products of one of naturally radioactive series: the uranium (^{238}U), actinium (^{235}U), thorium (^{232}Th), and neptunium (^{237}Np) series. With the exception of neptunium, each of the parent radionuclides is primordial in origin because they are so long lived that they still exist some 4.5 billion years after the solar system was formed.

Many ores are processed for their mineral content which enhances either the concentration of the radioactive elements in process residues or increases their environmental mobility; these processes result in materials that are no longer purely "natural." These materials are called NORM (naturally occurring radioactive material) or, more recently, TENORM (technologically enhanced NORM).

Radon is an important transformation product of ^{238}U, ^{235}U, and ^{232}Th, and it exists in various concentrations in all soils and minerals. Radon-222, which is a product of the ^{238}U series, is the most important radioisotope of radon because of its 3.82 d half-life and the 4.5 billion year half-life of its uranium parent. The inter-

mediate transformation products, ^{230}Th and ^{226}Ra (the immediate parent of ^{222}Rn), have half-lives of 75,380 and 1600 y; thus, they are in radioactive equilibrium with uranium and represent a perpetual source of radon. Whereas uranium and its intermediate products are solids and remain in the soils and rocks where they originate, ^{222}Rn is a radioactive noble gas which migrates through soil to zones of low pressure such as homes. Its 3.82 d half-life is long enough for it to diffuse into and build up in homes unless they are constructed in ways that preclude its entry, or provisions are made to remove it.

Naturally occurring radiation and radioactive materials account for a major portion of radiation dose received by members of the public, of the order of 100 mrem (1 mSv) per year to the average person in the USA. Cosmic rays contribute about 28 mrem/y, terrestrial radiation about 27 mrem/y, and radionuclides in the body, principally ^{40}K, about 35 mrem/y. Exposure to radon and its products produces dose primarily to lung tissue which varies widely with location and residence and can be substantial, representing a radiation risk well above that from other natural sources.

Acknowledgements

This chapter was prepared with major help from Chul Lee M.S. of the University of Michigan Radiological Health Program.

Other Suggested Sources

Evans, R. D. **1969**, Engineers guide to behavior of radon and daughters, *Health Physics*. 17, No. 2, August 1969.
Frame, P. W. **1996**, Radioactivity: conception to birth: the Health Physics Society 1995 radiology centennial Hartman oration, *Health Physics* April, 1996.
NCRP **1975**, Nature background radiation in the U.S., NCRP Report 45, 1975.
NCRP **1987**, Ionizing exposure of the US population, Report 93, (National Council on Radiation Protection and Measurements, Bethesda, MD).
NCRP **1993**, Radiation protection in the mineral extraction industry, Report 118, National Council on Radiation Protection and Measurements.
UNSCEAR **1988**, United Nations Scientific Committee on the Effects of Atomic Radiation. Sources, Effects, and Risks of Ionizing Radiation No. E 88.IX.7 (United Nations, New York).
USEPA **1987**, Standard Operating Procedures for Rn-222 measurement using charcoal canisters, NAREL, Montgomery, AL.

Problems – Chapter 6

6–1. When Becquerel separated uranium X (^{234}Th; $T_{1/2}$ = 24.1 d) from his uranium phosphor its radioactivity essentially vanished. When he measured it again 4 months later, the uranium had regained activity. What fraction of the original radioactivity due to UX had returned?

6–2. Rutherford and Soddy precipitated thorium nitrate and observed a phenomenon similar to that for uranium and UX. They found that essentially all the activity was removed in the precipitate that they called thorium X (^{224}Ra; $T_{1/2}$ = 3.66 d) but that the thorium regained its ThX activity much quicker. How long did it take for ThX to reach 99.9% of its original activity in thorium?

6–3. A sample of RaE (^{210}Bi) is freshly isolated and found to contain 1 μCi. What is the maximum activity of RaF (^{210}Po) that will exist in this naturally occurring mixture and when will it occur? (Hint: ignore the short-lived ^{206}Tl.)

6–4. The transition of ^{238}U to ^{206}Pb can be used to determine the age of minerals by determining the weight ratio of Pb to U by mass spectroscopy. (a) Show that the age of the mineral, if ^{238}U transformation is neglected, is the ratio (Pb/U × 7.45×10^9 y). (b) What is the age of a rock that contains 0.1 g of ^{206}Pb per gram of U? (c) What would be the age if corrected for the radioactive transformation of ^{238}U?

6–5. If 10 μCi of ^{223}Ra are eluted from an ^{227}Ac generator and tagged to monoclonal antibodies that in turn are incorporated into a 5 g cancerous mass, how much alpha particle energy would ultimately be delivered to the cancer (assume that ^{219}Rn does not diffuse out of the cancer and that all product atoms transform in the cancerous mass)?

6–6. Some of the carbon atoms in trees and lumber are ^{14}C. Why are there none among the carbon atoms in petroleum products?

6–7. If the activity of ^{14}C in wood grown prior to 1850 (before significant fossil fuel burning) was 15.3 d/m per gram of carbon, what would be the age of cinders found in an ancient fire pit that had an activity of 10 d/m per gram of carbon when discovered?

6–8. An old rock of volcanic origin is found and measured to contain 0.1 g of potassium. The rock is then heated and the ^{40}Ar from transformation of ^{40}K is collected and measured by mass spectroscopy to be 1.66 ××x 10^{-10} g. What is the age of the rock?

6–9. The bones of "Lucy" were found in 1974 in sedimentary rock containing trapped potassium with a typical sample yielding a total of 0.1 g. A fraction (0.0000118) of the trapped potassium was ^{40}K, which decays into ^{40}Ar. This sample contained 2.39×10^{-9} g of ^{40}Ar, of which 7.25×10^{-10} g was contamination from the air. What is the approximate age of "Lucy"?

6–10. Water from a deep well is measured and found to contain tritium that is only 40% of the tritium in fresh rainwater. If it can be assumed that the well water is isolated from surface flow, what is the approximate age of the water in the well, i.e., how long did it take to diffuse from the surface to the aquifer?

6–11. The average human is made up of 18% by weight of natural carbon. If a 70 kg person contains 0.1 μCi, what fraction of carbon in the body is ^{14}C? How does the activity per gram compare to that of living wood which contains 15.3 d/m per gram?

6–12. Regulations require that the concentration of ^{226}Ra in uranium tailings left at mill sites not exceed 15 pCi/g for a period of 1000 y. For soil that contains ^{230}Th, but no ^{226}Ra, what is the maximum concentration of ^{230}Th that can be left in the soil today such that the regulations are not exceeded in 1000 y?

6–13. A settling basin near an abandoned uranium processing site contains sediment with concentrations of 100 pCi/g of ^{230}Th and essentially no ^{226}Ra. (a) If the external gamma exposure rate is 2.5 mrem/y for 1 pCi/g of ^{222}Rn in equilibrium with its transformation products for the geometry of the sediment, what would be the exposure rate for 100% occupancy of the site 500 y hence? (b) If roughly 5 pCi/g of ^{226}Ra corresponds to 0.02 WL of ^{222}Rn and its products in a structure built upon soils containing ^{226}Ra, what would be the radon level in homes built upon the site in 200 y? In 500 y?

6–14. If ^{230}Th and ^{231}Pa are preferentially precipitated from seawater into silt with concentrations of 10 and 2 pCi/g, respectively, what is the age of a sediment sample at a 1 m depth if it contains 7 pCi/g of ^{226}Ra which is not brought down in the sediment? What would be the corresponding concentration of ^{223}Ra?

6–15. Determine the working level for 100 pCi/L of thoron (^{220}Ra) continuously in equilibrium with its short-lived decay products.

6–16. The average age of ^{222}Rn in a mineshaft is determined to be 20 min. What would be the WL in the mineshaft for a measured concentration of 100 pCi/L of ^{222}Rn?

6–17. Calculate the WL for air that contains 100 pCi/L of radon that is only 3 min old.

7
Interactions of Radiation with Matter

"Much of what we know of the Universe comes from information transmitted by photons."
John Hubbell (Ann Arbor, 1995)

When radiation is emitted, regardless of what type it is, it produces various interactions that deposit energy in the medium that surrounds it. This deposition of energy is characterized as radiation dose, and if it occurs in the living tissue of individuals, the endpoint effects will be biological changes, most of which are undesirable. Understanding these interactions leads naturally to the determination of radiation exposure and dose and the units used to define them.

The mechanisms by which different radiations interact in an absorbing medium are fundamental to describing the amount of deposited energy, how the characteristics of shields or other absorbers modify and affect radiation exposure and dose, and the design of detectors to measure the various types of radiation based on their respective interaction principles. The goals of this chapter are first to describe interaction processes that attenuate and absorb charged particles and photons and then to apply these concepts to the calculation of deposited energy, i.e., radiation exposure and dose. The design of radiation shields is covered in Chapter 8, and the detection of radiation is discussed Chapter 12. A similar treatment is provided in Chapter 14 for neutrons.

7.1
Radiation Dose and Units

The term *radiation dose*, or simply *dose*, is defined carefully in terms of two key concepts: (a) the energy deposited per gram in an absorbing medium, principally tissue, which is the absorbed dose, and (b) the damaging effect of the radiation type, which is characterized by the term effective dose equivalent. A related term is radiation exposure, which applies to air only and is a measure of the amount of ionization produced by x-rays and gamma radiation in air. Each of these is defined in the conventional system of units, which in various forms and refinements has been used for several decades, and in the newer SI system, which is gradually re-

Physics for Radiation Protection, Third Edition. James E. Martin

placing the conventional units. This presentation uses both sets, but for the most part emphasizes conventional units, which are firmly embedded in governmental standards and regulations, at least in the USA.

7.1.1 Radiation Absorbed Dose

The absorbed dose is defined as the amount of energy deposited per unit mass. The conventional unit for absorbed dose is the *rad* (radiation absorbed dose), and is equal to the absorption of 100 erg of energy in 1 g of absorbing medium, typically tissue:

$$1 \text{ rad} = 100 \text{ erg/g of medium}$$

The SI unit of absorbed dose is the gray (Gy) and is defined as the absorption of 1 J of energy per kilogram of medium:

$$1 \text{ Gy} = 1 \text{ J/kg}$$

$$= 100 \text{ rads}$$

A milligray (mGy) is 100 mrads, which is about the amount of radiation one receives in a year from natural background, excluding radon. This is a convenient relationship for translating between the two systems of units since the annual radiation dose due to natural background (equal to 1 mGy or 100 mrads) is a convenient reference point for radiation dose received by a person.

The rate at which an absorbed dose is received is quite often of interest. Common dose rates are rad/s, mrad/h, etc. In SI units, dose rates may be expressed as Gy/s, mGy/h, etc., and because the Gy is such a large unit compared to many common circumstances, the unit μGy/h is often used.

7.1.2 Radiation Dose Equivalent

The definition of dose equivalent is necessary because different radiations produce different amounts of biological damage even though the deposited energy may be the same. If the biological effects of radiation were directly proportional to the energy deposited by radiation in an organism, the radiation absorbed dose would be a suitable measure of biological injury, but this is not the case. Biological effects depend not only on the total energy deposited, but also on the way in which it is distributed along the path of the radiation. Radiation damage increases with the linear energy transfer (LET) of the radiation; thus, for the same absorbed dose, the biological damage from high-LET radiation (e.g., alpha particles, neutrons, etc.) is much greater than from low-LET radiation (beta particles, gamma rays, x-rays, etc.).

The dose equivalent, denoted by H, is defined as the product of the absorbed dose and a factor Q, the quality factor, that characterizes the damage associated with each type of radiation:

$$H \text{ (dose equivalent)} = D \text{ (absorbed dose)} \times Q \text{ (quality factor)}$$

In the conventional system of units, the unit of dose equivalent is the rem which is calculated from the absorbed dose as

$$\text{rem} = \text{rad} \times Q$$

The value of Q varies with the type of radiation: $Q = 1.0$ for x-rays, gamma rays, and electrons, $Q = 20$ for alpha particles and fission fragments, and $Q = 2$–10 for neutrons of different energies.

The SI unit of dose equivalent is the Sievert (Sv) or

$$\text{Sieverts} = \text{Gy} \times Q$$

The sievert, as is the gray, is a very large unit, corresponding to 100 rem in conventional units, and it is often necessary to abbreviate it to mSv or in some cases to μSv to describe the radiation dose equivalent (or rate) received by workers and the public.

7.1.3 Radiation Exposure

The term exposure is used to describe the quantity of ionization produced when x-rays or gamma rays interact in air because it can be conveniently measured directly by collecting the electric charge, whereas that which occurs in a person cannot be. The roentgen (R) is the unit of radiation exposure; it is defined only for air and applies only to x-rays and gamma rays up to energies of about 3 MeV. A milliroentgen (mR) is 0.001 R. Exposure rates are often expressed as roentgens per unit time, e.g., R/s, mR/h, etc. Since the roentgen is determined in air, it is not a radiation dose but with appropriate adjustment it can be converted to dose.

The roentgen was originally defined as that amount of x-radiation or gamma radiation such that the associated corpuscular emission produces in 0.001293 g of air (1 cm^3 of air at atmosphere pressure and 0 °C) 1 electrostatic unit (1 esu = 3.336×10^{-10} C) of charge of either sign. The ionization produced by the associated corpuscular emissions is due to photoelectric, Compton, and, if applicable, pair production interactions. In terms of charge produced per unit weight of air, the roentgen corresponds to

$$1\text{R} = \frac{1\,\text{esu} \times 3.336 \times 10^{-10}\text{C/esu}}{0.001293\,\text{g}} \times 10^3\,\text{g/kg}$$

$$= 2.58 \times 10^{-4}\ \text{C/kg of air}$$

The modern definition of the roentgen is based on this value; i.e., 1 R is that amount of x-radiation or gamma radiation that produces 2.58×10^{-4} C of charge in 1 kg of air.

The roentgen is not included in the SI system of units; the SI unit for exposure is the X unit, defined as the production of 1 C coulomb of charge in 1 kg of air, or

$$X = 1 \text{ C/kg of air}$$

The X unit corresponds to deposition of 33.97 J in 1 kg of air, and is equal to 3876 R. The X unit is a huge unit, and consequently most exposure measurements are made and reported in R which seems appropriate for the discoverer of x-rays.

Exposure and exposure rate apply *only* to x-rays and gamma rays and only in *air*, and neither the roentgen nor the X unit is appropriate for describing energy deposition from particles or for energy deposition in the body.

Energy deposition per roentgen is an important relationship because the deposition of energy in air is readily calculated. The amount of charge produced in air varies with energy, but is approximately linear for photons between about 70 keV and 3 MeV such that the amount of energy required to produce an ion pair is 33.97 eV on average. The roentgen thus corresponds to an energy deposition in air, the absorbing medium, of 87.64 erg/g of air (see Example 7-1).

Example 7-1. From the original definition of the roentgen, determine the energy deposition in air (a) in ergs per gram of air for an exposure of 1 R, and (b) in joules per kilogram of air for 1 R.

Solution. (a) Since 1 R = 1 esu in air at STP (0.001293 g),

$$\begin{aligned}\text{Exposure (erg/g)} &= \frac{1\text{ esu}}{0.001293\text{ g}} \times 33.97\text{ eV/ion pair} \\ &\quad \times \frac{1.6022 \times 10^{-12}\text{ erg/eV}}{1.6022 \times 10^{-19}\text{ C/ion pair}} \times 3.336 \times 10^{-10}\text{ C/esu} \\ &= 87.64\text{ erg/g R}\end{aligned}$$

(b) In SI units 1 R = 2.58×10^{-4} C/kg:

$$\text{Exposure (J/kg)} = 2.58 \times 10^{-4}\text{ C/kg} \times 33.97\text{ J/C}$$

$$= 8.764 \times 10^{-3}\text{ J/kg R}$$

7.2
Radiation Dose Calculations

Radiation dose can be calculated by a three-step procedure as follows:

1. First establish the number of radiation pulses (particles or photons) per unit area entering a volume of medium of known density.
2. Next, establish the mass of medium in which the energy is dissipated. For particles, this is just the depth of penetration. For photons, it is necessary to use a unit depth (e.g., 1 cm) due to the probabilistic pattern of interactions.
3. From the pattern(s) of interaction probabilities, determine the amount of energy deposited.

All emitted radiations must be considered in this process, and adjustments should be made for any attenuating medium between the source and the point of interest.

Since different radiations penetrate to different depths in tissue, radiation dose has been specified in regulations for three primary locations:

1. The shallow dose, which is just below the dead layer of skin that has a density thickness of 7 mg/cm^2, or an average thickness of 70 μm;
2. The eye dose just below the lens of the eye with a density thickness of 300 mg/cm^2.
3. The deep dose, which is located at a depth of 1 cm in tissue or at a density thickness of 1000 mg/cm^2, primarily to account for highly penetrating radiation such as x-rays or gamma rays or neutrons.

Precise determinations of absorbed energy at these depths requires an adjustment for any diminution in the flux due to energy losses in the overlying tissue layer.

Since energy deposition is dependent on the radiation type, its energy, and the absorbing medium, it will, for the sake of clarity, be discussed in the context of the interaction mechanisms of each type of radiation. Shielding of radiation, which is related to the same considerations, is discussed in the same manner in Chapter 8.

7.2.1
Inverse Square Law

The number of radiation pulses that enter and/or traverse a medium is governed by source strength and the geometry between the source and the medium of interest, a relationship that can often be conveniently expressed as a fluence

(number/cm^2) or a fluence rate or flux (number/cm^2 s). A radioactive point source of activity S (t/s) emits radiation uniformly in all directions, and at a distance r will pass through an area equal to that of a sphere of radius r. Therefore, the flux, ϕ_i, is

$$\phi(\text{number/cm}^2\ \text{s}) = \frac{S(\text{t/s})f_i}{4\pi r^2}$$

where f_i is the fractional yield per transformation of each emitted radiation. This relationship is the "inverse square law" which states that the flux of radiation emitted from a point source is inversely proportional to r^2, as shown in Example 7-2.

Example 7-2. What is the photon flux produced by a 1 mCi point source of ^{137}Cs at a distance of 100 cm? At 400 cm?

Solution. ^{137}Cs ($T_{1/2}$ = 30.07 y) emits 0.662 MeV gamma rays through ^{137m}Ba ($T_{1/2}$ = 2.52 min) in 85% of its transformations. The gamma flux is

$$\phi(\gamma/\text{cm}^2\ \text{s}) = \frac{1\,\text{mCi} \times 3.7 \times 10^7\ \text{t}/(\text{s mCi}) \times 0.85\,\gamma/\text{t}}{4\,\pi\,(100\,\text{cm})^2}$$

$$= 2.5 \times 10^2\ \gamma/\text{cm}^2\ \text{s}$$

At 400 cm

$$\phi(\gamma/\text{cm}^2\ \text{s}) = \frac{2.5 \times 10^2\,\gamma/\text{cm}^2\ \text{s} \times (100\,\text{cm}^2)}{(400\,\text{cm})^2}$$

$$= 15.625\ \gamma/\text{cm}^2\ \text{s}$$

Once the flux of radiation is known it can be converted to an energy flux by multiplying the flux by the average energy of each radiation emitted by the source. The energy flux due to particle emissions (betas, alphas, deuterons, neutrons, etc.) is calculated in a similar way using the average energy of each.

7.3 Interaction Processes

Radiation, either in the form of emitted particles or electromagnetic radiation, has properties of energy, mass, momentum, and charge which combine to determine how it interacts with matter. Various absorption and/or scattering interactions produce ionization or excitation of the medium, or the radiation may be converted into yet another type (e.g., photons from positron–electron annihilation). In general, charged particles lose considerable energy by ionization, whereas photons

and neutrons give up energy by scattering and absorption reactions. Table 7-1 summarizes various properties of the major types of radiation.

Table 7-1. Interaction properties of radiation.

Radiation	Charge	Energy	Range in air	Range in H_2O
α particles	+2	3–10 MeV	2–10 cm	20–125 μm
β^+, β^- particles	±1	0–3 MeV	0–10 m	<1 cm
Neutrons	0	0–10 MeV	0–100 m	0–1 m
X-rays	0	0.1–100 keV	m–10 m	mm–cm
Gamma rays	0	0.01–10 MeV	cm–100 m	mm–10s of cm

Several terms are used to describe the changes in energy of a particle and the absorbing medium.
The s*topping power*, *S*, is defined as the loss of energy *from* a particle over a path length *dx*:

$$S = -\frac{dE}{dx}$$

Linear energy transfer (LET), which is similar to stopping power but has a distinct property, is defined as the energy imparted *to the medium*:

$$\text{LET} = -\text{LET} = -\frac{dE}{dx}$$

Although the expression for LET appears to be the same as that for the stopping power, the LET is the energy imparted to the medium at or near the site of the collision. When bremsstrahlung is produced, as in beta absorption, LET will be different from *S* because the bremsstrahlung photons carry some of the energy lost by the particles away from the collision site.

Specific ionization is yet another energy-loss term. It is the number of ion pairs formed per unit path length, and is represented by

$$\text{SI} = \frac{dN}{dx}$$

where *N* is the number of ion pairs (or atoms ionized) produced per unit path length along the path of the radiation. The average amount of energy expended to create an ion pair in air is currently accepted to be 33.97 eV, which is often rounded to 34 eV/ion pair for most calculations; in other gases it ranges from 32 to 35 eV.

Example 7-3. Calculate the total number of ion pairs produced in air by a 4.78 MeV alpha particle emitted by ^{226}Ra.
Solution.

$$\text{Ion pairs} = \frac{E_a}{34} = \frac{4,780,000\,\text{eV}}{34\,\text{eV/ion pair}} = 140,600\,\text{ion pairs}$$

Example 7-3 illustrates the large number of energy-transferring interactions when alpha particles traverse a medium. In tissue, all of these occur in a few tens of micrometers.

Relative stopping power, S_{rel}, is used for comparing the energy loss in various substances to a reference medium such as air. When the relative stopping power is known, the range R_{m} in a medium can be determined by

$$S_{\text{rel}} = \frac{(dE/dx)_{\text{m}}}{(dE/dx)_{\text{air}}} = \frac{R_{\text{a}}}{R_{\text{m}}}$$

where R_{a} and R_{m} are the ranges in air and in the medium, respectively. An approximate relative stopping power can be calculated from densities; for example, the relative stopping power for aluminum relative to air is

$$S_{\text{Al}} = \frac{\rho_{\text{Al}}}{\rho_{\text{air}}} = \frac{2.669}{1.293 \times 10^{--3}} = 2064$$

Therefore, the stopping power of alpha particles in aluminum is almost 2100 times greater than that in air, or alternatively the range in aluminum is about 2100 times less.

Kerma (kinetic energy released in material) is also used to describe energy loss in a medium. It is a unit of exposure, expressed in rad, that represents the kinetic energy transferred to charged particles per unit mass of irradiated medium when indirectly ionizing (uncharged) radiations such as photons or neutrons traverse the medium. Kerma is thus the starting point for determining the energy deposition by a given type of radiation in an absorbing medium and varies according to radiation type and absorption medium. For this reason, it will be discussed as each type of radiation is presented.

7.4 Interactions of Alpha Particles and Heavy Nuclei

Alpha particles, heavy recoil nuclei, and fission fragments are highly charged and interact by ionization in traversing a medium. Because of their high charge, their paths of interaction are characterized by very dense patterns of ionized atoms, the energy transfer per millimeter of path length is large, and their depth of penetration in most absorbing media is of the order of micrometers; even in air the maximum range is only a few centimeters. Kerma and absorbed dose from alpha par-

ticles and heavy nuclei are essentially equal since the energy transferred is deposited very near the sites of interactions to produce absorbed dose.

An alpha particle does not have orbital electrons when it is ejected from the nucleus of a radioactive atom: it is a helium nucleus with a charge of +2 two. Sir Ernest Rutherford conducted an ingenious experiment that demonstrated that alpha particles are in fact helium nuclei. He placed radon in a tube with walls so thin that the alpha particles emitted by the radon could penetrate into a second tube surrounding the first (Figure 7-1). All the air was removed from the second tube (that vacuum pump again) before the experiment began, and after several days Rutherford induced an electrical discharge across the secondary chamber and observed the classic emission spectrum of helium thus proving that alpha particles were indeed helium nuclei stripped of their electrons.

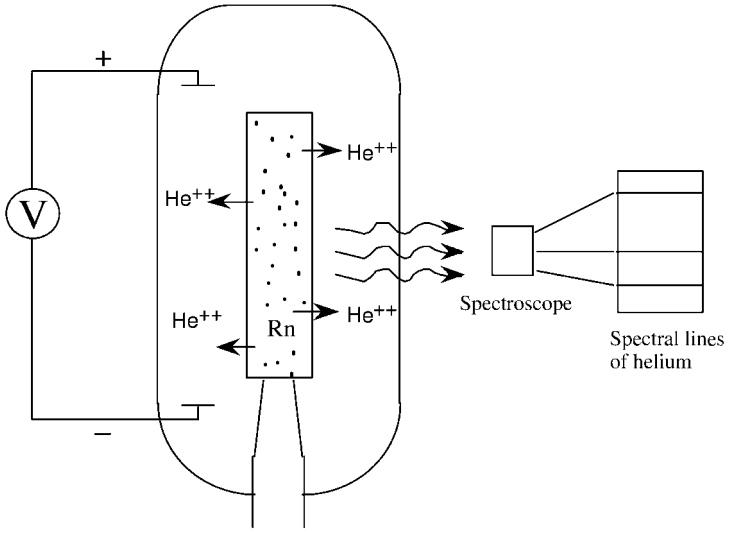

Fig. 7-1 Apparatus used to identify alpha particles as helium nuclei.

Alpha particles are emitted with several MeV of kinetic energy, typically 4–10 MeV, and because of their relatively large mass the product nucleus recoils with a significant amount of energy. Consequently, both the alpha particle with its +2 charge and the recoiling nucleus, which is also charged, produce considerable energy deposition in a very short distance. Such energy losses occur primarily by ionization and gradually reduce the velocity of the particle which allows it to spend more time in the vicinity of the target atoms with a greater probability of producing ionization. When it slows down and stops, it then picks up orbital electrons to become a neutral helium atom. This variation in specific ionization is shown in Figure 7-2 for highly ionizing alpha particles of ^{210}Po (E_α = 5.304 MeV) and radium C′ or ^{214}Po (E_α = 7.687 MeV). These particles produce on average about 50,000 ion pairs/cm and range up to about 80,000 ion pairs/cm near the end of their path. Such curves with increased ionization per unit path length near the

end of the particle track are called Bragg curves and are characterized by their shape, as shown in Figure 7-2. Beta particles produce a similar curve, but with a much reduced rate of ionization per millimeter, typically about 50 ion pairs/cm on average.

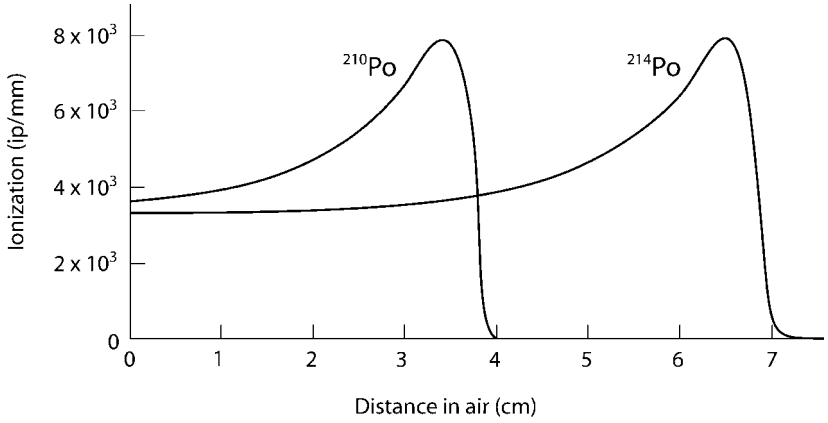

Fig. 7-2 Bragg curves of specific ionization (ion pairs/cm) of alpha particles from ^{210}Po and radium C′ (^{214}Po) in air at 760 mm and 15 °C.

7.4.1
Recoil Nuclei and Fission Fragments

Recoiling nuclei from nuclear fission also produce very short-range energy deposition. The two fission fragments share about 170 MeV of energy, which is usually apportioned as about 70 MeV of kinetic energy to a light fragment ($A \approx 94$) and about 100 MeV to a heavier one ($A \approx 140$). The fissioning nucleus supplies so much energy that the newly formed fragments that they repel each other with such force that they literally break loose from their respective electron clouds. Consequently, each fragment carries a charge of about +20 as they move through matter, and because of this excessive charge their range in most media is just a few micrometers. In uranium fuel rods, where they are commonly produced, their range is about 7–14 μm, and considerable heat is produced as the tremendous energy of the fission fragments is absorbed in the fuel matrix. Similar patterns occur for plutonium fission fragments and recoil nuclei from high-energy nuclear interactions.

7.4.2
Range of Alpha Particles

Alpha particles are emitted monoenergetically, and each particle will typically have the same range in air (or some other medium) except for some straggling about a mean range, $\bar{R}$, as shown in Figure 7-3. The straggling is statistical and

forms a normal distribution about the mean range $\bar{R}$. The range of an alpha particle is usually measured in and expressed as centimeters of air, which is roughly the same as its energy in MeV, as shown in Figure 7-4. An empirical fit of the data in Figure 7-4 shows a relationship between range and energy as

$$R = 0.325E^{3/2}$$

or

$$E = 2.12R^{2/3}$$

where R is in centimeters of standard air and E is in MeV.

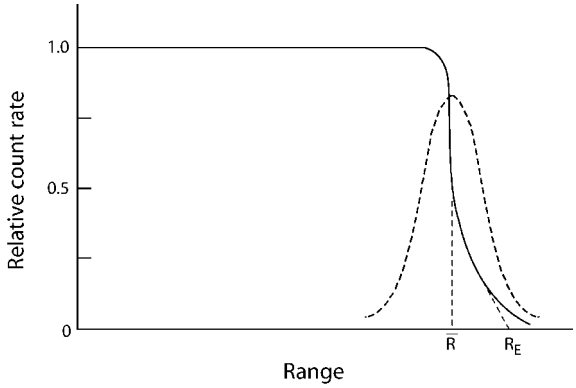

Fig. 7-3 Range in air of a collimated monoenergetic source of alpha particles showing straggling that is normally distributed about the mean range at $\bar{R}$. An extrapolated range, R_E, can be obtained by extending the straight-line portion of the curve to the x axis.

The range of an alpha particle in air can be used to determine its range in any other medium by the Bragg–Kleeman rule:

$$R_m = \frac{\rho_a}{\rho_m} R_a \sqrt{\frac{M}{M_a}}$$

The most useful relationship for the range of alpha particles in a medium is in terms of their range in air since these values have been well established. By inserting the molecular weight and density of air at 20 °C and 1 atm, one obtains

$$R_m = 3.2 \times 10^{-4} \times \frac{\sqrt{M}}{\rho_m} R_a$$

where R_m is the range in the medium in centimeters, R_a is the range of the alpha particle in centimeters of air, ρ_m is the density of the medium, and M is the atomic weight of the medium.

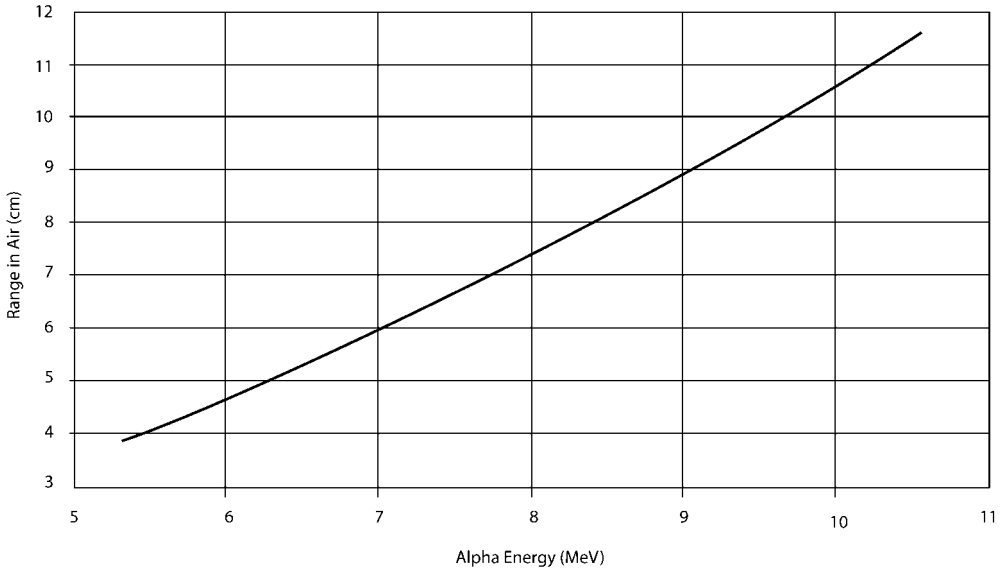

Fig. 7-4 Range versus energy of alpha particles in air.

Example 7-4. What thickness of aluminum ($\rho = 2.7$) is required to attenuate completely a source of 5 MeV alpha particles?
Solution. The range of a 5 MeV alpha particle in air is first obtained from Figure 7-4 or the empirical relationship $R = 0.325E^{3/2}$ to be 3.6 cm. The range in Al is

$$R_{\text{Al}} = 3.2 \times 10^{-4} \times \frac{\sqrt{27}}{2.7} \times 3.6\,\text{cm}$$

$$= 22.2 \times 10^{-4}\,\text{cm} = 22.2\,\mu\text{m}$$

For tissue, the mass stopping power is almost the same as in air since the composition of tissue is similar. The range of an alpha particle in tissue can be determined from the range in air R_a by adjusting it by the ratio of the densities of each:

$$R_t = \frac{\rho_a}{\rho_t} R_a$$

Thus the 5.0 MeV alpha particle in Example 7-4 would have a range in tissue of 4.65×10^{-3} cm or about 46.5 μm. The range of alpha particles in tissue is of particular interest in radiation protection, as illustrated in Example 7-5.

Example 7-5. If ^{218}Po is uniformly distributed on the lining of the bronchi (bronchial epithelium) of the human lung with an activity of 100 pCi/cm^2, what is the energy deposition per unit mass in the bronchial epithelium?

Solution. ^{218}Po emits 6.0 MeV alpha particles in 100% of its transformations, of which 50% would, due to geometry considerations, penetrate into the bronchial epithelium creating a flux of

$$\phi_a = 100 \text{ pCi/cm}^2 \times 2.22 \text{ (d/m)/pCi} \times 0.5 = 111 \ a/\text{cm}^2 \text{ min}$$

These alpha particles would dissipate their energy over the mean range in tissue ($\rho = 1.0$), which is determined from Figure 7-4 or from the equation for the range in air:

$$R_a = 0.325 E^{3/2} = 4.78 \text{ cm}$$

from which the range in tissue can be calculated:

$$R_t = \frac{1.293 \times 10^{-3}}{1} \times 4.78 \text{ cm} = 6.2 \times 10^{-3} \text{cm}$$

The energy deposition rate in rad/h over this depth of bronchial epithelium is

$$E_{dep} = \frac{111 \ a/\text{cm}^2 \text{ min} \times 6.0 \text{ MeV}/a \times 1.6022 \times 10^{-6} \text{ erg/MeV} \times 60 \text{ min/h}}{6.2 \times 10^{-3} \text{ cm} \times 1 \text{ g/cm}^3 \times 100 \text{ erg/g rad}}$$

$$= 0.104 \text{ rad/h}$$

Or, if the condition were to persist for a year due to continuous exposure to radon, the dose to the bronchial epithelium due to continuous emission of ^{218}Po alpha particles would be 911 rad (or 9.11 Gy, the unit of radiation absorbed dose in SI units).

7.5 Beta Particle Interactions and Dose

A beta particle is a high-speed electron that is so labeled because it originates from the nucleus of a radioactive atom. It has a rest mass m_0 of only 9.1×10^{-28} g and a charge Q of 1.6022×10^{-19} C. Its energy is dependent on its velocity, and conversely, and due to their small mass, beta particles with energies in the MeV range have velocities that approach the speed of light.

Beta particles lose energy to a medium in four ways: direct ionization, delta rays from electrons ejected by ionization, production of bremsstrahlung, and Cerenkov radiation. Although each mechanism can occur, the most important ones are direct ionization and bremsstrahlung production.

7.5.1
Energy Loss by Ionization

The kinetic energy of beta particles and their negative charge is such that coulombic forces dislodge orbital electrons in the absorbing medium to create ion pairs. Similar interactions occur for positrons. The particles thus lose energy by ionizing the absorbing medium, and the energy carried by these excited electrons is absorbed essentially at the interaction site. If the beta particles eject K-, L-, or M-shell electrons, characteristic x-rays will also be emitted as these vacancies are filled. These too are likely to be absorbed nearby.

Since beta particles and orbital electrons are about the same size, beta particles are deflected through a rather tortuous path, as shown in Figure 7-5a. The path length is much longer and both linear energy transfer and stopping power are relatively lower for electrons. A 3 MeV beta particle has a range in air of over 1000 cm and produces only about 50 ion pairs/cm of path length.

Delta rays are often formed along the ionization tracks of beta particles because some of the ionized electrons are ejected from target atoms with so much energy (of the order of 1 keV or so) that they can ionize other target atoms. These secondary ionizations form a short trail of ionization extending outward from the main path of the beta particle, as shown in Figure 7-5b.

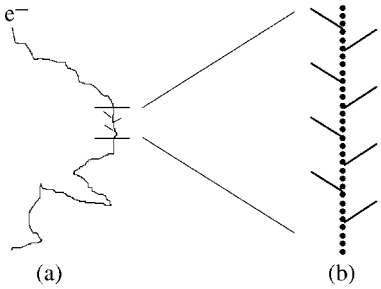

Fig. 7-5 (a) Range and ionization path of a beta particle in an absorbing medium; (b) amplified segment of ionization track showing delta ray tracks produced by ejected electrons.

7.5.2
Energy Losses by Bremsstrahlung

Since beta particles are high-speed electrons, they produce bremsstrahlung, or "braking radiation," in passing through matter, especially if the absorbing medium is a high-Z material. As electrons pass near a nucleus they experience acceleration due to the deflecting force and give up energy in producing bremsstrahlung, which in turn reduces the speed of the beta particle by an amount that corresponds to the energy lost to the bremsstrahlung photon. Whether a given beta particle converts part (or all) of its energy to radiation emission depends on the path

it takes toward a target nucleus, and the amount of deflection that occurs. The deflecting force is directly proportional to the nuclear charge (or Z) of the target, and since the beta particles can approach the nucleus of a target atom from many different angles, a source of beta particles will produce a spectrum of bremsstrahlung forming a continuous band of energies that extends up to the maximum energy of the beta particle. The process is the same one that occurs in an x-ray tube and is illustrated in Figure 7-6.

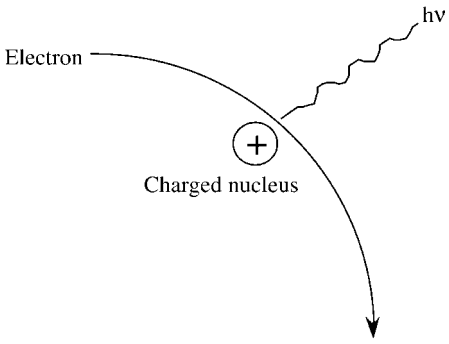

Fig. 7-6 Schematic of bremsstrahlung production by a high-speed electron.

The yield or fraction of bremsstrahlung produced is proportional to the atomic number of the target (or absorbing) material and the energy of the electrons striking the target, which of course rapidly decreases as the particles traverse the target material. Describing the process analytically is difficult; consequently best-fit models have been constructed of empirical data on the fraction of the beta energy from a source that is converted to photons in order to account for them in dosimetry or radiation shielding. Unfortunately, the measured data are for monoenergetic electrons which complicates the applicability for beta particles which are emitted as a spectrum of energies from a source. Berger and Seltzer have tabulated fractional yields for monoenergetic electrons (see Chapter 8) and these can be used with some discretion to estimate photon production for beta emitters. As much as 10% or so of the energy of 2 MeV particles can be converted to bremsstrahlung in heavy elements such as lead ($Z = 82$), an effect that must be recognized in choosing shield material (see Chapter 8). When beta particles are absorbed in tissue (which has a low atomic number), less than 1% of the interactions produce bremsstrahlung, and many of those that do are likely to escape the tissue medium because their probability of interaction is also low in this low-Z medium.

7.5.3 Cerenkov Radiation

High-speed beta particles (and other high-energy particles as well) can cause the emission of visible radiation with a blue tint that is called Cerenkov radiation after

the pioneer scientist who studied the effect. Cerenkov radiation occurs because charged particles moving through a medium experience deflections (and accelerations) which yield photons of electromagnetic radiation that must traverse the same medium. The velocity of these photons is equal to c/n where n is the index of refraction, which is specific for each medium ($n = 1.4$ for water). Since a medium such as water will refract electromagnetic radiation traveling in it, it is common for high-speed beta particles to have a velocity in the medium $\geq c/n$; when this happens, photons of electromagnetic energy are produced that cannot outrun the fast-moving beta particle. These photons will lag behind the beta particle which will produce other photons up ahead, and as the trailing photons overlap the new ones they constructively interfere with each other. The effect can be thought of as a charged-particle sonic boom, analogous to the compression wave created by an aircraft that, due to the physical constraint in traveling through air, simply cannot keep up with the aircraft that creates the shockwave (a similar analogy is the bow wave produced by a speedboat).

The constructive interference produced by high-speed beta particles (see Figure 7-7) yields photons in the ultraviolet region of the visible light spectrum and accounts for the blue glow that occurs from highly radioactive sources, e.g., multicurie cobalt sources and highly radioactive reactor fuel elements. Cerenkov radiation around nuclear reactor cores and other high-intensity radiation sources is fascinating to observe, but it accounts for little energy loss compared to that from ionization and bremsstrahlung production.

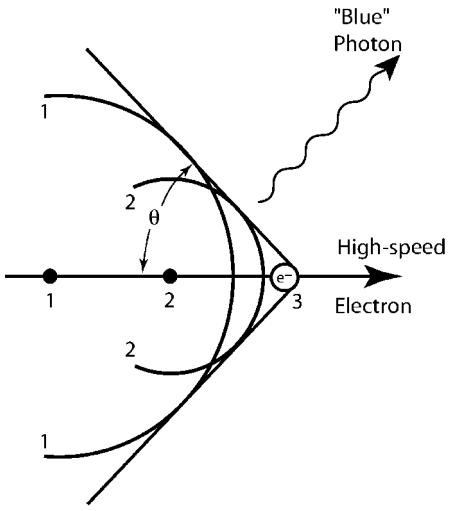

Fig. 7-7 Wavefronts produced by a particle with velocity $\geq c/n$ constructively interfere to produce blue photons of light, or Cerenkov radiation.

7.5.4 Attenuation of Beta Particles

Beta particles are attenuated in an absorption medium by the various interaction processes, primarily through ionization and radiative energy losses. The degree of absorption (or attenuation) is determined by observing the change in source strength due to insertion of different thickness of absorber (usually aluminum in units of mg/cm^2) in the beam (see Figure 12-19).

As shown in Figure 7-8, the counting rate, when plotted on a logarithmic scale, decreases as a straight line, or very nearly so, over a large fraction of the absorber thickness, eventually tailing off into another straight line region represented by the background, which is always present. The point where the beta absorption curve meets the background is the range, $R_{\beta\max}$, traversed by the most energetic particles emitted, and curves of this type can be used to determine $R_{\beta\max}$ and $E_{\beta\max}$ for a beta source. The measured range in mg/cm^2 in aluminum or other similar absorber is then used to determine the energy by an empirical range–energy curve

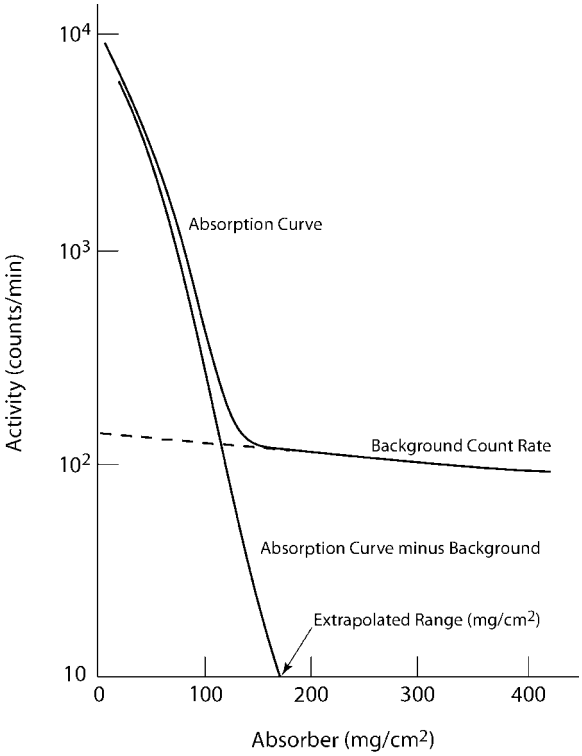

Fig. 7-8 Decrease in measured activity of a beta particle source versus mg/cm^2 of absorber thickness that trails off into the background of the detector system. Subtraction of the background portion from the total curve yields a curve that can be extrapolated to estimate the maximum range (in mg/cm^2) of the beta source.

as shown in Figure 7-9. Aluminum is the absorber medium most often used for determining ranges of beta particles, but most absorber materials will have essentially the same electron density since, with the exception of hydrogen, the Z/A ratio varies only slowly with Z. Consequently, the ranges in Figure 7-9 can be considered generic for most light absorbers, with a notable exception for air (see Figure 8-1), as long as the equivalent mg/cm^2 of absorber is known.

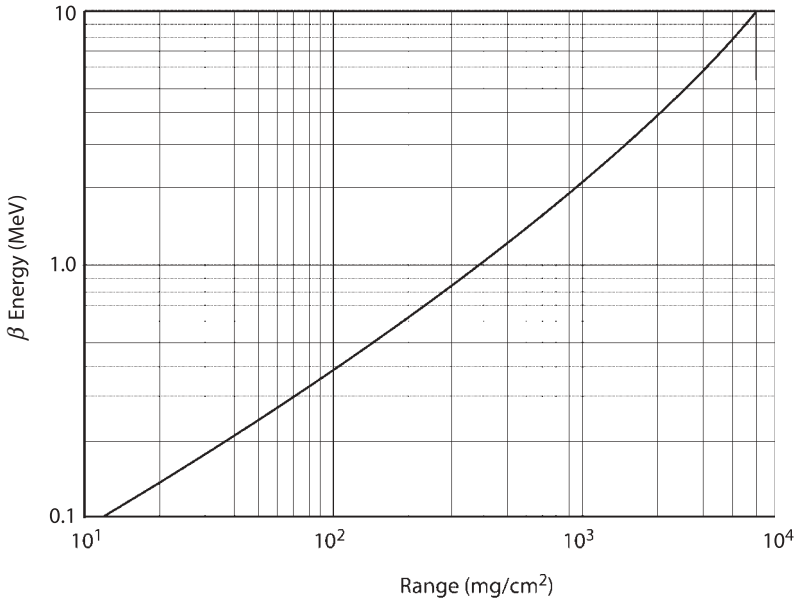

Fig. 7-9 Equivalent range of electrons in mg/cm^2 of low-Z absorbers.

7.5.5 Range Versus Energy of Beta Particles

Empirical relations have been developed from experimental data to relate range to beta particle energy. The range R in mg/cm^2 versus energy in MeV has been empirically derived for $0.01 \leq E \leq 2.5$ MeV as

$$R = 412E^{1.265 - 0.0954\ln E}$$

or alternatively for $R \leq 1200$ mg/cm^2

$$\ln E = 6.63 - 3.2376(10.2146 - \ln R)^{1/2}$$

Another empirical relationship between E in MeV and R in mg/cm^2 is Feather's rule for beta particles of $E \geq 0.6$ MeV:

$$R = 542E - 133$$

Although these relationships can be used to calculate ranges and energies for low-energy electrons, they can generally be obtained more accurately from the empirical range–energy curve in Figure 7-9 where range is determined in units of mg/cm^2.

The exponential decrease in the number of beta particles counted versus absorber thickness (Figure 7-8) is represented, to a good approximation, for the straight-line part of the curve as

$$N(x) = N_0 e^{-\mu_\beta(\rho x)}$$

where N_0 is the number of beta particles counted with zero thickness of absorber, $N(x)$ is the number observed for an absorber of thickness x, μ_β is the "beta absorption" coefficient in cm^2/g, and ρx is the density thickness (g/cm^2) of the absorber. Since the units of μ_β for various beta sources are determined (and expressed) in cm^2/g, it is necessary to specify the absorber as a density thickness with units of g/cm^2, which is obtained by multiplying the absorber thickness x by its density ρ.

The absorption of beta particles is not truly exponential, or probabilistic, as the expression for absorption would suggest. The exponential form of the curve is an artifact produced by a combination of the continually varying spectrum of beta energies and the scattering of the particles by the absorber. It can, however, be used with reasonable accuracy for density thicknesses less than the maximum range of the beta particles; there is no practical value in evaluating thicknesses greater than $R_{\beta\max}$.

Three techniques are generally used to obtain the range R_β from the net beta absorption curve: (a) extrapolation of the beta curve to intersect the residual radiation background; (b) a modified Feather analysis; and (c) a complete Feather analysis. The extrapolation technique, which is easiest, is only approximate but is often of sufficient accuracy to determine the energy, and hence the identity, of the beta emitter. The modified Feather analysis is, like the complete Feather analysis, based on an absorption curve obtained for a known standard such as ^{210}Bi which has a well-established value of R_β. In this technique the amount of absorber required to reduce the count rate of the standard by one half is compared to that required to reduce the unknown by one half and the two are compared as illustrated in Example 7-6.

It is common practice to extrapolate the straight-line portion of the curve in Figure 7-8 to the background and to use the extrapolated value as the maximum range. This procedure is often, but erroneously, called a *Feather analysis*. A true Feather analysis, named after its originator, is described by Lapp and Andrews as a more deliberate and accurate process which compares the absorption data from an unknown to a known beta standard, usually ^{210}Bi ($E_{\beta\max}$ = 1.162 MeV). The maximum range of ^{210}Bi has been carefully established as 510 mg/cm^2, and is thus used as a reference for calculating unknown ranges.

Example 7-6. A beta standard with a known range of 200 mg/cm^2 is counted with different thicknesses of absorber and from a data plot it is found that the count rate is reduced to one-half by 50 mg/cm^2 of aluminum. An unknown that is measured the same way requires 100 mg/cm^2 to reduce the count rate by one-half. What is the approximate beta range of the unknown and its energy?

Solution. For the standard, 50 mg/cm^2 corresponds to $0.25R_\beta$; therefore, since 100 mg/cm^2 is required to reduce the count rate of the unknown by one-half,

$$R_\beta = \frac{100 \text{ mg/cm}^2}{0.25} = 400 \text{ mg/cm}^2$$

From Figure 7-9, 400 mg/cm^2 corresponds to $E_{\beta\max} \cong 1.0$ MeV.

7.5.6 Radiation Dose from Beta Particles

Radiation dose calculations for beta particles are based on the number traversing a medium (usually tissue) per unit area, their range, which is energy dependent, and the energy deposition fraction per unit mass μ_β. When it is possible to establish a flux of beta particles impinging upon a mass of medium, then dose calculations are straightforward if the beta absorption coefficient and the average beta particle energy are known. The average beta particle energy can be obtained by equations in Chapter 5 or more accurately by the listed values for each radionuclide contained in Appendix D. The rule of thumb, $\bar{E} = \frac{1}{3}E_{\beta\max}$, can also be used as a first approximation, but for accurate calculation the weighted average values of $\bar{E}$ for each beta emitter should be used

Once the beta particle energy flux (MeV/cm^2 s) is known, the energy absorption in a medium (or dose) can be calculated by using the beta absorption coefficient for the medium and the particular beta particle energy. Approximate relationships for the beta absorption coefficient have been determined for air and tissue specifically because of their utility in radiation protection. Appropriate values of μ_β in cm^2/g can be determined for air and tissue as follows:

$$\mu_{\beta,\text{air}} = 16(E_{\beta\max} - 0.036)^{-1.4}$$

$$\mu_{\beta,\text{tissue}} = 18.6(E_{\beta\max} - 0.036)^{-1.37}$$

For any other medium,

$$\mu_{\beta,i} = 17(E_{\beta\max})^{-1.14}$$

where values of μ_β are in units of cm^2/g (based on measurements with aluminum absorbers) and $E_{\beta\max}$ is in units of MeV. It should be noted that μ_β is uniquely defined with units of cm^2/g instead of the more traditional units of cm^{-1} or as μ/ρ because the most practical uses of the beta absorption coefficients are in calculations of beta dose or beta attenuation.

The beta radiation dose rate, $\dot{D}_\beta$, for beta particles of average energy $\overline{E} = \frac{1}{3}E_{\beta\,\max}$ (MeV) is

$$\dot{D}_\beta(\text{rad/h}) = \frac{\phi_{\beta,\text{E}} \times \overline{E} \times 1.6022 \times 10^{-6}\,\text{erg/MeV} \times \mu_\beta(\text{cm}^2/\text{g}) \times 3600\,\text{s/h}}{100\,\text{erg/g rad}}$$

or

$$\dot{D}_\beta(\text{rad/h}) = 5.768 \times 10^{-5}\phi_\beta \overline{E} \times \mu_\beta$$

Example 7-7. What is the beta dose rate at the surface of a person 1 m from a 1 Ci source of ^{32}P ($E_{\beta\text{max}} = 1.710$ MeV and $\overline{E}_\beta \cong 0.695$ MeV) assuming no attenuation of the beta particles as they traverse the medium?
Solution. The beta flux is

$$\phi_{\beta,E} = \frac{3.7 \times 10^{10}\,\text{t/s Ci} \times 0.695\,\text{MeV/t}}{4\pi(100\,\text{cm})^2}$$

$$= 2.05 \times 10^5\ \text{MeV/cm}^2\,\text{s}$$

The beta absorption coefficient in tissue for ^{32}P beta particles is

$$\mu_{\beta,\text{tissue}} = 18.6(1.71 - 0.036)^{-1.37} = 9.183\,\text{cm}^2/\text{g}$$

and the beta dose rate due to beta particles with $\overline{E} = 0.695$ MeV is

$$\dot{D}_\beta = 5.768 \times 10^{-5} \times 2.94 \times 10^5\ \beta/\text{cm}^2\,\text{s} \times 0.695\ \text{MeV}/\beta \times 9.183\ \text{cm}^2/\text{g}$$

$$= 108.58\ \text{rad/h}$$

Most practical problems of beta radiation dose require adjustments of the energy flux. In Example 7-7 for instance, the dose rate from a point source would be more accurate if absorption of beta particles in the 1 m thickness of air were also considered since some absorption occurs in the intervening thickness of air before reaching the person. This is done by adjusting the energy flux for air attenuation using $\mu_{\beta,\text{air}}$ for the 1.71 MeV beta particles of ^{32}P, which is

$$\mu_{\beta,\text{air}} = 16(1.71 - 0.036)^{-1.4} = 7.78\,\text{cm}^2/\text{g}$$

The beta dose rate for ^{32}P beta particles after traversing a thickness x of air is then

$$\dot{D}_\beta(x) = \dot{D}_\beta^0 e^{-\mu_{\beta,\text{air}}(\rho x)}$$

$$= 108.58(0.3657) = 39.71\ \text{rad/h}$$

A further adjustment to Example 7-7 is appropriate to account for absorption of beta particles in the dead layer of skin with a density thickness of 0.007 g/cm^2; i.e., to calculate the dose where it matters, to living tissue. The dose rate just below the 7 mg/cm^2 skin layer is known as the "shallow dose." To make this adjustment, the beta dose rate is again calculated considering air attenuation and the density thickness of tissue (0.007 g/cm^2), or

$$\dot{D} = 39.71e^{-\mu_{\beta,t}(\rho x)}$$
$$= 39.71e^{-9.183\,\mathrm{cm^2/g}\times 0.007\,\mathrm{g/cm^2}} = 37.25\,\mathrm{rad/h}$$

To summarize, if ϕ_β, the flux of beta particles, is known, the general expression for the beta dose rate at the shallow depth in tissue after traversing a thickness x of air is

$$\dot{D}_\beta(\mathrm{rad/h}) = 5.768\times 10^{-5}\varphi_{\beta,\mathrm{E}}\,\mu_\beta\overline{E}[e^{-\mu_{\beta,\mathrm{a}}(\rho x)}][e^{-\mu_{\beta,\mathrm{t}}(0.007\,\mathrm{g/cm^2})}]$$

where ϕ is in units of β/cm^2 s, $\overline{E}$ is MeV/t, $\mu_{\beta,\mathrm{a}}$ and $\mu_{\beta,\mathrm{t}}$ are in units of cm^2/g, ρx is the density thickness of air, and 0.007 g/cm^2 is the density thickness of the dead skin layer.

Energy deposition of beta particles in a medium can be represented relative to air, as shown in Table 7-2. These factors can be useful for determining energy deposition (dose) or attenuation for a given medium from a beta dose rate measured in air. For example, when LiF is used as a dosimeter, its response can be estimated by multiplying the beta dose rate in air by 0.97 (from Table 7-2).

Table 7-2. Stopping powers and attenuation of beta particle dose, relative to air, for low-Z materials.

Medium	Z[a]	Stopping power	Attenuation relative to air
Polyethylene	4.75	1.205	1.12
Polystyrene	5.29	1.118	1.04
Carbon	6.00	1.007	0.96
Mylar	6.24	1.066	1.03
Water	6.60	1.150	1.12
Muscle	6.65	1.136	1.11
Air	7.36	1.00	1.00
LiF	7.50	0.965	0.97
Teflon (CF_2)	8.25	1.032	1.05
"Bone"	8.74	1.063	1.09

a Values of Z for compounds are weighted based on chemical composition.
Source: Atomic Energy of Canada Ltd. Cross et al. 1982. Adapted from *The Health Physics and Radiological Health Handbook*, with permission.

7.5.7 Beta Dose from Contaminated Surfaces

If a floor, wall, or other solid surface is uniformly contaminated with a beta emitter, the beta dose rate can be determined by establishing the beta flux and then proceeding as demonstrated in Example 7-8. For contaminated solid surfaces, the flux will be determined by the area contamination level (e.g., μCi/cm²), a geometry factor (usually $^1/_2$), and a backscatter factor to account for beta particles that penetrate into the surface but are scattered back out to increase the beta flux reaching a receptor near the surface. Table 7-3 contains backscatter factors versus beta energy for various materials. It is noticeable that the backscatter factor is highest for low-energy beta particles on dense (or high-Z) materials.

Table 7-3. Backscatter factors for beta particles on thick surfaces.

Beta energy (MeV)	Carbon	Aluminum	Concrete[a]	Iron	Copper	Silver	Gold
0.1	1.040	1.124	1.19	1.25	1.280	1.38	1.5
0.3	1.035	1.120	1.17	1.24	1.265	1.37	1.5
0.5	1.025	1.110	1.15	1.22	1.260	1.36	1.5
1.0	1.020	1.080	1.12	1.18	1.220	1.34	1.48
2.0	1.018	1.060	1.10	1.15	1.160	1.25	1.40
3.0	1.015	1.040	1.07	1.12	1.125	1.20	1.32
5.0	1.010	1.025	1.05	1.08	1.080	1.15	1.25

a Factors for concrete based on arithmetic average of factors for aluminum and iron.
Source: adapted from Tabata et al.

Example 7-8. What is the beta dose rate to skin and at the shallow depth (a) just above the surface (i.e., at contact) of a large copper shield uniformly contaminated with 10 μCi/cm² of ^{32}P, and (b) at a distance of 30 cm?

Solution. (a) The beta flux is presumed to be equal to the area emission rate, and since half of the beta particles would be directed into the surface, the geometry factor is 0.5. The backscatter factor for ^{32}P beta particles ranges between 1.18 and about 1.30 based on the average energy, which by interpolation yields a backscatter factor of 1.24. The surface-level beta dose rate at the air/tissue interface due to beta particles with $\overline{E}$ = 0.695 MeV/t is

$$\dot{D}_\beta \text{ (rad/h)} = 5.768 \times 10^{-5} \phi_\beta \overline{E} \times 0.5 \times \mu_{\beta,\text{t}}$$

$$= (5.768 \times 10^{-5})(10\ \mu\text{Ci/cm}^2 \times 3.7 \times 10^4\ \text{t/s} \times 0.5 \times 0.695\ \text{MeV/t})(9.183\ \text{cm}^2\text{/g})$$

$$= 84.7\ \text{rad/h}$$

and the beta dose at the shallow depth in tissue is

$$\dot{D}_{\beta,\text{sh}} = 84.7 e^{-9.183\,\text{cm}^2\text{/s} \times 0.007\,\text{g/cm}^2} = 79.4\,\text{rad/h}$$

(b) At 30 cm, the beta particles will be attenuated by 30 cm of air, and the beta dose rate at the skin is

$$\dot{D}_{\beta,\text{skin}} = 84.7\,\text{rad/h} \times e^{-\mu_{\beta,a}\rho_{\text{air}} \times 30\,\text{cm}}$$
$$= 63.94\,\text{rad/h}$$

and at the shallow depth, a dose of

$$\dot{D}_{\beta,\text{sh}} = 63.94\, e^{-9.183\,\text{cm}^2\text{/g} \times 0.007\,\text{g/cm}^2}$$
$$= 59.96\,\text{rad/h}$$

7.5.8 Beta Contamination on Skin or Clothing

Shallow dose from beta particles can occur from direct contamination of the skin or from contaminated protective clothing in contact with the skin. If an area energy flux can be established, calculation of the shallow dose is straightforward by assuming a geometry factor of 0.5 (one-half the activity goes outward) and adjusting the energy flux to account for beta energy absorption in the dead layer of skin. There will be some backscatter of beta particles by the tissue layer below the skin but since tissue is a low-Z material this is only a few percent and can be ignored for most radiation protection situations.

Example 7-9. Estimate the shallow dose rate from 5 mL of solution containing 10 μCi/mL of ^{32}P spilled onto the sleeve of a worker's lab coat and distributed uniformly over an area of about 50 cm^2.

Solution. Uniform absorption of the solution onto the lab coat would produce an area contamination of 1 μCi/cm^2. Assuming no attenuation of beta particles in the fabric, one-half of the beta particles emitted would impinge on the skin, and the energy flux just reaching the basal skin layer would be

$$\phi_{\beta,\text{E}} = 1\,\mu\text{Ci/cm}^2 \times 3.7 \times 10^4\,\text{t/s}\,\mu\text{Ci} \times 0.695\,\text{MeV/t} \times 0.5(e^{-\mu_{\beta,\text{t}}0.007})$$
$$= 1.23 \times 10^4\,\text{MeV/cm}^2\,\text{s}$$

and the beta dose rate at the shallow depth of tissue is

$$\dot{D}_{\beta,\mathrm{sh}} = (5.768 \times 10^{-5})(1.23 \times 10^{4}\,\mathrm{MeV/cm^2\ s})(9.183\,\mathrm{cm^2/g}) = 6.51\,\mathrm{rad/h}$$

A similar calculation can be made for direct contamination of the skin, although in most practical situations it is more difficult to determine the area contamination. The skin contamination may be estimated by careful measurements with a thin-window probe or by washing the wet area with a swab or liquid and measuring the activity removed.

7.5.9
Beta Dose from Hot Particles

Small, but very radioactive, particles that emit beta particles and gamma rays are occasionally found on the skin or clothing of persons in radiation areas. Because of their small size and intense radioactivity, small areas of tissue can receive significant energy deposition before the particles are detected and removed. Various computer codes such as VARSKIN have been developed to deal with the unusual and often diverse conditions presented by hot particles; however, it is possible to calculate the resultant beta doses by applying several general principles. The activity of the particle establishes the number of beta particles being emitted from a point, and since the particles are emitted uniformly in all directions from a point source, the emitted energy will be deposited into a hemispherical volume of tissue of radius equal to the range of the beta particles in tissue, as shown in Figure 7-10.

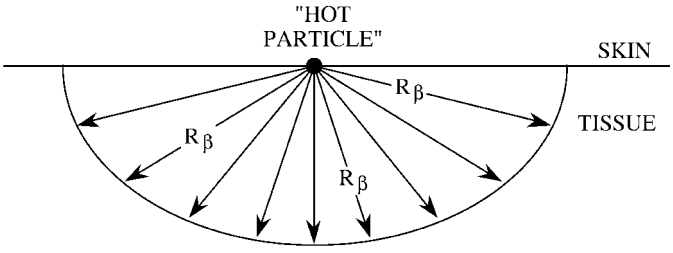

Fig. 7-10 Schematic of energy deposition of beta particles emitted by a point source "hot particle" on the surface of the skin. The energy of the beta particles is deposited uniformly in a three-dimensional hemispherical mass of tissue of radius equal to the maximum range R_β of the beta particles.

To determine the beta dose from a hot particle, it can be assumed that the average energy of the beta particles is distributed fairly uniformly throughout the tissue mass in the hemispherical volume of radius R_β, where R_β is based on the maximum energy of the emitted beta particles. The average energy is used to determine energy deposited rather than the maximum energy even though R_β is based on $E_{\beta\max}$. The interplay of the continuous energy spectrum of a beta emitter, the

maximum depth of penetration of each particle, and the Bragg absorption pattern for each beta particle combine to provide fairly uniform distribution of beta energy throughout the hemispherical mass. This is a reasonable determination since the continuous energy spectrum of beta particles and the random attenuation combine to produce an approximate exponential absorption pattern (see Figure 7-8). VARSKIN uses a value of $0.9R_\beta$ to account for these variables, thus conservatively assuming a smaller mass (and a somewhat higher absorbed dose) in which the energy deposition occurs. The beta dose rate to tissue, without correcting for absorption in the dead layer of skin, from a hot particle of activity q(μCi), one-half of which impinges on the skin, is

$$\dot{D}_\beta = \frac{0.5\,q\,(\mu\text{Ci}) \times 3.7 \times 10^4\ \text{t/s}\ \mu\text{Ci} \times \bar{E}\,\text{MeV/t} \times 1.6022 \times 10^{-6}\text{erg/MeV} \times 3600\,\text{s/h}}{{}^4\!/_3\,\pi R_\beta^3 \times {}^1\!/_2 \times 1\,\text{g/cm}^3 \times 100\,\text{erg/g rad}}$$

$$= \frac{0.51\bar{E}_\beta \times q\,(\mu\text{Ci})}{R_\beta^3}\ \text{rad/h}$$

where q is the activity of the hot particle in μCi, R_β is the range in centimeters of the beta particles of maximum energy, and $\bar{E}$ is the average energy in MeV of each beta particle emitted.

Example 7-10. Estimate the beta dose, ignoring the gamma emissions, due to a hot particle containing 1 μCi of ^{60}Co ($E_{\beta\text{max}}$ = 0.318 MeV; $\bar{E}$ = 0.106 MeV) on a person's skin.

Solution. The beta dose due to 1 μCi of ^{60}Co is assumed to be produced by deposition of the average beta energy of 0.106 MeV/t (Appendix D) uniformly in a hemispherical mass of radius R_β. The range R_β of 0.318 MeV beta particles is determined from Figure 7-9 to be 84 mg/cm^2 which corresponds to a distance in tissue of unit density of 0.084 cm. The beta dose from the "hot particle" is

$$D_\beta(\text{rad/h}) = \frac{0.51 \times 1\,\mu\text{Ci} \times 0.106\,\text{MeV/t}}{(0.084)^3}$$

$$= 91.1\ \text{rad/h}$$

7.6 Photon Interactions

Describing a photon is difficult, even though its roles in radiation protection are fairly well understood. Its more obvious properties are no rest mass, it always travels at the speed of light, and it can interact as a particle even though it is also a wave. The makeup or composition of a photon is unknown, but like the electron it

is a true "point" – it has no physical size and cannot be taken apart to yield subcomponents.

The energy of a photon is $h\nu$, its momentum is h/λ, and its energy can be described in terms of its momentum as $E = pc$. Einstein showed that a photon feels the pull of gravity as if it were a particle even though it has no rest mass. Photons are fundamental to physics because they transmit the electromagnetic force; two electric charges are believed to interact by "exchanging" photons (photons are emitted by one charge and absorbed by the other), even though these photons exist only in the mathematical framework of theoretical physics.

Photons originate in interesting ways; they simply appear when it is necessary to carry off excess energy (such as bremsstrahlung production, in radioactive transformation, or in nuclear interactions). The dichotomy of being both a wave and a particle is intriguing, but both properties are required to explain photon interactions in media. The origin and appearance of interference and diffraction phenomena are clearly wave properties, and its absorption to deposit energy and impart momentum requires a particle description as so effectively deduced by Einstein (photoelectric effect) and Compton (in explaining photon scattering). It is difficult to accept that both could exist simultaneously, yet both properties are required to completely describe photons. Neither the wave nor the particle theory is wholly correct all of the time, but both, as defined by Bohr, are "complementary" to each other.

The principal modes by which photons interact with matter to be attenuated and to deposit energy are by the photoelectric effect, the Compton effect, and pair production. Photons also undergo Rayleigh scattering, Bragg scattering, photodisintegration, and nuclear resonance scattering; however, these result in negligible attenuation or energy deposition and can generally be ignored for purposes of radiation protection.

7.6.1 Photoelectric Interactions

A low-energy photon can, by a process known as the photoelectric effect, collide with a bound orbital electron and eject it from the atom. The electron is ejected with an energy equal to that of the incoming photon, $h\nu$, minus the binding energy of the electron in its particular orbit, an energy that must be overcome to free the electron from the atom. The interaction must occur with a bound electron since the entire atom is necessary to conserve momentum, and it often occurs with one of the inner-shell electrons. Since a vacancy is created in the electron shell, a characteristic x-ray, typically from filling the K shell, will also be emitted. The kinetic energy of the ejected electron is almost always absorbed in the medium where photoelectric absorption occurs. Characteristic x-rays that are produced are also very likely to be absorbed in the medium, typically by another photoelectric interaction or by the ejection and absorption of Auger electrons (see Figure 4-6).

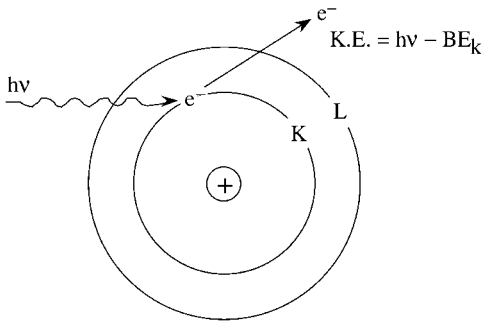

Fig. 7-11 Schematic of the photoelectric effect.

The *photoelectric absorption coefficient* τ is a function of the atomic number Z of the absorbing material (generally related to the density ρ of the absorbing medium) and the energy of the radiation as follows:

$$\tau \cong \text{constant} \times \frac{Z^5}{E^3}$$

It is evident that photoelectric absorption is most pronounced in high-Z materials and for low-energy photons (less than 0.5 MeV). In a high-Z material such as lead, L x-rays and M x-rays can also be prominent emissions from target atoms and these will either be absorbed in the absorbing medium or will contribute to the photon fluence. The photoelectric effect can be summarized as follows:

- It occurs only with bound electrons because the entire atom is necessary to conserve momentum.
- The interaction coefficient is greatest when the photon energy just equals the amount to overcome the binding energy of the orbital electron, causing it to be ejected from its shell.
- The photoelectric absorption coefficient is directly proportional to Z^5 and inversely proportional to $(h\nu)^3$ on average.
- In tissue the absorbed energy $E_{ab} \approx h\nu$, and the transfer, absorption, and attenuation coefficients are nearly equal.

7.6.2 Compton Interactions

Compton scattering interactions are especially important for gamma rays of medium energy (0.5–1.0 MeV), and, for low-Z materials such as tissue, can be the dominant interaction mechanism down to 0.1 MeV. Compton scattering involves a collision between a photon and a "free" or very loosely bound electron in which a part of the energy of the photon is imparted to the electron, as shown in Figure 7-12. Both energy and momentum are conserved in the collision.

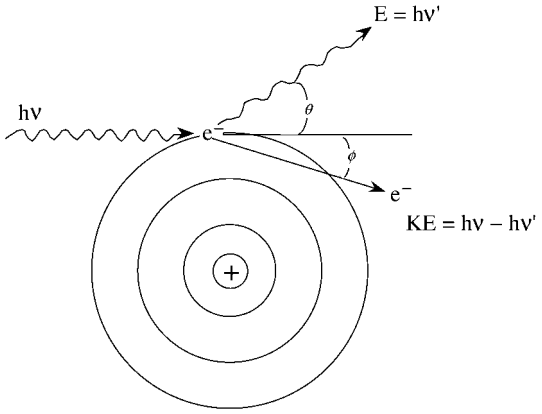

Fig. 7-12 Compton scattering with a "free" electron.

The Compton-scattered photon emerges from the collision in a new direction and with reduced energy and increased wavelength. The change in wavelength, $\lambda' - \lambda$, commonly referred to as the Compton shift, is

$$\lambda' - \lambda = \frac{h}{m_0 c}(1 - \cos\theta) = 0.024264(1 - \cos\theta)\ \text{Å}$$

It is notable that the change in wavelength (and decrease in energy) of the photon is determined only by the scattering angle. The term h/m_0c, often called the Compton wavelength, has the value 2.4264×10^{-10} cm.

Energy transfer to the recoiling electron is the most important consequence of Compton interactions since it will be absorbed locally to produce radiation dose. This is a variable quantity and can range from zero up to a maximum value for electrons ejected in the forward direction. The fraction of the photon energy $h\nu$ that is transferred to the Compton electron is shown in Figure 7-13; the value E_{tr} is dependent on the scattering angle, where $\bar{E}_{tr}$ is the average value due to random processes and $E_{tr,max}$ is the maximum value for a scattering angle of 180°.

The *Compton interaction coefficient* σ consists of two components:

$$\sigma = \sigma_a + \sigma_s$$

where σ is the total Compton interaction coefficient, σ_a is the Compton absorption coefficient for photon energy lost by collisions with electrons, and σ_s is the loss of energy due to the scattering of photons out of the beam. The Compton interaction coefficient is determined by electron density which is directly related to Z and inversely proportional to E as follows:

$$\sigma \cong \text{constant} \times \frac{Z}{E}$$

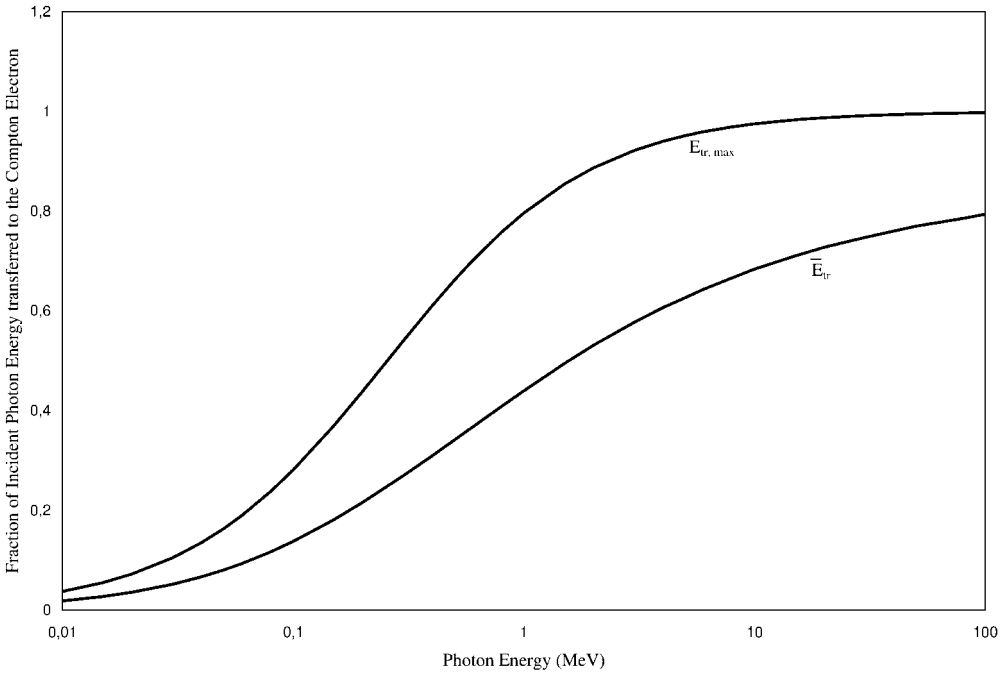

Fig. 7-13 Fraction of incident photon energy ($h\nu$) transferred to a Compton electron.

Compton scattering interactions can be summarized as follows:

- A Compton interaction occurs between a photon and a "free" electron producing a recoiling electron and a scattered photon of reduced energy.
- Kinetic energy transferred to the electron is directly proportional to the scattering angle of the scattered photon and, on average, increases with photon energy.
- The Compton interaction coefficient decreases with increasing energy and is almost independent of atomic number.
- For photons with energies above 100 keV, Compton interactions in soft tissue (low-Z material) are much more important than either the photoelectric or pair production interactions.

7.6.3 Pair Production

When a high-energy (>1.022 MeV) photon interacts with the strong electromagnetic field surrounding a nucleus as shown in Figure 7-14, its energy can be converted into a pair of electron masses, one of which is negatively charged (the electron) and the other, called the positron, is positively charged. Pair production can

also occur in the field of an electron yielding a triplet consisting of a positron, a negatron, and the recoiling electron.

Pair production is a classic example of Einstein's special theory of relativity in which the pure energy of the photon is converted into two electron masses, and since energy is conserved the positron and electron share the energy left over ($h\nu$ – 1.022) after the electron masses have been formed. This remaining energy appears as kinetic energy of the e^+ and e^- pair, but is not shared equally. The positively charged nucleus repels the positively charged positron which provides an extra "kick" while the negatron is attracted and thus slowed down with a decrease in its kinetic energy. Because of these circumstances, the positron should receive a maximum of about $0.0075Z$ more kinetic energy than the average negatron. The slight difference in energy shared by the positron and the electron in pair production interactions is of little consequence to radiation dosimetry or detection since the available energy, $h\nu$ – 1.022 MeV, will be absorbed in the medium with the same average result regardless of how it is shared.

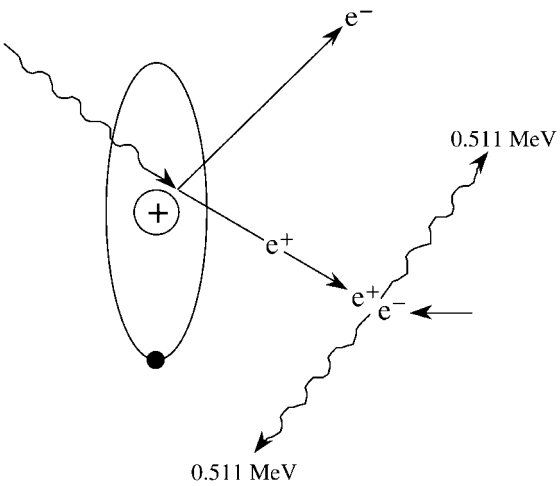

Fig. 7-14 Pair production.

Example 7-11. What energy sharing will exist for positrons and electrons when 2.622 MeV gamma rays from ThC′ produce a positron–electron pair?

Solution. The kinetic energy to be shared is 2.622 – 1.022 MeV = 1.6 MeV. If the energy were equally shared both the positron and negatron would each possess 0.80 MeV, but the positron energy should be 0.8 MeV + $0.0075Z$ = 1.06 MeV. The negatron energy is 1.6 – 1.06 = 0.54 MeV.

Pair production interactions are also accompanied by the emission of two annihilation photons of 0.511 MeV each, which are also shown in Figure 7-14. The positron will exist as a separate particle as long as it has momentum and kinetic energy. However, when it has been fully absorbed, being antimatter in a matter

world, it will interact with a negatively charged electron forming for a brief moment a "neutral particle" of "positronium" which then vanishes yielding two 0.511 MeV photons; i.e., mass becomes energy. The absorption of high-energy photons thus yields a complex pattern of energy emission and absorption in which the pure energy of the photon produces an electron and a positron which deposit $h\nu - 1.022$ MeV of kinetic energy along a path of ionization, followed in turn by positron annihilation with a free electron to convert mass back into energy. The absorption of a high-energy photon by pair production thus yields two new photons of 0.511 MeV which may or may not interact in the medium and an intermediate pair of electron masses which almost certainly do.

The p*air production interaction coefficient* κ is proportional to the square of the atomic number Z for photons with energy greater than 2×0.511 MeV (the energy required to form an electron–positron pair) and has the following relationship:

$$\kappa \cong \text{constant} \times Z^2(E - 1.022)$$

where Z is the atomic number and E is the photon energy in MeV. Pair production interactions can be summarized as follows:

- They occur for photons with $h\nu \geq 1.022$ MeV primarily in the field of the nucleus to produce two electron masses with kinetic energy, but can also occur with an orbital electron yielding a triplet of electron masses.
- The kinetic energy shared between the positron and the electron is $h\nu - 1.022$ MeV.
- The positron annihilates with a free electron after dissipating its kinetic energy to produce two 0.511 MeV annihilation photons.
- The absorption coefficient increases rapidly with energy above the 1.022 MeV threshold and varies approximately as Z^2.

7.6.4 Photodisintegration

Photodisintegration interactions can also deplete a beam of photons if the photon energy is sufficiently large. From a practical standpoint photodisintegration can generally be neglected in calculating the energy removed from a photon beam; however, such reactions are quite sharp at 1.66 MeV for ^{9}Be(γ,n) interactions and 2.225 MeV for ^{2}H(γ,n) interactions. Except for these two light elements, photodisintegration reactions require photon energies of 8 MeV or more. For photon energies above 20 MeV, the cross-sections for photodisintegration are sufficiently large and must be accounted for in shield designs. Large neutron fields are created at these energies and these neutrons will be mixed with a large number of unabsorbed photons, both of which must be considered in radiation dosimetry and shield designs.

7.7 Photon Attenuation and Absorption

Photon interactions with matter are very different from those of charged particles. When x-rays or gamma rays traverse matter, some are absorbed, some pass through without interaction, and some are scattered as lower energy photons in directions that are quite different from those in the primary beam.

The attenuation of a photon beam by an absorber is characterized as occurring in "good geometry" or "poor geometry," as shown in Figure 7-15. Good geometry exists when every photon that interacts is either absorbed or scattered out of the primary beam such that it will not impact a small receptor some distance away. When good geometry exists only those photons that have passed through the absorber without any kind of interaction will reach the receptor, and each one of these photons will have all of its original energy. This situation exists when the primary photons are confined to a narrow beam and the receptor (e.g., a detector) is small and sufficiently far away that scattered photons have a sufficiently large angle with the original narrowly focused beam that they truly leave the beam and do not reach the receptor. Because of this condition the geometry is also characterized as "narrow-beam" geometry. Readings taken with and without the absorber in place will yield the fraction of photons removed from the narrow beam, by whatever process.

In poor geometry or "broad-beam geometry," a significant fraction of the scattered photons will also reach the receptor of interest in addition to those transmitted without interaction. Poor geometry exists in most practical conditions. In addition to the configuration shown in Figure 7-15, other typical poor geometry configurations are a source enclosed by an absorber (e.g., a point source in a lead pig), a shielded detector, or any other condition where a broad beam of photons strike an absorber. Such conditions often exist when tissue is exposed or a shield is used to attenuate a photon source, and each scattered photon will be degraded in energy according to the angle through which it is scattered. The photons reaching a receptor will then have a complex energy spectrum, including scattered photons of many energies and unscattered photons originally present in the primary beam. The pattern of energy deposition in the receptor (e.g., a person or a detector) will be equally complex and governed by the energy distribution and the exact geometrical arrangement used. The amount of energy deposited in an absorber or a receptor under such conditions is very difficult to determine analytically.

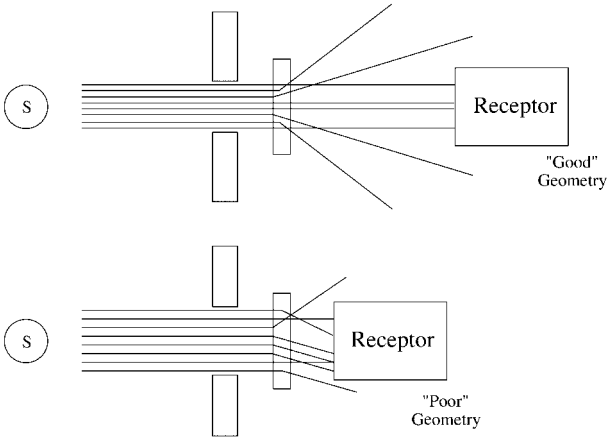

Fig. 7-15 Attenuation of a photon beam in "good geometry" in which all interactions reduce the number of photons reaching a small receptor, and in "poor geometry" in which the relationship between the beam and the receptor is such that the scattered photons reach the receptor. Attenuation coefficients for photons of a particular energy are determined under narrow beam or good geometry conditions.

The change in intensity of a photon in good geometry (as illustrated in Figure 7-16) is expressed mathematically as a decreasing function with thickness of absorber:

$$-\frac{dI}{dx} = \mu I$$

where the constant of proportionality μ is the total attenuation coefficient of the medium for the photons of interest. If all of the photons possess the same energy (i.e., the beam is monoenergetic) and if the photons are attenuated under conditions of good geometry (i.e., the beam is narrow and contains no scattered photons), then the number or intensity $I(x)$ of photons penetrating an absorber of thickness x (i.e., without interaction in the medium) is found by rearranging and integrating

$$\int_{I_0}^{I(x)} dI/I = \int_0^x -\mu dx$$

to yield

$$\ln I(x) - \ln I_0 = -\mu x$$

or

$$\ln I(x) = -\mu x + \ln I_0$$

which is an equation of a straight line with a slope of $-\mu$ and a y-intercept (i.e., with no absorber) of ln I_0 as shown in Figure 7-17a. This can be simplified by the law of logarithms to

$$\ln \frac{I(x)}{I_0} = -\mu x$$

and since the natural logarithm of a number is the exponent to which the base e is raised to obtain the number, this expression translates to

$$\frac{I(x)}{I_0} = e^{-\mu x}$$

or

$$I(x) = I_0 e^{-\mu x}$$

where I_0 is the intensity of the incident beam, $I(x)$ is the intensity after traversing a distance x through the absorbing medium, and μ, the *linear attenuation coefficient*, is the probability of interaction per unit distance in an absorbing medium. It is synonymous with the radioactive disintegration constant λ, which expresses the probability of transformation of radioactive atoms per unit time. The exponential relationship for photon absorption suggests that, theoretically, complete absorption of a beam of photon radiation never really occurs, but in a practical sense exponential attenuation and/or absorption can be used to reduce most the beam intensities to imperceptible levels.

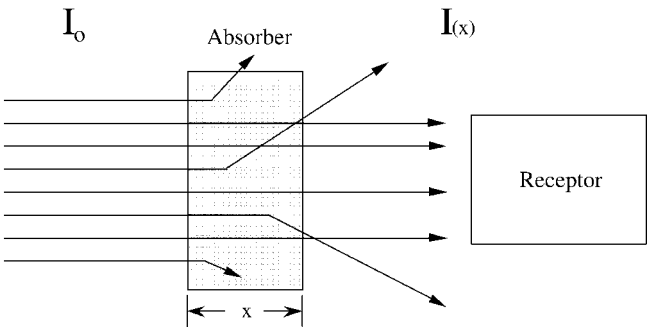

Fig. 7-16 Alteration of a beam of photons by attenuation processes.

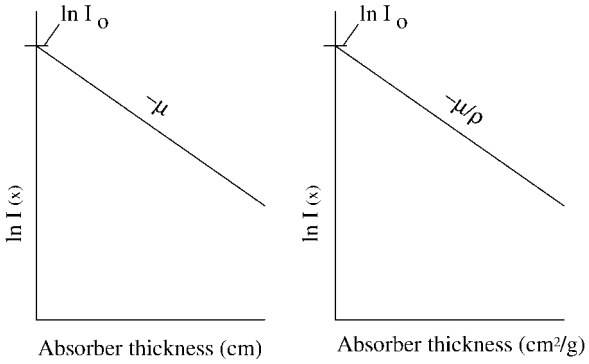

Fig. 7-17 (a) Linear attenuation and (b) mass absorption of photons.

7.7.1 Attenuation (μ) and Energy Absorption (μ_{En}) Coefficients

The relationship between beam intensity and the attenuation coefficient is valid for photoelectric, Compton, and, for photons of sufficient energy, pair production interactions. It also holds for each mode of attenuation separately, or in combination with each other; i.e., the total probability that a narrow beam of photons will interact with an absorber of thickness x and be depleted from the beam is obtained by multiplying the individual probabilities of each:

$$I(x) = I_0(e^{-\tau x} \times e^{-\sigma x} \times e^{-\kappa x}) = I_0 e^{-(\tau+\sigma+\kappa)x} = I_0 e^{-\mu x}$$

where μ, the total attenuation coefficient, is the sum of the coefficients of each of the principal modes of photon interaction in a medium,

$$\mu = \tau + \sigma + \kappa$$

where τ, σ, and κ are photoelectric, Compton, and pair production coefficients, respectively.

It is somewhat surprising that μ is a constant since it is the sum of the coefficients of individual interaction processes, each of which is a function of gamma ray energy, atomic number, and the mass and density of the absorbing medium; however, measured photon intensities versus absorber thickness consistently produce straight lines when plotted on semilog scales.

If other processes (e.g., photodisintegration) were to have a significant effect on the absorption of a beam of photons, these would need to be accounted for by an increase in μ or accomplished by a separate exponential term. Photodisintegration and Rayleigh (or coherent) scattering usually increase μ by only a small amount and are ignored.

Radiation exposure or absorbed dose from photons is determined by the amount of energy deposited by the various photon interactions as they traverse a medium such as tissue. Since some interactions produce radiant energy that carries energy out of the medium, the attenuation coefficient μ cannot be used to determine energy deposition in a medium. Consequently, a linear energy absorption coefficient μ_{en} has been defined that accounts for this loss:

$$\mu_{en} = \mu - (\sigma_s + \text{other low-probability interactions})$$

Processes that produce radiant energy that can escape the medium are Compton scattered photons that do not interact, bremmstrahlung from high-energy recoil electrons, annihilation radiation if $h\nu > 1.022$ MeV, and characteristic x-rays that do not interact. These depleting mechanisms and their effect on μ are shown in Figure 7-18.

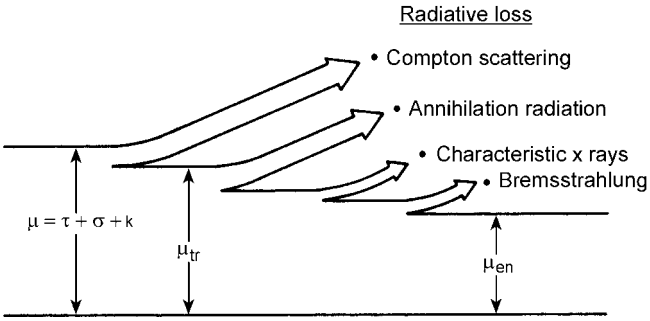

Fig. 7-18 Relationship of the photon attenuation coefficient μ the energy transfer coefficient $\mu_{tr} = \mu - \sigma_s$, and the energy absorption coefficient μ_{en}, and the radiative loss processes that propagate energy out of the absorbing medium.

The *mass energy absorption coefficient* μ_{en}/ρ with units of cm^2/g is the most useful form for determining radiation exposure or dose when a flux of x-rays or gamma rays is known or can be determined. Values of μ_{en}/ρ are provided along with values of μ and μ/ρ in Table 7-4 for air, tissue, muscle, and bone for determination of radiation exposure in air and radiation dose in tissue. These values are believed to be appropriate for a wide range of photon absorption problems, but the terminology for describing the various attenuation and absorption coefficients is not uniform, and care must be exercised to be sure that the proper coefficient is selected for a particular radiation protection problem. Values for various other media which are useful for radiation shielding and energy deposition in various materials, e.g., dosimeters, are included in Table 8-2.

Table 7-4. Photon attenuation (μ), mass attenuation (μ/ρ), and mass energy absorption (μ_{en}/ρ) coefficients for air, tissue, muscle, and bone (J. H. Hubbell and S. M. Seltzer)

	Dry air (sea level) (ρ = 0.001205 g/cm^3)			Tissue, ICRU (ρ = 1.00 g/cm^3)			Muscle (ICRP) (ρ = 1.05 g/cm^3)			Cortical bone (ICRP) (ρ = 1.92 g/cm^3)		
Energy (keV)	μ (cm^{-1})	μ/ρ (cm^2/g)	μ_{en}/ρ (cm^2/g)	μ (cm^{-1})	μ/ρ (cm^2/g)	μ_{en}/ρ (cm^2/g)	μ (cm^{-1})	μ/ρ (cm^2/g)	μ_{en}/ρ (cm^2/g)	μ (cm^2/g)	μ/ρ (cm^{-1})	μ_{en}/ρ (cm^2/g)
10	0.0062	5.120	4.742	4.937	4.937	4.564	5.6238	5.356	4.964	54.7392	28.51	26.80
15	0.0019	1.614	1.334	1.558	1.558	1.266	1.7777	1.693	1.396	17.3414	9.032	8.388
20	0.0009	0.7779	0.5389	0.7616	0.7616	0.5070	0.8615	0.8205	0.564	7.6819	4.001	3.601
30	4.26×10^{-4}	0.3538	0.1537	0.3604	0.3604	0.1438	0.3972	0.3783	0.1610	2.5555	1.331	1.070
40	2.99×10^{-4}	0.2485	0.0683	0.2609	0.2609	0.0647	0.2819	0.2685	0.0719	1.2778	0.6655	0.4507
50	2.51×10^{-4}	0.2080	0.0410	0.2223	0.2223	0.0399	0.2375	0.2262	0.0435	0.8145	0.4242	0.2336
60	2.26×10^{-4}	0.1875	0.0304	0.2025	0.2025	0.0305	0.2150	0.2048	0.0326	0.6044	0.3148	0.1400
70[a]	2.10×10^{-4}	0.1744	0.0255	0.1899	0.1899	0.0263	0.2006	0.1910	0.0276	0.4866	0.2534	0.0905
80	2.00×10^{-4}	0.1662	0.0241	0.1813	0.1813	0.0253	0.1914	0.1823	0.0262	0.4280	0.2229	0.0690
100	1.86×10^{-4}	0.1541	0.0233	0.1688	0.1688	0.0250	0.1778	0.1693	0.0254	0.3562	0.1855	0.0459
150	1.63×10^{-4}	0.1356	0.0250	0.1490	0.1490	0.0273	0.1567	0.1492	0.0275	0.2842	0.1480	0.0318
200	1.49×10^{-4}	0.1233	0.0267	0.1356	0.1356	0.0294	0.1426	0.1358	0.0294	0.2513	0.1309	0.0300
300	1.29×10^{-4}	0.1067	0.0287	0.1175	0.1175	0.0316	0.1235	0.1176	0.0316	0.2137	0.1113	0.0303
400	1.15×10^{-4}	0.0955	0.0295	0.1051	0.1051	0.0325	0.1105	0.1052	0.0325	0.1902	0.0991	0.0307
500	1.05×10^{-4}	0.0871	0.0297	0.0959	0.0959	0.0327	0.1008	0.0960	0.0327	0.1732	0.0902	0.0307
600	9.71×10^{-5}	0.0806	0.0295	0.0887	0.0887	0.0325	0.0932	0.0887	0.0325	0.1600	0.0833	0.0305

Energy (keV)	Dry air (sea level) (ρ = 0.001205 g/cm^3)			Tissue, ICRU (ρ = 1.00 g/cm^3)			Muscle (ICRP) (ρ = 1.05 g/cm^3)			Cortical bone (ICRP) (ρ = 1.92 g/cm^3)		
	μ (cm^{-1})	μ/ρ (cm^2/g)	μ_{en}/ρ (cm^2/g)	μ (cm^{-1})	μ/ρ (cm^2/g)	μ_{en}/ρ (cm^2/g)	μ (cm^{-1})	μ/ρ (cm^2/g)	μ_{en}/ρ (cm^2/g)	μ (cm^2/g)	μ/ρ (cm^{-1})	μ_{en}/ρ (cm^2/g)
662[a]	9.34×10^{-5}	0.0775	0.0293	0.0853	0.0853	0.0323	0.0896	0.0853	0.0323	0.1538	0.0801	0.0303
800	8.52×10^{-5}	0.0707	0.0288	0.0779	0.0779	0.0318	0.0818	0.0779	0.0318	0.1403	0.0731	0.0297
1,000	7.66×10^{-5}	0.0636	0.0279	0.0700	0.0700	0.0307	0.0736	0.0701	0.0307	0.1261	0.0657	0.0288
1,173[a]	7.05×10^{-5}	0.0585	0.0271	0.0644	0.0644	0.0299	0.0677	0.0644	0.0299	0.1160	0.0604	0.0279
1,250	6.86×10^{-5}	0.0569	0.0267	0.0626	0.0626	0.0294	0.0658	0.0627	0.0294	0.1127	0.0587	0.0275
1,333[a]	6.62×10^{-5}	0.0550	0.0263	0.0605	0.0605	0.0290	0.0636	0.0605	0.0290	0.1090	0.0568	0.0271
1,500	6.24×10^{-5}	0.0518	0.0255	0.0570	0.0570	0.0281	0.0599	0.0570	0.0281	0.1026	0.0535	0.0262
2,000	5.36×10^{-5}	0.0445	0.0235	0.0489	0.0489	0.0258	0.0514	0.0490	0.0258	0.0885	0.0461	0.0242
3,000	4.32×10^{-5}	0.0358	0.0206	0.0393	0.0393	0.0226	0.0413	0.0393	0.0226	0.0719	0.0375	0.0215
4,000	3.71×10^{-5}	0.0308	0.0187	0.0337	0.0337	0.0204	0.0354	0.0337	0.0205	0.0625	0.0326	0.0198
5,000	3.31×10^{-5}	0.0275	0.0174	0.0300	0.0300	0.0189	0.0315	0.0300	0.0190	0.0566	0.0295	0.0186
6,000	3.04×10^{-5}	0.0252	0.0165	0.0274	0.0274	0.0179	0.0288	0.0274	0.0179	0.0525	0.0273	0.0179
6,129[a]	3.01×10^{-5}	0.0250	0.0164	0.0271	0.0271	0.0178	0.0285	0.0271	0.0178	0.0520	0.0271	0.0178
7,000[a]	2.83×10^{-5}	0.0235	0.0159	0.0255	0.0255	0.0171	0.0267	0.0255	0.0170	0.0495	0.0258	0.0174
7,115[a]	2.82×10^{-5}	0.0234	0.0158	0.0253	0.0253	0.0170	0.0265	0.0253	0.0170	0.0492	0.0256	0.0173
10,000	2.46×10^{-5}	0.0205	0.0145	0.0219	0.0219	0.0155	0.0230	0.0219	0.0155	0.0444	0.0231	0.0164

a Coefficients for these energies were interpolated using polynomial regression.

7.7.2
Effect of *E* and *Z* on Photon Attenuation/Absorption

Most radiation protection work is done with the total attenuation coefficient μ (for radiation shielding) or the total mass energy absorption coefficient μ_{en}/ρ (for radiation dose calculations) instead of coefficients for the individual interactions; however, the features of each individual interaction process determine which is most important at various energies in different materials. Attenuation (or absorption) of photons varies considerably with photon energy and Z of the absorbing medium as shown in Figure 7-19 for water (similar to tissue) and lead because of the

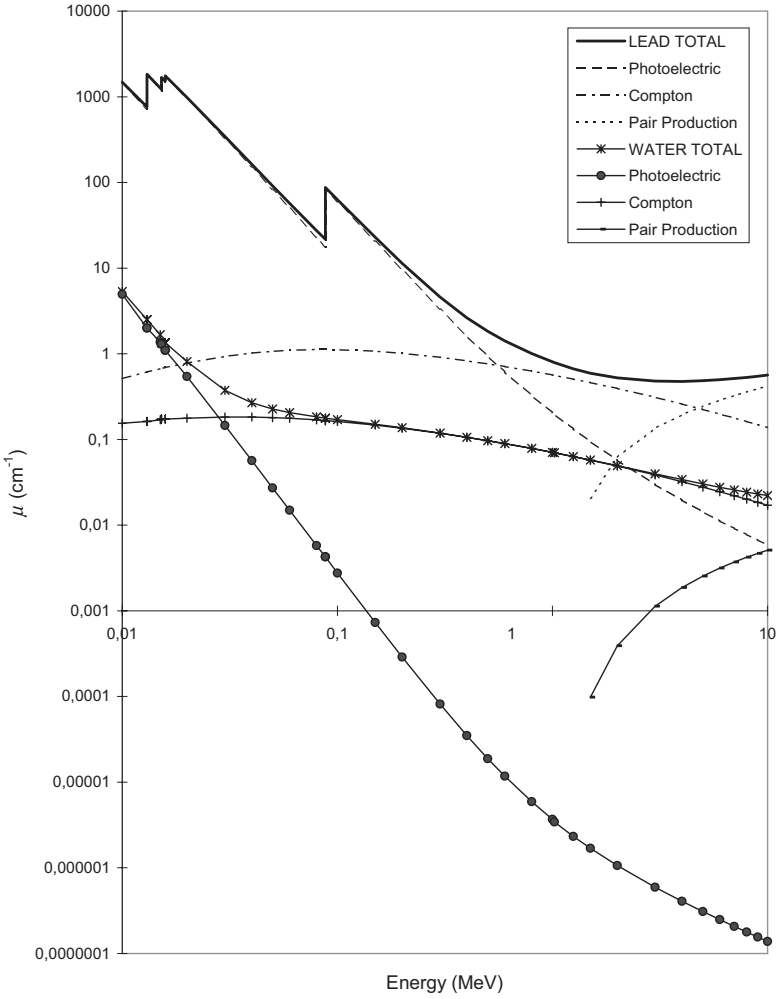

Fig. 7-19 Photon attenuation coefficients for (a) low-Z water and (b) high-Z lead, and the relative contributions of photoelectric, Compton, and pair production interactions versus photon energy.

influence of E and Z on the individual interaction coefficients. At low energies (<15 keV), the photoelectric effect accounts for virtually all of the interactions in water. As the photon energy increases, τ drops rapidly and Compton scattering interactions (σ) become dominant in water at about 100 keV and at about 500 keV in lead. The Compton scattering effect remains dominant up to several hundred keV where it decreases with energy and continues to do so until pair production becomes the dominant process.

In lead, a high-Z material, the photoelectric effect is the dominant interaction at low energies. Photoelectric absorption decreases rapidly with increasing photon energy, but rises abruptly when the photon energy is sufficient to eject a photoelectron from the K shell of the atom (Figure 7-19b). For photon energies above a few hundred keV, Compton scattering interactions dominate and continue to do so until photon energies are well above the 1.022 MeV pair production threshold. Figure 7-20 also shows the effect of increasing Z on the photon attenuation coefficient, which is relatively larger for lead (a high-Z material) than for iron and aluminum (a relatively low-Z material).

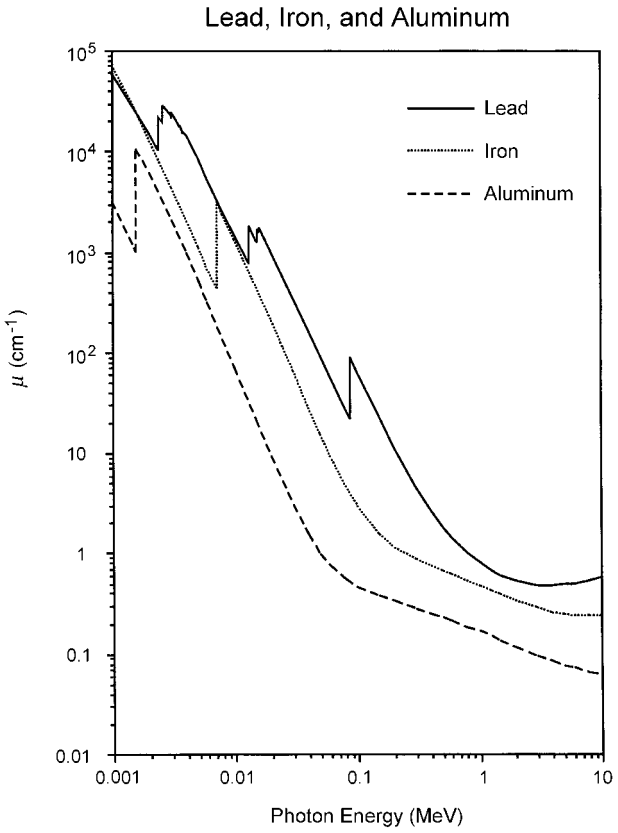

Fig. 7-20 Variation of μ versus Z which also illustrates the effect of Z on resonance absorption to create absorption "edges."

The relationship between values of μ and μ_{en} for lead is shown in Figure 7-21. They are similar at the intermediate energies because of the Z/E effect on Compton interactions, but μ_{en} is lower for energies above the K absorption edge and remains so above the pair production threshold. Both μ and μ_{en} for lead are quite large over the entire photon energy range, illustrating its effectiveness as a photon shield. The μ and μ_{en} values for air and tissue are almost the same as those for H_2O as would be expected because they consist of similar elements.

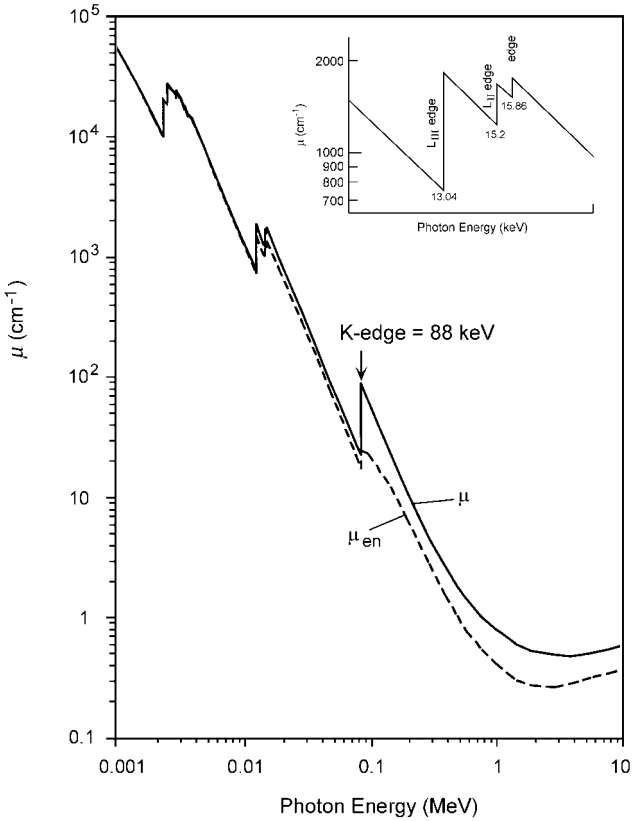

Fig. 7-21 Photon attenuation (μ) and energy (μ_{en}) absorption coefficients versus energies in lead; the K absorption edge is prominent at 88 keV and the substructures of the L shell (shown in detail) and the M shell are also visible.

7.7.3 Absorption Edges

When the energy of the incoming photon is the exact amount required to remove a K electron entirely from the atom, strong resonance absorption occurs. The attenuation (or absorption) cross-section increases sharply (see Figures 7-20 and

7-21) at this energy producing what is called an absorption edge. As long as the photon energy is below this amount, there can be no K resonance absorption, and the absorption cross-sections due to photoelectric and Compton interactions will decrease with increasing photon energy. Even at the exact K_{a1} energy, resonance absorption is still impossible, since there is only enough energy to move a K-shell electron up to the L shell, which by the Pauli principle is full; therefore, resonance absorption occurs only when the photon energy equals the electron binding energy. As photon energies increase above the absorption edge, the attenuation coefficient once again decreases. Similar interactions produce L absorption edges, which are also shown in detail in Figure 7-21 for lead (these edges also occur in other materials but they are difficult to observe). M absorption edges (shown in gross detail in Figure 7-21) also exist for lead, but observing their detail requires special techniques; they occur at such low energies for most materials that detection is difficult.

The energies at which absorption edges occur have practical value since they are determined uniquely by the atomic number of the absorber. This allows absorbers made of elements with adjacent atomic numbers to be used to "shape" photon beams by permitting the transmission of only those photons with a narrow band of energies, a circumstance that is very useful in x-ray beam quality (see Chapter 14).

Characteristic x-rays are emitted following the absorption of photons at and above the absorption edge of a material as the photoelectron vacancies are filled. The energies of these emissions are below the absorption edge of the material in which they are produced and hence are poorly absorbed by it. They can, however, be effectively removed by an absorber of slightly lower atomic number, and the characteristic x-rays produced can, in turn, be absorbed in materials with even lower atomic numbers. This principle is used to "harden" the beams generated by x-ray tubes by removing the low-energy portion of the x-ray emission spectrum. For example, a copper filter of 0.2–0.5 mm in an x-ray tube operating above 100 kV will effectively remove a large fraction of the lower energies, but in doing so will produce a considerable amount of 8 keV K_a x-rays from copper. These can in turn be absorbed by an aluminum ($Z = 13$) filter, but photoelectric absorption in aluminum will produce K_a photons of 1.5 keV which can in turn be absorbed in a bakelite filter ($Z = 6$). To be effective, filter combinations must be inserted in the proper order.

Checkpoints

Several things are worth noting about the exponential relationship for photon absorption:

- Since the radiation exposure rate or absorbed dose is proportional to flux, the attenuation coefficient and the thickness of absorber determine how much reduction occurs in the incident flux and in turn the exposure or dose.
- The value of μ depends on the absorbing medium and the energy of the photons; thus, extensive tabulations of μ are needed (as provided in Table 7-4) for calculations of flux changes.
- The values of μ are given for "good geometry," i.e., a narrow beam of photons where scattered photons are removed from the beam and do not reach a receptor of interest (either a detector or a person). Most real-world situations do not meet these ideal conditions and are characterized as "poor geometry."
- Values of μ_{en} are based only on the energy absorbed in the medium; therefore, energy losses due to Compton-scattered photons, bremsstrahlung, and other radiative processes following interaction have been subtracted because they are very likely to leave the medium.
- The most useful forms of the photon coefficients are μ_{en}/ρ (cm^2/g) for determining energy deposited in the absorbing medium and μ (cm^{-1}) for radiation shielding calculations.

7.8 Energy Transfer and Absorption by Photons

Energy transfer and absorption from a beam of photons takes place in two stages as shown in Figure 7-22. First, a photon interaction, which is probabilistic, produces an electron or electrons with kinetic energy; second, each ejected electron transfers energy to the medium through excitation and ionization all along its path. The first process is characterized by *kerma* (kinetic energy released in material (or matter)); the second is the absorbed dose. Kerma corresponds to energy transferred E_{tr}, and absorbed dose corresponds to energy absorbed E_{ab}. Both quantities are shown for air, various tissues, and lead for different photon energies in Table 7-5; their physical difference is illustrated in Example 7-12.

Table 7-5. Average energy transferred E_{tr} and absorbed E_{ab} by photons through interactions in various media (where the two are essentially the same only one entry is made).

	Air		Water		Muscle		Bone		Fat		Lead	
$h\nu$ (keV)	E_{tr} (keV)	E_{ab} (keV)	E_{tr} (keV)	E_{ab} (keV)	E_{tr} (keV)	E_{ab} (keV)	E_{tr} (keV)	E_{ab} (keV)	E_{tr} (keV)	E_{ab} (keV)	E_{tr} (keV)	E_{ab} (keV)
10	9.23		9.25		9.24		9.37		9.70		9.55	
20	13.5		13.2		13.4		17.5		18.0		16.0	
50	9.31		8.82		9.13		22.9		24.6		42.2	42.0
80	11.4		11.2		11.3		20.4		21.7		–	–
88	–		–		–		–		–		69.2[a]	68.5[a]
100	15.0		14.8		14.9		21.4		22.3		36.2	35.7
200	43.4		43.3		43.4		45.2		45.2		122	119
300	80.8		80.8		80.8		81.6		81.4		191	185
400	124		124		124		124		124		247	239
500	171		171		171		171		171		298	286
662	252		252		252		253		253		376	360
800	327		327		327		327		327		444	423
1000	440		440		440		440		440		550	520
1250	588	586	588	586	588	586	588	586	588	584	693	649

Table 7-5. Continued.

	Air		Water		Muscle		Bone		Fat		Lead	
$h\nu$ (keV)	E_{tr} (keV)	E_{ab} (keV)	E_{tr} (keV)	E_{ab} (keV)	E_{tr} (keV)	E_{ab} (keV)	E_{tr} (keV)	E_{ab} (keV)	E_{tr} (keV)	E_{ab} (keV)	E_{tr} (keV)	E_{ab} (keV)
1500	741	739	741	739	741	739	741	738	741	735	–	–
2000	1060	1050	1060	1060	1060	1060	1060	1060	1060	1050	1130	1040
3000	1740	1720	1740	1730	1740	1730	1740	1720	1750	1720	1860	1660
4000	2460	2430	2460	2430	2460	2430	2470	2430	2480	2430	2700	2350
5000	3220	3170	3210	3160	3210	3160	3230	3160	3270	3170	3600	3060
10,000	7370	7100	7330	7070	7320	7070	7430	7100	7610	7140	8450	6420
20,000	16,600	15,500	16,500	15,300	16,500	15,300	16,800	15,300	17,200	15,200	18,500	12,000

a Energy transferred and absorbed at the K edge in Pb; for photons with energy just below the K edge the values of E_{tr} and E_{ab} are 24.8 and 24.7 keV, respectively.
Source: adapted from H. E. Johns, J. R. Cunningham **1983**, *Physics of Radiology*, 4th edn, courtesy of C.C. Thomas Publisher, Springfield, IL.

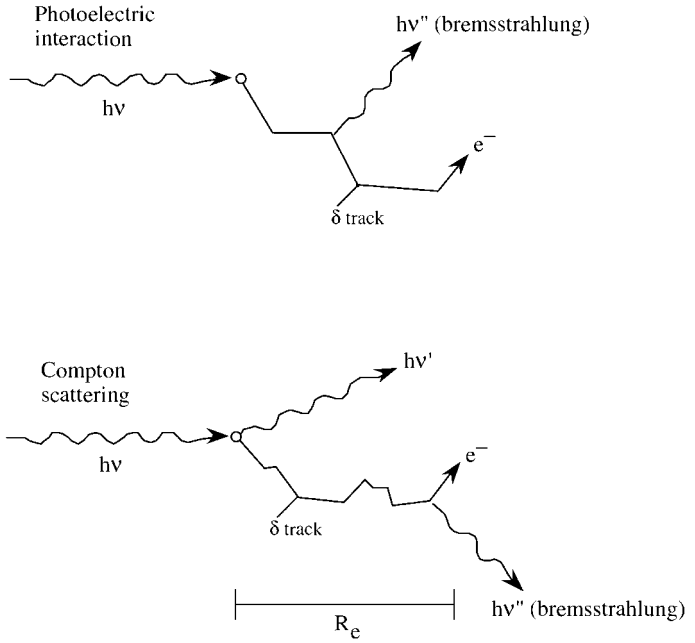

Fig. 7-22 Energy transfer and absorption is a two-stage process. First, a photon ($h\nu$) interacts with an atom of the medium, transferring all (photoelectric effect) or some of its energy (Compton scattering) to an electron, or in the case of pair production to the created electron and positron. The kinetic energy of these electrons is then deposited in the medium mostly by ionization, although some may be lost as bremsstrahlung and other radiative processes. The transfer of energy, or kerma, occurs at the point of interaction; the absorbed dose occurs, however, along the path of the recoiling electrons extending over their entire range R_e in the medium.

Kerma is directly related to the photon fluence, and the likelihood of interaction $(\mu/\rho)_{\text{med}}$ which causes energy to be released at the site of each interaction; it is calculated from the transfer of energy for a fluence ϕ of photons as

$$K_{\text{med}} = \phi \left(\frac{\mu}{\rho}\right)_{\text{med}} \bar{E}_{\text{tr}}(h\nu) \times 1.6022 \times 10^{-6} \text{erg/MeV}$$

where ϕ is the fluence (photons/cm^2), $(\mu/\rho)_{\text{med}}$ is the mass attenuation coefficient for the medium, and $\bar{E}_{\text{tr}}$ $(h\nu)$ is the average amount of the photon energy transferred to electrons in the medium.

Example 7-12. For a fluence of 10^{10} γ/cm^2 of 10 MeV photons on muscle tissue, calculate (a) kerma and (b) absorbed dose.
Solution. (a) From Table 7-4 $(\mu/\rho) = 0.0219$ cm^2/g for muscle tissue, and the average energy $\bar{E}_{\text{tr}}$ transferred by 10 MeV photons (Table 7-5) is 7.32 MeV.

$$\text{Kerma} = \frac{10^{10}\gamma}{\text{cm}^2} \times 0.0219\,\text{cm}^2/\text{g} \times 7.32\,\text{MeV} \times 1.6022 \times 10^{-6}\,\text{erg/MeV}$$

$$= 2.58 \times 10^3\,\text{erg/g of muscle}$$

(b) Absorbed dose is calculated in the same manner as kerma except that $\bar{E}_{ab}$ ($h\nu$) (from Table 7-5) is used instead of $\bar{E}_{tr}$ ($h\nu$). Since E_{ab} is 7.07 MeV, the absorbed dose is

$$\text{Dose} = 2.49 \times 10^3\,\text{erg/g}$$

which is somewhat less than the value of kerma because only 7.07 MeV of the 7.32 MeV transferred is absorbed along the electron track. The difference of 0.25 MeV is lost by radiative processes, principally bremsstrahlung. The 7.07 MeV actually absorbed is, at 34 eV/ion pair, sufficient to ionize about 208,000 atoms; i.e., although only one atom was ionized in the initial transfer of energy by a photon interaction, some 208,000 atoms were disrupted along the track of this energetic electron as it traversed the medium.

As illustrated in Figure 7-22, for photoelectric and Compton interactions, energy is transferred to an electron but not all of it is deposited in the medium since bremsstrahlung may be produced and radiated away (a small fraction of energy may also be lost in the form of characteristic x-rays that are not absorbed after photoelectric interactions) over the entire range R_e of the ejected electrons in the medium. Any pair production interactions that occur yield a positron and an electron which deposit their kinetic energy ($h\nu$ – 1.022 MeV) by similar processes, and if both annihilation photons are absorbed in the medium then most of the initial energy $h\nu$ is deposited. Because the length of the electron tracks may be appreciable, kerma and absorbed dose do not take place at the same location. The units of absorbed dose are joules per kilogram (or ergs per gram in conventional units); kerma has the same units, but there is no special designation (like the gray for absorbed dose) for kerma. It is just kinetic energy released or transferred per unit mass of medium.

An *energy transfer coefficient* μ_{tr} that represents the amount of energy transferred to a medium by photons of energy $h\nu$ can be calculated from listed values of μ_{en} as

$$\mu_{tr} = \frac{\mu_{en}}{1 - g}$$

where values of g, the fraction of energy lost by radiative processes, is numerically equal to $(E_{tr} - E_{ab})/E_{tr}$. Similarly, a *mass energy transfer coefficient* (μ_{tr}/ρ) can be calculated by dividing μ_{tr} by the density of the absorbing medium. Since values of E_{tr} and E_{ab} are identical below 1 MeV (see Table 7-5), and are essentially the same up to about 1.5 MeV, μ_{tr} and μ_{en} for a given medium are either identical or very nearly so for most photons emitted from radionuclides commonly encountered in radiation protection. They differ, however, for high-energy photons produced around

accelerators or in nuclear interactions, and it is essential to determine the appropriate value of E_{tr} (and μ_{tr} if it is used) for calculations of kerma or absorbed dose.

The value $(1 - g)$ slowly decreases with increasing photon energy as follows:

E (MeV)	$1 - g$
0.662	0.9984
1.25	0.9968
1.5	0.996
2.0	0.995
3.0	0.991
5.0	0.984
10.0	0.964

Because of their importance as gamma calibration sources for dosimetry, exact values of $(1 - g)$ have been determined for ^{137}Cs photons ($h\nu = 0.662$ MeV) and ^{60}Co photons ($h\nu = 1.332$ and 1.172 MeV) to be 0.9984 and 0.9968, respectively.

7.8.1 Electronic Equilibrium

Absorbed dose cannot be calculated unless a state of electronic equilibrium exists which, as shown in Figure 7-23, only occurs some distance into the medium as determined by the range of the ejected electrons. The curve in Figure 7-23 represents, for purposes of illustration, an idealized condition in which there is no attenuation of the photons as they pass through the medium. The deposition of energy by ionization along the path of the ejected electron starts at zero and reaches its maximum over a depth R called the buildup region; beyond R as many electrons stop in any volume as are set in motion in it. A condition known as "electronic equilibrium" is established where the kerma is constant with depth, and if no bremsstrahlung losses occur, the absorbed dose is equal to the kerma after electronic equilibrium is established.

The idealized conditions of Figure 7-23 do not exist in reality because, as shown in Figure 7-24, photons are in fact attenuated as they traverse the medium. Consequently, true "electronic equilibrium" is not attained, and kerma decreases with depth because the primary radiation is attenuated exponentially. The absorbed dose increases at first, reaches a maximum at R, and then decreases exponentially along with kerma. If bremsstrahlung losses are minimal the absorbed dose curve will be above the kerma curve because the absorbed energy will be due to kerma processes that occurred at the shallower depths. Even this more realistic condition is oversimplified because a spectrum of electrons of all energies is always set in

motion, and these travel in many different directions. Even more complexity exists when two different media are involved, such as for bone in soft tissue. Electrons set in motion in one material deposit their energy in the other, and kerma and absorbed dose will not be in equilibrium since path lengths of absorbed energy are determined by the range of the electrons in each.

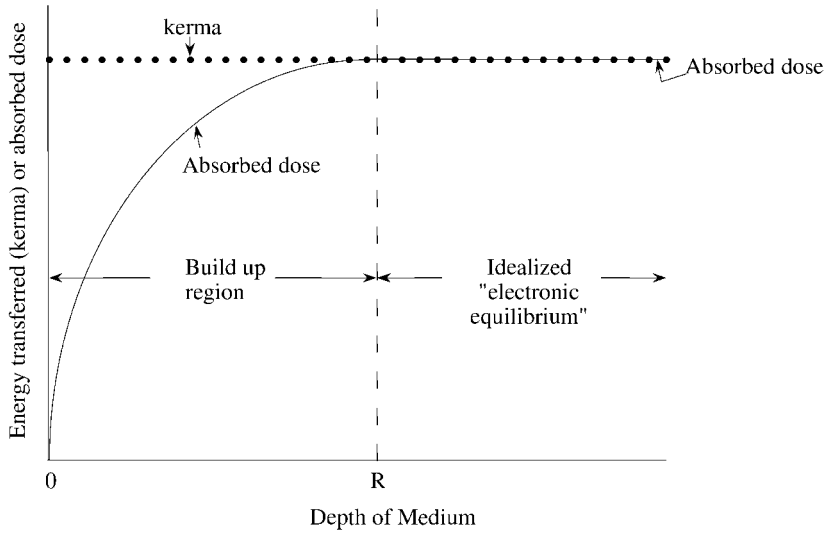

Fig. 7-23 Idealized conditions of electronic equilibrium.

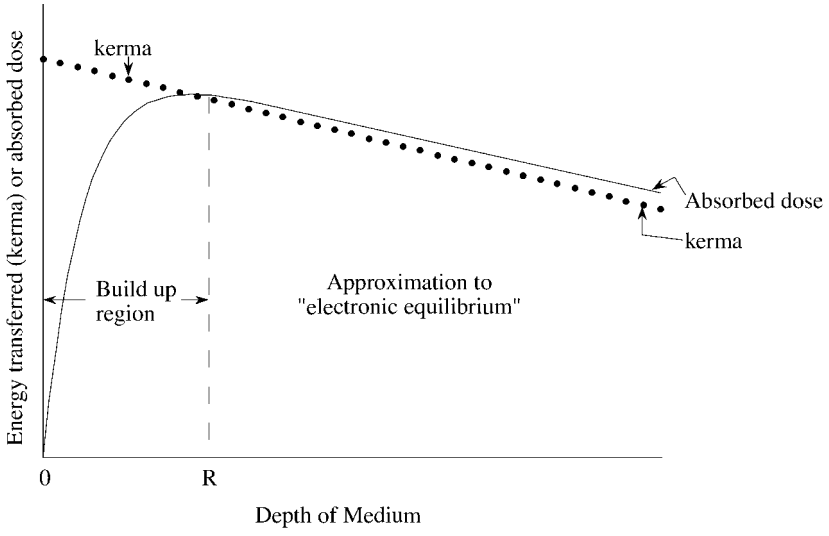

Fig. 7-24 Realistic equilibrium of kerma and absorbed dose where the primary photons are attenuated as they traverse the medium and thus both kerma and absorbed dose decrease with depth after equilibrium occurs.

Even though true electronic equilibrium does not occur, it is a common and reasonable practice to treat the region beyond R as being in equilibrium and to calculate absorbed dose using $\bar{E}_{ab}$ as follows:

$$D_{med} = \phi \left(\frac{\mu}{\rho}\right)_{med} \bar{E}_{ab}(h\nu) \times 1.6022 \times 10^{-6} = K(1-g)$$

where $\bar{E}_{ab}(h\nu)$ is the part of the average kinetic energy transferred to electrons that contributes to ionization (it excludes energy lost by radiative processes, principally bremsstrahlung) and K is the kerma. Although the absorbed dose beyond equilibrium is slightly larger than kerma, the calculated value of kerma is a reasonably accurate determination of absorbed dose for photons less than 5 MeV or so.

7.8.2 Bragg–Gray Theory

The Bragg–Gray theory is dependent on the same factors that relate kerma and energy absorption. A true measurement of absorbed dose can only be done with calorimetry, but the Bragg–Gray theory allows absorbed dose to be determined from the ionization produced by a beam of photons in a small gas cavity, usually air, imbedded in a tissue-equivalent medium of sufficient thickness to establish "electronic equilibrium." Under these conditions ionization will be produced in the cavity by the electrons ejected by photon interactions in the tissue medium, and under electronic equilibrium gas-produced electrons that are lost to the wall medium are compensated for by electrons produced in the medium and absorbed in the gas. The charge liberated in the gas is collected, and since the average energy required to cause one ionization in the gas is constant over a wide range of gas pressures and electron energies, the collected charge is directly proportional to the energy deposited in the gas. The dose absorbed in the enclosed gas cavity is therefore related to the ionization produced in the gas as

$$D_{gas} = \frac{Q}{m_{gas}} W$$

where Q is expressed in coulombs, m_{gas} in grams, and W has a value of 33.97 eV per ion pair, or 33.97 J/C.

Example 7-13. Determine the energy deposited in air if 3.336×10^{-10} C of charge is collected in a 1 cm^3 cavity of air at 0 °C and 1 atm (STP).
Solution. Since the density of air at STP is 1.293×10^{-3} g, the air dose is

$$D_{air} = \frac{3.336 \times 10^{-10}\ \text{C/cm}^3}{1.293 \times 10^{-3}\ \text{g/cm}^3} \times 33.97\ \text{J/C} \times 10^7\ \text{erg/J} = 87.64\ \text{erg/g}$$

$$= 0.8764\ \text{rad (or } 8.764\ \text{mGy)}$$

The charge liberated for the conditions of Example 7-13 and the energy deposited is that produced by an exposure of 1 R.

The Bragg–Gray relationship gives the energy imparted to the gas in the cavity, but the quantity of most interest is the energy deposited in the surrounding medium. Since the air cavity is assumed to be so small that it does not alter the electron spectrum, the gas in the cavity will "see" the same electron fluence as exists in the medium. The dose in the medium is related to the dose in air by the relative stopping power:

$$D_{\text{med}} = S_{\text{rel}} D_{\text{air}}$$

For tissue, bakelite, lucite, carbon, and most tissue-equivalent materials S_{rel} is currently accepted to be 1.12, although 1.14 has been used extensively.

7.9 Exposure/Dose Calculations

Calculations of radiation exposure or dose are straightforward if the source of photons is characterized in terms of a fluence, fluence rate, or flux (photons/cm^2 s), from which the energy fluence (MeV/cm^2) or energy fluence rate (MeV/cm^2 s) can be determined. The energy fluence can in turn be used to determine exposure in air or energy deposition in an absorbing medium.

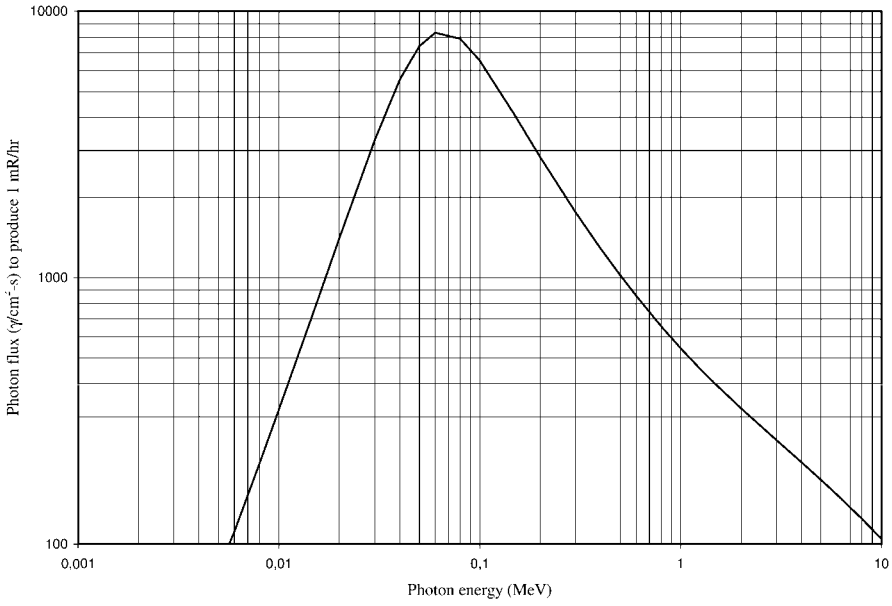

Fig. 7-25 Photon flux (γ/cm^2 s) to produce an exposure rate of 1 mR/h.

The exposure rate is directly proportional to photon flux. This relationship is plotted in Figure 7-25 as the flux at different energies that produces an exposure rate of 1 mR/h. It is noteworthy that the curve in Figure 7-25 is quite linear from about 70 keV up to about 2 MeV. Over this energy range μ_{en}/ρ for air varies little, and for air at STP is about 0.0275 cm^2/g. This range of approximate linearity allows two straightforward calculational tools: an inverse square exposure rate formula for point sources based on source strength, and a gamma constant for point sources of each of the gamma-emitting radionuclides.

7.9.1 Point Sources

Since a point source emits photons uniformly in all directions, the number passing through a unit area is inversely proportional to the square of the distance r (the inverse square law) and the point source exposure rate in R/h per curie at a distance r of 1 m is

$$\text{Exposure} = \frac{\text{Ci} \times 3.7 \times 10^{10}\text{t/s} \times f \times E(\text{MeV}) \times 1.6022 \times 10^{-6}\,\text{erg/MeV} \times 0.0275\text{cm}^2/\text{g} \times 3600\,\text{s/h}}{4\pi r^2 (100\,\text{cm/m})^2 \times 87.64\,\text{erg/g R}}$$

$$= \frac{0.533 \times \text{Ci} \times fE}{r^2}\,\text{R/h}$$

where Ci is in curies, r is the distance in meters from the point source, f is the number of photons emitted per transformation, and E is the photon energy in MeV between 0.07 and 3 MeV. The point source exposure rate is very useful since many sources can be represented as "points." If distance is measured in feet, this can be converted to the familiar and easy-to-remember approximation

$$\text{R/h at 1 ft} = 6CE$$

where C is in curies and E is MeV of gamma energy per transformation. When this expression is used, it is necessary to include the photon yield, f, in determining E, e.g., f = 0.85 for 0.662 MeV gamma rays from ^{137}Cs such that $E = 0.85 \times 0.662 = 0.563$ MeV/t and for the two gamma rays from ^{60}Co, $E = 1.33$ and $1.17 = 2.50$ MeV/t. Each of these expressions can be used to obtain the exposure rate at any other distance from a point source by dividing the result by the square of the actual distance (m^2 or ft^2).

7.9.2 Gamma Ray Constant, Γ

The exposure rate from a point source of each of several gamma-emitting radionuclides (as illustrated in Example 7-14) can be readily calculated because the photon emission rate and energy are unique for each; i.e., each one can be represented as a "gamma ray constant" (Γ) for a unit of activity (usually Ci or Mbq) and at a unit distance (usually 1 m) as tabulated in Table 7-6. A separate calculation was performed for each gamma ray emitted by the nuclide and the results were summed. For example, ^{60}Co has two gamma rays, one at 1.332 MeV in 100% of transformations and one at 1.173 MeV in 99.9% of transformations; Γ was determined for each gamma ray and the two were added together (see Problem 7-10).

Example 7-14. Determine Γ, the exposure gamma ray constant (R/h mCi at 1 cm) for a point source of ^{137}Cs.

Solution. The gamma yield of 0.662 MeV gamma rays from ^{137}Cs is 0.85/t, and the photon flux produced by the 1 mCi ^{137}Cs source at 1 cm is

$$\phi = \frac{1\,\text{mCi} \times 3.7 \times 10^7\,\text{t/s mCi} \times 0.85\,\gamma/\text{t}}{4\pi(1\,\text{cm})^2}$$

$$= 2.503 \times 10^6\ \text{photons/cm}^2\,\text{s}$$

The mass energy absorption coefficient for air is 0.0293 cm^2/g, and

$$E_{ab} = \phi \times E\,(\text{MeV}/\gamma) \times \mu_{en}/\rho$$

$$= (2.503 \times 10^6\,\gamma/\text{cm}^2\ \text{s})(0.662\,\text{MeV}/\gamma)(1.602 \times 10^{-6}\,\text{erg/MeV})$$

$$\times (0.0293\,\text{cm}^2/\text{g})(3600\,\text{s/h})$$

$$= 2.8 \times 10^2\ \text{erg/g h}$$

and since 1 R = 87.64 erg/g of air

Exposure = 3.193 R/h for 1 mCi of ^{137}Cs at 1 cm or 0.319 R/h per Ci at 1 m.

The gamma constant Γ is generally given in units of R/h at 1 m per curie but has also been tabulated as R/h at 1 cm per mCi.

Table 7-6. The gamma ray constant Γ (R/h at 1 m) for 1 Ci of selected radionuclides.

Nuclide	Γ	Nuclide	Γ	Nuclide	Γ
Antimony-122	0.304	Europium-155	0.067	Platinum-197	0.021
Antimony-124	1.067	Gallium-67	0.111	Potassium-40	0.082
Antimomy-125	0.380	Gallium-72	1.456	Praseodymium-144[a]	0.017
Arsenic-72	1.165	Gold-198	0.292	Radium-226	0.012
Arsenic-76	0.545	Hafnium-181	0.393	Rhodium-106[a]	0.138
Barium-133	0.455	Iodine-123	0.277	Rubidium-86	0.054
Barium-140	0.165	Iodine-125	0.275	Scandium-46	1.167
Beryllium-7	0.034	Iodine-130	1.403	Scandium-47	0.080
Bromine-82	1.619	Iodine-131	0.283	Selenium-75	0.860
Cadmium-115m	0.013	Iodine-132	1.427	Silver-110m	1.652
Calcium-47	0.585	Iridium-192	0.592	Sodium-22	1.339
Carbon-11	0.717	Iron-59	0.662	Sodium-24	1.938
Cerium-141	0.073	Krypton-85	0.002	Strontium-85	0.759
Cerium-144	0.023	Lanthanum-140[a]	1.253	Tantalum-182	0.772
Cesium-134	0.999	Magnesium-28	0.879	Tellerium-132	0.279
Cesium-137	0.319	Manganese-54	0.463	Thallium-208[a]	1.704
Chlorine-38	0.719	Manganese-56	0.924	Tin-113	0.179
Chromium-51	0.023	Mercury-197	0.069	Tungsten-187	0.329
Cobalt-56	1.926	Mercury-203	0.253	Vanadium-48	1.701
Cobalt-57	0.151	Molybdenum-99	0.113	Xenon-133	0.010
Cobalt-58	0.614	Neodymium-147	0.139	Xenon-133m	0.112
Cobalt-60	1.370	Nickel-65	0.297	Xenon-135	0.189
Copper-64	0.132	Niobium-95	0.480	Yttrium-88	1.783
Europium-152	0.744	Nitrogen-13	0.708	Zinc-65	0.330
Europium-154	0.756	Nitrogen-16	1.474	Zirconium-95	0.465

a Short-lived transformation product in equilibrium with longer-lived parent.

7.9.3 Exposure and Absorbed Dose

The point source formulas and the gamma ray constant are based on exposure, usually in R/h per curie at 1 m. The absorbed dose in rad to a person is usually of primary interest, however, and this can be obtained from exposure by the relative stopping power, S_{rel}, of photons in air and tissue which has the value of 1.12. In order to use S_{rel} to obtain absorbed dose, it is necessary to convert exposure rate to an energy deposition rate in air since S_{rel} relates energy loss per unit path length:

$$\text{Dose (rad)} = S_{rel} \times \frac{\text{Exposure (R/h)} \times 87.64\ \text{erg/g R}}{100\ \text{erg/g rad}}$$

or

$$\text{Tissue dose (rad)} = 1.12 D_a$$

where D_a is the air dose in rad.

The absorbed dose in tissue can also be calculated directly from the energy deposition rate in the medium of interest (usually tissue) by using the μ_{en}/ρ value for the tissue medium of interest and the appropriate photon energy. In this direct method, one proceeds as before to determine an energy flux impinging on a person, which is multiplied by the appropriate μ_{en}/ρ value to establish the energy deposition rate and the absorbed dose as illustrated in Example 7-15.

Example 7-15. Determine the dose to muscle tissue at 1 m from a 1 mCi point source of ^{137}Cs by (a) the indirect method (i.e., relative stopping power) and (b) the direct method.

Solution. (a) The gamma ray constant for ^{137}Cs is 0.319 R/h Ci at 1 m:

$$D_a = \frac{0.319\ \text{R/h Ci} \times 0.001\ \text{Ci} \times 87.64\ \text{erg/g R}}{100\ \text{ergs/g rad}}$$

$$= 2.8 \times 10^{-4}\ \text{rad/h} = 0.28\ \text{mrad/h}$$

The dose to muscle tissue is obtained from the relative stopping power of tissue to air of 1.12, or

$$D = 1.12 \times D_a = 1.12 \times 0.28\ \text{mrad/h} = 0.31\ \text{mrad/h}$$

(b) ^{137}Cs emits 0.662 MeV gamma rays in 85% of its transformations and produces a flux at 1 m of 2.5×10^2 g/cm^2 s. The energy flux is

$$\phi_{en} = 2.5 \times 10^2\ \gamma/\text{cm}^2\ \text{s} \times 0.662\ \text{MeV} = 1.66 \times 10^2\ \text{MeV/cm}^2\ \text{s}$$

The mass energy absorption coefficient μ_{en}/ρ, for muscle is 0.0323 cm^2/g; therefore, the energy deposition rate in muscle tissue is determined directly as

$$D = \frac{1.66 \times 10^2 \text{ MeV/cm}^2 \text{ s} \times 0.0323 \text{ cm}^2/\text{g} \times 1.6022 \times 10^{-6} \text{ erg/MeV} \times 3600 \text{ s/h}}{100 \text{ erg/g rad}}$$

$$= 3.1 \times 10^{-4} \text{ rad/h} = 0.31 \text{ mrad/h}$$

7.9.4 Exposure, Kerma, and Absorbed Dose

The absorbed dose at various tissue depths is dependent on the photon flux reaching the depth, the interaction fraction that occurs by the various attenuation/absorption mechanisms, and the paths and distribution of charged particles released in the tissue layer including those backscattered from interactions in deeper layers. A very practical approach for radiation dosimetry has been developed in which all these factors are incorporated into a factor C_k that relates air kerma, K_a, and the absorbed dose, D_i, at various depths as

$$D_i = C_{ki} K_a$$

where C_{ki} is a coefficient for a particular depth in tissue and has units of Sv/Gy (or rem/rad). Values of C_{ki} are provided in Table 7-7 for tissue depths of 7 mg/cm^2, 300 mg/cm^2, and 1000 mg/cm^2. The absorbed doses at each of these tissue depths is determined by first calculating or measuring the air kerma at the interface of a tissue of sufficient thickness for electronic equilibrium to exist and then multiplying it by the appropriate C_{ki} value.

Air kerma can be calculated from the incident photon flux as

$$K_a = 1.6022 \times 10^{-10} \phi \left(\frac{\mu_{en}}{\rho}\right)_{air} \frac{E_{h\nu}}{1-g}$$

where K_a is in units of gray (100 rad), ϕ is the photon flux ($h\nu/cm^2$ s), μ_{en}/ρ or μ_{tr}/ρ is in units of cm^2/g, and $E_{h\nu}$ is in MeV. The quantity g is unitless, and is negligible for photons below 1.5 MeV or so. A mass energy transfer coefficient μ_{tr}/ρ can also be used to calculate K_a; it is more convenient to use the mass energy absorption coefficient μ_{en}/ρ and to adjust it with the value of $1/(1-g)$ since values of μ_{en}/ρ are more readily available.

Table 7-7. Factors of C_k to convert air kerma K_a to tissue dose equivalent in a 30 cm thick semi-infinite tissue slab at 7 mg/cm^2 (shallow dose), 300 mg/cm^2 (eye dose), and 1000 mg/cm^2 (deep dose), also defined as H(10) by ICRU (1992).

Photon source	$\bar{E}_{Avg}$ (keV)	C_k (shallow)	C_k (eye)	C_k (deep)
X rays[a] (mm Al, Cu, Sn)				
M30 (0.5, 0, 0)	20	1.02		0.42
M60 (1.5, 0, 0)	35	1.21		1.00
M100 (5.0, 0, 0)	53	1.49		1.52
M150 (5.0, 0.25, 0)	73	1.64		1.78
H150 (4.0, 4.0, 1.5)	118	1.60		1.71
Monoenergetic photons (keV)				
10	10	0.949	0.251	0.010
20	20	1.040	0.910	0.616
25	25	1.124	1.071	0.886
30	30	1.228	1.221	1.115
50	50	1.657	1.737	1.803
70	70	1.821	1.913	2.026
90	90	1.798	1.879	1.990
120	120	1.702	1.766	1.852
150	150	1.616	1.670	1.731
300	300	1.405	1.431	1.459
500	500	1.299	1.312	1.325
^{137}Cs	662	1.210	1.210	1.210
1000	1000	1.205	1.209	1.208
^{60}Co	1250	1.180	1.180	1.170
2000	2000	1.140	1.149	1.140

a X ray sources are standard beam designations established by the National Institute of Standards and Technology (NIST) for x-ray spectra obtained with noted filtration; M denotes moderate filtration, H denotes heavy filtration, and the number is the x-ray tube voltage in kilovolts.

The *air kerma/exposure relationship* represents a practical means of determining absorbed dose in tissue because the exposure or exposure rate in free air can be readily measured. The air kerma rate is calculated from the exposure rate measurement as

$$K_a = K_a = \mathrm{Exp(R)}\frac{W}{e}\frac{1}{1-g} = \frac{\mathrm{Exp(R)} \times 33.97\,\mathrm{J/C}}{(1-g)} \times 2.58 \times 10^{-4}\,\mathrm{C/kg\ R}$$

$$= \frac{87.64 \times 10^{-3} \times \mathrm{Exp(R)}}{1-g}$$

where K_a is in units of Gy, Exp(R) is the measured exposure in R, and g is unitless. The value of K_a is then multiplied by the appropriate C_{ki} value (from Table 7-7) to obtain the absorbed dose. These relationships are particularly useful in calibrating dosimeters or other devices in terms of absorbed dose.

7.10 Summary

Radiation interacts in an absorbing medium to deposit energy which is defined as the absorbed dose, and, when weighted according to the damaging effect of the radiation type, the term effective dose equivalent. A related term is radiation exposure, which applies to air only and is a measure of the amount of ionization produced by x-rays and gamma radiation in air.

Radiation dose can be calculated if three things are known: (a) the mass of the medium being irradiated, (b) the number of "radiations" per unit area (the flux) that impinge on the mass, and (c) the amount or rate of energy deposition in the mass specified. For particles, the mass in which the energy is dissipated is just the depth of penetration; for photons, it is necessary to use a unit depth (e.g., 1 cm) due to the probabilistic pattern of interactions represented by the mass energy absorption coefficient, μ_{en}/ρ. All emitted radiations must be considered in this process, and adjustments should be made for any attenuating medium between the source and the point of interest.

Acknowledgments

Many of the data resources in this chapter came from the very helpful people at the National Institute of Standards and Technology, in particular Dr. John H. Hubbell and his colleagues M. J. Berger and S. M. Seltzer. Its assembly is due in large measure to the patient, careful, and untiring efforts of Chul Lee M.S., a graduate of the University of Michigan Radiological Health Program.

Other Suggested Sources

Hubbell, J. H., Seltzer, S. M. **1995**, *Tables of X-ray Attenuation Coefficients and Mass Absorption Coefficients 1 keV to 20 MeV for Elements Z = 1 io 92 and 48 Additional Substances of Dosimetric Interest*, NIST, Gaithersburg, MD.
Knoll, G. F. *Nuclear Radiation Detection*, 2nd edn, Wiley Interscience, New York.
Lamarsh, J. R. **1983**, *Introduction to Nuclear Engineering*, Addison-Wesley, Reading, MA, Chapters 5 and 9.
Lapp, R. E., Andrews, H. L. **1972**, *Nuclear Radiation Physics*, 4th edn, Prentice-Hall, Upper Saddle River, NJ.

Problems – Chapter 7

7–1. What energy must (a) an alpha particle and (b) a beta particle have to just penetrate the dead layer of a person's skin?
7–2. The binding energies of electrons in different shells of an element may be determined by measuring the transmission of a monoenergetic beam of photons through a thin foil of the element as the energy of the beam is varied. Explain how this method works.
7–3. A gamma ray of 2.75 MeV from ^{24}Na undergoes pair production in a lead shield. How much kinetic energy is shared by the two electron masses and how is it distributed among them?
7–4. A ^{90}Sr–^{90}Y point source contains an activity due to ^{90}Sr of 10^6 t/s (i.e., 1 Mbq). Determine (a) the beta particle flux at 40 cm; (b) the energy flux due to ^{90}Y at 40 cm; (c) the absorbed dose rate in tissue at 40 cm if air attenuation is not a factor; and (d) the effect of air attenuation on the absorbed dose.
7–5. A "hot particle" containing 1 μCi of ^{192}Ir was found on a person's lab coat which was next to the skin. What was the absorbed dose rate in rad/h?
7–6. The following data were recorded for identical samples mounted on different holders: a "weightless" mylar mount, 2038 cpm; a silver disc, 3258 cpm. Compute the backscatter factor for silver.
7–7. What is the kinetic energy of the Compton electron for photons scattered at 45° during a Compton interaction, if the energy of the incident photon is 150 keV? What effect does an increase in the photon scattering angle have on the scattered photon?
7–8. A narrow beam of 40 keV photons which initially contains 500,000 photons is passed through three different filters. One filter is 5 mm of Al, one is 3 mm of Cu, and one is 1 mm of Pb. How many photons interact in each of the three filters?
7–9. For ^{54}Mn, determine (a) the gamma ray constant (R/h Ci at 1 m) and (b) the absorbed dose rate per Ci in tissue at 50 cm.
7–10. Determine Γ for 1 mCi of ^{60}Co which emits 1.17 MeV (μ_{en} in air of 3.43×10^{-5} cm^{-1}) and 1.33 MeV gamma rays assuming each is emitted 100% of the time.

7–11. A solution of 10 μCi of ^{32}P was spilled on a wooden tabletop but was not discovered until it dried. If the area of contamination was a circle 30 cm in diameter and the solution dried uniformly over it, what would be the beta flux, the energy flux, and the dose rate just over the tabletop? How would these change if the tabletop were stainless steel?

7–12. An exposure rate was measured some distance from a point source as 100 mR/h. What would be the absorbed dose rate (rad/h) to a person that stood at the exact spot? What would be the dose equivalent rate (rem/h)?

7–13. A source of 1 MeV gamma rays produces a uniform flux of 10^6 γ/cm^2 s at a distance of 150 cm. What is the absorbed dose rate to a person at that distance? What would it be at 200 cm?

8
Radiation Shielding

"Eureka! I have found it."
Archimedes (ca. 250 BC);
W. A. Mills (1970)

Various materials, placed between a source and a receptor, can affect the amount of radiation transmitted from the source to the receptor. Such effects are due to attenuation and absorption of the emitted radiation in the source itself, in material used for encapsulation of the source, or in a shielding barrier. Regardless of how it occurs, shielding is an important aspect of radiation protection since it can be a form of radiation control; therefore, the features of shields and their design, use, and effectiveness warrant specific consideration.

The presentation in this chapter builds upon the interaction principles described in Chapter 7. It is worth noting that even though various aspects are straightforward, radiation shielding is a very complex discipline for many radiation sources and the many geometric configurations in which they may occur. Therefore, this presentation focuses on straightforward configurations of point sources, line sources, and area and volume sources which fortunately can be used conservatively to address most of the situations encountered in practical radiation protection. Many shielding problems can be treated in terms of one of these configurations, and in general the exposure will be slightly overestimated such that shield designs would be conservative.

8.1
Shielding of Alpha-Emitting Sources

Alpha particles are easy to shield since their relatively large mass and charge limit their range in most media to a few tens of micrometers and to just a few centimeters in air. Only the most energetic ones are capable of penetrating the 7 mg/cm^2 dead layer of human skin. However, inside the body, they do considerable damage because of these same properties.

Most shielding problems for alpha emitters involve fixing the material in place so it cannot become a source of contamination taken into the body by touch or as airborne particles. A layer of paint or other fixative can be used to reduce even

Physics for Radiation Protection, Third Edition. James E. Martin

highly contaminated areas to non-detectable levels. Caution and continuous vigilance through inspections and surveys are required to ensure that the fixative remains intact, especially on floors or high-use areas.

In a similar vein, the very short range of alpha particles makes their detection very difficult because they must be able to penetrate detector coverings or windows to reach the sensitive volume of the detector and be registered. It is easy to miss highly contaminated areas by failing to get close enough (most alphas are absorbed in a few centimeters of air), using the wrong detector, or using a detector with a window that is too thick.

8.2 Shielding of Beta-Emitting Sources

Beta particles have a limited range in most media because they are charged particles and will dissipate all their energy as they traverse a medium by ionization and bremsstrahlung production. The path of ionization can be rather long and tortuous because of the smallness of the electrons, but limited nonetheless. The mean range of most beta particles is no more than a few meters in air (see Figure 8-1), thus air can significantly attenuate beta particles; shielding properties of other media are even better since the range of most beta particles is only a few millimeters in dense materials. Because of this behavior, all of the beta particles emitted by a source can be stopped by determining the maximum range of the highest energy beta particles and choosing a thickness of medium that matches or exceeds the range. Most beta shields are based on this very practical approach, usually with a little more thickness just to be sure.

8.2.1 Attenuation of Beta Particles

The exponential decrease in the number of beta particles for absorber thicknesses less than the maximum range $R_{\beta\max}$ as shown in Figure 7-8 can be used to determine beta particle attenuation as long as the absorber thickness (mg/cm^2) is less than the maximum range of the beta particles in the particular medium I:

$$I(x) = I_0 e^{-\mu_{\beta,i}(\rho x)}$$

where $\mu_{\beta,i}$ (cm^2/ g) is a function of maximum beta particle energy, I_0 is the intensity (or number) of beta particles, $I(x)$ is the intensity (or number) observed for an absorber of thickness x, and ρx is the density thickness (g/cm^2) of the absorber. Since the units of μ_β for various beta sources are determined (and expressed) in cm^2/g, it is necessary to specify the absorber as a density thickness with units of g/cm^2, which is obtained by multiplying the absorber thickness x by its density ρ.

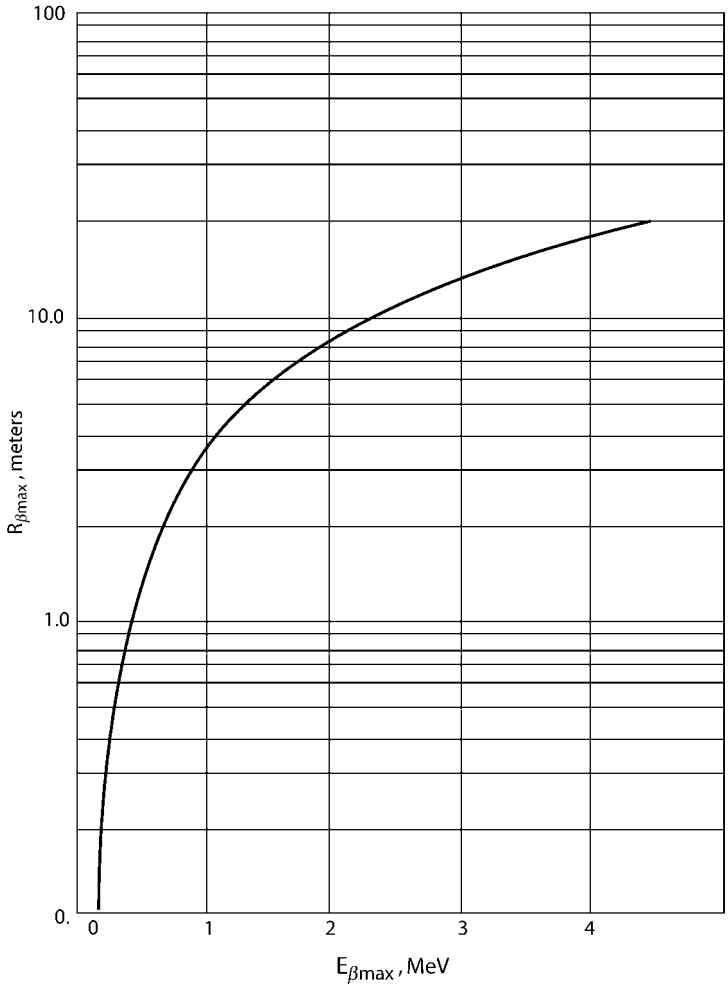

Fig. 8-1 Maximum range $R_{\beta max}$ versus maximum energy $E_{\beta max}$ of beta particles in air at STP.

As developed in Chapter 7, beta absorption coefficients for air, tissue (or water), and solid materials as a function of $E_{\beta max}$ are, respectively

$$\mu_{\beta,\text{air}} = 16(E_{\beta\max} - 0.036)^{-1.4}$$

$$\mu_{\beta,\text{tissue}} = 18.6(E_{\beta\max} - 0.036)^{-1.37}$$

$$\mu_{\beta,i} = 17(E_{\beta\max})^{-1.14}$$

where values of μ_β are in units of cm^2/g and $E_{\beta max}$ is in units of MeV. It should be noted that μ_β is uniquely defined with units of cm^2/g instead of the more tradi-

tional units of cm^{-1} or as μ/ρ because the most practical uses of the "beta absorption" coefficients are in calculations of beta attenuation in materials with density thickness ρx.

Example 8-1. Beta particles with $E_{\beta max}$ of 2.0 MeV produce a flux of 1000 beta particles/cm^2 s incident on an aluminum (ρ = 2.7 g/cm^3) absorber 0.1 mm thick. What will be the flux of beta particles reaching a receptor just beyond the foil?
Solution. The beta absorption coefficient μ_β is

$$\mu_\beta = 17 \times (2)^{-1.14} = 17 \times (0.45376)$$

$$= 7.714 \text{ cm}^2/\text{g}$$

The density thickness of the aluminum absorber is

$$2.7 \text{ g/cm}^3 \times 0.01 \text{ cm} = 0.0274 \text{ g/cm}^2$$

Therefore, the flux of beta particles penetrating the foil and striking the receptor is

$$I(x) = I_0 e^{-\mu_\beta(\rho x)} = 1000 e^{-7.714 \text{ cm}^2/\text{g} \times 0.0274 \text{ g/cm}^2}$$

$$= 809.5 \ \beta/\text{cm}^2 \text{ s}$$

It is important to consider all the attenuating materials that may be present between the beta source and the point of interest. For example, as shown in Figure 8-2, a given configuration may contain, in addition to the shield material enclosing the beta emitter, a thickness of air, and yet another layer between the air gap and the sensitive volume of interest (e.g., a dead layer of skin or a detector window). And of course geometry factors for a given configuration and a backscatter factor if appropriate also influence the dose rate from a source. These, with the exception of backscatter, tend to add additional conservatism in the effectiveness of beta shields, but not always if bremsstrahlung is considered.

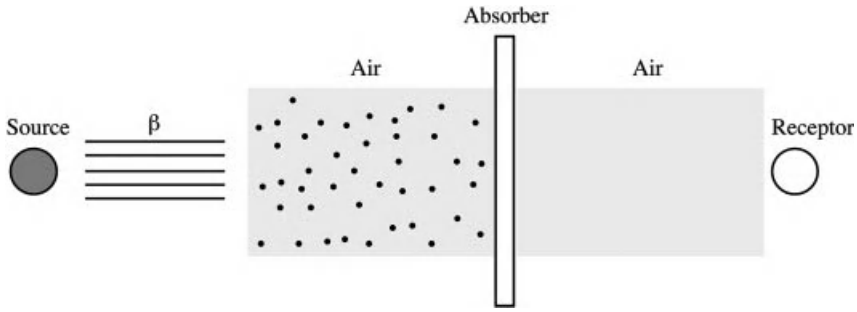

Fig. 8-2 Schematic of various absorbing materials between a beta-emitting source and a layer or volume of interest.

8.2.2 Bremsstrahlung Effects for Beta Shielding

Since beta particles are high-speed electrons, they produce bremsstrahlung, or "braking radiation," in passing through matter, especially if the absorbing medium is a high-Z material. Consequently, the design of shields for beta particle sources or accelerated monoenergetic electrons needs to consider the fraction of the beta particle energy emitted by a source that is converted to photons in order to account for them. The most accurate data on the fraction of the beta energy that is converted to bremsstrahlung have been provided by Berger and Seltzer for monoenergetic electrons; these are listed in Table 8-1 and plotted in Figure 8-3 and illustrate the effects of changes in electron energy and Z of absorber on the energy fraction converted to photons. Since beta particles emitted from a radionuclide exhibit a spectral effect (where the average beta energy is $\sim\frac{1}{3} E_{\beta\max}$), it is more difficult to determine the bremsstrahlung yield for beta sources.

Table 8-1. Percent radiation yield of electrons of initial energy E on different absorbers.

	Absorber (Z)					
E (MeV)	Water	Air	Al (13)	Cu (29)	Sn (50)	Pb (82)
0.100	0.058	0.066	0.135	0.355	0.658	1.162
0.200	0.098	0.111	0.223	0.595	1.147	2.118
0.300	0.133	0.150	0.298	0.795	1.548	2.917
0.400	0.166	0.187	0.368	0.974	1.900	3.614
0.500	0.198	0.223	0.435	1.143	2.224	4.241
0.600	0.229	0.258	0.501	1.307	2.530	4.820
0.700	0.261	0.293	0.566	1.467	2.825	5.363
0.800	0.293	0.328	0.632	1.625	3.111	5.877
0.900	0.325	0.364	0.698	1.782	3.391	6.369
1.000	0.358	0.400	0.764	1.938	3.666	6.842
1.250	0.442	0.491	0.931	2.328	4.340	7.960
1.500	0.528	0.584	1.101	2.720	4.998	9.009
1.750	0.617	0.678	1.274	3.113	5.646	10.010
2.000	0.709	0.775	1.449	3.509	6.284	10.960
2.500	0.897	0.972	1.808	4.302	7.534	12.770
3.000	1.092	1.173	2.173	5.095	8.750	14.470

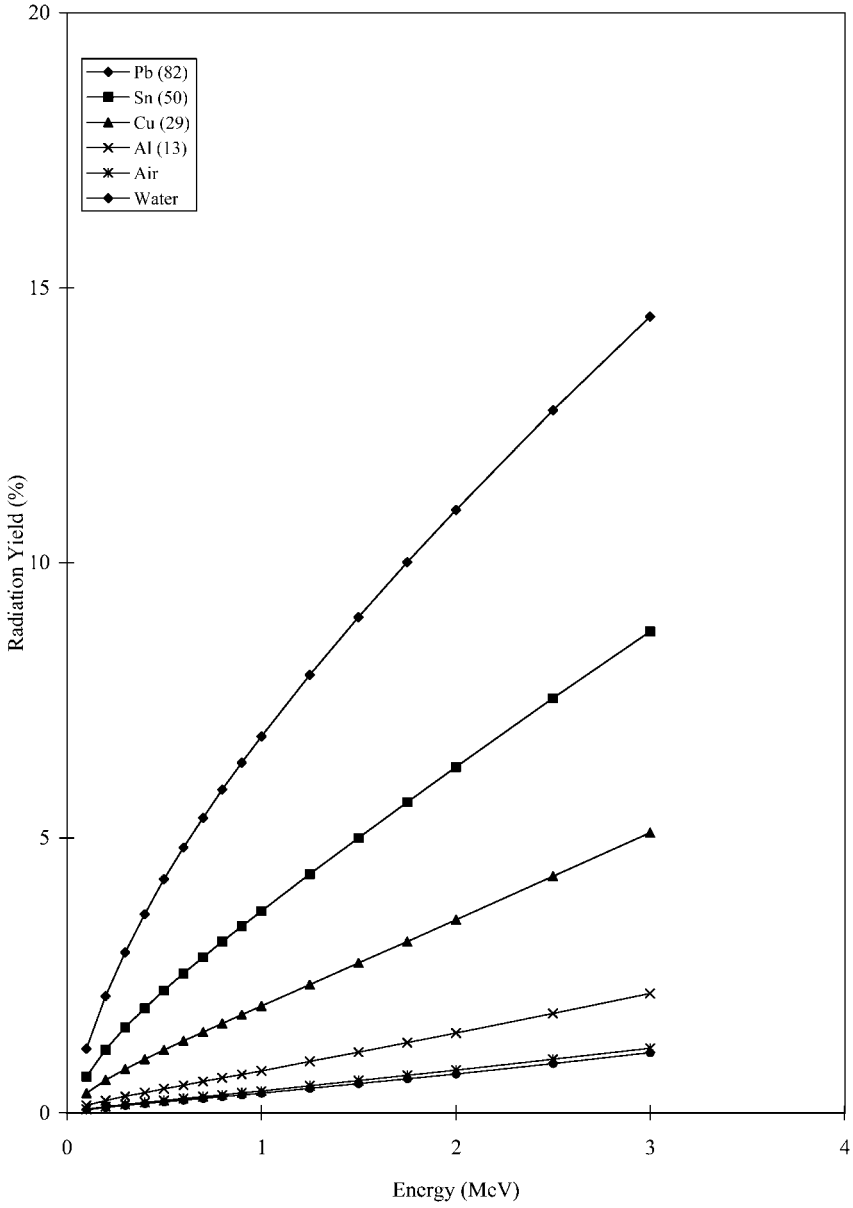

Fig. 8-3 Percent radiation yield of electrons of initial energy E on different absorbers.

Empirical relations have been developed for the fraction of the total electron energy that is converted to photon production; however, these too are based on the experimental data for monoenergetic electrons. One such relation, expressed as an energy yield fraction Y_i for monoenergetic electrons is

$$Y_i = \frac{6 \times 10^{-4}\, EZ}{1 + 6 \times 10^{-4}\, EZ}$$

where E is the maximum energy of the electrons in MeV before striking a target and Z is the atomic number of the target material.

For a beta particle source it is appropriate to multiply the value of Y_i for monoenergetic electrons of energy $E = E_{\beta\max}$ on an absorber by a factor of 0.3 to obtain the total energy converted to photons. The total energy converted to photons can then be divided by an energy value assumed for each bremsstrahlung photon to obtain a beta flux for use in determining beta dose. This can be done conservatively by assuming that each bremsstrahlung photon has an energy equal to the maximum energy of the beta particles emitted by the source; however, it may be more reasonable but less conservative to assign the average beta particle energy to each bremsstrahlung photon produced.

Beta shield designs must account for the yield of bremsstrahlung photons. High-Z materials such as lead ($Z = 82$) should not be used to shield high-activity sources such as ^{32}P ($E_{\beta\max} = 1.71$ MeV) and ^{90}Sr–Y ($E_{\beta\max} = 2.28$ MeV) because 8–12% of the emitted energy could be in the form of bremsstrahlung photons. Since the bremsstrahlung yield is higher in high-Z materials, the most practical approach for shielding beta sources is to use a layer of plastic, aluminum, or other low-Z material to absorb all the beta particles and minimize bremsstrahlung production, then to add a layer of lead or other dense material to absorb any bremsstrahlung and characteristic x-rays that are produced in the beta shield, as shown in Example 8-2.

Example 8-2. One curie of ^{32}P ($E_{\beta\max} = 1.71$ MeV) is dissolved in 50 mL of water for an experiment. If it is to be kept in a polyethylene ($\rho = 0.93$) bottle, how thick should the wall be to stop all the beta particles emitted by ^{32}P and what thickness of lead would be required to ensure that the dose equivalent rate due to bremsstrahlung photons will be less than 2 mrem/h at 1 m?

Solution. (a) From Figure 7-9, the maximum range of 1.71 MeV beta particles is 810 mg/cm^2 or 0.81 g/cm^3; therefore, the thickness of polyethylene required to absorb the 1.71 MeV beta particle is

$$\frac{0.81\ \text{g/cm}^2}{0.93\ \text{g/cm}^3} = 0.87\ \text{cm}$$

Essentially all of the bremsstrahlung can be assumed to be produced in the water solution since the thin polyethylene walls are of similar density. From Table 8-1, about 0.6% of 1.7 MeV beta energy (fractional yield of about 6×10^{-3}) is converted to photons due to absorption in water, and since the average beta energy for ^{32}P (Appendix D) is 0.695 MeV the photon emission rate is

$$E_{\text{rad}} = 3.7 \times 10^{10}\ \text{t/s} \times 0.695\ \text{MeV/t} \times 6 \times 10^{-3}$$
$$= 1.55 \times 10^{8}\ \text{MeV/s due to bremsstrahlung production}$$

If this beta energy converted to bremsstrahlung is assumed to produce photons equal to the maximum beta energy of 1.71 MeV, a conservative assumption, then the photon emission rate is

$$\frac{1.55 \times 10^8}{1.71\,\text{MeV/photon}} = 9.1 \times 10^7 \text{photons}$$

or 7.24×10^2 photons/cm^2 s at 1 m. From Table 8-2, the *mass energy* absorption coefficient by interpolation for 1.71 MeV photons in tissue is 0.027 cm^2/g; therefore, this flux produces an energy absorption rate in tissue of

$$E_{ab} = 7.24 \times 10^2/\text{cm}^2\ \text{s} \times 1.71\ \text{MeV} \times 0.027\ \text{cm}^2/\text{g} \times 1.6022 \times 10^{-6}\ \text{erg/MeV} \times 3600\ \text{s/h}$$

$$= 0.193\ \text{erg/g h}$$

which corresponds to an absorbed dose rate of 1.93 mrad/h, or a dose equivalent rate of 1.93 mrem/h. The attenuation coefficient μ for 1.71 MeV photons in lead is given in Table 8-2 as 0.565 cm^{-1}; thus, the thickness of lead needed to attenuate the photon flux to 1 mrem/h is found from

$$1\ \text{mrem/h} = 1.93\ \text{mrem/h} \times e^{-0.565x}$$

and $x = 1.16$ cm. As will be shown later, it is usually necessary to account for scattered photons that are produced in the absorber by a buildup factor; however, since it is assumed that all the bremsstrahlung is produced with an energy of $E_{\beta\text{max}}$, a conservative assumption, buildup can be reasonably ignored. Consideration of buildup due to Compton scattering could result in a somewhat thicker shield.

8.3 Shielding of Photon Sources

As discussed in Chapter 7, photon interactions with matter are very different from those of charged particles. When x-rays or gamma rays traverse matter, some are absorbed, some pass through without interaction, and some are scattered as lower energy photons in directions that are quite different from those in the primary beam. The attenuation of a photon beam by an absorber is characterized, as shown in Figure 7-16, as occurring in "good geometry" or "poor geometry." In g*ood geometry* attenuation, every photon that interacts is either absorbed or scattered out of the primary beam such that those that reach the receptor have all of their original energy. In *poor geometry* (also called broad-beam geometry), a significant fraction of scattered photons will also reach the receptor of interest, and the energy spectrum will be quite complex with multiple scattered photon ener-

gies in addition to unattenuated photons that retain all of their initial energy. Poor geometry exists in most practical conditions when tissue is exposed or a shield is used to attenuate a photon source, and it is necessary to account for these scattered photons.

8.3.1 Shielding of Good Geometry Photon Sources

The attenuation of photons by various absorbing materials under ideal narrow-beam conditions satisfy the relationship

$$I(x) = I_0 e^{-\mu x}$$

where I_0 is the initial photon intensity (usually expressed as a fluence or flux), $I(x)$ is the photon intensity after passing through an absorber of thickness x in narrow-beam geometry, and μ (cm^{-1}) is the total attenuation coefficient, which accounts for all interaction processes, including scattering reactions, that remove photons from the beam. The attenuation coefficient μ is dependent on the particular absorber medium and the photon energy; therefore, extensive listings are required as provided in Table 8-2 along with mass attenuation and mass energy absorption coefficients. The values of μ listed in Table 8-2 were obtained with collimated narrow beams of monoenergetic photons incident on the different absorbers with a detector placed behind each absorber such that scattered photons were not detectable.

Values of μ generally increase as the Z of the absorber increases (see Figure 7-20) because photoelectric interactions are increased in high-Z materials especially for low-energy photons, and high-Z materials yield increases in pair production interactions for high-energy photons. Because of the high-Z effect, lead is often used to line the walls of x-ray rooms, made into lead aprons for personnel protection, and incorporated into leaded glass, and $BaSO_4$ is incorporated into concrete (called barite or barytes concrete) to increase its effectiveness as a photon shield.

Photon attenuation coefficients in various materials can be calculated from measurements of the intensity of a narrow beam of photons of a given energy as shown in Example 8-3.

Table 8-2. Photon attenuation (μ), mass attenuation (μ/ρ), and mass energy absorption (μ_{en}/ρ) coefficients for selected elements and compounds/mixtures (J. H. Hubbell and S. M. Seltzer).

	Dry air (sea level) (ρ = 0.001205 g/cm^3)			Water, liquid (ρ = 1.00 g/cm^3)			Aluminum (ρ = 2.699 g/cm^3)			Iron (ρ = 7.874 g/cm^3)		
Energy (keV)	μ (cm^{-1})	μ/ρ (cm^2/g)	μ_{en}/ρ (cm^2/g)	μ (cm^{-1})	μ/ρ (cm^2/g)	μ_{en}/ρ (cm^2/g)	μ (cm^{-1})	μ/ρ (cm^2/g)	μ_{en}/ρ (cm^2/g)	μ (cm^{-1})	μ/ρ (cm^2/g)	μ_{en}/ρ (cm^2/g)
10	0.0062	5.120	4.742	5.329	5.329	4.944	70.795	26.23	25.43	1343.304	170.6	136.90
15	0.0019	1.614	1.334	1.673	1.673	1.374	21.4705	7.955	7.487	449.4479	57.08	48.96
20	0.0009	0.7779	0.5389	0.8096	0.8096	0.5503	9.2873	3.441	3.094	202.2043	25.68	22.60
30	4.26×10^{-4}	0.3538	0.1537	0.3756	0.3756	0.1557	3.0445	1.128	0.8778	64.3778	8.176	7.251
40	2.99×10^{-4}	0.2485	0.0683	0.2683	0.2683	0.0695	1.5344	0.5685	0.3601	28.5747	3.629	3.155
50	2.51×10^{-4}	0.2080	0.0410	0.2269	0.2269	0.0422	0.9935	0.3681	0.1840	15.4173	1.958	1.638
60	2.26×10^{-4}	0.1875	0.0304	0.2059	0.2059	0.0319	0.7498	0.2778	0.1099	9.4882	1.2050	0.9555
70[a]	2.10×10^{-4}	0.1744	0.0255	0.1948	0.1948	0.0289	0.6130	0.2271	0.0713	6.2318	0.7914	0.5836
80	2.00×10^{-4}	0.1662	0.0241	0.1924	0.1924	0.0272	0.5447	0.2018	0.0551	4.6866	0.5952	0.4104
100	1.86×10^{-4}	0.1541	0.0233	0.1707	0.1707	0.0255	0.4599	0.1704	0.0379	2.9268	0.3717	0.2177
150	1.63×10^{-4}	0.1356	0.0250	0.1505	0.1505	0.0276	0.3719	0.1378	0.0283	1.5465	0.1964	0.0796
200	1.49×10^{-4}	0.1233	0.0267	0.1370	0.1370	0.0297	0.3301	0.1223	0.0275	1.1496	0.1460	0.0483
300	1.29×10^{-4}	0.1067	0.0287	0.1186	0.1186	0.0319	0.2812	0.1042	0.0282	0.8654	0.1099	0.0336
400	1.15×10^{-4}	0.0955	0.0295	0.1061	0.1061	0.0328	0.2504	0.0928	0.0286	0.7402	0.0940	0.0304
500	1.05×10^{-4}	0.0871	0.0297	0.0969	0.0969	0.0330	0.2279	0.0845	0.0287	0.6625	0.0841	0.0291
600	9.71×10^{-5}	0.0806	0.0295	0.0896	0.0896	0.0328	0.2106	0.0780	0.0285	0.6066	0.0770	0.0284

	Dry air (sea level) (ρ = 0.001205 g/cm^3)			Water, liquid (ρ = 1.00 g/cm^3)			Aluminum (ρ = 2.699 g/cm^3)			Iron (ρ = 7.874 g/cm^3)		
Energy (keV)	μ (cm^{-1})	μ/ρ (cm^2/g)	μ_{en}/ρ (cm^2/g)	μ (cm^{-1})	μ/ρ (cm^2/g)	μ_{en}/ρ (cm^2/g)	μ (cm^{-1})	μ/ρ (cm^2/g)	μ_{en}/ρ (cm^2/g)	μ (cm^{-1})	μ/ρ (cm^2/g)	μ_{en}/ρ (cm^2/g)
662[a]	9.34×10^{-5}	0.0775	0.0293	0.0862	0.0862	0.0326	0.2024	0.0750	0.0283	0.5821	0.0739	0.0280
800	8.52×10^{-5}	0.0707	0.0288	0.0787	0.0787	0.0321	0.1846	0.0684	0.0278	0.5275	0.0670	0.0271
1000	7.66×10^{-5}	0.0636	0.0279	0.0707	0.0707	0.0310	0.1659	0.0615	0.0269	0.4720	0.0600	0.0260
1173[a]	7.05×10^{-5}	0.0585	0.0271	0.0650	0.0650	0.0301	0.1526	0.0565	0.0261	0.4329	0.0550	0.0251
1250	6.86×10^{-5}	0.0569	0.0267	0.0632	0.0632	0.0297	0.1483	0.0550	0.0257	0.4213	0.0535	0.0247
1333[a]	6.62×10^{-5}	0.0550	0.0263	0.0611	0.0611	0.0292	0.1435	0.0532	0.0253	0.4071	0.0517	0.0243
1500	6.24×10^{-5}	0.0518	0.0255	0.0575	0.0575	0.0283	0.1351	0.0501	0.0245	0.3845	0.0488	0.0236
2000	5.36×10^{-5}	0.0445	0.0235	0.0494	0.0494	0.0261	0.1167	0.0432	0.0227	0.3358	0.0427	0.0220
3000	4.32×10^{-5}	0.0358	0.0206	0.0397	0.0397	0.0228	0.0956	0.0354	0.0202	0.2851	0.0362	0.0204
4000	3.71×10^{-5}	0.0308	0.0187	0.0340	0.0340	0.0207	0.0838	0.0311	0.0188	0.2608	0.0331	0.0199
5000	3.31×10^{-5}	0.0275	0.0174	0.0303	0.0303	0.0192	0.0765	0.0284	0.0180	0.2477	0.0315	0.0198
6000	3.04×10^{-5}	0.0252	0.0165	0.0277	0.0277	0.0181	0.0717	0.0266	0.0174	0.2407	0.0306	0.0200
6129[a]	3.01×10^{-5}	0.0250	0.0164	0.0274	0.0274	0.0180	0.0713	0.0264	0.0173	0.2403	0.0305	0.0200
7000[a]	2.83×10^{-5}	0.0235	0.0159	0.0258	0.0258	0.01723	0.0683	0.0253	0.0170	0.2370	0.0301	0.0202
7115[a]	2.82×10^{-5}	0.0234	0.0158	0.0256	0.0256	0.0172	0.0680	0.0252	0.0170	0.2368	0.0301	0.0203
10,000	2.46×10^{-5}	0.0205	0.0145	0.0222	0.0222	0.0157	0.0626	0.0232	0.0165	0.2357	0.0299	0.0211

a Coefficients for these energies were interpolated using polynomial regression.

Table 8-2. Continued.

	Copper (ρ = 8.96 g/cm^3)			Lead (ρ = 11.35 g/cm^3)			Polyethylene (ρ = 0.93 g/cm^3)			Concrete, ordinary (ρ = 2.3 g/cm^3)		
Energy (keV)	μ (cm^{-1})	μ/ρ (cm^2/g)	μ_{en}/ρ (cm^2/g)	μ (cm^{-1})	μ/ρ (cm^2/g)	μ_{en}/ρ (cm^2/g)	μ (cm^{-1})	μ/ρ (cm^2/g)	μ_{en}/ρ (cm^2/g)	μ (cm^{-1})	μ/ρ (cm^2/g)	μ_{en}/ρ (cm^2/g)
10	1934.464	215.9	148.4	1482.31	130.6	124.7	1.9418	2.088	1.781	47.04	20.45	19.37
15	663.4880	74.05	57.88	1266.66	111.6	91.0	0.6930	0.7452	0.4834	14.61	6.351	5.855
20	302.7584	33.79	27.88	980.1860	86.36	68.99	0.4013	0.4315	0.1936	6.454	2.806	2.462
30	97.8432	10.92	9.349	344.1320	30.32	25.36	0.2517	0.2706	0.0593	2.208	0.9601	0.7157
40	43.5635	4.862	4.163	162.9860	14.36	12.11	0.2116	0.2275	0.0320	1.163	0.5058	0.2995
50	23.4125	2.613	2.192	91.2654	8.041	6.740	0.1938	0.2084	0.0244	0.7848	0.3412	0.1563
60	14.2733	1.5930	1.2900	56.9884	5.0210	4.1490	0.1832	0.1970	0.0224	0.6118	0.2660	0.0955
70[a]	9.2401	1.0313	0.7933	35.0670	3.0896	2.6186	0.1754	0.1886	0.0221	0.5131	0.2231	0.0638
80	6.8365	0.7630	0.5581	27.4557	2.4190	1.9160	0.1695	0.1823	0.0227	0.4632	0.2014	0.0505
100	4.1073	0.4584	0.2949	62.9812	5.5490	1.9760	0.1599	0.1719	0.0242	0.3997	0.1738	0.0365
150	1.9864	0.2217	0.1027	22.8589	2.0140	1.0560	0.1427	0.1534	0.0279	0.3303	0.1436	0.0290
200	1.3969	0.1559	0.0578	11.3330	0.9985	0.5870	0.1304	0.1402	0.0303	0.2949	0.1282	0.0287
300	1.0026	0.1119	0.0362	4.5752	0.4031	0.2455	0.1132	0.1217	0.0328	0.2523	0.1097	0.0297
400	0.8434	0.0941	0.0312	2.6366	0.2323	0.1370	0.1013	0.1089	0.0337	0.2250	0.0978	0.0302
500	0.7492	0.0836	0.0293	1.8319	0.1614	0.0913	0.0925	0.0995	0.0339	0.2050	0.0892	0.0303
600	0.6832	0.0763	0.0283	1.4165	0.1248	0.0682	0.0855	0.0920	0.0338	0.1894	0.0824	0.0302
662[a]	0.6555	0.0732	0.0279	1.2419	0.1094	0.0587	0.0823	0.0885	0.0335	0.1822	0.0792	0.0299

	Copper (ρ = 8.96 g/cm^3)			Lead (ρ = 11.35 g/cm^3)			Polyethylene (ρ = 0.93 g/cm^3)			Concrete, ordinary (ρ = 2.3 g/cm^3)		
Energy (keV)	μ (cm^{-1})	μ/ρ (cm^2/g)	μ_{en}/ρ (cm^2/g)	μ (cm^{-1})	μ/ρ (cm^2/g)	μ_{en}/ρ (cm^2/g)	μ (cm^{-1})	μ/ρ (cm^2/g)	μ_{en}/ρ (cm^2/g)	μ (cm^{-1})	μ/ρ (cm^2/g)	μ_{en}/ρ (cm^2/g)
800	0.5918	0.0661	0.0268	1.0067	0.0887	0.0464	0.0751	0.0808	0.0330	0.1662	0.0723	0.0294
1000	0.5287	0.0590	0.0256	0.8061	0.0710	0.0365	0.0675	0.0726	0.0319	0.1494	0.0650	0.0284
1173[a]	0.4840	0.0540	0.0246	0.7020	0.0619	0.0315	0.0621	0.0668	0.0310	0.1374	0.0598	0.0276
1250	0.4714	0.0526	0.0243	0.6669	0.0588	0.0299	0.0604	0.0650	0.0305	0.1336	0.0581	0.0272
1333[a]	0.4553	0.0508	0.0239	0.6369	0.0561	0.0285	0.0584	0.0628	0.0300	0.1291	0.0561	0.0268
1500	0.4303	0.0480	0.0232	0.5927	0.0522	0.0264	0.0550	0.0591	0.0291	0.1216	0.0529	0.0260
2000	0.3768	0.0421	0.0216	0.5228	0.0461	0.0236	0.0471	0.0506	0.0268	0.1048	0.0456	0.0240
3000	0.3225	0.0360	0.0202	0.4806	0.0423	0.0232	0.0376	0.0405	0.0233	0.0851	0.0370	0.0212
4000	0.2973	0.0332	0.0199	0.4764	0.0420	0.0245	0.0320	0.0344	0.0209	0.0740	0.0322	0.0195
5000	0.2847	0.0318	0.0200	0.4849	0.0427	0.0260	0.0283	0.0305	0.0192	0.0669	0.0291	0.0184
6000	0.2785	0.0311	0.0203	0.4984	0.0439	0.0274	0.0257	0.0276	0.0179	0.0620	0.0270	0.0176
6129[a]	0.2781	0.0310	0.0203	0.5002	0.0441	0.0276	0.0254	0.0273	0.0178	0.0616	0.0268	0.0175
7000[a]	0.2757	0.0308	0.0206	0.5141	0.0453	0.0287	0.0236	0.0254	0.0169	0.0585	0.0254	0.0171
7115[a]	0.2755	0.0307	0.0207	0.5161	0.0455	0.0289	0.0235	0.0252	0.0168	0.0582	0.0253	0.0170
10,000	0.2780	0.0310	0.0217	0.5643	0.0497	0.0318	0.0199	0.0215	0.0151	0.0524	0.0228	0.0162

a Coefficients for these energies were interpolated using polynomial regression.

Table 8-2. Continued.

	Concrete, barite (type BA) (ρ = 3.35 g/cm^3)			Leaded glass (ρ = 6.22 g/cm^3)			Borosilicate glass (ρ = 2.23 g/cm^3)			Gypsum (ρ = 2.69 g/cm^3)		
Energy (keV)	μ (cm^{-1})	μ/ρ (cm^2/g)	μ_{en}/ρ (cm^2/g)	μ (cm^{-1})	μ/ρ (cm^2/g)	μ_{en}/ρ (cm^2/g)	μ (cm^{-1})	μ/ρ (cm^2/g)	μ_{en}/ρ (cm^2/g)	μ (cm^{-1})	μ/ρ (cm^2/g)	μ_{en}/ρ (cm^2/g)
10	357.45	106.70	99.60	640.04	102.90	98.21	38.02	17.05	16.42	124.62	42.1000	39.7700
15	120.63	36.01	33.63	532.25	85.57	69.91	11.63	5.217	4.828	39.3384	13.2900	12.4700
20	55.44	16.55	15.27	408.53	65.68	52.52	5.122	2.297	1.995	17.2598	5.8310	5.3520
30	18.60	5.551	4.912	143.37	23.05	19.27	1.781	0.7987	0.5684	5.5530	1.8760	1.5870
40	39.70	11.85	4.439	67.98	10.93	9.198	0.9680	0.4341	0.2361	2.6427	0.8928	0.6645
50	22.35	6.671	3.206	38.15	6.134	5.118	0.6739	0.3022	0.1235	1.5928	0.5381	0.3403
60	13.88	4.143	2.266	23.9035	3.843	3.152	0.5390	0.2417	0.0765	1.1212	0.3788	0.2001
70[a]	9.04	2.699	1.630	15.0524	2.420	1.930	0.4623	0.2073	0.0523	0.8594	0.2903	0.1256
80	6.593	1.968	1.211	11.6252	1.869	1.458	0.4215	0.1890	0.0423	0.7323	0.2474	0.0929
100	3.759	1.122	0.7138	26.2235	4.216	1.498	0.3695	0.1657	0.0321	0.5808	0.1962	0.0573
150	1.482	0.4423	0.2659	9.641	1.550	0.8042	0.3097	0.1389	0.0273	0.4402	0.1487	0.0344
200	0.8603	0.2568	0.1369	4.8640	0.7820	0.4508	0.2779	0.1246	0.0276	0.3827	0.1293	0.0306
300	0.4891	0.1460	0.0641	2.0507	0.3297	0.1934	0.2384	0.1069	0.0289	0.3220	0.1088	0.0298
400	0.3698	0.1104	0.0447	1.2340	0.1984	0.1114	0.2127	0.0954	0.0295	0.2857	0.0965	0.0299
500	0.3119	0.0931	0.0372	0.8888	0.1429	0.0768	0.1939	0.0870	0.0296	0.2598	0.0878	0.0299
600	0.2762	0.0825	0.0334	0.7078	0.1138	0.0592	0.1792	0.0804	0.0294	0.2398	0.0810	0.0296
662[a]	0.2635	0.0787	0.0325	0.6602	0.1061	0.0551	0.1723	0.0773	0.0292	0.2293	0.0775	0.0294

	Concrete, barite (type BA) (ρ = 3.35 g/cm^3)			Leaded glass (ρ = 6.22 g/cm^3)			Borosilicate glass (ρ = 2.23 g/cm^3)			Gypsum (ρ = 2.69 g/cm^3)		
Energy (keV)	μ (cm^{-1})	μ/ρ (cm^2/g)	μ_{en}/ρ (cm^2/g)	μ (cm^{-1})	μ/ρ (cm^2/g)	μ_{en}/ρ (cm^2/g)	μ (cm^{-1})	μ/ρ (cm^2/g)	μ_{en}/ρ (cm^2/g)	μ (cm^{-1})	μ/ρ (cm^2/g)	μ_{en}/ρ (cm^2/g)
800	0.2324	0.0694	0.0295	0.5238	0.0842	0.0425	0.1573	0.0705	0.0287	0.2102	0.0710	0.0288
1000	0.2048	0.0611	0.0274	0.4301	0.0691	0.0347	0.1413	0.0634	0.0277	0.1888	0.0638	0.0279
1173[a]	0.1851	0.0553	0.0256	0.3803	0.0611	0.0307	0.1300	0.0583	0.0269	0.1743	0.0589	0.0270
1250	0.1810	0.0540	0.0254	0.3624	0.0583	0.0293	0.1264	0.0567	0.0265	0.1687	0.0570	0.0266
1333[a]	0.1744	0.0521	0.0248	0.3467	0.0557	0.0281	0.1221	0.0548	0.0261	0.1633	0.0552	0.0262
1500	0.1647	0.0492	0.0240	0.3239	0.0521	0.0264	0.1151	0.0516	0.0253	0.1537	0.0519	0.0254
2000	0.1439	0.0430	0.0223	0.2841	0.0457	0.0237	0.0992	0.0445	0.0234	0.1328	0.0449	0.0235
3000	0.1231	0.0368	0.0208	0.2539	0.0408	0.0228	0.0805	0.0361	0.0207	0.1089	0.0368	0.0210
4000	0.1135	0.0339	0.0204	0.2449	0.0394	0.0234	0.0700	0.0314	0.0190	0.0957	0.0323	0.0196
5000	0.1085	0.0324	0.0205	0.2438	0.0392	0.0244	0.0633	0.0284	0.0180	0.0874	0.0295	0.0187
6000	0.1059	0.0316	0.0207	0.2462	0.0396	0.0254	0.0587	0.0263	0.0172	0.0820	0.0277	0.0181
6129[a]	0.1056	0.0315	0.0207	0.2468	0.0397	0.0255	0.0581	0.0261	0.0171	0.0815	0.0275	0.0181
7000[a]	0.1047	0.0313	0.0210	0.2504	0.0403	0.0263	0.0553	0.0248	0.0167	0.0783	0.0265	0.0178
7115[a]	0.1046	0.0312	0.0211	0.2510	0.0403	0.0264	0.0549	0.0246	0.0166	0.0779	0.0263	0.0178
10,000	0.1051	0.0314	0.0221	0.2671	0.0430	0.0288	0.0496	0.0222	0.0158	0.0719	0.0243	0.0173

a Coefficients for these energies were interpolated using polynomial regression.

Example 8-3. If a narrow beam of 2000 monoenergetic photons of 1.0 MeV is reduced to 1000 photons by a slab of copper 1.31 cm thick, determine (a) the total linear attenuation coefficient of the copper slab for these photons and (b) the total mass attenuation coefficient.

Solution. (a) Since $I(x) = I_0 e^{-\mu x}$, μ is determined by taking the natural logarithm of each side of the equation:

$$\ln(0.5) = -\mu(1.31\ \text{cm})$$

$$\mu = \frac{0.69315}{1.31\ \text{cm}} = 0.5287\ \text{cm}^{-1}$$

(b) Copper has a density of 8.9 g/cm^3; therefore, the mass attenuation coefficient μ/ρ is

$$\frac{\mu}{\rho} = \frac{0.5287\ \text{cm}^{-1}}{8.9\ \text{g/cm}^3} = 0.0594\ \text{cm}^2/\text{g}$$

8.3.2 Half-Value and Tenth-Value Layers

As was done in Chapter 3 for radioactivity, it is also useful to express the exponential attenuation of photons in terms of a half-thickness, $x_{1/2}$, or half-value layer (HVL). The HVL (sometimes called the half-value thickness) is the thickness of absorber required to decrease the intensity of a beam of photons to one-half its initial value, or

$$\frac{I(x)}{I_0} = \frac{1}{2} = e^{-\mu x_{1/2}}$$

which can be solved for $x_{1/2}$ to yield

$$x_{1/2} = \text{HVL} = \frac{\ln 2}{\mu}$$

Since a thickness of 1.31 cm of copper reduces the beam intensity of 1.0 MeV photons in Example 8-3 by one-half, it is also the HVL of copper for 1.0 MeV photons.

Similarly, the tenth-value layer (TVL) is

$$\text{TVL} = \frac{\ln 10}{\mu} = \frac{2.3026}{\mu}$$

The HVLs for various materials are listed in Table 8-3. The HVL can be used in calculations for photon attenuation in much the same way half-life is used for radioactive transformation as shown in Example 8-4.

Table 8-3. Half-value layers (in cm) versus photon energy for various materials[a].

Energy (MeV)	Lead (11.35 g/cm^3)	Iron (7.874 g/cm^3)	Aluminum (2.699 g/cm^3)	Water (1.00 g/cm^3)	Air (0.001205 g/cm^3)	Stone concrete (2.30 g/cm^3)
0.1	0.011	0.237	1.507	4.060	3.726×10^3	1.734
0.3	0.151	0.801	2.464	5.843	5.372×10^3	2.747
0.5	0.378	1.046	3.041	7.152	6.600×10^3	3.380
0.662	0.558	1.191	3.424	8.039	7.420×10^3	3.806
1.0	0.860	1.468	4.177	9.802	9.047×10^3	4.639
1.173	0.987	1.601	4.541	10.662	9.830×10^3	5.044
1.332	1.088	1.702	4.829	11.342	1.047×10^4	5.368
1.5	1.169	1.802	5.130	12.052	1.111×10^4	5.698
2.0	1.326	2.064	5.938	14.028	1.293×10^4	6.612
2.5	1.381	2.271	6.644	15.822	1.459×10^4	7.380
3.0	1.442	2.431	7.249	17.456	1.604×10^4	8.141
3.5	1.447	2.567	7.813	19.038	1.747×10^4	8.828
4.0	1.455	2.657	8.270	20.382	1.868×10^4	9.366
5.0	1.429	2.798	9.059	22.871	2.094×10^4	10.361
7.0	1.348	2.924	10.146	26.860	2.449×10^4	11.846
10.0	1.228	2.940	11.070	31.216	2.817×10^4	13.227

a Calculated from attenuation coefficients listed in Table 8-2.
Source: Data from Hubbell and Seltzer (1995).

Example 8-4. If the HVL for iron is 1.47 cm for 1 MeV photons and the exposure rate from a source is 800 mR/h, calculate (a) μ (cm^{-1}), (b) the thickness of iron required to reduce the exposure rate to 200 mR/h, and (c) the thickness of iron required to reduce it to 150 mR/h.
Solution. (a)

$$\mu = \frac{\ln 2}{\text{HVL}} = \frac{0.69315}{1.47\,\text{cm}} = 0.47\,\text{cm}^{-1}$$

(b) It is observed that $800/2^n = 200$ when $n = 2$; therefore, 2 HVLs, or 2.94 cm of iron, will reduce an 800 mR/h exposure rate to 200 mR/h.

(c) Since $I = I_0 e^{-\mu x}$, the thickness of iron required to reduce an 800 mR/h exposure rate to 150 mR/h in good geometry conditions is

$$150 = 800e^{-0.47x}$$

$$\ln(150/800) = -1.674 = -0.47x$$

$$x = 3.55 \text{ cm}$$

This can also be solved by determining the number of HVLs (1.47 cm) necessary to reduce 800 mR/h to 150 mR/h, or

$$150 = 800/2^n \quad \text{or} \quad 2^n = 800/150$$

Taking the logarithm of both sides yields

$$n\ln 2 = \ln(800/150) = 1.674$$

$$n = 1.674/(\ln 2) = 2.4156 \text{ HVL}$$

and since $x = n\text{HVL}$,

$$x = 2.4156 \text{ HVL} \times 1.47 \text{ cm/HVL} = 3.55 \text{ cm}$$

8.3.3 Shielding of Poor Geometry Photon Sources

When a significant absorbing medium such as a metal shield is placed between a photon source and a receptor, the photon flux (or fluence) will be altered significantly because of Compton scattered photons produced in the absorber, many of which will reach the receptor. The scattered photons are also reduced in energy, and the flux of photons reaching the receptor becomes a complicated function of beam size, photon-energy distribution, absorber material, and geometry. The conditions that include these complexities are called poor geometry and represent most practical situations in radiation protection. A calculated value of $I(x)$ based on the attenuation coefficient μ determined in good geometry conditions will thus underestimate the number of photons reaching the receptor which implies that absorption is greater than what actually occurs, and a shield designed on this basis will not be thick enough.

The effect of scattered photons, in addition to unscattered primary photons, is best dealt with by a buildup factor B, which is greater than 1.0 to account for photons scattered towards the receptor from regions outside the primary beam. When buildup is included, the radiation intensity is

$$I(x) = I_0 B e^{-\mu x}$$

Experimentally determined values of B for photons of different energies absorbed in various media are listed in Table 8-4 for point sources (earlier compilations also included buildup factors for broad beams, but these are out of date).

Table 8-4. Exposure buildup factors for photons of energy E versus μx (for various absorbers).

	Energy (MeV)									
μx	0.1	0.5	1	2	3	4	5	6	8	10
Al										
0.5	1.91	1.57	1.45	1.37	1.33	1.32	1.28	1.26	1.22	1.19
1.0	2.86	2.28	1.99	1.78	1.68	1.62	1.54	1.49	1.41	1.35
2.0	4.87	4.07	3.26	2.66	2.38	2.19	2.04	1.94	1.76	1.64
3.0	7.07	6.35	4.76	3.62	3.11	2.78	2.54	2.37	2.11	1.93
4.0	9.47	9.14	6.48	4.64	3.86	3.38	3.04	2.81	2.46	2.22
5.0	12.1	12.4	8.41	5.72	4.64	3.99	3.55	3.26	2.82	2.52
6.0	14.9	16.3	10.5	6.86	5.44	4.61	4.08	3.72	3.18	2.83
7.0	18.0	20.7	12.9	8.05	6.26	5.24	4.61	4.19	3.55	3.14
8.0	21.3	25.7	15.4	9.28	7.1	5.88	5.14	4.66	3.92	3.46
10.0	28.7	37.6	21.0	11.9	8.83	7.18	6.23	5.61	4.68	4.12
15.0	51.7	78.6	37.7	18.9	13.4	10.5	9.03	8.09	6.64	5.87
20.0	81.1	137	57.9	26.6	18.1	14.0	11.9	10.7	8.68	7.74
25.0	117	213	81.3	34.9	23.0	17.5	14.9	13.3	10.8	9.74
30.0	159	307	107	43.6	28.1	21.0	18.0	16.0	13.0	11.8
Fe										
0.5	1.26	1.48	1.41	1.35	1.32	1.3	1.27	1.25	1.22	1.19
1.0	1.4	1.99	1.85	1.71	1.64	1.57	1.51	1.47	1.39	1.33
2.0	1.61	3.12	2.85	2.49	2.28	2.12	1.97	1.87	1.71	1.59
3.0	1.78	4.44	4	3.34	2.96	2.68	2.46	2.3	2.04	1.86
4.0	1.94	5.96	5.3	4.25	3.68	3.29	2.98	2.76	2.41	2.16
5.0	2.07	7.68	6.74	5.22	4.45	3.93	3.53	3.25	2.81	2.5
6.0	2.2	9.58	8.31	6.25	5.25	4.6	4.11	3.78	3.24	2.87
7.0	2.31	11.7	10.0	7.33	6.09	5.31	4.73	4.33	3.71	3.27
8.0	2.41	14.0	11.8	8.45	6.96	6.05	5.38	4.92	4.2	3.71
10.0	2.61	19.1	15.8	10.8	8.8	7.6	6.75	6.18	5.3	4.69
15.0	3.01	35.1	27.5	17.4	13.8	11.9	10.7	9.85	8.64	7.88

Table 8-4. Continued.

	Energy (MeV)									
μx	**0.1**	**0.5**	**1**	**2**	**3**	**4**	**5**	**6**	**8**	**10**
20.0	3.33	55.4	41.3	24.6	19.4	16.8	15.2	14.2	12.9	12.3
25.0	3.61	79.9	57.0	32.5	25.4	22.1	20.3	19.3	18.2	18.1
30.0	3.86	108	74.5	40.9	31.7	27.9	25.9	25.1	24.5	25.7
Sn										
0.5	1.35	1.32	1.33	1.27	1.29	1.28	1.31	1.31	1.33	1.31
1.0	1.38	1.61	1.69	1.57	1.56	1.51	1.55	1.54	1.6	1.57
2.0	1.41	2.15	2.4	2.17	2.07	1.96	1.97	1.94	2.04	2.05
3.0	1.43	2.68	3.14	2.82	2.64	2.45	2.43	2.38	2.51	2.61
4.0	1.45	3.16	3.86	3.51	3.25	3.0	2.54	2.87	3.05	3.27
5.0	1.47	3.63	4.6	4.23	3.92	3.6	3.52	3.43	3.69	4.09
6.0	1.49	4.14	5.43	5.03	4.68	4.29	4.19	4.09	4.45	5.07
7.0	1.5	4.64	6.27	5.87	5.48	5.04	4.93	4.83	5.34	6.26
8.0	1.52	5.13	7.11	6.74	6.32	5.84	5.74	5.65	6.36	7.69
10.0	1.54	6.13	8.88	8.61	8.19	7.65	7.63	7.63	8.94	11.5
15.0	1.58	8.74	13.8	14.0	13.8	13.5	14.1	14.9	19.7	29.6
20.0	1.61	11.4	19.1	20.1	20.5	21.1	23.5	26.4	40.7	72.1
25.0	1.64	14.0	24.5	26.9	28.1	30.6	36.2	43.9	79.7	168
30.0	1.66	16.5	30.0	34.2	36.6	42.1	53.0	69.3	150	377
Pb										
0.5	1.51	1.14	1.2	1.21	1.23	1.21	1.25	1.26	1.3	1.28
1.0	2.04	1.24	1.38	1.4	1.4	1.36	1.41	1.42	1.51	1.51
2.0	3.39	1.39	1.68	1.76	1.73	1.67	1.71	1.73	1.9	2.01
3.0	5.6	1.52	1.95	2.14	2.1	2.02	2.05	2.08	2.36	2.63
4.0	9.59	1.62	2.19	2.52	2.5	2.4	2.44	2.49	2.91	3.42
5.0	17.0	1.71	2.43	2.91	2.93	2.82	2.88	2.96	3.59	4.45
6.0	30.6	1.8	2.66	3.32	3.4	3.28	3.38	3.51	4.41	5.73
7.0	54.9	1.88	2.89	3.74	3.89	3.79	3.93	4.13	5.39	7.37
8.0	94.7	1.95	3.1	4.17	4.41	4.35	4.56	4.84	6.58	9.44

Table 8-4. Continued.

	Energy (MeV)									
μx	**0.1**	**0.5**	**1**	**2**	**3**	**4**	**5**	**6**	**8**	**10**
10.0	294	2.1	3.51	5.07	5.56	5.61	6.03	6.61	9.73	15.4
15.0	5800	2.39	4.45	7.44	8.91	9.73	11.4	13.7	25.1	50.8
20.0	1.33×10^5	2.64	5.27	9.98	12.9	15.4	19.9	26.6	62.0	161
25.0	3.34×10^6	2.85	5.98	12.6	17.5	23.0	32.9	49.6	148	495
30.0	8.87×10^7	3.02	6.64	15.4	22.5	32.6	52.2	88.9	344	1470
U										
0.5	1.04	1.11	1.17	1.19	1.2	1.19	1.23	1.24	1.28	1.27
1.0	1.06	1.19	1.31	1.35	1.35	1.32	1.37	1.38	1.48	1.49
2.0	1.08	1.3	1.53	1.65	1.64	1.6	1.64	1.66	1.85	1.97
3.0	1.1	1.39	1.73	1.95	1.95	1.89	1.94	1.98	2.27	2.56
4.0	1.11	1.45	1.9	2.25	2.28	2.21	2.27	2.33	2.78	3.31
5.0	1.12	1.52	2.07	2.56	2.62	2.55	2.63	2.74	3.39	4.26
6.0	1.13	1.58	2.23	2.88	2.99	2.93	3.04	3.19	4.11	5.43
7.0	1.14	1.63	2.38	3.19	3.38	3.33	3.49	3.71	4.96	6.9
8.0	1.14	1.68	2.52	3.51	3.78	3.76	3.99	4.28	5.97	8.73
10.0	1.16	1.77	2.78	4.17	4.64	4.72	5.14	5.68	8.61	13.9
15.0	1.18	1.96	3.35	5.84	7.06	7.72	9.1	11.0	20.8	43.4
20.0	1.2	2.11	3.82	7.54	9.8	11.6	15.1	20.1	48.6	131
25.0	1.22	2.23	4.23	9.27	12.8	16.5	23.7	35.4	110	385
30.0	1.23	2.33	4.59	11.0	16.0	22.5	36.0	60.4	244	1100
H_2O										
0.5	2.37	1.6	1.47	1.38	1.34	1.31	1.28	1.27	1.23	1.2
1.0	4.55	2.44	2.08	1.83	1.71	1.63	1.56	1.51	1.43	1.37
2.0	11.8	4.88	3.62	2.81	2.46	2.24	2.08	1.97	1.8	1.68
3.0	23.8	8.35	5.5	3.87	3.23	2.85	2.58	2.41	2.15	1.97
4.0	41.3	12.8	7.68	4.98	4	3.46	3.08	2.84	2.46	2.25
5.0	65.2	18.4	10.1	6.15	4.8	4.07	3.58	3.27	2.82	2.53
6.0	96.7	25.0	12.8	7.38	5.61	4.68	4.08	3.7	3.15	2.8

Table 8-4. Continued.

	Energy (MeV)									
μx	**0.1**	**0.5**	**1**	**2**	**3**	**4**	**5**	**6**	**8**	**10**
7.0	137	32.7	15.8	8.65	6.43	5.3	4.58	4.12	3.48	3.07
8.0	187	41.5	19.0	9.97	7.27	5.92	5.07	4.54	3.8	3.34
10.0	321	62.9	26.1	12.7	8.97	7.16	6.05	5.37	4.44	3.86
15.0	938	139	47.7	20.1	13.3	10.3	8.49	7.41	5.99	5.14
20.0	2170	252	74.0	28	17.8	13.4	10.9	9.42	7.49	6.38
25.0	4360	403	104	36.5	22.4	16.5	13.3	11.4	8.96	7.59
30.0	7970	594	139	45.2	27.1	19.7	15.7	13.3	10.4	8.78
Air										
0.5	2.35	1.6	1.47	1.38	1.34	1.31	1.29	1.27	1.23	1.2
1.0	4.46	2.44	2.08	1.83	1.71	1.63	1.57	1.52	1.43	1.37
2.0	11.4	4.84	3.6	2.81	2.46	2.25	2.09	1.97	1.8	1.68
3.0	22.5	8.21	5.46	3.86	3.22	2.85	2.6	2.41	2.15	1.97
4.0	38.4	12.6	7.6	4.96	4	3.46	3.11	2.85	2.5	2.26
5.0	59.9	17.9	10.0	6.13	4.79	4.07	3.61	3.28	2.84	2.54
6.0	87.8	24.2	12.7	7.35	5.6	4.69	4.12	3.71	3.17	2.82
7.0	123	31.6	15.6	8.61	6.43	5.31	4.62	4.14	3.51	3.1
8.0	166	40.1	18.8	9.92	7.26	5.94	5.12	4.57	3.84	3.37
10.0	282	60.6	25.8	12.6	8.97	7.19	6.13	5.42	4.49	3.92
15.0	800	134	47.0	20	13.4	10.3	8.63	7.51	6.08	5.25
20.0	1810	241	72.8	27.9	17.9	13.5	11.1	9.58	7.64	6.55
25.0	3570	385	103	36.2	22.5	16.7	13.6	11.6	9.17	7.84
30.0	6430	567	136	45	27.2	19.9	16.1	13.6	10.7	9.11
Concrete										
0.5	1.89	1.57	1.45	1.37	1.33	1.31	1.27	1.26	1.22	1.19
1.0	2.78	2.27	1.98	1.77	1.67	1.61	1.53	1.49	1.41	1.35
2.0	4.63	4.03	3.24	2.65	2.38	2.18	2.04	1.93	1.76	1.64
3.0	6.63	6.26	4.72	3.6	3.09	2.77	2.53	2.37	2.11	1.93
4.0	8.8	8.97	6.42	4.61	3.84	3.37	3.03	2.8	2.45	2.22

Table 8-4. Continued.

	Energy (MeV)									
μx	**0.1**	**0.5**	**1**	**2**	**3**	**4**	**5**	**6**	**8**	**10**
5.0	11.1	12.2	8.33	5.68	4.61	3.98	3.54	3.25	2.81	2.51
6.0	13.6	15.9	10.4	6.8	5.4	4.6	4.05	3.69	3.16	2.8
7.0	16.3	20.2	12.7	7.97	6.2	5.23	4.57	4.14	3.51	3.1
8.0	19.2	25.0	15.2	9.18	7.03	5.86	5.09	4.6	3.87	3.4
10.0	25.6	36.4	20.7	11.7	8.71	7.15	6.15	5.52	4.59	4.01
15.0	44.9	75.6	37.2	18.6	13.1	10.5	8.85	7.86	6.43	5.57
20.0	69.1	131	57.1	26.0	17.7	13.9	11.6	10.2	8.31	7.19
25.0	97.9	203	80.1	33.9	22.5	17.4	14.4	12.7	10.2	8.86
30.0	131	290	106	42.2	27.4	20.9	17.3	15.2	12.2	10.6

The *buildup factor B* is dependent on the absorbing medium, the photon energy, the attenuation coefficient for specific energy photons in the medium, and the absorber thickness x. The latter two are depicted in Table 8-4 as μx which is dimensionless and is commonly referred to as the number of mean free paths or the number of relaxation lengths, the value that reduces the initial flux (or exposure) by $1/e$ (the mean free path can be thought of as the mean distance a photon travels in an absorber before it undergoes an absorption or scattering interaction that removes it from the initial beam). It is also clear from Table 8-4 that B can be quite large, especially for low-energy photons, and that calculations of the radiation exposure associated with a beam of photons would be significantly in error if it were not included.

The buildup factors presented in Table 8-4 are for exposure in air after penetration through the absorber or shielding material. Other types of buildup factors also exist, in particular energy absorption buildup factors for energy deposition in an absorbing medium and dose buildup factors for absorbing media. Since a primary assessment in radiation protection is the exposure field before and after use of a radiation shield, exposure buildup factors (as provided in Table 8-4) are of most general use with appropriate adjustments of the air exposure to obtain absorbed dose.

8.3.4 Use of Buildup Factors

Estimates of photon fields under poor geometry conditions are made by first using good geometry conditions and then adjusting the results to account for the buildup of scattered photons, as follows:

1. First, determine the total attenuation of the beam in good geometry by calculating the change in intensity for the energy/absorber combination as

$$I(x) = I_0 e^{-\mu x}$$

where $I(x)$ is the unscattered intensity (flux, exposure, etc.) and μ is the linear attenuation coefficient (cm^{-1}).

2. Next, the unscattered intensity is multiplied by the buildup factor for the particular photon energy/absorber combination:

$$I_b(x) = B I_0 e^{-\mu x}$$

where B is obtained for the absorber in question, the photon energy, and the particular value of μx (or number of mean free paths (mfp)). It is usually necessary to interpolate between the energies and the μx values (sometimes both) to obtain the proper value. This procedure is illustrated in Example 8-5.

Example 8-5. A beam of 1.0 MeV gamma rays is emitted from a point source and produces a flux of 10,000 γ/cm^2 s. If 2 cm of iron is placed in the beam, what is the best estimate of the flux after passing through the shield?
Solution. First determine the flux based on narrow beam conditions. The attenuation coefficient for 1 MeV photons in iron is 0.472 cm^{-1} and the value of μ (or mfp) for 2 cm of iron is 0.944; therefore, the attenuated unscattered flux would be

$$I(x) = I_0 e^{-\mu x} = 10{,}000\ \gamma/cm^2\ s \times e^{-0.472 \times 2\ cm}$$

$$= 3890\ \gamma/cm^2\ s$$

This needs to be adjusted by the buildup factor which is determined by interpolation from Table 8-4 as ~1.8, and the best estimate of $I_b(x)$ is

$$I_b(x) = 1.8 \times 3890 \cong 7000\ \gamma/cm^2\ s$$

This same approach is also used if $I(x)$ is in units of exposure rate, energy flux, or absorbed dose rate since these quantities are based on the photon flux which is the quantity that is measured in determining values of μ for different absorbers.

Example 8-6. A fluence of 10^5 γ/cm^2 of 1.5 MeV photons strikes a 2 cm thick piece of lead. What is the best estimate of the total energy that reaches a receptor beyond the lead shield?

Solution. The linear attenuation coefficient μ for 1.5 MeV photons in lead is 0.5927 cm^{-1}, and for good geometry

$$I(x) = 10^5\ \gamma/cm^2 \times e^{-(0.5927)(2)}$$

$$= 3.06 \times 10^4\ \gamma/cm^2$$

From Table 8-4, the buildup factor for 1.5 MeV photons in lead for $\mu x = 1.185$ is found by interpolation to be 1.45, and the buildup fluence is

$$I_b(x) = BI_0e^{-\mu x} = 1.45(3.06 \times 10^4) = 4.43 \times 10^4\ \gamma/cm^2$$

which contains primary beam photons and scattered photons of lower energy; however, despite the presence of lower energy scattered photons, the best estimate of the energy fluence is, conservatively

$$I_b(x)_E = 4.43 \times 10^4\ \gamma/cm^2 \times 1.5\ MeV = 6.65 \times 10^4\ MeV/cm^2$$

8.3.5 Effect of Buildup on Shield Thickness

The exposure rate in air for unscattered photons of energy E is

$$\text{Exposure}(mR/h) = \frac{\phi E \times 1.6022 \times 10^{-6}\ erg/MeV \times (3600\ s/h) \times (\mu_{en}/\rho)_{air}}{87.64\ erg/g\ R \times 10^{-3}\ R/mR}$$

or

$$\text{Exposure (mR/h)} = 0.0658\ \phi E(\mu_{en}/\rho)_{air}$$

where ϕ = flux of photons/cm^2 s and $(\mu_{en}/\rho)_{air}$ is the energy absorption coefficient in air for photons of energy E. If a shield or other absorber is placed between the photon source and a receptor, it is necessary to introduce a buildup factor B to account for an increase in the exposure due to buildup of scattered photons:

$$\text{Exposure (mR/h)} = 0.0658\ \phi BE(\mu_{en}/\rho)_{air}e^{-\mu x}$$

such that the exposure is directly proportional to $(\mu_{en}/\rho)_{air}$, B, and $e^{-\mu x}$ of the absorber, all of which vary with photon energy. The buildup factor B and the exponential attenuation factor $e^{-\mu x}$ are also a function of μx which can complicate calculations of the shield thickness x to reduce a photon intensity from I_0 to $I(x)$.

The appropriate thickness for a given reduction usually requires successive approximations, and the process becomes one of homing in on the correct value of x by iterative calculations. For most circumstances B increases slowly with x while the exposure rate decreases exponentially and at a faster rate; these various complexities are illustrated in Example 8-7.

Example 8-7. Determine the thickness of an iron shield needed to reduce the exposure rate from a point source that emits 10^8 1 MeV photons to 1 mR/h at 60 cm.
Solution. First, determine the thickness x of a shielding material for narrow-beam geometry with $B = 1$; this underestimates the shield thickness, but it can then be increased by adding thicknesses of absorber until the appropriate values of x and B are obtained and the exponential function yields the desired reduction in I_0.

The value of $(\mu_{en}/\rho)_{air}$ for 1 MeV photons in air from Table 8-2 is 0.0279 cm^2/g and the flux that produces 1 mR/h is

$$\phi = \frac{1\,\text{mR/h}}{0.0658 \times 1\,\text{MeV} \times 0.0279} = 544.7\,\gamma/\text{cm}^2\ \text{s}$$

The flux at 60 cm from a point source that emits 10^8 photons (i.e., without shielding) is

$$\phi = \frac{10^8\,\gamma/\text{cm}^2\ \text{s}}{4\,\pi(60)^2} = 2.21 \times 10^3\,\gamma/\text{cm}^2\ \text{s}$$

The linear attenuation coefficient for 1 MeV photons in iron is 0.472 cm^{-1} and the value of x required without a buildup factor is determined as

$$544.7 = 2.21 \times 10^3 e^{-0.472\,\text{cm}^{-1}x}$$

or

$$x = 2.97\ \text{cm}$$

and

$$\mu x = 1.40$$

The buildup factor is found by interpolation in Table 8-4 to be 2.25, and the calculated exposure based on good geometry attenuation is, as expected, well above 1 mR/h. If the amount of iron used is 6.0 cm, μx becomes 2.83, B is about 3.8 and the flux is

$$\phi = 2.2 \times 10^3 \times 3.8 e^{-2.83}$$

$$= 493\ \gamma/\text{cm}^2\ \text{s}$$

which is just below the flux (545 γ/cm^2 s) that produces 1 mR/h; thus, the appropriate shield thickness is about 6 cm of iron.

The iterative process in Example 8-7 can be made more exact by a computer program or by plotting ϕ versus μx on semilog paper. Such plots produce a near-straight line from which the appropriate value of μx that corresponds to the desired flux can be determined.

8.3.6 Mathematical Formulations of the Buildup Factor

Buildup factors can be calculated by using one of several mathematical approximations, each of which is developed as an equation-of-fit for the experimental data. The primary use of the mathematical formulation is in analytical solutions for complex geometries where it is useful to include a formulation of B as a varying quantity in the solution; if, however, the conditions of the problem are fixed, it is easier and more accurate to use tables of B. Two approximations, known as the Berger or Taylor forms after their developers, are widely used. The Berger form is somewhat complex to use even though it is one of the more accurate formulations for B. The Taylor form which is based on a sum of exponentials, however, has found wide use for problems in which values of x, which influences both attenuation and buildup, are to be determined. The Taylor form of the buildup factor as a function of photon energy E and μx is

$$B(E,\mu x) = Ae^{-\alpha_1 \mu x} + (1 - A)e^{-\alpha_2 \mu x}$$

where A, α_1 and α_2 are fitting parameters for the particular absorber and photon energy. These are listed in Table 8-5. The Taylor form of the buildup factor is generally accurate but needs to be used with caution for low-energy photons in low-Z material. It should also be remembered that the fitting parameters are based on older data whereas the buildup factors listed in Table 8-4 are much more recent.

Table 8-5. Values of fitting parameters for the Taylor form of the buildup factor.

Material	E (MeV)	A	α_1	α_2
Water	0.5	100.845	0.12687	–0.10925
	1	19.601	0.09037	–0.02520
	2	12.612	0.53200	0.01932
	3	11.110	0.03550	0.03206
	4	11.163	0.02543	0.03025
	6	8.385	0.01820	0.01640
	8	4.635	0.02633	0.07097
	10	3.545	0.02991	0.08717

Table 8-5. Continued.

Material	*E* (MeV)	A	α_1	α_2
Aluminum	0.5	38.911	0.10015	–0.06312
	1	28.782	0.06820	–0.02973
	2	16.981	0.04588	0.00271
	3	10.583	0.04066	0.02514
	4	7.526	0.03973	0.03860
	6	5.713	0.03934	0.04347
	8	4.716	0.03837	0.04431
	10	3.999	0.03900	0.04130
Barytes concrete	0.5	33.026	0.06129	–0.02883
	1	23.014	0.06255	–0.02217
	2	9.350	0.05700	0.03850
	3	6.269	0.06064	0.04440
	4	4.730	0.06500	0.05883
	6	3.240	0.08000	0.06407
	8	2.167	0.09514	0.07857
	10	1.433	0.11201	0.13021
Ferrophosphorus concrete	0.5	61.341	0.07292	–0.05264
	1	46.087	0.05202	–0.02845
	2	14.790	0.04720	0.00867
	3	10.399	0.04290	0.02211
	4	6.240	0.05280	0.03765
	6	4.425	0.05880	0.04262
	8	3.000	0.06750	0.05730
	10	2.279	0.07575	0.06438
Ordinary concrete	0.5	38.225	0.14824	–0.10579
	1	25.507	0.07230	–0.01843
	2	18.089	0.04250	0.00849
	3	13.640	0.03200	0.02022
	4	11.460	0.02600	0.02450

Table 8-5. Continued.

Material	*E* (MeV)	A	α_1	α_2
	6	10.781	0.01520	0.02925
	8	8.972	0.01300	0.02979
	10	4.015	0.02880	0.06844
Magnetite concrete	0.5	75.471	0.07479	–0.05534
	1	49.916	0.05195	0.02796
	2	14.260	0.04692	0.01531
	3	8.160	0.04700	0.04590
	4	5.580	0.05200	0.05728
	6	3.437	0.06000	0.11520
	8	2.480	0.06645	0.14002
	10	1.743	0.08082	0.27209
Iron	0.5	31.379	0.06842	–0.03742
	1	24.957	0.06086	–0.02463
	2	17.622	0.04627	–0.00526
	3	13.218	0.04431	–0.00087
	4	9.624	0.04698	0.00175
	6	5.867	0.06150	–0.00186
	8	3.243	0.07500	0.02123
	10	1.747	0.09900	0.06627
Lead	0.5	1.677	0.03084	0.30941
	1	2.984	0.03503	0.13486
	2	5.421	0.03482	0.04379
	3	5.580	0.05422	0.00611
	4	3.897	0.08468	–0.02383
	6	0.926	0.17860	–0.04635
	8	0.368	0.23691	–0.05684
	10	0.311	0.24024	0.02783

Table 8-5. Continued.

Material	*E* (MeV)	A	α_1	α_2
Tin	0.5	11.440	0.01800	0.03187
	1	11.426	0.04266	0.01606
	2	8.783	0.05349	0.01505
	3	5.400	0.07440	0.02080
	4	3.496	0.09517	0.02598
	6	2.005	0.13733	–0.01501
	8	1.101	0.17288	–0.01787
	10	0.708	0.19200	0.01552
Tungsten	0.5	2.655	0.01740	0.11340
	1	3.234	0.04754	0.13058
	2	3.504	0.06053	0.08862
	3	4.722	0.06468	0.01404
	4	5.520	0.08857	–0.04570
	6	1.273	0.17257	–0.12178
	8	664.000	0.20710	0.04692
	10	0.509	0.21743	0.05025
Uranium	0.5	1.444	0.02459	0.35167
	1	2.081	0.03862	0.22639
	2	3.287	0.03997	0.08635
	3	4.883	0.04950	0.00981
	4	2.800	0.08240	0.00370
	6	0.975	0.15886	0.21101
	8	0.602	0.19189	0.02774
	10	0.399	0.21314	0.02083

A *single-term Taylor formulation of the buildup factor* in which a single exponential term accounts for absorber/thickness combinations is

B (E, μx) $B(E,\mu x) \approx A_1 e^{-\alpha_x \mu x}$

in which A_1 and α_x are fitting parameters (shown in Table 8-6) that depend on the initial gamma ray energy E, the attenuating medium, and μx. This approximation is almost exact for μx values of between 3 and 8 and within a few percent up to $\mu x = 12$. Below $\mu x = 3$, the one-term Taylor approximation overestimates the exposure by as much as a factor of 1.5.

Table 8-6. Fitting parameters for the single-term Taylor form of the buildup factor for $3 \le \mu x \le 8$.

E_0 (MeV)	Water		Concrete		Iron		Lead	
	A_1	α_x	A_1	α_x	A_1	α_x	A_1	α_x
0.2	5.5	–0.40	3.8	–0.28	2.2	–0.15		
0.5	3.7	–0.31	3.0	–0.27	2.4	–0.22	1.4	–0.06
1.0	2.9	–0.24	2.6	–0.23	2.3	–0.21	1.5	–0.10
1.5	2.6	–0.21	2.4	–0.20	2.2	–0.19	1.5	–0.11
2.0	2.4	–0.18	2.2	–0.18	2.1	–0.18	1.5	–0.13
5.0	1.8	–0.13	1.8	–0.14	1.6	–0.15	1.1	–0.17

A linear formulation of the buildup factor has also been developed and is expressed as

$$B(E, \mu x) = 1 + a_\ell(\mu x)$$

where E is the incident photon energy, μx is the number of mean free paths in the absorber material, and a_ℓ is a fitting parameter which is sometimes taken to be unity, a practice which should be eschewed except in special instances. Values of a_ℓ for water, aluminum, concrete, iron, tin, and lead are listed in Table 8-7 for values of $\mu x = 7$ and 20; however, since the expression is linear, these may be plotted in order to interpolate values of a_ℓ for other values of μx. This simpler formulation is not quite as accurate as the Taylor or Berger formulations, but is less cumbersome to use and generally produces acceptable results.

Table 8-7. Values of the fitting parameter a_ℓ for the linear buildup factor approximation $B(E, \mu x) \cong 1 + a_\ell(\mu x)$ for different absorbers.

Energy (MeV)	Values of a_ℓ in					
	Water	Concrete	Aluminum	Iron	Tin	Lead
$\mu x = 7$						
0.5	4.680	3.744	2.646	1.428	0.5153	0.1549
1.0	1.995	1.906	1.609	1.237	0.7199	0.2990
2.0	1.030	1.023	0.9686	0.8556	0.6731	0.3796
3.0	0.7397	0.7303	0.7197	0.6691	0.5837	0.3810
4.0	0.5884	0.5736	0.5663	0.5403	0.5146	0.3523
6.0	0.4321	0.4329	0.4334	0.4297	0.4153	0.3034
8.0	0.3406	0.3376	0.3476	0.3391	0.3317	0.2419
10	0.2877	0.2923	0.2847	0.2681	0.2550	0.1933
$\mu x = 20$						
0.5	13.093	5.012	5.737	2.377	0.5090	0.1043
1.0	3.479	2.992	2.539	1.864	0.8495	0.2549
2.0	1.255	1.233	1.193	1.119	0.8521	0.3947
3.0	0.7863	0.7857	0.8061	0.8446	0.8509	0.5123
4.0	0.5951	0.5942	0.6075	0.6942	0.8643	0.6378
6.0	0.4030	0.4145	0.4626	0.6134	1.079	1.125
8.0	0.3085	0.3200	0.3697	0.5245	1.171	1.417
10	0.2584	0.2737	0.3087	0.4759	1.108	1.237

Source: ORNL (1966).

The various mathematical formulations can be quite useful for calculations of complex geometries such as discs, slabs, and areal and volume sources as discussed in the next section.

8.4 Gamma Flux for Distributed Sources

Many calculations of radiation exposure/dose from photon sources are straightforward once the flux is known. A useful formulation is the flux at a distance r from an attenuated point source:

$$\phi(x) = \phi_0 \frac{e^{-\mu x}}{4\pi r^2}$$

The expression $e^{-\mu x}/4\pi r^2$ is referred to as the "point kernel" which is the response at a point r from a source of unit strength. The point kernel is used extensively in developing relationships between flux and exposure for various source geometries and absorbing media.

Although many radiation sources can, with its ease and utility, be represented as a point or an approximate point source, many real-world exposure conditions cannot. Typical examples are a long pipe or tube containing radioactive material which approximates a line source, a contaminated area that is representative of a disc or infinite planar source, and various volume sources. Practical approaches can be used to determine the photon flux from point kernels spread over such geometries, and once the flux has been determined it can then be applied in the usual way to calculate radiation exposure.

8.4.1 Line Sources

Line sources can often be practically considered as infinitely long with respect to a point P, located a distance x away from the lineal source as shown in Figure 8-4a. The differential flux $d\phi_\ell$ at a point P located a distance r from a point-sized element $d\ell$ that emits S_L gamma rays per centimeter of length is

$$d\phi_\ell = \frac{S_L}{4\pi r^2} d\ell$$

which can be integrated by substituting $\ell^2 + x^2$ for r^2. For an "infinite line" source the limits of integration are $-\infty$ and $+\infty$ and the flux at P is

$$\phi_{\ell,\infty}(\gamma/\text{cm s}) = S_L/4x$$

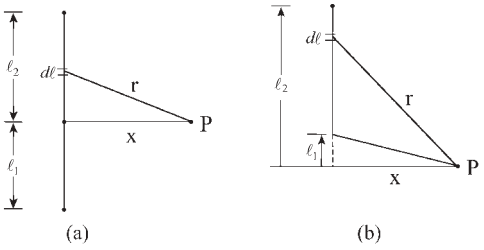

Fig. 8-4 Schematic of a line source of radioactive material that emits S_L gamma rays/s per centimeter over a finite length (ℓ_1 to ℓ_2) or is infinitely long ($\ell = \infty$) to produce a flux at P with (a) coordinates along the line, or (b) some distance from one end of the line source.

The photon flux for a "finite line" source is obtained by integration between $-\ell_1$ and $+\ell_2$, or

$$\phi_\ell = \frac{S_L}{4\pi x}\left[\tan^{-1}\left(\frac{\ell_2}{x}\right) + \tan^{-1}\left(\frac{\ell_1}{x}\right)\right]$$

where the $\tan^{-1}$ solutions are expressed in radians. For the geometry shown in Figure 8-4 the solution is such that the second term is $-\tan^{-1}(\ell_1/x)$ since in this case ℓ_1 is a fictitious source and thus must be subtracted.

Thus, the fluence or fluence rate from line sources of photon emitters varies as $1/x$, a very useful general rule.

Example 8-8. A worker must enter a 100 ft pipe tunnel to repair a valve 30 ft from one end. The pipe is estimated to emit 1.0 MeV gamma rays at a lineal rate of 10 γ/cm s. What is the flux (a) at 1 m from the pipe at the location of the valve, and (b) how much does the flux change if the pipe is assumed to be an infinite line source?

Solution. (a) The gamma flux at 30 ft from one end is

$$\phi_\ell = \frac{10\,\gamma/\text{cm s}}{4\pi(100\,\text{cm})}\left[\tan^{-1}\left(\frac{70\,\text{ft}}{3.281\,\text{ft}}\right) + \tan^{-1}\left(\frac{30\,\text{ft}}{3.281\,\text{ft}}\right)\right]$$

$$= 7.96 \times 10^{-3}\ (87.32\ + 83.76°)$$

and since one radian = 57.3°

$$\phi\ = 7.96 \times 10^{-3} \times 2.986 \text{ radians}$$

$$= 2.38 \times 10^{-2}\ \gamma/\text{cm}^2\ \text{s}$$

(b) An infinite line source with the same lineal emission rate would produce a flux of

$$\phi_{\ell,\infty} = \frac{S_L}{4x} = \frac{10\,\gamma/\text{cm}\ \cdot \text{s}}{4 \times 100\,\text{cm}} = 2.5 \times 10^{-2}\,\gamma/\text{cm}^2\ \text{s}$$

which overestimates the flux by about 5%.

Shielding of a line source is often done by placing a sheet of metal close to a pipe or rod containing the radioactive material or constructing an annular ring around the lineal source. Interposing shielding material between the line source and the receptor point of interest not only attenuates the photons emitted but introduces a scattered component that must be accounted for by an appropriate buildup factor. An *approximation* to the shielded photon flux at a point P away from the lineal source can be made by assuming that all photons penetrate through the shield in a perpendicular direction even though the true direction

from most points along the line will be along an angular (and longer) path through the shield. This approximation overestimates the flux and the resultant exposure rate by only a few percent and is reasonable to use in lieu of the more complex integration necessary to account for an angular distance that constantly varies.

Exact calculations of shield thicknesses for line sources and other distributed sources involve the Sievert integral function $F(\theta_i, \mu x)$, which adds more complexity than is necessary for most shielding problems in radiation protection. Such detailed calculations are justified in the design of shields for very high radiation areas such as hot cells and reactor walls where more exact solutions may represent considerable cost savings for building materials and supporting structures. LaMarsh has provided the elements of such calculations as has Morgan and Turner, and computer programs are available from the Radiation Shielding Information Center at Oak Ridge National Laboratory (see other suggested sources at the end of the chapter).

Example 8-9. What would be the photon flux in Example 8-8 if the 100 ft line source were to be enclosed in a 2 cm thick annular shield constructed of lead?
Solution. It is reasonable to assume all photons are emitted perpendicular to the pipe which simplifies the consideration of buildup; therefore,

$$\phi_s = \phi_{us} B e^{-\mu x}$$

where B is determined from Table 8-4 to be 1.56 for 1 MeV photons that penetrate 1.61 mean free path lengths of lead ($\mu x = 0.8061\ \text{cm}^{-1} \times 2\ \text{cm}$). The shielded flux is

$$\phi_s = (2.38 \times 10^{-2}\ \gamma/\text{cm}^2\ \text{s})(1.56)(e^{-1.61})$$

$$= 7.4 \times 10^{-3}\ \gamma/\text{cm}^2\ \text{s}$$

If, as shown in part (b) of example 8-8, an infinite line source is assumed, the flux would be $7.8 \times 10^{-3}\ \gamma/\text{cm}^2$ s. Since the primary beam contains 1 MeV photons, it can be conservatively estimated that the combination of scattered and unscattered photons yields an energy flux of 7.8×10^{-3} MeV/cm^2 s. The actual energy flux will be a mixture of 1 MeV photons and many lower-energy photons.

8.4.2 Ring Sources

Some sources are or can be modeled as a linear source in the shape of a ring of radius R and length $\ell = 2\pi R$. Such a ring source, if thin enough, is simply a curved line source, and if the photon emission rate is $S_L\ \gamma$/s per centimeter of length the differential flux $d\phi_\ell(P)$ at a point P in the center of the ring at a distance r from each differential segment $d\ell$ along the line is

$$d\phi_\ell(P) = \frac{S_L}{4\pi r^2} d\ell$$

and the total flux at P is

$$\phi_\ell(P) = \frac{S_L}{4\pi r^2} \ell$$

and since $\ell = 2\pi R$

$$\phi_\ell(P) = \frac{S_L}{2r^2} R$$

where $r^2 = x^2 + R^2$

Example 8-10. A 5 cm diameter pipe containing ^{60}Co with a lineal emission rate of 10^6 photons/cm s curves half-way around the ceiling of a circular room 6 m in diameter. What is the flux 1.5 m below the pipe in the center of the room?
Solution. Since the pipe is a half-circle, the flux can be computed for a ring source of radius $R = 3$ m, and the estimated flux for the half-circle will be one-half of this value; thus

$$\phi_\ell(P = 1.5\,\text{m}) = \frac{1}{2} \frac{10^6\ \gamma/\text{cm s} \times 3000\,\text{cm}}{2(1,500^2 + 3000^2)}$$

$$= 66.7\ \gamma/\text{cm}^2\ \text{s}$$

8.4.3 Disc and Planar Sources

Spill areas on floors and/or contaminated sites can produce a flux of gamma rays and an exposure field at points above them. These area sources can be modeled as a disc source made up of a series of annular rings as shown in Figure 8-5. If the activity is uniformly spread over the area such that gamma rays are emitted isotropically as S_A γ/cm^2 s, the differential flux contributed by each ring at a point P a distance x away from the center of the disc is

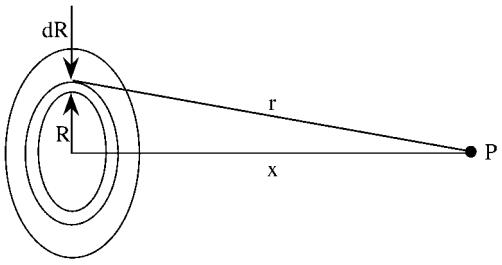

Fig. 8-5 Disc source with a uniform emission rate of S_A photons/s per unit area produces a differential flux at point P a distance r from a thin ring of width dR and area $2\pi RdR$.

$$d\phi = S_A \frac{2\pi R dR}{4\pi r^2} = S_A \frac{R dR}{2r^2}$$

The total unscattered flux at P is obtained by integrating over all annuli encompassed in the disc of radius R:

$$\phi(P) = \frac{S_A}{2} \int_0^R \frac{R dR}{r^2}$$

and since $r^2 = x^2 + R^2$

$$\phi_u(P)_A = \frac{S_A}{4} \ln\left(1 + \frac{R^2}{x^2}\right)$$

This is the general solution for all values of x, which is the distance of P from the center of a disc-shaped source with radius R. When the area source is very much larger than the distance x, as it typically is, the flux is

$$\phi_u(P)_A = \frac{S_A}{2} \ln\left(\frac{R}{x}\right), \quad R \gg x$$

Therefore, for large-area sources the gamma flux (and radiation exposure) decreases as $1/x$, and once the flux is determined it is used in the usual way for determining radiation exposure or absorbed dose.

8.4.4
Shield Designs for Area Sources

Shielding an area source with a slab to reduce gamma exposure is often the more practical problem since the unshielded exposure rate is usually measured after contamination occurs rather than calculated (an exposure level may also be forecast for a disposal location or a work area). In such cases, it may be necessary to determine the required thickness of a layer of concrete or other material that may be used to reduce an exposure rate to a desired level or perhaps a layer of soil to be placed atop a contaminated site for the same purpose.

If a shield of thickness a is placed between the disc source and the point P shown in Figure 8-5, the flux, minus any buildup effect, is obtained as before by integrating over a series of annular rings of radius R and width dR for S_A γ/cm^2 s emitted isotropically by the disc. The integration must also account for the exponential attenuation of the gamma rays by the shield; therefore, the unscattered flux at P from a ring of width dR and radius R with the shield in place is

$$\phi_u(P) = \frac{S_A 2\pi R dR e^{-\mu r_s}}{4\pi r^2}$$

where r_s is that segment of r that is taken up by the shield. The shield path length r_s equals a only when P is directly over the center of the disc; for all other paths through the shield $r_s > a$. It can be shown that r_s is related to ar, and since $r^2 = x^2 + R^2$ and $rdr = RdR$, the integral becomes

$$\phi_u(P)_{A,\infty} = \frac{S_A}{2}\int_0^\infty \frac{e^{-\mu r_s} RdR}{r^2} = \frac{S_A}{2}\int_0^\infty \frac{e^{-\mu r_s} dr}{r}$$

The integral, though simplified in terms of r, cannot be evaluated analytically. Such integrals are known as exponential integrals, and E-function tables of its solutions for values of x have been prepared for integer values of n where

$$E_n(x) = x^{n-1}\int_x^\infty \frac{e^{-t}}{t} dt$$

A *shielded infinite area source* can be expressed in terms of the E_1 function since the integral in the relationship for the uncollided flux $\phi(P)_{A,\infty}$ matches the case where $n = 1$ and $x = \mu a$; therefore

$$\phi_u(P)_{A,\infty} = \frac{S_A}{2} E_1(\mu a)$$

where $E_1(\mu a)$ is obtained for the value $x = \mu a$ from a table of the function. Plots of $E_n(x)$ can also be used but tables are more accurate, especially when it is necessary to interpolate between values of $E_n(x)$ as x changes. Values of the $E_1(x)$ function, which is encountered in many shielding problems, are contained in Table 8-8 along with the $E_2(x)$ function which is also encountered in such problems.

Values of $E_1(\mu x)$ when μx is very small or very large are often needed, and these can be obtained fairly accurately by a series calculation. For very small values of μx (≤0.1), the following approximation can be used

$$E_1(\mu x) = -0.577216 - \ln(\mu x)$$

For large values of μx (≥10)

$$E_1(\mu x) = e^{-\mu x}\left[\frac{1}{(\mu x + 1)} + \frac{1}{(\mu x + 1)^3}\right]$$

These approximations are accurate to a few percent, however, the best accuracy is obtained from the tabulations of $E_1(x)$ in Table 8-8.

Table 8-8. Tabulations of the $E_1(x)$ and $E_2(x)$ functions for photons where $x = \mu a$.

x	$E_1(x)$	$E_2(x)$	x	$E_1(x)$	$E_2(x)$	x	$E_1(x)$	$E_2(x)$	x	$E_1(x)$	$E_2(x)$
0.00	0.000	1.000	0.40	7.024	3.894	0.80	3.106	2.009	1.20	1.584	1.111
0.01	4.038	9.497	0.41	6.859	3.824	0.81	3.050	1.978	1.21	1.559	1.095
0.02	3.355	9.131	0.42	6.700	3.756	0.82	2.996	1.948	1.22	1.535	1.080
0.03	2.959	8.817	0.43	6.546	3.690	0.83	2.943	1.918	1.23	1.511	1.065
0.04	2.681	8.535	0.44	6.397	3.626	0.84	2.891	1.889	1.24	1.487	1.050
0.05	2.468	8.278	0.45	6.253	3.562	0.85	2.840	1.860	1.25	1.464	1.035
0.06	2.295	8.040	0.46	6.114	3.500	0.86	2.790	1.832	1.26	1.441	1.020
0.07	2.151	7.818	0.47	5.979	3.440	0.87	2.742	1.804	1.27	1.419	1.006
0.08	2.027	7.610	0.48	5.848	3.381	0.88	2.694	1.777	1.28	1.397	9.920
0.09	1.919	7.412	0.49	5.721	3.323	0.89	2.647	1.750	1.29	1.376	9.781
0.10	1.823	7.225	0.50	5.598	3.266	0.90	2.602	1.724	1.30	1.355	9.645
0.11	1.737	7.048	0.51	5.478	3.211	0.91	2.557	1.698	1.31	1.334	9.510
0.12	1.660	6.878	0.52	5.362	3.157	0.92	2.513	1.673	1.32	1.313	9.378
0.13	1.589	6.715	0.53	5.250	3.104	0.93	2.470	1.648	1.33	1.293	9.247
0.14	1.524	6.560	0.54	5.140	3.052	0.94	2.429	1.623	1.34	1.274	9.119
0.15	1.464	6.410	0.55	5.034	3.001	0.95	2.387	1.599	1.35	1.254	8.993
0.16	1.409	6.267	0.56	4.930	2.951	0.96	2.347	1.576	1.36	1.235	8.868
0.17	1.358	6.128	0.57	4.830	2.902	0.97	2.308	1.552	1.37	1.216	8.746
0.18	1.310	5.995	0.58	4.732	2.855	0.98	2.269	1.530	1.38	1.198	8.625
0.19	1.265	5.866	0.59	4.636	2.808	0.99	2.231	1.507	1.39	1.180	8.506
0.20	1.223	5.742	0.60	4.544	2.762	1.00	2.194	1.485	1.40	1.162	8.389
0.21	1.183	5.622	0.61	4.454	2.717	1.01	2.157	1.463	1.41	1.145	8.274
0.22	1.145	5.505	0.62	4.366	2.673	1.02	2.122	1.442	1.42	1.128	8.160
0.23	1.110	5.393	0.63	4.280	2.630	1.03	2.087	1.421	1.43	1.111	8.048
0.24	1.076	5.283	0.64	4.197	2.587	1.04	2.052	1.400	1.44	1.094	7.938
0.25	1.044	5.177	0.65	4.115	2.546	1.05	2.019	1.380	1.45	1.078	7.829
0.26	1.014	5.074	0.66	4.036	2.505	1.06	1.986	1.360	1.46	1.062	7.722
0.27	9.849	4.974	0.67	3.959	2.465	1.07	1.953	1.340	1.47	1.046	7.617
0.28	9.573	4.877	0.68	3.883	2.426	1.08	1.922	1.321	1.48	1.030	7.513

Table 8-8. Continued.

x	$E_1(x)$	$E_2(x)$	x	$E_1(x)$	$E_2(x)$	x	$E_1(x)$	$E_2(x)$	x	$E_1(x)$	$E_2(x)$
0.29	9.309	4.783	0.69	3.810	2.387	1.09	1.890	1.302	1.49	1.015	7.411
0.30	9.057	4.691	0.70	3.738	2.349	1.10	1.860	1.283	1.50	1.000	7.310
0.31	8.815	4.602	0.71	3.668	2.312	1.11	1.830	1.264	1.51	9.854	7.211
0.32	8.583	4.515	0.72	3.599	2.276	1.12	1.801	1.246	1.52	9.709	7.113
0.33	8.361	4.430	0.73	3.532	2.240	1.13	1.772	1.228	1.53	9.567	7.017
0.34	8.147	4.348	0.74	3.467	2.205	1.14	1.743	1.211	1.54	9.426	6.922
0.35	7.942	4.267	0.75	3.403	2.171	1.15	1.716	1.193	1.55	9.288	6.828
0.36	7.745	4.189	0.76	3.341	2.137	1.16	1.688	1.176	1.56	9.152	6.736
0.37	7.554	4.112	0.77	3.280	2.104	1.17	1.662	1.160	1.57	9.019	6.645
0.38	7.371	4.038	0.78	3.221	2.072	1.18	1.635	1.143	1.58	8.887	6.555
0.39	7.194	3.965	0.79	3.163	2.040	1.19	1.609	1.127	1.59	8.758	6.467

x	$E_1(x)$	$E_2(x)$	x	$E_1(x)$	$E_2(x)$	x	$E_1(x)$	$E_2(x)$	x	$E_1(x)$	$E_2(x)$
1.60	8.631	6.380	2.0	4.890	3.753	6.0	3.601	3.183	10.0	4.157	3.830
1.61	8.506	6.295	2.1	4.261	3.297	6.1	3.211	2.842	10.1	3.727	3.436
1.62	8.383	6.210	2.2	3.719	2.898	6.2	2.864	2.539	10.2	3.342	3.083
1.63	8.261	6.127	2.3	3.250	2.550	6.3	2.555	2.268	10.3	2.997	2.767
1.64	8.142	6.045	2.4	2.844	2.246	6.4	2.279	2.027	10.4	2.687	2.483
1.65	8.025	5.964	2.5	2.491	1.980	6.5	2.034	1.811	10.5	2.410	2.228
1.66	7.909	5.884	2.6	2.185	1.746	6.6	1.816	1.619	10.6	2.162	2.000
1.67	7.796	5.806	2.7	1.918	1.541	6.7	1.621	1.447	10.7	1.939	1.795
1.68	7.684	5.729	2.8	1.686	1.362	6.8	1.448	1.294	10.8	1.740	1.611
1.69	7.574	5.652	2.9	1.482	1.203	6.9	1.293	1.157	10.9	1.561	1.446
1.70	7.465	5.577	3.0	1.305	1.064	7.0	1.155	1.035	11.0	1.400	1.298
1.71	7.359	5.503	3.1	1.149	9.417	7.1	1.032	9.259	11.1	1.256	1.166
1.72	7.254	5.430	3.2	1.013	8.337	7.2	9.219	8.283	11.2	1.127	1.047
1.73	7.151	5.358	3.3	8.939	7.384	7.3	8.239	7.411	11.3	1.012	9.398
1.74	7.049	5.287	3.4	7.891	6.544	7.4	7.364	6.632	11.4	9.080	8.439
1.75	6.949	5.217	3.5	6.970	5.802	7.5	6.583	5.935	11.5	8.150	7.578

Table 8-8. Continued.

x	$E_1(x)$	$E_2(x)$	x	$E_1(x)$	$E_2(x)$	x	$E_1(x)$	$E_2(x)$	x	$E_1(x)$	$E_2(x)$
1.76	6.850	5.148	3.6	6.160	5.146	7.6	5.886	5.312	11.6	7.315	6.805
1.77	6.753	5.080	3.7	5.448	4.567	7.7	5.263	4.756	11.7	6.566	6.112
1.78	6.658	5.013	3.8	4.820	4.054	7.8	4.707	4.258	11.8	5.895	5.490
1.79	6.564	4.947	3.9	4.267	3.600	7.9	4.210	3.812	11.9	5.292	4.931
1.80	6.471	4.882	4.0	3.779	3.198	8.0	3.767	3.414	12.0	4.751	4.429
1.81	6.380	4.817	4.1	3.349	2.842	8.1	3.370	3.057	12.1	4.266	3.979
1.82	6.290	4.754	4.2	2.969	2.527	8.2	3.015	2.738	12.2	3.830	3.574
1.83	6.202	4.691	4.3	2.633	2.247	8.3	2.699	2.453	12.3	3.440	3.211
1.84	6.115	4.630	4.4	2.336	1.999	8.4	2.415	2.198	12.4	3.089	2.885
1.85	6.029	4.569	4.5	2.073	1.779	8.5	2.162	1.969	12.5	2.774	2.592
1.86	5.945	4.509	4.6	1.841	1.583	8.6	1.936	1.764	12.6	2.491	2.329
1.87	5.862	4.450	4.7	1.635	1.410	8.7	1.733	1.581	12.7	2.238	2.093
1.88	5.780	4.392	4.8	1.453	1.255	8.8	1.552	1.417	12.8	2.010	1.881
1.89	5.700	4.335	4.9	1.291	1.118	8.9	1.390	1.270	12.9	1.805	1.690
1.90	5.620	4.278	5.0	1.148	9.965	9.0	1.245	1.138	13.0	1.622	1.519
1.91	5.542	4.222	5.1	1.021	8.881	9.1	1.115	1.020	13.1	1.457	1.365
1.92	5.465	4.167	5.2	9.086	7.917	9.2	9.988	9.149	13.2	1.309	1.227
1.93	5.390	4.113	5.3	8.086	7.060	9.3	8.948	8.203	13.3	1.176	1.103
1.94	5.315	4.059	5.4	7.198	6.296	9.4	8.018	7.356	13.4	1.057	9.914
1.95	5.241	4.007	5.5	6.409	5.617	9.5	7.185	6.596	13.5	9.495	8.912
1.96	5.169	3.955	5.6	5.708	5.012	9.6	6.439	5.916	13.6	8.532	8.011
1.97	5.098	3.903	5.7	5.085	4.473	9.7	5.771	5.306	13.7	7.667	7.202
1.98	5.027	3.853	5.8	4.532	3.992	9.8	5.173	4.759	13.8	6.890	6.475
1.99	4.958	3.803	5.9	4.039	3.564	9.9	4.637	4.269	13.9	6.193	5.821

Table 8-8. Continued.

x	$E_1(x)$	$E_2(x)$	x	$E_1(x)$	$E_2(x)$	x	$E_1(x)$	$E_2(x)$
14.0	5.566	5.234	18.2	6.511(–10)	6.201(–10)	22.4	8.004	7.687
14.1	5.002	4.706	18.3	5.860(–10)	5.582(–10)	22.5	7.212	6.927
14.2	4.496	4.232	18.4	5.275(–10)	5.027(–10)	22.6	6.498	6.242
14.3	4.042	3.805	18.5	4.749(–10)	4.526(–10)	22.7	5.854	5.625
14.4	3.633	3.422	18.6	4.275(–10)	4.075(–10)	22.8	5.275	5.069
14.5	3.266	3.077	18.7	3.848(–10)	3.669(–10)	22.9	4.753	4.568
14.6	2.936	2.767	18.8	3.464(–10)	3.304(–10)	23.0	4.283	4.117
14.7	2.640	2.489	18.9	3.119(–10)	2.975(–100	23.1	3.859	3.710
14.8	2.373	2.238	19.0	2.808(–10)	2.679(–10)	23.2	3.477	3.344
14.9	2.134	2.013	19.1	2.528(–10)	2.413(–10)	23.3	3.133	3.014
15.0	1.919	1.811	19.2	2.276(–10)	2.173(–10)	23.4	2.824	2.716
15.1	1.725	1.629	19.3	2.049(–10)	1.957(–10)	23.5	2.544	2.448
15.2	1.551	1.465	19.4	1.845(–10)	1.762(–10)	23.6	2.293	2.206
15.3	1.395	1.318	19.5	1.661(–10)	1.587(–10)	23.7	2.066	1.988
15.4	1.255	1.186	19.6	1.496(–10)	1.429(–10)	23.8	1.862	1.792
15.5	1.128	1.067	19.7	1.347(–10)	1.287(–10)	23.9	1.678	1.615
15.6	1.015	9.595	19.8	1.213(–10)	1.159(–10)	24.0	1.512	1.456
15.7	9.126	8.633	19.9	1.092(–10)	1.044(–10)	24.1	1.363	1.312
15.8	8.208	7.767	20.0	9.836	9.405	24.2	1.228	1.183
15.9	7.383	6.988	20.1	8.857	8.471	24.3	1.107	1.066
16.0	6.640	6.287	20.2	7.976	7.630	24.4	9.977	9.611
16.1	5.973	5.657	20.3	7.183	6.873	24.5	8.992	8.664
16.2	5.373	5.090	20.4	6.469	6.191	24.6	8.105	7.810
16.3	4.834	4.581	20.5	5.826	5.577	24.7	7.305	7.040
16.4	4.348	4.122	20.6	5.247	5.023	24.8	6.584	6.346
16.5	3.912	3.709	20.7	4.726	4.525	24.9	5.934	5.721
16.6	3.519	3.338	20.8	4.257	4.077	25.0	5.349	5.157

A *finite shielded area source* can also be represented in terms of the $E_1(x)$ function. An area source of radius R will produce an unscattered (uncollided) photon flux through a shield of thickness of

$$\phi_u(P)_{A,R} = \frac{S_A}{2}[E_1(\mu a) - E_1(\mu r)]$$

where r is the distance from P to the edge of the disc. The value of r can be calculated from $r^2 = x^2 + R^2$ or as $x\sec\theta$ (or $a\sec\theta$), where θ is the angle between x and r.

A *shielded infinite area source with a buildup factor* is used when scattered photons, which can be quite significant, combine with unscattered photons to produce a buildup flux $\phi_b(P)$ at P. An analytical solution of this situation requires one of the approximations for $B(\mu x)$ such as the Taylor form, which contains two exponential terms. This formulation yields an expression for the buildup flux at P for an infinite disc or planar source in terms of E_1 functions, or

$$\phi_b(P)_{A,\infty} = \frac{S_A}{2}\{AE_1[(1+a_1)\mu a] + (1-A)E_1[(1+a_2)\mu a]\}$$

where A, a_1, and a_2 are selected from Table 8-5 for the particular absorber and photon energy, and values of the E_1 function are obtained from Table 8-8.

Example 8-11. A large isotropic planar source emits 1 MeV gamma rays with a fluence rate of 10^7 γ/cm^2 s. If a 30 cm layer of concrete ($\rho = 2.35$) is poured over the area, what would be the adjusted fluence rate?

Solution. Since the planar source is large, it can be treated as a shielded infinite plane in which the buildup flux above the concrete layer using the Taylor approximation is

$$\phi_b(P)_{A,\infty} = \frac{S_A}{2}\{AE_1[(1+a_1)\mu a] + (1-A)E_1[(1+a_2)\mu a]\}$$

From Table 8-5, $A = 97.0$, $a_1 = -0.0396$, and $a_2 = -0.02710$; and from Table 8-2 $\mu/\rho = 0.0635$ cm^2/g (or $\mu = 0.14923$ cm^{-1}), and $\mu a = 4.4768$. Therefore

$$\phi_b(P)_{A,\infty} = \frac{10^7}{2}\{97.0E_1[(1-0.0396)4.4768] - 96.0E_1[(1-0.02710)4.4768]\}$$

$$= 5\times10^6[97.0E_1(4.30) - 5\times10^6\times96.0E_1(4.355)]$$

$$= 5\times10^6[(97.0\times2.633\times10^{-3}) - (96.0\times2.47\times10^{-3})]$$

$$= 5\times10^6[0.2554 - 0.2371] = 9.15\times10^4\ \gamma/cm^2\ s$$

As shown in the above example, it is relatively straightforward to obtain $\phi_b(P)_{A,\infty}$ when the shield thickness and the emission rate for photons of a given energy are

known; it is much more complex to obtain the shield thickness required to yield a predetermined flux (or exposure rate). The latter requires iterative calculations which are facilitated by plotting solutions of the equation on semilog paper for incremental values of μx. Iterative calculations of $\phi_b(P)_{A,\infty}$ for values of μx can also be performed by computer; in either case, once the appropriate value of μx is determined, the shield thickness x can be obtained directly.

A *shielded finite area source of radius R with buildup* also uses the Taylor approximation to obtain the buildup flux

$$\phi_b(P)_{A,R} = \frac{S_A A}{2}\{E_1[(1+\alpha_1)\mu a] - E_1[(1+\alpha_1)\mu r]\} + \frac{S_A}{2}(1-A) \times \{E_1[(1+\alpha_2)\mu a] - E_1[(1+\alpha_2)\mu r]\}$$

where r can be obtained from $r^2 = x^2 + R^2$ or $r = x\sec\theta$ where θ is the angle subtended between the line x perpendicular from the center of the area and the line from P to the outside edge. In essence this more detailed calculation is the same expression as for the infinite area source minus the portion that lies outside the radius R. Fortunately, most practical problems can be considered "infinitely large" and this refinement can often be neglected. Exposures calculated on the basis of infinite planar or area sources will be somewhat conservative for radiation protection purposes, i.e., higher than what actually occurs.

8.4.5
Gamma Exposure from Thick Slabs

Many sources are not strictly area sources because they may be a thick source (e.g., slab) that contains a uniformly distributed gamma-emitting isotope, with the effective surface activity being very much a function of the amount of self-absorption within the source. A thick slab is essentially a volume source that emits S_V γ/cm^3 s; however, this volume source can be adjusted to a surface source by accounting for self-absorption of radiation in the slab. If the linear absorption coefficient of the slab material is μ, the activity on the surface due to radioactivity in a differential layer dx at a depth of x in the slab is

$$dS_V = S_V \times dx \times e^{-\mu x}$$

which can be integrated over the total thickness t of the slab to obtain an effective surface activity of

$$S_A = \int_0^t S_V e^{-\mu x} dx = \frac{S_V}{\mu}(1 - e^{-\mu t})$$

This expression can then be used in the above relationship for the gamma flux at a point P above the slab:

$$\phi(P)_{V,t} = \frac{S_V}{4\mu}(1 - e^{-\mu t}) \ln\left(1 + \frac{R^2}{x^2}\right)$$

or for very large slabs where $R \gg x$

$$\phi(P)_{V,t} = \frac{S_V}{2\mu}(1 - e^{-\mu t}) \ln\left(\frac{R}{x}\right), \quad R \gg x$$

where $\phi(P)_{V,t}$ is the unscattered flux that exits from the thick slab. It does not, however, account for scattered photons produced within the slab itself, which requires a buildup factor again based on one of the mathematical formulations of B.

An *"infinite" slab source* is representative of a number of typical sources encountered in radiation protection. Such sources can be represented as a homogenous concentration in a slab of material, many of which are large enough to be considered as infinitely thick and infinite in area. Of course they are not, but if they are several inches thick and a few tens of square feet in area their detailed solution approaches one with infinite dimensions in which reasonable accuracy is obtained and the mathematics is much easier. Contaminated soils at a site are generally representative of this condition.

Schiager (1974) published a classic paper in which the unscattered flux above large-area thick slabs of gamma-emitting radioactive material can be represented in terms of the soil volume concentration S_V as

$$\phi(\gamma/\text{cm}^2\ s) = \frac{S_V}{2\mu}[1 - E_2(\mu x)]$$

where ϕ is the emission rate of gamma rays per unit area (γ/cm^2 s), S_V is the soil-volume emission rate (γ/cm^3 s), μ is the linear attenuation coefficient, and x is the slab thickness. The term in brackets has a rather difficult solution because $E_2(\mu x)$ is the second-order exponential integral (also listed in Table 8-8); however, when plotted as shown in Figure 8-6 for this special case of a very thick infinite plane its use is rather straightforward.

An *"infinite slab" buildup factor* is also necessary to obtain the total exposure rate because more scattered photons exit a large slab than uncollided primary photons. Unfortunately buildup factors are only available for point sources; however, a buildup factor for slab sources based on empirical data can be approximated as

$$B_{\text{Slab}} = e^{\mu x/(1 + \mu x)}$$

With these considerations, the total flux is

$$\phi(\gamma/\text{cm}^2\ \text{s}) = \frac{S_V}{2\mu}[1 - E_2(\mu x)]e^{\mu x/(1+\mu x)}$$

where the relationship $[1 - E_2(\mu x)]$ is readily obtained from Figure 8-6 (or calculated using the data in Table 8-8).

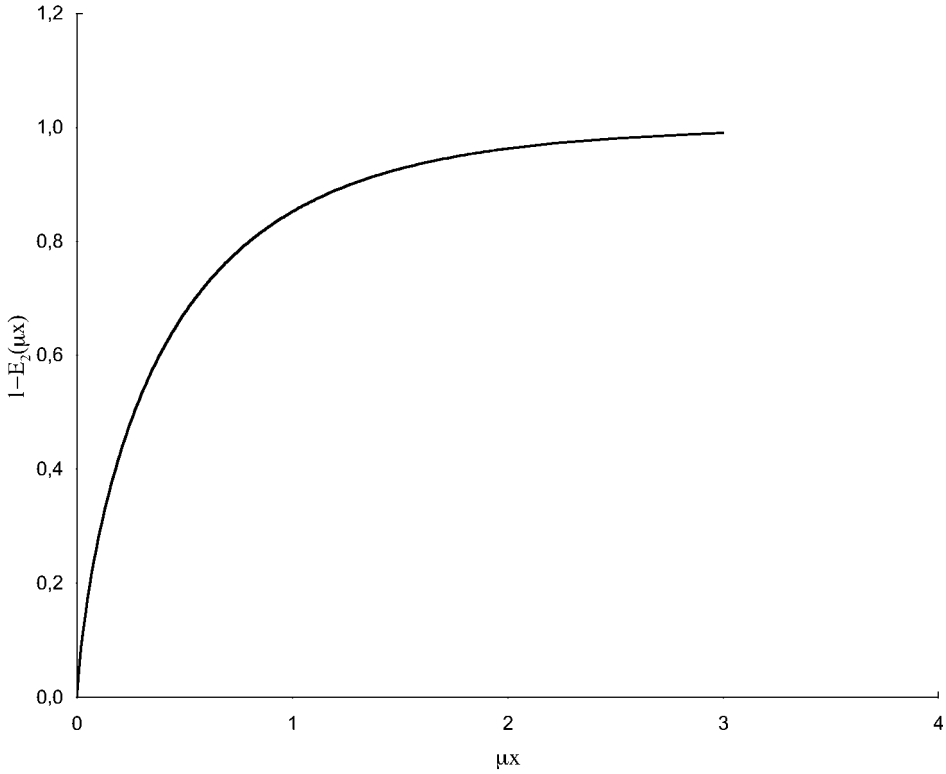

Fig. 8-6 Plot of the function $(1 - E_2)$ versus μx for large infinitely thick slab sources of gamma-emitting radioactive material.

The value of μ for dry or moist soils ($\rho = 1.6$) is about 0.11 cm^{-1} for 0.8 MeV photons and about 0.16 cm^{-1} for concrete ($\rho = 2.35$) and varies very slowly for thicknesses of these materials where x is greater than 30–60 cm. Many site conditions are typical of such depths, and for such conditions both $[1 - E_2(\mu x)]$ and B are essentially unity and the expression for the flux reduces to

$$\phi(\gamma/\mathrm{cm}^2\ \mathrm{s}) = \frac{S_V}{2\mu} e$$

This is not the case, however, when the thickness of the radioactive layer (typically soil or sediment) is less than 20 cm or so, and it is necessary to use the general equation with the factor $[1 - E_2(\mu x)]$ and the approximation for the slab buildup factor.

Radium-contaminated soils are a special case, although a fairly common one. The radioactive progeny of ^{226}Ra produce 2.184 photons per transformation of ^{226}Ra and these photons have an average energy of 0.824 MeV (Schiager 1974). The gamma constant for radium progeny photons is 0.84 R/h Ci of ^{226}Ra at 1 m and

2300 photons/cm^2 yield 1 μR; therefore, 1 pCi/g of ^{226}Ra will produce an unscattered flux of

$$\phi = 0.59\ \gamma/\text{cm}^2\ \text{s per pCi/g of } ^{226}\text{Ra}$$

The exposure rate due to the unscattered photons is $0.92C_{Ra}\ \mu$R/h, which needs to be adjusted by a buildup factor B to account for the importance of scattered photons. Since B can be approximated by $B = e^{\mu x/(1+\mu x)}$, the exposure rate for a ^{226}Ra concentration, C_{Ra} (pCi/g), is

$$\text{Exposure } (\mu\text{R/h}) = 0.92C_{Ra}e^{\mu x/(1+\mu x)}$$

When the thickness of the contaminated soil layer is 30–60 cm or more, μx becomes very large such that B changes very little and $B \approx e$, therefore

$$\text{Exposure}_{Ra}\ (\mu\text{R/h}) = 0.92eC_{Ra} = 2.5C_{Ra}$$

where C_{Ra} is in pCi/g. If, however, the radium soil layer is less than 30 cm or so, the practical approach would be to first calculate the exposure rate for an "infinitely thick" layer and adjust it by the factor Exp(x)/Exp(∞) obtained from Figure 8-7. It is important to note in Figure 8-7 the rapid change of Exp(x)/Exp(∞) for thin layers of contaminated soils; therefore, the accuracy of exposure determinations very much depend on accurate determinations, usually by field measure-

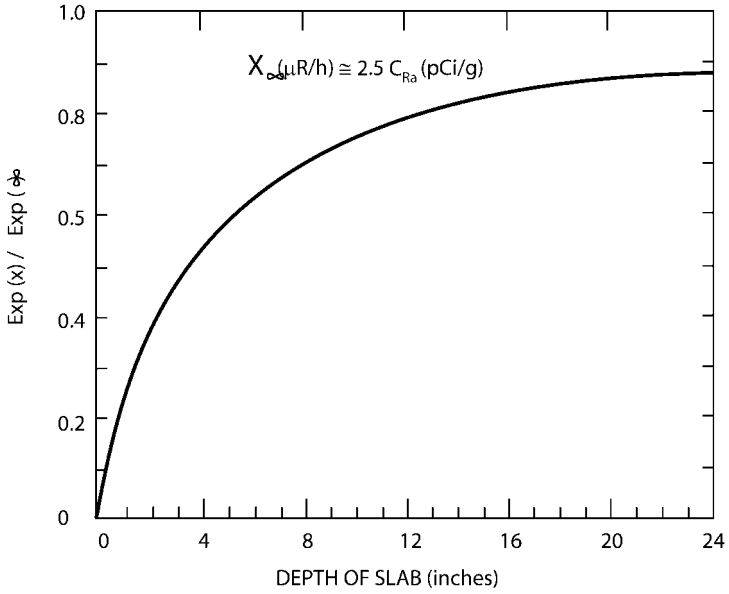

Fig. 8-7 Ratio of exposure rate Exp(x) for a slab of thickness x of gamma-emitting material and Exp(∞) for an infinitely thick and infinitely large slab of the same concentration.

Table 8-9. Parameters and exposure calculations for a 10 cm diameter pipe modeled as five 1 Ci "point" sources[a].

Point Source	Distance (cm)			μx		$B(\mu x)$		Attenuated flux at P (γ/cm^2 s)			Exposure in air (mR/h) × B	
	to P	in H_2O	in Pb	for H_2O	for Pb	for H_2O	for Pb	by air	by H_2O	by Pb	H_2O only	H_2O + Pb
1	116.6	5.83	3.50	0.503	4.51	1.58	1.76	1.84×10^5	1.11×10^5	2.02×10^3	224	4.53
2	104.4	5.22	3.13	0.450	4.03	1.56	1.71	2.29×10^5	1.46×10^5	4.07×10^3	290	8.88
3	100	5.00	3.00	0.631	3.87	1.55	1.70	2.5×10^5	1.62×10^5	5.21×10^3	321	11.30
4	104.4	5.22	3.13	0.450	4.03	1.56	1.71	2.29×10^5	1.46×10^5	4.07×10^3	290	8.88
5	116.6	5.83	3.50	0.503	4.51	1.58	1.76	1.84×10^5	1.11×10^5	2.02×10^3	224	4.53
										Total	1349	38.12

a Exposure rate in air for 0.662 MeV gamma rays is 1.276×10^{-6} R/h γ.

ments, of the thickness of the contaminated layer. These determinations have more influence on the calculated results than the analytical solutions used. If the contamination layer is covered with soil, H_2O, concrete, or other material it is necessary to determine the exposure rate as though the shielding material were absent and then calculate the exposure rate as a shielded area source (see above) where the shield is the thickness of cover material.

8.4.6 Volume Sources

Volume sources such as large drums or tanks of radioactive material produce scattered photons due to self-absorption by the medium in which they are produced. Radiation exposure calculations for these various cylindrical and spherical geometries is fairly complex; however, good information can be obtained for such geometries by dividing them up into several point source subdivisions and summing the contributions of each. Such calculations are generally conservative in that they tend to overestimate exposure, but considerable simplification of the calculations is obtained and errors in the estimates are not large. Detailed integration over many differential volume sources is of course more precise, and computerized calculations can be performed for numerous small-volume elements to increase accuracy and reduce the calculational burden.

Example 8-12. Estimate the exposure rate in air at 1 m (a) from the center of a 10 cm diameter plastic pipe if the pipe is 1.5 m long and contains 5 Ci of ^{137}Cs in H_2O, and (b) with a 3 cm thick lead shield between the pipe and the receptor.
Solution. The 1.5 m pipe is divided into 5 segments of 30 cm, each of which contains 1 Ci as shown in Figure 8-8.

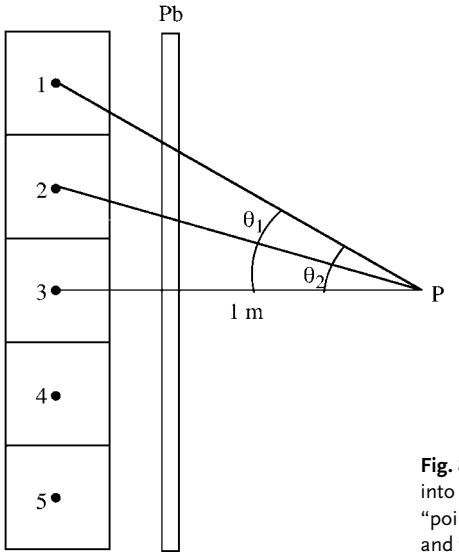

Fig. 8-8 Volume source of 5 Ci of ^{137}Cs divided into five segments and modeled as five 1 Ci "point" sources producing exposure at P with and without a lead shield.

The activity of each subvolume is assumed to be concentrated at a point in the center and the exposure at P is calculated for the "point sources" at 1, 2, and 3, and because of symmetry the exposures for 4 and 5 are the same as those of 1 and 2. The individual exposures are added to obtain the total. It is necessary to determine the distance between each point source and P, the angular thickness of water and Pb to be penetrated, the attenuation of flux by each of these thicknesses, and the buildup flux for each thickness. The results of these determinations, which are shown in Table 8-9, yield the following results: (a) exposure at P without the Pb shield is 1350 mR/h due to photon absorption and the buildup effect in the H_2O solution; (b) with the lead shield in place, the exposure rate is reduced to 38.1 mR/h.

Better accuracy and somewhat less conservatism (slightly lower total exposure) could be obtained by further subdividing the segments, perhaps into two lengthwise segments and then further dividing each of these into 9 segments.

8.4.7 Buildup Factors for Layered Absorbers

Example 8-12 is also illustrative of the influence of two different absorber media on photon absorption and transmission. When different photon absorbers are used in tandem even more complexity occurs because of the different effect presented by each. The most important consideration is the production of Compton scattered photons which can be quite large for low- to medium-energy photons in low-Z absorbers, factors which in turn also influence the buildup factor.

There are no precise methods for dealing with the complexities of absorber materials of different Z but a few general principles can be applied. First, a low-Z material (such as water) will result in a higher fraction of scattered photons than high-Z materials (e.g., lead); therefore, the low-Z absorber should be placed closest to the source and the high-Z material placed outside it to absorb the Compton scattered photons produced in the first absorber. If, for example, a source is shielded with a layer of lead and then enclosed in water the buildup flux would be considerably higher than the inverse because the photons entering the water would produce relatively more scattered photons (due to the dominance of the Compton interaction coefficient in water for low- to medium-energy photons (Figure 7-20), and these would not be absorbed in the water because photoelectric absorption is relatively low in a low-Z medium. If, however, the water shield is placed closest to the source, the scattered photons produced in it will be highly absorbed in lead by photoelectric interactions since it is a high-Z material. Although the buildup factor is higher in lead for low- to intermediate-energy photons, this is more than offset by its greater effect on attenuation and absorption. Therefore, when there is a choice, one should put the low-Z material first.

Similarly, the choice of a buildup factor for layered absorbers can be generalized as follows:

- If the atomic numbers of the two media do not differ by more than 5 to 10, then use the buildup factor of the medium for which this factor is the larger, but compute the overall buildup factor for the sum of both thicknesses since (except at low energy) the buildup factors do not vary rapidly with the Z of the medium.
- If the media are different, with the low-Z medium first, then use the buildup factor of the second medium as if the first medium were not there because the Compton scattered radiation from the first is of lower energy and can be expected to be absorbed in the second.
- If the media are significantly different, with the high-Z medium first, the procedure to be followed in this case depends upon whether the gamma ray energy is above or below the minimum in the μ-curve, which occurs at about 3 MeV for heavy elements. If $E < 3$ MeV, then

$$B(Z_1 + Z_2) = B_{Z1}(\mu_1 a_1) \times B_{Z2}(\mu_2 a_2)$$

This is because the energy of the photons emerging from a high-Z shield is little different from that of the source, and in the second medium the photons can be treated as if they were source gamma rays. If, however, $E > 3$ MeV, then

$$B(Z_1 + Z_2) = B_{Z1}(\mu_1 a_1) \times \mathrm{B}_{Z2}(\mu_2 a_2)_{\min}$$

where $\mathrm{B}_{Z2}(\mu_2 a_2)_{\min}$ is the value of B_{Z2} at 3 MeV. This assumes that the gamma rays penetrating the first layer have energies clustered about the minimum in μ, so that their penetration through the second layer is determined by this energy rather than by the actual source energy.

8.5 Shielding of Protons and Light Ions

Beams of protons, deuterons, tritons, and helium ions can be present around accelerators. Since all of these are charged particles with considerable mass they will ionize atoms in a shielding material and can be completely stopped in a short distance after giving up all of their energy. Since attenuation occurs by ionization (and not by probabilistic exponential processes) the range is definitive. Therefore, shielding for these particles follows the same principles as for beta and alpha particles, i.e., by determining the maximum range of the most energetic particles in the beam. Being charged particles, some bremsstrahlung may be produced, but this is very minor except perhaps for highly energetic particles (say above several tens of MeV).

Shield designs for high-energy protons are based on their range in matter as shown in Figure 8-9 for selected materials. Example 8-13 demonstrates the utility of these data.

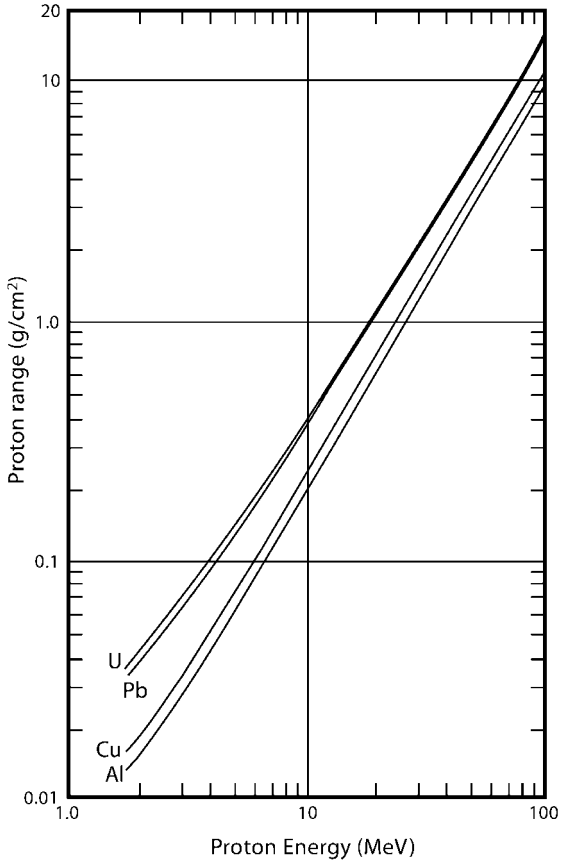

Fig. 8-9 Range versus energy of protons in uranium, lead, copper, and aluminum. (From NCRP 1977.)

Example 8-13. What thicknesses of lead and of aluminum are necessary to each attenuate completely a beam of 20 MeV protons?
Solution. From Figure 8-9, the range of 20 MeV protons in lead is 0.9 g/cm^2; therefore

$$x = \frac{R}{\rho} = \frac{0.9\,\text{g/cm}^2}{11.34\,\text{g/cm}^2} = 0.079\,\text{cm}$$

For aluminum, the range of 20 MeV protons is approximately 0.5 g/cm^2, and

$$x = \frac{R}{\rho} = \frac{0.5\,\text{g/cm}^2}{2.7\,\text{g/cm}^2} = 0.185\,\text{cm}$$

Obviously even light materials are effective in shielding energetic protons. One must be careful, however, to consider the production of other radiations by proton absorption interactions in the material chosen.

Shield designs for light ions are based on a reference thickness of penetration for a proton of a given energy. This reference value is then adjusted to account for the different mass and charge for deuterons, tritons, and helium ions.

The range of deuterons, tritons, and doubly charged helium ions of a given energy E are related to the range of protons in an absorber as follows:

$$R\,(^2\text{H}^+) = 2R_\text{p} \text{ at } E/2$$

$$R\,(^3\text{H}^+) = 3R_\text{p} \text{ at } E/3$$

$$R\,(\text{He}^{2+}) = R_\text{p} \text{ at } E/4$$

where the range of the respective particle of energy E is obtained by determining the proton range R_p at a lower energy and adjusting it by the appropriate factor, as shown in Example 8-14.

Example 8-14. What thickness of copper is required to attenuate completely 30 MeV tritons?
Solution. First determine the range of protons at $E/3$ = 10 MeV which is 0.23 g/cm^2. The range of 30 MeV tritons in copper is

$$R\,(^3\text{H}^+) = 3R_\text{p} = 0.695\ \text{g/cm}^2$$

which is provided by a thickness of

$$x = \frac{0.695\,\text{g/cm}^2}{8.92\,\text{g/cm}^2} = 0.077\,\text{cm}$$

8.6 Summary

Radiation shielding, which is a very complex discipline, is a form of radiation protection for many radiation sources and the many geometric configurations in which they may occur. Alpha particles and other light ions are easy to shield, usually by a sealer, since their relatively large mass and charge limit their range in most media to a few tens of micrometers. Shielding of beta particles from a source is also straightforward by choosing a thickness of medium that matches or exceeds the maximum range; however, since high-energy beta particles can produce bremsstrahlung, especially in high-Z materials, beta shields should use plastic, aluminum, or other low-Z material followed by lead or some other dense material to absorb any bremsstrahlung and characteristic x-rays that are produced in the beta shield.

Photon shields, unlike those for charged particles, are governed by the exponential, or probabilistic, attenuation of electromagnetic radiation, and the flux of shielded photons is a complex mixture of scattered and unscattered photons characterized as "poor geometry." A calculated value of $I(x)$ based on the attenuation coefficient μ, which is determined in "good geometry" conditions, will thus underestimate the number of photons reaching the receptor which implies that absorption is greater than what actually occurs. A buildup factor, $B > 1.0$, is used to correct good geometry calculations to more accurately reflect actual or poor geometry conditions.

Many radiation sources can, with its ease and utility, be represented as a point or an approximate point source; however, many real-world situations cannot, e.g., long pipes or tubes approximate a line source, a contaminated area that is representative of a disc or infinite planar source, and various volume sources. Fortunately, various practical calculations, some of which are fairly complex, can be used to determine the photon flux, which can then be applied in the usual way to calculate radiation exposure. Such calculations are generally conservative in that they tend to overestimate exposure, but considerable simplification of the calculations is obtained and errors in the estimates are not large.

Acknowledgments

Many of the data resources in this chapter came from the very helpful people at the National Institute of Standards and Technology, in particular Dr. John H. Hubbell and his colleagues M. J. Berger and S. M. Seltzer. Its assembly is due in large measure to the patient, careful, and untiring efforts of Chul Lee M.S., a graduate of the University of Michigan Radiological Health Program.

Other Suggested Sources

Berger, M. J., Selzer S. M. **1983**, *Stopping Powers and Ranges of Electrons and Positrons*, NBSIR 82-2550A, National Bureau of Standards, Washington, DC.
Chilton, A. B. **1977**, *Nucl. Sci. Eng.*, 64, 799–800.
Hubbell, J. H., Seltzer S. M. **1995**, *Tables of X-Ray Attenuation Coefficients and Mass Absorption Coefficients 1 keV to 20 MeV for Elements Z = 1 to 92 and 48 Additional Substances of Dosimetric Interest*, NIST, Gaithersburg, MD.
Lamarsh J. R. **1983**, *Introduction to Nuclear Engineering*, 2nd edn, Addison-Wesley, Reading, MA, Chapters 5 and 9.
Morgan, K. Z., Turner J. E. **1967**, *Principles of Radiation Dosimetry*, John Wiley, New York.
NCRP **1977**, *Radiation Protection Design Guidelines for 0.1–100 MeV Particle Accelerator Facilities*, Report No. 51, National Council on Radiation Protection and Measurements, Bethesda, MD.
Oak Ridge National Laboratory **1966**, Radiation Shielding and Information Center, Report 10, Oak Ridge, TN.
Schaeffer, N. M. (ed.) **1973**, *Reactor Shielding for Nuclear Engineers*, Report TID 25951, US Atomic Energy Commission.
Schiager K. J. **1974**, Analysis of radiation exposures on or near uranium tailings piles, *Radiation Data and Reports*, pp. 411–425.

Problems – Chapter 8

8–1. A surface is contaminated with alpha-emitting ^{239}Pu. If it is to be sealed with fiberglass resin ($\rho \approx 1.0$), how thick must it be to absorb all the alpha particles emitted?
8–2. A point source that emits beta particles at a rate of 10^7/s is to be shielded. If the maximum beta energy is 3.0 MeV, what thickness of aluminum would be required to attenuate the beta particles, and what thickness of lead would need to be included to reduce the photon flux at 50 cm by a factor of 10^3?
8–3. A 30 mL solution containing 2 Ci of ^{90}Sr in equilibrium with ^{90}Y is to be put into a small glass bottle, which will then be placed in a lead container having walls 1.5 cm thick. (a) How thick must the walls of the glass bottle be in order to prevent any beta rays from reaching the lead? (b) Estimate the bremsstrahlung dose rate at a distance of 1.5 m from the center of the lead container.
8–4. A small vial (approximately a point source) containing 200 Ci of ^{32}P in aqueous solution is enclosed in an 8 mm thick aluminum can. Calculate the thickness of lead shielding needed to reduce the exposure rate to 2.0 mR/h at a distance of 2 m from the can.
8–5. Show that the tenth-value layer for photons equals $2.30/\mu$, where μ is the total linear attenuation coefficient.

8–6. Assume that the exponent μx in the equation $I(x) = I_0 e^{-\mu x}$ is equal to or less than 0.1. Show that, with an error less than 1%, the number of photons transmitted is $I_0(1 - \mu x)$ and the number attenuated is $I_0 \mu x$. (Hint: expand the term $e^{-\mu x}$ into a series).

8–7. By what fraction will 2 cm of aluminum reduce a narrow beam of 1.0 MeV photons?

8–8. What thickness of copper is required to attenuate a narrow beam of 500 keV photons to one-half of the original number?

8–9. Calculate the thickness of lead shielding needed to reduce the exposure rate 2.5 m from a 16 Ci point source of ^{137}Cs to 1.0 mR/h if scattered photons are not considered, i.e., without buildup.

8–10. Recalculate the exposure rate for the shield design in Problem 8-9 when the buildup of scattered photons is considered.

8–11. How thick must a spherical lead container be in order to reduce the exposure rate 1 m from a small 100 mCi ^{24}Na source to 2.0 mR/h?

8–12. A beam of 500 keV photons is normally incident on a uranium sheet that is 1.5 cm thick. If the exposure rate in front of the sheet is 60 mR/h, what is it behind the sheet?

8–13. What thickness of lead shielding is needed around a 2000 Ci point source of ^{60}Co to reduce the exposure rate to 10 mR/h at a distance of 2 m?

8–14. An ion exchange column that contains radioactive materials that emits 5.5×10^6 1 MeV gamma rays per centimeter of length rests on the floor of a plant. This column is 9 m long and has a diameter of 0.5 m. What is the unshielded exposure rate at a point 12 m away and 1 m above the floor (ignore air attenuation and scatter from the floor and walls) if the gamma ray constant is 1.55 R/h per Ci at 1 m?

8–15. For Problem 8-14, estimate the approximate exposure rate behind a 2 cm thick lead shield placed around the ion exchange column.

8–16. A solution of ^{131}I containing an activity of 10^7 t/s is spilled on an approximately circular area 1 m in diameter. Determine the exposure rate 1 m above the center of the contaminated area.

8–17. A solution of ^{137}Cs with a concentration of 0.16 μCi/mL is to be mixed with concrete in a cylindrical plastic container 30 cm in diameter and 28 cm long. What exposure rate will the ^{137}Cs concrete mixture ($\rho = 2.35$) produce at 1 m from the 30 cm diameter surface?

8–18. Radioactive fresh fission products from an atomic explosion contaminate the surface at 1 μCi/cm^2 with an average gamma ray energy of 0.7 MeV per transformation. A person enters a fallout shelter that has a 30 cm thick concrete roof. What is the exposure rate inside the shelter?

8–19. A shallow circular impoundment roughly 10 m in diameter was drained exposing a thin sediment layer containing ^{137}Cs which dried. If the estimated activity of the thin sediment layer is 1 mCi/cm^2, what is the gamma dose rate 1 m above the center?

8–20. Residues from processing thorium ores in monazite sands and from which all the ^{232}Th has been removed are to be stored in a cylindrical tank 40 cm in diameter and 2 m high. The ^{228}Ra concentration of 20 pCi/g maintains an equilibrium concentration of ^{208}Tl which emits photons of 0.583 MeV in 4.5% and 2.614 MeV in 94.16% of transformations. Perform a simplified volume source estimation of the exposure rate 1 m from the tank due to the 2.614 MeV gamma rays by segmenting the volume into two parallel subvolumes each of which contains 5 segments.

8–21. A very large basin has a 10 cm sediment layer (ρ = 1.6) containing ^{137}Cs that emits 10^3 0.662 MeV gamma rays per second per gram. What is the exposure rate (a) 1 m above the exposed sediment layer, and (b) 1 m above the area if it is covered with 60 cm of water?

8–22. An old radium site contains a large area of debris with an average concentration of 5 pCi/g of ^{226}Ra. It is about 50 cm thick but is covered with a layer of soil. If the soil layer is removed, what would be the exposure rate above the radium debris?

9
Internal Radiation Dose

"Madame Curie died of aplastic pernicious anemia...the bone marrow did not react, probably because it had been injured by a long accumulation of radiations."
Dr. Tobé (July 4, 1934)

An internal radiation dose can occur due to inhalation or ingestion of radionuclides, a direct injection for diagnosis or treatment of disease, a puncture wound, or skin absorption. Internal radiation doses cannot be measured; they must be calculated based on an estimated/measured intake, an estimated/measured quantity in an organ, or an amount eliminated from the body. Submersion in an atmosphere containing a noble gas such as xenon, krypton, or radon may also irradiate internal organs, but external exposure is usually dominant. Submersion exposure is, however, typically treated as a special case of internal exposure.

9.1
Absorbed Dose in Tissue

Internal radiation dose calculations begin with the definition of absorbed dose, which is energy (joules or ergs) deposited per unit mass, and several key assumptions. First, it is assumed that the deposited radionuclide (expressed as its activity q in μCi or Bq) is uniformly distributed throughout the tissue mass of a source organ. Second, the radionuclide emits energy while in a source organ S that is absorbed in a target tissue T which is characterized by an absorbed fraction, AF(T ← S). The source organ is also a target organ, and if the deposited radionuclide is a pure alpha or beta emitter, it will be the only target organ and all of the energy emitted will be deposited in it, i.e., AF(T ← S) = 1.0. For x-rays and gamma rays, AF(T ← S) will generally be less than 1.0 and will vary considerably depending on the photon energy and the masses of the source organ and target tissues. Since many radionuclides produce more than one form of radiation emission per transformation, it is necessary to account for the energy absorbed due to each emitted radiation and its fraction Y_i of the number of transformations that occur.

If the transformation rate $q(t)$ of a radionuclide uniformly deposited in a tissue mass m_T is in units of t/s, the energy deposition rate per transformation is

Physics for Radiation Protection, Third Edition. James E. Martin

$$\dot{D}(\text{erg/g s}) = 1.6022 \times 10^{-6} q(t) \frac{\sum Y_i \bar{E}_i \text{AF}(\text{T} \rightarrow \text{S})_i}{m_\text{T}}$$

where $q(t)$ = activity (t/s) of the radionuclide in the tissue at any time t, Y_i = fractional yield per transformation of each radiation emitted, $\overline{E}_i$ = average energy (MeV) of each emitted radiation, $\text{AF}(\text{T} \leftarrow \text{S})_i$ = fraction of energy emitted by a source tissue S that is absorbed in a target tissue T, and m_T = mass (g) of target tissue T. This expression yields the "instantaneous" energy deposition (or dose) rate; it is a direct function of the amount of activity $q(t)$ that exists at any time t in a source organ.

Example 9-1. Calculate the instantaneous dose rate (rad/h) for 1 μCi of ^{32}P uniformly deposited in the liver (m_T = 1800 g).
Solution. An activity of 1 μCi = 3.7×10^4 t/s, and since ^{32}P is a pure beta emitter (Y_i = 1.0) with $E_{\beta,\text{avg}}$ = 0.695 MeV/t, it is reasonable to assume that all of the emitted beta energy is uniformly absorbed in the liver (m_T = 1800 g). Therefore

$$\dot{D}(\text{Liv} \leftarrow \text{Liv}) = 1.6022 \times 10^{-6} \times 3.7 \times 10^4 \text{t/s} \times \frac{\sum Y_i \bar{E}_i \text{AF}(\text{T} \leftarrow \text{S})_i}{m_\text{T}}$$

$$= 2.29 \times 10^{-5} \text{ erg/g s}$$

$$= 8.24 \times 10^{-4} \text{ rad/h}$$

9.2 Accumulated Dose

Although the "instantaneous" dose rate is of some interest, it is the accumulation of dose delivered over a period of time (usually the total dose) that is of most importance. All of the parameters that determine the instantaneous dose rate are constant for a given exposure situation except $q(t)$ which varies with time after deposition in an organ due to the combined effects of radioactive transformation (physical loss) and biological turnover. Both processes steadily decrease the number of radioactive atoms in an organ or tissue, as shown schematically in Figure 9-1.

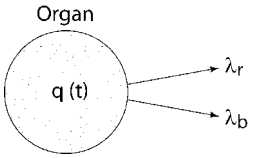

Fig. 9-1 Radionuclide consisting of N atoms with activity $q(t) = \lambda N$ is assumed to be distributed uniformly in an organ mass from which radioactive atoms are cleared by both radioactive transformation (λ_r) and biological removal (λ_b).

The rate constants λ_r (radioactive transformation) and λ_b (biological removal) are additive, and thus their sum is an "effective" removal constant λ_{eff}:

$$\lambda_{eff} = \lambda_r + \lambda_b$$

Since $\lambda_i = \ln 2/T_i$, an effective half-life (T_e) can be determined from the radiological (T_r) and biological (T_b) half-lives as

$$T_e = \frac{T_r T_b}{T_r + T_b}$$

The radiological half-life T_r is a well-known quantity for each radionuclide; however, T_b is characteristic of the radionuclide, its physical/chemical form, and the physiological dynamics of the organ in which it is deposited. Values of T_b for various tissues have been determined experimentally for a number of compounds and these are listed in various compilations, the most useful of which are metabolic models. Values of T_b and T_r for selected radionuclides are listed in Table 9-6 (see below).

Since the only factor in the instantaneous dose equation that changes with time is the activity $q(t)$, the dose rate will diminish with time as shown in Figure 9-2 as a function of $q(t)$, which is in turn a function of q_0, the activity initially deposited, and the effective removal constant λ_{eff}:

$$q(t) = q_0 e^{-\lambda_{eff} t}$$

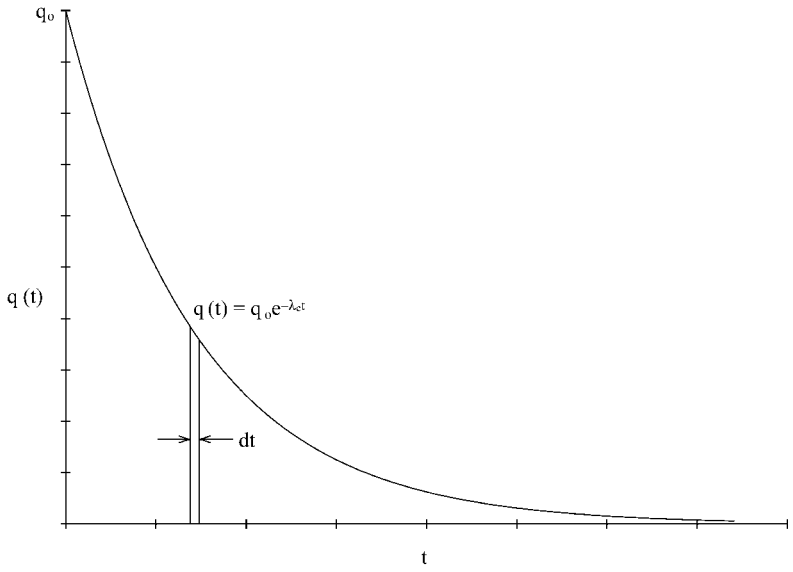

Fig. 9-2 Variation of the instantaneous dose rate with time after deposition in a tissue from which it is removed by radioactive transformation and biological processes, or with an effective removal constant $\lambda_{eff} = \lambda_r + \lambda_b$.

The *accumulated radiation dose* is obtained by integrating the instantaneous dose rate equation from the time of initial deposition ($t = 0$) in the tissue to a later time t. If the initial activity deposited in a source organ S is q_0, the total energy deposition (erg/g) in a target tissue T is

$$D_{\mathrm{TOT}} = 1.6022 \times 10^{-6} \frac{\sum Y_i \bar{E}_i \mathrm{AF}(\mathrm{T} \leftarrow \mathrm{S})_i}{m_{\mathrm{T}}} q_0 \int_0^t e^{-\lambda_{\mathrm{eff}} t}$$

which can be integrated directly. Since $\lambda_{\mathrm{eff}} = \ln 2/T_{\mathrm{e}}$, the total energy deposition is

$$D_{\mathrm{TOT}}(\mathrm{erg/g}) = 1.6022 \times 10^{-6} \left[\frac{q_0}{\lambda_{\mathrm{e}}} \left(1 - \exp\left(-\frac{\ln 2}{T_{\mathrm{e}}} t\right)\right)\right] \times \left[\frac{\sum Y_i f_i \bar{E}_i \mathrm{AF}(\mathrm{T} \leftarrow \mathrm{S})_i}{m_{\mathrm{T}}}\right]$$

where the first term in brackets represents the total number of transformations that occur for a time t following the initial deposition of an activity q_0; the second term is the energy deposition (or dose) per transformation (erg/g t) in the tissue mass m_{T}; and the constant accounts for the units. D_{TOT} can also be expressed as J/kg by multiplying by 10^{-7} J/erg and 10^3 g/kg.

In *SI units*, the total dose D_{TOT} is defined as the committed dose equivalent, $H_{50,\mathrm{T}}$, in units of sieverts (Sv) delivered over a 50 y period following the initial deposition of an activity q_0 in t/s or Bq:

$$H_{50,\mathrm{T}}(\mathrm{Sv}) = 1.6 \times 10^{-10} \left[\frac{q_0}{\lambda_{\mathrm{e}}} \left(1 - \exp\left(-\frac{\ln 2}{T_{\mathrm{e}}} t\right)\right)\right] \times \left[\frac{\sum f_i \bar{E}_i \mathrm{AF}(\mathrm{T} \leftarrow \mathrm{S})_i Q_i}{m_{\mathrm{T}}}\right]$$

where the first term in brackets is defined as U_{s}, the total number of transformations that occur due to an initially deposited activity q_0 (Bq), the second (or energy deposition) term in brackets is defined as the specific effective energy (SEE) with units of MeV/t g adjusted by the quality factor Q_i for each form of emitted radiation, and the constant 1.6×10^{-10} converts MeV/t g to J/kg t to yield, in sieverts (Sv), the 50 y committed dose equivalent (CDE) in SI units; or

$$H_{50,\mathrm{T}}\ (\mathrm{Sv}) = 1.6 \times 10^{-10} U_{\mathrm{s}} \times \mathrm{SEE}(\mathrm{T} \leftarrow \mathrm{S})$$

U_{s} is calculated from an initially deposited activity of q_0 (Bq) where T_{e} is in seconds. Since $\lambda_{\mathrm{e}} = \ln 2/T_{\mathrm{e}}$, it is

$$U_{\mathrm{s}}(\text{no. of transformations}) = 1.443 q_0 T_{\mathrm{e}} \left[1 - \exp\left(-\frac{\ln 2}{T_{\mathrm{e}}} t\right)\right]$$

The exposure period for a radionuclide deposited in a tissue is usually assumed to be 50 y, or a working lifetime, which is much longer than biological clearance for most radionuclides. Thus the total number of transformations that occur in an organ due to an uptake q_0 (t/s) reduces to

$$U_{\mathrm{s}}\ (\text{no. of transformations}) = 1.443 q_0 T_{\mathrm{e}}$$

with an error of less than 1% for exposure times that are 7–10 times the effective half-life T_e. This simplified expression of the total number of transformations can be used for internal dose calculations if, and only if, the integrated period of exposure is 7–10 times greater than the effective half-life T_e, which is the case for most radionuclides in tissue. Possible exceptions are long-lived radionuclides such as ^{90}Sr, ^{226}Ra, and long-lived isotopes of thorium and the transuranic elements that are deposited in bone and lymph tissues that have very slow biological clearance. In these cases it is necessary to integrate the dose over the period of interest, usually a working lifetime of 50 y.

9.2.1
Internal Dose: Medical Uses

Medical applications usually determine q_0 in microcuries and T_e in hours, and the result is called the cumulative activity $\tilde{q}$. The Medical Internal Radiation Dose (MIRD) Committee of the Society of Nuclear Medicine has incorporated these parameters into a straightforward schema as

$$D_{TOT} = \tilde{A}S(T \leftarrow S)$$

where $\tilde{A}$ is the cumulative activity in μCi h (1 μCi h = 1.332×10^8 t) due to an initial deposition of q_0 μCi in a source tissue and $S(T \leftarrow S)$ incorporates the energy deposition parameters and conversion constants to yield rad/μCi h of the deposited radionuclide. The S-value is fixed for a given radionuclide and source–target; therefore, use of the MIRD schema is basically a process of determining $\tilde{A}$ due to a deposited radionuclide and use of the respective S-value table to determine dose(s) to a relevant tissue(s).

Checkpoints

All internal radiation dose determinations involve three quantities, which vary only to account for the units of dose (rad or Sv):

- the total number of transformations that occur following the deposition of an initial activity q_0 in a source organ;
- the amount of energy (MeV) deposited per gram of target tissue for each transformation that occurs in a source organ;
- a constant to adjust units: for D_{TOT} in erg/MeV g it is 1.6022×10^{-6}; in SI units it is rounded to 1.6×10^{-10} J/MeV kg to obtain J/kg (or Sv).

9.3 Factors In The Internal Dose Equation

The internal dose equation can be generalized in terms of the total number of transformations that occur in a source organ, which is a function of q_0 and λ_{eff}, and three key factors, m_T, $\sum Y_i \bar{E}_i$, and $AF(T \leftarrow S)_i$, which are constants for any given radionuclide and a selected source–target organ pair.

The *initial activity* q_0 in a source organ is commonly derived from stated conditions, measured by whole-body or tissue counting, or estimated from the amount entering the body based on established models and uptake fractions.

The e*ffective removal constant* λ_{eff} is calculated as $\ln 2/T_e$, where T_e is calculated from the radiological (T_r) and biological (T_b) half-lives(listed in Table 9-6).

The *target tissue mass* m_T (in grams) is used in the calculation when actual values are available; otherwise the values in Table 9-1, which are based on a 70 kg reference person, are used.

Table 9-1. Tissue masses (g) for a reference 70 kg adult male (unique source organs are denoted as S, and specific target tissues, which are usually irradiated by source organ contents, are denoted as T).

Tissue	Mass (g)
Ovaries	11
Testes	35
Muscle	28,000
Red marrow	1500
Lungs	1000
Thyroid	20
Stomach contents (S)	250
Small intestine contents (S)	400
Upper large intestine contents (S)	220
Lower large intestine contents (S)	135
Stomach wall (T)	150
Small intestine wall (T)	640
Upper large intestine wall (T)	210
Lower large intestine wall (T)	160
Kidneys	310
Liver	1800
Pancreas	100
Cortical bone	4000
Trabecular bone	1000
Bone surfaces (T)	120

Table 9-1. Continued.

Tissue	Mass (g)
Skin	2600
Spleen	180
Adrenals	14
Thymus	20
Uterus	80
Bladder contents (S)	200
Bladder wall (T)	45
Total body	70,000

The *energy emission per transformation* $\sum Y_i \bar{E}_i$ is combined with the absorbed fraction AF(T ← S) to obtain the energy deposition in a target tissue T for each transformation that occurs in a source organ S. Energy emission and deposition from pure beta or alpha emitters that have a single energy are straightforward, but many radionuclides undergo transformation by emitting one or more particles and one or more photons. Whereas the emission energies of alpha particles and photons are discrete, the average energy $\bar{E}_\beta$ for beta radiation and positron emission is dependent upon the shape of the beta particle energy spectrum and weighted average energy values (as tabulated in Appendix D) should be used in dose calculations; when weighted values of $\bar{E}_\beta$ are not available it is common to use the approximation $\bar{E}_\beta = 0.33 E_{\beta\max}$.

The *absorbed fraction* AF(T ← S) is a dimensionless quantity to account for the fraction of the energy emitted by a source organ S that is actually absorbed in a target tissue T, which may be the source organ itself. For most practical purposes it is 1.0 for alpha particles and electrons (beta particles and positrons) and the source organ and the target organ will be the same (the range of a 5 MeV alpha particle is about 50 μm in tissue and the range of most beta particles in tissue is at most a few millimeters). Complete absorption of all emitted photons in a source organ is unlikely (possible exceptions are those with very low energies) and the absorbed fraction AF(T ← S) accounts for the energy deposited when photons from a source organ S irradiate a target organ some distance away; it is a function of the energy of the radiation and the size, shape, and relative locations of the source organ(s) and the target organ(s) as illustrated in Figure 9-3.

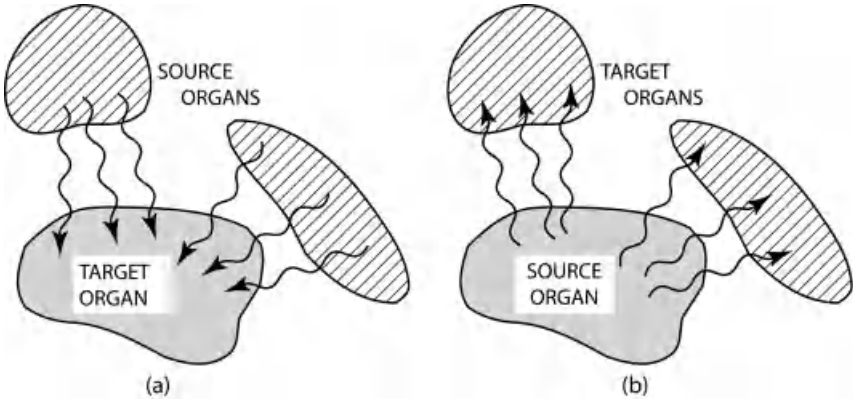

Fig. 9-3 A radionuclide may be deposited such that (a) more than one source organ produces absorption of energy in a target tissue, or (b) a source organ can produce energy absorption in more than one target tissue.

Absorbed fractions for photon energies between 0.02 and 4 MeV are listed in Tables 9-2–9-4 for the lungs, liver, and whole body as source organs. Similar data have been compiled by the MIRD Committee for up to 25 source–target organ pairs and are available at www.nndc.bnl.gov. Specific absorbed fractions, which already include tissue masses based on a reference person, are also available and are easier to use in detailed internal dose calculations.

Energy absorption in source organs is often the largest contributor to the internal dose from a radionuclide. All of the energy emitted in the form of particles will be deposited in the source organ; however, only a fraction of the photon energy will be absorbed. Absorbed fractions of photon energies produced in tissues that are both the source and target are listed in Table 9-5; e.g., thyroid to thyroid, whole body to whole body, etc. The dose coefficient (erg/g t or J/kg t) associated with the source organ can be calculated by absorbing all of the particle energy in the source organ mass and adding that due to the fractional absorption of the photon(s).

The parameters in the internal dose equation and their use are shown in Example 9-2.

Table 9-2. Absorbed fractions AF(T ← Lu) for photons emitted from radionuclides deposited in the lungs.

Target organ	Photon energy, *E* (MeV)									
	0.020	**0.030**	**0.050**	**0.100**	**0.200**	**0.500**	**1.000**	**1.500**	**2.000**	**4.000**
Adrenals	–	1.59×10^{-4}	1.55×10^{-4}	1.64×10^{-4}	1.03×10^{-4}	1.57×10^{-4}	1.25×10^{-4}	1.07×10^{-4}	1.85×10^{-4}	1.22×10^{-4}
Bladder	–	–	–	4.79×10^{-5}	1.45×10^{-4}	1.61×10^{-4}	1.58×10^{-4}	1.77×10^{-4}	3.25×10^{-4}	2.95×10^{-4}
GI (stom)	8.75×10^{-4}	2.63×10^{-3}	3.62×10^{-3}	2.63×10^{-3}	2.50×10^{-3}	2.28×10^{-3}	1.84×10^{-3}	1.90×10^{-3}	2.02×10^{-3}	1.68×10^{-3}
GI (SI)	–	1.70×10^{-4}	8.79×10^{-4}	1.37×10^{-3}	1.60×10^{-3}	1.72×10^{-3}	1.95×10^{-3}	2.47×10^{-3}	1.90×10^{-3}	2.03×10^{-3}
GI (ULI)	–	–	2.94×10^{-4}	4.46×10^{-4}	4.53×10^{-4}	4.32×10^{-4}	4.01×10^{-4}	6.26×10^{-4}	4.34×10^{-4}	5.17×10^{-4}
GI (LLI)	–	–	–	5.17×10^{-5}	9.73×10^{-5}	6.22×10^{-5}	1.43×10^{-4}	1.25×10^{-4}	1.46×10^{-4}	2.09×10^{-4}
Heart	9.83×10^{-3}	2.28×10^{-2}	2.03×10^{-2}	1.39×10^{-2}	1.30×10^{-2}	1.11×10^{-2}	1.02×10^{-2}	8.98×10^{-3}	9.40×10^{-3}	7.18×10^{-3}
Kidneys	–	3.26×10^{-4}	9.23×10^{-4}	9.01×10^{-4}	9.34×10^{-4}	1.16×10^{-3}	8.14×10^{-4}	9.15×10^{-4}	9.39×10^{-4}	6.32×10^{-4}
Liver	1.42×10^{-2}	2.58×10^{-2}	2.39×10^{-2}	1.73×10^{-2}	1.55×10^{-2}	1.54×10^{-2}	1.38×10^{-2}	1.33×10^{-2}	1.17×10^{-2}	1.06×10^{-2}
Lungs	4.75×10^{-1}	2.31×10^{-1}	8.92×10^{-2}	4.93×10^{-2}	4.98×10^{-2}	5.14×10^{-2}	4.52×10^{-2}	4.13×10^{-2}	3.82×10^{-2}	3.14×10^{-2}
Marrow	1.33×10^{-2}	3.86×10^{-2}	4.66×10^{-2}	2.54×10^{-2}	1.61×10^{-2}	1.33×10^{-2}	1.25×10^{-2}	1.14×10^{-2}	1.13×10^{-2}	9.80×10^{-3}
Pancreas	–	3.79×10^{-4}	5.73×10^{-4}	6.07×10^{-4}	4.30×10^{-4}	4.62×10^{-4}	5.71×10^{-4}	5.69×10^{-4}	6.47×10^{-4}	2.40×10^{-4}
Skel (rib)	3.12×10^{-2}	7.01×10^{-2}	5.77×10^{-2}	2.43×10^{-2}	1.45×10^{-2}	1.19×10^{-2}	1.10×10^{-2}	1.04×10^{-2}	1.01×10^{-2}	8.58×10^{-3}
Skel (pelvis)	–	–	1.96×10^{-4}	4.07×10^{-4}	3.48×10^{-4}	4.34×10^{-4}	4.72×10^{-4}	3.46×10^{-4}	4.98×10^{-4}	6.37×10^{-4}
Skel (spine)	1.28×10^{-3}	1.48×10^{-2}	3.55×10^{-2}	2.35×10^{-2}	1.53×10^{-2}	1.21×10^{-2}	1.07×10^{-2}	1.02×10^{-2}	9.91×10^{-3}	8.27×10^{-3}
Skel (total)	3.31×10^{-2}	9.52×10^{-2}	1.13×10^{-2}	6.11×10^{-2}	3.89×10^{-2}	3.24×10^{-2}	3.07×10^{-2}	2.78×10^{-2}	2.78×10^{-2}	2.42×10^{-2}
Skull	–	2.64×10^{-4}	1.37×10^{-3}	1.20×10^{-3}	9.70×10^{-4}	1.50×10^{-3}	1.37×10^{-3}	1.23×10^{-3}	1.58×10^{-3}	1.07×10^{-3}
Skin	1.76×10^{-3}	5.73×10^{-3}	5.99×10^{-3}	5.41×10^{-3}	5.47×10^{-3}	6.37×10^{-3}	6.12×10^{-3}	6.68×10^{-3}	6.10×10^{-3}	4.71×10^{-3}
Spleen	8.91×10^{-4}	1.82×10^{-3}	2.05×10^{-3}	1.46×10^{-3}	1.46×10^{-3}	1.19×10^{-3}	1.13×10^{-3}	1.08×10^{-3}	1.03×10^{-3}	8.54×10^{-4}
Thyroid	–	–	3.83×10^{-5}	3.29×10^{-5}	5.39×10^{-5}	6.49×10^{-5}	6.33×10^{-5}	–	–	–
Uterus	–	–	–	1.53×10^{-5}	1.57×10^{-5}	2.25×10^{-5}	–	–	9.76×10^{-5}	–
Total body	9.81×10^{-1}	8.78×10^{-1}	6.10×10^{-1}	3.92×10^{-1}	3.59×10^{-1}	3.54×10^{-1}	3.29×10^{-1}	3.01×10^{-1}	2.88×10^{-1}	2.41×10^{-1}

Source: Society of Nuclear Medicine, August 1969.

Table 9-3. Absorbed fractions AF(T ← Liv), for photons emitted from radionuclides deposited in the liver.

Target organ	Photon energy, *E* (MeV)									
	0.020	**0.030**	**0.050**	**0.100**	**0.200**	**0.500**	**1.000**	**1.500**	**2.000**	**4.000**
Adrenals	1.83×10^{-4}	4.40×10^{-4}	3.92×10^{-4}	2.70×10^{-4}	2.37×10^{-4}	1.98×10^{-4}	2.21×10^{-4}	2.33×10^{-4}	3.27×10^{-4}	2.65×10^{-4}
Bladder	–	–	1.69×10^{-4}	2.75×10^{-4}	3.89×10^{-4}	3.58×10^{-4}	5.21×10^{-4}	5.15×10^{-4}	7.35×10^{-4}	4.74×10^{-4}
GI (stom)	1.71×10^{-4}	1.51×10^{-3}	3.60×10^{-3}	3.00×10^{-3}	2.71×10^{-3}	2.80×10^{-3}	2.40×10^{-3}	2.54×10^{-3}	2.10×10^{-3}	1.50×10^{-3}
GI (SI)	1.17×10^{-4}	4.93×10^{-3}	1.08×10^{-2}	1.09×10^{-2}	1.00×10^{-2}	9.17×10^{-3}	9.25×10^{-3}	9.04×10^{-3}	7.91×10^{-3}	6.46×10^{-3}
GI (ULI)	9.27×10^{-4}	3.18×10^{-3}	4.48×10^{-3}	4.01×10^{-3}	3.87×10^{-3}	3.64×10^{-3}	3.20×10^{-3}	2.87×10^{-3}	3.40×10^{-3}	2.32×10^{-3}
GI (LLI)	–	–	6.13×10^{-5}	1.49×10^{-4}	2.11×10^{-4}	3.91×10^{-4}	2.68×10^{-4}	2.86×10^{-4}	3.34×10^{-4}	3.91×10^{-4}
Heart	1.32×10^{-3}	5.31×10^{-3}	7.62×10^{-3}	6.74×10^{-3}	5.70×10^{-3}	5.73×10^{-3}	5.01×10^{-3}	4.98×10^{-3}	3.92×10^{-3}	0.37×10^{-2}
Kidneys	1.06×10^{-3}	4.37×10^{-3}	5.66×10^{-3}	4.37×10^{-3}	3.90×10^{-3}	3.86×10^{-3}	3.35×10^{-3}	2.94×10^{-3}	3.01×10^{-3}	2.56×10^{-3}
Liver	7.84×10^{-1}	5.43×10^{-1}	2.78×10^{-1}	1.65×10^{-1}	1.58×10^{-1}	1.57×10^{-1}	1.44×10^{-1}	1.32×10^{-1}	1.22×10^{-1}	1.01×10^{-1}
Lungs	8.59×10^{-2}	1.65×10^{-3}	1.47×10^{-2}	1.01×10^{-2}	9.23×10^{-3}	8.38×10^{-3}	8.25×10^{-3}	6.96×10^{-3}	6.01×10^{-3}	5.68×10^{-3}
Marrow	8.19×10^{-3}	2.28×10^{-2}	3.25×10^{-2}	2.06×10^{-2}	1.33×10^{-2}	1.07×10^{-2}	9.35×10^{-3}	9.24×10^{-3}	8.88×10^{-3}	7.20×10^{-3}
Pancreas	1.86×10^{-4}	1.07×10^{-3}	1.30×10^{-3}	1.05×10^{-2}	1.02×10^{-3}	8.22×10^{-4}	8.64×10^{-4}	5.87×10^{-4}	7.65×10^{-4}	6.12×10^{-4}
Skel (rib)	1.83×10^{-2}	4.02×10^{-2}	3.66×10^{-2}	1.81×10^{-2}	1.11×10^{-2}	8.67×10^{-3}	7.60×10^{-3}	7.48×10^{-3}	6.35×10^{-3}	5.27×10^{-3}
Skel (pelvis)		5.23×10^{-4}	2.65×10^{-3}	3.08×10^{-3}	2.16×10^{-3}	1.82×10^{-3}	1.71×10^{-3}	1.81×10^{-3}	2.07×10^{-3}	1.57×10^{-3}
Skel (spine)	3.93×10^{-4}	5.66×10^{-3}	2.17×10^{-2}	1.67×10^{-2}	1.08×10^{-2}	0.857×10^{-2}	6.94×10^{-3}	6.70×10^{-3}	7.01×10^{-3}	5.21×10^{-3}
Skel (skull)	–	–	–	6.29×10^{-5}	1.40×10^{-4}	1.87×10^{-4}	2.62×10^{-4}	3.60×10^{-4}	4.20×10^{-4}	3.70×10^{-4}
Skel (total)	2.09×10^{-2}	5.87×10^{-2}	8.03×10^{-2}	4.98×10^{-2}	3.24×10^{-2}	2.60×10^{-2}	2.31×10^{-2}	2.29×10^{-2}	2.17×10^{-2}	1.79×10^{-2}
Skin	1.36×10^{-3}	4.68×10^{-3}	5.58×10^{-3}	4.99×10^{-3}	5.07×10^{-3}	5.61×10^{-3}	5.81×10^{-3}	5.67×10^{-3}	5.60×10^{-3}	5.43×10^{-3}
Spleen	–	6.17×10^{-5}	5.33×10^{-4}	6.06×10^{-4}	6.45×10^{-4}	6.19×10^{-4}	6.33×10^{-4}	3.96×10^{-4}	3.36×10^{-4}	5.03×10^{-4}
Thyroid	–	–	–	–	–	–	–	–	2.38×10^{-5}	–
Uterus	–	–	5.64×10^{-5}	1.15×10^{-4}	1.36×10^{-4}	1.30×10^{-4}	1.27×10^{-4}	7.29×10^{-5}	9.20×10^{-5}	–
Total body	9.84×10^{-1}	9.05×10^{-1}	6.61×10^{-1}	4.54×10^{-1}	4.15×10^{-1}	4.07×10^{-1}	3.81×10^{-1}	3.55×10^{-1}	3.36×10^{-1}	2.82×10^{-1}

Source: Society of Nuclear Medicine, August 1969.

Table 9-4. Absorbed fractions AF(T ← TB) for photons emitted from radionuclides deposited in the whole body.

Target organ	Photon energy, *E* (MeV)									
	0.020	**0.030**	**0.050**	**0.100**	**0.200**	**0.500**	**1.000**	**1.500**	**2.000**	**4.000**
Adrenals	1.75×10^{-4}	2.09×10^{-4}	1.31×10^{-4}	1.01×10^{-4}	3.52×10^{-5}	1.38×10^{-4}	1.00×10^{-4}	1.07×10^{-4}	1.14×10^{-4}	–
Bladder	6.83×10^{-3}	6.25×10^{-3}	4.45×10^{-3}	3.25×10^{-3}	3.27×10^{-3}	3.41×10^{-3}	2.74×10^{-3}	2.91×10^{-3}	2.31×10^{-3}	1.47×10^{-3}
GI (stom)	5.73×10^{-3}	5.60×10^{-3}	3.91×10^{-3}	2.73×10^{-3}	2.18×10^{-3}	2.58×10^{-3}	1.81×10^{-3}	1.99×10^{-3}	2.12×10^{-3}	1.19×10^{-3}
GI (SI)	2.34×10^{-2}	2.09×10^{-2}	1.63×10^{-2}	1.20×10^{-2}	1.06×10^{-2}	1.14×10^{-2}	1.09×10^{-2}	9.15×10^{-3}	8.20×10^{-3}	4.09×10^{-3}
GI (ULI)	6.47×10^{-3}	5.33×10^{-3}	3.74×10^{-3}	2.62×10^{-3}	2.56×10^{-3}	3.06×10^{-3}	2.28×10^{-3}	2.09×10^{-3}	1.97×10^{-3}	1.60×10^{-3}
GI (LLI)	4.57×10^{-3}	2.85×10^{-3}	2.56×10^{-3}	1.87×10^{-3}	1.51×10^{-3}	1.84×10^{-3}	1.78×10^{-3}	1.81×10^{-3}	1.57×10^{-3}	6.73×10^{-4}
Heart	7.69×10^{-3}	6.35×10^{-3}	4.69×10^{-3}	4.20×10^{-3}	3.37×10^{-3}	3.72×10^{-3}	3.01×10^{-3}	3.45×10^{-3}	3.12×10^{-3}	1.45×10^{-3}
Kidneys	4.12×10^{-3}	3.38×10^{-3}	2.33×10^{-3}	1.83×10^{-3}	1.71×10^{-3}	1.42×10^{-3}	1.61×10^{-3}	1.52×10^{-3}	1.54×10^{-3}	9.04×10^{-4}
Liver	2.49×10^{-2}	2.21×10^{-2}	1.54×10^{-2}	1.20×10^{-2}	1.11×10^{-2}	1.01×10^{-2}	8.96×10^{-3}	9.12×10^{-3}	8.47×10^{-3}	5.60×10^{-3}
Lungs	1.38×10^{-2}	1.22×10^{-2}	8.08×10^{-3}	5.51×10^{-3}	5.07×10^{-3}	4.96×10^{-3}	4.66×10^{-3}	4.66×10^{-3}	4.27×10^{-3}	5.68×10^{-3}
Marrow	–	7.40×10^{-2}	6.13×10^{-2}	3.29×10^{-2}	2.21×10^{-2}	1.94×10^{-2}	1.82×10^{-2}	1.64×10^{-2}	1.56×10^{-2}	9.69×10^{-3}
Pancreas	8.28×10^{-4}	7.80×10^{-4}	5.67×10^{-4}	4.49×10^{-4}	4.44×10^{-4}	3.82×10^{-4}	5.34×10^{-4}	3.48×10^{-4}	3.58×10^{-4}	1.42×10^{-4}
Skel (rib)	2.47×10^{-2}	2.63×10^{-2}	1.76×10^{-2}	7.64×10^{-3}	5.05×10^{-3}	4.35×10^{-3}	4.21×10^{-3}	4.05×10^{-3}	3.50×10^{-3}	3.38×10^{-3}
Skel (pelvis)	1.63×10^{-2}	2.20×10^{-2}	1.99×10^{-2}	1.03×10^{-2}	6.68×10^{-3}	5.69×10^{-3}	5.62×10^{-3}	5.11×10^{-3}	4.22×10^{-3}	2.56×10^{-3}
Skel (spine)	2.34×10^{-2}	2.53×10^{-2}	2.29×10^{-2}	1.44×10^{-2}	9.10×10^{-3}	7.63×10^{-3}	7.51×10^{-3}	6.10×10^{-3}	6.06×10^{-3}	3.41×10^{-3}
Skel (total)	1.67×10^{-1}	1.88×10^{-1}	1.53×10^{-1}	8.10×10^{-2}	5.50×10^{-2}	4.88×10^{-2}	4.56×10^{-2}	4.13×10^{-2}	3.96×10^{-2}	2.52×10^{-2}
Skull	1.23×10^{-2}	1.28×10^{-2}	7.22×10^{-3}	3.13×10^{-3}	2.77×10^{-3}	3.04×10^{-3}	2.80×10^{-3}	2.54×10^{-3}	2.92×10^{-3}	2.24×10^{-3}
Skin	1.69×10^{-2}	1.16×10^{-2}	7.58×10^{-3}	5.85×10^{-3}	6.77×10^{-3}	7.57×10^{-3}	7.45×10^{-3}	7.59×10^{-3}	6.64×10^{-3}	1.23×10^{-2}
Spleen	2.42×10^{-3}	2.23×10^{-3}	1.49×10^{-3}	1.11×10^{-3}	7.98×10^{-4}	1.16×10^{-3}	9.14×10^{-4}	9.03×10^{-4}	7.40×10^{-4}	3.68×10^{-4}
Thyroid	6.02×10^{-5}	1.11×10^{-4}	1.14×10^{-4}	8.73×10^{-5}	4.18×10^{-5}	–	–	–	8.10×10^{-5}	–
Uterus	–	–	1.22×10^{-3}	9.24×10^{-4}	4.08×10^{-4}	4.73×10^{-4}	5.17×10^{-4}	3.23×10^{-4}	3.64×10^{-4}	2.38×10^{-4}
Total body	8.92×10^{-1}	7.74×10^{-1}	5.48×10^{-1}	3.70×10^{-1}	3.38×10^{-1}	3.40×10^{-1}	3.21×10^{-1}	3.02×10^{-1}	2.84×10^{-1}	2.40×10^{-1}

Source: Society of Nuclear Medicine, August 1969.

Table 9-5. Absorbed fractions AF(S ← S) for photon energies released in and absorbed in a source organ.

Source/target tissue	Photon energy (MeV)									
	0.020	**0.030**	**0.050**	**0.100**	**0.200**	**0.500**	**1.000**	**1.500**	**2.000**	**4.000**
Bladder	7.45×10^{-1}	4.64×10^{-1}	2.01×10^{-1}	1.17×10^{-1}	1.16×10^{-1}	1.16×10^{-1}	1.07×10^{-1}	1.00×10^{-1}	9.10×10^{-2}	7.22×10^{-2}
Brain	8.03×10^{-1}	5.55×10^{-1}	2.68×10^{-1}	1.61×10^{-1}	1.59×10^{-1}	1.60×10^{-1}	1.49×10^{-1}	1.36×10^{-1}	1.26×10^{-1}	1.00×10^{-1}
GI (stom)	7.05×10^{-1}	4.14×10^{-1}	1.76×10^{-1}	1.01×10^{-1}	1.01×10^{-1}	1.01×10^{-1}	9.32×10^{-2}	8.46×10^{-2}	7.92×10^{-2}	6.43×10^{-2}
GI (SI)	7.56×10^{-1}	5.17×10^{-1}	2.64×10^{-1}	1.59×10^{-1}	1.54×10^{-1}	1.50×10^{-1}	1.40×10^{-1}	1.25×10^{-1}	1.17×10^{-1}	9.36×10^{-2}
GI (ULI)	6.25×10^{-1}	3.35×10^{-1}	1.34×10^{-1}	7.83×10^{-2}	8.04×10^{-2}	8.11×10^{-2}	7.49×10^{-2}	7.00×10^{-2}	6.38×10^{-2}	4.89×10^{-2}
GI (LLI)	5.56×10^{-1}	2.76×10^{-1}	1.05×10^{-1}	6.24×10^{-2}	6.31×10^{-2}	6.49×10^{-2}	6.01×10^{-2}	5.61×10^{-2}	4.93×10^{-2}	4.04×10^{-2}
Kidneys	5.82×10^{-1}	2.98×10^{-1}	1.12×10^{-1}	6.61×10^{-2}	6.76×10^{-2}	7.30×10^{-2}	6.70×10^{-2}	6.00×10^{-2}	5.59×10^{-2}	4.49×10^{-2}
Liver	7.84×10^{-1}	5.43×10^{-1}	2.78×10^{-1}	1.65×10^{-1}	1.58×10^{-1}	1.57×10^{-1}	1.44×10^{-1}	1.32×10^{-1}	1.22×10^{-1}	1.01×10^{-1}
Lungs	4.75×10^{-1}	2.31×10^{-1}	8.92×10^{-2}	4.93×10^{-2}	4.98×10^{-2}	5.14×10^{-2}	4.52×10^{-2}	4.13×10^{-2}	3.82×10^{-2}	3.14×10^{-2}
Ovaries	2.72×10^{-1}	9.84×10^{-2}	2.94×10^{-2}	1.74×10^{-2}	1.96×10^{-2}	2.29×10^{-2}	1.99×10^{-2}	1.76×10^{-2}	1.70×10^{-2}	1.37×10^{-2}
Pancreas	4.42×10^{-1}	1.95×10^{-1}	6.76×10^{-2}	3.83×10^{-2}	4.18×10^{-2}	4.37×10^{-2}	4.01×10^{-2}	3.74×10^{-2}	3.41×10^{-2}	2.67×10^{-2}
Skeleton	8.30×10^{-1}	6.81×10^{-1}	4.00×10^{-1}	1.73×10^{-1}	1.23×10^{-1}	1.18×10^{-1}	1.10×10^{-1}	1.02×10^{-1}	9.40×10^{-2}	7.97×10^{-2}
Spleen	6.25×10^{-1}	3.31×10^{-1}	1.28×10^{-1}	7.09×10^{-2}	7.35×10^{-2}	7.69×10^{-2}	6.99×10^{-2}	6.50×10^{-2}	5.99×10^{-2}	4.83×10^{-2}
Testes	4.69×10^{-1}	2.08×10^{-1}	7.03×10^{-2}	3.99×10^{-2}	4.33×10^{-2}	4.46×10^{-2}	4.12×10^{-2}	3.83×10^{-2}	3.54×10^{-2}	2.89×10^{-2}
Thyroid	3.66×10^{-1}	1.49×10^{-1}	4.80×10^{-2}	2.78×10^{-2}	3.06×10^{-2}	3.19×10^{-2}	2.95×10^{-2}	2.76×10^{-2}	2.54×10^{-2}	2.00×10^{-2}
Total body	8.92×10^{-1}	7.74×10^{-1}	5.48×10^{-1}	3.70×10^{-1}	3.38×10^{-1}	3.40×10^{-1}	3.21×10^{-1}	3.02×10^{-1}	2.84×10^{-1}	2.40×10^{-1}

Example 9-2. An amount of 20 μCi of ^{32}P ($T_{1/2}$ = 14.3 d) is injected into the bloodstream of a reference adult. Calculate (a) the absorbed dose constant (erg/g t) for ^{32}P irradiating the whole body uniformly, (b) the total number of transformations that occur in the total body as a source organ, and (c) the total body dose.
Solution. (a) The energy deposition rate per transformation is

$$\dot{D}(\text{TB} \leftarrow \text{TB}) = 1.6022 \times 10^{-6}\ \text{erg/MeV} \times \frac{1.0 \times 0.695\ \text{MeV/t} \times 1.0}{70,000\ \text{g}}$$

$$= 1.59 \times 10^{-11}\ \text{erg/g t}$$

(b) As shown in Table 9-6, ^{32}P is metabolized in such a way that 40% is uniformly distributed throughout the whole body where it is cleared with a biological half-life of 19 d; thus, the total number of transformations that occur in the total body from an injection of 20 μCi is determined from the initial activity distributed in the total body (q_0 = 0.40 × 20 μCi = 8 μCi) and the effective half-life of ^{32}P in the total body:

$$T_{\text{eff}} = \frac{19\ \text{d} \times 14.3\ \text{d}}{19\ \text{d} + 14.3\ \text{d}} = 8.16\ \text{d} = 196\ \text{h}$$

And since T_{eff} is quite short compared to 50 y,

$$\text{No. of transformations} = 1.443 \times (196\ \text{h} \times 3600\ \text{s/h}) \times (8\ \mu\text{Ci} \times 3.7 \times 10^4\ \text{t/s}\ \mu\text{Ci})$$

$$= 3.014 \times 10^{11}\ \text{t}$$

(c) The total dose to the whole body is obtained by multiplying the absorbed dose constant (erg/g t) and the total number of transformations, or

$$D_{\text{TOT}}\ (\text{TB} \leftarrow \text{TB}) = (1.59 \times 10^{-11}\ \text{erg/G t}) \times 3.014 \times 10^{11}\ \text{t}$$

$$= 4.79\ \text{erg/g} = 47.9\ \text{mrad}$$

9.3.1 The Dose Reciprocity Theorem

Reciprocity can be used to determine the absorbed energy per gram in a tissue that is not listed as a target organ but may be listed as a source organ or vice versa. Under the dose reciprocity theorem the energy absorbed per gram is the same for radiation traveling from T to S as it is for radiation traveling from S to T. Therefore, if AF(T ← S) is known, then AF(S ← T) can be obtained from the dose reciprocity theorem by adjusting the known quantity to account for the different masses:

$$\text{AF}(\text{S} \leftarrow \text{T})/m_{\text{S}} = \text{AF}(\text{T} \leftarrow \text{S})/m_{\text{T}}$$

Therefore

$$\mathrm{AF}(\mathrm{S} \leftarrow \mathrm{T}) = (m_S/m_T) \times \mathrm{AF}(\mathrm{T} \leftarrow \mathrm{S})$$

as illustrated in Example 9-3.

Example 9-3. Use the dose reciprocity theorem and the data in Table 9-2 to determine the absorbed fraction of 1 MeV photons emitted from the thyroid and absorbed in the lung.
Solution. From Table 9-2, AF(Thy ← Lung) = 0.0000633, and from Table 9-1 the masses of the lung and the thyroid are 1000 and 20 g, respectively. Therefore

$$\begin{aligned}\mathrm{AF}(\mathrm{Lung} \leftarrow \mathrm{Thy}) &= 0.0000633 \times (1000\ \mathrm{g}/20\ \mathrm{g}) \\ &= 0.003165\end{aligned}$$

9.3.2 Deposition and Clearance Data

Calculations of internal dose require information on the fractional uptake of a radionuclide from the bloodstream to a source organ and the pattern and rate(s) of clearance from it. These data have been summarized and compiled by the International Commission on Radiological Protection (ICRP) in ICRP Publication 30 and supplements and are provided in Table 9-6 for selected radioelements. As indicated in Table 9-6, deposition can occur in various tissues and clearance can be rather complex.

9.3.3 Multicompartment Retention

When a given radionuclide is eliminated from an organ or tissue at different rates, it is usually due to two or more biological compartments of retention with different effective removal half-lives (see Table 9-6). In such cases, it is necessary to calculate the number of transformations (or cumulative activity) that occur in each compartment separately and to sum them to determine the total dose delivered to the tissue. For example, it has been established from biological studies that 10% of cesium that is deposited in the whole body is cleared from a subcompartment with a biological half-life of 2 d and the remaining 90% is cleared with a biological half-life of 110 d (see Table 9-6). The amount $q(t)$ of cesium in the total body at any time after a deposition of q_0 is called the retention function, and is expressed for cesium as

$$q(t) = 0.1q_0\exp\left(-\frac{\ln 2}{2\,\mathrm{d}}t\right) + 0.9q_0\exp\left(-\frac{\ln 2}{110\,\mathrm{d}}t\right)$$

where, as indicated by the first term, $0.1q_0$ is cleared with a biological half-life of 2 d and, as shown by the second term, $0.9q_0$ is cleared with a biological half-life of 110 d.

Table 9-6. Distribution of radioelements in adults from the transfer compartment (blood) to tissue in the body, the percentage (%) clearance, subcompartments of each tissue, and the biological half-life (T_b) for each.

Element (f_1) **Nuclide ($T_{1/2}$)**	**Transfer from blood**		**Clearance from tissue**		
	Tissue	**%**	**Compartment**	**% [a]**	**T_b**
Carbon (f_1 = 1.0)	Tot. body	100%	Tot. body	100%	40 d
^{11}C (20.3 m)					
^{14}C (5715 y)					
Phosphorus (f_1 = 0.8)	Tot. body	70%	T. body exc.	21.5%	0.5 d
^{32}P (14.1 d)	Bone	30%	Tot. body A	21.5%	2 d
^{33}P (25.34 d)			Tot. body B	57%	19 d
			Bone	100%	∞
Sulfur (f_1 = 0.8)	Tot. body	100%	T. body Exc.	80%	0.3 d
^{35}S (87.44 d)			Tot. body A	15%	20 d
			Tot. body B	5%	200 d
Manganese (f_1 = 0.1)	Bone	35%	Bone	100%	40 d
^{54}Mn (312.12 d)	Liver	25%	Liver A	10%	4 d
^{56}Mn (2.5785 h)	Other Tiss.	40%	Liver B	15%	40 d
			Other tiss. A	20%	4 d
			Other tiss. B	20%	40 d
Cobalt (f_1 = 0.1)	Excretion	50%	Excretion	100%	0.5 d
^{57}Co (270.9 d)	Tot. body	45%	Tot. body A	60%	6 d
^{58}Co (70.8 d)			Tot. body B	20%	60 d
^{60}Co (5.27 y)			Tot. body C	20%	800 d
	Liver	5%	Liver A	60%	6 d
			Liver B	20%	600 d
			Liver C	20%	800 d

Table 9-6. Continued.

Element (f_1) Nuclide ($T_{1/2}$)	Transfer from blood		Clearance from tissue		
	Tissue	%	Compartment	% [a]	T_b
Nickel ($f_1 = 0.05$)	Kidneys	2%	Kidneys	100%	0.2 d
^{59}Ni (75,000 y)	Other tiss.	30%	Other tiss.	100%	1200 d
Zinc ($f_1 = 0.5$)		Tot. body	100%	Skeleton A	19.5%
^{65}Zn (245 d)			Skeleton B	0.5%	10,000 d
			Tot. body A	24%	20 d
			Tot. body B	56%	400 d
Selenium ($f_1 = 0.8$)	Liver	25%	All tiss. A	10%	3 d
^{75}Se (119.8 d)	Kidneys	10%	All tiss. B	40%	30 d
	Spleen	1%	All tiss. C	50%	200 d
	Pancreas	0.5%			
	Testes	0.1%			
	Ovaries	0.02%			
	Other tiss.	63.4%			
Strontium ($f_1 = 0.3$)	Soft tiss.	100%	S. tiss. A	80%	2 d
^{89}Sr (50.5 d)			S. tiss. B	15%	30 d
^{90}Sr (29.1 y)			S. tiss. C	5%	200 d
Zirconium ($f_1 = 0.01$)	Skeleton	50%	Skeleton	100%	10,000 d
^{95}Zr (64.02 d)	Other tiss.	50%	Other tiss.	100%	7 d
Molybdenum ($f_1 = 1.0$)	Skeleton	10%	Skeleton	100%	10,000 d
^{99}Mo (66 h)	Liver	25%	Other tiss. A	10%	1 d
	Kidney	5%	Other tiss. B	90%	50 d
	Other tissue	60%			
Technetium ($f_1 = 0.5$)	Thyroid	4%	Thyroid	100%	0.5 d
^{99m}Tc (6.0 h)	Stom. wall	10%	Other tiss. A	75%	1.6 d
^{99}Tc (2.1×10^5 y)	Liver	3%	Other tiss. B	20%	3.7 d
	Tot. body	83%	Other tiss. C	5%	22 d

Table 9-6. Continued.

Element (f_1) Nuclide ($T_{1/2}$)	Transfer from blood		Clearance from tissue		
	Tissue	%	Compartment	% [a]	T_b
Ruthenium (f_1 = 0.05)	Tot. body	100%	T. body exc.	15%	0.3 d
^{103}Ru (39.28 d)			Tot. body A	35%	8 d
^{106}Ru (368.2 d)			Tot. body B	30%	35 d
			Tot. body C	20%	1000 d
Silver (f_1 = 0.05)	Liver	50%	Liver A	10%	3.5 d
^{110m}Ag (249.9 d)	Other tiss.	50%	Liver B	80%	50 d
			Liver C	10%	500 d
			Other tiss. A	10%	3.5 d
			Other tiss. B	80%	50 d
			Other tiss. C	10%	500 d
Antimony (f_1 = 0.1)	Excretion	20%	All tiss. A	85%	5 d
^{124}Sb (60.2 d)	Skeleton	40%	All tiss. B	10%	100 d
^{125}Sb (2.77 y)	Liver	5%	All tiss. C	5%	5000 d
	Other tiss.	35%			
Iodine (f_1 = 1.0)	Thyroid	30%	Thyroid	100%	80 d
^{125}I (60 d)					
^{129}I (1.57×10^7 y)					
^{131}I (8.02 d)					
Cesium (f_1 = 1.0)	Tot. body	100%	Tot. body A	10%	2 d
^{134}Cs (2.065 y)			Tot. body B	90%	110 d
^{137}Cs (30.07 y)					
Cerium (f_1 = 0.0005)	Skeleton	30%	All tissues		3500 d
^{141}Ce (32.5 d)	Liver	50%			
^{144}Ce (284.3 d)	Other tiss.	20%			

a Listed value represents percent clearance of amount deposited in the listed tissue, e.g., for ^{32}P 70% of that entering the blood (transfer compartment) distributes to the whole body and 21.5%, 21.5%, and 57% of that is cleared with half-lives of 0.5 d , 2 d, and 19 d, respectively, and the remaining 30% goes to bone where all of it (100%) is retained with an infinite half life.

Retention functions are provided in various compilations for stable elements as sums of exponential functions (e.g., cesium with two compartments); i.e., the clearance half-lives are due to biological removal only (e.g., all cesium, whether radioactive or not, clears the same way). It is necessary, therefore, to multiply through by $e^{-\lambda_r t}$ to account for radioactive removal as well as biological turnover for each compartment of retention/clearance; however, for long-lived radionuclides such as ^{137}Cs ($T_{1/2}$ = 30.04 y) the biological half-life for each retention compartment is, for all practical purposes, the effective half-life.

The number of transformations due to deposition of an initial activity q_0 is obtained by integrating each term of the retention function over the period of interest (usually 50 y). For example, for ^{137}Cs distributed in the total body

$$U_s(\text{no. of transformations}) = \frac{0.1q_0}{\ln 2/2\,\text{d}}(1 - e^{-(\ln 2/2\,\text{d})t}) + \frac{0.9q_0}{\ln 2/110\,\text{d}}(1 - e^{-(\ln 2/110\,\text{d})t})$$

which for $t \geq$ 7–10 effective half-lives for each compartment simplifies to

$$U_s\ (\text{no. of } t) = [(0.1q_0)(1.443 \times 2\ \text{d}) + (0.9q_0)(1.443 \times 110\ \text{d})] \times 86{,}400\ \text{s/d}$$

if q_0 is in units of t/s.

Example 9-4. For 2 μCi of ^{137}Cs deposited in the total body, determine (a) the total number of transformations that occur over a 50 y working career, (b) the energy deposition constant (MeV/g t), and (c) the total body dose.

Solution. (a) From Table 9-6, cesium is distributed uniformly in the body, but is cleared from two compartments with biological half-lives of 2 and 110 d, respectively, and since the exposure time t is long compared to the effective half-lives, the number of transformations in the two compartments is

$$U_s = 1.443 \times (2\ \mu\text{Ci} \times 3.7 \times 10^4\ \text{t/s}\ \mu\text{Ci}) \times [(0.1 \times 2\ \text{d}) + (0.9 \times 110\ \text{d})] \times 86{,}400\ \text{s/d}$$

$$= 9.15 \times 10^{11}\ \text{t}$$

(b) The decay scheme (Appendix D) for ^{137}Cs lists beta emissions ($\bar{E}_\beta$ = 0.1734 MeV at 94.4% and 0.4163 MeV at 5.6%), two primary conversion electron transitions (E = 0.6242 MeV at 7.66% and 0.6557 MeV at 1.12%), and one gamma emission of 0.662 MeV at 85.1%. (Note: other lesser emissions are neglected.) The energy deposition constant for nonpenetrating particle emissions, where AF(T ← S) = 1.0, is

$$\sum \frac{Y_i \bar{E}_i \times 1.0}{70,000\,\text{g}} = \frac{1}{70,000}[(0.1734 \times 0.944) + (0.4163 \times 0.056) + (0.6242 \times 0.076) + (0.6557 \times 0.0112)]$$
$$= \frac{0.24216}{70,000} = 3.4594 \times 10^{-6}\ \text{MeV/g t}$$

and for the penetrating gamma energy where AF(T. body ← T. body) = 0.334 (Table 9-5)

$$= \frac{0.662 \times 0.851 \times 0.334}{70,000\,\text{g}} = 2.688 \times 10^{-6}\ \text{MeV/g t}$$

for a total energy deposition per transformation of 6.1474×10^{-6} MeV/g t.

(c) The whole body dose is

$$H_{50,\text{T}} = 1.6 \times 10^{-6}\ \text{erg/MeV} \times 6.1474 \times 10^{-6}\ \text{MeV/g t} \times 9.15 \times 10^{11}\ \text{t}$$
$$= 9.0122\ \text{erg/g} = 0.09\ \text{rad} = 90\ \text{mrad}$$

9.4 Radiation Dose from Radionuclide Intakes

Inhalation or ingestion of radionuclides introduces complexity to internal dose determinations because radionuclides must first pass through the respiratory system and/or the gastrointestinal (GI) tract before entering the bloodstream from which uptake to an organ occurs. These circumstances are quite different from those where the amount of a radionuclide in the organ of interest is known or can be reasonably determined (e.g., in medical uses); thus, it is necessary to consider the mechanisms by which they are deposited and the physiological mechanisms by which they are translocated to other tissues which become source organs. It is also necessary to determine radiation doses to the lung and the various segments of the GI tract as the radioactive material passes through them as well as doses to tissues where they subsequently deposit and those that surround them.

Internal radiation dose and intake are directly related, and because of this direct correlation controls for internal radiation dose have been based on establishing an annual limit of intake (ALI) for each particular radionuclide. Such limits, which have varied over the years, are now based on an explicit consideration of risk. Previous standards for internal dose (since the 1940s) were to a large extent also based on risk; however, it was not explicitly stated, at least not numerically. Risk has thus become the primary protection standard, and dose, whether received internally or externally or both, is a physical surrogate, or secondary standard, for meeting the risk standard.

9.4.1 Risk-Based Radiation Standards

Internal dose limits were, prior to 1977, devised for a critical organ, which depending on its sensitivity, was limited to 15 rad/y for most tissues, a factor of 3 greater than the total body dose limit. For special tissues such as the thyroid, the skin, and the gonads, the limits were 30, 30, and 5 rad/y, respectively, and as much as 50 rad/y to skeletal tissue for bone seekers. Dose limits for specific tissues were allowed to be higher than those for the total body because they posed an overall lesser risk to the total organism, and perhaps more significantly, organ doses were considered singly and separately from external dose on the presumption that one or the other would dominate in an occupational setting.

The ICRP, in 1977, estimated that a whole body dose of 1 rem (0.01 Sv) to 10^6 exposed persons would produce a lifetime risk of 165 serious health effects. These effects were observed to occur in 6 major tissue groups plus other tissues (referred to as the remainder), and would produce a total body risk that could be considered acceptable if the total effective dose equivalent (TEDE) to each individual was ≤0.05 Sv (5 rem) in a year. The ICRP schema also limited the 50 y committed dose for any tissue to 50 rem (0.05 Sv)/y to preclude nonstochastic effects such as fibrous tissue, etc. Both stochastic and nonstochastic dose limits presume that no external or other doses occur.

The ICRP revisited the risk data in 1990 (ICRP Report 60) and concluded that a linear nonthreshold model was a more appropriate descriptor of risk than the linear quadratic model used in its 1977 analysis. Although the number of health effects in the study populations was essentially the same, this change in the extrapolation model (see Chapter 6) yielded a risk factor of about 5×10^{-4}/rem, or about a factor of 3 higher than 1.65×10^{-4}/rem as previously. Rather than raise the level of risk that had been so arduously justified in 1977, the ICRP chose to recommend an overall lower (by a factor of about 3) standard of 10 rem for 5 y periods of exposure not to exceed 5 rem in any year. Two major effects of the 1990 recommendations are that they limit the average annual dose to 2 rem and they affirm the previous level of 0.05 Sv (5 rem) in one year, but restrict its application such that a 5 y average would be ≤0.1 Sv (or 10 rem).

Radiation protection standards in the USA are also now based on an assessment of risk in accordance with Federal Radiation Guidance recommended by EPA and approved by the president in 1987. EPA analyses of the risk data have consistently used the linear nonthreshold model, which yields a risk value of the order of 5×10^{-4}/rem, and US standards have remained at

$$\text{TEDE} \leq 5 \text{ rem } (0.05 \text{ Sv})/\text{y}$$

which limits radiation risk regardless of whether the dose was received internally, externally, or the sum of both. Also, consistent with ICRP recommendations, the annual committed dose to any individual tissue is also limited to 50 rem (0.5 Sv) to preclude nonstochastic effects.

9.4.2 Committed Effective Dose Equivalent (CEDE)

Since the basic protection standards were derived from risk data based on whole-body doses, a mechanism is necessary to adjust doses to internal organs to an effective whole-body dose. Such doses produce varying levels of risk to the person; thus the aggregate (or whole-body) risk is determined by assigning a relative weighting factor w_T to each of the major tissues at risk and the aggregate risk is obtained by summing these to obtain a dose equivalent to that of the total body irradiated uniformly.

The 1977 schema assigned values of w_T for six major tissues and the next five highest (the remainder); however, by 1990 sufficient risk data were available to derive w_T values (in ICRP 60) for several additional tissues. Values of w_T for tissues at risk are given in Table 9-7.

Table 9-7. Values of w_T for tissues at risk.

	w_T (ICRP 26)	w_T (ICRP 60)
Gonads	0.25	0.20
Breast	0.15	0.05
Colon	–	0.12
Red marrow	0.12	0.12
Lung	0.12	0.12
Stomach	–	0.12
Ur. bladder	–	0.05
Liver	–	0.05
Esophagus	–	0.05
Thyroid	0.03	0.05
Bone surfaces	0.03	0.01
Skin	–	0.01
Remainder ($w_T \times 5$)	0.06×5	0.01×5
Total	1.00	1.00

The w_T values for the six tissue groups plus the next five highest remaining tissues ($w_T = 5 \times 0.06 = 0.30$ or $5 \times 0.01 = 0.05$) have a total weighted risk of 1.0, as do the 12 tissues addressed in ICRP 60. Values of w_T can thus be used to convert

internal doses to organs and tissues to an effective whole-body dose; e.g., a dose to the lung of 10 rad (0.1 Sv) times a weighing factor of 0.12 yields a CEDE of 1.2 rad; i.e. it represents the same risk as 1.2 rad delivered to the total body, and under the risk-based scheme, is considered as an effective dose of 1.2 rad (or 1.2 rem if $Q = 1.0$).

Each tissue-specific committed dose equivalent ($H_{50,T}$) due to an intake is weighted and summed to obtain a committed effective dose equivalent (CEDE) to the whole body, and since the risk-based TEDE standard is 5 rem/y (0.05 Sv/y) this weighted sum is limited to

$$\sum w_T H_{50,T} \leq 5 \text{ rem } (0.05 \text{ Sv}) \text{CEDE/y}$$

where $H_{50,T}$ is the 50 y committed dose equivalent to a target tissue T due to the intake of a radionuclide.

Two tertiary requirements are used to ensure that internal doses do not exceed the TEDE limit: the ALI and a derived air concentration (DAC) which, as the name implies, is derived from the ALI and is the concentration of a radionuclide in air which, if breathed by a reference person, will result in an intake just equal to the ALI. The ALI for each radionuclide taken into the body is calculated from the weighted sum of tissue doses as

$$\text{ALI (Bq)} = \frac{0.05 \text{ Sv}}{\sum w_T H_{50,T} \text{ Sv/Bq of intake}}$$

where 0.05 Sv (5 rem) is the limiting CEDE for stochastic risks (for nonstochastic risks the ALI would be based on 0.5 Sv, or 50 rem to the maximum tissue exposed). The DAC is calculated as

$$\text{DAC (Bq/m}^3\text{)} = \frac{\text{ALI (Bq)}}{2.4 \times 10^3 \text{m}^3}$$

where 2.4×10^3 m^3 is the amount of air breathed by a reference person during light activity (20 L/min) for a working year of 2000 h, and the ALI is the most restrictive value for either stochastic or nonstochastic effects.

US regulations for internal emitters currently include ALIs and DACs based on a TEDE of 5 rem/y (see Tables 9-9 and 9-10). The ICRP has also used its recommended 2 rem/y average value to develop new calculations of ALIs and DACs which are provided in ICRP Report 61.

9.4.3 Biokinetic Models: Risk-Based Internal Dosimetry

Fairly extensive models have been developed for calculating doses for inhalation and ingestion of radionuclides, in particular a respiratory deposition/clearance model and a GI tract model which are shown together in Figure 9-4. Both assume

an initial deposition of radioactive material that is translocated to various tissues to produce a tissue dose according to the chemical and physical characteristics of the radionuclide. It is necessary therefore to determine radiation doses to the lung and various sections of the GI tract as the radioactive material passes through them as well as doses to tissues where they subsequently deposit and those that surround them. A special model has also been developed for bone dosimetry because of the unique distribution and deposition of bone-seeking radionuclides.

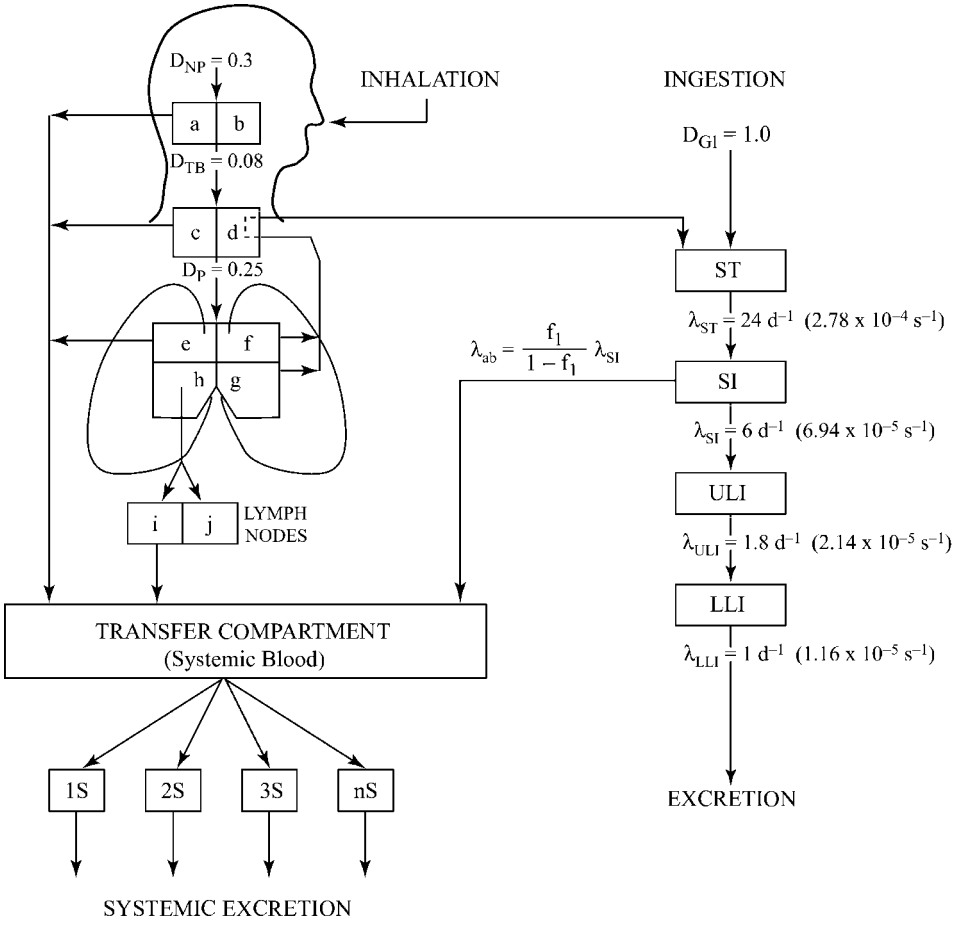

Fig. 9-4 Deposition and clearance routes of inhaled and ingested materials according to ICRP 30 schema.

Inhaled radionuclides are first deposited in various lung compartments (shown in Figure 9-4) followed by clearance to other tissues in the body either by direct absorption to the bloodstream or clearance to the GI tract. Radioactive material translocated from the lung to the GI tract clears the same as ingested material; therefore, both are shown in Figure 9-4 as interconnected routes. The GI tract

consists of four compartments, the stomach (ST), the small intestine (SI), and the upper (ULI) and lower (LLI) large intestines. A fifth compartment accounts for fecal elimination, and since it is treated as a holding compartment, it is euphemistically referred to as a "bucket" compartment. A radionuclide entering the stomach can produce a radiation dose to the stomach wall while it clears to the small intestine where it then produces a dose to the small intestine wall. Also, depending on its solubility (denoted by f_1), the radionuclide can be absorbed into the bloodstream and translocate to other organs and tissues, producing a dose to them. The remaining portion passes to the upper and lower large intestine where it delivers a dose to the ULI and LLI walls as the material is translocated for eventual excretion. The GI tract is thus an important route for translocation of both inhaled and ingested radioactive material to other tissues and organs of the body.

9.4.4 Radiation Doses Due to Inhaled Radionuclides

Two models, both of which were developed by the ICRP Task Group on Lung Dynamics, are used to describe the deposition and clearance of radionuclides in the lung. These models (shown schematically in Figure 9-4) are summarized in ICRP Report 30 (published in 1976) and provide the basis of ICRP calculations of internal dose for inhaled radionuclides. The lung model was updated in 1996 (ICRP Publication 66) but has not yet been incorporated into US regulations for controlling internal radiation dose, although it has been used by ICRP in calculations of revised dose factors for intakes of inhaled radionuclides (ICRP Report 72).

The *ICRP-30 respiratory model* assigns the deposition of inhaled radioactive materials to four major regions: the nasal–pharangeal (or NP) region, the trachea and bronchial tree (TB), the pulmonary parenchyma (P), and the lymphatic (L) system which is considered separately as a tissue compartment connected to the pulmonary region. The deposited material is assigned to one of three broad clearance classes based on the chemical and physical characteristics:

- Class D (daily) particles are quite soluble and have a half-time in the lung of less than about 10 d.
- Class W (weekly) particles are slightly soluble and have a half-time in the lung of 10–100 d (or several weeks).
- Class Y (yearly) particles are largely insoluble and can remain in the lung with half-times greater than 100 d (i.e., of the order of years).

Each region of the ICRP-30 lung model has two or more compartments (see Figure 9-4) each of which has unique deposition fractions and clearance routes and rates depending on the clearance class (D, W, Y) of the element. Material deposited in each subregion of the lung is cleared as follows:

- Material deposited in compartments a, c, and e is absorbed directly into the systemic blood, defined as the transfer compartment.
- Material deposited in compartments b, d, f, and g is transported by mucociliary action to the oropharynx where it is swallowed, thus entering the stomach where it is translocated through the rest of the GI tract where, depending on its solubility, it can either be absorbed into the systemic blood through the small intestine wall or/and moved through the upper and lower large intestines.
- Material deposited in compartment h is translocated via phagocytosis and absorption to the pulmonary lymph nodes (region L) which contains two compartments, i and j. Material transferred to compartment i is slowly translocated to body fluids, and some class Y aerosols (i.e., highly insoluble particulate matter) may be translocated to compartment j where they are assumed to be retained indefinitely.

Radioactive material that is cleared to the systemic blood supply (mathematically labeled the transfer compartment) can be taken up in various amounts by systemic organs and tissues, can circulate in the intercellular fluid, or be excreted directly. The time-dependent rate of translocation and retention in the lung, the blood, and various interconnected tissues can be modeled as a system of first-order kinetics using a series of differential equations.

The clearance class of each radiocompound and relevant metabolic data are listed in the various parts and supplements of ICRP Publication 30. The 1996 (or ICRP 66) model has more regions to account for complexities learned since 1966 (see below); however, it also designates clearance of radiocompounds in three classes that are similar to those in the ICRP 30 model: fast (F), medium (M), and slow (S).

Lung deposition of radionuclides is determined by the particle size of the inhaled aerosols expressed as the activity median aerodynamic diameter (AMAD). Deposition fractions for 1 μm AMAD particles in the nasal–pharangeal, the trachea–bronchial, and the pulmonary regions are $D_{NP} = 0.30$, $D_{TB} = 0.08$, and $D_P = 0.25$, respectively, which totals less than 1.0, indicating that the remaining fraction (0.37 for 1.0 μm AMAD particles) is exhaled. The deposition of different sized AMAD particles can also be determined from the deposition model (see Figure 9-5) for particles ranging from 0.1 to 20 μm (particles greater than 20 μm are assumed to deposit only in the NP region).

The deposition fractions for each clearance class are listed in Table 9-8 for each compartment of the lung for 1.0 μm AMAD aerosols along with the corresponding clearance half-lives and clearance constants.

Inhalation dose factors (Sv/Bq of intake) corresponding to inhalation of nominal 1 μm AMAD particles have been calculated for radionuclides in one or more clearance classes; values of these (in CDE) for selected radionuclides are listed in

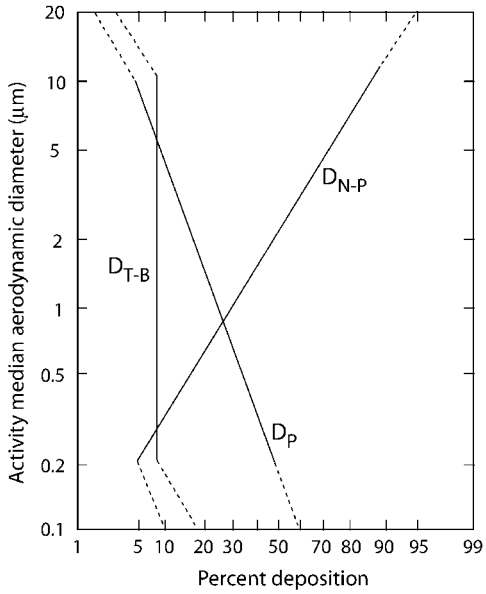

Fig. 9-5 Percent deposition of different AMAD aerosols in the nasal–phrangeal (NP), trachea–bronchial (TB), and pulmonary (P) regions of the lung of an adult male.

Table 9-8. Deposition fractions, clearance half-lives (d), and clearance constants (s^{-1}) for 1 μm AMAD aerosols in each subregion of the lung.

Region/ compartment		Class D			Class W			Class Y		
		F	*T* (d)	λ (s^{-1})	*F*	*T* (d)	λ (s^{-1})	*F*	*T* (d)	λ (s^{-1})
Nasal–pharynx ($D_{NP} = 0.30$)	a	0.5	0.01	8.02×10^{-4}	0.1	0.01	8.02×10^{-4}	0.01	0.01	8.02×10^{-4}
	b	0.5	0.01	8.02×10^{-4}	0.9	0.4	2.01×10^{-5}	0.99	0.4	2.01×10^{-5}
Trachea–bronchi ($D_{TB} = 0.08$)	c	0.95	0.01	8.02×10^{-4}	0.5	0.01	8.02×10^{-4}	0.01	0.01	8.02×10^{-4}
	d	0.95	0.2	4.01×10^{-5}	0.5	0.2	4.01×10^{-5}	0.99	0.2	4.01×10^{-5}
Pulmonary ($D_P = 0.25$)	e	0.8	0.5	1.60×10^{-5}	0.15	50	1.60×10^{-7}	0.05	500	1.60×10^{-8}
	f	n.a.	n.a.	n.a.	0.4	1.0	8.02×10^{-6}	0.4	1.0	8.02×10^{-6}
	g	n.a.	n.a.	n.a.	0.4	50	1.60×10^{-7}	0.4	500	1.60×10^{-8}
	h	0.2	0.5	1.60×10^{-5}	0.05	50	1.60×10^{-7}	0.15	500	1.60×10^{-8}
Lymph	i	1.0	0.5	1.60×10^{-5}	1.0	50	1.60×10^{-7}	0.9	1000	8.02×10^{-9}
	j	n.a.	n.a.	n.a.	n.a.	n.a.	n.a.	0.1		n.a.

Table 9-9 for the six major tissue groups which have specific weighting factors, plus up to five remainder tissues, each of which has a weighting factor of 0.06. These CDE values for the specific tissues and the "remainder" tissue(s) have been multiplied by their respective weighting factors w_T and summed to obtain the committed effective dose equivalent (CEDE) per unit intake (Sv/Bq). If the limiting CEDE is the effective dose (0.05 Sv or 5 rem), which it quite often is, it is shown in bold type; if however, the controlling effect is due to nonstochastic effects (i.e., 0.5 Sv or 50 rem) in one of the tissues, then the dose per unit intake is shown in bold type for the particular tissue that is limiting.

Table 9-9 also lists the ALI for each radionuclide which is calculated by dividing the effective dose per unit of intake into 0.05 Sv (5 rem) if the effective dose is controlling or 0.5 Sv (50 rem) if the nonstochastic tissue dose is limiting (see Example 9-5). Once the ALI is known, the corresponding DAC can be obtained by dividing the ALI by the annual breathing rate of 2.4×10^3 m^3; DAC values are also listed for the selected radionuclides in Table 9-9.

Example 9-5. From the data in Table 9-9, calculate the ALI and DAC for (a) class Y ^{60}Co, and (b) class D ^{131}I.

Solution. (a) As shown in Table 9-9, the limiting dose (shown by the bold type) for ^{60}Co is the effective dose which is 5.91×10^{-8} Sv/Bq; thus, the ALI is based on stochastic effects and is

$$\text{ALI}_S = \frac{0.05 \text{ Sv}}{5.91 \times 10^{-8} \text{ Sv/Bq}} = 8.46 \times 10^5 \text{ Bq}$$

The DAC to preclude inhalation of one ALI in 2000 work hours in a year is

$$\text{DAC (Bq/m}^3) = \frac{\text{ALI}}{2.4 \times 10^3 \text{ m}^3} = 3.53 \times 10^2 \text{ Bq/m}^3$$

(b) For ^{131}I, Table 9-9 shows the thyroid dose per Bq in bold type as 2.92×10^{-7} Sv/Bq; thus, the ALI_{NS} is based on a capping dose of 0.5 Sv to the thyroid to preclude nonstochastic effects, or

$$\text{ALI}_{NS} \text{ (Bq)} = \frac{0.5 \text{ Sv}}{2.92 \times 10^{-7} \text{ Sv/Bq}} = 1.7 \times 10^6 \text{ Bq}$$

The data in Table 9-9 can also be used to calculate the stochastic ALI for ^{131}I; this is based on the listed effective dose of 8.89×10^{-9} Sv/Bq, or

$$^{131}\text{I ALI}_S = \frac{0.05 \text{ Sv}}{8.89 \times 10^{-9} \text{ Sv/Bq}} = 5.6 \times 10^6 \text{ Bq}$$

Obviously, the nonstochastic ALI is the more limiting condition and is the one chosen to limit intakes of ^{131}I; the DAC is derived from it as

$$\text{DAC} = \frac{1.7 \times 10^6 \text{ Bq}}{2.4 \times 10^3 \text{ m}^3} = 7.1 \times 10^2 \text{ Bq/m}^3$$

Table 9-9. Inhalation dose factors (Sv/Bq inhaled), annual limits on intakes (Al5 in Bq) od derived air concentrations (ΔAl in Bq/m^3) for different classes (D, W, Y) of selected radionuclides.

Nuclide	Class	f_1	Gonad	Breast	Lung	R marrow	B surface	Thyroid	Remainder	Effective	ALI (Bq)	DAC (Bq/m^3)
H-3	V	1.0	1.73×10^{-11}	1.73×10^{-11}	1.73×10^{-11}	1.73×10^{-11}	1.73×10^{-11}	1.73×10^{-11}	1.73×10^{-11}	$\mathbf{1.73 \times 10^{-11}}$	2.89×10^{9}	1.20×10^{6}
Be-7	Y	0.005	3.17×10^{-11}	3.82×10^{-11}	3.73×10^{-10}	3.99×10^{-11}	2.98×10^{-11}	3.10×10^{-11}	7.23×10^{-11}	$\mathbf{8.67 \times 10^{-11}}$	5.77×10^{8}	2.40×10^{5}
C-11		1.0	3.41×10^{-12}	2.98×10^{-12}	3.09×10^{-12}	3.18×10^{-12}	3.03×10^{-12}	2.97×10^{-12}	3.54×10^{-12}	$\mathbf{3.29 \times 10^{-12}}$	1.52×10^{10}	6.33×10^{6}
C-14		1.0	5.64×10^{-10}	5.64×10^{-10}	5.64×10^{-10}	5.64×10^{-10}	5.64×10^{-10}	5.64×10^{-10}	5.64×10^{-10}	$\mathbf{5.64 \times 10^{-10}}$	8.87×10^{7}	3.69×10^{4}
F-18	D	1.0	2.17×10^{-12}	3.88×10^{-12}	1.09×10^{-10}	2.76×10^{-11}	2.79×10^{-11}	3.47×10^{-10}	1.37×10^{-11}	$\mathbf{2.26 \times 10^{-11}}$	2.21×10^{9}	9.22×10^{5}
Na-22	D	1.0	1.77×10^{-9}	1.65×10^{-9}	2.47×10^{-9}	2.73×10^{-9}	3.51×10^{-10}	1.60×10^{-9}	2.00×10^{-9}	$\mathbf{2.07 \times 10^{-9}}$	2.42×10^{7}	1.01×10^{4}
Na-24	D	1.0	1.78×10^{-10}	1.61×10^{-10}	1.25×10^{-9}	2.13×10^{-10}	2.58×10^{-10}	1.53×10^{-10}	2.35×10^{-10}	$\mathbf{3.27 \times 10^{-10}}$	1.53×10^{8}	6.37×10^{4}
P-32	W	0.8	3.37×10^{-10}	3.37×10^{-10}	2.56×10^{-8}	4.17×10^{-9}	4.05×10^{-9}	3.37×10^{-10}	1.18×10^{-9}	$\mathbf{4.19 \times 10^{-9}}$	1.19×10^{7}	4.97×10^{3}
S-35	W	0.1	4.54×10^{-11}	4.54×10^{-11}	5.07×10^{-9}	4.54×10^{-11}	4.54×10^{-11}	4.54×10^{-11}	1.15×10^{-10}	$\mathbf{6.69 \times 10^{-10}}$	7.47×10^{7}	3.11×10^{4}
Cl-36	W	1.0	5.04×10^{-10}	5.04×10^{-10}	4.56×10^{-8}	5.04×10^{-10}	5.04×10^{-10}	5.04×10^{-10}	5.36×10^{-10}	$\mathbf{5.93 \times 10^{-9}}$	8.43×10^{6}	3.51×10^{3}
K-40	D	1.0	3.19×10^{-9}	3.08×10^{-9}	4.66×10^{-9}	3.10×10^{-9}	3.07×10^{-9}	3.06×10^{-9}	3.21×10^{-9}	$\mathbf{3.34 \times 10^{-9}}$	1.50×10^{7}	6.24×10^{3}
Ca-45	W	0.3	4.49×10^{-11}	4.49×10^{-11}	9.67×10^{-9}	2.92×10^{-9}	4.39×10^{-9}	4.49×10^{-11}	4.27×10^{-10}	$\mathbf{1.79 \times 10^{-9}}$	2.79×10^{7}	1.16×10^{4}
Cr-51	Y	0.1	2.21×10^{-11}	1.50×10^{-11}	3.77×10^{-10}	1.87×10^{-11}	1.50×10^{-11}	1.00×10^{-11}	4.93×10^{-11}	$\mathbf{7.08 \times 10^{-11}}$	7.06×10^{8}	2.94×10^{5}
Mn-54	W	0.1	7.09×10^{-10}	8.59×10^{-10}	6.66×10^{-9}	1.10×10^{-10}	1.25×10^{-9}	7.40×10^{-10}	1.72×10^{-9}	$\mathbf{1.81 \times 10^{-9}}$	2.76×10^{7}	1.15×10^{4}
Mn-56	D	0.1	9.46×10^{-12}	7.79×10^{-12}	5.37×10^{-10}	1.02×10^{-11}	8.23×10^{-12}	6.18×10^{-12}	6.50×10^{-11}	$\mathbf{8.91 \times 10^{-11}}$	5.61×10^{8}	2.34×10^{5}
Fe-55	D	0.1	5.23×10^{-10}	5.09×10^{-10}	5.19×10^{-10}	5.17×10^{-10}	5.14×10^{-10}	5.42×10^{-10}	1.21×10^{-9}	$\mathbf{7.26 \times 10^{-10}}$	6.89×10^{7}	2.87×10^{4}

Nuclide	Class	f_1	Gonad	Breast	Lung	R marrow	B surface	Thyroid	Remainder	Effective	ALI (Bq)	DAC (Bq/m^3)
Fe-59	D	0.1	3.32×10^{-9}	3.01×10^{-9}	3.50×10^{-9}	3.18×10^{-9}	2.91×10^{-9}	2.95×10^{-9}	5.81×10^{-9}	$\mathbf{4.00 \times 10^{-9}}$	1.25×10^{7}	5.21×10^{3}
Co-57	Y	0.05	1.24×10^{-10}	3.75×10^{-10}	1.69×10^{-8}	5.88×10^{-10}	4.52×10^{-10}	2.71×10^{-10}	8.22×10^{-10}	$\mathbf{2.45 \times 10^{-9}}$	2.04×10^{7}	8.50×10^{3}
Co-58	Y	0.05	6.17×10^{-10}	9.37×10^{-10}	1.60×10^{-8}	9.23×10^{-10}	6.93×10^{-10}	8.72×10^{-10}	1.89×10^{-9}	$\mathbf{2.94 \times 10^{-9}}$	1.70×10^{7}	7.09×10^{3}
Co-60	Y	0.05	4.76×10^{-9}	1.84×10^{-8}	3.45×10^{-7}	1.72×10^{-8}	1.35×10^{-8}	1.62×10^{-8}	3.60×10^{-8}	$\mathbf{5.91 \times 10^{-8}}$	8.46×10^{5}	3.53×10^{2}
Ni-59	D	0.05	3.59×10^{-10}	3.46×10^{-10}	3.59×10^{-10}	3.54×10^{-10}	3.51×10^{-10}	3.77×10^{-10}	3.63×10^{-10}	$\mathbf{3.58 \times 10^{-10}}$	1.40×10^{8}	5.82×10^{4}
Ni-63	D	0.05	8.22×10^{-10}	8.22×10^{-10}	8.74×10^{-10}	8.22×10^{-10}	8.22×10^{-10}	8.22×10^{-10}	8.59×10^{-10}	$\mathbf{8.39 \times 10^{-10}}$	5.96×10^{7}	2.48×10^{4}
Ni-65	D	0.05	8.46×10^{-12}	6.48×10^{-12}	3.11×10^{-10}	6.70×10^{-12}	5.79×10^{-12}	5.54×10^{-12}	7.98×10^{-11}	$\mathbf{6.55 \times 10^{-11}}$	7.63×10^{8}	3.18×10^{5}
Cu-64	Y	0.5	1.24×10^{-11}	6.38×10^{-12}	3.50×10^{-10}	7.12×10^{-12}	5.29×10^{-12}	4.98×10^{-12}	9.20×10^{-11}	$\mathbf{7.48 \times 10^{-11}}$	6.68×10^{8}	2.79×10^{5}
Zn-65	Y	0.5	2.03×10^{-9}	3.08×10^{-9}	2.10×10^{-8}	3.62×10^{-9}	3.36×10^{-9}	3.02×10^{-9}	4.66×10^{-9}	$\mathbf{5.51 \times 10^{-9}}$	9.07×10^{6}	3.78×10^{3}
Ga-67	Y	0.001	6.12×10^{-11}	1.83×10^{-11}	5.37×10^{-10}	3.71×10^{-11}	7.84×10^{-11}	9.43×10^{-12}	2.04×10^{-10}	$\mathbf{1.51 \times 10^{-10}}$	3.31×10^{8}	1.38×10^{5}
Ga-68	D	0.001	5.49×10^{-12}	4.40×10^{-12}	1.88×10^{-10}	5.71×10^{-12}	4.91×10^{-12}	3.77×10^{-12}	3.95×10^{-11}	$\mathbf{3.74 \times 10^{-11}}$	1.34×10^{9}	5.57×10^{5}
Ge-67	D	1.0	1.22×10^{-12}	1.63×10^{-12}	1.01×10^{-10}	1.66×10^{-12}	1.49×10^{-12}	1.47×10^{-12}	1.16×10^{-11}	$\mathbf{1.64 \times 10^{-11}}$	3.05×10^{9}	1.27×10^{6}
Ge-68	W	1.0	2.16×10^{-10}	7.50×10^{-10}	1.11×10^{-7}	7.17×10^{-10}	5.94×10^{-10}	6.90×10^{-10}	1.43×10^{-9}	$\mathbf{1.40 \times 10^{-8}}$	3.57×10^{6}	1.49×10^{3}
As-76	W	0.5	7.54×10^{-11}	5.33×10^{-11}	5.02×10^{-9}	5.59×10^{-11}	4.90×10^{-11}	4.80×10^{-11}	1.24×10^{-9}	$\mathbf{1.01 \times 10^{-9}}$	4.95×10^{7}	2.06×10^{4}
Br-82	W	1.0	1.69×10^{-10}	2.10×10^{-10}	1.68×10^{-10}	2.18×10^{-10}	1.92×10^{-10}	2.06×10^{-10}	3.31×10^{-10}	$\mathbf{4.13 \times 10^{-10}}$	1.21×10^{8}	5.04×10^{4}
Rb-86	D	1.0	1.34×10^{-9}	1.33×10^{-9}	3.30×10^{-9}	2.32×10^{-9}	4.27×10^{-9}	1.33×10^{-9}	1.38×10^{-9}	$\mathbf{1.79 \times 10^{-9}}$	2.79×10^{7}	1.16×10^{4}
Sr-85	Y	0.3	3.34×10^{-10}	4.65×10^{-10}	7.15×10^{-9}	4.65×10^{-10}	3.50×10^{-10}	3.85×10^{-10}	9.05×10^{-10}	$\mathbf{1.36 \times 10^{-9}}$	3.68×10^{7}	1.53×10^{4}
Sr-89	Y	0.3	7.95×10^{-12}	7.96×10^{-12}	8.35×10^{-8}	1.07×10^{-10}	1.59×10^{-10}	7.96×10^{-12}	3.97×10^{-9}	$\mathbf{1.12 \times 10^{-8}}$	4.46×10^{6}	1.86×10^{3}
Sr-90	Y	0.3	2.69×10^{-10}	2.69×10^{-10}	2.86×10^{-6}	3.28×10^{-8}	7.09×10^{-8}	2.69×10^{-10}	5.73×10^{-9}	$\mathbf{3.51 \times 10^{-7}}$	1.42×10^{5}	5.94×10^{1}

Table 9-9. Continued.

Nuclide	Class	f_1	Gonad	Breast	Lung	R marrow	B surface	Thyroid	Remainder	Effective	ALI (Bq)	DAC (Bq/m^3)
Zr-95	W	0.02	8.40×10^{-10}	9.32×10^{-10}	1.86×10^{-8}	3.24×10^{-9}	2.17×10^{-8}	7.82×10^{-10}	2.13×10^{-9}	**4.29×10^{-9}**	1.17×10^{7}	4.86×10^{3}
Nb-94	Y	0.01	4.42×10^{-9}	2.24×10^{-8}	7.48×10^{-7}	2.26×10^{-8}	1.97×10^{-8}	2.22×10^{-8}	4.45×10^{-8}	**1.12×10^{-7}**	4.46×10^{5}	1.86×10^{2}
Nb-95	Y	0.01	4.32×10^{-10}	4.07×10^{-10}	8.32×10^{-9}	4.42×10^{-10}	5.13×10^{-10}	3.58×10^{-10}	1.07×10^{-9}	**1.57×10^{-9}**	3.18×10^{7}	1.33×10^{4}
Mo-99	Y	0.8	9.51×10^{-11}	2.75×10^{-11}	4.29×10^{-9}	5.24×10^{-11}	4.13×10^{-11}	1.52×10^{-11}	1.74×10^{-9}	**1.07×10^{-9}**	4.67×10^{7}	1.95×10^{4}
Tc-99	W	0.8	3.99×10^{-11}	3.99×10^{-11}	1.67×10^{-8}	3.99×10^{-11}	3.99×10^{-11}	1.07×10^{-9}	6.26×10^{-10}	**2.25×10^{-9}**	2.22×10^{7}	9.26×10^{3}
Tc-99m	D	0.8	2.77×10^{-12}	2.15×10^{-12}	2.28×10^{-11}	3.36×10^{-12}	2.62×10^{-12}	5.01×10^{-11}	1.02×10^{-11}	**8.80×10^{-12}**	5.68×10^{9}	2.37×10^{6}
Ru-103	Y	0.05	3.07×10^{-10}	3.11×10^{-10}	1.56×10^{-8}	3.19×10^{-10}	2.37×10^{-10}	2.57×10^{-10}	1.25×10^{-9}	**2.42×10^{-9}**	2.07×10^{7}	8.61×10^{3}
Ru-106	Y	0.05	1.30×10^{-9}	1.78×10^{-9}	1.04×10^{-6}	1.76×10^{-9}	1.61×10^{-9}	1.72×10^{-9}	1.20×10^{-8}	**1.29×10^{-7}**	3.88×10^{5}	1.61×10^{2}
Ag-110m	Y	0.05	2.43×10^{-9}	7.10×10^{-9}	1.20×10^{-7}	6.74×10^{-9}	5.19×10^{-9}	6.39×10^{-9}	1.51×10^{-8}	**2.17×10^{-8}**	2.30×10^{6}	9.60×10^{2}
Cd-109	D	0.05	2.71×10^{-9}	2.97×10^{-9}	3.34×10^{-9}	3.45×10^{-9}	3.14×10^{-9}	2.66×10^{-9}	9.59×10^{-8}	3.09×10^{-8}	1.62×10^{6}	6.74×10^{2}
									3.95×10^{-7}	**Kidneys**	1.27×10^{6}	5.29×10^{2}
In-115	Y	0.02	1.17×10^{-7}	1.17×10^{-7}	1.17×10^{-7}	3.67×10^{-6}	1.89×10^{-6}	1.17×10^{-7}	1.49×10^{-6}	**1.01×10^{-6}**	4.95×10^{4}	2.06×10^{1}
Sn-113	W	0.02	3.16×10^{-10}	2.99×10^{-10}	1.84×10^{-8}	7.71×10^{-10}	1.32×10^{-9}	2.27×10^{-10}	1.38×10^{-9}	**2.88×10^{-9}**	1.74×10^{7}	7.23×10^{3}
Sb-124	W	0.01	1.04×10^{-9}	8.94×10^{-10}	4.14×10^{-8}	1.09×10^{-9}	1.24×10^{-9}	6.74×10^{-10}	4.18×10^{-9}	**6.80×10^{-9}**	7.35×10^{6}	3.06×10^{3}
Sb-125	W	0.01	3.60×10^{-10}	4.16×10^{-10}	2.17×10^{-8}	5.35×10^{-10}	9.78×10^{-10}	3.24×10^{-10}	1.45×10^{-9}	**3.30×10^{-9}**	1.52×10^{7}	6.31×10^{3}
I-123	D	1.0	2.89×10^{-12}	4.87×10^{-12}	6.57×10^{-11}	5.97×10^{-12}	5.18×10^{-12}	**2.25×10^{-9}**	7.89×10^{-12}	8.01×10^{-11}	**2.22×10^{8}**	9.25×10^{4}
I-125	D	1.0	1.84×10^{-11}	9.25×10^{-11}	1.19×10^{-10}	4.41×10^{-11}	4.27×10^{-11}	**2.16×10^{-7}**	3.33×10^{-11}	6.53×10^{-9}	**2.31×10^{6}**	9.63×10^{2}
I-129	D	1.0	8.69×10^{-11}	2.09×10^{-10}	3.14×10^{-10}	1.40×10^{-10}	1.38×10^{-10}	**1.56×10^{-6}**	1.18×10^{-10}	4.69×10^{-8}	**3.21×10^{5}**	1.34×10^{2}
I-130	D	1.0	2.81×10^{-11}	4.87×10^{-11}	6.03×10^{-10}	4.55×10^{-11}	4.03×10^{-11}	**1.99×10^{-8}**	8.02×10^{-11}	7.14×10^{-10}	**2.51×10^{7}**	1.05×10^{4}

Nuclide	Class	f_1	Gonad	Breast	Lung	R marrow	B surface	Thyroid	Remainder	Effective	ALI (Bq)	DAC (Bq/m^3)
I-131	D	1.0	2.53×10^{-11}	7.88×10^{-11}	6.57×10^{-10}	6.26×10^{-11}	5.73×10^{-11}	$\mathbf{2.92 \times 10^{-7}}$	8.03×10^{-11}	8.89×10^{-9}	$\mathbf{1.71 \times 10^{6}}$	7.13×10^{2}
Cs-134	D	1.0	1.30×10^{-8}	1.08×10^{-8}	1.18×10^{-8}	1.18×10^{-8}	1.10×10^{-8}	1.11×10^{-8}	1.39×10^{-8}	$\mathbf{1.25 \times 10^{-8}}$	4.00×10^{6}	1.67×10^{3}
Cs-137	D	1.0	8.76×10^{-9}	7.84×10^{-9}	8.82×10^{-9}	8.30×10^{-9}	7.94×10^{-9}	7.93×10^{-9}	9.12×10^{-9}	$\mathbf{8.63 \times 10^{-9}}$	5.79×10^{6}	2.41×10^{3}
Cs-138	D	1.0	3.28×10^{-12}	4.02×10^{-12}	1.59×10^{-10}	3.95×10^{-12}	3.55×10^{-12}	3.57×10^{-12}	2.06×10^{-11}	$\mathbf{2.74 \times 10^{-11}}$	1.82×10^{9}	7.60×10^{5}
Ba-133	D	0.1	1.07×10^{-9}	1.10×10^{-9}	1.29×10^{-9}	6.56×10^{-9}	9.51×10^{-9}	9.99×10^{-10}	1.41×10^{-9}	$\mathbf{2.11 \times 10^{-9}}$	2.37×10^{7}	9.87×10^{3}
Ba-140	D	0.1	4.30×10^{-10}	2.87×10^{-10}	1.66×10^{-9}	1.29×10^{-9}	2.41×10^{-9}	2.56×10^{-10}	1.41×10^{-9}	$\mathbf{1.01 \times 10^{-9}}$	4.95×10^{7}	2.06×10^{4}
La-140	W	0.001	4.54×10^{-10}	1.45×10^{-10}	4.21×10^{-9}	2.14×10^{-10}	1.41×10^{-10}	6.87×10^{-11}	2.12×10^{-9}	$\mathbf{1.31 \times 10^{-9}}$	3.82×10^{7}	1.59×10^{4}
Ce-141	Y	0.0003	5.54×10^{-11}	4.46×10^{-11}	1.67×10^{-8}	8.96×10^{-11}	2.54×10^{-10}	2.55×10^{-11}	1.26×10^{-9}	$\mathbf{2.42 \times 10^{-9}}$	2.07×10^{7}	8.61×10^{3}
Ce-144	Y	0.0003	2.39×10^{-10}	3.48×10^{-10}	7.91×10^{-7}	2.88×10^{-9}	4.72×10^{-9}	2.92×10^{-10}	1.91×10^{-8}	$\mathbf{1.01 \times 10^{-7}}$	4.95×10^{5}	2.06×10^{2}
Pr-144	Y	0.0003	2.41×10^{-15}	1.05×10^{-14}	9.40×10^{-11}	1.38×10^{-14}	1.47×10^{-14}	8.47×10^{-15}	1.40×10^{-12}	$\mathbf{1.17 \times 10^{-11}}$	4.27×10^{9}	1.78×10^{6}
Nd-147	Y	0.0003	8.41×10^{-11}	3.45×10^{-11}	1.06×10^{-8}	9.19×10^{-11}	3.26×10^{-10}	1.82×10^{-11}	1.76×10^{-9}	$\mathbf{1.85 \times 10^{-9}}$	2.70×10^{7}	1.13×10^{4}
Pm-147	Y	0.0003	8.25×10^{-15}	3.60×10^{-14}	7.74×10^{-8}	1.61×10^{-9}	2.01×10^{-8}	1.98×10^{-14}	1.56×10^{-9}	$\mathbf{1.06 \times 10^{-8}}$	4.72×10^{6}	1.97×10^{3}
Eu-152	W	0.001	1.31×10^{-8}	1.74×10^{-8}	5.76×10^{-8}	7.91×10^{-8}	2.40×10^{-7}	8.25×10^{-9}	9.99×10^{-8}	$\mathbf{5.97 \times 10^{-8}}$	8.38×10^{5}	3.49×10^{2}
Eu-154	W	0.001	1.17×10^{-8}	1.55×10^{-8}	7.92×10^{-8}	1.06×10^{-7}	5.23×10^{-7}	7.14×10^{-9}	1.13×10^{-7}	$\mathbf{7.73 \times 10^{-8}}$	6.47×10^{5}	2.70×10^{2}
Gd-148	D	0.0003	0.00×10^{0}	0.00×10^{0}	1.98×10^{-7}	1.41×10^{-4}	$\mathbf{1.76 \times 10^{-3}}$	0.00×10^{0}	6.45×10^{-5}	8.91×10^{-5}	$\mathbf{2.84 \times 10^{2}}$	1.18×10^{-1}
Gd-152	D	0.0003	0.00×10^{0}	0.00×10^{0}	1.33×10^{-7}	1.04×10^{-4}	$\mathbf{1.30 \times 10^{-3}}$	0.00×10^{0}	4.77×10^{-5}	6.58×10^{-5}	$\mathbf{3.85 \times 10^{2}}$	1.60×10^{-1}
Lu-176	D	0.0003	3.86×10^{-9}	1.10×10^{-8}	9.99×10^{-7}	1.21×10^{-7}	1.19×10^{-6}	8.24×10^{-9}	2.10×10^{-8}	$\mathbf{1.79 \times 10^{-7}}$	2.79×10^{5}	1.16×10^{2}
Lu-177	W	0.0003	1.93×10^{-11}	5.79×10^{-12}	3.33×10^{-9}	1.82×10^{-11}	1.03×10^{-10}	2.47×10^{-12}	8.42×10^{-10}	$\mathbf{6.63 \times 10^{-10}}$	7.54×10^{7}	3.14×10^{4}
Ta-182	Y	0.001	8.99×10^{-10}	1.79×10^{-9}	8.28×10^{-8}	1.92×10^{-9}	1.51×10^{-9}	1.53×10^{-9}	4.37×10^{-9}	$\mathbf{1.21 \times 10^{-8}}$	4.13×10^{6}	1.72×10^{3}

Table 9-9. Continued.

Nuclide	Class	f_1	Gonad	Breast	Lung	R marrow	B surface	Thyroid	Remainder	Effective	ALI (Bq)	DAC (Bq/m^3)
W-188	D	0.3	7.97×10^{-12}	4.88×10^{-12}	1.36×10^{-9}	5.54×10^{-10}	1.65×10^{-9}	2.72×10^{-12}	2.75×10^{-9}	$\mathbf{1.11 \times 10^{-9}}$	4.50×10^{7}	1.88×10^{4}
Re-186	W	0.8	4.53×10^{-11}	4.48×10^{-11}	4.42×10^{-9}	4.72×10^{-11}	4.59×10^{-11}	2.19×10^{-9}	8.10×10^{-10}	$\mathbf{8.64 \times 10^{-10}}$	5.79×10^{7}	2.41×10^{4}
Ir-192	Y	0.01	6.08×10^{-10}	8.63×10^{-10}	5.24×10^{-8}	9.38×10^{-10}	7.00×10^{-10}	6.51×10^{-10}	2.94×10^{-9}	$\mathbf{7.61 \times 10^{-9}}$	6.57×10^{6}	2.74×10^{3}
Pt-193	D	0.01	1.43×10^{-11}	1.33×10^{-11}	3.86×10^{-11}	1.36×10^{-11}	1.35×10^{-11}	1.42×10^{-11}	1.62×10^{-10}	$\mathbf{6.14 \times 10^{-11}}$	8.14×10^{8}	3.39×10^{5}
Pt-193m	D	0.01	3.78×10^{-11}	3.55×10^{-11}	4.09×10^{-10}	3.86×10^{-11}	3.70×10^{-11}	3.50×10^{-11}	5.55×10^{-10}	$\mathbf{2.37 \times 10^{-10}}$	2.11×10^{8}	8.79×10^{4}
Pt-195m	D	0.01	6.80×10^{-11}	5.42×10^{-11}	5.65×10^{-10}	7.24×10^{-11}	6.29×10^{-11}	5.04×10^{-11}	7.48×10^{-10}	$\mathbf{3.29 \times 10^{-10}}$	1.52×10^{8}	6.33×10^{4}
Pt-197	D	0.01	1.64×10^{-11}	1.45×10^{-11}	4.55×10^{-10}	1.59×10^{-11}	1.50×10^{-11}	1.41×10^{-11}	2.97×10^{-10}	$\mathbf{1.53 \times 10^{-10}}$	3.27×10^{8}	1.36×10^{5}
Pt-197m	D	0.01	3.24×10^{-12}	2.80×10^{-12}	1.40×10^{-10}	3.28×10^{-12}	2.92×10^{-12}	2.62×10^{-23}	4.83×10^{-11}	$\mathbf{3.31 \times 10^{-11}}$	1.51×10^{9}	6.29×10^{5}
$Pt^{-19}9$	D	0.01	1.09×10^{-12}	9.87×10^{-13}	6.61×10^{-11}	1.07×10^{-12}	9.66×10^{-13}	9.03×10^{-13}	1.26×10^{-11}	$\mathbf{1.23 \times 10^{-11}}$	4.07×10^{9}	1.69×10^{6}
Au-195	Y	0.1	7.67×10^{-11}	2.29×10^{-10}	2.65×10^{-8}	4.35×10^{-10}	3.39×10^{-10}	1.08×10^{-10}	6.63×10^{-10}	$\mathbf{3.50 \times 10^{-9}}$	1.43×10^{7}	5.95×10^{3}
Au-198	Y	0.1	1.40×10^{-10}	4.16×10^{-11}	3.51×10^{-9}	5.40×10^{-11}	3.19×10^{-11}	2.37×10^{-11}	1.39×10^{-9}	$\mathbf{8.87 \times 10^{-10}}$	5.64×10^{7}	2.35×10^{4}
Hg-197	W	0.02	3.38×10^{-11}	1.20×10^{-11}	7.21×10^{-10}	2.65×10^{-11}	1.62×10^{-11}	6.98×10^{-12}	2.84×10^{-10}	$\mathbf{1.86 \times 10^{-10}}$	2.69×10^{8}	1.12×10^{5}
Hg-197	W	vapor	3.15×10^{-11}	3.47×10^{-11}	1.12×10^{-9}	5.34×10^{-11}	4.70×10^{-11}	3.09×10^{-11}	1.18×10^{-10}	$\mathbf{1.92 \times 10^{-10}}$	2.60×10^{8}	1.09×10^{5}
Hg-203	W	0.02	2.74×10^{-10}	2.14×10^{-10}	8.78×10^{-9}	2.63×10^{-10}	2.09×10^{-10}	1.77×10^{-10}	1.19×10^{-9}	$\mathbf{1.55 \times 10^{-9}}$	3.23×10^{7}	1.34×10^{4}
Hg-203	W	vapor	8.65×10^{-10}	7.90×10^{-10}	3.32×10^{-9}	9.45×10^{-10}	8.49×10^{-10}	7.32×10^{-10}	2.77×10^{-9}	$\mathbf{1.73 \times 10^{-9}}$	2.89×10^{7}	1.20×10^{4}
Tl-201	D	1.0	3.66×10^{-11}	3.32×10^{-11}	1.69×10^{-10}	5.37×10^{-11}	4.77×10^{-11}	3.14×10^{-11}	6.71×10^{-11}	$\mathbf{6.34 \times 10^{-11}}$	7.89×10^{8}	3.29×10^{5}
Tl-204	D	1.0	4.14×10^{-10}	4.14×10^{-10}	1.13×10^{-9}	4.15×10^{-10}	4.15×10^{-10}	4.14×10^{-10}	9.14×10^{-10}	$\mathbf{6.50 \times 10^{-10}}$	7.69×10^{7}	3.21×10^{4}
Pb-210	D	0.2	3.18×10^{-7}	3.18×10^{-7}	3.18×10^{-7}	3.75×10^{-6}	$\mathbf{5.47 \times 10^{-5}}$	3.18×10^{-7}	4.69×10^{-6}	3.67×10^{-6}	$\mathbf{9.14 \times 10^{3}}$	3.81×10^{0}
Bi-210	D	0.05	6.47×10^{-11}	6.47×10^{-11}	4.26×10^{-7}	6.47×10^{-11}	6.47×10^{-11}	6.47×10^{-11}	5.66×10^{-9}	$\mathbf{5.29 \times 10^{-8}}$	9.45×10^{5}	3.94×10^{2}

Nuclide	Class	f_1	Gonad	Breast	Lung	R marrow	B surface	Thyroid	Remainder	Effective	ALI (Bq)	DAC (Bq/m^3)
Po-210	D	0.1	4.04×10^{-7}	4.04×10^{-7}	7.29×10^{-7}	4.04×10^{-7}	4.04×10^{-7}	4.04×10^{-7}	7.40×10^{-6}	$\mathbf{2.54 \times 10^{-6}}$	1.97×10^{4}	8.20×10^{0}
Ra-226	W	0.2	1.02×10^{-7}	1.02×10^{-7}	1.61×10^{-5}	6.64×10^{-7}	7.59×10^{-6}	1.02×10^{-7}	1.07×10^{-7}	$\mathbf{2.32 \times 10^{-6}}$	2.16×10^{4}	8.98×10^{0}
Ra-227	W	0.2	2.27×10^{-12}	2.36×10^{-12}	3.32×10^{-10}	4.81×10^{-11}	$\mathbf{9.59 \times 10^{-10}}$	2.30×10^{-12}	4.60×10^{-12}	7.68×10^{-11}	$\mathbf{5.21 \times 10^{8}}$	2.17×10^{5}
Ra-228	W	0.2	1.83×10^{-7}	1.84×10^{-7}	7.22×10^{-6}	7.38×10^{-7}	6.51×10^{-6}	1.83×10^{-7}	1.87×10^{-7}	$\mathbf{1.29 \times 10^{-4}}$	3.88×10^{2}	1.61×10^{-1}
Th-230	W	0.0002	4.08×10^{-7}	4.08×10^{-7}	1.61×10^{-5}	1.73×10^{-4}	$\mathbf{2.16 \times 10^{-3}}$	4.08×10^{7}	1.05×10^{-6}	8.80×10^{-5}	$\mathbf{2.31 \times 10^{2}}$	9.63×10^{-2}
Th-232	W	0.0002	7.62×10^{-7}	7.72×10^{-7}	1.44×10^{-5}	8.93×10^{-4}	$\mathbf{1.11 \times 10^{-2}}$	7.44×10^{-7}	1.87×10^{-6}	4.43×10^{-4}	$\mathbf{4.50 \times 10^{1}}$	1.88×10^{-2}
Pa-231	W	0.001	6.90×10^{-9}	8.79×10^{-9}	1.72×10^{-5}	6.97×10^{-4}	$\mathbf{8.70 \times 10^{-3}}$	7.64×10^{-9}	2.87×10^{-7}	3.47×10^{-4}	$\mathbf{5.75 \times 10^{1}}$	2.40×10^{-2}
U-235	Y	0.002	2.84×10^{-9}	5.37×10^{-9}	2.76×10^{-4}	7.15×10^{-8}	1.05×10^{-6}	4.11×10^{-9}	1.02×10^{-7}	$\mathbf{3.32 \times 10^{-5}}$	1.51×10^{3}	6.28×10^{-1}
U-238	Y	0.002	2.42×10^{-9}	2.91×10^{-9}	2.66×10^{-4}	6.88×10^{-8}	1.01×10^{-6}	2.73×10^{-9}	9.61×10^{-8}	$\mathbf{3.20 \times 10^{-5}}$	1.56×10^{3}	6.51×10^{-1}
Np-237	W	0.001	2.96×10^{-5}	1.69×10^{-8}	1.61×10^{-5}	2.62×10^{-4}	$\mathbf{3.27 \times 10^{-3}}$	1.34×10^{-8}	2.34×10^{-5}	1.46×10^{-4}	$\mathbf{1.53 \times 10^{2}}$	6.38×10^{-2}
Pu-238	Y	0.00001	1.04×10^{-5}	4.40×10^{-10}	3.20×10^{-4}	5.80×10^{-5}	7.25×10^{-4}	3.86×10^{-10}	2.74×10^{-5}	$\mathbf{7.79 \times 10^{-5}}$	6.42×10^{2}	2.67×10^{-1}
Pu-239	Y	0.001	3.18×10^{-5}	9.22×10^{-10}	1.73×10^{-5}	1.69×10^{-4}	$\mathbf{2.11 \times 10^{-3}}$	9.03×10^{-10}	7.56r-5	1.16×10^{-4}	$\mathbf{2.37 \times 10^{2}}$	9.88×10^{-2}
Pu-241	W	0.001	6.82×10^{-7}	3.06×10^{-11}	7.42×10^{-9}	3.36×10^{-6}	$\mathbf{4.20 \times 10^{-5}}$	1.24×10^{-11}	1.31×10^{-6}	2.23×10^{-6}	$\mathbf{1.19 \times 10^{2}}$	4.96×10^{-2}
Pu-242	W	0.001	3.02×10^{-5}	9.45×10^{-10}	1.64×10^{-5}	1.61×10^{-4}	$\mathbf{2.01 \times 10^{-3}}$	8.79×10^{-10}	7.18×10^{-5}	1.11×10^{-4}	$\mathbf{2.49 \times 10^{2}}$	1.04×10^{-1}
Am-241	W	0.001	3.25×10^{-5}	2.67×10^{-9}	1.84×10^{-5}	1.74×10^{-4}	$\mathbf{2.17 \times 10^{-3}}$	1.60×10^{-9}	7.82×10^{-5}	1.20×10^{-4}	$\mathbf{2.30 \times 10^{2}}$	9.58×10^{-2}
Cm-244	W	0.001	1.59×10^{-5}	1.04×10^{-9}	1.93×10^{-5}	9.38×10^{-5}	$\mathbf{1.17 \times 10^{-3}}$	1.01×10^{-9}	4.78×10^{-5}	6.70×10^{-5}	$\mathbf{4.27 \times 10^{2}}$	1.78×10^{-1}
Cf-252	W	0.001	5.43×10^{-6}	6.56×10^{-8}	3.74×10^{-5}	5.50×10^{-5}	$\mathbf{6.86 \times 10^{-4}}$	3.38×10^{-8}	1.33×10^{-5}	3.70×10^{-5}	$\mathbf{7.29 \times 10^{2}}$	3.04×10^{-1}

Source: Adapted from Federal Guidance Report 11, EPA 520/11-88-020 1988.

9.4.5
Radiation Doses Due to Ingested Radionuclides

A dynamic GI tract model, as illustrated in Figure 9-6 and based on linear first-order kinetics, has been used to determine translocation and retention of radioactive material deposited in the stomach (ST) which in turn passes through the small intestine (SI) and the upper (ULI) and lower (LLI) large intestines. The GI tract model includes absorption through the small intestine wall into the bloodstream where it can be taken up by organs and tissues, circulated in intercellular fluids, or excreted directly.

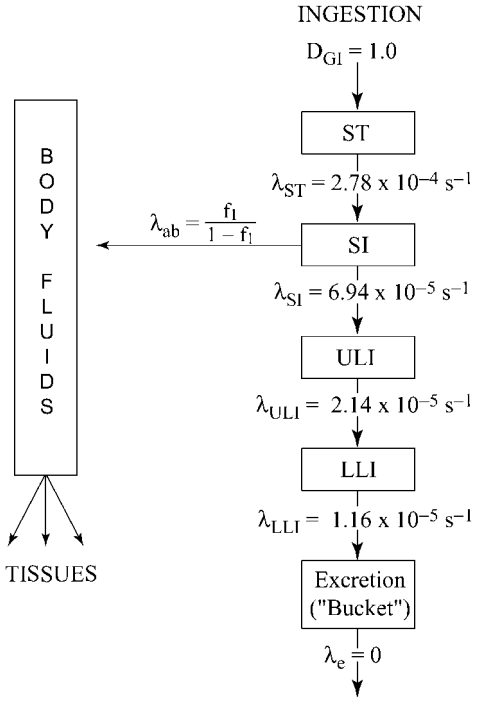

Fig. 9-6 Model of the gastrointestinal (GI) tract used for determining radiation dose to segments of the GI tract and for dynamic translocation of ingested radionuclides to other tissues.

Ingestion dose factors (Sv/Bq of intake) are provided in Table 9-10 for selected radionuclides that are ingested into the body along with the corresponding ALI values. No concentration values have been calculated since it is doubtful that workers would consume contaminated water, and certainly not continuously over a year. Such a limiting concentration for a radionuclide in water might be more appropriate for the general public; however, national and international standards organizations do not recommend the use of these derived values for the general public since they are based on a reference male adult worker and not a typical member of the public. Regardless of these cautions, various groups, and in particular the US Nuclear Regulatory Commission, have used inhalation and ingestion ALIs, appropriately adjusted, to derive concentration values in air and water for the general public.

Table 9-10. Ingestion dose factors (Sv/Bq ingested) and annual limits on intake (Bq) for ingestion of selected radionuclides (ALIs marked with * are based on limiting nonstochastic risks).

Nuclide	Class	f_1	Gonad	Breast	Lung	R. marrow	B. surface	Thyroid	Remainder	Effective	ALI (Bq)
H-3	V	1.0	1.73×10^{-11}	1.73×10^{-11}	1.73×10^{-11}	1.73×10^{-11}	1.73×10^{-11}	1.73×10^{-11}	1.73×10^{-11}	$\mathbf{1.73 \times 10^{-11}}$	2.89×10^{9}
Be-7	Y	0.005	5.67×10^{-11}	6.97×10^{-12}	1.41×10^{-12}	1.23×10^{-11}	5.03×10^{-12}	6.08×10^{-13}	5.83×10^{-11}	$\mathbf{3.45 \times 10^{-11}}$	1.45×10^{9}
C-11		1.0	3.41×10^{-12}	2.98×10^{-12}	3.09×10^{-12}	3.18×10^{-12}	3.03×10^{-12}	2.97×10^{-12}	3.54×10^{-12}	$\mathbf{3.29 \times 10^{-12}}$	1.52×10^{10}
C-14		1.0	5.64×10^{-10}	5.64×10^{-10}	5.64×10^{-10}	5.64×10^{-10}	5.64×10^{-10}	5.64×10^{-10}	5.64×10^{-10}	$\mathbf{5.64 \times 10^{-10}}$	8.87×10^{7}
F-18	D	1.0	4.97×10^{-12}	6.36×10^{-12}	6.54×10^{-12}	5.94×10^{-11}	6.02×10^{-11}	4.52×10^{-12}	7.03×10^{-11}	$\mathbf{3.31 \times 10^{-11}}$	1.51×10^{9}
									$\mathbf{2.87 \times 10^{-10}}$	**ST wall**	1.74×10^{9}*
Na-22	D	1.0	2.81×10^{-9}	2.58×10^{-9}	2.51×10^{-9}	4.29×10^{-9}	5.54×10^{-9}	2.50×10^{-9}	3.18×10^{-9}	$\mathbf{3.10 \times 10^{-9}}$	1.61×10^{7}
Na-24	D	1.0	3.43×10^{-10}	2.71×10^{-10}	2.60×10^{-10}	3.74×10^{-10}	4.68×10^{-10}	2.60×10^{-10}	5.31×10^{-10}	$\mathbf{3.84 \times 10^{-10}}$	1.30×10^{8}
P-32	W	0.8	6.55×10^{-10}	6.55×10^{-10}	6.55×10^{-10}	8.09×10^{-9}	7.87×10^{-9}	6.55×10^{-10}	2.67×10^{-9}	$\mathbf{2.37 \times 10^{-9}}$	2.11×10^{7}
S-35	W	0.1	9.53×10^{-12}	9.53×10^{-12}	9.53×10^{-12}	9.53×10^{-12}	9.53×10^{-12}	9.53×10^{-12}	6.39×10^{-10}	$\mathbf{1.98 \times 10^{-10}}$	2.53×10^{8}
									$\mathbf{2.23 \times 10^{-9}}$	**LLI wall**	2.24×10^{8}*
Cl-36	W	1.0	7.99×10^{-10}	7.99×10^{-10}	7.99×10^{-10}	7.99×10^{-10}	7.99×10^{-10}	7.99×10^{-10}	8.61×10^{-10}	$\mathbf{8.18 \times 10^{-10}}$	6.11×10^{7}
K-40	D	1.0	5.07×10^{-9}	4.89×10^{-9}	4.85×10^{-9}	4.91×10^{-9}	4.88×10^{-9}	4.85×10^{-9}	5.18×10^{-9}	$\mathbf{5.02 \times 10^{-9}}$	9.96×10^{6}
Ca-45	W	0.3	5.36×10^{-11}	5.36×10^{-11}	5.36×10^{-11}	3.47×10^{-9}	5.23×10^{-9}	5.36×10^{-11}	8.40×10^{-10}	$\mathbf{8.55 \times 10^{-10}}$	5.85×10^{7}
Cr-51	Y	0.1	4.00×10^{-11}	7.51×10^{-12}	4.38×10^{-12}	1.25×10^{-11}	7.86×10^{-12}	3.71×10^{-12}	8.75×10^{-11}	$\mathbf{3.98 \times 10^{-11}}$	1.26×10^{9}
Mn-54	W	0.1	9.48×10^{-10}	2.77×10^{-10}	2.29×10^{-10}	4.89×10^{-10}	5.71×10^{-10}	1.33×10^{-10}	1.21×10^{-9}	$\mathbf{7.48 \times 10^{-10}}$	6.68×10^{7}
Mn-56	D	0.1	8.53×10^{-11}	1.76×10^{-11}	8.00×10^{-12}	2.43×10^{-11}	1.06×10^{-11}	2.40×10^{-12}	7.84×10^{-10}	$\mathbf{2.64 \times 10^{-10}}$	1.89×10^{8}

Table 9-10. Continued.

Nuclide	Class	f_1	Gonad	Breast	Lung	R. marrow	B. surface	Thyroid	Remainder	Effective	ALI (Bq)
Fe-55	D	0.1	1.07×10^{-10}	1.04×10^{-10}	1.02×10^{-10}	1.05×10^{-10}	1.05×10^{-10}	1.10×10^{-10}	3.00×10^{-10}	**1.64×10^{-10}**	3.05×10^{8}
Fe-59	D	0.1	1.66×10^{-9}	7.37×10^{-10}	6.35×10^{-10}	8.45×10^{-10}	6.61×10^{-10}	6.03×10^{-10}	3.56×10^{-9}	**1.81×10^{-9}**	2.76×10^{7}
C0-57	Y	0.05	1.83×10^{-10}	4.10×10^{-11}	2.89×10^{-11}	8.84×10^{-11}	4.92×10^{-11}	1.93×10^{-11}	4.42×10^{-10}	**2.01×10^{-10}**	2.49×10^{8}
C0-58	Y	0.05	1.04×10^{-9}	1.79×10^{-10}	8.53×10^{-11}	2.60×10^{-10}	1.25×10^{-10}	6.31×10^{-11}	1.58×10^{-9}	**8.09×10^{-10}**	6.18×10^{7}
C0-60	Y	0.05	3.19×10^{-9}	1.10×10^{-9}	8.77×10^{-10}	1.32×10^{-9}	9.39×10^{-10}	7.88×10^{-10}	4.97×10^{-9}	**2.77×10^{-9}**	1.81×10^{7}
Ni-59	D	0.05	3.83×10^{-11}	3.58×10^{-11}	3.50×10^{-11}	3.66×10^{-11}	3.62×10^{-11}	3.90×10^{-11}	1.03×10^{-10}	**5.67×10^{-11}**	8.82×10^{8}
Ni-63	D	0.05	8.50×10^{-11}	8.50×10^{-11}	8.50×10^{-11}	8.50×10^{-11}	8.50×10^{-11}	8.50×10^{-11}	3.20×10^{-10}	**1.56×10^{-10}**	3.21×10^{8}
Ni-65	D	0.05	2.43×10^{-11}	5.63×10^{-12}	2.75×10^{-12}	7.26×10^{-12}	2.89×10^{-12}	6.79×10^{-13}	5.32×10^{-10}	**1.68×10^{-10}**	2.98×10^{8}
Cu-64	Y	0.5	4.78×10^{-11}	1.59×10^{-11}	1.28×10^{-11}	1.94×10^{-11}	1.39×10^{-11}	1.13×10^{-11}	3.57×10^{-10}	**1.26×10^{-10}**	3.97×10^{8}
Zn-65	Y	0.5	3.56×10^{-9}	3.28×10^{-9}	3.08×10^{-9}	4.50×10^{-9}	4.50×10^{-9}	3.21×10^{-9}	4.59×10^{-9}	**3.90×10^{-9}**	1.28×10^{7}
Ga-67	Y	0.001	1.58×10^{-10}	1.70×10^{-11}	2.38×10^{-11}	4.14×10^{-11}	1.40×10^{-11}	2.43×10^{-13}	5.49×10^{-10}	**2.12×10^{-10}**	2.36×10^{8}
Ga-68	D	0.001	1.95×10^{-11}	4.56×10^{-12}	2.79×10^{-12}	5.81×10^{-12}	2.18×10^{-12}	2.61×10^{-13}	2.86×10^{-10}	**9.24×10^{-11}**	5.41×10^{8}
Ge-67	D	1.0	2.71×10^{-12}	3.25×10^{-12}	3.64×10^{-12}	3.09×10^{-12}	2.63×10^{-12}	2.17×10^{-12}	1.10×10^{-10}	**3.52×10^{-11}**	1.42×10^{9}
									5.09×10^{-10}	**ST wall**	9.82×10^{8}*
Ge-68	W	1.0	2.42×10^{-10}	2.23×10^{-10}	2.28×10^{-10}	2.33×10^{-10}	2.25×10^{-10}	2.22×10^{-10}	4.22×10^{-10}	**2.89×10^{-10}**	1.73×10^{8}
As-76	W	0.5	2.16×10^{-10}	1.09×10^{-10}	9.83×10^{-11}	1.20×10^{-10}	1.02×10^{-10}	9.35×10^{-11}	4.35×10^{-9}	**1.41×10^{-9}**	3.55×10^{7}
Br-82	W	1.0	4.48×10^{-10}	3.81×10^{-10}	3.84×10^{-10}	4.14×10^{-10}	3.80×10^{-10}	3.83×10^{-10}	5.80×10^{-10}	**4.62×10^{-10}**	1.08×10^{8}
Rb-86	D	1.0	2.15×10^{-9}	2.14×10^{-9}	2.14×10^{-9}	3.72×10^{-9}	6.86×10^{-9}	2.14×10^{-9}	2.33×10^{-9}	**2.53×10^{-9}**	1.98×10^{7}
Sr-85	Y	0.3	6.25×10^{-10}	2.53×10^{-10}	2.06×10^{-10}	5.97×10^{-10}	6.06×10^{-10}	2.05×10^{-10}	7.31×10^{-10}	**5.34×10^{-10}**	9.36×10^{7}
Sr-89	Y	0.3	2.40×10^{-10}	2.40×10^{-10}	2.40×10^{-10}	3.23×10^{-9}	4.81×10^{-9}	2.40×10^{-10}	6.11×10^{-9}	**2.50×10^{-9}**	2.00×10^{7}

Nuclide	Class	f_1	Gonad	Breast	Lung	R. marrow	B. surface	Thyroid	Remainder	Effective	ALI (Bq)
Sr-90	Y	0.3	1.51×10^{-9}	1.51×10^{-9}	1.51×10^{-9}	1.94×10^{-7}	**4.19×10^{-7}**	1.51×10^{-9}	6.14×10^{-9}	3.85×10^{-8}	1.19×10^{6}*
Zr-95	W	0.02	8.16×10^{-10}	1.05×10^{-10}	2.34×10^{-11}	2.14×10^{-10}	4.86×10^{-10}	8.27×10^{-12}	2.53×10^{-9}	**1.02×10^{-9}**	4.90×10^{7}
Nb-94	Y	0.01	1.80×10^{-9}	3.47×10^{-10}	1.72×10^{-10}	7.39×10^{-10}	7.65×10^{-10}	1.23×10^{-10}	4.30×10^{-9}	**1.93×10^{-9}**	2.59×10^{7}
Nb-95	Y	0.01	8.05×10^{-10}	1.07×10^{-10}	2.74×10^{-11}	1.99×10^{-10}	2.94×10^{-10}	1.18×10^{-11}	1.47×10^{-9}	**6.95×10^{-10}**	7.19×10^{7}
Mo-99	Y	0.8	2.21×10^{-10}	1.83×10^{-10}	1.93×10^{-10}	5.33×10^{-10}	7.69×10^{-10}	1.64×10^{-10}	2.08×10^{-9}	**8.22×10^{-10}**	6.08×10^{7}
Tc-99	W	0.8	6.04×10^{-11}	6.04×10^{-11}	6.04×10^{-11}	6.04×10^{-11}	6.04×10^{-11}	1.62×10^{-9}	1.02×10^{-9}	**3.95×10^{-10}**	1.27×10^{8}
Tc-99m	D	0.8	9.75×10^{-12}	3.57×10^{-12}	3.14×10^{-12}	6.29×10^{-12}	4.06×10^{-12}	8.46×10^{-11}	3.34×10^{-11}	**1.68×10^{-11}**	2.98×10^{9}
Ru-103	Y	0.05	5.72×10^{-10}	1.20×10^{-10}	7.31×10^{-11}	1.66×10^{-10}	9.63×10^{-11}	6.25×10^{-11}	2.10×10^{-9}	**8.24×10^{-10}**	6.07×10^{7}
Ru-106	Y	0.05	1.64×10^{-9}	1.44×10^{-9}	1.42×10^{-9}	1.46×10^{-9}	1.43×10^{-9}	1.41×10^{-9}	2.11×10^{-8}	**7.40×10^{-9}**	6.76×10^{6}
Ag-110m	Y	0.05	2.99×10^{-9}	7.51×10^{-10}	8.30×10^{-10}	9.42×10^{-10}	4.93×10^{-10}	1.81×10^{-10}	6.08×10^{-9}	**2.92×10^{-9}**	1.71×10^{7}
Cd-109	D	0.05	3.46×10^{-10}	3.10×10^{-10}	3.17×10^{-10}	3.70×10^{-10}	3.28×10^{-10}	2.75×10^{-10}	1.10×10^{-8}	3.55×10^{-9}	1.41×10^{7}
									4.08×10^{-8}	**Kidneys**	1.22×10^{7}*
In-115	Y	0.02	4.86×10^{-9}	4.86×10^{-9}	4.86×10^{-9}	1.53×10^{-7}	7.91×10^{-8}	4.86×10^{-9}	6.41×10^{-8}	**4.26×10^{-8}**	1.17×10^{6}
Sn-113	W	0.02	3.88×10^{-10}	5.68×10^{-10}	2.54×10^{-11}	1.78×10^{-10}	2.34×10^{-10}	2.16×10^{-11}	2.32×10^{-9}	**8.33×10^{-10}**	6.00×10^{7}
									7.91×10^{-9}	**LLI wall**	6.32×10^{7}*
Sb-124	W	0.01	1.78×10^{-9}	2.30×10^{-10}	5.40×10^{-11}	3.81×10^{-10}	1.89×10^{-10}	1.76×10^{-11}	7.34×10^{-9}	**2.74×10^{-9}**	1.82×10^{7}
Sb-125	W	0.01	5.27×10^{-10}	6.22×10^{-11}	1.36×10^{-11}	1.21×10^{-10}	9.05×10^{-11}	5.58×10^{-12}	1.99×10^{-9}	**7.57×10^{-10}**	6.61×10^{7}
I-123	D	1.0	5.61×10^{-12}	7.23×10^{-12}	6.66×10^{-12}	8.68×10^{-12}	7.65×10^{-12}	**4.42×10^{-9}**	2.01×10^{-11}	1.43×10^{-10}	1.13×10^{8}*

Table 9-10. Continued.

Nuclide	Class	f_1	Gonad	Breast	Lung	R. marrow	B. surface	Thyroid	Remainder	Effective	ALI (Bq)
I-125	D	1.0	2.93×10^{-11}	1.45×10^{-10}	4.08×10^{-11}	6.82×10^{-11}	6.63×10^{-11}	**3.44×10^{-7}**	5.80×10^{-11}	1.04×10^{-8}	1.45×10^{6}*
I-129	D	1.0	1.38×10^{-10}	3.31×10^{-10}	1.65×10^{-10}	2.21×10^{-10}	2.17×10^{-10}	**2.48×10^{-6}**	1.99×10^{-10}	7.46×10^{-8}	2.02×10^{5}*
I-130	D	1.0	5.52×10^{-11}	7.32×10^{-11}	7.18×10^{-11}	6.74×10^{-11}	6.12×10^{-11}	**3.94×10^{-8}**	1.97×10^{-10}	1.28×10^{-9}	1.27×10^{7}*
I-131	D	1.0	4.07×10^{-11}	1.21×10^{-10}	1.02×10^{-10}	9.44×10^{-11}	8.72×10^{-11}	**4.76×10^{-7}**	1.57×10^{-10}	1.44×10^{-8}	1.05×10^{6}*
Cs-134	D	1.0	2.06×10^{-8}	1.72×10^{-8}	1.76×10^{-8}	1.87×10^{-8}	1.74×10^{-8}	1.76×10^{-8}	2.21×10^{-8}	**1.98×10^{-8}**	2.53×10^{6}
Cs-137	D	1.0	1.39×10^{-8}	1.24×10^{-8}	1.27×10^{-8}	1.32×10^{-8}	1.26×10^{-8}	1.26×10^{-8}	1.45×10^{-8}	**1.35×10^{-8}**	3.70×10^{6}
Cs-138	D	1.0	8.00×10^{-12}	8.00×10^{-12}	8.53×10^{-12}	7.37×10^{-12}	6.47×10^{-12}	5.73×10^{-12}	1.57×10^{-10}	5.25×10^{-11}	9.52×10^{8}
									7.01×10^{-10}	**ST wall**	7.13×10^{8}*
Ba-133	D	0.1	7.33×10^{-10}	2.73×10^{-10}	2.19×10^{-10}	1.46×10^{-9}	1.97×10^{-9}	2.03×10^{-10}	1.43×10^{-9}	**9.19×10^{-10}**	5.44×10^{7}
Ba-140	D	0.1	9.96×10^{-10}	1.59×10^{-10}	6.63×10^{-11}	4.39×10^{-10}	5.53×10^{-10}	5.25×10^{-11}	7.37×10^{-9}	2.56×10^{-9}	1.95×10^{7}
									2.64×10^{-8}	**LLI wall**	1.89×10^{7}*
La-140	W	0.001	1.34×10^{-9}	1.80×10^{-10}	4.01×10^{-11}	2.81×10^{-10}	9.77×10^{-11}	6.40×10^{-12}	6.26×10^{-9}	**2.28×10^{-9}**	2.19×10^{7}
Ce-141	Y	0.0003	1.08×10^{-10}	1.11×10^{11}	1.43×10^{-12}	3.39×10^{-11}	2.30×10^{-11}	1.80×10^{-13}	2.50×10^{-9}	7.83×10^{-10}	6.39×10^{7}
									8.64×10^{-9}	**LLI wall**	5.79×10^{7}*
Ce-144	Y	0.0003	6.98×10^{-11}	1.22×10^{-11}	6.52×10^{-12}	8.92×10^{-11}	1.28×10^{-10}	5.15×10^{-12}	1.88×10^{-8}	5.68×10^{-9}	8.80×10^{6}
									6.64×10^{-8}	**LLI wall**	7.53×10^{6}*
Pr-144	Y	0.0003	7.38×10^{-14}	3.38×10^{-14}	3.15×10^{-14}	3.22×10^{-14}	1.52×10^{-14}	3.59×10^{-15}	1.05×10^{-10}	3.15×10^{-11}	1.59×10^{9}*
									4.09×10^{-10}	**ST wall**	1.22×10^{9}*
Nd-147	Y	0.0003	1.79×10^{-10}	1.87×10^{-11}	2.44×10^{-12}	5.05×10^{-11}	2.22×10^{-11}	2.64×10^{-13}	3.76×10^{-9}	1.18×10^{-9}	4.24×10^{7}*
									1.28×10^{-8}	**LLI wall**	3.91×10^{7}*

Nuclide	Class	f_1	Gonad	Breast	Lung	R. marrow	B. surface	Thyroid	Remainder	Effective	ALI (Bq)
Pm-147	Y	0.0003	6.86×10^{-15}	7.45×10^{-16}	1.96×10^{-16}	2.09×10^{-11}	2.61×10^{-10}	3.12×10^{-17}	9.08×10^{-10}	2.83×10^{-10}	1.77×10^{8}
									3.17×10^{-9}	**LLI wall**	1.58×10^{8}*
Eu-152	W	0.001	1.33×10^{-9}	2.85×10^{-10}	2.40×10^{-10}	9.19×10^{-10}	2.09×10^{-9}	6.66×10^{-11}	3.92×10^{-9}	**1.75×10^{-9}**	2.86×10^{7}
Eu-154	W	0.001	1.37×10^{-9}	2.79×10^{-10}	2.16×10^{-10}	1.15×10^{-9}	4.46×10^{-9}	5.71×10^{-11}	6.32×10^{-9}	**2.58×10^{-9}**	1.94×10^{7}
Gd-148	D	0.0003	0.00×10^{0}	0.00×10^{0}	0.00×10^{0}	8.90×10^{-8}	**1.11×10^{-6}**	0.00×10^{0}	4.98×10^{-8}	5.89×10^{-8}	4.50×10^{5}*
Gd-152	D	0.0003	0.00×10^{0}	0.00×10^{0}	0.00×10^{0}	6.57×10^{-8}	**8.21×10^{-7}**	0.00×10^{0}	3.62×10^{-8}	4.34×10^{-8}	6.09×10^{5}*
W-188	D	0.3	3.31×10^{-11}	5.57×10^{-12}	2.76×10^{-12}	3.25×10^{-10}	9.52×10^{-10}	1.42×10^{-12}	6.78×10^{-9}	2.11×10^{-9}	2.37×10^{7}
									2.33×10^{-8}	**LLI wall**	2.15×10^{7}*
Re-186	W	0.8	1.00×10^{-10}	9.54×10^{-11}	9.53×10^{-11}	9.89×10^{-11}	9.69×10^{-11}	4.79×10^{-9}	1.95×10^{-9}	**7.95×10^{-10}**	6.29×10^{7}
Ir-192	Y	0.01	1.03×10^{-9}	1.51×10^{-10}	6.54×10^{-11}	2.54×10^{-10}	1.11×10^{-10}	3.78×10^{-11}	4.08×10^{-9}	**1.55×10^{-9}**	3.23×10^{7}
Pt-193	D	0.01	2.02×10^{-12}	2.95×10^{-13}	2.73×10^{-13}	3.35×10^{-13}	2.94×10^{-13}	2.97×10^{-13}	1.05×10^{-10}	3.21×10^{-11}	1.56×10^{9}
									3.60×10^{-10}	**LLI wall**	1.39×10^{9}*
Au-195	Y	0.1	1.33×10^{-10}	1.98×10^{-11}	9.07×10^{-12}	6.29×10^{-11}	2.56×10^{-11}	7.43×10^{-12}	8.05×10^{-10}	**2.87×10^{-10}**	1.74×10^{8}
Au-198	Y	0.1	3.43×10^{-10}	5.51×10^{-11}	2.44×10^{-11}	8.57×10^{-11}	4.06×10^{-11}	1.85×10^{-11}	3.44×10^{-9}	**1.14×10^{-9}**	4.39×10^{7}
Hg-197	W	0.02	8.26×10^{-11}	9.43×10^{-12}	2.15×10^{-12}	3.53×10^{-11}	1.14×10^{-11}	1.27×10^{-12}	7.72×10^{-10}	**2.59×10^{-10}**	1.93×10^{8}
Hg-203	W	0.02	3.30×10^{-10}	5.41×10^{-11}	2.69×10^{-11}	9.38×10^{-11}	4.61×10^{-11}	2.15×10^{-11}	1.71×10^{-9}	**6.21×10^{-10}**	8.05×10^{7}
Tl-201	D	1.0	6.19×10^{-11}	5.41×10^{-11}	5.78×10^{-11}	8.71×10^{-11}	7.76×10^{-11}	5.19×10^{-11}	1.21×10^{-10}	**8.11×10^{-11}**	6.17×10^{8}
Tl-204	D	1.0	6.57×10^{-10}	6.57×10^{-10}	6.57×10^{-10}	6.59×10^{-10}	6.59×10^{-10}	6.57×10^{-10}	1.49×10^{-9}	**9.08×10^{-10}**	5.51×10^{7}

Table 9-10. Continued.

Nuclide	Class	f_1	Gonad	Breast	Lung	R. marrow	B. surface	Thyroid	Remainder	Effective	ALI (Bq)
Pb-210	D	0.2	1.25×10^{-7}	1.25×10^{-7}	1.25×10^{-7}	1.48×10^{-6}	**2.16×10^{-5}**	1.25×10^{-7}	1.85×10^{-6}	1.45×10^{-6}	2.31×10^{4}*
Bi-210	D	0.05	1.97×10^{-11}	1.97×10^{-11}	1.97×10^{-11}	1.97×10^{-11}	1.97×10^{-11}	1.97×10^{-11}	5.72×10^{-9}	**1.73×10^{-9}**	2.89×10^{7}
Po-210	D	0.1	8.23×10^{-8}	8.23×10^{-8}	8.23×10^{-8}	8.23×10^{-8}	8.23×10^{-8}	8.23×10^{-8}	1.52×10^{-6}	**5.14×10^{-7}**	9.73×10^{4}
Ra-226	W	0.2	9.16×10^{-8}	9.17×10^{-8}	9.16×10^{-8}	5.98×10^{-7}	**6.83×10^{-6}**	9.15×10^{-8}	1.03×10^{-7}	3.58×10^{-7}	7.32×10^{4}*
Ra-227	W	0.2	3.65×10^{-12}	2.31×10^{-12}	2.16×10^{-12}	4.30×10^{-11}	**8.54×10^{-10}**	1.84×10^{-12}	9.56×10^{-11}	6.10×10^{-11}	5.85×10^{8}*
Ra-228	W	0.2	1.58×10^{-7}	1.57×10^{-7}	1.57×10^{-7}	6.53×10^{-7}	**5.82×10^{-6}**	1.57×10^{-7}	1.63×10^{-7}	3.88×10^{-7}	8.59×10^{5}*
Th-230	W	0.0002	6.82×10^{-10}	6.80×10^{-10}	6.80×10^{-10}	2.89×10^{-7}	**3.60×10^{-6}**	6.80×10^{-10}	1.54×10^{-8}	1.48×10^{-7}	1.39×10^{5}*
Th-232	W	0.0002	1.25×10^{-9}	1.26×10^{-9}	1.25×10^{-9}	1.48×10^{-6}	**1.85×10^{-5}**	1.21×10^{-9}	1.47×10^{-8}	7.38×10^{-7}	2.70×10^{4}*
Pa-231	W	0.001	1.21×10^{-10}	7.81×10^{-11}	6.80×10^{-11}	5.78×10^{-6}	**7.22×10^{-5}**	6.33×10^{-11}	1.71×10^{-8}	2.86×10^{-6}	6.93×10^{3}*
U-235	Y	0.002	3.34×10^{-10}	1.21×10^{-10}	1.01×10^{-10}	2.78×10^{-9}	4.20×10^{-8}	9.82×10^{-11}	1.84×10^{-8}	**7.22×10^{-9}**	6.93×10^{6}
U-238	Y	0.002	1.02×10^{-10}	9.33×10^{-11}	9.22×10^{-11}	2.72×10^{-9}	4.04×10^{-8}	9.20×10^{-11}	1.61×10^{-8}	**6.42×10^{-9}**	7.79×10^{6}
Np-237	W	0.001	2.46×10^{-7}	1.45×10^{-10}	1.53×10^{-10}	2.18×10^{-6}	**2.72×10^{-5}**	1.10×10^{-10}	2.10×10^{-7}	1.20×10^{-6}	1.84×10^{4}*
Pu-238	Y	0.00001	2.33×10^{-9}	1.80×10^{-13}	8.64×10^{-14}	1.27×10^{-8}	**1.58×10^{-7}**	7.99×10^{-14}	2.18×10^{-8}	1.34×10^{-8}	3.16×10^{6}*
Pu-239	Y	0.001	2.64×10^{-7}	7.69×10^{-12}	7.74×10^{-12}	1.41×10^{-6}	**1.76×10^{-5}**	7.49×10^{-12}	6.43×10^{-7}	9.56×10^{-7}	2.84×10^{4}*
Pu-241	W	0.001	5.66×10^{-9}	2.52×10^{-13}	4.45×10^{-13}	2.78×10^{-8}	**3.48×10^{-7}**	1.01×10^{-13}	1.10×10^{-8}	1.85×10^{-8}	1.44×10^{6}*
Pu-242	W	0.001	2.51×10^{-7}	8.00×10^{-12}	7.88×10^{-12}	1.34×10^{-6}	**1.67×10^{-5}**	7.29×10^{-12}	6.10×10^{-7}	9.08×10^{-7}	2.99×10^{4}*
Am-241	W	0.001	2.70×10^{-7}	2.62×10^{-11}	3.36×10^{-11}	1.45×10^{-6}	**1.81×10^{-5}**	1.32×10^{-11}	6.66×10^{-7}	9.84×10^{-7}	2.76×10^{4}*
Cm-244	W	0.001	1.33×10^{-7}	8.82×10^{-12}	8.81×10^{-12}	7.82×10^{-7}	**9.77×10^{-6}**	8.44×10^{-12}	4.15×10^{-7}	5.45×10^{-7}	5.12×10^{4}*
Cf-252	W	0.001	5.39×10^{-8}	1.49×10^{-9}	4.67×10^{-10}	4.69×10^{-7}	**5.84×10^{-6}**	2.68×10^{-10}	1.58×10^{-7}	2.93×10^{-7}	8.56×10^{4}*

Source: Adapted from Federal Guidance Report 11, EPA 520/11-88-020 1988.

Example 9-6. Consumption of milk following a release of ^{131}I from a nearby facility resulted in an ^{131}I intake of 10 μCi (3.7×10^5 Bq). Estimate for an adult (a) the committed dose to the thyroid and (b) the committed effective whole-body dose.
Solution. (a) From Table 9-10, the CDE to thyroid from ^{131}I ingestion is 4.76×10^{-7} Sv/Bq; thus, the thyroid dose is

$$\text{CDE} = (4.76 \times 10^{-7}\ \text{Sv/Bq})(3.7 \times 10^5\ \text{bq}) = 0.176\ \text{Sv}\ (17.6\ \text{rem})$$

(b) The committed effective dose equivalent (CEDE) factor from Table 9-10 is 1.44×10^{-8} Sv/Bq; thus, the effective whole-body dose for the intake of 3.7×10^5 Bq (10 μCi) is

$$\text{CEDE} = (1.44 \times 10^{-8}\ \text{Sv/Bq})(3.7 \times 10^5\ \text{Bq}) = 5.3 \times 10^{-3}\ \text{Sv}\ (0.53\ \text{rem})$$

Note: the CEDE dose factor incorporates the weighing factor w_T for all tissues which is dominated by $w_T = 0.03$ for thyroid.

9.5 Operational Determinations of Internal Dose

A straightforward operational practice for assigning internal radiation doses to persons is to determine the intake, which is then used with the data in Tables 9-9 and 9-10 to determine the internal radiation dose to individual tissues or the committed effective whole-body dose (or CEDE). For airborne radioactivity, the inhalation intake (or alternatively the dose due to submersion) can be determined by measuring the air concentration and combining it with a standard breathing rate and the time of exposure. The ingestion intake due to radioactivity in water or food can be determined by similar means.

Example 9-7. A person ingests food and water over a period of several weeks for an estimated intake of 3.7×10^5 Bq (10 μCi) of ^{60}Co. Determine the committed dose equivalent (CDE) to the lung and the committed effective dose equivalent (CEDE) to the whole body.
Solution. Since the intake period is relatively short compared to a year, it is reasonable to consider it as an acute intake. From Table 9-10, the CDE to lung due to ingested ^{60}Co is 8.77×10^{-10} Sv/Bq and the total body effective dose is 2.77×10^{-9} Sv/Bq. Therefore

$$\text{CDE (lung)} = 8.77 \times 10^{-10}\ \text{Sv/Bq} \times 3.7 \times 10^5\ \text{Bq} = 3.25 \times 10^{-4}\ \text{Sv}\ (32.5\ \text{mrem})$$

and for the total body

$$\text{CEDE (TB)} = 2.77 \times 10^{-9}\ \text{Sv/Bq} \times 3.7 \times 10^5\ \text{Bq} = 1.02 \times 10^{-3}\ \text{Sv}\ (102.5\ \text{mrem})$$

9.5.1 Submersion Dose

Exposure of persons immersed in a cloud of radioactive material (submersion) can also be considered a form of internal radiation exposure; however, in most cases a total body external exposure is received due to the concentration of the radionuclide in the air surrounding the person. Noble gases and tritium are the most important radionuclides for submersion exposure, and the air concentration is the limiting condition to preclude exceeding the TEDE limit. Values of dose equivalent rates (Sv/h) per unit air concentration (Bq/m^3) are provided in Table 9-11. The effective whole-body dose is usually limiting but the nonstochastic effect for skin or the lens of the eye may be the dominant effect in some cases; when the limiting concentration is based on nonstochastic effects, the particular tissue is also listed in Table 9-11 for the particular gaseous radionuclide (see Example 9-7).

Example 9-8. A worker is exposed to an atmosphere of ^{85}Kr for 2000 h per year. What limiting concentration of ^{85}Kr could be allowed such that radiation protection limits are not exceeded?

Solution. As shown in bold type in Table 9-11, the limiting dose rate for ^{85}Kr is 4.66×10^{-11} Sv/h per Bq/m^3 of ^{85}Kr which is based on precluding nonstochastic effects in skin. The limiting air concentration that corresponds to a skin dose of 0.5 Sv (50 rem) in 2000 h of exposure (a nominal working year) is

$$0.5 \text{ Sv} = \chi \text{ (Bq/m}^3\text{)} \times 4.66 \times 10^{-11} \text{ Sv/h per Bq/m}^3 \times 2000 \text{ h}$$

$$\chi = 5.36 \times 10^6 \text{ Bq/m}^3$$

which, because of the 2000 h exposure period, is also the DAC for ensuring that an occupational dose to skin does not exceed the 50 rem nonstochastic limit.

Checkpoints

- A direct link exists between an inhaled or ingested intake of a radionuclide and the subsequent committed effective dose equivalent (CEDE) as summarized in Tables 9-9 and 9-10 for selected radionuclides.
- Submersion in a cloud of a radioactive gas produces exposure of the whole body and various tissues which may be limiting, especially for noble gas radionuclides and tritium; therefore, a direct relationship also exists between the air concentration and tissue dose, values of which are summarized in Table 9-11.

Table 9-11. Exposure-to-dose conversion factors for submersion exposure to airborne concentrations of tritium and noble gases.

Nuclide	Dose equivalent rates per unit air concentration (Sv/h per Bq/m^3)							
	Gonad	Breast	Lung	R. marrow	B surface	Thyroid	Remainder	Effective
H-3			9.90×10^{-15}					$\mathbf{1.19 \times 10^{-15}}$
Ar-41	1.90×10^{-10}	2.32×10^{-10}	2.20×10^{-10}	2.28×10^{-10}	2.47×10^{-10}	2.07×10^{-10}	2.24×10^{-10}	$\mathbf{2.17 \times 10^{-10}}$
Kr-85	5.18×10^{-13}	4.52×10^{-13}	4.31×10^{-13}	5.75×10^{-13}	6.15×10^{-13}	2.50×10^{-13}	4.20×10^{-13}	4.70×10^{-13}
							4.66 × 10^{-11}	*Skin*
Kr-85m	3.35×10^{-11}	2.66×10^{-11}	2.57×10^{-11}	4.43×10^{-11}	4.72×10^{-11}	2.95×10^{-11}	2.25×10^{-11}	$\mathbf{2.98 \times 10^{-11}}$
Kr-87	1.26×10^{-10}	1.48×10^{-10}	1.41×10^{-10}	1.52×10^{-10}	1.67×10^{-10}	1.42×10^{-10}	1.46×10^{-10}	$\mathbf{1.42 \times 10^{-10}}$
Kr-88	3.48×10^{-10}	3.65×10^{-10}	3.49×10^{-10}	3.48×10^{-10}	3.85×10^{-10}	3.74×10^{-10}	3.72×10^{-10}	$\mathbf{3.60 \times 10^{-10}}$
Xe-133	6.30×10^{-12}	5.62×10^{-12}	4.84×10^{-12}	1.08×10^{-11}	1.18×10^{-11}	7.12×10^{-12}	4.03×10^{-12}	$\mathbf{6.07 \times 10^{-12}}$
Xe-133m	6.80×10^{-12}	4.88×10^{-12}	4.33×10^{-12}	7.37×10^{-12}	7.95×10^{-12}	4.89×10^{-12}	3.84×10^{-12}	$\mathbf{5.38 \times 10^{-12}}$
Xe-135	5.63×10^{-11}	4.21×10^{-11}	4.07×10^{-11}	6.16×10^{-11}	6.59×10^{-11}	3.80×10^{-11}	3.67×10^{-11}	$\mathbf{4.68 \times 10^{-11}}$
Xe-135m	8.27×10^{-11}	7.32×10^{-11}	7.04×10^{-11}	8.62×10^{-11}	9.21×10^{-11}	3.32×10^{-11}	7.04×10^{-11}	$\mathbf{7.53 \times 10^{-11}}$
Xe-138	1.65×10^{-10}	2.06×10^{-10}	1.98×10^{-10}	2.11×10^{-10}	2.31×10^{-10}	1.91×10^{-10}	1.95×10^{-10}	$\mathbf{1.92 \times 10^{-10}}$

9.6 Tritium: a Special Case

Persons can be exposed to tritium either as elemental ^3H or by ingestion of tritiated water in the form of HTO or tritium oxide, ^3H_2O. Exposure to elemental ^3H deposits a minimal amount in the body water due to inhalation and very little is absorbed through the skin; the remainder, which is difficult to know exactly, will be exhaled where it may become oxidized and be available for other exposure. The form of tritium can change rapidly; thus it is a perplexing radionuclide due to such variability.

Most radiation protection determinations for tritium are based on the oxide form since it is incorporated directly into body water to produce a whole-body exposure. For a person exposed to airborne tritium oxide, an amount equal to 50% of the inhaled intake is assumed to also be absorbed through skin; therefore, a person in a tritium atmosphere that inhales 200 Bq of ^3H_2O will also absorb 100 Bq through the skin for a total intake to the body water of 300 Bq.

Tritium entering the body distributes rapidly and uniformly in 42 L of body water where it is uniformly distributed in and irradiates 63 kg of soft tissue. The daily intake of fluids by a reference male adult is 3 L/d, and an equal amount is eliminated each day (see Figure 9-7) to maintain a tidal volume of 42 L of water in the body; thus, the biological removal coefficient for water in the body is

$$\lambda_b = \frac{3\ \text{L/d}}{42\ \text{L}} = 7.14 \times 10^{-2}\ \text{d}^{-1}$$

which is also the biological removal constant for tritium uniformly distributed in body water, which yields a biological half-life of

$$T_b = \ln 2/\lambda_b = 9.7\ \text{d}$$

or about 10 days. For an acute intake of tritium, its initial concentration in body water is

$$C_0 = \frac{I}{42\ \text{L}}$$

and as shown schematically in Figure 9-7, the concentration of tritium in body water at any time t following an acute intake I is

$$C(t) = \frac{I}{42\ \text{L}} e^{-(\lambda_b + \lambda_r)t}$$

where $\lambda_b + \lambda_r$ is the effective removal constant λ_{eff} which is effectively λ_b since the radiological half-life of ^3H is 12.3 y. Therefore

$$C(t) = C_0 e^{-\lambda_b t} = C_0 e^{-(\ln 2/T_b)t}$$

Since tritium (as HTO) spreads uniformly and quickly throughout the body water, this is also the concentration in urine at a time t following an accute intake.

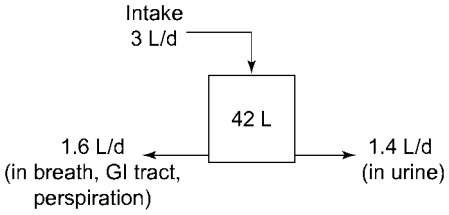

Fig. 9-7 Fluid balance in the total body of a reference adult male represented by a tidal pool of 42 L in which a daily intake of 3 L/d replenishes average daily losses of 1.4 L/d in urine and 1.6 L/d through the GI tract, breath moisture, and perspiration.

The *dose due to an intake of tritium* is, as described previously, the product of a unit-conversion constant, the total number of transformations that are associated with an initial deposition of activity q_0, and the absorbed energy per transformation. In SI units

$$D_{\mathrm{TOT}}(\mathrm{J/kg}) = 1.6022 \times 10^{-10} \frac{q_0}{\lambda_e}\left[1 - \exp\left(-\frac{\ln 2}{T_e}t\right)\right]\left[\frac{\sum Y_i \bar{E}_i \mathrm{AF}(\mathrm{T} \leftarrow \mathrm{S})_i Q_i}{m_{\mathrm{T}}}\right]$$

where the first term in brackets is the total number of transformations U_s that occur due to an intake of q_0 (Bq), or $1.443 q_0$ (Bq) $\times T_b$ since $T_e = T_b = 9.7$ d (due to the long radiological half-life of tritium), or for each Bq of a tritium intake

$$U_s \text{ (no. of transformations)} = 1.443 \times 1 \text{ Bq} \times 1 \text{ t/s Bq} \times 9.7 \text{ d} \times 86{,}400 \text{ s/d}$$

$$= 1.21 \times 10^6 \text{ t}$$

Since ^{3}H is a pure beta emitter, Y_i, Q_i, and AF(T ← S) = 1.0 and the average energy per transformation is 5.685×10^{-3} MeV; thus the specific effective energy (SEE) for tritium uniformly distributed in 63 kg of soft tissue is

$$\mathrm{SEE}(\mathrm{TB} \leftarrow \mathrm{TB}) = \frac{\sum Y_i \overline{E_i} \times \mathrm{AF}(\mathrm{TB} \leftarrow \mathrm{TB})_i Q_i}{m_{\mathrm{T}}(\mathrm{g})}$$

$$= \frac{5.685 \times 10^{-3} \mathrm{MeV/t} \times 1 \times 1}{63{,}000 \mathrm{g}}$$

$$= 9 \times 10^{-8} \text{ MeV/g t}$$

The committed effective dose equivalent, $H_{50,\mathrm{T}}$, due to an intake of 1 Bq of ^{3}H is

$$H_{50,\mathrm{T}}(\mathrm{TB} \leftarrow \mathrm{TB}) = 1.6 \times 10^{-10} \times 1.21 \times 10^6 \text{ t} \times 9 \times 10^{-8} \text{ MeV/g t}$$

$$= 1.74 \times 10^{-11} \text{ Sv/Bq of intake}$$

Example 9-12. If the whole-body dose limit for a reference person is 0.05 Sv (5 rem) per year, what is the maximum intake of tritium (i.e., the ALI) that could occur without exceeding the dose limit?

Solution. The committed effective dose equivalent for 1 Bq of tritium in oxide form (HTO) is 1.74×10^{-11} Sv/Bq, and the intake that corresponds to the stochastic limit of 0.05 Sv in 1 y is

$$I = \frac{0.05\ \text{Sv/y}}{1.74 \times 10^{-11}\ \text{Sv/Bq}} = 2.9 \times 10^{9}\ \text{Bq/y}$$

which is usually expressed to one significant figure. Thus the annual limit on intake is

$$\text{ALI}_s\ (^3\text{H}) = 3 \times 10^{9}\ \text{Bq}$$

The *derived air concentration* (or DAC) for limiting exposure to an air concentration of ^3H_2O must recognize that one-third of the body burden of ^3H_2O will enter through the skin; i.e., a person in a tritium atmosphere who inhales 200 Bq of ^3H_2O will also absorb 100 Bq into the body water by absorption through the skin such that only two-thirds of the ALI can be by inhalation, or

$$\text{DAC}\ (^3\text{H}) = \frac{\frac{2}{3}\ \text{ALI(Bq)}}{2.4 \times 10^{3}\text{m}^3\ \text{of air}} = 8 \times 10^{5}\ \text{Bq/m}^3$$

9.6.1 Bioassay of Tritium: a Special Case

Since tritium in oxide form mixes rapidly in the body water, and since λ_r is very small relative to λ_b, its concentration in body fluids, including urine, at any time t following an acute intake I is

$$C_u(t) = \frac{I}{42\ \text{L}} e^{-(\lambda_b + \lambda_r)t} = C_0 e^{-\lambda_b t}$$

where C_0 is the initial tritium concentration (Bq/L) in urine and $C_u(t)$ is the concentration at any time t post-intake. A bioassay measurement of the tritium concentration in urine can thus be used to determine the intake of tritium by first determining C_0 and multiplying by 42 L of body water, and this value is used in calculating the dose.

Example 9-10. An adult male worker was put on a high liquid intake (cheap beer?) and subjected to intense physical exercise following an acute inhalation intake of HTO. Tritium concentrations in urine were measured during this period and were found to fit an exponential function yielding a biological (actually effective) half-life of 5.96 d. Extrapolation of the urine concentration data back to the time of

intake for this clearance rate yielded an initial concentration C_0, of 9×10^7 Bq/L. If the worker was otherwise typical of a reference person, what was his dose?
Solution. The worker's intake was

$$\text{Intake} = 9 \times 10^7 \text{ Bq/L} \times 42 \text{ L} = 3.78 \times 10^9 \text{ Bq}$$

and based on the measured biological half-life of 5.96 d, the number of transformations is

$$U_s = 1.443 \times 3.78 \times 10^9 \text{ t/s} \times (5.96 \text{ d})(86{,}400 \text{ s/d})$$

$$= 2.81 \times 10^{15} \text{ t}$$

Since the specific effective energy (SEE) for tritium in body water is 9×10^{-8} MeV/g t (see above) the CEDE is

$$H_{50,T} = 1.6 \times 10^{-10} U_s \times \text{SEE}$$

$$= 1.6 \times 10^{-10}(2.81 \times 10^{15} \text{ t})(9 \times 10^{-8} \text{ MeV/g t})$$

$$= 0.04 \text{ Sv (4 rem)}$$

which is close enough to the limiting CEDE for the whole body of 0.05 Sv (5 rem) that an overexposure would be assigned if the lower measured effective half-life had not been used; i.e., the high liquid intake and exercise regimen was to the benefit of the worker (see Problem 9-14).

9.7 Summary

Internal radiation doses are calculated as the product of three quantities: (a) the number of transformations produced by a radionuclide in a source organ in a given time period, which is a function of the activity of the deposited radionuclide and the time it remains in the source organ; (b) the energy deposition per nuclear transformation, which is a constant for a specific radionuclide and a source–target organ pair; and (c) a constant to adjust the units. Since energy deposition is a constant for a specific radionuclide and source–target organ pair, calculation of internal dose thus becomes an exercise in determining how much of a radionuclide is deposited in a source organ and the subsequent number of transformations associated with the deposited activity. Both are very much determined by human biology; thus, internal dose determinations can be complex because radionuclides must first pass through the respiratory system and/or the GI tract before entering the bloodstream from which uptake to an organ occurs. Radiation doses also occur to source organs, other surrounding target tissues, and to the lung and the

various segments of the GI tract as the radioactive material passes through them. Fairly extensive biokinetic models have been developed for calculating doses due to intakes by inhalation and ingestion of radionuclides, in particular a respiratory deposition/clearance model and a GI tract model. Both assume an initial deposition of radioactive material that is, depending on chemical and physical characteristics, translocated to various tissues to produce a tissue dose.

Other Suggested Sources

EPA Federal Guidance Report 11.
International Commission on Radiological Protection (ICRP) publications, in particular ICRP Reports 26, 30 (all parts with supplements), 60, 61, 66, and 71.
Lessard, E. T. et al. **1987**, *Interpretation of Bioassay Measurements*, US Nuclear Regulatory Commission NUREG/CR-4884.

Problems – Chapter 9

9–1. Determine (a) the effective half-life of ^{131}I ($T_{1/2}$ = 8.02 d) in the thyroid if its biological half-life is 80 d; and (b) explain the magnitude of the calculated value.
9–2. A researcher working with $^{14}CO_2$ was found to have a body burden of 20 μCi of ^{14}C ($\bar{E}$ = 0.049 MeV; T_b = 40 d). (a) What dose rate (rad/h) would be delivered to soft tissue (m = 63,000 g) from this body level; and (b) if removed from the work, what total dose would be delivered due to the amount of ^{14}C accumulated in the body?
9–3. Determine (a) the instantaneous dose rate (rad/h) due to the principal beta emission ($\bar{E}_\beta$ = 0.192 MeV) of ^{131}I which occurs in 89.4% of transformations for 1 mCi of ^{131}I (T_r = 8.02 d and T_b = 80 d) deposited in the 12 g thyroid gland of a 10-year-old person; and (b) the total accumulated dose delivered due to this emission.
9–4. Use the dose reciprocity theorem to determine the absorbed fraction AF(Liver ← Kidney) for 0.5 MeV photons.
9–5. Calculate (a) the photon dose to the lung and the total body from 1 μCi of ^{60}Co deposited in the lung and cleared with a biological half-life of 60 d, and (b) the photon dose to the lung and the total body for 1 μCi of ^{60}Co deposited uniformly in the total body that clears with a biological half-life of 800 d.
9–6. Inorganic compounds of metallic mercury are presumed from metabolic studies to distribute uniformly after inhalation or ingestion with 8% going to the liver (f = 0.08) and 92% to the total body (f = 0.92). Biological clearance of mercury in each of these tissues occurs by two compartments, 95% with a biological half-life of 40 d and the remaining 5% with a biological half-life of 10,000 d. For an intake of 1 Bq of ^{203}Hg ($T_{1/2}$ = 46.61 d), determine how many transformations occur (a) in the liver and (b) in the total body.

9–7. For ^{137}Cs–^{137m}Ba distributed uniformly in the total body, the specific effective energy is 6.31×10^{-6} MeV/g t. If an initially measured amount in the body of an adult is 4×10^5 Bq, determine (a) the total number of transformations based on the retention function for ^{137}Cs and (b) the 50 y integrated whole-body dose.

9–8. For the first 8 months of a calendar year, an adult worker inhales 2×10^6 Bq of ^{137}Cs, 10^6 Bq of ^{131}I, and 6×10^5 Bq of ^{60}Co. The appropriate ALIs are 6×10^6, 2×10^6, and 6×10^6 Bq, respectively. (a) If the worker is reassigned to an area where only external gamma exposure is possible, how much exposure (if any) could the worker receive without exceeding the stochastic risk limit? (b) if the worker were exposed to ^{131}I aerosols instead of external gamma radiation, how many Bq could the worker take in without exceeding ICRP-30 recommended limits?

9–9. For the ICRP-30-derived DAC (Table 9-9), how many DAC-hours could the worker in Example 9-9 be exposed to without exceeding a stochastic dose limit of 0.05 Sv?

9–10. A lung burden of 2.45×10^7 Bq of ^{51}Cr is measured in an adult male worker following exposure to class Y ^{51}Cr aerosols. Estimate the committed effective dose equivalent due to this intake and the major tissue to which it occurs.

9–11. Use the data in Table 9-2 to determine the ALI and DAC for inhalation of 1 μm AMAD aerosols of (a) ^{59}Ni and (b) ^{125}I.

9–12. Use the data in Table 9-2 to determine the ALI for ingestion of (a) ^{32}P and (b) ^{35}S.

9–13. A routine *annual* whole-body measurement of a worker identified a whole-body accumulation of 190 Bq of ^{60}Co assumed to be due to exposure to Class D 1 μm AMAD aerosols. Determine (a) a best estimate of the intake; (b) the CEDE based on the ^{60}Co ALI (6×10^6 Bq); and (c) the CEDE using the data in Table 9-2 (from Federal Guidance Report No. 11). (d) Compare the results.

9–14. What would be the estimated dose to the worker in Example 9-10 due to the intake of tritium if the worker had not been on the high liquid diet and exercise regimen?

9–15. Assuming reference person radiobiology, determine the initial intake of tritium for a person whose urine concentration was 2×10^{-4} μCi/L six days post-intake.

9–16. Urine samples from an adult male worker who was placed on a high-liquid diet after exposure to airborne tritium (assumed to be in oxide form) were 65, 40 and 22 Bq/L at 2, 5, and 9 d after exposure. (a) Plot the data and determine the effective half-life for elimination. (b) Estimate the initial intake of HTO. (c) Determine the whole-body dose due to the intake.

10
Environmental Dispersion

"Persons generally east and northeast of the Hanford reservation who were exposed to releases from the site after 1944 refer to themselves as 'downwinders'."

National Cancer Institute (1995)

The behavior of radionuclides released to environmental pathways is based on empirical models that account for their distribution and dilution in air, surface water, groundwater, and terrestrial ecosystems. Such models provide radioactivity concentrations that can then be used to determine intakes and radiation doses to persons (see Chapter 9). Such intakes are often governed by a complex interlinked chain, e.g., downwind air concentrations produced by a source followed by exposure of persons due to various habits and patterns of occupancy.

The concentration of a radionuclide in an environmental medium is determined by: a source (or input) term in units of activity per unit of time (Ci/s, g/h, etc), a dispersion (or mixing) term, a velocity term for the rate of input of the diluting medium (wind speed, stream flow rate, etc.), and, most important, an expression that describes the area through which the released material flows. These key factors are illustrated in Figure 10-1 in which a substance is introduced at a known rate Q (per s), into a diluting medium that has a flow rate of u (m/s) and a flowthrough area of width y (m) and height z (m) at a specified location. The resulting concentration (per m^3) of the discharged material in the respective medium is

$$\text{Conc (per m}^3\text{)} = \frac{\text{Q(per s)}}{u(\text{m/s}) \times y(\text{m}) \times z(\text{m})}\,[\text{DF}]$$

where DF is a dimensionless dispersion factor between 0 and 1.0. The product of u and the area (yz) yields the volume of material that dilutes the pollutant in a unit of time, and if Q is the amount of pollutant released into the flowing diluent in the same unit of time then the equation yields the concentration at the specific point downstream (or downwind for a release into the atmosphere). The concentration of a radiocontaminant released into an environmental medium is thus: (a) directly proportional to the release rate; (b) inversely proportional to the flow

Physics for Radiation Protection, Third Edition. James E. Martin

(velocity) of the mixing medium; and (3) inversely proportional to the area through which the contaminant–diluent mixture flows.

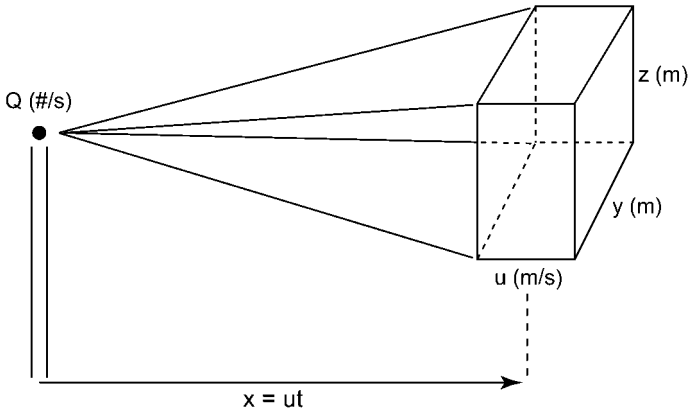

Fig. 10-1 Simple box model for dispersion of a contaminant emitted at a rate Q (per s) into a diluent stream (e.g., air or H_2O) that has a linear flow rate u (m/s) such that uniform mixing occurs as it flows through the area of width y (m) and height z (m) to produce a concentration $\chi = Q/uyz$ (per m^3).

Surface water dispersion may be represented as the mixing of discharged radioactivity into a liquid stream confined by a conduit, channel, culvert, or a naturally flowing stream. A typical example is a known amount of radioactivity in a holding tank that is discharged at a constant rate into flowing water over several hours. In such circumstances the material will form a mixing zone of nonuniform concentration near the discharge point but can be presumed to become uniformly mixed a short distance downstream. The concentration beyond the mixing zone is determined by the input rate, the stream flow rate, and the width and depth of the stream after it leaves the mixing zone, as in Example 10-1.

Example 10-1. A 12,000 L holding tank containing 0.1 Ci of a radionuclide is discharged over a period of 2 h into a small stream that is 10 m wide and 3 m deep that flows past the discharge point at a rate of 0.5 m/s. What is the average concentration (Ci/m^3) of the radiocontaminant over the 2 h period at a location downstream and beyond the mixing zone?

Solution. The activity concentration in the tank is 0.1 Ci/12,000 L = 8.33×10^{-6} Ci/L or 8.33 μCi/L. The discharge rate is

$$Q = Q = \frac{12{,}000\,\text{L}}{2\,\text{h} \times 3600\,\text{s}} \times 8.33\,\mu\text{Ci/L}$$

$$= 13.89\ \mu\text{Ci/s}.$$

It can be assumed that the volume of the fluid added by the tank is minimal compared to the volume of stream flow into which the material is diluted and that sufficient turbulence exists in the stream to provide uniform mixing of the radioactivity into the stream volume; therefore, the downstream concentration is

$$\text{Conc. } (\mu\text{Ci/m}^3) = \frac{13.89\,\mu\text{Ci/s}}{0.5\,\text{m/s} \times 10\,\text{m} \times 3\,\text{m}}$$

$$= 0.926\,\mu\text{Ci/m}^3\ (3.43 \times 10^4\ \text{Bq/m}^3)$$

or 9.26×10^{-7} μCi/mL.

Dispersion of contaminants in groundwater is also represented by the three general principles, and can be reasonably modeled using simplified parameters. Such an approach is often sufficient for modeling such releases because they are conservative; however, groundwater flow can be quite complex and accurate models require sophisticated techniques.

10.1 Atmospheric Dispersion

Atmospheric releases of a pollutant are usually assumed to emanate from a source that can be reasonably approximated as a "point" emitting material at a steady rate of Q (per s). The emitted material enters an atmospheric volume with a particular turbulence profile that flows past the release point with a velocity u (m/s) causing it to be mixed therein. If there is uniform turbulence in the atmospheric volume that flows past the point of release, the contaminant emitted in one second will, under these confined circumstances, be diluted in a volume of air equal to width y (m) and height z (m) multiplied by the translocation rate of air downwind, which is just u (m/s). The volume of diluent that passes the point in one second is thus $u(yz)$ m^3 and the concentration of the contaminant is just the amount released in the same second divided by the volume (in m^3) of flowing air, or

$$\chi(\text{per m}^3) = \frac{Q(\text{per s})}{u(yz)}$$

where Q is any quantity (mass, activity, etc.) expressed as a release rate (per s). The concentration downwind is thus directly proportional to the release rate and inversely proportional to the wind speed; i.e., doubling the wind speed halves the concentration if Q remains constant. A plume trapped in a channeled valley of width y and depth z is representative of this circumstance.

For a radionuclide release expressed as Ci/s, this general relationship becomes

$$\chi(\text{Ci/m}^3) = \frac{Q(\text{Ci/s})}{u(yz)}$$

which is reasonably accurate for plumes released at a steady rate and confined to flow through a specific area such as a plume trapped in a channeled valley of width y and height z.

Gaussian-distributed plumes represent most releases from "point" sources because the free atmosphere is not confined. The concentration χ will still be directly proportional to Q and inversely proportional to the wind speed; however, the concentration varies across an areal segment of the plume at some point x downwind and it is necessary to introduce a dispersion term to account for the nonuniform distribution of concentration. Measurements of concentration profiles at distances downwind from elevated point sources have demonstrated that the concentration varies both horizontally and vertically across the plume according to a Gaussian distribution, and because of this the dispersion term has been chosen accordingly. For continuously emitting sources, diffusion in the downwind (or x) direction is completely dominated by the wind speed u; however, both the vertical and horizontal spread of the plume increase with distance downwind (as shown in Figure 10-2) and are represented by the Gaussian dispersion coefficients σ_y and σ_z, which also vary with the downwind distance x.

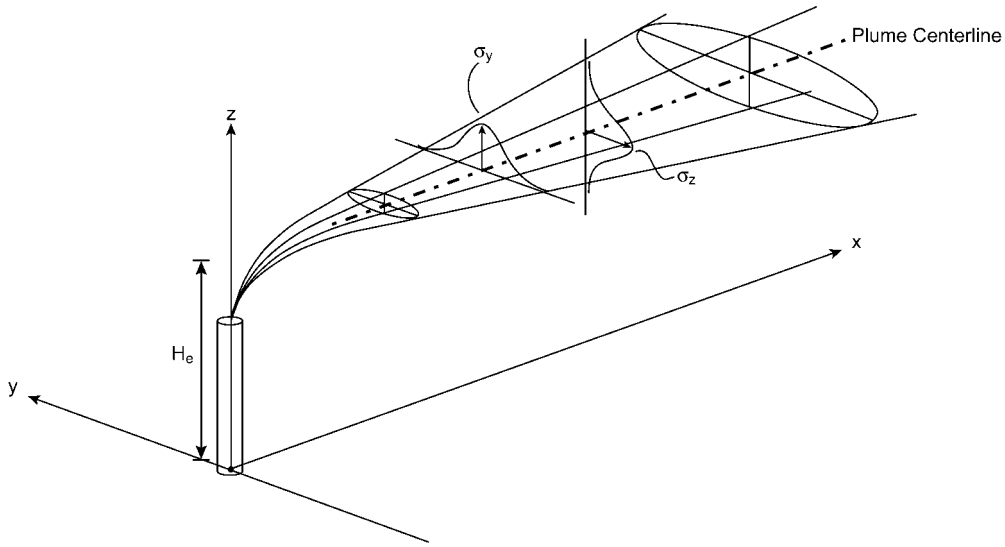

Fig. 10-2 Atmospheric dispersion of material released from a point source of height H above the ground that produces Gaussian-distributed concentration profiles both horizontally and vertically. A "virtual" source located at $-H$ accounts for reflection of the plume by the ground surface.

The general form of the Gaussian probability distribution across the plume (i.e., in the y direction) is

$$P(y) = \frac{1}{\sqrt{2\pi}\sigma_y} \exp\left(-\frac{y^2}{2\sigma_y^2}\right)$$

and vertically (in the z direction)

$$P(z) = \frac{1}{\sqrt{2\pi}\sigma_z}\exp\left(-\frac{z^2}{2\sigma_z^2}\right)$$

If the dispersion term for the y and z dimensions is expressed as the product of these two Gaussian probability distributions, the downwind concentration produced by a point source emission is

$$\chi(\text{per m}^3) = \frac{Q(\text{per s})}{2\pi\sigma_y\sigma_z u}\exp\left(-\frac{y^2}{2\sigma_y^2}\right)\exp\left(-\frac{z^2}{2\sigma_z^2}\right)$$

This equation has the same features as the general form equation, but with the exponential terms added to account for plume shape. The product of the two Gaussian distribution terms yields a denominator containing $2\pi\sigma_y\sigma_z u$ which also has units of area (m^2) since both σ_y and σ_z, the horizontal and vertical distribution coefficients, have units of length (m). Combining this Gaussian-distributed area with the wind speed (m/s) yields the volume into which the emitted contaminant is diluted. It is important to note that this equation is for "idealized" free space with no barriers. Most real-world situations consist of a release point above the ground and the ground surface represents a barrier that reflects the plume.

Plume reflection by the ground is accounted for mathematically by adding a "virtual source" also emitting contaminant at a rate Q an equal distance, $-H$, below the ground to produce a concentration above the ground surface (see Figure 10-2); this virtual source represents the above-ground concentration due to reflection of the "real" plume by the ground. The virtual source emits the contaminant at the same rate Q, thus producing a general solution for the concentration of the contaminant throughout the free space above the plane $z = 0$ (the reflecting barrier or the ground level) due to the virtual source; thus

$$\chi(x, y, z, H) = \frac{Q(\text{per s})}{2\pi\bar{u}\sigma_y\sigma_z}\exp\left(-\frac{y^2}{2\sigma_y^2}\right)\left[\exp\left(-\frac{(z-H)^2}{2\sigma_z^2}\right) + \exp\left(-\frac{(z+H)^2}{2\sigma_z^2}\right)\right]$$

where χ = concentration (per m^3) of the contaminant at a distance x downwind and at coordinates y = horizontal distance from the plume centerline and z = height above ground; Q = release rate of contaminants (per s); $\bar{u}$ = mean wind speed, typically measured at 10 m above the ground; H = height (+ and –) of release for the real and the virtual sources; σ_y = horizontal dispersion coefficient (m), and σ_z = vertical dispersion coefficient (m)

This general equation for the concentration in a ground-reflected plume is the sum of the concentrations χ produced by both the real and virtual sources and is for any value of y and z. Since the ground level concentration (i.e., where $z = 0$) is usually of interest, the solution is further simplified as

$$\chi(x, y, 0, H) = \frac{Q(\text{per s})}{\pi\sigma_y\sigma_z u}\exp\left(-\frac{y^2}{2\sigma_y^2}\right)\exp\left(-\frac{H^2}{2\sigma_z^2}\right) \tag{10-1}$$

which is twice as large (i.e., the value of 2 is no longer in the denominator) due to reflection of the plume; i.e., it essentially folds over on itself to double the ground-level concentration. The concentration at the point (x, y, 0) is a function of the height of release, H.

If the main concentration of interest is along the centerline (where $y = 0$), the equation further simplifies to

$$\chi(x, 0, 0, H) = \frac{Q(\text{per s})}{\pi\sigma_y\sigma_z u}\exp\left[-\frac{1}{2}\left(\frac{H}{\sigma_z}\right)^2\right] \tag{10-2}$$

and when the release is at ground level ($H = 0$) the concentration χ is very similar to the general flow equation developed earlier but now with the flowthrough area expressed in terms of the Gaussian plume dispersion coefficients σ_y and σ_z:

$$\chi = (x, 0, 0, 0) = \frac{Q(\text{per s})}{\pi\sigma_y\sigma_z\bar{u}} \tag{10-3}$$

where the values of σ_y and σ_z that fit a Gaussian plume concentration profile are governed by atmospheric properties, principally the vertical temperature profile.

10.1.1 Atmospheric Stability Effects on Dispersion

The values of σ_y and σ_z that fit a Gaussian plume concentration profile are governed by atmospheric properties, principally the effect of the vertical temperature profile on the turbulence field. Classes of atmospheric stability have, therefore, been defined in terms of the temperature profile with height and variations in wind speed/direction each of which affects the turbulence field. Various combinations of these parameters yield different types of plumes as shown in Figure 10-3 relative to the dry adiabatic lapse rate, which is –9.86 °C/km or about –1 °F/100 m or –5.4 °F/1000 ft.

As shown in Figure 10-3a, a vertical temperature profile that is steeper than the dry adiabatic lapse rate causes a displaced parcel of the air/contaminant mixture to continue to rise or sink. If the atmospheric temperature profile is the same as the dry adiabatic lapse rate (Figure 10-3b), the temperature of a parcel that is displaced either up or down will experience an adiabatic temperature change and will thus be dispersed only as far as the disturbing force moves it. This "neutral" condition (Figure 10-3b) results in plumes that spread in the shape of a cone. If, as shown in Figure 10-3c, the vertical temperature profile is less than the dry adiabatic lapse rate, the parcel will tend to be restored to its original position.

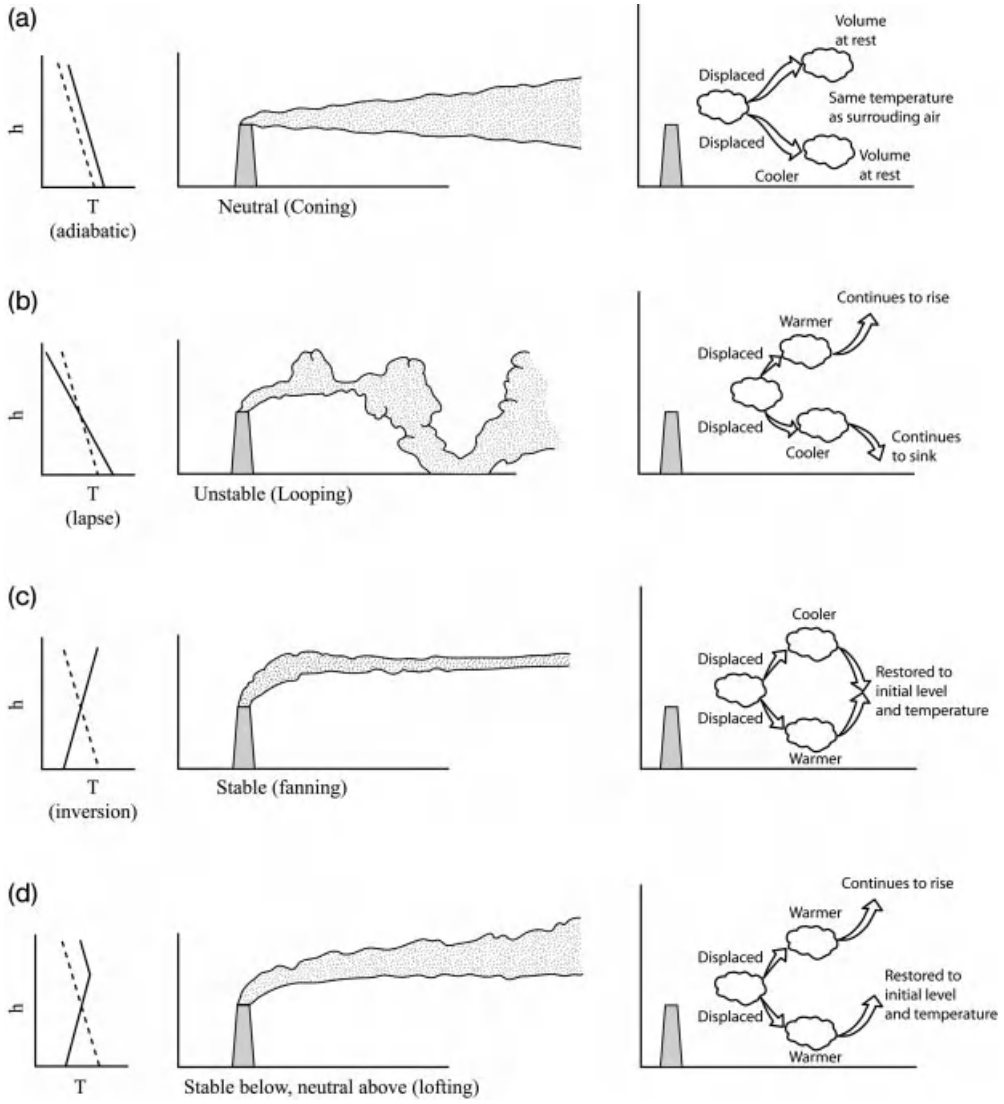

Fig. 10-3 Effects of the vertical temperature profile on plume shape: (a) lapse conditions yield looping plumes; (b) neutral conditions produce cone-shaped plumes; (c) inversion conditions result in long thin plumes; (d) inversion below/unstable above produces a condition known as lofting.

Lapse conditions occur when the atmospheric temperature profile is steeper than the dry adiabatic lapse rate (Figure 10-3a). If a parcel of the air/contaminant mixture in a plume is quickly displaced upward its temperature will decrease in absolute terms due to adiabatic cooling but its temperature relative to the surrounding atmosphere will be warmer causing it to be increasingly buoyant. If the parcel is

displaced downward its temperature will fall more rapidly than that of the surrounding atmosphere and its relatively greater density will cause it to settle even further. Strong lapse (superadiabatic temperature profile) conditions produce looping plumes that spread out over a wide area; thus, they are inherently *unstable* and are highly favorable for the dispersal of pollutants.

Temperature inversions yield very thin plumes, as shown in Figure 10-3c, due to highly stable conditions. Fluctuations that displace the parcel upward produce adiabatic cooling of the parcel such that it is denser than the surrounding atmosphere, consequently its upward motion stops and it returns to its original level. Likewise, any movement of the parcel downward causes its temperature to increase relative to the atmosphere and its buoyancy causes it to return to its original level. The atmosphere in this case is said to be stable and pollutant dispersion is minimal. This circumstance also occurs for releases into an isothermal profile, but is not as pronounced. Light winds are generally associated with stable conditions and if the wind direction is steady the plume becomes a long, meandering ribbon that extends downwind at the altitude of the stack, but if it fluctuates significantly, the plume spreads out in the horizontal plane like a fan – hence the term *fanning*. A fanning plume is not necessarily an unfavorable condition for the dispersion of effluents since the plume is quite wide and does not touch the ground.

Lofting is a condition that occurs when a temperature inversion exists below the plume height (Figure 10-3d). It typically occurs just after sunset as radiant cooling of the earth builds up a nighttime temperature inversion such that stable air exists below the plume and unstable or neutral conditions continue to exist above it. Lofting is a most favorable condition because effluents can disperse vertically but are kept away from the ground by the stable air below; dispersion thus occurs for great distances throughout large volumes of air.

10.1.2 Atmospheric Stability Classes

Seven categories of atmospheric stability have been defined, each of which can be described qualitatively in terms of the general atmospheric conditions under which they occur:

- Class A: extremely unstable conditions (bright sun, daytime)
- Class B: moderately unstable conditions (sunny, daytime)
- Class C: slightly unstable conditions (light cloudiness, daytime)
- Class D: neutral conditions (overcast sky, brisk wind, day or night)
- Class E: slightly stable conditions (early evening, light winds, relatively clear sky)
- Class F: moderately stable conditions (late night, light wind, clear sky)
- Class G: very stable (predawn, very light wind, clear sky)

These general conditions can also be summarized in terms of wind speed and the amount of sunshine or cloudiness, as shown in Table 10-1, but they are still mostly qualitative.

Table 10-1. Atmospheric stability class as a function of wind speed and amount of solar insolation.

Wind speed (m/s at 10 m)	Daytime conditions			Nighttime conditions	
	Strong sun	Moderate sun	Cloudy	>4/8 clouds	Clear sky
<2	A	A–B	B	E or F	F or G
2–3	A–B	B	C	E	F
3–5	B	B–C	C	D	E
5–6	C	C–D	D	D	D
>6	C	D	D	D	D

A more quantitative determination of stability class is based on measured values of temperature versus elevation and/or the standard deviation σ_θ of the mean wind direction. Stability classes that correspond to measured values of these parameters are listed in Table 10-2.

Table 10-2. Stability class (or Pasquill category)[a] versus vertical temperature profiles ($\Delta T/\Delta z$) and the standard deviation in the horizontal wind direction σ_θ.

Stability class	$\Delta T/\Delta z$ (°C/100 m)	σ_θ (degrees)[b]
A	< -1.9	>22.5°
B	$-1.9 \le -1.7$	$17.5 \le 22.5$
C	$-1.7 \le -1.5$	$12.5 \le 17.5$
D	$-1.5 \le -0.5$	$7.5 \le 12.5$
E	$-0.5 \le +1.5$	$3.8 \le 7.5$
F	$+1.5 \le +4.0$	$2.1 \le 3.8$
G	$> +4.0$	<2.1

a From Regulatory Guide 1.23, US Nuclear Regulatory Commission, 1980.
b Measured at wind speeds ≥ 1.5 m/s.

10.1.3
Calculational Procedure: Uniform Stability Conditions

The first step in performing atmospheric dispersion calculations is to determine the stability class that exists during the period of consideration which in turn establishes the dispersion coefficients σ_y and σ_z for a specific downwind distance x. The stability class can be chosen by one of three methods: (a) a qualitative determination based on the general conditions listed in Table 10-1; (b) measured values of temperature change with elevation as listed in Table 10-2; or (c) the standard deviation σ_θ of the mean wind vector, also listed in Table 10-2. Once the stability class is known, dispersion coefficients σ_y and σ_z are determined from Figures 10-4 and 10-5 for stability classes A to F. For extremely stable class G conditions, the dispersion coefficients σ_y and σ_z are computed from class F values since Figures 10-4 and 10-5 do not contain curves for stability class G (which, though not defined in the original work by Hay-Pasquill, was later added by the Nuclear Regulatory Commission (NRC)):

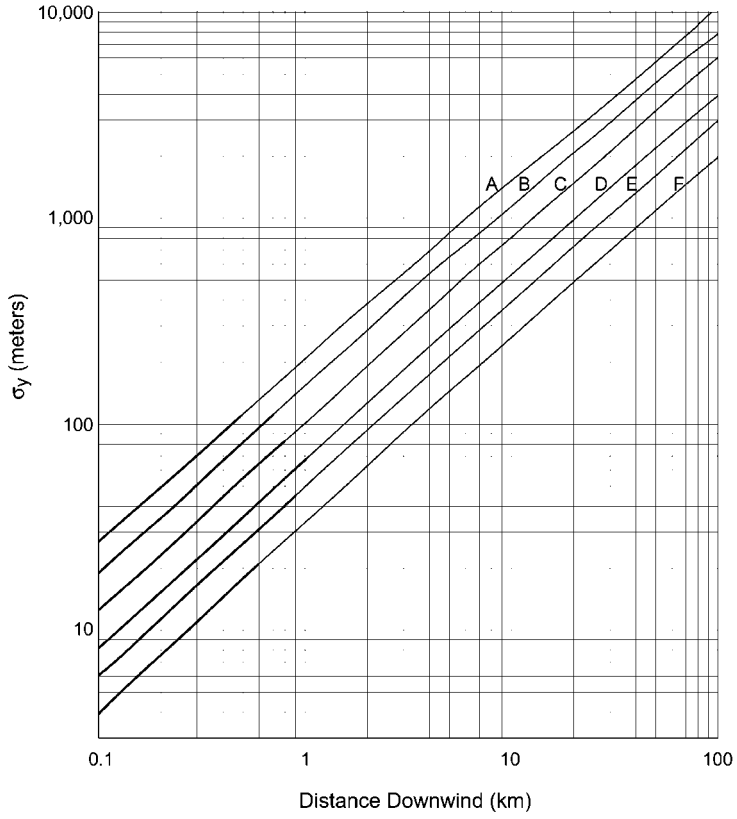

Fig. 10-4 Values of the horizontal Gaussian dispersion coefficient σ_y (m) versus distance and atmospheric stability class (A to F).

σ_y (G) = $2/3\sigma_y$ (F)

σ_z (G) = $3/5\sigma_z$ (F)

The emission rate Q, the stack height H, and the coordinates x, y, z are usually known and/or can be selected. The general procedure for calculating atmospheric dispersion is illustrated in Example 10-2.

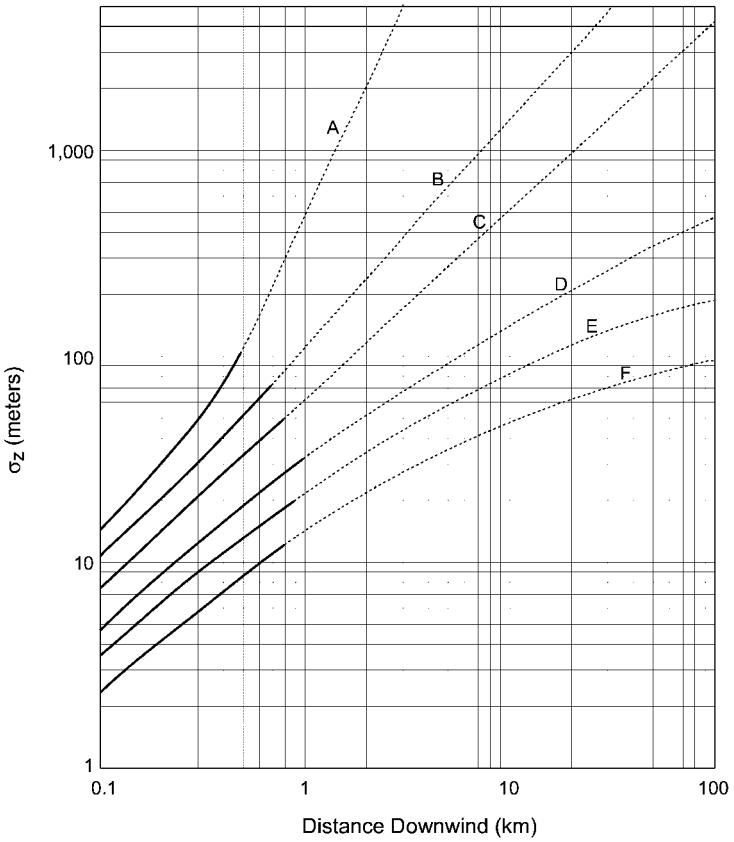

Fig. 10-5 Values of the vertical Gaussian dispersion coefficient σ_z (m) versus distance and atmospheric stability class (A to F).

Example 10-2. A stack 60 m high discharges a radionuclide at a rate of 80 Ci/s into a 6 m/s wind during the afternoon under overcast skies. Determine the ground-level concentration (a) 500 m downwind and 50 m off the plume centerline, and (b) at the same downwind distance but along the centerline.

Solution. (a) From Table 10-1, the atmospheric stability is judged to be class D due to overcast conditions and the relatively brisk wind. From Figure 10-4, it is deter-

mined that σ_y is 36 m for class D stability at 500 m and σ_z (from Figure 10-5) is 18.5 m; therefore, for $x = 500$ m, $y = 50$ m, and $H = 60$ m:

$$\chi(500, 50, 0, 60) = \frac{80\ \text{Ci/s}}{(3.14)(36\ \text{m})(18.5\ \text{m})(6\ \text{m/s})} \exp\left(-\frac{(60)^2}{2(18.5)^2}\right) \exp\left(-\frac{(50)^2}{2(36)^2}\right)$$

$$= 1.27 \times 10^{-5}\ \text{Ci/m}^3$$

(b) For $x = 500$ m and $y = 0$, the second exponential term is equal to 1.0, and

$$\chi(500, 0, 0, 60) = \frac{80\ \text{Ci/s}}{(3.14)(36\ \text{m})(18.5\ \text{m})(6\ \text{m/s})} \exp\left(-\frac{(60)^2}{2(18.5)^2}\right)$$

$$= 3.34 \times 10^{-5}\ \text{Ci/m}^3$$

yielding , as expected, a higher concentration.

10.1.4 Distance x_{max} of Maximum Concentration (χ_{max})

The point at which the maximum ground-level concentration occurs is often of interest especially for design purposes and emergency planning. Solution of the general dispersion equation for the point of maximum downwind concentration indicates that it occurs along the centerline when the vertical dispersion coefficient σ_z has the value

$$\sigma_z = 0.707H$$

which is of course dependent on the stability class. This specific value of σ_z is found in Figure 10-5 for the particular stability class and the corresponding value of x (i.e., x_{max}) at which χ_{max} occurs is determined. Once the location x_{max} is established, the maximum concentration can then be calculated using the values of σ_y and σ_z that correspond to that distance (it is only necessary to determine σ_y since σ_z has already been calculated based on x_{max} and the stability class). The maximum concentration is

$$\chi_{max} = \frac{Q(\text{per s})}{\pi \bar{u} \sigma_{y,max} \sigma_{z,max}} \times \frac{1}{e}$$

or, by inserting the values for π and $e = 2.7183$,

$$\chi_{max} = 0.117 \frac{Q(\text{per s})}{\bar{u} \sigma_{y,\,max} \sigma_{z,\,max}}$$

where $\sigma_{y,\max}$ and $\sigma_{z,\max}$ are determined for the point downwind where the maximum concentration occurs. These relationships are applicable to elevated stack releases only; the maximum concentration for a ground-level release is at the point of release and the downwind concentration gradually decreases with increasing x.

Example 10-3. Estimate (a) the downwind point of maximum concentration for effluent released at 10 Ci/s at a height of 30 m under class F stability into a steady wind of 1 m/s; and (b) the maximum concentration at that location.

Solution. (a) For these conditions, $\sigma_z = 0.707H = 21.2$ m; therefore, as shown in Figure 10-5, σ_z has the value 21.2 m at about 1900 m (1.2 miles) which is $x_{\max}$.

(b) At $x = 1900$ m, $\sigma_y = 60$ m and $\sigma_z = 21.2$ m (already determined); thus the maximum concentration is

$$\chi_{\max} = \frac{0.117 \times 10\,\text{Ci/s}}{1\,\text{m/s} \times 21.2\,\text{m} \times 60\,\text{m}} = 9.2 \times 10^{-4}\,\text{Ci/m}^3$$

10.1.5 Stack Effects

The Gaussian plume model can be used for stack releases if the release approximates a "point" and the wind field has homogeneous turbulence. These conditions can be assumed for tall slender stacks located such that the turbulence induced by surrounding structures and terrain is minimal: a general rule of thumb is that the top of the stack should be 2.5 times higher than any surrounding obstructions that may induce turbulence that would produce inhomogeneities at the point of release. Gaussian plume conditions may also exist for shorter stacks if releases occur during moderate to light winds but they may fail to exist even for tall stacks if wind speeds are very high.

The stack itself exerts effects on plume dispersion, some of which may promote dispersion while others may reduce it. The temperature of the effluent can induce buoyancy (positive or negative) and the momentum of the effluent can affect the height at which the plume levels off. Such effects are considered in terms of effective stack height, stack concentration effects, and stack turbulence effects.

The *effective stack height* is that elevation above the physical stack height where the plume levels off (see Figure 10-2), which is often referred to as plume rise. The amount of plume rise, or dH, is governed by the efflux velocity which gives momentum to the effluent as it leaves the stack, the horizontal wind speed, and the differential temperature of the effluent versus that of the receiving air stream. For example, a hot plume will be buoyant and if ejected with a high efflux velocity may rise quite a bit above the physical stack height before being leveled off by a combination of the wind speed and the cooling effect of the receiving air. The effective stack height H_{eff} is obtained by adding the calculated plume rise dH to the physical stack height:

$$H_{\text{eff}} = H + dH$$

Various models have been devised for determining dH. One of the most straightforward was devised by Davidson using Bryant's data:

$$dH = d\left(\frac{v_s}{\bar{u}}\right)^{1.4}\left(1 + \frac{T_s - T_a}{T_s}\right)$$

where dH = differential plume rise (m); d = inside diameter of stack (m); v_s = efflux velocity of stack (m/s); $\bar{u}$ = mean wind velocity (m/s) at the top of the stack; T_s = temperature in the stack (K); and T_a = temperature of the atmosphere (K). The first term in the Davidson–Bryant model accounts for momentum effects due to the velocity of the discharged effluent and the horizontal translation due to the wind field; the second term accounts for the temperature differential between the two fluids.

Example 10-4. An effluent of 100 °C is released from a stack 100 m high with an inside diameter of 2.44 m and at an efflux velocity of 13.7 m/s into the atmosphere which has a mean wind speed of 3 m/s and a temperature of 18 °C. Calculate the effective stack height ($H + dH$).
Solution.

$$dH = 2.44\,\text{m} \times \left(\frac{13.7\,\text{m/s}}{3\,\text{m/s}}\right)^{1.4}\left(1 + \frac{(100 + 273) - (18 + 273)}{273 + 100}\right)$$

$$= 20.456(1.22) = 25\ \text{m}$$

and

$$H_{\text{eff}} = H + dH = 100 + 25\ \text{m}$$

$$= 125\ \text{m}$$

Changing the stack concentration by increasing the air flow in the stack has little effect on the resulting downwind concentration which is not intuitively obvious. The calculated value of χ is governed primarily by the emission rate Q which would stay the same. The increased air flow may, however, increase the effective stack height, but in general this has minimal influence on χ.

Mechanical turbulence induced by a stack can cause significant tip vortices and a zone of low pressure may develop on the lee side of the stack, especially during high winds. If the plume is discharged at a relatively low velocity or is not particularly buoyant, it can be drawn into the lee of the stack creating a negative dH. In very high winds, the plume appears to exit the stack several feet below the top. Large stacks often have discoloration several feet below the top due to these combined effects.

Checkpoints

The Gaussian plume model for point source releases is based on very specific conditions; therefore, it is applicable *only* for the following essential conditions:

- for points of release 2.5 times the height of any surrounding structures;
- a steady-state release rate into an atmosphere with homogeneous turbulence;
- unobstructed releases over flat, open terrain where complete reflection of the plume by the ground (i.e., minimal plume depletion) can be assumed;
- diffusion times of 10 min or more;
- positive values of wind speed (equations fail for zero windspeed).

Despite these restrictions, the models are often used for other conditions because they are the only ones available. It must be recognized, however, that the quality of the results will be influenced by the degree to which conditions deviate from the model, and the results should be used accordingly.

10.2 Nonuniform turbulence: Fumigation, Building Effects

Various conditions can occur in which the turbulence associated with an airborne plume will be nonuniform and it is not appropriate to use a Gaussian plume model to determine the plume concentration. Two common situations are fumigation and mechanical turbulence induced by buildings or other obstructions, and a different model is required for each.

10.2.1 Fumigation

Plume concentrations can be quite high during temperature inversions, which typically occur during low winds and clear nights. These conditions promote radiant cooling of the earth's surface and the temperature of the air near the ground becomes relatively cooler than layers above thus creating a zone of very stable air. When the sun comes up it heats the ground which in turn produces a zone of turbulent air, which occurs at first near the ground but grows in height due to thermal eddies. When the turbulent air zone ascends to the height of the plume, the trapped plume material is rapidly dispersed to ground level, producing relatively high concentrations at ground level, as illustrated in Figure 10-6. Effluents emitted during this period continue to be confined by the inversion overhead, and will be dispersed toward the ground by the turbulence in the newly heated unstable air. Such events are called fumigation; the ground-level concentration during fumigation is

$$\chi_{\text{fum}}(H_e > 10\text{m}) = \frac{Q(\text{per s})}{(2\pi)^{1/2}\bar{u}_h\sigma_y H_e}$$

$$= 0.4\frac{Q(\text{per s})}{\bar{u}_h\sigma_y H_e}$$

where $\bar{u}_h$ = average wind speed for the layer at H_e (m/s); σ_y = lateral plume spread (m), typically for class F stability; and H_e = effective stack height (m). This fumigation equation cannot be used when H_e becomes small (of the order of 10 m or less) because calculated χ/Q values will become unrealistically large. For releases <10 m, it is more realistic to model the dispersion as a ground-level release where H_e is replaced by the appropriate value of σ_z.

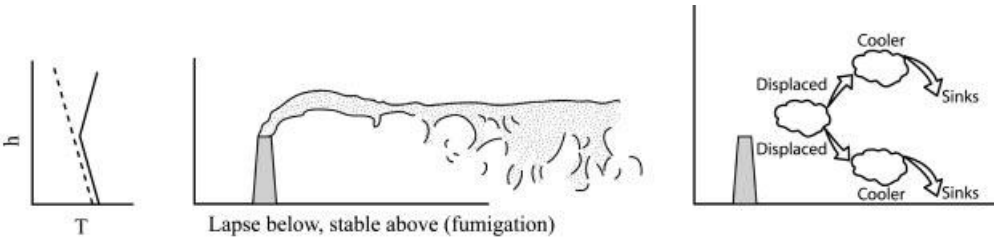

Fig. 10-6 Fumigation breakup of a trapped plume producing a zone of relatively high concentration between the ground and the bottom of the inversion layer, typically at H_e.

Example 10-5. If a unit of radioactivity is released from a 100 m stack during class F stability during which the wind speed is 2 m/s, what is the χ/Q value for a plume centerline location 3000 m downwind for (a) normal conditions and (b) during fumigation?

Solution. (a) For non-fumigation (i.e., normal Gaussian plume dispersion), H_e=100 m, σ_y = 100 m, and σ_z = 280 m.

$$\frac{\chi}{Q} = \frac{1}{\pi\bar{u}\sigma_y\sigma_z}\exp\left(-\frac{H_e^2}{2\sigma_z^2}\right)$$

$$= \frac{1}{\pi(2\,\text{m/s})(100\,\text{m})(280\,\text{m})}\exp\left[-\frac{(100\,\text{m})^2}{2(280\,\text{m})^2}\right]$$

$$= 5.33\times10^{-6}\ \text{s/m}^3$$

(b) For fumigation conditions where H_e = 100 m, and σ_y = 100 m (Figure 10-4),

$$\frac{\chi}{Q} = \frac{1}{(2\pi)^{1/2}\bar{u}_h\sigma_y H_e}$$

$$= \frac{1}{(2\pi)^{1/2}(2\,\text{m/s})(100\,\text{m})(70\,\text{m})}$$

$$= 2.8 \times 10^{-5}\ \text{s/m}^3$$

which, as expected, is considerably larger than that calculated for non-fumigation conditions.

10.2.2 Dispersion for an Elevated Receptor

A receptor location may exist at an elevation above the base of the stack (a knoll or a small hill perhaps) but below the effective stack height. Plume concentrations at such a location can be calculated by modifying the basic dispersion equation for the concentration along the centerline (i.e., $y = 0$) as follows:

$$\chi = \frac{Q(\text{per s})}{\pi \bar{u}_h \sigma_y \sigma_z} \exp\left[\frac{-(H_e - h_t)^2}{2\sigma_z^2}\right]$$

where $\bar{u}_h$ = wind speed representing conditions at the release height; H_e = effective stack height above plant grade (m); and h_t = maximum terrain height (m) above plant grade between the release point and the point for which the calculation is made (h_t cannot exceed H_e). If ($H_e - h_t$) is less than about 10 m, then the condition should be modeled as a ground-level release. An example of the ground-level concentration for an elevated receptor point is shown in Example 10-6.

Example 10-6. Assuming non-fumigation conditions, what is the χ/Q value 3000 m downwind for a receptor located 30 m above plant grade if the point of release is a 100 m stack, the wind speed is 2 m/s, and the stability is class F?
Solution. Since the height of the receptor h_t = 30 m, the effective release point is 100 m – 30 m = 70 m, and σ_y (Figure 10-4) and σ_z (Figure 10-5) are 100 m and 280 m, respectively; thus

$$\frac{\chi}{Q} = \frac{1}{\pi \bar{u}_h \sigma_y \sigma_z} \exp\left[\frac{-(H_e - h_t)^2}{2\sigma_z^2}\right]$$

$$= \frac{1}{\pi(2\,\text{m/s})(100\,\text{m})(280\,\text{m})} \exp\left[\frac{-(70\,\text{m})^2}{2(280\,\text{m}^2)}\right]$$

$$= 5.5 \times 10^{-6}\ \text{s/m}^3$$

which is essentially the same as result obtained in part (a) of Example 10-5 for level terrain; i.e., a slightly elevated receptor has less effect than other conditions of the dispersion field.

Fumigation dispersion for an elevated receptor can also be modeled by adjusting the value of H_e in the fumigation equation similar to that done in Example 10-6 to account for the elevated point of interest. This in effect decreases the area through which the plume material flows at the receptor location which in turn increases the ground-level concentration due to the "trapped" plume. For protection purposes, this is a conservative approach because the actual vertical dispersion depth is likely to be greater due to the elevated receptor location, especially if it is on a small hill or due to a gradual change in the terrain.

10.2.3
Building Wake Effects: Mechanical Turbulence

The Gaussian diffusion equations were developed for idealized conditions of point source releases over relatively flat undisturbed terrain where atmospheric turbulence, as characterized by the vertical temperature profile, is fairly homogeneous. These idealized conditions rarely exist, but as a practical matter the point source equations can be used for flat and relatively unobstructed terrain and release points that are 2.5 times higher than surrounding buildings or terrain disturbances (e.g., cliffs or rock outcrops).

Mechanical turbulence induced by buildings or other structures can completely dominate the dispersion pattern due to a combination of moderate to strong winds, a low efflux velocity, and fairly short release points. A common situation is a short stack or vent atop a sizeable building as shown in Figure 10-7. Effluent released under such conditions will be drawn into the building wake, and special considerations are required for determining plume concentrations.

Fig. 10-7 Photograph of building wake entrapment of a plume released in a 6 m/s wind from a stack 3 m above a research reactor building approximately 15 m high with a width projection of about 15 m.

10.2.4 Concentrations of Effluents in Building Wakes

Building turbulence thoroughly mixes any effluent introduced into a building wake and the resulting concentration will be uniform throughout the wake volume. Three methods can be used to determine the concentration of a plume confined to flow in the lee of a building: (a) determining the building wake volume and the dilution it provides for the emission rate Q; (b) a modified ground-release equation; and (c) a virtual source method.

The *building wake volume* is, as shown in Example 10-7, a function of the area the building projects downwind and the wind speed.

Example 10-7. Estimate the street-level concentration at approximately 120 m downwind of the 3 m stack atop the large building in Figure 10-7 ($h = 15$ m; $w = 15$ m) due to a steady-state release of 5 μCi/s of ^{41}Ar when the wind speed is 5 m/s.

Solution. The smoke test in Figure 10-7 was conducted during 5 m/s winds and clearly shows building wake entrapment due to mechanical turbulence induced by the large building; therefore, the plume flows near the ground where its height, as estimated from the figure, is about the same as that of the stack. Its width, which is more uncertain from the figure, can be assumed to be the width of the building projected downwind; i.e., no channeling due to windstreaming. The calculated concentration at ~120 m is

$$\chi = \frac{Q}{\bar{u}hw} = \frac{5\,\mu\text{Ci/s}}{5\,\text{m/s} \times 18\,\text{m} \times 15\,\text{m}}$$

$$= 3.7 \times 10^{-3}\,\mu\text{Ci/m}^3$$

The ground-level release equation has been modified in various ways to account for mechanical turbulence, one of which has been proposed by Fuquay as

$$\chi = \frac{Q(\text{per s})}{u(\pi\sigma_y\sigma_z + cA)}$$

where A, the area of the building on the lee side, is adjusted by the factor c to obtain the area through which the plume flows due to the dominant influence of the mechanical turbulence caused by the building. For downwind distances within about 10 building heights, c ranges between 0.5 and 2.0. Use of small values of c (i.e., $c = 0.5$) yields conservative (i.e., higher) estimates of plume concentrations because of the small flowthrough area of the wake. The quantity cA has the greatest effect on the plume concentration at short distances downwind because $cA \gg \pi\sigma_y\sigma_z$; however, at larger distances $\pi\sigma_y\sigma_z$ will dominate such that the equation accounts for wake effects both close to the building and at locations further downwind. Values of σ_y and σ_z are determined for distances of x measured from the center of the building.

A *virtual source method* can also be used because mechanical turbulence produced by the obstruction causes the released contaminant to flow along the ground. The plume concentration can thus be modeled as though it were a ground-level release by placing a ground-level virtual source at a location upwind of the point of release such that the plume produced by the virtual source would have a height and horizontal spread that just envelops the building as it passes it. The downwind concentration is then modeled as a Gaussian-distributed ground-level release at the point of interest downwind as though the building were not present; i.e., the fictitious source would produce a concentration

$$\chi = \frac{Q(\text{per s})}{\pi \bar{u} \sigma_{y,x_0} \sigma_{z,x_0}}$$

where σ_{y,x_0} and σ_{z,x_0} are determined for downwind distances measured from the location of the ground-level virtual source. The values of σ_{y,x_0} and σ_{z,x_0} that correspond to a plume that just envelops a building of height H_b and width W are

$$\sigma_{z,x_0} = \frac{H_b}{2.14}$$

$$\sigma_{y,x_0} = \frac{W}{4.28}$$

and these calculated values of σ_{y,x_0} and σ_{z,x_0} are used to obtain the upwind virtual-source distances x_{z0} and x_{y0} by entering them separately into the curves in Figures 10-4 and 10-5 for the particular stability class that exists. These two values are added to the downwind distance of interest to establish the value of x at which σ_{y,x_0} and σ_{z,x_0} are determined. One can use either or both distances for locating the virtual source, but for buildings it is usually based on x_{z0}, as shown in Example 10-8.

Example 10-8. Use the virtual source method to estimate the concentration of radiocesium 200 m downwind of a source that emits 0.5 Ci/s from a 2 m vent atop a building that is 30 m tall and 20 m wide during class D stability and a wind speed of 6 m/s.

Solution. A ground-level source emitting a plume that would just engulf a 30 m high building when it reaches the building corresponds to a σ_{z,x_0} value of

$$\sigma_{z,x_0} = \frac{30\,\text{m}}{2.14} = 14\,\text{m}$$

As shown in Figure 10-4, this value for class D stability corresponds to a downwind distance of 350 m; therefore, the concentration 200 m downwind of the building is modeled as if it were emitted from a ground-level "virtual" source located 350 m + 200 m upwind. At 550 m σ_{y,x_0} = 40 m and σ_{z,x_0} = 20 m and the concentration at 200 m downwind of the release point is

$$\chi = \frac{0.5\ \text{Ci/s}}{\pi \times 6\ \text{m/s} \times 40\ \text{m} \times 20\ \text{m}}$$

$$= 3.32 \times 10^{-5}\ \text{Ci/m}^3$$

10.2.5 Ground-level Area Sources

The virtual source method is also useful for determining downwind concentrations for emissions from contaminated areas such as a waste disposal site, or a treatment pit or lagoon. The virtual source distance for these circumstances is based on the width of the area and it is this dimension that is used to establish x_{y_0} and thus σ_{y,x_0} as shown in Example 10-9. The same value (i.e., $x_{y_0} = x_{z_0}$) is generally used for determining σ_{z,x_0} unless the height of the plume above the area is known.

Example 10-9. Radon gas is exhaled from a roughly circular area 50 m in diameter at a flux of 10 pCi/m^2 s. Estimate the concentration of radon in air 400 m downwind for an average wind speed of 4 m/s and an assumed condition of neutral (class D) atmospheric stability.

Solution. The total emission rate for the area is 19,635 pCi/s which can be modeled as coming from a virtual ground-level point source located upwind such that the plume width during class D stability conditions just envelops the area as it passes over it. This value of σ_{y,x_0} is

$$\sigma_{y,x_0} = \frac{W}{4.28} = \frac{50\ \text{m}}{4.28} = 11.7\ \text{m}$$

From Figure 10-4 this value of σ_{y,x_0} occurs ~100 m downwind of a point source during class D stability; therefore, the concentration at all other distances is modeled as emanating from a virtual point source located 100 m upwind of the center of the area. For a location 400 m downwind, or x_0 = 500 m, σ_{y,x_0} = 36 m and σ_{z,x_0} = 18.5 m from Figures 10-4 and 10-5, respectively, and radon concentration is

$$\chi = \frac{Q}{\pi u(\sigma_{y,x_0})(\sigma_{z,x_0})}$$

$$= \frac{19{,}365\ \text{pCi/s}}{\pi \times 4\ \text{m/s} \times 18.5\ \text{m} \times 36\ \text{m}} = 2.3\ \text{pCi/m}^3$$

10.2.6
Effect of Mechanical Turbulence on Far-field Diffusion

The US Nuclear Regulatory Commission has provided guidance (NRC Regulatory Guide1.145) that uses selection rules to determine the effect of mechanical turbulence on plume concentrations in the far field of buildings (i.e., at distances greater than 10 building heights). Three modified ground-release equations are used with values of σ_y and σ_z determined for a downwind distance x measured from the center of the building:

$$\frac{\chi}{Q} = \frac{1}{\bar{u}_{10}(\pi\sigma_y\sigma_z + 0.5A)} \tag{10-4}$$

$$\frac{\chi}{Q} = \frac{1}{\bar{u}_{10}(3\pi\sigma_y\sigma_z)} \tag{10-5}$$

$$\frac{\chi}{Q} = \frac{1}{\bar{u}_{10}\pi\Sigma_y\sigma_z} \tag{10-6}$$

where χ/Q = dispersion factor per unit release (s/m^3); $\bar{u}_{10}$ = mean wind speed (m/s) at 10 m above the ground; A = smallest vertical plane cross-sectional area (m^2), and Σ_y = lateral plume spread based on meander and building wake effects (m). This approach, which is described in NRC Regulatory Guide 1.145, eliminates the need to find an upwind virtual source distance; it does, however, rely on *selection rules* which are:

- For neutral (class D) or stable (class E, F, G) atmospheric conditions the *higher* of the two values calculated by Equations (10-4) and (10-5) is compared to the value from Equation (10-6) and the *lower* of these two values is selected as the appropriate dispersion coefficient, or χ/Q value.
- For unstable conditions (class A, B, C) the appropriate χ/Q value is the higher of the two values obtained from Equation (10-4) or (10-5).

The value of Σ_y in Equation (10-6) is a calculated quantity that accounts for horizontal (lateral) plume meander, which should be considered during neutral (class D) or stable (class E, F, or G) atmospheric stability conditions when the wind speed at the 10 m level is less than 6 m/s; it is thus a function of atmospheric stability, the wind speed $\bar{u}_{10}$, and the downwind distance. For downwind distances of 800 m or less, $\Sigma_y = M\sigma_y$, where M is a plume meander factor determined from Figure 10-8; for downwind distances greater than 800 m, $\Sigma_y = (M - 1)\sigma_{y800\text{m}} + \sigma_y$, where $\sigma_{y800\text{m}}$ is the value of σ_y determined from Figure 10-4 at 800 m for the respective stability class. It is not necessary to consider plume meander during

unstable atmospheric conditions (class A, B, or C stability) and/or wind speeds of 6 m/s or more because building wake mixing becomes more effective in dispersing effluents than meander effects.

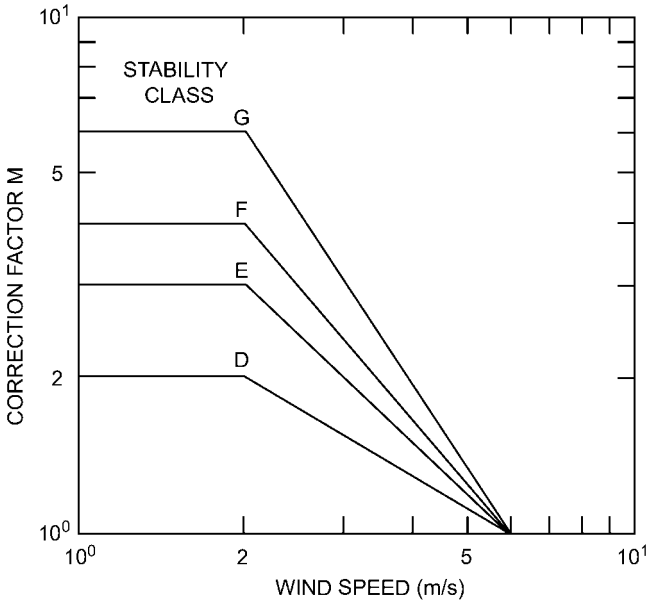

Fig. 10-8 Meander factor M for determining Σ_y for far-field dispersion downwind of buildings and obstacles.

Example 10-10. Determine the appropriate χ/Q value for radioactivity released from a short vent on a building with a cross-sectional area of 2000 m² during class F atmospheric stability conditions and a wind speed of 2 m/s at (a) 100 m and (b) 1000 m downwind.

Solution. This type of dispersion is considered a ground-level release for calculational purposes using Equations (10-4)–(10-6) in accord with the selection rules. (a) For a downwind distance of 100 m, $\sigma_y = 4$ m and $\sigma_z = 2.4$ m; $M = 4$ (Figure 10-8) and $\Sigma_y = M\sigma_y = 16$ m; and the area-modifying factor is conservatively chosen as $c = 0.5$. By Equation (10-4)

$$\frac{\chi}{Q} = \frac{1}{(2\,\text{m/s})[\pi(4\,\text{m})(2.4\,\text{m}) + (2000\,\text{m}^2 \times 0.5)]}$$

$$= 4.9 \times 10^{-4}\ \text{s/m}^3$$

and by Equation (10-5)

$$\frac{\chi}{Q} = \frac{1}{(2\,\text{m/s})[(3)\pi(4\,\text{m})(2.4\,\text{m})]}$$

$$= 5.5 \times 10^{-3}\ \text{s/m}^3$$

and by Equation (10-6) where $\Sigma_y = 4\sigma_y = 16$ m

$$\frac{\chi}{Q} = \frac{1}{(2\,\text{m/s})[\pi(16\,\text{m})(2.4\,\text{m})]}$$

$$= 4.1 \times 10^{-3}\ \text{s/m}^3$$

Application of the selection rules for class F stability yields a choice of 4.1×10^{-3} s/m^3 for the dispersion factor.

(b) similar calculations for 1000 m yield χ/Q values of 1.8×10^{-4} s/m^3 (Equation (10-4)), 9.5×10^{-5} s/m^3 (Equation (10-5)), and 8.7×10^{-5} s/m^3 (Equation (10-6)) and the selected value based on the selection rules is 8.7×10^{-5} s/m^3.

10.3 Puff Releases

Contaminants can also be released in a single burst during emergencies when overpressurization occurs (perhaps even an explosion) or as a result of a sudden spillage. Such releases are characterized as puffs of very short duration in which a discrete volume of material travels downwind, expanding in all directions due to atmospheric effects. Such an expansion causes the quantity of the contaminant Q_p to be diluted in a continually expanding volume. The release Q_p is a discrete amount (i.e., it does occur at a continuous rate) and the Gaussian distribution of the concentration at any point (x, y, z) measured from the center of the puff is

$$\chi(x,y,z) = \frac{Q_p}{(2\pi)^{3/2}\sigma_x{}^*\sigma_y{}^*\sigma_z{}^*}\exp\left\{-\frac{1}{2}\left[\left(\frac{x-\bar{u}t}{\sigma_x{}^*}\right)^2+\left(\frac{y}{\sigma_y{}^*}\right)^2+\left(\frac{z-z_0}{\sigma_z{}^*}\right)^2\right]\right\}$$

where Q_p is the total release of material and values of σ^* are distinct for expansion of the puff as it moves downwind. In contrast to continuous releases, there is no dilution due to wind speed and u does not appear in the denominator of the equation; its only effect is translocation of the puff downwind which is determined by the term ut, or the position of the center of puff downwind. Dispersion in the x direction is accounted for by the dispersion coefficient $\sigma_x{}^*$, and it and the dispersion coefficients $\sigma_y{}^*$ and $\sigma_z{}^*$ are uniquely determined for a contaminant released in a puff based on data for two downwind distances at 100 and 4000 m, as in Table 10-3. Figure 10-9 shows the diffusion of a single puff with Gaussian concentration distributions.

Table 10-3. Puff release data (in m) for two downwind distances x = 100 and 4000 m.

	x = 100 m		x = 4000 m	
Atmospheric condition	$\sigma_x^* = \sigma_y^*$	σ_z^*	$\sigma_x^* = \sigma_y^*$	σ_z^*
Unstable (A–C)	10	15	300	220
Neutral (D)	4	3.8	120	50
Very stable (E–F)	1.3	0.75	35	7

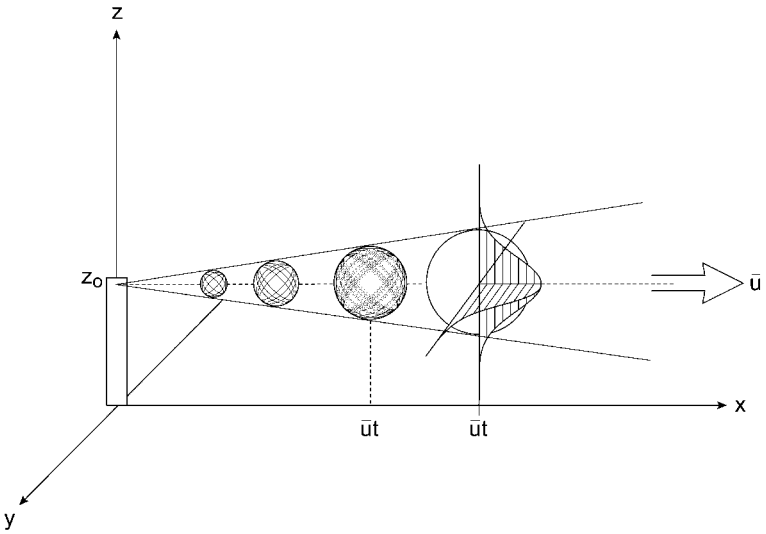

Fig. 10-9 Diffusion of a single puff with Gaussian concentration distributions, vertically (z), laterally (y), and horizontally (x) from an elevated point where $\bar{u}t$ indicates the distance of travel of the center of the puff in the downwind direction x.

10.4 Sector-Averaged χ/Q Values

In practice, most radiological assessments for facilities that release radioactive (or other) materials to the atmosphere are of long duration. Atmospheric conditions, especially wind direction and stability conditions, will obviously vary for extended periods, and it is necessary to account for such changes by determining a sector-averaged χ/Q value. This is done typically on an annual or quarterly basis by distributing the released material into several sections of a downwind sector grouped according to wind speed and stability class for an average release quantity Q.

These long-term average χ/Q values are based on accumulated meteorological data.

Many nuclear facilities provide one or more meteorological towers equipped to measure wind speed and direction and the vertical temperature profile from which stability class is determined. These are accumulated in real time and a computer program sorts them into the categories needed for determining long-term sector-averaged $\bar{\chi}/\bar{Q}$ values calculated as

$$\frac{\bar{\chi}}{\bar{Q}}(\mathrm{s/m^3}) = \left(\frac{2}{\pi}\right)^{1/2} \frac{f_i}{\beta x} \sum_{jk} \frac{F_{jk}}{\sigma_{zj}\bar{u}_k} \exp\left(-\frac{1}{2}\frac{H^2}{\sigma_{zj}^2}\right)$$

where the quantity βx (m) replaces σ_y in the general dispersion equation. The value of x is the downwind distance to the midpoint of a subsection of the sector of interest (e.g., the subsection extending from 1 to 3 km has a midpoint of 2 km) and when multiplied by the sector width $\beta = 2\pi/n$ radians yields the horizontal width through which the plume flows; it is thus a reasonable surrogate value of σ_y for that distance based on averaged conditions.

The number of downwind sectors for plume averaging is usually chosen to be $n = 16$ which consists of sector arcs of 22.5° each extending from the point of release as shown in Figure 10-10. For example, material released when the wind is from due west ±11.25° is presumed to diffuse into sector 4 which is ascribed by a pie-shaped wedge extending due east ±11.25°. Likewise, for winds from due south ±11.25° the material is transported into sector 16, a pie-shaped wedge extending due north ±11.25°. All winds blowing into a given sector are thus recorded for the sector and over time will constitute a fraction f_i of the total amount of material dispersed into a given sector. The fraction of wind blowing into a given subsection of a sector is further subdivided into wind speed groupings (0–2 m/s, 2–4 m/s, etc.) which are further subdivided into each of the stability classes recorded for each wind speed grouping yielding another fraction F_{jk}. If the released material is distributed into $n = 16$ sectors each of 22.5° then $\beta = 2\pi/16$ or 0.3927, and each sector-averaged χ/Q is thus (USNRC, Reg. Guide 1.111, 1977)

$$\frac{\bar{\chi}_i}{\bar{Q}_i}(\mathrm{s/m^3}) = \frac{2.032 f_i}{x} \sum_{jk} \frac{F_{jk}}{\bar{u}_k \sigma_{zj}} \exp\left(-\frac{H^2}{2\sigma_{zj}^2}\right)$$

where $\bar{\chi}_i/\bar{Q}_i$ = the sector-averaged dispersion factor for a downwind subsection of sector i; f_i = the fraction of the time (e.g., month, year) the wind blows toward sector i; F_{jk} = the fraction of f_i during which each stability class j exists for wind class k (direction and speed) in sector i; x = the median downwind distance for a subsection of sector i; $\bar{u}_k$ = the median wind speed for a chosen group (e.g., $\bar{u}_k = 1$ m/s for winds of 0 to 2 m/s); σ_{zj} = the vertical diffusion coefficient (m) for each stability class j; and H = the effective stack height (m). The interrelationships of these variables are illustrated in very simplified form in Example 10-11 in order to demonstrate the underlying concepts.

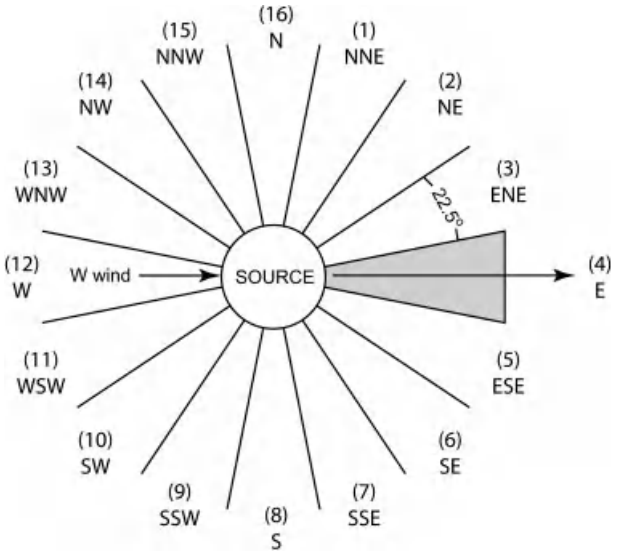

Fig. 10-10 Schematic of a 16-sector wind rose for distributing wind direction data into downwind sectors of 22.5° each.

Example 10-11. Meteorological data were accumulated for one month (720 h) at a facility that releases a radionuclide at an average rate Q (Ci/s) from a 50 m stack. During the one-month period winds were from due west ±11.25° for 240 h which blew released material into sector 4. Wind speeds occurred between 0 and 2 m/s for 60 h, 2–4 m/s for 80 h, and 4–8 m/s for 100 h. Stability classes existed for each wind speed group as follows:

- For 0–2 m/s winds: class F for 60 h.
- For 2–4 m/s winds: class B for 40 h; and class C for 40 h.
- For 4–8 m/s winds: class C for 20 h; and class D for 80 h.

Determine the monthly sector-averaged χ/Q for a downwind subsection of sector 4 between 1.0 and 3.0 km.

Solution. The median downwind distance for the subsection is 2 km, for which the vertical diffusion coefficients σ_{zj} for each stability class from Figure 10-5 are: 22 m for class F; 230 m for class B; 120 m for class C; and 50 m for class D. When these σ_{zj} values are combined with the effective stack height of 50 m, the exponential dispersion term, $\exp(-H^2/2\sigma_{zj}^2)$, for each (F, B, C, and D) is 0.0756, 0.977, 0.917, and 0.607, respectively.

The median speed $\bar{u}_k$ and the F_{jk} fractions for each wind speed group and stability class are:

1. For class F stability and wind class 0–2 m/s, $F_{jk} = 60/240 = 0.25$ and the median wind speed $\bar{u}_k = 1$ m/s.
2. For class B stability and wind class 2–4 m/s, $F_{jk} = 40/240 = 0.167$ and the median wind speed $\bar{u}_k = 3$ m/s.
3. For class C stability and wind class 2–4 m/s, $F_{jk} = 40/240 = 0.167$ and the median wind speed $\bar{u}_k = 3$ m/s.
4. For class C stability and wind class 4–8 m/s, $F_{jk} = 20/240 = 0.0833$ and the median wind speed $\bar{u}_k = 6$ m/s.
5. For class D stability and wind class 4–8 m/s, $F_{jk} = 80/240 = 0.333$ and the median wind speed $\bar{u}_k = 6$ m/s.

Since the sector-averaged $\bar{\chi}_i/\bar{Q}_i$ is to be determined for the midpoint of one subsection of sector 4 which is at a median distance $x = 2000$ m and $f_i = 240/720$, the sector-averaged $\bar{\chi}/\bar{Q}$ value for sector 4 is

$$\frac{\bar{\chi}}{\bar{Q}} = 2.032\frac{240}{720\times 2000\,\text{m}}\left[\frac{0.25}{1\,\text{m/s}\times 22\,\text{m}}\times 0.0756 + \frac{0.167}{3\,\text{m/s}\times 230\,\text{m}}\times 0.997 + \frac{0.167}{3\,\text{m/s}\times 120\,\text{m}}\times 0.917 + \frac{0.0833}{6\,\text{m/s}\times 120\,\text{m}}\times 0.917 + \frac{0.333}{6\,\text{m/s}\times 50\,\text{m}}\times 0.607\right]$$

$$= 7.79\times 10^{-7}\ \text{s/m}^3$$

Example 10-11 demonstrates several important observations: first, the fraction f_i merely allocates the average release rate $\bar{Q}$ into the sector of interest; second, choosing a location of interest within a sector at a particular median downwind distance simplifies the calculation considerably; and third, the complexity of accumulating and allocating large amounts of data into sector averages makes a computer almost indispensable for such tasks. Sector-averaged $\bar{\chi}_i/\bar{Q}_i$ values can often be made more accurate and useful by selecting a particular subsection(s) of interest within a sector (e.g., a pasture or a small community) and calculating specific values for these downwind locations. One or more such locations may in fact be controlling and if it is possible to limit a release(s) to certain periods (e.g., venting only under specified wind conditions) the effects of the release(s) can be optimized to the most favorable sectors and/or meteorological conditions especially if real-time systems and computer sorting are available.

It is common practice in siting and licensing a nuclear facility (e.g., a nuclear power plant) to use meteorological data from local weather stations in projecting the potential impact of estimated releases. These data are then supplemented with several years of on-site meteorological data, prior to and during operations,

from towers equipped to measure wind direction and speed and vertical temperature profiles. Many facilities do not have such data for periods of interest and it may be necessary to retrospectively construct them, typically from local weather stations at airports or in nearby urban areas. Such information may be adequate if the data can be shown to be representative of the site conditions; however, they are a compromise between no data and the more desirable on-site measurements.

10.5 Deposition/Depletion: Guassian Plumes

As plumes migrate downwind they are subject to various influences, in addition to dispersion and dilution, that tend to reduce the concentration of material in them. Large particles may settle out and plume contaminants may be deposited on vegetation, ground surfaces, or other objects due to physical and chemical processes. The effects of such processes on plume concentrations are overall quite small compared to inputs from the source of release, and they are generally ignored in computations of downwind concentrations. Their more important effect is an accumulation of contaminants on vegetation and the ground where they may become entrained in food pathways and/or become a source of direct exposure from the ground surface.

10.5.1 Dry Deposition

Dry deposition (fallout) of contaminants onto vegetation and ground surfaces is represented as an areal contamination $C_{A,dry}$ that is related to the air concentration by a constant of proportionality v_d called the deposition velocity, or

$$C_{A,dry}(\text{per m}^2) = v_d \frac{\bar{\chi}_i}{\bar{Q}_i} \times Q_{TOT}$$

where Q_{TOT} is the total amount of material released over the period that the average $\bar{\chi}_i/\bar{Q}_i$ factor is determined for a subsection of a downwind sector i. The areal deposition is given in terms of $\bar{\chi}_i/\bar{Q}_i$ because the conditions of interest are relatively long-term processes and it is a common practice to determine a weighted average of the dispersion factor for a particular downwind direction, e.g., over a pasture.

The proportionality constant v_d is termed the deposition velocity because it has units of m/s; however, it is not a true velocity. Values of v_d have been determined experimentally by measuring the areal contamination (e.g., $\mu Ci/m^2$) during periods of known air concentration over an area; these are provided in Table 10-4 for selected radioelements and for different types of vegetation and soils. Deposition velocities are also a function of wind velocity because the vertical profile of concentration changes with wind velocity and the amount of deposition is greatly influ-

enced by sorption characteristics, roughness of the underlying surface, and the chemical composition of a given effluent. Even the best measured values of deposition velocity have an uncertainty that may vary by an order of magnitude or more. Consequently, values of v_d are limited and must be used with caution for the particular circumstances encountered; e.g., the physical and chemical forms of the radionuclide, the deposition medium (grass, food crops, or ground surfaces), and atmospheric conditions such as stability and wind speed, each of which can markedly influence deposition.

Table 10-4. Dry deposition velocities v_d for selected forms of radioactive materials on soils and vegetation for several atmospheric stability conditions.

Radioelement	Medium	Atm. stability	v_d (m/s)
I_2	Grass/wheat	A, B	1.4×10^{-2}
	Grass	C, D	8×10^{-3}
	Clover	C, D	$(1–2) \times 10^{-2}$
	Dry grass	E, F	1×10^{-2}
	Grass/wheat	E, F	3×10^{-3}
	Snow	–	3.4×10^{-3}
	Soil	–	3.3×10^{-3}
CH_3I	Grass	A, B	1×10^{-4}
	Grass	E, F	1×10^{-5}
SO_2	Vegetation	–	1×10^{-2} [a]
CO_2	Grass	–	2×10^{-4}
Ru	Grass	–	1×10^{-5}
	Soil	–	4×10^{-3}
Cs	Grass	–	2×10^{-3}
	Soil	–	4×10^{-4}
Zr–Nb	Soil	–	3×10^{-2}
1 μm aerosols	Grass/soil	–	1×10^{-3}
Fission products	Sagebrush	–	3×10^{-2}
Weapons fallout	Grass	–	2×10^{-3}
	Sticky ppr	–	5×10^{-3} [a]

a Average value.

Example 10-12. Estimate the areal contamination due to dry deposition of iodine-131 (a) on the ground downwind of a 100 m stack that releases 10^9 Bq (2.7×10^{-2} Ci) of iodine-131 if the average $\bar{\chi}_i/\bar{Q}_i$ value over the period of release is 1.55×10^{-7} s/m^3 and (b) on grass for the same conditions.

Solution. (a) From Table 10-4, the deposition velocity for elemental iodine on soil is 3.3×10^{-3} m/s. Thus the areal contamination is

$$C_A\ (\text{Bq/m}^2) = 3.3 \times 10^{-3}\ \text{m/s} \times 1.55 \times 10^{-7}\ \text{s/m}^3 \times 10^9\ \text{Bq}$$

$$= 0.51\ \text{Bq/m}^2\ (27.1\ \text{pCi/m}^2)$$

(b) For long-term deposition on grass, it is appropriate to assume an average atmospheric stability condition of class D (neutral) such that $v_d = 8 \times 10^{-3}$. Thus

$$C_A\ (\text{Bq/m}^2) = 8 \times 10^{-3} \times 1.55 \times 10^{-7}\ \text{s/m}^3 \times 10^9\ \text{Bq}$$

$$= 1.24\ \text{Bq/m}^2\ (33.5\ \text{pCi/m}^2)$$

Material deposited onto a surface (e.g., grass or soil) is also subject to removal by weathering and biological processes denoted as a biological half-life T_b. If the material is radioactive the combined effect of these processes is described by an effective half-life T_{eff}, values of which are listed in Table 10-5 for selected radionuclides on selected surfaces often considered in radiological assessments. The effective half-life can be used in the usual way to determine an effective removal constant λ_{eff}, which is calculated as $\lambda_{eff} = \ln 2/T_{eff}$.

For an airborne concentration of some duration, the areal contamination $C_{A,dry}$ (per m^2) is

$$C_{A,dry}(\text{per m}^2) = v_d \frac{\bar{\chi}}{\lambda_{eff}}\left(1 - e^{-\lambda_{eff} t}\right)$$

which will reach an equilibrium value in 7–10 effective half-lives, or

$$C_{A,dry}(\text{per m}^2) = v_d \frac{\bar{\chi}}{\lambda_{eff}}$$

Table 10-5. Measured biological (T_b) and effective (T_{eff}) half-lives of radionuclides on vegetation and soil for spring (SP), summer (S), fall (F), and winter (W) seasons.

Radionuclide	Medium	T_b (d)[a]	T_{eff} (d)
^{131}I (8.02 d)	Pasture (F)	13.9	5.08
	Pasture (W)	34.6	6.51
	Grass (S)	6.8	3.68
	Grass (F)	~24	6.01
	Grass (SP, S)	7.5	3.87
	Sagebrush	8.0	4.00
	Hay	16.4	5.39
	Clover (S)	4.6	2.93
	Clover (F)	13.4	5.02
	Dry Soil	18.2	5.57
	Grass washoff	4.1	2.72
^{90}Sr (28.78 y)	Rye grass/clover	30.8	30.8
^{89}Sr (50.52 d)	Cabbage	24	16.4
	Grass	17	12.7
^{137}Cs (30.04 y)	Pasture	31	31.0
	Rye grass/clover	25.9	25.9
^{103}Ru (39.27 d)	Grass	8.4	6.92

a Includes multiple environmental/biological processes that diminish deposited radioactivity over time.
Source: Peterson, H. T., NUREG-Cr-3332, 1983.

Example 10-13. If a plume that contains a concentration of 10^{-6} μCi/m^3 of ^{131}I ($T_{1/2}$ = 8.02 d) exists during the fall season over dry pasture grass for 2 h following an incident, estimate (a) the areal contamination on the pasture for the 2 h period, and (b) the equilibrium value of the areal contamination if the airborne concentration persists over the area.

Solution. (a) From Table 10-4, v_d is 10^{-2} m/s, and from Table 10-5, the radiological and biophysical effective half-lives are 8.02 and 13.9 d, respectively. The effective half-life is thus 5.08 d and the effective removal constant is 0.1364 d^{-1}. The areal deposition for the 2 h period is

$$C_{A,dry} = 10^{-2}\,\mathrm{m/s} \times \frac{10^{-6}\,\mu\mathrm{Ci/m^3}}{0.1364\,\mathrm{d^{-1}}} \times 86,400\,\mathrm{s/d} \times (1 - e^{-0.1364 \times (2/24)})$$

$$= 7.16 \times 10^{-5}\,\mu\mathrm{Ci/m^2}$$

(b) The equilibrium value which occurs after about 35 d is

$$C_{A,dry}\,(t > 35\,\mathrm{d}) = 10^{-2}\,\mathrm{m/s} \times \frac{10^{-6}\,\mu\mathrm{Ci/m^3}}{0.1364\,\mathrm{d^{-1}}} \times 86,400\,\mathrm{s/d}$$

$$= 6.33 \times 10^{-3}\,\mu\mathrm{Ci/m^2}$$

Reaching such an equilibrium condition would be highly unlikely, since it is doubtful, because of atmospheric variability, that a constant air concentration would be maintained over the area for 35 days. If, however, the concentration is a weighted average $\bar{\chi}$, the areal deposition would be of this order.

10.5.2
Air Concentration Due to Resuspension

Long-lived (or stable) contaminants that build up over time may also become resuspended to produce elevated concentrations of the material above the immediate area or perhaps translocated to other areas. Resuspension of deposited material that persists near the surface is largely governed by wind speed and surface roughness (e.g., loose soil) and surface creep processes which widen the area of contamination. Of particular interest has been various land areas contaminated with plutonium due to incidents, e.g., leakage of plutonium from stored drums at the Rocky Flats Plant in Colorado and partial detonation of nuclear weapons in Spain, the Nevada test site, and Johnston Atoll. A similar circumstance is redistributed uranium tailings that may be re-entrained into the atmosphere. Both are, of course, long-lived insoluble materials that remain near the surface of the ground unless covered in some way.

The air concentration of resuspended long-lived materials is directly related to the areal contamination of the soil and its depth of distribution. Obviously, surface-level contamination is of most significance especially if the soils are loose and dry and the area is open and subject to high winds. The airborne concentration of resuspended materials is thus

$$\chi_{res}\,(\mathrm{per\ m^3}) = k_s C_{A,dry}$$

where k_s is the resuspension factor (m^{-1}) and $C_{A,dry}$ is the areal concentration (per m^2). Values of k are scant but a few have been determined, primarily for plutonium and uranium; resuspension factors for relatively short-lived or highly mobile radionuclides in soils would be not only difficult to establish, but highly uncertain for air concentration estimations. Several typical values are listed in Table 10-6, but even these should be used with caution.

Table 10-6. Resuspension factors k_s for deposited radionuclides for various soils and soil depths.

Radionuclide	Medium	Depth (cm)	k (m^{-1})
Plutonium	Rocky Flats soil[a]	0.02	1×10^{-6}
	Rocky Flats soil[a]	20	1×10^{-9}
	Nevada test site	3.0	1×10^{-11}
	Moist soil	1.0	2×10^{-10}
	Mud flats	0.1	4×10^{-8}
	Fields	5.0	1×10^{-9}
Uranium	Soil (Surrey, UK)	1.0	5×10^{-9}
	Soil (New York, USA)	1.0	5×10^{-8}
Iodine	Vegetation	–	2×10^{-6}
Fallout	Desert soil	–	3×10^{-7}

a k for Rocky Flats soils varied from 10^{-5} to 10^{-9} m^{-1} for surfaces ranging from vehicular traffic on dusty roads to soil layers contaminated to a depth of 20 cm.

It is apparent that material will weather due to various environmental effects and that the resuspension factor will thus change with time following deposition of the material. One of the most widely used calculational models for determining a weathered value for k_s is

$$k_s\ (m^{-1}) = 10^{-9} + 10^{-5}e^{-0.6769t}$$

where t is the amount of time in years after deposition. This empirical relationship is based on desert-type soil and should be used with caution. For example, if applied for initial contamination ($t = 0$) a resuspension factor of 10^{-5} m^{-1} is obtained that is a factor of 10 greater than resuspension observed for semi-arid Rocky Flats soil/vegetation (Table 10-6). Application of this relationship is shown in Example 10-14.

Example 10-14. For plutonium in air above a desert-like plot uniformly contaminated at an initial level of 0.2 μCi/m^2, calculate the air concentration of plutonium (a) initially, (b) at 1 y after the initial deposition, and (c) at 10 y after the initial deposition.

Solution. (a) At $t = 0$, $k_s = 10^{-5}$ and the airborne concentration is

$$C_{A,dry} = (10^{-5}\ m^{-1})(0.2\ \mu Ci/m^2) = 2 \times 10^{-6}\ \mu Ci/m^3$$

(b) At 1 y, $k_s = 5.08 \times 10^{-6}$, and the airborne concentration is 1.02×10^{-6} μCi/m³.
(c) At 10 y, $k_s = 1.25 \times 10^{-8}$, and the resulting airborne concentration is 2.5×10^{-9} μCi/m³.

For locations with moist soils and vegetation a smaller resuspension factor would need to be chosen and the relationship used in Example 10-14 would not be applicable.

10.5.3 Wet Deposition

Contaminants can also be removed from a plume by precipitation, a process that results in wet deposition of the plume material on vegetation, the ground, and other exposed surfaces. Both wet deposition and dry deposition contribute to areal contamination; however, each is considered separately even though both may occur during a precipitation period. The amount of wet deposition is similar to that used for dry deposition, but in this case the constant of proportionality is a combination of the rainfall rate R and the washout ratio W_v, values of which are listed in Table 10-7 for selected radionuclides. The amount of washout is a function of the size and distribution of raindrops and the physiochemical features of the plume. These parameters, themselves functions of the space coordinates (x, y, z), cause the amount of washout to be a space-dependent parameter; however, as a practical matter it is assumed to be constant with respect to space because of scant empirical data.

The areal contamination $C_{A,wet}$ (per m²) due to wet deposition is

$$C_{A,wet}(t) = \frac{RW_v e^{-mR}}{\lambda_e + kR} \chi \left[1 - e^{-(\lambda_e + kR)t}\right]$$

where χ = the contaminant concentration (Ci/m³) in the air above the area; R = rainfall rate (mm/h); W_v = volumetric washout rate (volume of air/volume of rain); m = the plume depletion constant (h/mm) which is related to rainfall rate; k = vegetation washoff coefficient (mm⁻¹); λ_e = effective removal constant that accounts for radioactive removal and biological processes other than washoff; and t = duration of precipitation (h). The areal contamination $C_{A,wet}(t)$ will thus build up to an equilibrium condition as a function of the rainfall rate R, the removal coefficient k, and the effective removal constant λ_e. The areal ground concentration is also a function dry deposition, which is often ignored for precipitation events.

Table 10-7. Vegetation washoff constant k and volumetric washout factors W_v for selected radionuclides.

Radionuclide	Washoff constant		Washout factor	
	Vegetation	k (mm^{-1})	Form	W_v (m^3 air/m^3 rain)
^{89}Sr, ^{90}Sr	Grass/cabbage	0.017[a]	Fallout	5.9×10^5
^{95}Zr	Cabbage	0.022	Fallout	4.2×10^5
^{106}Ru	Lettuce	0.063	Fallout	5.6×10^6
	Cabbage	0.026	–	–
^{131}I	Grass	0.020	Fallout	3.5×10^5
	Cabbage	0.026	I_2	8.3×10^4
			Alkyl (pH 5)	4.2×10^3
^{137}Cs	Cabbage	0.02	Fallout	4.6×10^5
^{140}Ba	–	–	Fallout	4.0×10^5
^{144}Ce	Cabbage	0.025	Fallout	4.6×10^5
Particles (~1 μm)	Grass	0.063	Soluble	1.0×10^6
	Grain	0.069	Insoluble	3.0×10^5

a Median value; reported values range between 0.009 and 0.024.
Source: NUREG/CR-3332, 1983.

Example 12-15. Calculate the equilibrium deposition of radioiodine by rainout for an average atmospheric concentration of 10^{-5} μCi/m^3 when the rainfall rate R = 2.5 mm/h, the washoff constant k = 0.025 mm^{-1}, m = 0.025 h/mm, the washout coefficient W_v = 8.3×10^4 m^3 air per m^3 of rain, and the effective removal constant = 0.1364 d^{-1}.

Solution. Since the equilibrium value is sought, the exponential buildup term = 1; thus

$$C_{A,wet}(\infty) = \frac{RW_v e^{-mR}}{(\lambda_e + kR)}\bar{\chi}$$

$$RW_v = (2.5 \text{ mm/h})(24 \text{ h/d})(10^{-3} \text{ m/mm})(8.3 \times 10^4 \text{ m}^3 \text{ of air/m}^3 \text{ of rain})$$

$$= 4.98 \times 10^3 \text{ m}^3/\text{m}^2 \text{ d}$$

$$(\lambda_e + kR) = 0.1364 \text{ d}^{-1} + (0.025 \text{ mm}^{-1})(2.5 \text{ mm/h})(24 \text{ hr/d}) = 1.6364 \text{ d}^{-1}$$

And

$$C_{A,wet}(\infty) = \frac{4.98 \times 10^3\ \mathrm{m^3/m^2\ d}}{1.6364\ \mathrm{d^{-1}}} \times 10^{-5}\ \mu\mathrm{Ci/m^3} \times e^{-0.025 \times 2.5}$$

$$= 0.286\ \mu\mathrm{Ci/m^2}$$

It is worth noting that the areal deposition due to precipitation is directly related to the volumetric washoff factor W_v, and its selection is key to such calculations.

Short-term plume washout due to precipitation effects on a plume can be determined by use of a washout rate coefficient similar to that for dry deposition. The areal contamination using a washout rate is

$$C_{A,wet}(\mathrm{per\ m^2\ s}) = \frac{\Lambda Q(\mathrm{per\ s})}{(2\pi)^{1/2}\bar{u}\sigma_y} \exp\left(-\frac{y^2}{2\sigma_y^2}\right)$$

where Λ is the washout rate (s^{-1}) for relatively short measurement intervals and single individual precipitation situations, typically of the order of 1 h. The value of σ_y is, of course, location dependent and should be selected for the specific downwind distance where the precipitation event occurs.

Nominal values of Λ for both aerosols and gases are 10^{-4} s^{-1} for stable conditions and 10^{-3} s^{-1} for unstable conditions. If the rainfall rate R is known, a somewhat better value of Λ can be calculated based on data for nuclear power plant releases, which for elemental iodine is

$$\Lambda\ (\mathrm{s^{-1}}) = 8.0 \times 10^{-5} R^{0.6}$$

and for aerosols

$$\Lambda\ (\mathrm{s^{-1}}) = 1.2 \times 10^{-4} R^{0.4}$$

where R is the actual precipitation intensity in mm/h.

Plume depletion due to wet deposition can be significant for persistent precipitation rates and the areal contamination rate will be reduced exponentially as the plume moves downwind. This effect is accounted for by introducing an additional exponential removal term:

$$C_{A,wet}(\mathrm{per\ m^2\ s}) = \frac{\Lambda \dot{Q}}{(2\pi)^{1/2}\bar{u}\sigma_y} \exp\left(-\frac{y^2}{2\sigma_y^2}\right) \exp\left(-\frac{\Lambda x}{\bar{u}}\right)$$

where the factor $x/\bar{u}$ accounts for the effective time of plume travel and the duration of washout by precipitation.

It is important to recognize that both wet and dry deposition parameters are quite site specific; thus, the quality of any given estimate of areal contamination is determined by how well the available parameters fit the situation being modeled.

10.6 Summary

The environmental dispersion of radionuclides and associated doses can be quite complex; therefore many assessments are done for a hypothetical maximum or a typical individual. These rarely fit any given person potentially or actually exposed but can provide a range of exposures/doses that can be used to judge the significance of radionuclides associated with a given activity/facility.

Dispersion modeling usually assumes a release that emanates from a "point" source such as a pipe, an elevated stack, or a small area. The concentration χ at a downstream distance is directly proportional to Q and inversely proportional to the diluent (e.g., air or water) speed. Atmospheric concentrations across an areal segment of the plume located at some point x downwind fit a Gaussian distribution and are modeled accordingly for idealized conditions of point source releases over relatively flat undisturbed terrain. Atmospheric turbulence under such conditions can be characterized by the vertical temperature profile, and is fairly uniform for flat and relatively unobstructed terrain and release points that are 2.5 times higher than surrounding buildings or terrain disturbances (e.g., cliffs or rock outcrops). The models are also often used for other conditions because they are the only ones available; however, the quality of the results will be influenced by the degree to which conditions deviate from those specified for the model.

Various conditions can occur in which the turbulence associated with an airborne plume will be nonuniform and it is not appropriate to use Gaussian plume models to determine air concentrations. Two common situations are fumigation and mechanical turbulence induced by buildings or other obstructions; the turbulence associated with each can completely dominate the dispersion of an effluent released under such conditions. Determinations of areal contamination due to deposition processes are also influenced by highly variable factors, and are at best estimates that can be expected to have considerable uncertainty. The degree to which these can be supplemented with, or better yet replaced with measured values offers considerable improvement in the reliability of the results.

Other Suggested Sources

Hanna, S. R., Briggs, Hosker **1982**, *Handbook on Atmospheric Diffusion*, DOE/TIC-11223.

Peterson, H.T., Jr. **1983**, Terrestrial and aquatic food chain pathways, in *Radiological Assessment*, ed. J. E. Till and H. R. Meyer, TID Information Service, NUREG/CR-3332.

Randerson, D. **1984**, *Atmospheric Science and Energy Production*, DOE/TIC-27601.

Slade, D. H. **1968**, *Meteorology and Atomic Energy – 1968*, Report TID-24190, Clearinghouse for Federal Scientific and Technical Information, US Department of Commerce, Springfield, VA.

Turner, D.B. **1970**, *Workbook on Atmospheric Dispersion Estimates*, EPA Publications, AP26.
US Nuclear Regulatory Commission, Regulatory Guides 1.109, 1.111, and 1.145.

Problems – Chapter 10

10–1. What is the ground level concentration directly downwind of a nuclear facility that emits 80 Ci/s from a 60 m stack over relatively flat terrain during overcast daytime conditions when the wind is 6 m/s (a) at 500 m along the centerline and (b) at 1500 m downwind and 50 m off the centerline?
10–2. For the conditions in Problem 10-1, find (a) the location of the point of maximum concentration along the plume centerline and (b) the concentration at that maximum distance.
10–3. Calculate the effective stack height for a 50 m stack with an inside diameter of 5 m that emits effluent at 200 °C and at an efflux velocity of 8 m/s into an atmosphere that has an ambient temperature of 20 °C and a wind speed of 3 m/s.
10–4. Effluent is emitted at 100 g/s from a 6 ft high vent atop a building that is 80 ft high and 100 ft wide on the lee side. Atmospheric conditions are overcast, it is late afternoon, and the wind speed is 5 m/s. What is the ground-level air concentration (a) 50 m downwind and (b) 300 m downwind?
10–5. A major reactor accident occurs around noon on a bright sunny June day releasing halogens and noble gases into the wake of a containment building that is 30 m wide and 50 m high. If ^{131}I escapes from the containment building at a rate of 9.0×10^{-4} Ci/s during the first 2 h of the accident and the wind speed is 6 m/s, what is the average air concentration at Joe Panic's house 3000 m directly downwind?
10–6. Solve Problem 10-5 using the virtual source method and compare the results. Comment on the accuracy of each method and which should be selected.
10–7. Effluent released from a 50 m stack contains ^{85}Kr released at a rate of 0.1 Ci/s into a 4 m/s wind during stability class F conditions. What is the ground-level concentration 5000 m downwind?
10–8. Calculate the ground-level concentration for the conditions in Problem 10-7 if the release occurs during fumigation conditions when the wind speed is 2 m/s at the height of the stack.
10–9. Estimate the areal contamination of cesium-137 (assumed to form aerosols) on the ground due to dry deposition downwind of a 100 m stack that releases 10^9 Bq (2.7×10^{-2} Ci) of cesium-137 into a sector for which the average value of $\bar{\chi}/\bar{Q} = 1.55 \times 10^{-7}$ s/m^3.
10–10. Using the conditions of Example 10-11, determine the sector-averaged χ/Q value in sector 4 for a subsection with a midpoint located at 1200 m downwind if the effective stack height is 60 m.

10–11. What would be the χ/Q value at 100 m for the release considered in Example 10-12 for (a) stability category D instead of category F, and (b) category A stability conditions?

10–12. For the conditions in Example 10-7, estimate the ground-level concentration of ^{41}Ar at 120 m downwind and during neutral atmospheric stability conditions using (a) the Fuquay method and a building area correction factor $c = 0.8$ and (b) the virtual source method.

10–13. For the conditions in Example 10-7, determine the far-field concentration of ^{41}Ar at 600 m downwind using selection rules (a) for class D atmospheric stability conditions and (b) for class E stability conditions.

11
Nuclear Criticality

"If the radiance of a thousand suns were to burst into the sky, that would be the splendor of the Mighty One." Bhagavad-Gita

Anyone who has witnessed the explosion of a nuclear device will attest that the emitted light is indeed brighter than "a thousand suns," a connection easily made by many of the physicists who saw the first nuclear explosion on July 16, 1945. J. Robert Oppenheimer, who led the development of the atomic bomb, learned Sanskrit so he could read the ancient 700-stanza Bhagavad-Gita in the original. His recollection of the phrase, "Now I have become death, destroyer of worlds" from the ancient scripture is frequently cited to characterize the new age the world entered that day; however, the Gita's reference to "the radiance of a thousand suns" also captured the awe-inspiring splendor, and the physics, of the event.

This author, after shivering with Morgan Seal and R. H. Neill in the early morning darkness on a plateau above Yucca Flats in Nevada, was struck by the blinding brilliance, felt the heat, and saw the changing colors of the nuclear fireball as it spread and rose into the dawn of a September day in 1957; experienced several months later the persistent energy of "Oak," the largest of several multi-megaton devices exploded in the Marshall Islands in 1958; and saw the brightness of day burst upon and persist for tens of seconds in the night sky above Fiji from a high-altitude detonation some 2500 miles away at Johnston Island in the pacific. The light of nuclear criticality, once seen, is like no other. It is unfortunate that it has also been seen, as detailed in several accounts that follow, by those exposed to the burst of neutrons and gamma rays that also accompany the light of nuclear excursions.

Prevention of inadvertent criticality of fissionable material events requires consideration of the same factors that must be met to obtain an explosive release of fission energy in nuclear devices or in a controlled fashion in nuclear reactors. The purpose of this chapter is to describe the features of criticality events, the factors related to their occurrence, and the relevant radiation protection issues associated with each.

Physics for Radiation Protection, Third Edition. James E. Martin

11.1
Nuclear Reactors and Criticality

A *"natural reactor" criticality event* occurred in Gabon, Africa, some 2 billion years ago. It was discovered when assays of uranium ore from the region found that the ^{235}U content was well below 0.72% found in most current-day natural uranium, which suggested that the ^{235}U had been depleted by fission. The Gabon natural reactor provides a good example of the interplay of various parameters essential for nuclear criticality to occur. First, the ore body was more than large enough to provide a critical mass. Second, with arid conditions the surface layer would dry out and crack so that rainwater could settle in the cracks and provide a zone of moderator to slow any neutrons to thermal energies for enhanced fission of ^{235}U in the ore. Third, the ^{235}U content was sufficient to overcome neutron absorption losses in hydrogen atoms present in light water. Fourth, spontaneous fission in uranium would provide neutrons to begin the reaction. Fifth, the heat of the reaction would boil the water to steam forcing it out of the matrix to stop the reaction, which would start up again when more water accumulated in the cracks and a spontaneous fission event occurred to begin a new chain reaction. It appears that this sequence was repeated many times over hundreds to thousands of years until the semi-ideal conditions changed, perhaps by rearrangement of the ore body due to the energy of the reactions, changes in climate, and/or reduction of the percent abundance of ^{235}U below that necessary to sustain a chain reaction with a light water moderator.

The first human-induced sustained chain reaction was achieved by Enrico Fermi on December 2, 1942, which duplicated many of the conditions that occurred naturally some 2 billion years ago. Since the ^{235}U content of present-day uranium is much less, Fermi chose to intersperse natural uranium metal slugs in a graphite moderator (ordinary water absorbs too many neutrons) in a size and configuration to keep the reaction going once started (in this case with a Ra–Be neutron source). The results of Fermi's genius led to the design and operation of nuclear reactors, first to generate plutonium for nuclear weapons and later for electricity production.

11.1.1
Three Mile Island Accident

On March 28, 1979 a defining event in the history of nuclear power occurred at the Three Mile Island (TMI) unit 2 reactor near Harrisburg, Pennsylvania. The reactor was operating at near its full power level of 2700 MWt (850 MWe), having reached that level about three months earlier. It had gone critical for the first time exactly one year before the incident. The coolant temperature was 600 °F and the system pressure was 2200 psig, both normal conditions for a pressurized water reactor.

The incident that occurred was not a criticality event, but rather involved overheated fuel which then led to the release of fission products within the reactor,

and some of these escaped to the environment. The incident was defining in nature because it highlighted design deficiencies, but more importantly it demonstrated that operator training, procedures, and communications of information are essential elements to offset human frailty.

At approximately 4:00 am on March 28, a condensate pump on the secondary loop stopped, which is not unusual. When this occurred, there was a loss of flow to the feedwater pumps that circulate water to the steam generators. Without suction, they too stopped, as designed. This produced an automatic shutdown of the turbine – with no feedwater, no steam is produced, and the turbine shuts down to protect itself. PWRs are designed with auxiliary feedwater pumps to supply feedwater to the steam generators in such events. These in fact came on automatically to supply water to the steam generators, but the valves had been left closed by the last maintenance crew, a circumstance that could be called the first human frailty in the event. Without coolant water, the secondary side began to boil dry. Eight minutes elapsed before the closed valves were discovered and opened, but by this time the steam generators had boiled dry, and trouble had begun. Safety systems designed into the reactor would have righted the situation; however, more confounding events, many of which were induced by the operators, followed.

Without water in the secondary system the reactor heat could not be removed, and since the reactor was still running, the primary loop pressure began to build up. This caused the pressure relief value on top of the pressurizer to open, as designed. This allowed primary coolant water to flow out the valve and into a discharge tank, put there for just such occurrences. But without feedwater to the steam generators to remove heat from the primary loop, the pressure started to increase again, and the reactor shut down automatically. At this point, a malfunction exists but the reactor is still safe. But unfortunately the pressure relief valve had stuck in the open position. If the valve had closed, the system pressure would have leveled off, the automatic shutdown system would have stabilized, and the operator could have proceeded to a stable shutdown (and power could have been restored after the feedwater pumps, etc., were returned to normal function). But with the pressure valve stuck open, the system pressure continued to drop, and as per design the emergency core cooling system (ECCS) came on to remove the fission product decay heat (about 200 MWt) which was still being produced in the fuel.

A second human frailty occurred when the operators did not notice the stuck valve (and may have had no telemetry to indicate its position). Fearing a flooding of the loop with soiled water, they shut down the ECCS, a grave mistake. The primary system pressure dropped even further with the ECCS off, and steam bubbles began to form, which in turn caused a troubling vibration in the coolant pumps. The operators then further exacerbated the situation when they decided to shut the pumps off (the third human frailty) with the idea that cooling could be established with natural convection. However, the steam voids prevented convection flow and the core began to overheat since all means of removing the fission product decay heat (which as shown in Figure 5-11 is about 7% of total energy production) were now out of commission. The water level dropped significantly, exposing the fuel. Without cooling the fuel cladding began to fail, and fission products

were released. At the same time, water began to react with the overheated metal (a dreaded metal–water reaction), releasing hydrogen. This actually led to an explosion later on, but it was contained so well by the containment structure that it went unnoticed.

The coolant containing fission products continued to flow out of the stuck pressure relief valve, first overflowing the discharge tank and then onto the containment floor and into a sump. The sump pump came on and contaminated water was pumped to the auxiliary building outside the containment structure, where volatile fission products could vent directly to the atmosphere. This pathway released about 10–20 Ci of ^{131}I and about 10^6 Ci of ^{133}Xe. The highest dose to the public was estimated to be 80 mrem for an individual assumed to be outdoors at the site boundary for 11 days. The rest of the fission products, and surprisingly most of the ^{131}I, were contained in the primary coolant water that remained in the containment building. At 7:04 am (three hours later) the Pennsylvania Health Department was notified and emergency crews began to descend on the scene.

The TMI accident was the result of operator error, which was compounded by design deficiencies and equipment failure, especially the stuck pressurizer valve. Operator errors were numerous, including the closed valves in the feedwater line to the steam generators, misreading the condition of the pressurizer, and shutting off both the emergency core cooling pumps and the reactor cooling pumps.

The TMI accident led to significant actions that have improved the safety and performance of all nuclear power reactors. Among these are: (a) an increase in the number of qualified operating personnel; (b) upgrading of training and operator licensing practices; (c) reviews of control room design to take account of human factors; (d) new detectors and instruments that would permit operators to know the status of the reactor at all times; (e) hydrogen detecting equipment; (f) improvement in monitoring of accident conditions, including inadequate core cooling; (g) improved intercommunications between regulators and the plants; and (h) better emergency preparedness. These actions were taken by the nuclear industry as a whole primarily through the formation of the Institute of Nuclear Power Operations in which senior managers share experiences and knowledge. If the industry had not imposed these improvements, the US Nuclear Regulatory Commission most certainly would have.

11.1.2 Chernobyl Accident

A very serious reactor accident occurred at Unit 4 of the Chernobyl reactor station near Kiev, Ukraine, on April 26, 1986. The Chernobyl-4 reactor was an RBMK design with a graphite moderator pierced by over 1600 pressure-tube fuel channels spaced 25 cm apart in the graphite. Clusters of 18 slightly enriched (2% ^{235}U) uranium oxide fuel assemblies were placed inside each pressure tube and the heat of fission was removed by ordinary light water. Separate channels contained 222 control and shutdown rods, and the reactor could be refueled on line by a refueling machine above the core.

The sequence of events leading to the accident began with an experiment conducted by a group not responsible for operations of the reactor. The test sought to determine if electricity produced during the coastdown of the turbine could be used to run emergency core cooling systems until diesel generators could be started to produce emergency power. This separate organization was not familiar with the reactor, and apparently placed more attention on the test than on safety measures. The operators were under some pressure to complete the test because the next maintenance period was over a year away, a situation made even more stressful when the local dispatcher requested a delay of 8 hours. The emergency core cooling system was deactivated for the test.

The first step in the test was to reduce the power from 3200 MWt to about 800 MWt, but it was inadvertently reduced to 30 MWt, which was too low to offset the ingrowth of ^{135}Xe fission product poison. The rapid ingrowth of ^{135}Xe made it very difficult to bring the power level back up. In violation of all rules the operators pulled out most of the control rods in an attempt to override the ^{135}Xe poison and overcome their earlier error; however, they were unable to bring the power level back to 800 MWt, and in fact could not get it above 200 MWt. The RBMK reactor is unstable at 200 MWt, a situation made even worse because various safety systems had been disabled to prevent circuit trips while the experiment was in progress. Under these conditions steam voids began to form in the coolant flowing in the pressure tubes which adds positive reactivity because fewer hydrogen atoms are present to absorb neutrons (i.e., the RBMK has an inherent positive void coefficient, in sharp contrast to US BWRs and PWRs which have a negative void coefficient).

The positive reactivity coefficient was a fatal design flaw. As shown in Figure 11-1, an increase in temperature reduces the density of the cooling water in the pressure tubes which results in fewer neutrons being absorbed in hydrogen atoms. However, these extra neutrons would still be thermalized in the graphite moderator; thus, any increase in fuel temperature produces a net increase in fissioning reactions (and an increase in power level), an effect that multiplies rapidly unless neutron absorption is added quickly. Even in normal conditions an elaborate system of detectors, circuits, and control rods was required to control the power level in the RBMK reactor.

When steam voids began to form, the result was a sudden insertion of positive reactivity. This caused a power surge to around 30,000 MWt, which was ten times normal, and it could not be reduced quickly because too many rods were too far out to have any effect. The power surge pulverized the fuel and the increased steam pressure ruptured the coolant tubes. Chemical reactions between steam, graphite, and zirconium produced large amounts of carbon monoxide and hydrogen which exploded through the roof (designed to provide confinement, but not containment). The hot graphite caught fire and burned for several days, melting the core. Large amounts of fission products were carried high into the atmosphere to drift over Scandinavia and Eastern Europe and eventually worldwide. All of the noble gases were released, 3% of the transuranic elements, 13% of the ^{137}Cs, and 20% of the ^{131}I. Exposures of emergency workers ranged between 100 and

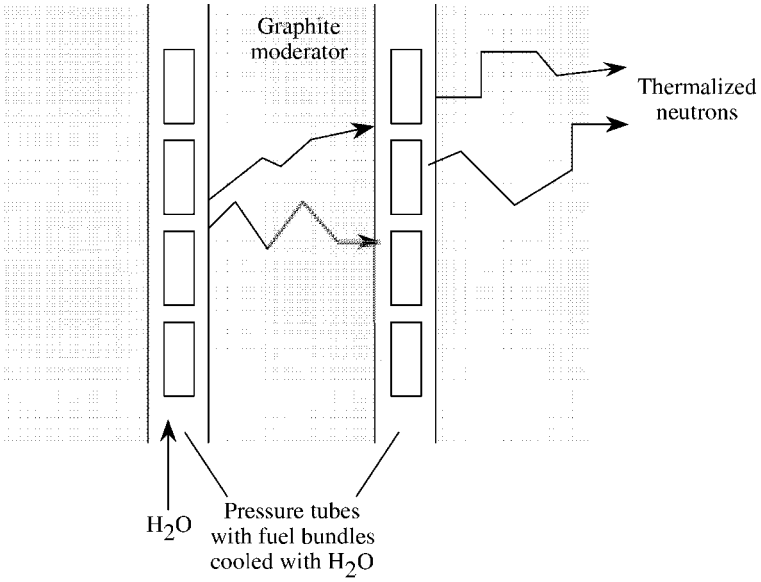

Fig. 11-1 Schematic of fuel channels in a graphite-moderated, light water-cooled RBMK-type reactor in which an increase in fuel temperature causes a reduction of neutron absorption by coolant, thus inducing positive reactivity.

1500 rems, and 31 persons, mainly fire fighters, died. Thousands of people were evacuated, including 45,000 from the town of Pripyat, many of whom were permanently relocated with great cost and undoubtedly much distress. Most of these people received less than 25 rems. Although the amount of radiation exposure to workers and the public (1.6 million person-rems has been estimated) is not precisely known, the collective dose to the public has been projected to increase significantly the cancer risk. An International Chernobyl Project, which involves more than 200 specialists from around the globe, continues to follow the accident.

Many factors contributed to the Chernobyl accident, but the fatal flaw was the positive void coefficient, which has since been changed in the other Chernobyl-type reactors in the region. The hard lesson learned at Chernobyl was the consequence of urgent actions by well-intentioned persons who were so focused on a different agenda that considerations by experts in criticality and nuclear safety were either not sought or were ignored or overridden. Similar human frailties have contributed to most criticality incidents, particularly those that have occurred with aqueous solutions and critical assembly tests.

11.1.3
NRX Reactor: Chalk River, Ontario, December 1952

The NRX reactor was developed in Canada during World War II to demonstrate the use of D_2O, or "heavy" water, as a moderator for a reactor fueled with natural uranium. It has the distinction of being the forerunner of a very useful nuclear power reactor, the CANDU (see Chapter 5). The uranium rods in the NRX were contained in a pressure tube and were cooled by a thin sheath of light water flowing between the aluminum-clad fuel rods and the pressure tube wall, a slightly larger concentric aluminum cylinder. The heavy water moderator that flowed in the space between the pressure tubes was sufficient to moderate all neutrons to thermal energies; therefore, the light water coolant was effectively a poison in that it slightly depleted the number of neutrons available for fissioning uranium atoms.

The NRX accident occurred while experiments were underway that required a reduced flow of the light water coolant for several of the fuel rods. Operator errors and electrical and mechanical safety circuit failures also contributed to the incident. With the experiments in process, a rapid power increase began on December 12, 1952, but it appeared that it would level off at about 20 MW as a slowly moving control rod took effect. Normally this would have been a high, but tolerable, power level and the situation probably would have been controllable if low-flow conditions had not been imposed. At a power of about 17 MW, the cooling water commenced to boil in the channels with reduced coolant flow, which effectively removed some of the water poison due to the decreased density, causing the power to rise once more. The power increased to 60 and then to 90 MW, at which point the heavy water moderator was automatically dumped and the reaction stopped. About 1.2×10^{20} fissions had occurred and the core and calandria (fuel element support structure) were damaged beyond repair. Some 104 Ci of long-lived fission products were flushed to the basement in about 10^6 gal of cooling water which had to be cleaned up. Personnel exposures were low, and the reactor was restarted about a year later.

The NRX accident also demonstrated the positive reactivity effect when light water is used to cool pressure-tube fuel channels, a situation that was similar in some respects to the RBMK Chernobyl reactor. It is also yet another example of the violence of the steam explosion that accompanies a rapid power surge. Also noteworthy is the ability to stop the fission reaction by dumping the D_2O moderator, which is one advantage a heavy water reactor has that a graphite-moderated reactor does not.

11.1.4
SL-1 Accident

A severe nuclear criticality accident, with three deaths, occurred at the stationary low-power unit one (SL-1) reactor in Idaho on January 3, 1961. The reactor had been designed for the US Army to provide power in remote regions and had mini-

mal containment and fixed systems to allow portability. The reactor had been shut down for maintenance, and three operators (the only three people at the plant) came in on the night shift to reconnect the control rods to the drive mechanisms so the reactor could be restarted the next morning. It was necessary physically to lift the control rods to reconnect them. No one knows exactly what happened, but it is believed that the central rod was stuck and when they pulled on it, it let go with a large and sudden injection of reactivity. The steam explosion from the excursion blew out all of the control rods and lifted the heavy reactor vessel some 9 ft. All three operators were killed.

Alarms sounded in the fire station some miles away, and the responding firefighters found the plant deserted, but followed procedures and took radiation readings before entering the building. The radiation levels pegged their survey meters, and they called for backup and initiated emergency response procedures. The plant health physicist responded to the site and entered the building to try and save the one person still alive – he and the medical personnel who attempted to treat the person received doses of a few rads up to 27 rad. The reactor was so badly damaged that it was dismantled and buried on site, a recovery process that took several weeks.

11.1.5
K-reactor, Savannah River Site, 1988

K-reactor is one of several heavy water-moderated reactors built in the early 1950s to produce tritium by neutron irradiation of ^{6}Li targets. The reactor had operated successfully for about 25 years when it was shut down in mid-cycle for various safety upgrades, primarily for improved seismic stability. These upgrades took about a year, which was longer than expected, and during this period tritium in the targets decayed to ^{3}He, a significant neutron absorber with a cross-section of 5330 b. When the reactor was restarted, the operators had to withdraw the control rods considerably more than normal. When this was noted, the Department of Energy official ordered the reactor to be shut down until this unusual condition was formally evaluated. It was at this point that the poisoning effect of the ingrown ^{3}He was determined, but further questions on the formality of procedures for identifying and reviewing off-normal circumstances (even self-imposed ones without prior consideration of effect on reactor criticality) were raised.

The event is yet another example of poisoning materials affecting reactor criticality and the need to consider these when circumstances change. Even though the operators were very familiar with their reactor and brought it to power safely, it was done so without full understanding of the conditions that existed. The K-reactor remained shut down for several years after 1988, was restarted after costly upgrades in equipment and formality of operations, and was then placed in a standby condition. It is questionable whether further operations at this relatively old reactor will ever resume; other means of producing tritium for nuclear weapons are likely to be developed.

11.1.6 Fukushima-Daichi Plant—Japan, March 11, 2011

The Fukushima-Daichi plant consists of six Mark I boiling water reactors manufactured by the General Electric company. The Mark I design is an early version BWR with a water-filled torus that surrounds and is connected to the pressure vessel to provide a pressure suppression pool should incidents occur. Several of the reactors were in operation on March 11, 2011 when a 9.0 magnitude earthquake occurred several miles offshore. The earthquake was detected at the complex and triggered automatic shutdowns of those reactors that were in operation which was the normal procedure. But, the earthquake triggered a huge tsunami some nine meters high that arrived at the site a few hours later and completely swamped seawalls, flooded the reactors, and knocked out all offsite power. Although each unit was provided with backup diesel generators to keep systems and cooling pumps operational, these were located below ground level and were completely swamped by the tsunami. Operators rushed to bring in offsite power for the pumps which were crucial for removing residual heat from the core as well as from fuel in spent fuel pools. As shown in figure 5-11 core cooling is necessary for several days after reactor shutdown to prevent fuel damage, including melting. Despite these efforts the fuel overheated causing a water-metal reaction that oxidized fuel cladding releasing hydrogen that built up in containment. Operators appear to have been reluctant to vent the hydrogen because the local population was understandably fearful of radiation and radioactivity because of the bombings of Hiroshima and Nagasaki. Consequently, an explosive concentration built up and hydrogen explosions occurred on March 14 (some three days later) that blew off the roof and walls at units 1 and 3, followed by releases of airborne radioactive material. Radioactivity levels several times established limits were detected in milk, fish, and spinach several days later.

An electric cable feed was finally arranged on March19 to provide power to cooling pumps at two of the reactors, some eight days after the automatic shutdowns. By then significant damage to fuel had occurred both in the core and in spent fuel pools despite heroic efforts by plant operators that included use of seawater to provide emergency cooling. The seawater was damaging to all systems and especially reactor fuel both in the core and in spent fuel pools, each of which contained between 50 and 151 tons of spent fuel causing concern that fuel cooling could be lost. Pool-water levels were reduced to about half at reactors 1 and 3 but were higher at reactor 2. Reactor fuel had recently been added to the pool at reactor 4 which presented a higher thermal loading that boiled water off and exposed the zirconium clad fuel to an exothermic reaction which could occur above 1800 degrees C.

Pumps were eventually restored and the fuel pools secured, and after a year or so all nuclear fuel was cool enough that melting was no longer likely. However, significant damage at the reactors compounded by the emergency uses of seawater created major cleanup problems that are expected to require years to resolve. Some offsite areas were also contaminated which requires some decon-

tamination and restrictions of land use. Fortunately, much of the released material went offshore and away from populated areas. The Fukushima- Daichi incident again reminds the nuclear industry of the importance of dependable emergency power to assure fuel cooling at all times.

11.2
Nuclear Explosions

The detailed information on nuclear weapons is highly classified, but the general physical concepts of the two major types are fairly well known: the first, based on fission, uses plutonium or highly enriched uranium; the second depends on thermonuclear fusion to produce a hydrogen bomb.

11.2.1
Fission Weapons

The physical principles of modern fission weapons are shown schematically in Figure 11-2. The predetonation configuration arrays a critical mass of plutonium or uranium in a thin spherical geometry which prevents criticality by providing a large surface area to promote neutron leakage. A supercritical configuration is produced by the use of high explosives to compress rapidly a uranium tamper across a gap into the spherical shell of fissionable material with pressures of 10^7 psi or more. Compression reduces the core radius which increases the surface to volume ratio, and even though this increases neutron leakage the increased density decreases the mean free path of the neutrons, which is the dominant effect.

Nuclear weapons are designed to hold the fissionable material together long enough to fission the maximum possible number of uranium or plutonium atoms. Such designs depend on fast neutrons; there is not enough time to moderate neutrons to thermal energies and moderating material is intentionally kept out of these devices. As postulated in Figure 11-2, a burst of neutrons is required at the moment of compression. This could be provided by an (α,n) source of neutrons (called an initiator) or acceleration of deuterons into a beryllium target. Under these conditions the neutron multiplication accelerates, and power increases rapidly as the fission energy is released. Tritium released into the center space fuses under the intense heat and releases additional neutrons to boost the fission yield. The rapid increase in power produces an enormous burst of photons and neutrons that quickly leave the exploding mass and the material is eventually blown apart.

An unreflected plutonium assembly has a critical mass of about 16 kg, which can be reduced to about 10 kg by surrounding it with a 1-inch reflecting layer of natural uranium. Devices composed of unreflected ^{235}U require about 23 kg for 93% enriched metal; below 20% enrichment they are impractically large.

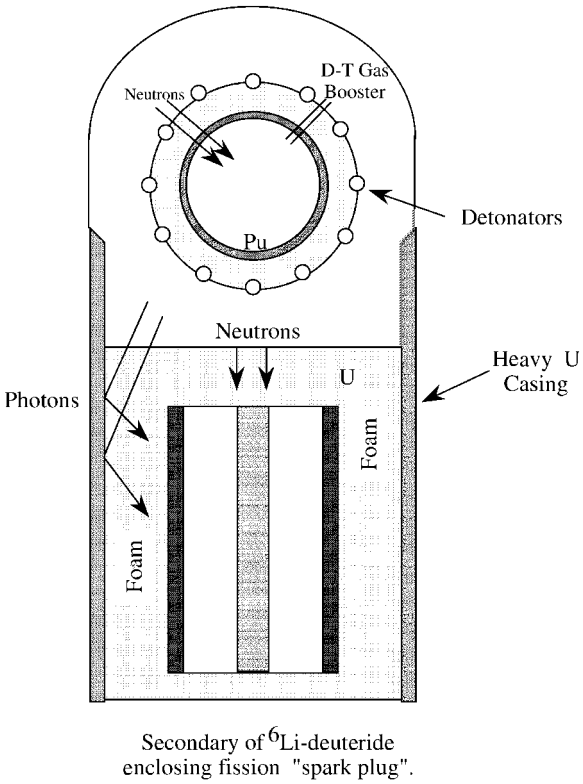

Fig. 11-2 Hypothetical configuration of a nuclear weapon containing a tritium-boosted primary that fissions when imploded, and a secondary of $^{6}Li^{2}H$ around a fission "spark plug" that is compressed by radiation to fusion temperature.

11.2.2 Fusion Weapons

The fission trigger (or primary) can be used to produce the intense heat necessary for fusion reactions (as described in Chapter 4): hence the term thermonuclear weapons. X-rays and gamma rays from the primary travel at the speed of light down the channel surrounding the secondary and flash a polyethylene lining to a plasma yielding low-energy photons that create enormous heat and pressure. This intense radiation pressure compresses and ablates the heavy uranium tamper driving it into the lithium-6 deuteride assembly which is wrapped around a fission "spark plug" that may also enclose a tritium booster. The intense radiation pressure heats the LiD causing fusion of deuterium atoms and yielding ^{3}He plus a neutron or tritium and a proton. The kinetic energy of the products is absorbed in the mass adding additional heat. Neutrons interact with ^{6}Li in the assembly of

lithium deuteride ($^6Li^2H$) to produce ^3H via (n,α) reactions. This tritium in turn fuses with deuterium atoms in the lithium deuteride yielding 17.6 MeV/fusion, 14.1 MeV of which is carried by the emitted neutrons. All of these events occur in a few shakes (a shake = 10 ns, so called by the physicists as mimicking the shaking of a lamb's tail) during which some of the relatively slower neutrons escaping the fission primary and others from fusion and lithium fission reactions induce fission in the spark plug. The imploding LiD assembly in the secondary is thus squeezed from the center as well, which creates enormous pressure and heat in the mass. Neutrons also contribute to tritium production by (n,a) reactions in ^6Li which has a large cross-section (741 b for thermal neutrons) and thus the lithium deuteride assembly is enriched to 30–40% ^6Li to optimize tritium production. Although less probable, the (n,2n) reaction in ^7Li also adds ^6Li and numerous additional neutrons for tritium-producing and fission reactions in the exploding secondary. These various physics processes have been optimized in designs of nuclear weapons based on numerous tests of configurations and materials and such designs remain highly classified.

The high temperatures created by the radiation pressure gives the charged deuterons and tritons enough energy to overcome the electrostatic repulsion between the nuclei and fuse via the D–D and D–T fusion reactions, thus yielding energy, additional tritium, and more neutrons. The neutrons from D–D and D–T reactions can be used to induce more fissions or produce more tritium in ^6Li which in turn yields additional fusions with deuterium to produce yet more neutrons and energy. The (n,p) cross-section in ^3He is huge (5330 b for thermal neutrons) and would poison the fission sequence, and since it is the decay product of tritium the booster gas is held outside and the helium content minimized before being added.

The 14.1 MeV neutrons produced in D–T reactions can induce fast neutron fission in ^{238}U, which is sometimes provided expressly for this purpose thus creating a fission–fusion–fission weapon. The explosive yields of fusion weapons range between 100 kilotons (kT) and a few megatons (MT) of TNT equivalent; fission–fusion–fission weapons can yield explosive energies of several megatons or more, apparently limited only by the amount of material added to the design.

11.2.3
Products of Nuclear Explosions

The energy released in nuclear explosions is commonly expressed in kilotons or megatons of TNT equivalent. Since each fission represents about 200 MeV of energy release, the explosive energy yield of a weapon is directly related to the number of fissions that occur. One kiloton of TNT is equivalent to 9.1×10^{11} cal, and the number of fissions per kiloton can be calculated as

$$\text{No. of fissions} = \frac{9.1 \times 10^{11}\,\text{cal/kT}}{(3.83 \times 10^{-14}\,\text{cal/MeV})(200\,\text{MeV/fission})}$$

$$= 1.19 \times 10^{23}\ \text{fissions/kT}$$

The number of atoms of a given fission product is determined by its fission yield Y_i:

$$N_i = (1.19 \times 10^{23} \text{ fissions/kT of fission yield}) Y_i$$

This relationship holds only for the fission yield of nuclear weapons. For weapons in which a substantial fraction of the explosive yield is due to fusion, it is necessary to know the fission yield to compute the inventory of fission products. The fission yield Y_i of an element is directly related to the material fissioned and the energy of the fissioning neutrons; therefore, these also need to be known if precise calculations are to be made. Reasonable values can be calculated with the thermal neutron fission yield data given in Appendix C for ^{235}U and ^{239}Pu.

Example 11-1. The Hiroshima explosion was estimated at 14 kT. If all the ^{137}Cs produced fell out over Japan, how many curies of ^{137}Cs were deposited on the ground?
Solution. The number of fissions that occurred is

$$\text{Fissions} = 1.19 \times 10^{23} \text{ fissions/kT} \times 14 = 1.663 \times 10^{24} \text{ fissions}$$

The nuclear device had a core of ^{235}U, and since the fission yield of ^{137}Cs in ^{235}U is 6.189%, the number of atoms of ^{137}Cs formed is

$$N(^{137}\text{Cs}) = 1.663 \times 10^{24} \times 0.06189 = 1.03 \times 10^{23} \text{ atoms}$$

$$\text{Activity} = \lambda N = 7.53 \times 10^{13} \text{ t/s} = 2035 \text{ Ci}$$

11.2.4 Fission Product Activity and Exposure

The beta emission rate from fission can be used to determine the activity associated with a single fission which varies with time after formation as

$$A_{FP} = 1.03 \times 10^{-16} t^{-1.2} \text{ Ci/fission}$$

Consequently, the radiation exposure rate from fission products will also vary as a function of $t^{-1.2}$, which is very useful for determining the exposure rate from deposition of fresh fission products in an area following a criticality or reactor incident, or perhaps a nuclear detonation. The exposure rate changes with time t according to the relationship

$$R_t = R_1 t^{-1.2}$$

where R_t = exposure rate at a time t after fission products are formed; R_1 = exposure rate at 1 h, 1 d, etc.; and t = time after formation of fission products. This relationship, which is plotted in Figure 11-3, holds reasonably well for fission products with ages between 1 min and about 200 d. Exposure rates at various times after the production of fresh fission products can be determined from Figure 11-3; however, direct calculations are relatively straightforward as shown in Example 11-2.

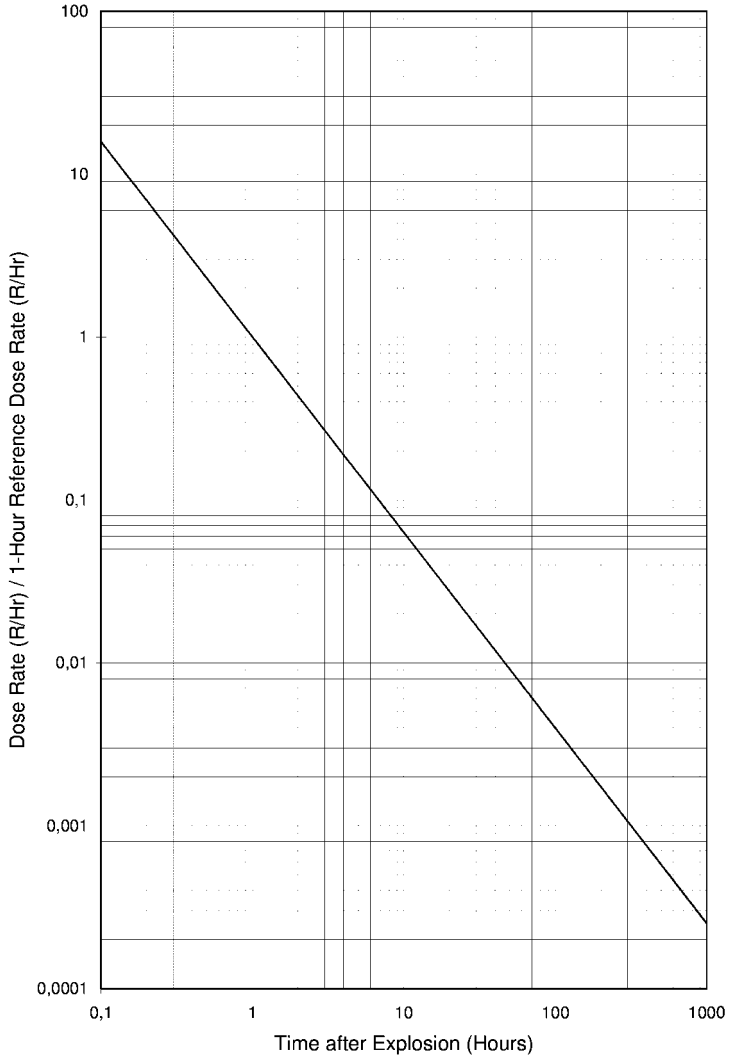

Fig. 11-3 Decrease of dose rate from fission products with time.

Example 11-2. The exposure rate downwind from an atmospheric nuclear explosion is measured to be 100 mrem/h 4 h after detonation. What will be the exposure rate 24 h later?
Solution. First, the exposure rate at 1 h is calculated:

$$100 \text{ mrem} = R_1(4)^{-1.2} \quad \text{or} \quad R_1 = 528 \text{ mrem/h}$$

and the exposure rate at 4 h + 24 h is

$$R_t = 528 \text{ mrem/h} \times (28 \text{ h})^{-1.2}$$

Although Example 11-2 yields the exposure rate for fission products at a given time t after their formation, the actual radiation exposure received depends on the exposure time. Since the exposure rate changes with time, it is necessary to integrate the instantaneous exposure rate over the period of actual exposure to obtain the total exposure E_{TOT}, which is

$$E_{TOT} = 5R_1(t_1^{-0.2} - t_2^{-0.2})$$

If R_1 is per hour, then t_1 and t_2 must be in hours also. It has also been demonstrated (Glasstone 1957) that the total exposure from a few seconds after formation of fresh fission products to infinity is 11.3 times the 1 h exposure rate.

Example 11-3. For the conditions of Example 11-2 calculate the total exposure a person would receive between 4 h and 28 h.
Solution. Since the exposure rate at 1 h is 528 mrem/h

$$E_{TOT} = 5 \times 528[(4)^{-0.2} - (28)^{-0.2}] = 645 \text{ mrem}$$

Checkpoints

There are two rules of thumb that are very useful in radiation protection considerations for fresh fission products:

- *Rule of thumb*: for every sevenfold increase in time, the exposure rate will decrease by a factor of 10 for times between 1 min and about 200 d (i.e., R_1 at 1 h will equal $0.1R_1$ at 7 h; R_1 at 1 d will be $0.1R_1$ in 7 d, etc.).
- *Rule of thumb*: the total dose to infinity will be about 11.3 times the 1 h dose rate.

The first Rule of thumb ($7t = 0.1R_1$) is illustrated by Example 11-3 where a sevenfold increase in time from 4 h to 28 h reduced the 100 mrem/h exposure rate to about 10 mrem/h (actually 9.7). Application of the second rule of thumb for total

exposure from a few seconds after detonation to infinity would yield an infinity dose of 5966 mrem.

It is important to remember that the exposure rate and decay relations for fission products are empirical and are based on a uniform mixture of fresh fission products such as that produced in a criticality event or nuclear detonation. Any given fission product mixture is affected by many factors such as plateout on surfaces before being released and alteration or selective depletion of reactive components during transport to the location where they are deposited. Even with such caveats, these relationships can be quite useful for assessing radiation exposures due to fission products and how they vary over time.

11.3 Criticality Accidents

There have been numerous supercritical accidents worldwide, many of which involved mixing of ^{235}U or ^{239}Pu with liquid which provided a moderator/reflector for neutrons thus promoting thermal neutron fission because of the higher fission cross-section at thermal energies. Eight of these, seven of which occurred in the USA, involved aqueous solutions in chemical processing operations: five with highly enriched uranium and three with plutonium. These caused two deaths and nineteen significant overexposures of personnel to radiation, but negligible loss of fissile material, equipment damage, or impact on the general public. Three of the excursions took place in shielded areas designed for processing irradiated fuel, and consequently personnel were protected from the direct radiation released. Each accident was related to misuse of equipment, procedural inadequacies or violations, or various combinations of each. Most of these accidents resulted in prompt criticality in which there was a "fission spike" with an exponential increase in energy generation, and some were followed by secondary spikes or pulses. Such spikes were terminated when bubbles formed or the energy release and radiolytic dissociation of water resulted in subcritical concentrations and/or configurations.

11.3.1 Y-12 Plant, Oak Ridge National Laboratory, TN: June 16, 1958

A bank of geometrically subcritical storage vessels for highly enriched uranium (HEU) recovered from scrap had been disassembled, cleaned, and reassembled for leak testing with water. The leak test was to be done some time after reassembly; however, during this interval, and unbeknownst to the operators, an isolation valve between the vessels and process equipment upstream leaked, which allowed HEU to drain into the vessels. Unfortunately, the presence of the HEU did not affect the leak test and it went unnoticed. After the leak tests were done the water was drained into a 55 gal drum, and the HEU solution containing about 2.1 kg of ^{235}U was suddenly present in an unsafe geometry, and criticality occurred. A suc-

cession of pulses then produced a total of 1.3×10^{18} fissions (in about 2.8 min). The reaction was terminated after about 20 min by additional water which continued to flow into the drum diluting the uranium density to a subcritical concentration.

An initial "blue flash" was observed from the first pulse (estimated at 10^{16} fissions) but the solution stayed within the open container. One person who was about 2 m away received a whole-body dose of ~461 rem; other exposures were 428 rem at ~5.5 m, 413 rem at ~4.9 m, 341 rem at ~4.6 m, 298 rem at 6.7 m, 86.5 rem at 9.4 m, 86.5 rem at 11 m, and 28.8 rem at 15.2 m. All responded to the evacuation alarm within 5–15 s, which is roughly the interval between the first two pulses, which apparently limited exposures considerably. After the accident it became standard practice to disconnect transfer lines containing fissile material instead of relying on valves, and "always safe" containers were required for use with ^{235}U-enriched solutions.

11.3.2
Los Alamos Scientific Laboratory, NM: December 30, 1958

An accident involving plutonium occurred at Los Alamos under conditions that were very similar to those at the Y-12 plant just six months earlier. Four vessels were to be emptied and cleaned individually, but somehow the residues and acidic wash solutions from the four vessels were combined into a single 850 L, 96.5 cm diameter tank. The wash solutions contained 3.10 kg of plutonium that had accumulated gradually in the process vessels and transfer lines over a period of about 7.5 y. The solution in the tank was subcritical at first because the plutonium had stratified into an organic layer that was about 20 cm thick and represented about 160 L of the total volume in the tank.

A stirrer in the tank was started to mix the solution for sampling before further transfer. When the stirrer blades, which were near the bottom of the tank, began to rotate, solution was forced up the walls of the tank which squeezed the aqueous plutonium layer toward the center, increasing its thickness and decreasing its lateral dimension. This created a cube-like or oblong spherical geometry, which was more favorable for criticality and an excursion estimated at 1.5×10^{17} fissions occurred. This supercritical condition only lasted a few seconds before the stirrer created a vortex in the liquid and the configuration quickly became subcritical, perhaps aided by the energy of the excursion. The excursion lasted only a few seconds because further stirring rapidly mixed the two phases to a subcritical concentration. The operator who started the stirrer received an exposure of about 12,000 rem and died 36 h later. Two men who went to his aid received doses of 134 and 53 rem.

The entire recovery plant, which had been scheduled for rebuilding after another six months of operation, was retired immediately. The replacement facility used geometrically subcritical equipment, eliminated unnecessary solution-transfer lines, auxiliary vessels were "poisoned" with borosilicate glass Rasching rings, and written procedures and nuclear safety training were improved.

11.3.3
Idaho Chemical Processing Plant: October 16, 1959, January 25, 1961, and October 17, 1978

Three incidents involving HEU solutions occurred in Idaho, all of them behind heavy shielding. In the first, a bank of geometrically subcritical storage cylinders was inadvertently siphoned into a large waste tank. About 200 L of solution containing 34 kg of ^{235}U were transferred into the tank with about 600 L of water. The large geometry with H_2O moderator and reflector went critical and produced about 4×10^{19} fissions over a period of about 20 min. An initial spike of ~10^{17} fissions was followed by smaller pulses, then by more-or-less stable boiling that distilled 400 L of water into another tank. The exceptionally large yield was the result of the large solution volume and long duration of the reaction. Fission products were vented into working areas which resulted in doses of 50 and 32 rem to two people, mostly in the form of beta radiation to the skin.

The second event occurred some 15 months later, again inside shielding, when a large air bubble forced 40 L of solution containing 8 kg of ^{235}U out the top of a "geometrically safe" 12.7 cm diameter section of an evaporator into a large (61 cm diameter) cylinder. The resulting excursion, probably a single pulse, had a magnitude of 6×10^{17} fissions. Personnel were protected from direct radiation and the ventilation system prevented airborne activity from entering work areas. The 61 cm diameter cylinder ultimately was "poisoned" by a grid of stainless steel plates containing 1.0 wt% natural boron. The incident provided valuable, if unintended, information that led to steps to prevent the introduction of air into solution lines that could contain fissionable material.

In the third criticality incident (October 17, 1978) a dilute aqueous solution of dissolved reactor fuel was introduced into the first of a series of pulsed columns for extracting and purifying HEU. Uranium was to be extracted into an organic stream which then flowed to a second column for removal of fission products into a stream of water. Under normal operations, the water in the second column was buffered with aluminum nitrate to prevent significant entrainment of uranium, and after fission products were removed the solution was then reintroduced along with feedstock into the first column to remove traces of uranium. The uranium was supposed to remain in the organic stream flushed from the second column. However, water had leaked into the aluminum nitrate makeup tank, and it was too dilute to prevent appreciable uptake of uranium. Instead of leaving with the organic, as it was supposed to, the uranium was entrained into the water and recycled successively through the first and second columns building up to an estimated 10 kg in the second column and with H_2O moderation and reflection, a criticality condition was eventually established. About 2.7×10^{18} fissions occurred over a 30 min period. The flow of HEU feed material was stopped and the reaction terminated due to improved mixing.

11.3.4
Hanford Recuplex Plant: April 7, 1962

A liquid, unidentified at the time and containing some 1400–1500 g of plutonium, was collected from a large glove-box sump into a 45.7 cm diameter vessel. Apparently, 46 L of the concentrated liquid had overflowed from a favorable geometry tank and was sucked into the vessel through a temporary line used for cleanup operations that were in progress. This change in geometry produced an excursion of 8.2×10^{17} fissions that occurred over 37 h, 20% of which occurred in the first half hour. The initial pulse (estimated at 10^{16} fissions) was followed by smaller pulses for about 20 min, after which boiling ultimately distilled off enough water to stop the reaction. The initial pulse, accompanied by the usual blue flash, triggered a criticality accident alarm, and the area was evacuated promptly, presumably before a second pulse. Exposures of 110, 43, and 19 rem were received by personnel at distances of about 2.1, 3.2, and 7 m, respectively.

11.3.5
Wood River Junction RI: July 24, 1964

This plant recovered HEU from scrap. Startup difficulties led to an unusual accumulation of trichloroethane (TCE) solution containing low concentrations of uranium which was recovered by tedious hand agitation with sodium carbonate solution. An easier process was improvised in which the TCE was treated in a 46 cm diameter tank which was normally used only for making up sodium carbonate solution. Neither the plant superintendent nor one of three shift supervisors was aware of this improvisation. Unbeknownst to these operators, a plug of uranium nitrate crystals containing 240 g of ^{235}U per liter had been drained the previous day from a connecting line into polyethylene bottles identical to those they were using for the low-concentration TCE solution. Thinking it was TCE solution, an operator poured a bottle of the concentrated solution into the large-diameter makeup tank which was being agitated by an electric stirrer. This configuration of highly concentrated ^{235}U in solution produced a criticality excursion of 10^{17} fissions with the usual flash of light, splashed about 8 L (20% of the total) out of the makeup tank, and knocked the operator to the floor. He received about 10,000 rad and died 49 h later.

The loss of solution and the vortex created by the stirrer, which continued to run, was sufficient to maintain subcriticality. Two men entered the area 90 min later to drain the solution into safe containers. As they were leaving, they turned off the stirrer, and the change in geometry created by the collapse of the stirrer-induced vortex apparently caused at least one more excursion of $2 \times \times 10^{16}$ to 3×10^{16} fissions. They received radiation doses estimated at between 60 and 100 rad. Modifications were made in operating and emergency procedures, criticality limits and controls, uranium accountability and material balance practices, and training. Favorable geometry equipment was installed for recovering uranium from TCE.

11.3.6
UKAEA Windscale Works, UK: August 24, 1970

An unsuspected buildup of plutonium occurred in an organic solvent layer similar to the Los Alamos accident. The excursion took place at the head end of a process for recovering plutonium by solvent extraction from an aqueous solution of about 6 g Pu/L. Forty liters of organic solvent from an unknown source entered a vacuum transfer vessel, and was then transferred to a trap which isolated the floating layer of solvent instead of permitting it to drain. Although the trap had been provided for safety, it allowed the solvent gradually to accumulate plutonium, and aqueous batches pouring through it eventually built up a concentration of 55 g Pu/L in the solvent. It appears that an emulsion layer formed between the solvent and the aqueous solutions which led to a criticality of about 10^{15} fissions during the brief period after the flow stopped and before the two phases of emulsion separated. Exposures were less than 2 rad for the two closest workers, who were protected somewhat by shielding.

11.3.7
Bare and Reflected Metal Assemblies

Two fatal accidents occurred at Los Alamos in 1945 and 1946 to scientists working with a bare assembly of two hemispheres of delta-phase plutonium (density of about 15.7 g/cm^3). In the first accident, a critical assembly was being created by hand stacking 4.4 kg tungsten carbide reflector bricks around the plutonium hemispheres. The experimenter was working alone, in violation of procedures. As he was moving the final brick over the assembly (he was supposed to add it from below) he noticed, from the nearby neutron counters, that the addition of this brick would make the assembly supercritical and he began to withdraw it. However, he dropped it onto the center of the assembly, which added sufficient reflection to make the system super-prompt critical. He quickly pushed off the final brick and proceeded to unstack the assembly, but an excursion estimated at 10^{16} fissions had already occurred. The experimenter received an estimated exposure of 510 rems and died 28 d later.

In the second accident, an experimenter was demonstrating a metal critical assembly using the same plutonium sphere which, in this case, was reflected by beryllium, a better neutron reflector. The top and final hemispherical beryllium shell was being slowly lowered into place; one edge was touching the lower beryllium hemisphere while the edge 180° away was resting on the tip of a screwdriver. The person conducting the demonstration was holding the top shell with his left thumb inserted in an opening at the polar point, while slowly working the screwdriver out with his right hand when the screwdriver slipped and the shell seated on the lower hemisphere creating a supercritical assembly and a power excursion of 3×10^{15} fissions which blew the shell off the assembly and onto the floor. The eight people in the room received doses of about 2100, 360, 250, 160, 110, 65, 47, and 37 rem. The man who performed the experiment died 9 d later.

These types of experiments were characterized by Richard Feynman, the Nobel prize-winning physicist, as "tickling the dragon's tail" – get too close and the beast will breathe fire on you.

11.4
Radiation Exposures in Criticality Events

Figure 11-4 shows a general picture of personnel dose versus distance from the criticality event; the exposures are normalized to 10^{17} fissions and exposure times of ~15 s. The relationships are based on empirical data rather than calculable parameters, which can vary considerably from one event to another, and hence the exposures should be regarded as representing typical excursions. The short exposure times presume rapid evacuation, a major factor in the dose received. Good alarms and personnel training to ensure rapid response are essential elements of criticality safety programs. Our first knowledge that the $LD_{50,30}$ for humans was 450–500 rad came from the fatality associated with the Los Alamos criticality accident in 1946.

The criticality accidents involving aqueous solutions, six of which occurred in a six-year period between 1958 and 1964, appear to be related to a wider variety of tasks associated with an increased demand for plutonium and enriched uranium

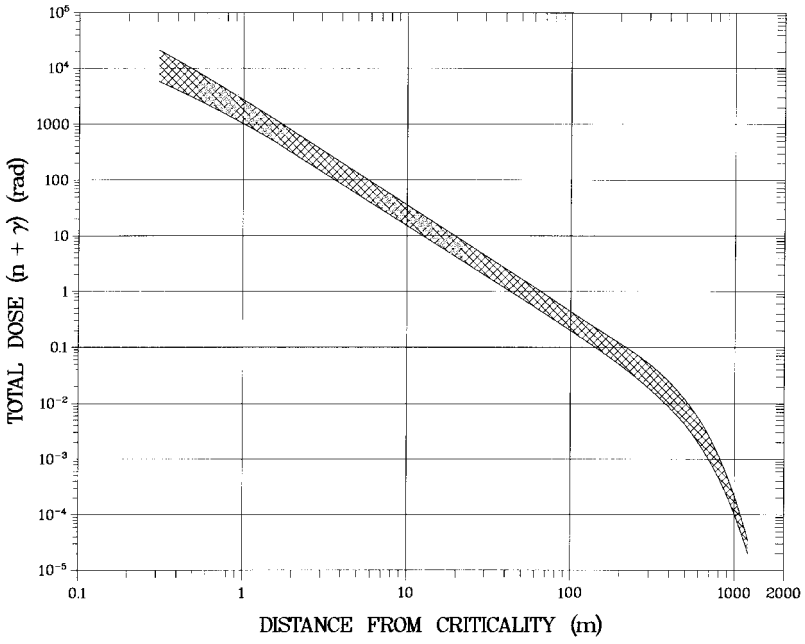

Fig. 11-4 Radiation dose versus distance from the criticality event.

production. They are also dramatic examples of the consequences of major changes in operations without a corresponding reassessment of criticality control.

Facilities left over from the Cold War have interesting inventories and arrays of fissionable material and the potential for criticality conditions. Particular attention needs to be paid to anticipate and prevent criticality events when solutions of plutonium or HEU are processed by the non-routine circumstances that are associated with stabilizing, dismantling, and recovering old sites and facilities.

11.5 Criticality Safety

Preventing a criticality of fissile material is based on a consideration of the same factors that must be overcome if a supercritical condition is to be achieved in controlled nuclear reactors or nuclear weapons. The mass, volume, and density/concentration of fissionable material, its geometrical shape and configuration, and the moderation/reflection, absorption, and leakage of neutrons are all important factors in achieving or preventing a supercritical system. Criticality safety depends on the following:

- Limiting the quantity of fissile material to less than the critical mass under any conceivable configuration.
- Restricting the geometry of the fissile material, preferably to one that is "always safe," i.e., one where the surface to volume ratio is such that excessive neutron leakage makes it impossible to attain a multiplication factor of 1.00 or more.
- Limiting the concentration of any fissile material that may be in a solution of moderating material such as H_2O, D_2O, or other liquids, and considering the presence or absence of neutron reflecting material(s).
- Preventing the interaction between two or more subcritical arrays of fissile materials, especially in transport and storage.

Mass/density effects influence the critical mass of a fissile material. The critical mass of a sphere of ^{239}Pu metal is much less than that of a sphere containing unmoderated ^{239}Pu filings or chips. Nuclear weapon designs take advantage of this fact by compressing a spherical mass to high density.

Geometry effects can be used in an "always safe" configuration to prevent inadvertent criticality by promoting neutron loss even if sufficient mass and/or moderation and reflection are available. If a given volume of fissile solution departs from spherical shape, there is an increase of surface area through which neutrons can escape; therefore, two practical "always safe" geometries are an elongated cylinder of sufficiently small diameter or an extensive slab of restricted thickness; para-

Table 11-1. Minimum critical safety parameters for fissionable materials in moderated and reflected[a] conditions and as unmoderated[b] metal.

Fissile material	Parameter	Minimum critical value	
		Moderated and reflected[a]	Unmoderated[b]
Always-safe	^{235}U enrichment	≤0.93 wt%	5.0 wt%
	Aqueous ^{235}U	≤11.94 g/L	–
	$^{235}UO_2(NO_3)_2$ at 2.88 wt%	≤595 g/L	–
	$^{235}UO_2(NO_3)_2$	≤1.96 wt%	–
	Dry oxides Pu + U	≤4.4 wt% Pu	–
	Damp oxides (H/Pu + U) ≤ 0.45	≤1.8 wt% Pu	–
^{235}U – 93%	Mass	830 g	22.8 kg
	Diameter of infinite cylinder	8.0 cm	–
	Thickness of infinite slab	1.80 cm	–
^{235}U – 100%[c]	Mass (ρ = 17.484)	760 g	20.1 kg
	Diameter of infinite cylinder	13.7 cm	7.3 cm
	Thickness of infinite slab	4.4 cm	1.3 cm
	Volume of solution	5.5 L	–
	Concentration (aqueous)	11.6 g/L	–
^{233}U – 100%	Mass (ρ = 18.05)	540 g	7.5 kg
	Diameter of infinite cylinder	10.5 cm	5.0 cm
	Thickness of infinite slab	2.5 cm	0.6 cm
	Volume of solution	2.8 L	–
	Concentration (aqueous)	10.8 g/L	–
^{239}Pu – 100%[d]	Mass (ρ = 19.74)	480 g	5.0 kg
	Diameter of infinite cylinder	15.4 cm	4.40 cm
	Thickness of infinite slab	5.5 cm	0.65 cm
	Volume of solution	7.3 L	–
	Concentration (aqueous)	7.3 g/L	–

a Moderation and reflection by H_2O is assumed.
b Unmoderated values assume water reflection.
c Values for moderated and reflected solutions are based on $^{235}UO_2F_2$; for $^{235}UO_2(NO_3)_2$, these may be increased to 780 g, 14.4 cm, 4.9 cm, 6.2 L, and 11.6 g U/L, respectively.
d Values based on moderated and reflected pure ^{239}Pu metal or $^{239}Pu(NO_3)_4$ solutions; if ≥5 wt% of ^{240}Pu is present, the values increase to 570g, 17.4 cm, 6.7 cm, 10.0 L, and 7.8 g Pu/L.
Source: Adapted from *Nuclear Criticality Safety Guide*, Los Alamos National Laboratory, Report LA-12808, 1996.

meters for these shapes, reflected by a thick layer of water, are provided in Table 11-1.

Another very important geometric factor is separation of subcritical units to preclude mutual exchange of neutrons between them. Such separation is especially important in facility design and in the storage and transport of subcritical units.

Moderator/reflector effects of light materials, especially water, can greatly influence the critical configuration of fissile material, reducing its critical mass to as little as a few hundred grams. On the other hand, very dilute solutions in which neutron absorption by hydrogen predominates can contain unlimited quantities of fissionable material without criticality. A close-packed subcritical array may become critical if flooded; and conversely, a flooded subcritical array of large, less closely packed units may become critical if the water is removed, since the water, as a neutron absorber, may diminish neutron coupling of the units.

Subcritical systems may also become critical if a reflector such as beryllium, H_2O, or tissue is added that returns escaping neutrons into the array. For example, Yuli Khariton recalled that as Vannikov, who was a rather large fat man, "went back and forth to read the gauges...during (a test of critical assembly for the first Soviet nuclear weapon) we understood: the bomb would definitely work" (described by Richard Rhodes in *Dark Sun*, Simon and Schuster, New York, 1995).

11.5.1 Criticality Safety Parameters

The interrelationships of mass, moderator, and reflector are shown in Figures 11-5 and 11-6 for spherical shapes containing ^{235}U and ^{239}Pu and in Figure 11-7 and 11-8 for slabs of various concentrations of the two materials. These two geometries are conservative ones, and the relationships determined for them provide indices for preventing criticality conditions. For example, spherical geometries of fully reflected pure uranium or plutonium metal will be safe (Figures 11-5 and 11-6) as long as the total mass of each is less than 1.5 and 0.9 kg, respectively; any other shape will also be safe since this is an optimal geometrical configuration requiring the least amount of fissionable material. Without reflection an assembly can contain more mass without becoming critical. If, however, the ^{235}U or ^{239}Pu is in a solution that provides moderation and reflection, the critical mass is reduced considerably, and can be as low as 0.76 kg of ^{235}U or 0.48 kg of ^{239}Pu in solution. If the mass of either is kept below these quantities, they will always be subcritical regardless of how they are mixed; therefore, a minimum critical mass of material can be stated that will be always safe. These various limiting parameters and several other useful data are also listed in Table 11-1.

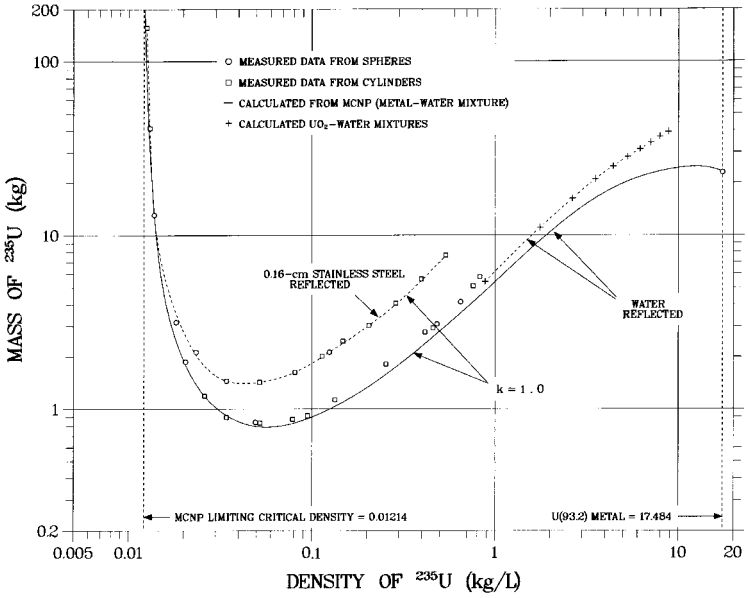

Fig. 11-5 Critical masses of spherical shapes of 93.2% ^{235}U in homogeneous water-moderated solution as function of ^{235}U density and reflection by thick water and stainless steel. (Adapted from *Criticality Safety Guide* with permission.)

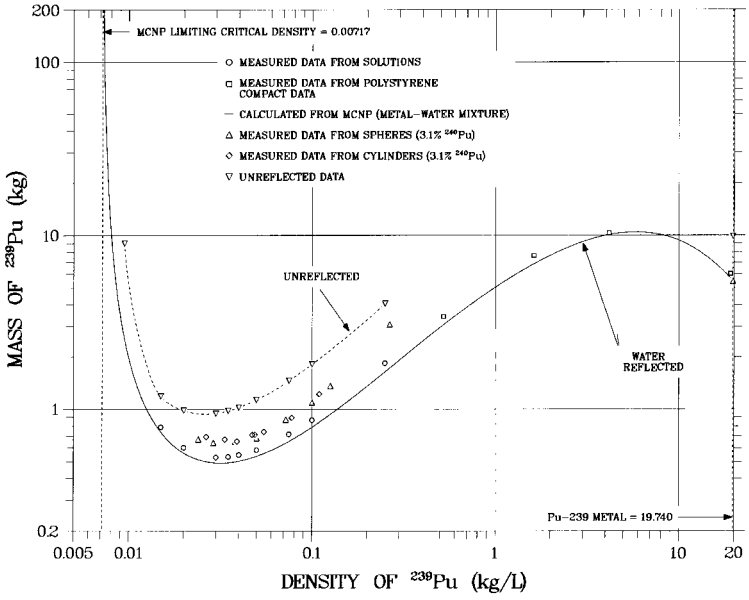

Fig. 11-6 Critical masses of spherical shapes of ^{239}Pu in homogeneous water-moderated solution as function of ^{239}Pu density with and without water reflection. (Adapted from *Criticality Safety Guide* with permission.)

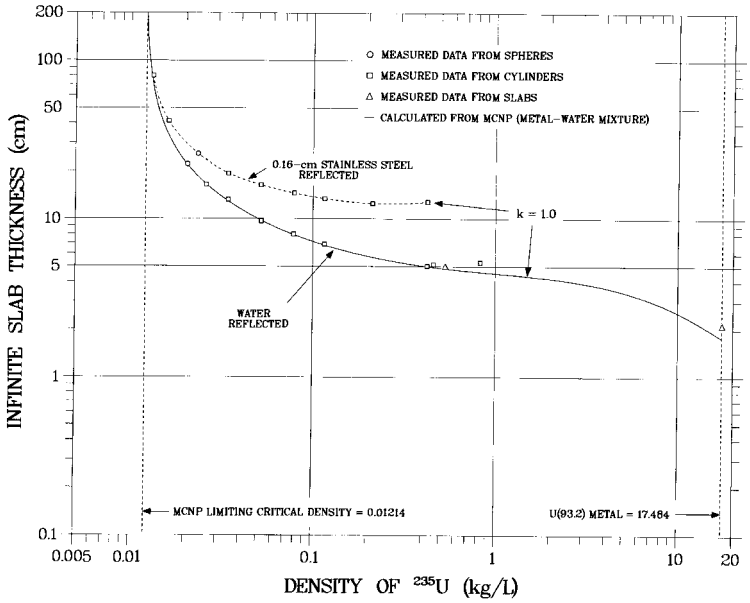

Fig. 11-7 Thicknesses of infinite slabs of 93.2% ^{235}U in homogeneous water moderator as function of ^{235}U density and reflection by water and stainless steel. (Adapted from *Criticality Safety Guide* with permission.)

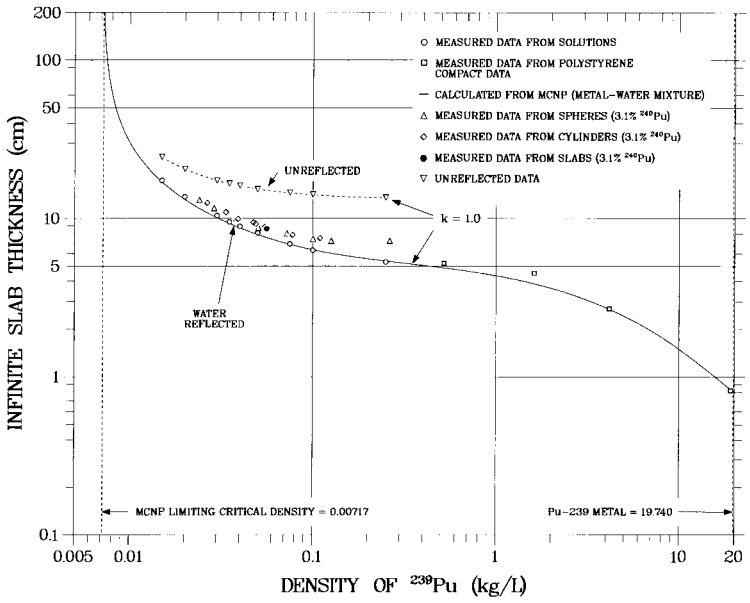

Fig. 11-8 Thicknesses of infinite slabs of 93.2% ^{239}Pu in homogeneous water moderator as function of ^{239}Pu density with and without water reflection. (Adapted from *Criticality Safety Guide* with permission.)

Similar interpretations can be made for slab geometries in which layered material containing ^{235}U or ^{239}Pu will always be subcritical (Figures 11-7 and 11-8) if the thickness of a fully reflected slab of a very large ("infinite") area is less than 1.9 or 0.8 cm, respectively. If a reflector is absent, the layer of fissionable material could be thicker, but most criticality assessments of layered material would want it to be safe even if flooded with water.

A cylindrical geometry of ^{235}U will be "always safe" regardless of the concentration or reflection if the diameter is less than 7.3 cm (100% ^{235}U, fully reflected and unmoderated); a cylindrical geometry of fully reflected pure ^{239}Pu will be "always safe" if the diameter is less than 4.4 cm (100% ^{239}Pu, fully reflected and unmoderated). Most processes developed for solutions of fissionable material use these dimensions because, as the accidents described above demonstrate, fissionable materials have a way of accumulating in concentrations that would be undesirable if "always safe" geometries are not ensured.

Most real-world situations are not represented by spherical or infinite slab geometries nor are they fully reflected or moderated. For such configurations a larger mass of fissionable material could be present without criticality, but allowing these conditions to exist should be done with the utmost care.

Separation of subcritical units is also an important consideration in assessing criticality safety, especially if either could contribute significant neutrons to the other. Such separation is essential between "always safe" vessels, transfer lines, and pipes, lest they assume a critical configuration, and care needs to be exercised in placing either near materials that are good reflectors of neutrons. Densely formed concrete can be a good reflector; therefore, placement of vessels containing concentrated fissionable material next to a wall or floor of such concrete could cause subcritical concentrations to become critical.

Containers that ensure "always safe" spacing are commonly called "bird cages". A 55 gal drum with an "always safe" unit container welded into the center by appropriate spacers provides an excellent bird cage. The drum becomes the spacing container, ensuring that the closest distance between the surfaces of fissile materials is always less than a safe separation distance even if the containers are immersed in water.

Criticality safety practices limit at least one, and preferably two, of the factors that determine criticality below the specified minimum values in Table 11-1. The limiting values in Table 11-1 are independent of each other and restriction of any one of the parameters is protective; however, processes and equipment are generally designed such that at least two of these independent parameters are met to provide additional safety, the "double contingency" principle. It is also good practice to rely on equipment designs rather than to rely principally on a process to ensure safety. A process designed to meet a concentration or enrichment criterion could well fail if the wrong material inadvertently appears in the process, circumstances that can be precluded by equipment designs that provide an "always safe" geometry.

Limiting the degree of enrichment of fissionable material (^{235}U, ^{239}Pu, ^{233}U) in a concentration of liquid is also an effective practice. It is not possible for an aqueous mixture or solution of uranium to attain criticality unless the ^{235}U is enriched

to above 0.95% or more; therefore, no criticality restrictions need be made for transportation or storage of natural uranium or homogeneous aqueous mixtures containing less than 0.95% ^{235}U. Similarly, uranium metal with an enrichment of less than 5% ^{235}U cannot achieve criticality provided the metal is not interspersed as chunks or rods in hydrogenous material.

Example 11-4. Vessels containing highly enriched (>93%) $UO_2(NO_3)_2$ solutions are located above a bermed concrete floor area of 9 m^2. What conditions should be required for an overflow line above the floor to limit the thickness of solution should the vessels leak?

Solution. The configuration of the solution can be conservatively approximated by an effectively infinite uniform slab with a thick concrete reflector on one side and incidental reflection on the other side. From Table 11-1 the subcritical thickness of an infinite slab of $UO_2(NO_3)_2$ fully reflected by water is 4.9 cm. Assumption of a thick water reflector on both surfaces is more conservative than concrete reflection by the floor and the berm; therefore, an overflow pipe placed 4.9 cm above the lowest portion of the floor would ensure that a critical configuration of $^{235}UO_2(NO_3)_2$ solution could not occur in the bermed area regardless of the areal extent.

11.6 Fission Product Release in Criticality Events

Criticality events yield fission products in addition to the high exposure field of neutrons and gamma rays. Volatile fission products such as iodines, bromines, and noble gases usually escape because of the heat generated and these can produce airborne levels in buildings or be released to the environment. Others remain in the medium where the criticality occurred and can be used to characterize the magnitude of the event, usually in terms of the number of fissions that occurred.

A calculation of fission product releases from criticality events first must recognize that such events occur instantaneously, which means that any gaseous and volatile fission products available for release will be those formed instantaneously which is determined by their independent fission yields. The inventory will of course change with time as the fission products undergo transformation and transition down the fission product mass chain, in some cases to produce other gaseous and volatile radionuclides. Alternatively, those volatiles that were formed directly and released in the excursion will not yield their usual products from radioactive transformation associated with fission products chains.

Example 11-5. A criticality event occurs in a container which overpressurizes causing all the ^{138}Xe produced to be vented. The container is sampled 3 h later and found to contain 10 Ci of ^{138}Cs. How many fissions occurred in the event?

Solution. The formation of ^{138}Cs (see Appendix C) occurs by radioactive transformation of ^{138}Xe, its precursor, and by independent yield. Since all of the ^{138}Xe formed at the instant of the excursion can be assumed to have been vented from the container due to the overpressurization, the only ^{138}Cs in the container would be formed by direct fission yield (6.7080 – 6.2973).

The amount of ^{138}Cs that existed when the excursion occurred (i.e., 3 h earlier) is

$$10 \text{ Ci} = A_0 e^{-(\ln 2/32.2\,\text{m}) \times 180\,\text{m}} \quad \text{or} \quad A_0 = 481.3 \text{ Ci}$$

The number of atoms in 481.3 Ci is

$$N_{\text{Cs}} = \frac{1.78 \times 10^{13}\,\text{t/s}}{3.588 \times 10^{-4}\,\text{s}^{-1}} = 4.96 \times 10^{15} \text{ atoms of } ^{138}\text{Cs}$$

and the number of fissions is

$$\frac{4.96 \times 10^{15} \text{ atoms}}{0.00411} = 1.21 \times 10^{18} \text{ fissions}$$

11.6.1 Fast Fission in Criticality Events

Many criticality events occur with fast neutrons, especially nuclear explosions. The fission product yield spectrum for fast neutron fission is somewhat different from that due to thermal fission as shown in Figure 5-22; therefore, the most accurate calculations of yield of a given fission product for such events is obtained if the fission yield spectrum for fast neutrons is used. Fast fission yields for ^{239}Pu and ^{235}U for some of the more important mass chains are shown in Figure 11-9, using the same nomenclature as in Appendix C. The fission yields in Appendix C for thermal neutron fission can be used for fission with an accuracy within 10–20% if fast fission yields are not otherwise available. Fast fission yields are available for other mass chains from the National Nuclear Data Center website as referenced in Appendix C.

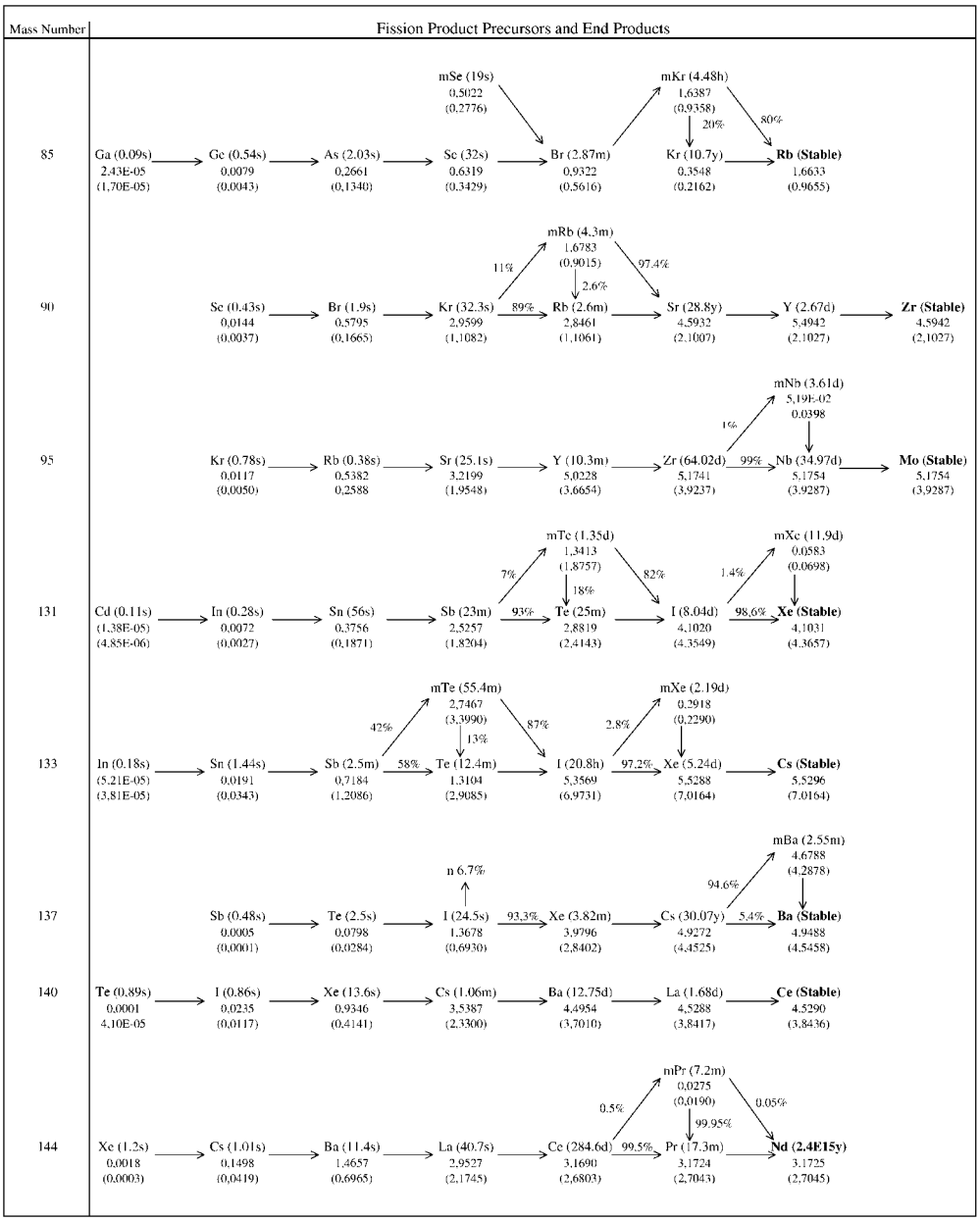

Fig. 11-9 Cumulative percent fission yields for fast neutrons in ^{235}U and (^{239}Pu) for each isotope in selected mass chains.

Example 11-6. Estimate the amount of ^{131}I produced from a 1 kT ^{239}Pu-fueled weapon based on fast fission. How does this compare with an assumption based on the thermal neutron fission yield in ^{239}Pu?

Solution. From Figure 11-9, the cumulative fast fission yield in ^{239}Pu for ^{131}I atoms is 4.355%, and since 1 kT of weapon yield corresponds to 1.19×10^{23} fissions, the number of atoms of ^{131}I formed is

$$^{131}I_f \text{ atoms} = 1.19 \times 10^{23} \text{ fissions} \times 0.04355 \text{ atoms/fission}$$
$$= 5.18 \times 10^{21} \text{ atoms or } 140{,}000 \text{ Ci}$$

If the thermal fission yield for ^{239}Pu were assumed (Appendix C, 3.856%), the number of atoms of ^{131}I would be

$$^{131}I_t \text{ atoms} = 1.19 \times 10^{23} \text{ fissions} \times 0.03856 \text{ atoms/fission}$$
$$= 4.59 \times 10^{21} \text{ atoms or } 124{,}000 \text{ Ci}$$

Example 11-6 shows the importance of the type of fission event in determining fission product inventories from criticality events. The calculated ^{131}I activity is a factor of about 1.13 larger (or about 13%) when the fast fission yield is used, which is just the ratio of the fast and thermal fission yields.

11.7 Summary

Criticality safety is an important consideration in radiation protection because exposures and consequences can be very high. Criticality events are generally of three types: (a) the intentional assembly of fissionable material to release energy such as in nuclear weapons; (b) supercritical conditions in reactors; and (c) unintended accumulations or configurations of fissionable materials such as enriched ^{235}U or ^{239}Pu in solution. Preventing a criticality of fissile material is based on a consideration of the same factors that must be overcome to achieve a sustained supercritical condition in a nuclear reactor or the explosive release of energy in nuclear weapons. The mass, volume, and density/concentration of fissionable material; its geometrical shape and configuration; and the moderation/reflection, absorption, and leakage of neutrons are all important factors in achieving or preventing a supercritical system.

Processes and equipment are generally designed such that at least two of the independent parameters that determine criticality are met. Equipment designs are more reliable for ensuring safety than a process or a procedure since these could fail if the wrong material inadvertently appears in the process. Equipment designs that provide an "always safe" geometry preclude the occurrence of an accidental critically even if concentration limits are exceeded and a good reflector is present. Whenever possible, fissionable material should be processed and/or stored in cylindrical containers with safe diameters, and these should be physical-

ly spaced with "bird cages" or other fixed arrays far enough apart that they could not go critical even if flooded with water.

Criticality events produce high exposure fields of neutrons and gamma rays and the release of volatile fission products such as iodines, bromines, and noble gases. The fission products available for release will be those formed instantaneously which is determined by their independent fast fission yields; however, thermal neutron fission yields can be used for such determinations with an accuracy within 10–20% if fast fission yields are not otherwise available.

Acknowledgments

N. L. Provost and H. C. Paxton of the Criticality Safety Group at Los Alamos National Laboratory were especially helpful in providing comprehensive information on criticality safety, to which the author hopes he did justice in the summary of a very complex subject.

Other Suggested Sources

Glasstone, S. **1957**, *Effects of Nuclear Weapons*, US Department of Defense (US Atomic Energy Commission).
Provost, N. L., Paxton, H. C. **1996**, *Nuclear Criticality Safety Guide*, Report LA-12808, Los Alamos National Laboratory.
Stratton, W. R. **1989**, *A Review of Criticality Accidents*, Report DOE/NCT-04, US Department of Energy.

Problems – Chapter 11

11–1. In 1000 atoms of present-day natural uranium, 993 are ^{238}U and 7 are ^{235}U. What would have been the percentage of ^{235}U in natural uranium 2 billion years ago, and could it have yielded a natural reactor?
11–2. If the Earth is 4.5 billion years old, what would have been the percentage of ^{235}U in uranium at that time, and how might this have contributed to early changes in the Earth's crust?
11–3. Careful measurement of the soil around the Gabon natural reactor site established the current inventory of ^{129}I formed in the soils at 10 mCi. If it can be assumed that none of the ^{129}I initially has left the site, estimate the number of fissions that occurred some 2 billion years ago. If humans existed and could recover the energy, how much thermal energy (kW) was available for their use?
11–4. A 100 kT nuclear fission device is exploded underground in Nevada and the iodines produced vent through a fissure. How many curies of ^{131}I would be available for release?

11–5. A foreign country tests a nuclear device in the atmosphere. The exposure rate measured downwind was 10 mR/h 3 h later. What would be the exposure rate 24 h after the test? What would be the total dose from 3 h onward if people remained in the area indefinitely?

11–6. It has been estimated that 20 Ci of ^{131}I was released to the environment from the Three Mile Island incident, which occurred when the reactor had been running at full power (2700 MWt) for 3 months. How many curies of ^{131}I were released in the reactor system/containment structure?

11–7. The Chernobyl reactor had operated at 3200 MWt for about a year before the explosion. The inventory of ^{133m}Xe and ^{133}Xe was released as a large puff that drifted over the nearby area to produce external exposure by sky shine and submersion. How many curies of ^{133m}Xe and ^{133}Xe would form the source term in this puff?

11–8. A nuclear criticality incident occurred instantaneously in a tank containing enriched uranyl nitrate and water when a mixer was turned on. It was determined that 10^{20} fissions occurred. (a) What would be the activity (in Ci) of ^{138}Xe 10 s after the incident? (b) What would be the activity of ^{138}Xe 1 h later (use exact solution)?

11–9. A criticality occurred in a tank containing a solution of fissionable material producing 2×10^{17} fissions. Estimate the radiation exposure to a worker standing 2 m away who responded quickly to the criticality alarm and exited the area within 15 s.

11–10. A solution containing highly enriched uranium was processed after a criticality of 10^{18} fissions had occurred to recover the uranium. How many curies of ^{137}Cs would be in the residual radioactive waste process solution?

12
Radiation Detection and Measurement

"When you can measure what you are speaking about and express it in numbers, you know something about it; when you cannot...your knowledge is of a meager and unsatisfactory kind."
Lord Kelvin (1889)

The interactions of various types of radiation in matter provide mechanisms for measuring the amount of radiation emitted and absorbed by a source(s), and with careful techniques the identity of the radiation source or radionuclide producing it. Radiation instruments include portable survey instruments that are designed to detect radiation and measure exposure or absorbed dose and laboratory instruments that allow precise quantitation and identification of the radiation source. Various detectors are used in them, and these can be roughly divided into two categories: gas-filled chambers and crystalline materials. Each of these various devices is based on the liberation of electrons in a medium and the collection and processing of the ions by electronic means. Although many of these same considerations apply to neutrons, their detection and measurement require special considerations which are described in Chapter 14.

12.1
Gas-Filled Detectors

Absorption of radiation in a gas-filled chamber is accomplished by establishing an electrostatic field between the wall of the chamber and a positive electrode located on the axis of the chamber and insulated from it as illustrated in Figure 12-1. The gas is usually at a pressure of one atmosphere or less, but with appropriate care can be pressurized to enhance interactions. When radiation is absorbed in the gas contained by the chamber, ion pairs (a positive ion and an electron) are produced, which are collected and amplified for recording the signal produced.

Physics for Radiation Protection, Third Edition. James E. Martin

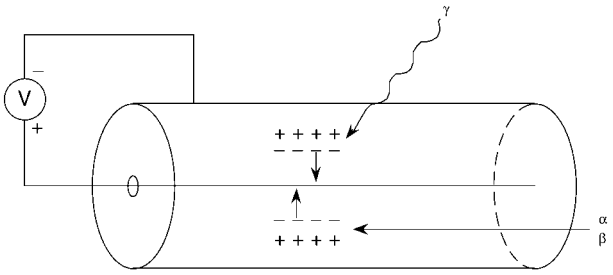

Fig. 12-1 Schematic of gas-filled detector operated with a varying voltage applied between the chamber wall (cathode) and a central collecting electrode (anode).

The collection of ion pairs in a gas-filled detector is a function of the applied voltage as shown in Figure 12-2, which characterizes the operation of such detectors for beta particles (lower curve) and for alpha particles (upper curve). If there is no voltage across the chamber, the ion pairs will recombine, and no charge will flow in the external circuit for either type of radiation. As the voltage is increased, say to a few volts, some ion pairs will still recombine but others will flow to the electrodes and be collected. At a voltage of perhaps 10 V or more, recombination becomes negligible, and all of the electrons produced by ionization will reach the central electrode. As the voltage is increased to several tens of volts the number of ion pairs collected is independent of the applied voltage, and the curve will remain horizontal as long as the radiation source produces ionizing radiation at a steady rate. If 10 ion pairs are formed initially, the response will be steady as shown by the lower curve; if the source strength or ionizing rate (e.g., an alpha emitter) is a factor of 10 higher, 100 ion pairs will be formed, and the detector response will also be a factor of 10 higher as shown in the upper curve. These curves are parallel to each other, i.e., the current collected is directly related to the ionization produced by the incoming radiation. This region in which the current measured is directly related to the amount of ionization produced is called the *ionization region*; its magnitude will be quite different for equal source strengths of alpha particles, beta particles, x-rays, and gamma rays due to differences in the number of ion pairs produced by each as they interact in the medium.

Increasing the voltage of a gas-filled detector above the ionization region causes the electrons released by the primary ionizations to acquire enough energy to produce additional ionizations as they collide with the gas molecules in the chamber. The number of electrons collected increases roughly exponentially with the applied voltage because each initial electron is then accelerated to produce a small "avalanche" of electrons, most of which are liberated close to the central electrode. Each electron liberated by the incoming radiation produces its own independent avalanche such that at a given voltage of the detector the ionization produced is amplified by a constant amount, i.e., the number of ion pairs collected is proportional to the initial ionization. Gas-filled detectors operated at these voltages are characterized as being operated in the *proportional region*. When the voltage across

the chamber reaches several hundred volts the gas multiplication effect increases very rapidly, and as more electrons produce avalanches, the latter begin to interact with one another creating a region of limited proportionality. As voltage is increased further the charge collected becomes independent of the ionization initiating it, and the two curves not only become identical but form a plateau as voltage is increased. This is the *Geiger–Mueller region* and it is characterized by the plateau. At voltages above the plateau the detector produces a region of continuous discharge.

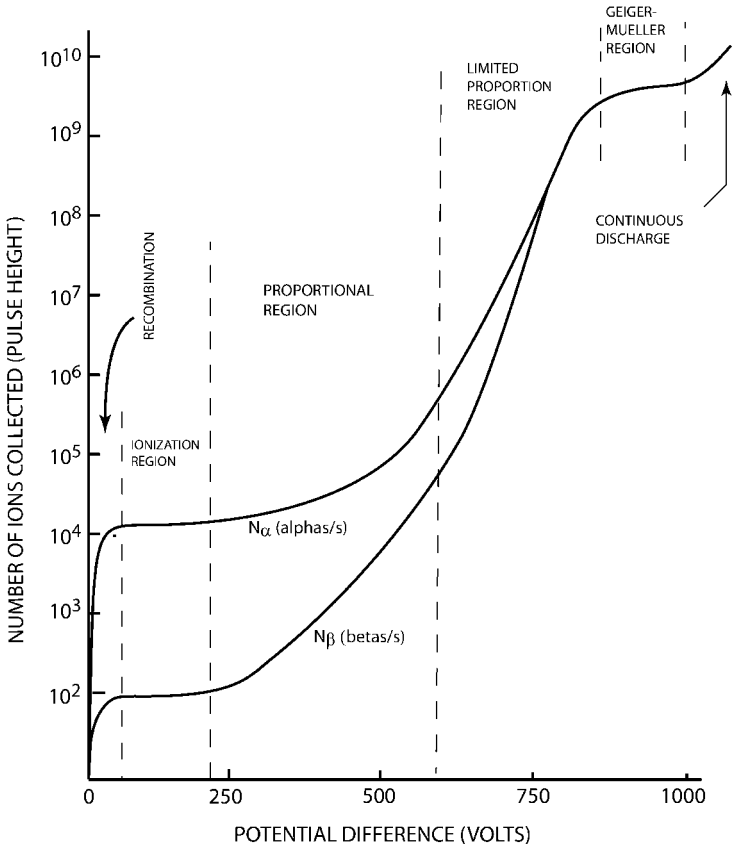

Fig. 12-2 Ionization rates for constant source strengths of a beta emitter and an alpha emitter in a gas-filled detector operated in different voltage ranges.

Three radiation detector types have been developed based on the regions of applied voltage illustrated in Figure 12-2: the ionization chamber (based on the ionization region), the proportional counter (based on the proportional region), and the Geiger–Mueller (GM) counter (based on the GM region).

The *ionization chamber*, operated at voltages in the ionization region, is characterized by complete collection, without gas amplification, of all the electrons liberated by the passage of the ionizing radiation, either in the form of particles or photons. The electrodes of an ionization chamber are typically cylindrical with a center electrode, but it may also be a parallel-plate design. The applied voltage is selected to ensure collection of all the ions formed; i.e., it is high enough to prevent recombination of the ions produced but still on the plateau where current amplification does not occur. The current pulse is proportional to the number of ionizing events produced, and the collected charge can be used directly to establish radiation exposure.

The *proportional counter*, which is operated at voltages in the proportional region, is characterized by gas multiplication which produces a pulse proportional to the initial ionization. Since alpha particles are highly ionizing relative to beta particles, proportional counters are useful to both count the particles and to discriminate between them based on the size of the pulse each produces. The proportional counter thus offers a particular advantage for pulse-type measurements of beta radiation, and can be used in conjunction with electronics to sort the smaller beta pulses from the larger ones produced by alpha particles. With modern electronics samples that contain both alpha and beta particles can be easily sorted and measured at the same time.

The *Geiger–Mueller (GM) counter*, is operated in the Geiger region and is characterized by a plateau voltage which produces an avalanche of discharge throughout the counter for each ionizing radiation that enters the chamber. This avalanche of charge produces a pulse, the size of which is independent of the initial ionization, therefore the GM counter is especially useful for counting lightly ionizing radiations such as beta particles or gamma rays and is specially designed to take advantage of this effect. Since it is difficult to make tubes with windows thin enough for alpha particles to penetrate into the gas chamber, GM counters are used mainly for the more penetrating beta and gamma radiations. A thin end-window is often incorporated in GM tubes to enhance detection of beta particles. A GM tube usually consists of a fine wire electrode (e.g., tungsten) mounted along the axis of a tube containing a mixture of 90% argon and 10% ethyl alcohol (for quenching) at a fraction of atmospheric pressure. A potential difference of 800–2000 V (nominally 900 V) is applied to make the tube negative with respect to the wire. Because of their mode of operation, they cannot be used to identify the type of radiation being detected nor its energy.

In summary, gas-filled radiation detectors respond to incoming radiation by the ionization it produces. The ions, either multiplied in number or not, are collected to produce a voltage pulse which may be as small as 10 μV. These small pulses are amplified to 5 to 10 V and fed to a galvanometer for a direct reading or to a pulse counter (or scaler) so that their rates can be measured. The magnitude of the pulses produced can also be measured in the proportional region and sorted according to their energy, e.g., alpha particles from beta particles.

12.2
Crystalline Detectors/Spectrometers

Various crystals and solid-state detectors can be used with electronic instrumentation to quantitate the number of radiations of a given energy that activate the detector and the rate at which such events occur. A scintillating crystal such as sodium iodide with a thallium additive, NaI(Tl), will produce a "flash" of light proportional to the energy deposited by a photon that interacts in the crystal. The light (also a photon with a wavelength in the visible region of the electromagnetic spectrum) is reflected onto a photocathode connected to a photomultiplier (PM) tube. When these photons strike the light-sensitive cathode a small number of electrons (Figure 12-3) proportional to the energy of the absorbed photon are emitted. These are accelerated by a potential difference across the first dynode, which emits approximately four secondary electrons for each incident electron. A series of 10 dynodes gives an amplification factor of 4^{10}, or approximately a mil-

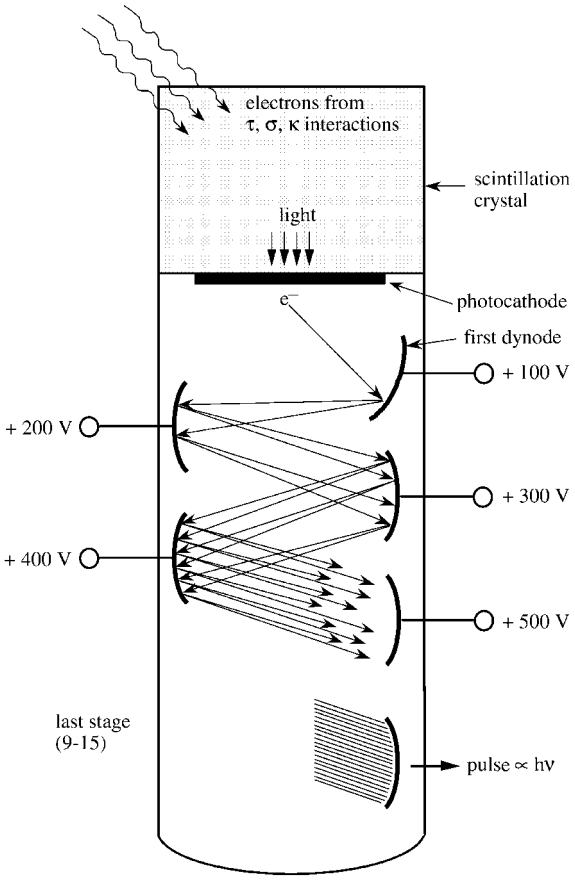

Fig. 12-3 Scintillation detector with associated photomultiplier tube.

lion. Each pulse leaving the 10th dynode is proportional to the amount of energy absorbed, which in turn is proportional to the energy of the photon striking the crystal. These pulses are sorted according to their size and stored in corresponding channels of a multichannel analyzer as counts, allowing the source to be identified by its unique gamma energy.

Sodium iodide crystals have a high efficiency for detecting gamma rays (because of their density and the large Z of iodine), and their pulse resolving time of about 0.25 μs permits their use for high count rates. Plastic scintillators have even shorter resolving times (several nanoseconds) but their detection efficiency for photons is low and the light output with energy is not linear resulting in spectra with poor resolution.

12.3 Semiconducting Detectors

The deposition of energy in a semiconducting material such as intrinsically pure germanium excites electrons from filled valence bands to conduction bands producing pairs of conduction electrons and electron vacancies, or holes. A bias voltage is applied across the semiconductor which causes these charge carriers to move, producing a current pulse. The energy needed to produce an electron–hole pair in a semiconductor is typically about 1 eV, which is considerably less than that required to produce ionizations in a scintillator; therefore, a relatively large number of charge carriers is produced for each photon absorbed. Consequently, the statistical fluctuations in the number of atoms excited or ionized is much less for a semiconductor detector, and when used with a multichannel analyzer very sharp peaks (high resolution) are obtained which allow energies to be determined very accurately. This technology has advanced to a stage that high-efficiency germanium detectors are routinely produced that provide excellent photon resolution (an example of a spectrum obtained with such a detector is shown in Figure 12-7).

Semiconductor detectors have several advantages over scintillators. They are very efficient in detecting photons because of their density, and produce fast pulses (typically a few nanoseconds) with excellent resolution. Germanium and lithium-drifted germanium, Ge(Li), detectors must be operated at liquid nitrogen temperatures to reduce thermal noise, which can be a disadvantage. Ge(Li) (sometimes called "jelly") detectors will quickly deteriorate if not stored at liquid nitrogen temperature due to unwanted drifting of the Li into the germanium matrix, and for this reason Ge(Li) detectors have been supplanted by intrinsically pure germanium detectors, which can be stored at room temperature between uses; however, they must be cooled during use.

Other semiconductor detectors are made of silicon with lithium additives to detect electrons and alpha particles, and when coupled with pulse height analyzers are used for spectral analysis. These detectors also provide excellent resolution and can be stored at room temperatures because the mobility of Li is less in Si than it is in Ge.

12.4
Gamma Spectroscopy

Gamma ray spectrometers use photon detectors designed to take advantage of the various absorptive processes in a high-Z medium to maximize sensitivity and provide spectral information about the photons being detected. The complexities of photon interactions are evident in the energy spectra of gamma emitters. The most distinctive features can be roughly divided as those that occur below the threshold for pair production ($h\nu \leq 1.022$ MeV) and those that occur above it.

12.4.1
Gamma-Ray Spectra: $h\nu \leq 1.022$ MeV

A crystal of NaI(Tl) is a commonly used scintillation detector that produces light scintillations that are proportional to absorbed photon energy. The light scintillations are due solely to ionizations and excitations produced by the electrons that are released when photons interact in the crystal. Being charged particles, virtually all of the electrons so released are absorbed in the crystal to produce an output pulse that corresponds to the amount of photon energy absorbed, thus counting the photons that interact and their energy. A typical NaI(Tl) detector/spectrometer is shown in Figure 12-4.

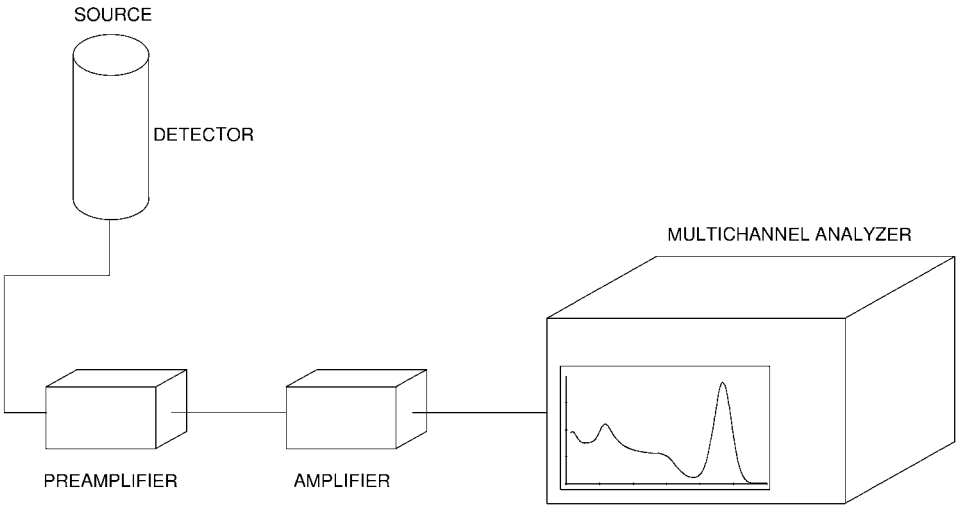

Fig. 12-4 Schematic of a NaI(Tl) photon detector/spectrometer.

The interaction probability of photons in NaI(Tl) is determined by the attenuation coefficient, which is dominated by the presence of high-Z iodine atoms. As shown in Figure 12-5, the photoelectric effect is the dominant interaction with the iodine atoms ($Z = 53$) in NaI at all energies up to about 250 keV. Some interactions occur in sodium, but with $Z = 11$ these are considerably less probable.

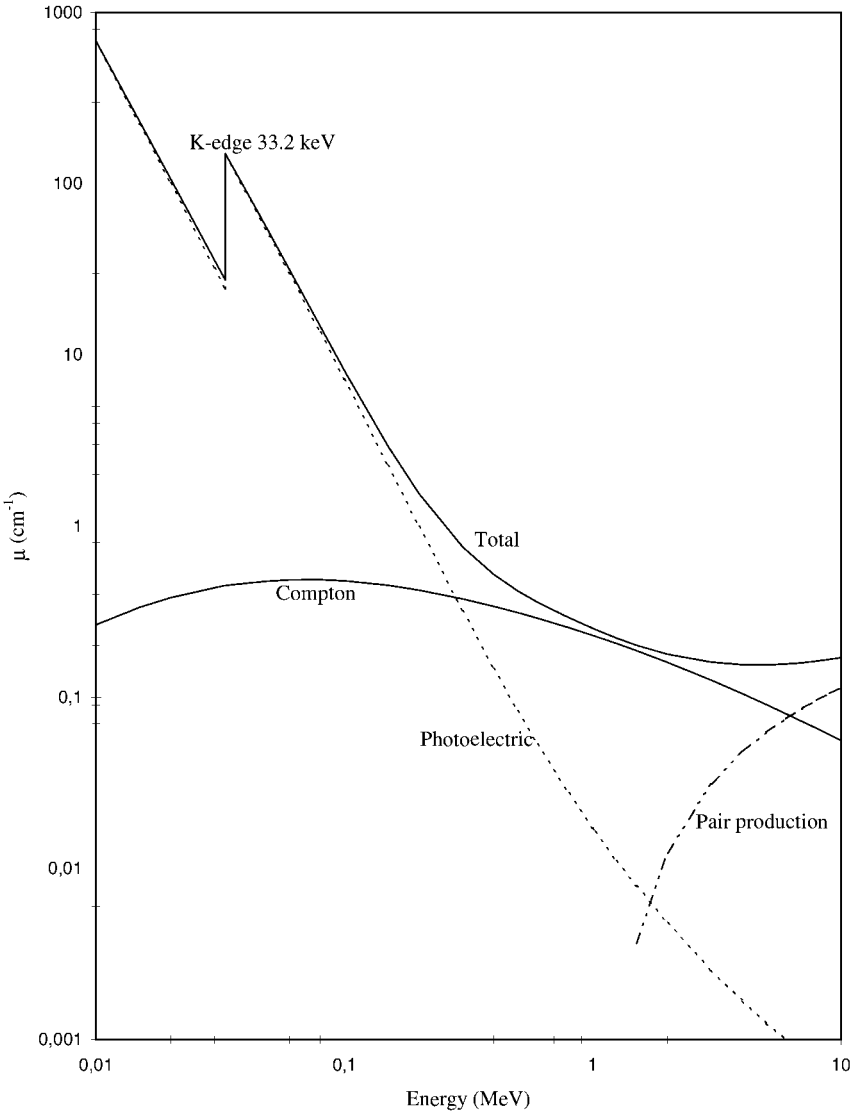

Fig. 12-5 Linear absorption coefficients for photons in sodium iodide.

Electrons ejected by photoelectric absorption will contain the photon energy minus 33.17 keV supplied to overcome the binding energy of K-shell electrons in iodine atoms. The orbital vacancy thus produced will be promptly filled followed by characteristic iodine x-rays. Since these are very soft, they are highly likely to be absorbed in the crystal by other photoelectric interactions. If all of these processes (absorption of the photoelectron and the subsequent photoelectron liberated by the K_a x-ray) take place within the luminous lifetime of the phosphor, the visible

light produced will correspond to that of the original photon energy $h\nu$. This in fact occurs for a large fraction of absorbed photons (determined by crystal size and efficiency) and yields a full-energy photopeak as illustrated in Figure 12-6 for ^{137}Cs.

The full-energy "photopeak" is the most prominent feature of the gamma ray spectrum. It is spread over several channels because the number of electrons produced in the photocathode of the photomultiplier tube is relatively small, and is subject to statistical fluctuations which are nearly normally distributed and serve to broaden the peak (Figure 12-6). About 12% of the energy of an incident photon will be deposited in NaI, and since each light photon produced will have an energy of about 3 eV the number of photoelectrons produced in the photocathode of the photomultiplier tube can be determined as well as the statistical fluctuation. As shown in Example 12-1, the number of photoelectrons produced will be relatively low, of the order of a few thousand.

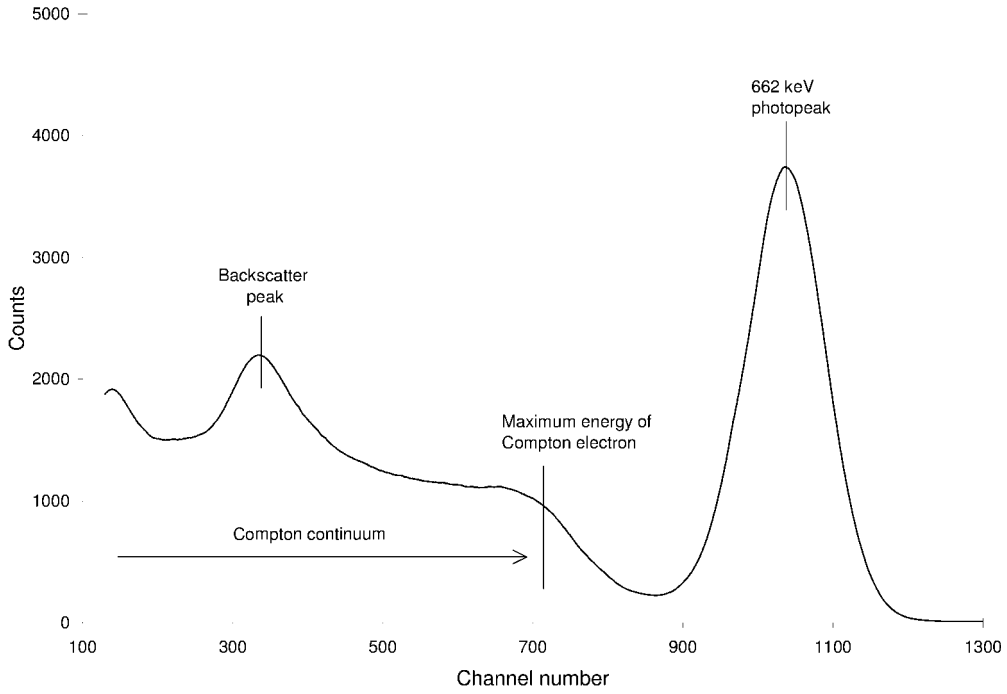

Fig. 12-6 Gamma ray spectrum obtained with a sodium iodide crystal exposed to 662 keV gamma rays of ^{137}Cs.

Example 12-1. For 0.364 MeV gamma rays from ^{131}I, determine the number of photoelectrons in NaI(Tl) for each gamma ray at the photocathode of the photomultiplier tube (see Figure 12-3). Assume a 12% scintillation efficiency, an average light photon energy of 3 eV, 25% loss of light photons in the crystal/photomultiplier assembly, and a conversion efficiency in the photocathode of 20%.

Solution. At 12% efficiency, a 0.364 MeV gamma ray will deposit 43,800 eV of energy in NaI yielding 14,600 light photons of 3 eV each, 11,000 of which strike the photocathode. Twenty percent (or 0.2) of these will produce photoelectrons in the photocathode, or

$$\text{No. of photoelectrons} = 11{,}000 \times 0.2 = 2200 \text{ photoelectrons}$$

Energy resolution of a gamma spectrometer is an important parameter. If the spread of the data points that make up a measured peak is small, then energy resolution is good and peak identification is reasonably accurate; if the spread is wide, then energy resolution is much less, perhaps even poor, and identification of the peak energy suffers. Qualitatively, sharp peaks have good resolution; wide peaks do not.

Energy resolution is defined as the ratio of the full width of the spectral energy peak measured at half the height of the peak center (both expressed as counts or a count rate) which is known as full width at half maximum (FWHM):

$$\text{Resolution} = \text{FWHM}/E_0$$

where E_0 is the energy value at the center of the peak and FWHM is the number of energy units encompassed by the peak measured at one-half the peak height. It is important to note that the peak height is determined as the net count (or count rate) above any background spectrum or Compton continuum upon which it may be superimposed.

Example 12-2. The centroid of a gamma peak obtained with a NaI(Tl) detector is observed at 0.662 MeV to have a height of 10,000 counts above the spectrum background at the peak. At a half-height of 5000 counts (FWHM) the peak width varies from 0.630 MeV to 0.694 MeV. What is the energy resolution?
Solution.

$$\text{Resolution} = \frac{\text{FWHM}}{E_0} = \frac{0.694 - 0.630}{0.662} = 0.097$$

or 9.7%. The energy resolution for NaI(Tl) detectors is usually in the range of a few percent because of the statistical variability due to the relatively small number of photoelectrons produced in the photocathode of the photomultiplier tube (the energy resolution of the peak in Figure 12-6 is about 9%).

By contrast, deposition of photon energy in a semiconductor produces ion pairs that are collected directly (i.e., without the need to produce light photons which in turn produce photoelectrons with inherent losses along the way). If the 0.364 MeV gamma rays in Example 12-1 were to be absorbed in germanium at about 1 eV per ion pair then about 360,000 electrons would be produced and collected. Statistical fluctuations in the energy peaks thus produced are much less in a semiconductor such as germanium and excellent resolution is obtained.

Prominent features of spectra for photons with $h\nu \leq 1.022$ MeV in NaI(Tl) are the Compton continuum, the Compton edge, a lead x-ray peak, and a backscatter peak. All are shown in Figure 12-6. Compton interactions, which are prominent in NaI(Tl) above about 250 keV (Figure 12-6) yield multistage processes each of which can produce light scintillations that enter the photomultplier tube either as separate events or summed in various combinations to produce features of the gamma spectrum. The Compton electron will be completely absorbed, and if the Compton-scattered photon is also absorbed in the crystal along with it, the light output will be due to the energy dissipated in both events and will correspond to the total energy of the photon, thus producing a pulse that appears in the full-energy photopeak. This is quite likely if the crystal is fairly large since many of the scattered photons will be of lower energy and photoelectric absorption is favorable. If, however, the Compton-scattered photon escapes from the crystal, the light output will correspond only to the energy transferred to the Compton electron. These electrons form a continuum of light scintillations and output pulses that are registered in the spectrometer (labeled as the Compton continuum in Figure 12-6). The energies range from zero up to the maximum that the photon in question can transfer to an electron in a Compton interaction which occurs when the photon is scattered backward towards the source or when $\theta = 180°$ in the equation for the energy of a Compton-ejected electron:

$$E_{ce} = h\nu \frac{a(1 - \cos\theta)}{1 + a(1 - \cos\theta)}$$

where $a = h\nu/m_0c^2$. When this happens the electron recoils along the original direction of the photon and will receive a maximum energy

$$E_{ce,\,max} = h\nu \frac{2a}{1 + 2a}$$

The Compton continuum drops off sharply at this maximum energy to form the "Compton edge." The ratio of the Compton continuum to the photopeak expresses this likelihood, which varies with each detector.

Compton interactions may also cause a "backscatter peak" to appear in the spectrum at an energy of about 0.25 MeV. This peak, which is also shown in Figure 12-6, occurs because some of the primary photons from a source miss the detector and are scattered from the tube mount and nearby shielding material. Because they must undergo large-angle scattering to reach the detector, the energy of these Compton backscattered photons approaches $m_0c^2/2$ or about 0.25 MeV, or slightly less. These lower energy backscattered photons are very likely to be detected separately by photoelectric interactions to produce a small backscatter peak near the low-energy end of the continuum.

A "lead x-ray peak" at about 88 keV is often observed in gamma spectra because most gamma detectors are shielded with lead. Primary photons from the source interact in the lead shield, as do cosmic rays and other background radiation. Since lead is a high-Z material, many of these photons are absorbed in lead atoms

by photoelectric interactions which are followed by the emission of 88 keV K_α x-rays which can exit the shield and be absorbed in the detector, thus producing a separate peak. Low background shields are often lined with copper and aluminum to absorb lead K_α x-rays; the K_α x-rays from copper and aluminum are low energy which generally do not penetrate the detector cover, or if they do so they appear very near the low-energy end of the spectrum.

The various interactions and the spectral results produced will be random events for any individual photon; however, the average effect of a large number of photon events for a given source/detector produces predictable and reproducible spectra. Such results allow photon sources to be identified and quantified with reasonable accuracy.

12.4.2 Gamma-Ray Spectra: $h\nu \geq 1.022$ MeV

More complicated spectra occur when the energy of the primary photon is sufficient to undergo absorption by pair production, i.e., $h\nu \geq 1.022$ MeV. If the detector is relatively large, the full-energy photopeak will be seen as usual, but other features will also be present as illustrated in the gamma spectrum of ^{24}Na (Figure 12-7), which was measured with an intrinsically pure germanium crystal. Sodium-24 emits two high-energy gamma rays at 1.369 and 2.754 MeV, both of which produce photopeaks at these energies in the gamma spectrum. Figure 12-7 also shows the excellent resolution provided by an intrinsically pure germanium detector, which is much larger than that obtained with a NaI(Tl) detector (as shown in Figure 12-8 for ^{22}Na).

All three of the primary photon interactions can occur for ^{24}Na gamma rays, but most interactions occur as Compton scattering or pair production since the photoelectric absorption coefficient in germanium is low for these high energies. When Compton interactions occur and all the processes following such interactions are completed within the luminous lifetime of the crystal, these will yield two photopeaks at 1.369 and 2.754 MeV. These peaks are produced by pulses corresponding to deposition of all of the energy of the photons by the various processes that can occur in the crystal. A Compton continuum of pulses produced by the absorption of the Compton electrons exists below each photopeak because some of the respective Compton-scattered photons are lost from the crystal and only the energy transferred to each ejected electron is absorbed and registered.

Pair production interactions are also prominent for the 1.369 and 2.754 MeV photons of ^{24}Na since they are well above the pair production threshold. When these occur, the total kinetic energy shared between the positron and electron pair ($h\nu - 1.022$ MeV) will be absorbed in the crystal followed by positron annihilation. If both of the annihilation photons are absorbed in the crystal, their energy adds to that of the absorbed electron pair and the pulse from the detector will correspond to the full energy of the original photon; the summation of these events will be registered in the full photopeak. Since the annihilation photons are fairly

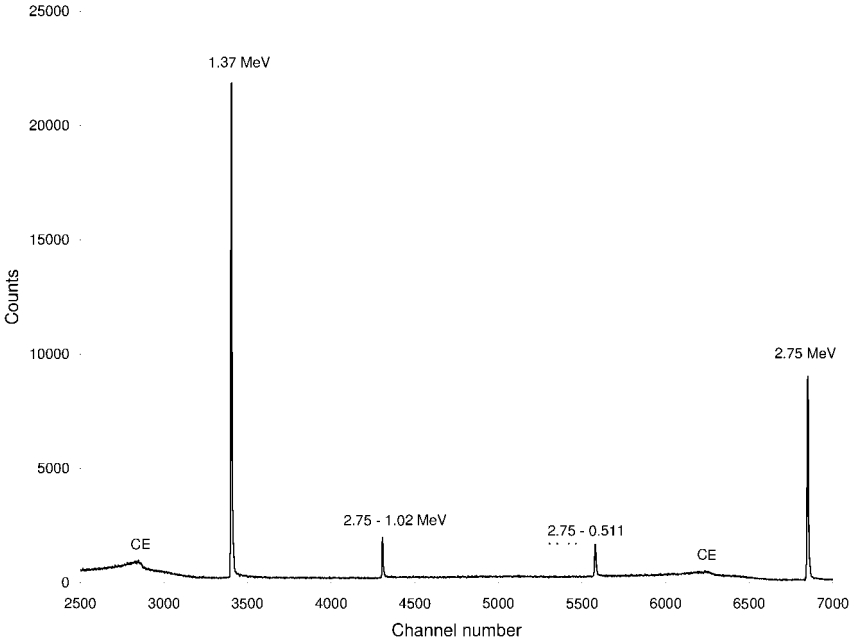

Fig. 12-7 Pulse height spectrum of ^{24}Na measured with a germanium detector with excellent resolution.

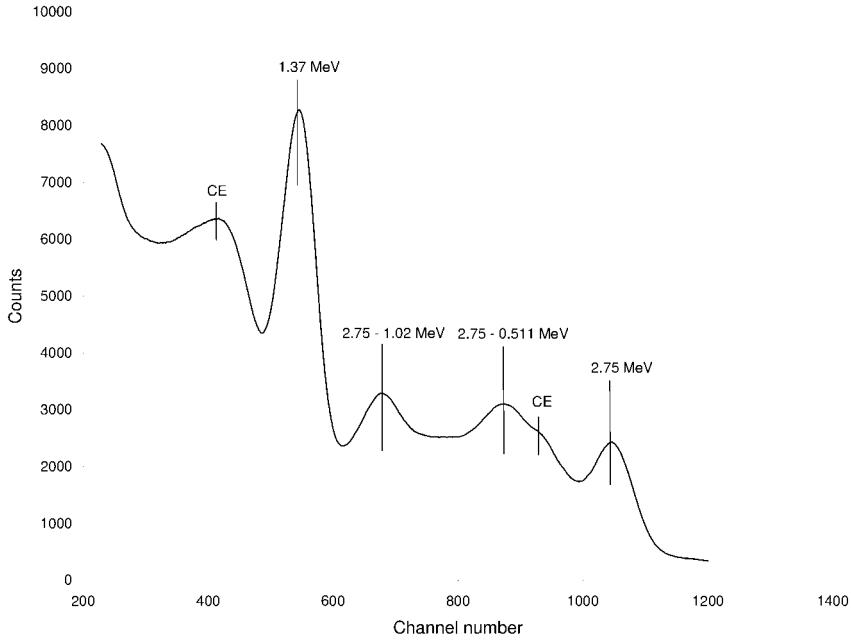

Fig. 12-8 Pulse height spectrum of ^{24}Na measured with a NaI(Tl) detector.

energetic at 0.511 MeV, one or both may escape the crystal such that this energy is absent in forming the photopeak.

Gamma emitters that produce pair production interactions also produce a strong peak at 0.511 MeV. This peak occurs because many of the photons emitted by the source will miss the crystal entirely and be absorbed in the shield around the crystal, and due to the 180° separation between the two annihilation photons thus produced, only one will strike the crystal and be detected.

12.4.3 Escape Peaks and Sum Peaks

Escape peaks are those peaks in a gamma spectrum that occur separate and distinct from the full-energy photopeak and are due to the net photon energy absorbed; i.e., the escape peak energy is that of the interacting photon minus that carried off by the "escaping" photon(s). The escape of annihilation photons following pair production interactions in a crystal causes the production of either a single escape peak or a double escape peak. If both of the annihilation photons escape from the crystal, a peak will be seen at an energy of $h\nu$ – 1.022 MeV. If only one of the 0.511 MeV photons escapes and the other is absorbed, a peak will occur at an energy of $h\nu$ – 0.511 MeV.

The peak shown in Figure 12-7 at 2.75 – 0.511 MeV is termed a single escape peak due to escape of one of the annihilation photons, and the one at 2.75 – 1.022 MeV is the double escape peak because both annihilation photons escape the detector without depositing energy. The Compton continuum in a gamma spectrum is also due to escape photons, but since Compton-scattered photons represent many energies an escape continuum is produced rather that an escape peak even though each point in the continuum is due to $h\nu$ minus the energy of the escaping Compton-scattered photon.

Escape peaks are distinct, but they do not represent primary photon energies and do not enter into the primary identification of the gamma emitter; they are only observable consequences of the patterns of photon interactions and losses in the detector itself. Consequently, their size and shape are unique features of an individual detector system because their patterns of interaction and detection are determined by the size and configuration of the detector system which can be quite variable. Detector size has perhaps the greatest influence on whether secondary photons escape detection.

Characteristic x-ray escape peaks may be observed when detectors are quite small and photon energies are low, say <0.5 MeV or so, where photoelectric interactions are dominant. For low-energy photons and small NaI(Tl) detectors, the 33.17 keV characteristic x-rays produced in iodine atoms may well leave the detector such that the actual photon energy deposited is at $h\nu$ – 0.033 MeV; thus, an "iodine escape peak" is produced below the full-energy photopeak at $h\nu$ – 0.033 MeV. By a similar process a "germanium escape peak" can occur for low-energy photons in a small germanium detector at $h\nu$ – 0.011 MeV.

Sum peaks are another feature of gamma ray spectra. These are produced when two or more photons are emitted in quick succession such that they are absorbed within the luminous lifetime of the crystal (i.e., simultaneously, or very nearly so). When this happens they are recorded as a single event but at an energy equal to the sum of the two energies. Sum peaks are often observed for high-activity sources that emit two or more photons per transformation, or for photon sources with $h\nu \geq 1.022$ MeV which yield annihilation photons; these peaks will be much smaller than the photopeaks since they depend upon the simultaneous detection in coincidence of two emission events which is much less probable.

12.4.4
Gamma Spectroscopy of Positron Emitters

Positron emitters that also emit gamma rays produce gamma spectra with distinct features and other complexities. These additional features are illustrated in Figure 12-9 in the spectrum for ^{22}Na, which emits positrons followed by emission of a 1.275 MeV gamma ray.

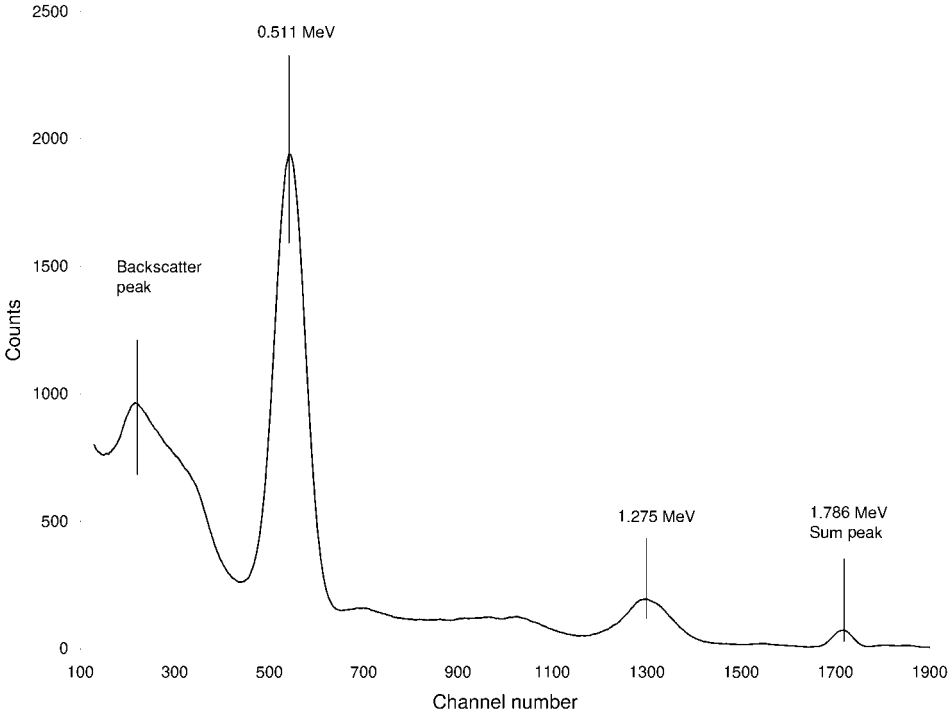

Fig. 12-9 Gamma ray spectrum of ^{22}Na measured with a NaI(Tl) detector. The spectrum shows the typical 0.511 MeV annihilation peak of a positron emitter, the photopeak of the 1.275 MeV gamma ray emitted, a sum peak, the Compton continuum, and the backscatter peak.

A positron emitter will always show a peak at 0.511 MeV due to the annihilation of the positron. The strong peak at 0.511 MeV occurs because most of the annihilation events occur within the source itself, outside the crystal, or at the surface of the crystal where the positrons are absorbed. Since the annihilation photons are emitted 180° from each other, only one of them is likely to be absorbed in the crystal and thus it will be detected as a separate event with an energy of 0.511 MeV. The Compton continuum also occurs below the 0.511 MeV photopeak (and the 1.275 MeV photopeak as well), as does the usual backscatter peak, and if two annihilation peaks are detected simultaneously a sum peak at 1.022 MeV will be produced.

The 1.275 MeV gamma ray of ^{22}Na will also be detected by photoelectric, Compton, and pair production interactions. If the sequence of electron-producing events for each interaction all occur within the luminous lifetime of the crystal, the pulses will produce a photopeak at 1.275 MeV, as shown in Figure 12-9. If these events are detected simultaneously with an annihilation photon, a small sum peak will be produced at 1.786 MeV due to the reduced probability of both sequences occurring simultaneously. This sum peak is evident in the spectrum shown in Figure 12-9, in addition to the strong peak at 0.511 MeV produced when ^{22}Na positrons are annihilated and the full energy photopeak produced by the 1.275 MeV gamma rays.

12.5 Portable Field Instruments

The general principles of radiation detection discussed above can be incorporated into portable field instruments, and instruments based on GM detectors, proportional counting, and ionization are available. The portability of such instruments makes field measurements convenient and reliable, though with differing degrees of sensitivity compared to laboratory instruments where greater shielding of detectors is practicable.

12.5.1 Geiger Counters

Geiger counters, especially with pancake probes, are very useful for general surveys of personnel contamination, area contamination, and the presence of external radiation fields (see Figure 12-10). In making personnel surveys, the GM probe should normally be moved slowly to allow time for the instrument to respond. An energy correction factor may need to be applied to GM measured readings if the photon field contains a large fraction of low-energy gamma rays because it will overrespond in this region because the photoelectric cross-section is high for low-energy photons. The shield assembly provided by the manufacturer flattens out this overresponse by selectively filtering out lower energy photons more than medium energy photons, and the instrument should be used

with the shield closed when low-energy photons are dominant. GM detectors should be used with care in high exposure fields because they can saturate yielding a reading near zero when in fact the exposure rate is well above the highest range on the survey meter. In such circumstances, an ion chamber should be used.

Fig. 12-10 Geiger counter with a thin "beta window."

12.5.2 Ion Chambers

Ion chambers have a very flat energy response for gamma ray measurements, and although they are less sensitive than the Geiger counter, they respond correctly in much higher fields. They are, however, subject to *zero drift*, especially on the more sensitive ranges; therefore, they are provided with a control to set the meter scale to zero before an exposure is read.

A typical ion chamber survey instrument contains a chamber of about 200 cm^3 filled with ambient air, though other gases can be used. The chamber is sealed at one end with aluminized mylar with a density thickness of 7 mg/cm^2 and a sliding plastic shield is provided to protect the mylar window. The sliding shield is commonly made of phenolic plastic (ρ = 1.25) about 0.34 cm thick which has a density thickness of about 0.439 g/cm^2 which stops all beta particles of energy below about 1 MeV (see Figure 12-12). When operated with the shield closed, only gamma radiation and high-energy beta particles are detected; when the shield is open beta particles of sufficient energy to penetrate the dead skin layer are detected as well as gamma radiation. These features allow detection of mixed fields of gamma and beta emitters when both are present which they often are, especially in various nuclear facilities. As a practical matter, the gamma reading should be significantly smaller than the beta + gamma reading or else large uncertainties are introduced.

The basic survey procedure is to take two readings: one with the window open and the other with the window closed. The beta component can then be deter-

mined by subtraction of the gamma reading (taken with the cap on) from the open window reading. The open window reading may need to be adjusted to account for the energies of the beta particles and the density of air in the chamber due to atmospheric pressure changes, but this is usually a minor effect except perhaps at high altitudes. If the ion chamber is exposed to a highly collimated beam of radiation so that only part of the chamber volume is irradiated, the instrument will read low by an amount equal to the ratio of the volume exposed to the total chamber volume.

12.5.3 Microrem Meters

Microrem meters are used to obtain accurate measurements of low-level gamma radiation (e.g., near background level). Commercial microrem survey meters use a scintillation crystal as the detector to increase sensitivity, and these are typically about 10 times more sensitive than commercial Geiger counters. The microrem meter consists of a suitable phosphor, which is optically coupled to a photomultiplier tube, which in turn is connected to an electronic circuit. If the counter is used simply to detect radiation, the output circuit often consists of a battery-operated power supply, an amplifier and pulse shaper, and a rate meter. If the device is used for energy analysis, the output circuit includes a pulse-height analyzer and a scaler and can be operated as a single or multichannel analyzer.

12.5.4 Alpha Radiation Monitoring

Generally, alpha radiation is only encountered as a result of surface contamination or in the form of airborne particulates, both of which may be taken internally by workers or others. Two types of instruments are in practical use for locating surface contamination: the portable proportional counter and a portable scintillation counter. Ion chamber survey meters with thin windows can also be used, but since they also respond to both photons and beta particles, they are best used for monitoring sources of pure alpha emitters.

Portable alpha proportional counters are of two types: one uses air at ambient pressure as the counting gas while the other is supplied by propane gas, usually by a small cylinder attached to the counter. Both must have an extremely thin window in order for the alpha particles to penetrate to the sensitive region of the detector; they also require special discriminator circuits, very stable high-voltage supplies, and, in some cases, very sensitive amplifiers. Alpha particles produce a rather large electrical pulse in a proportional counter and good discrimination is possible against beta and gamma ray interference or fast neutrons, if present. Such interference can be detected by simply moving the alpha probe about 10 cm away from the surface being monitored; if the counts cease, then they are due to true alpha contamination.

An air-proportional counter does not require the gas cylinder and associated plumbing necessary for a propane proportional counter; consequently, it is lighter and less cumbersome to set up and use though it is generally less efficient and sensitive to changes in humidity, a condition that is avoided with the propane counter. The propane regulator and needle valve tend to plug up after long use, and the counter is not suitable for monitoring large quantities of plutonium because the propane released can be a hazard since plutonium is pyrophoric.

Alpha scintillation counters use a silver-activated zinc sulfate, ZnS(Ag), phosphor that is quite sensitive to alpha particles; however, it is less rugged than either the air- or propane-proportional counters because of the fragile photomultiplier assembly (see Figure 12-11). It does have good detection efficiency, ranking between the air-proportional counter and the propane-proportional counter.

Fig. 12-11 Portable alpha scintillation counter.

A ZnS alpha probe has a sensitive area of about 50 cm^2 and a total efficiency ((c/m)/(d/m)) of 25%; thus, 100 d/m spread uniformly over 100 cm^2 will produce a count rate of about 12 counts per minute. In a practical sense, alpha monitoring of a large area must be done slowly and carefully because the meter will not have time to respond to a small spot of contamination, a circumstance that can be overcome somewhat by using earphone or an audio output.

12.5.5 Beta Radiation Surveys

The proper instrument for measuring the beta dose rate is a thin-window ion chamber because it responds to actual energy deposited and the electrical signal produced is directly proportional to the energy deposited in the chamber gas. These instruments can be converted for use in gamma surveys by covering the window with a shield cap (see Figure 12-12). The Geiger counter cannot quantita-

tively measure the dose rate or the dose equivalent rate in a beta field although it can be used to detect the presence of beta radiation.

Ion chamber instruments are usually calibrated for photons rather than beta particles; therefore, it is necessary to multiply the ion chamber reading by a beta correction factor CF (expressed in units of mrad/mR) to obtain surface contact beta dose rates. The actual CFs for beta surface contamination depend on the chamber geometry (size and shape), the chamber wall thickness, and the size of the beta source; small spots of beta contamination require CFs substantially greater than unity.

Fig. 12-12 Portable ion chamber instrument with a removable beta shield cap.

12.5.6 Removable Radioactive Surface Contamination

The smear, swipe, or wipe test is universally used to measure removable surface contamination whereas survey instrument measurements of alpha, beta, and/or gamma surface contamination include the total contamination whether fixed or removable. In the usual technique a surface area of 100 cm^2 is swiped by a cloth, paper, plastic, foam, or fiberglass disk. These smears are in turn counted for alpha contamination or higher energy beta emitters in a gas flow proportional counter, or for gamma contamination with a scintillation or semiconductor detector. Low-energy beta emitters such as tritium or ^{14}C are counted in liquid scintillation counters, which can be used to count other beta emitters, and with appropriate adjustment, alpha emitters as well.

12.5.7 Instrument Calibration

Calibration of an instrument involves a determination of its response or reading relative to a series of known radiation values covering the range of the instrument, and adjusting the instrument to provide a correct response. Three levels of "calibration" are generally recognized. These include a full characterization (usually done by the instrument manufacturer), a calibration for specific, perhaps unusual, conditions, and a routine calibration for normal working conditions using an appropriate source.

In general, two approaches are used in the calibration of portable instruments. A radiation field produced by a standard source calibrated by the National Institute of Standards and Technology (NIST) can be used, or the field can be measured with an instrument that is a secondary standard. A secondary (or "transfer") standard instrument is an instrument that has been calibrated by comparison with a national standard by placing the instrument in the radiation field and noting the response. The instrument to be calibrated is then substituted for the original instrument, and calibration is based upon a comparison of the two readings.

Ion chambers and GM counters are calibrated with ^{60}Co, ^{137}Cs, and ^{226}Ra to provide a known exposure rate at distances that allow the source to be treated as a point source. Calibration of ion chambers requires uniform irradiation of the detector volume; therefore, the distance between the source and the calibration point should be at least three times the chamber's longest dimension which should be perpendicular to the source.

12.6 Personnel Dosimeters

Personnel dosimeters consist of film badges which contain photographic film or thermoluminescent dosimeters (TLDs) to measure the radiation dose received by persons over a period of time, usually a month or a quarter. For short-term monitoring of work, a pocket ion chamber dosimeter is worn or an electronic dosimeter. Electronic dosimeters can be useful for this purpose because they can be set to indicate an alert or warning level of exposure.

12.6.1 Film Badges

Film badges continue to be used in personnel monitoring because they are relatively inexpensive, the processed film provides a permanent record, and they provide sufficient accuracy to meet accreditation requirements, especially for x-rays and gamma radiation. Film badges use dental x-ray film shielded in places (called windows) by thin absorbers to distinguish beta rays from gamma radiation. An unshielded area (the "open window") gives the total dose from beta and gamma

rays and this can be apportioned by the amount of film density behind the shielded strip. Double emulsion film is used for high sensitivity (in the mR range); and conversely high-range film is made with a single emulsion. Film can also be used to measure neutrons if the film is impregnated or covered with a material such as lithium or boron which readily absorbs neutrons.

The response of film is independent of energy above 200 keV or so; however, at low photon energies, the film may overrespond by as much as a factor of 20–40. With proper calibration and appropriate corrections for low-energy response, the film badge can report doses from about 0.1 mSv (10 mrem) to about 10 Sv (1000 rem).

12.6.2 Thermoluminescence Dosimeters (TLDs)

The phenomenon of thermoluminescence (TL) was rediscovered in the 1960s and was perfected as a dosimetry technique in the 1970s when is was found that the chemical makeup of lithium fluoride (LiF) or calcium fluoride (CaF_2) phosphors could be made uniform by good quality control.

As indicated in Figure 12-13, exposure of a TLD to radiation causes electrons to be excited to the conduction band from which they can fall into one of the isolated levels provided by impurities in the crystal and be "trapped"; they will remain so until energy is supplied (usually by heat) to free it. Heating the crystal elevates the trapped electrons back to the conduction band, and when they return to a valence "hole," a photon of visible light is emitted. The total light emitted is a measure of the number of trapped electrons and therefore of the total absorbed radiation even after months of storage. TLDs are aptly named because thermal heating (thermo-) produces luminescence emitted by the crystal. TLDs are generally more accurate than film badges, are less subject to fading, are usable over a much larger range of radiation levels, can be used over and over, and processing does not require film development but can be done by a one-step electronic reader.

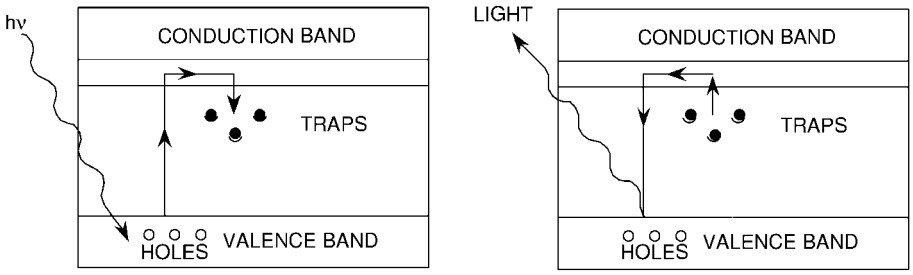

Fig. 12-13 Energy level diagram of a TLD crystal. Absorption of radiation excites valence electrons up to electron "traps" thus storing information on the amount of radiation absorbed; heating the TLD de-excites the trapped electrons with the emission of light photons with intensity that is proportional to the amount of radiation absorbed.

The TLD phosphor can be reset by heating it to a high temperature to release all trapped electrons, a process known as *annealing*. After proper annealing, the phosphor has the same sensitivity as previously, so it can be reused as a dosimeter, which offers some advantage versus film. This feature can be a disadvantage because once the traps release their electrons, the information is lost; however, the glow curve from the TLD reader can be stored electronically or run out on a strip chart recorder to provide a permanent record if such is required or desirable.

12.6.3 Pocket Dosimeters

The pocket dosimeter, often used in conjunction with a TLD or film badge, is a small electroscope, about the size and shape of a fountain pen. The dosimeter is usually fitted with an eyepiece and a calibrated scale so that an individual user can read the amount of exposure received. The dosimeter is charged before use and exposure to radiation causes it to lose charge proportional to the radiation exposure received. Since any leakage of charge produces a reading, good insulation of the electrode is needed. The response of the dosimeter is seldom linear, except in the region of the calibrated scale; therefore, exposures should not be estimated if the device reads slightly above the full-scale reading. When reading the dosimeter the fiber image should be vertical to reduce the geotropic effect, the tendency to give a reading that depends on the orientation of the device.

12.7 Laboratory Instruments

12.7.1 Liquid Scintillation Analysis

Liquid scintillation analysis (LSA) of samples is achieved by mixing the radioactive sample into a liquid scintillant made up of chemicals that produce visible light when radiation is absorbed. Liquid scintillation solutions contain low-Z materials (typically $Z = 6–8$), and consequently have relatively low counting efficiency for x-rays and gamma rays above 40 keV or so. On the other hand, good efficiency is obtained for low-energy x-rays and gamma rays and especially so for most beta particles because of their short range in liquids. The liquid scintillation counter (LSC) is often the best, and perhaps the only practical detector for measuring low-energy beta emitters such as ^{3}H and ^{14}C. It is also useful for measuring beta-emitting radionuclides on wipe and leak test samples.

Liquid scintillation counting is done by placing a sample and the scintillating chemicals into vials that transmit light. The light flashes, which are proportional to the energy of the radiation source, are measured by one or more photomultiplier (PM) tubes as shown in Figure 12-14 for two PM tubes. These are placed in a darkened chamber with a tight lid made of materials that excludes ultraviolet radi-

ation so that only the light produced by the sample is observed. Background electronic noise due to thermal emission of electrons from the photocathode of the PM tube can be significant, and thus it also is essential to use low-noise PM tubes with coincidence circuitry to eliminate extraneous pulses electronically. This is done by coincidence detection using two PM tubes placed 180° apart as shown in Figure 12-14. Optical reflectors around the counting vials direct the emitted light produced in the liquid scintillant to the two PM tubes with outputs routed to a coincidence circuit that accepts only those pulses that arrive simultaneously (Figure 12-14). Since the light emitted from a radiation event will be reflected into both PM tubes two pulses are produced in coincidence and the event will be detected and registered; thermal noise that occurs randomly in the PM tube photocathode will produce only a single pulse and will be rejected.

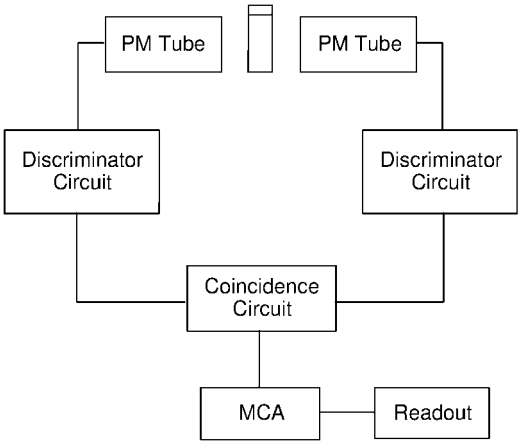

Fig. 12-14 Schematic of a liquid scintillation counter in which two photomultiplier tubes measure light produced by absorption of emitted radiations in the liquid scintillation sample. The signals from each of the PM tubes pass through discriminators and are registered as a function of energy if they arrive in coincidence; if not the signal is presumed to be noise and is rejected.

The signal from the PM tubes is proportional to the light energy collected which in turn is directly proportional to the radiation energy absorbed; thus the pulses that are produced can be sorted to produce a spectrum. Most modern LSCs have several thousand channels and the data can be accumulated and displayed electronically as well as plotted. With appropriate calibration, the endpoint beta energy or $E_{\beta\max}$ can be determined and this is often a good determinant of the radionuclide. Another technique is to compare the spectrum obtained with reference spectra obtained with pure standards, many of which have unique shapes. For example, a full spectrum of ^{137}Cs will show the sharp conversion electron peak above the continuous spectrum of beta particles (see Figure 3-22) and a ^{60}Co spectrum will show a unique feature at the upper energies due to absorption of its gamma rays.

Two or more beta emitters in a sample can be identified and quantified in the presence of each other. The spectrum obtained is the sum of both as shown in Figure 12-15 for tritium and ^{14}C, and the counts from each beta emitter can be accumulated by setting appropriate energy windows. This approach requires counting of a standard of each radionuclide to set the energy window, determining the counting efficiency in each set window, and determining the fractional overlap of each into the other window so that it may be subtracted as shown in Example 12-3.

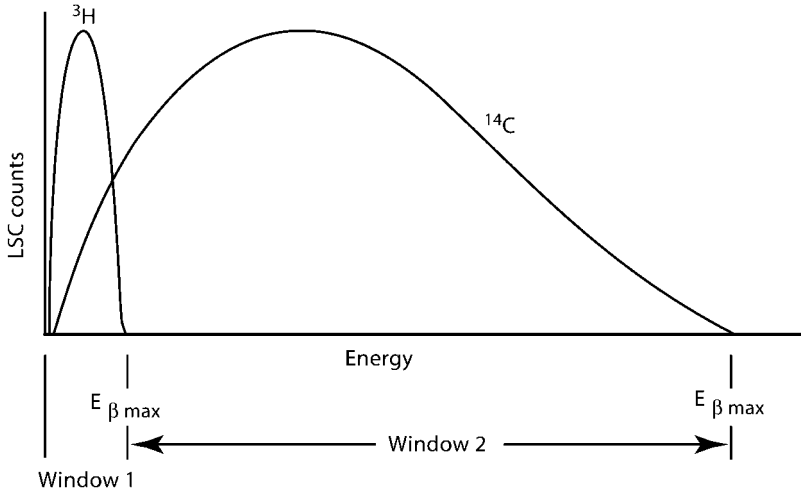

Fig. 12-15 Typical beta spectra of ^{3}H and ^{14}C obtained by liquid scintillation counting.

Example 12-3. A mixed sample containing ^{3}H and ^{14}C is counted in an LSC system with two window settings with upper level discriminator settings just above 18.6 keV for ^{3}H beta particles and 156 keV for ^{14}C beta particles. The measured counting efficiencies are 36% for the ^{3}H window and 80% for ^{14}C, and it is determined that 8% of the counts observed from a ^{14}C standard will be registered in the ^{3}H window. A sample that contains both ^{3}H and ^{14}C is counted with a net (minus background) count rate of 2000 c/m in the ^{3}H window and 6000 c/m in the ^{14}C window. Determine the activity of each in the sample.

Solution. First, subtract the number of counts in the ^{3}H window due to the spectral distribution of ^{14}C counts:

$$^{3}H \text{ (net c/m)} = 2000 - (0.08)6000 = 1520 \text{ c/m}$$

And since ^{3}H beta particles are not energetic enough to exceed the lower setting of the ^{14}C window, the net count rate for ^{14}C is 6000 c/m. The activity of each is

^{3}H (t/m) = 1520/0.36 = 4222 t/m

^{14}C (t/m) = 6000/0.80 = 7500 t/m

The spectral analysis method shown in Example 12-3 can be developed and used, with appropriate standards and technique, for various other beta-emitting radionuclides.

Sample quenching, which is the term applied to any process which reduces the emitted light output, is a major consideration in liquid scintillation counting. There are two general subclasses: chemical and optical quenching. The effect of sample quench, as shown in Figure 12-16, is to shift the beta spectrum toward lower energies and thus reduce the overall number of counts observed. This problem is dealt with by measuring the amount of quench and applying a "quench correction" to the counter results.

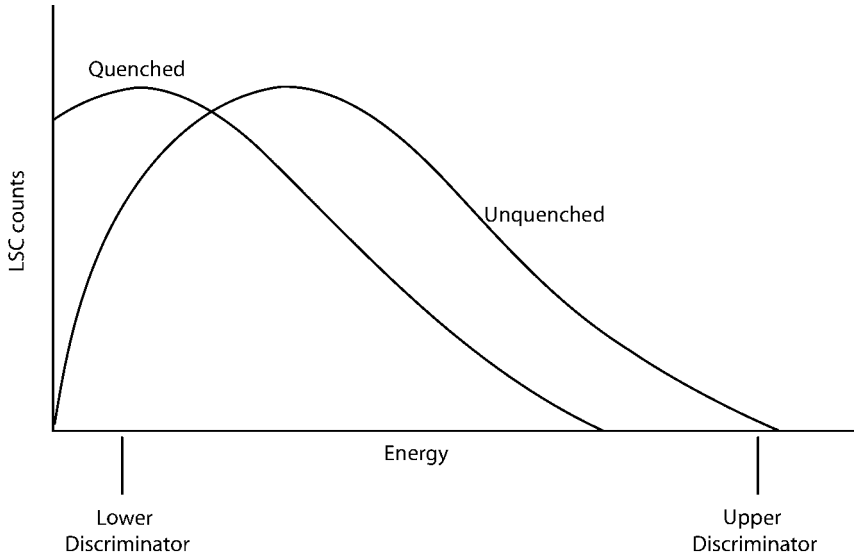

Fig. 12-16 Effect of sample quench in liquid scintillation counting is to lower the number of counts observed in a set window.

Sample quench can be minimized by ensuring good mixing of the sample in the liquid scintillant. If incompatible liquids are used the sample may phase-separate and accurate quantitation will be difficult. Use of a small sample volume can reduce this phenomenon, but may not eliminate it; therefore, each sample should be examined before counting.

The amount of quench in each sample is usually measured by briefly exposing it to a high-activity radiation standard (e.g., ^{133}Ba) located next to the sample chamber. The measured light output produced by such exposure is calculated as a

"quench number," which has been given various designations by equipment manufacturers. A plot of a series of such measurements made on a known quantity of sample yields a quench curve of counter efficiency versus quench number that is in turn used to adjust the count rate for each sample to the true count rate. The known sample is mixed with distilled water, added to the LSC cocktail and counted. A chemical contaminant such as carbon tetrachloride is then added to the "known" in the LSC cocktail in increasing amounts and the quench number and count rate are recorded and plotted to produce the quench curve. Modern LSC instruments can store quench correction curves and such corrections can be made electronically to increase the number of recorded counts to those that would have been recorded if quench losses had not occurred.

12.7.2 Proportional Counters

Gas proportional counters take advantage of the amplification obtained when radiation is absorbed in the counting gas to provide good sensitivity as well as to discriminate charged particles on the basis of the proportional pulse sizes produced; e.g., beta emitters from alpha emitters. Because of these factors and their relatively poor sensitivity to x-rays and gamma radiation, proportional counters are used primarily for counting charged particles, principally beta particles, alpha particles, or one in the presence of the other. A hemispherical counting chamber (Figure 12-17) with a central electrode, or anode, usually in the form of a small wire loop, is used that encloses an optimal counting gas in intimate contact with the sample to be counted. The electric field changes rapidly with distance in the immediate

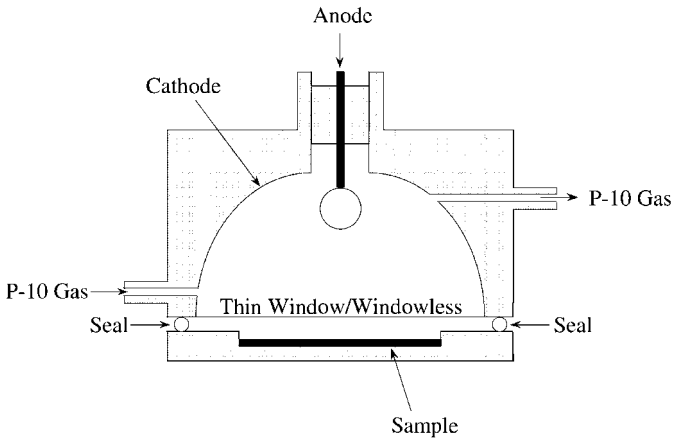

Fig. 12-17 A 2π proportional counter with a window; if used without a window in either 2π or 4π geometry, it is necessary to provide a mechanism to reseal the chamber after samples are inserted and to provide rapid flushing with the counting gas to replace any outside air.

vicinity of the anode, and most of the amplification occurs in the vicinity of the anode wire. In this configuration (typically referred to as a "2π chamber" or "2π geometry"), the counter may be windowless, or more typically it will have a thin window such that the sample to be counted is placed just outside the window. Both designs have advantages and disadvantages in terms of sensitivity and control of contamination.

Proportional counters have good counting efficiency and can be used at very high counting rates because the negative ions, which are moving in the most intense field in the counter, have to move only a few mean free paths to be collected. The movement of the negative ions is little influenced by the presence of the positive ions. When operated in the proportional region, secondary electrons are formed in the immediate vicinity of the primaries produced by the incoming radiation as it is absorbed, and with a typical gas amplification of 10^3, the absorption of an alpha particle might lead to a pulse containing 10^8 ions, while a pulse initiated by a beta particle or a gamma ray would contain more nearly 10^5 ions. These pulses are in turn amplified to a desired output level, but the relative pulse sizes remain the same and a discriminator can be set to reject all pulses below some desired level allowing alpha particles to be counted in the presence of beta and gamma radiation. These characteristics lead to different degrees of amplification versus detector voltage for alpha particles and beta particles, producing two distinct "plateaus" for counter operation as shown in Figure 12-18. The counter can be operated to just detect alpha particles or at a higher voltage to detect both alpha particles and beta particles. Electronic circuitry can be used to register one or the other or both.

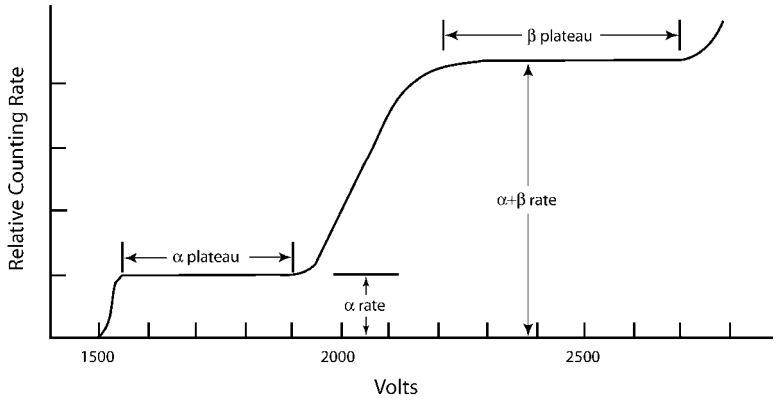

Fig. 12-18 Response of a proportional counter versus applied voltage showing a voltage plateau for counting energetic alpha particles and a much higher voltage plateau for beta particles. Whereas beta particles, because of insufficient energy, are not registered in the alpha counter region, both are registered when the counter is operated in the beta particle region; however, the sizes of the pulses are significantly different and can be sorted electronically for a separate alpha count in the alpha region where beta particles are excluded and subtracted from the beta plus alpha count.

Proportional counting is usually done at atmospheric pressure because the voltages, which range from 1000 to 5000 V, present no technical problems and there are advantages to a counter that can be readily opened for the insertion of samples, a necessity for windowless counters. If a windowless chamber is used, it is necessary to provide a mechanism to reseal the chamber after samples are inserted. This is usually done by causing the sample tray to press against an o-ring or similar sealing device when the sample holder brings the sample into the detector volume (or under it for a thin-window detector). It is also necessary to flush the windowless chamber with counting gas to ensure that no outside air remains in the chamber. A detector with a window does not require flushing since a steady gas flow is maintained; however, the window must be quite thin to minimize absorption of alpha and beta particles.

Various gases and mixtures are suitable for proportional counting but a mixture of 90% argon and 10% methane is often used. Argon has good performance because of its high density but it has long-lived excited states which may trigger spurious discharges; therefore, methane is added to counteract these. The 90% argon–10% methane mixture is known as P-10 gas.

Windowless proportional counters can be used to eliminate absorption of particles to be counted, and they are essential for proportional counting of very low-energy beta emitters. If 4π geometry is used, the chamber volume is a complete sphere, typically with two anode loops. The sample is placed on a thin suspension in the center, and in a double chamber with a suitable sample mount, essentially all of the particles emitted will be counted. Such counters are used in absolute counting where it is necessary to determine the absolute disintegration rate of a radioactive sample. Consequently, 4π measurements are a special technique and are generally used primarily for standardization of sources.

Contamination of the windowless chamber surfaces can be problematic because the surfaces are much more difficult to clean should they become contaminated. This can be controlled to some extent by ensuring that the sample remains fixed, perhaps by a fixative of some type. After a sample is in position in the chamber volume, the counter is flushed rapidly with the counting gas until any room air inside the chamber has been displaced. After stable counting conditions have been established, the gas flow can be reduced to provide a slight positive pressure in the chamber to prevent the inward diffusion of room air.

12.7.3
End-window GM Counters

A laboratory version of the GM counter is used for counting various samples such as smears or determining beta particle absorption. The GM tube has been replaced in many applications by newer devices because of its inability to distinguish between radiations. It was, however, the first practical detector used in the development of radiation physics and is still widely used.

The GM counter can be made quite sensitive for laboratory conditions by providing a stable mount for a high-quality thin-window GM tube and enclosing it in

a shield to both reduce background radiation and provide physical protection of the GM tube itself. Samples are placed just below the end window and the output routed to a scaler unit, often with a timer, to record the counts. The operating voltage is set in the GM plateau region (see Figure 12-2) and the counter is usually calibrated for efficiency with a medium energy beta source, or a standard of the radionuclide that is routinely counted. Such systems provide good sensitivity for routine counting of many types of samples.

12.7.4 Surface Barrier Detectors

Specially constructed silicon surface barrier semiconductors are used for alpha and beta spectroscopy. A pure silicon crystal will normally have an equal number of electrons and holes, but impurities can be added to create an excess number of electrons (an n-region) or an excess number of holes (a p-region). Silicon (and germanium) is in group IV of the periodic table. If atoms of group V, each of which has five valence electrons, are added, four of the five electrons in each of the added atoms will be shared by silicon atoms to form a covalent bond. The fifth electron from the impurity is thus an excess electron and is free to move about in the crystal and to participate in the flow of electric current. Similarly, adding an impurity from group III with three valence electrons creates bonds with a missing electron, or hole: a p-type crystal.

Surface barrier detectors are constructed to provide a junction between an n-type and a p-type crystal. When a voltage bias is applied to a silicon layered crystal with an n–p junction, the excess electrons are swept in one direction and the "holes" in the opposite direction. This creates a depletion layer between the two that is nonconducting. If, however, an alpha (or beta) particle is absorbed in the depletion layer, it creates numerous charge pairs by ionizing silicon atoms and these migrate quickly to create a pulse. The size of the pulse is directly proportional to the energy deposited and can be processed electronically to provide a spectrum for identification and quantification of the source. A large number of charge units is produced because only 1 eV or so is required to ionize silicon; thus excellent resolution is obtained because the statistical fluctuation of the collected ions is minimal.

The depletion layer can be constructed just thick enough to equal the maximum range of the particles to be detected, and thus minimize interference by other types of radiation. A detector with a very thin depletion layer is used for alpha spectroscopy, and these detectors have essentially zero background since the probability of photon interactions is minimal. Beta spectroscopy is achieved by increasing the depletion layer, and both alpha and beta particles will be detected with such a detector. When used for alpha spectroscopy, silicon surface barrier detectors provide good energy resolution because alpha particles are emitted monoenergetically. Any self-absorption of the alpha particles in the source will degrade their energy before they reach the detector, and only the energy actually deposited will be recorded; therefore, sharp peaks will only be attained if the alpha source is

deposited in a thin layer to minimize self-absorption. Beta particles, which are less subject to self-absorption, will be detected and displayed as a continuous energy spectrum up to $E_{\beta\max}$ because of the mode of beta transformation. Since no peaks will be formed, except perhaps for conversion elections activated with gamma emission (e.g., ^{137}Cs), beta spectroscopy with silicon detectors must be done with the entire spectrum as in liquid scintillation analysis.

12.7.5 Range Versus Energy of Beta Particles

Proportional counters and laboratory-type end-window GM counters are used to determine the range of beta particles. Since the amount of beta absorption is related to its energy, the amount of absorber required to just stop all of the particles emitted by a source is also a measure of the beta particle energy. A range–energy plot for a given beta source is obtained by placing different thicknesses of an absorber such as aluminum between the source and a thin-window detector as shown in Figure 12-19 and measuring the change in activity for each absorber thickness. A plot of these measurements versus absorber thickness (usually in units of g/cm^2 or mg/cm^2) produces a beta absorption curve that can be used to determine the beta energy of the source (see Figure 7-8).

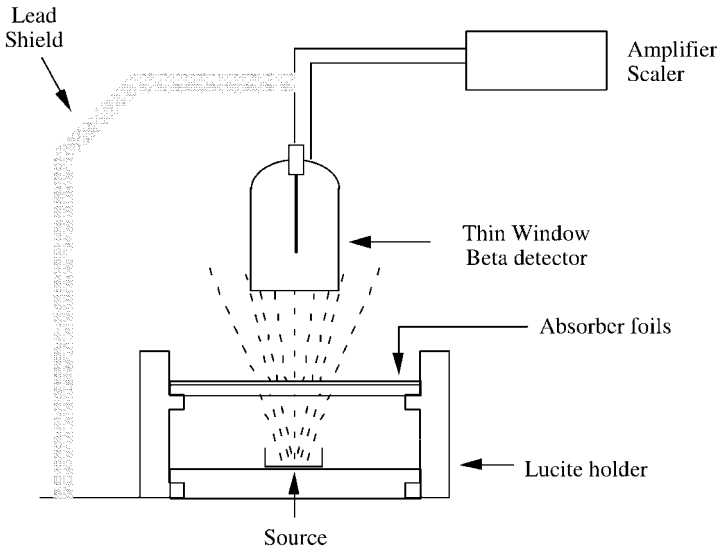

Fig. 12-19 Experimental arrangement for measuring the absorption of beta particles.

The counting rate, when plotted on a logarithmic scale, decreases as a straight line, or very nearly so, over a large fraction of the absorber thickness, eventually tailing off into another straight line region represented by the background, which is always present, and any gamma rays that may be emitted by the source (many

beta-emitting radionuclides also emit photons). The point where the corrected beta absorption curve meets the residual radiation level is the range R_β traversed by the most energetic beta particles emitted by the source. The measured range in mg/cm^2 in aluminum or other similar absorber is then used to determine the energy by an empirical range–energy curve (see Figure 7-9), or alternatively from a listing (usually provided in mg/cm^2) for different beta-emitting sources. This extrapolation technique which is fairly easy is only approximate but is often of sufficient accuracy to determine the energy, and hence the identity, of the beta emitter. Another technique is to determine the amount of absorber required to reduce the count rate of a known standard by one-half and then compare that value to the amount of absorber required to reduce the unknown by one-half, as illustrated in Example 12-4.

Example 12-4. A beta standard with a known range of 200 mg/cm^2 is counted with different thicknesses of absorber and from a data plot it is found that the count rate is reduced to one-half by 50 mg/cm^2 of aluminum. An unknown that is measured the same way requires 100 mg/cm^2 to reduce the count rate by one-half. What is the approximate beta range of the unknown and its energy?
Solution. For the standard, 50 mg/cm^2 corresponds to $0.25R_\beta$; therefore, since 100 mg/cm^2 is required to reduce the count rate of the unknown by one-half,

$$R_\beta = \frac{100\,\text{mg/cm}^2}{0.25} = 400\,\text{mg/cm}^2$$

From Figure 7-9, 400 mg/cm^2 corresponds to $E_{\beta\max} \cong 1.0$ MeV.

It is common practice to extrapolate the straight-line portion of a beta absorption curve to the background and to use the extrapolated value as the maximum range. This procedure is often, but erroneously, called a *Feather analysis*. A true Feather analysis, after its originator, is described by Lapp and Andrews as a more deliberate and accurate process which compares the absorption data from an unknown to a known beta standard, usually ^{210}Bi ($E_{\beta\max}$ = 1.162 MeV). The maximum range of ^{210}Bi has been carefully established as 510 mg/cm^2, and is thus used as a reference for calculating unknown range.

Other Suggested Sources

Knoll, G. F. **1989**, *Nuclear Radiation Detection*, 2nd edn, Wiley Interscience, New York.
Lapp, R. E., Andrews, H.L. **1972**, *Nuclear Radiation Physics*, 4th edn, Prentice Hall, New York.
Moe, H. G. **1988**, *Operational Health Physics Training*, Argonne National Report ANL-88-26, Argonne, IL.

Problems – Chapter 12

12–1. K- and L-shell binding energies for cesium are 28 and 5 keV, respectively. What are the kinetic energies of photoelectrons released from the K and L shells when 40 keV photons interact in cesium?
12–2. Calculate the number of electrons entering the first stage of a photonmultiplier tube from the interaction of a 0.46 MeV photon in a 12% efficient NaI(Tl) crystal.
12–3. Calculate the energy of the Compton edge for 1 MeV photons.
12–4. For a small NaI(Tl) detector exposed to 0.2 MeV photons, calculate the energy of the "iodine escape peak" and provide an approximate plot of the energy spectrum.
12–5. For ^{88}Y photons incident on an intrinsically pure germanium detector/spectrometer, calculate the energies of the "single escape" and "double escape" peaks.
12–6. A biomedical research laboratory uses ^{14}C and ^{32}P in tracer experiments. Devise a method for setting up a liquid scintillation counter to quantitate each radionuclide separately and in the presence of each other.
12–7. An LSC is calibrated such that a low-energy window has a counting efficiency of 30% for ^{3}H and a higher-energy window has a counting efficiency of 72% for ^{32}P. When a ^{32}P standard is counted, it is noted that 12% of the counts in window 2 are recorded in window 1. A mixed sample containing ^{3}H and ^{32}P yields 3800 counts in window 1 and 5800 counts in window 2. Determine the activity of each radionuclide.
12–8. What count rate will be observed by a portable air-proportional alpha counter above a surface uniformly contaminated with an alpha emitter that emits 200 5.16 MeV alpha particles per 100 cm^2 if the probe area is 60 cm^2 and the overall counting efficiency is 22%?
12–9. An ionization chamber detector has been calibrated at STP to provide accurate measurements of dose from photons ranging from about 1 to 3 MeV. If the counter is taken to an elevation of 6000 ft, what modifications would need to be made in interpreting the dose measurements to obtain accurate results? If a proportional counter calibrated at STP is substituted, what modifications would need to be made to properly interpret the results?
12–10. What relative meaning does the term "quench" have in regard to a proportional counter, a GM counter, and a liquid scintillation counter?
12–11. The absorption of beta particles from a source was measured with aluminum and the results shown in Table 12-1 were obtained. (a) Plot the data and estimate, using Figure 7-9, the maximum range of the beta particles in the source. (b) From the range versus energy plot, determine $E_{\beta\max}$. (c) Determine the maximum energy from Feather's empirical formula: $R = 543E - 150$, where R is in mg/cm^2 and E is in MeV.

Table 12-1. Data for Problem 12-11.

Al (mg/cm^2)	c/m	Al (mg/cm^2)	c/m
0	1000	550	8
100	600	600	3.5
200	375	650	1.5
250	250	700	0.75
300	165	750	0.5
350	110	800	0.4
400	65	850	0.35
450	37	900	0.33
500	18	950	0.32

12–12. From the data in Problem 12–11, determine the range using the approximate Feather analysis method if the count rate of a ^{210}Bi standard ($R_\beta = 510$ mg/cm^2) is reduced to one-half by 115 mg/cm^2 of absorber.

13
Statistics in Radiation Physics

"A statistic is worthless unless you know its use."

John Thompson
(Georgetown University)

Many nuclear processes are random, i.e., statistical in nature. The transformation of any given radioactive atom is subject to the laws of chance and as such each has the same probability for transformation in an interval of time regardless of the past history. The science of statistics is used to describe radioactive transformation in several important ways:

- specifying the amount of uncertainty at a given level of confidence in a measurement of radioactivity;
- determining whether a sample actually contains radioactivity, especially if the measured activity level in the sample is very close to the natural background;
- checking whether a counting instrument is functioning properly by comparing the statistically predicted variance of the sample counts to that obtained experimentally.

Practical circumstances dominate these determinations, and much of the presentation that follows emphasizes applications; however, it is important to recognize that all such applications are due to the random statistical behavior of radioactive atoms and to focus to some degree on the fundamental statistical principles that support the rather straightforward applications that can be carried out once the statistical basis of the phenomena and models used are understood.

13.1
Nature of Counting Distributions

If one makes successive measurements of a steady radiation source in a fixed geometry with a stable counting system, it is found that the source does not consis-

Physics for Radiation Protection, Third Edition. James E. Martin

tently produce the same count, but that the counts vary, sometimes considerably, due to the random nature of radioactive transformations. Figure 13-1, which is a scatter plot of 1000 one-minute counts of a sample containing a long-lived radionuclide, demonstrates two important features of such data sets: (a) the one-minute counts cluster around a central value which is likely to be the true count rate of the sample; and (b) the values around the central value form a fairly symmetrical distribution pattern. If one additional count is made on the sample, it is highly likely that it would be one of the values obtained before; however, it is also possible, but not as likely, that the new value would be outside the distribution of the data.

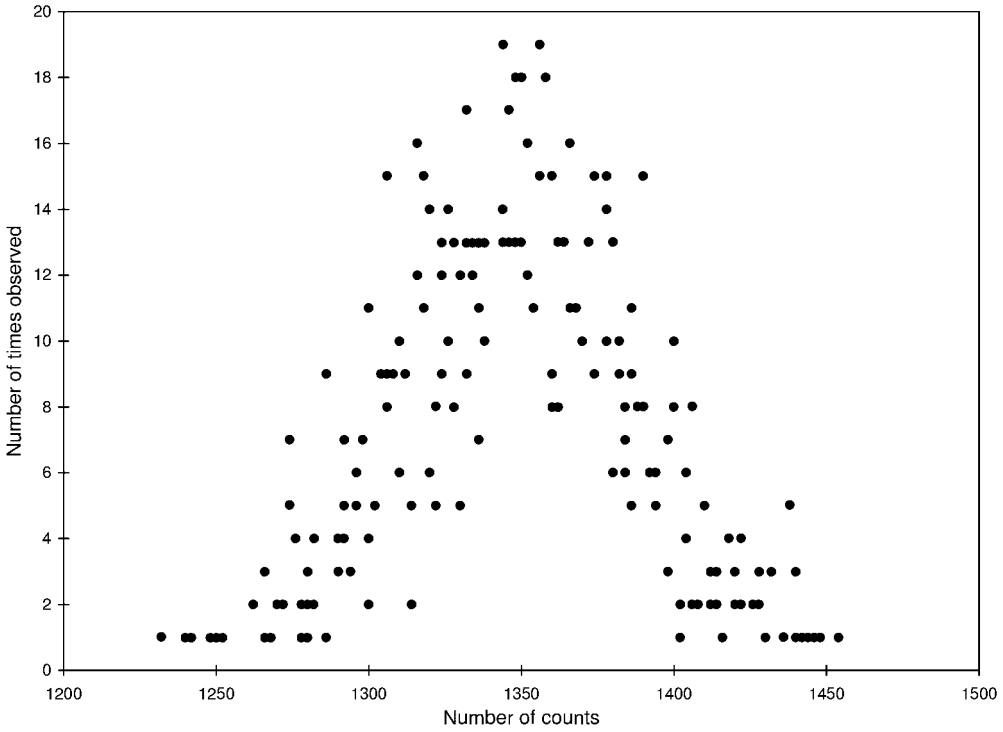

Fig. 13-1 Plot of the number of times (i.e., the frequency) a given count was observed when a sample was counted repeatedly for a 1 min period.

When a radioactive sample is measured it is not generally practical to make more than one or at most a few repeat measurements. Obviously, the objective is to arrive at a value as close to the true transformation rate, or activity, of the sample as possible. It is a fact of nature that the true value cannot be determined exactly unless an infinite number of measurements is made which is not practical. It is possible, however, due to the random nature of radioactive transformation to use one or several measurements to describe the measurement and its

reliability through the use of statistical models. The features of the binomial, Poisson, and normal (or Gaussian) distributions, each of which is summarized briefly, are appropriate for this purpose.

13.1.1 Binomial Distribution

The binomial distribution is the most general statistical model and is widely applicable to processes that occur with a constant probability p; for example, the flip of a coin, choosing a card, or an atom that may or may not disintegrate in a set time. If n is the number of events, each of which has a probability p, then the predicted probability of observing exactly x events (e.g., transformed atoms) in an interval (or a number of trials) is

$$P(x) = \frac{n!}{(n-x)!x!} p^x (1-p)^{n-x}$$

where $P(x)$ is the predicted binomial probability distribution function. It is important to recognize that $P(x)$ is defined only for integer values of n and x.

13.1.2 Poisson Distribution

The binomial distribution, despite its fundamental applicability to random events, is too complex to use for describing the distribution of radioactive events. Most observations of radioactive transformations of interest in radiological protection involve relatively large numbers of events that are produced by a large number of atoms each of which has a very small probability (i.e., $p \ll 1.0$) of transformation in a practical time interval, say minutes or hours. When $p \ll 1.0$ the binomial distribution can be simplified mathematically into a quite useful function, the Poisson distribution:

$$P_n = \frac{x^n e^{-x}}{n!}$$

where, for radioactivity determinations, P_n is the probability of obtaining a count n and x is the "true" average count for the sample. Since the true average count or "true mean" for the sample cannot be measured, the average measured count (properly termed the estimated or "sample mean", $\bar{x}$) is used for x. When the sample mean, $\bar{x}$, is substituted in the general expression for the Poisson distribution of a set of events, then

$$P_n = \frac{\bar{x}^n e^{-\bar{x}}}{n!}$$

This expression can be used to characterize the distribution of measured data for a radioactive source as shown in Example 13-1.

Example 13-1. What is the probability of obtaining a count of 12 for a radioactive source when the "true" average count is 15?
Solution. Since $p \ll 1.0$ for radioactive transformation of a large number of radioactive atoms, the Poisson distribution can be used. This yields

$$P_n = \frac{\bar{x}^n e^{-\bar{x}}}{n!}$$

$$P_{12} = \frac{(15)^{12} e^{-15}}{12!}$$

$$= \frac{(129.7 \times 10^{12})(30.6 \times 10^{-8})}{(4.79 \times 10^{8})}$$

$$P_{12} = 0.0829$$

The probability is 0.0829 (or 8.29%) that a count of 12 will be obtained when the "true" average count is 15.

Use of the Poisson distribution law is fairly straightforward when n is small (as in Example 13-1); however, it too can be quite cumbersome for determining the probability of observing a given count from a source when n is large. Obviously, a simpler function that accurately represents the random statistical events that occur in radioactive transformation is desirable. Such a function is the normal distribution which can be used to represent Poisson-distributed events if n is greater than 16. Figure 13-2 illustrates the application of the Poisson distribution for intervals of counts from a ^{137}Cs sample.

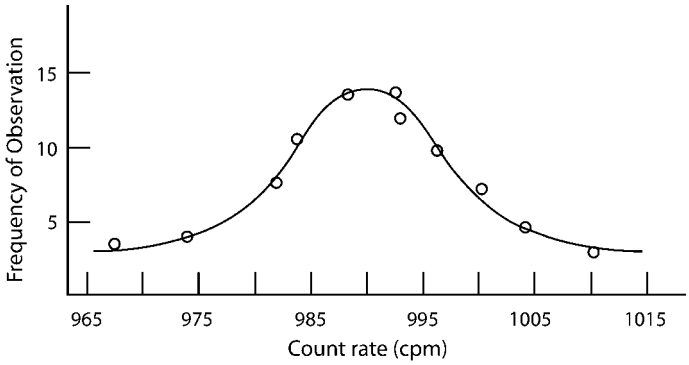

Fig. 13-2 Data from 100 ten-minute measurements of a ^{137}Cs source with a mean count rate of about 990 c/m plotted as a function of the number of times that the count rate fell within successive increments of 5 (i.e., between 975 and 980, or 980 to 985, etc.). The Poisson curve of best fit is drawn through the central values of the data increments.

13.1.3 Normal Distribution

If a large number of measured counts produced by a radioactive sample are grouped into smaller and smaller intervals of incremental counts, a plot of the frequency of occurrence of a given counting interval becomes very symmetrical, as illustrated in Figure 13-3. The symmetry of such a plot for events where $n \geq 17$ allows statement of a very fortunate principle: Poisson-distributed events such as radioactive transformation can be represented by the normal distribution which is completely described by two parameters, the true mean μ and the standard deviation σ, which in turn is derived from the estimated mean by $\sqrt{\bar{x}}$.

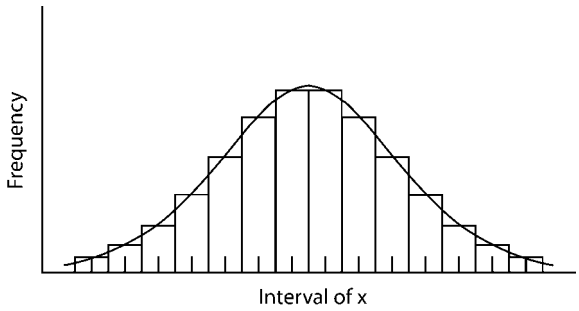

Fig. 13-3 Histogram illustrating the conceptual basis of a normal curve.

The variation in a large number of repeated measurements (e.g., in Figure 13-3) can be described by plotting a histogram of the number of measurements observed for a given interval (frequency) versus that interval. The intervals still represent discrete events (i.e., an atom transforms or it does not); however, if the counting intervals are made very small, the discrete values can be replaced by a continuous function that fits the data points. The equation for the function (or curve) that fits the data points is the normal (or Gaussian) distribution:

$$P_N(n) = \frac{1}{\sqrt{2\pi\bar{x}}} e^{-(x_i-\bar{x})^2/2\bar{x}}$$

where $P_N(n)$ is the probability of observing a count n when the true count (estimated as the average count) is $\bar{x}$ ($\bar{x} = \sigma_{\bar{x}}^2$ which can be substituted). This, like the binomial and Poisson distributions, is a distribution function for integer values of x; however, the continuous function of the normal distribution makes the interpretation and description of probabilistic events considerably easier.

Example 13-2. Apply the normal distribution function to Example 13-1.
Solution. The probability $P_N(n)$ of obtaining a count of 12 when the true average count is 15 is

$$P_N(n) = \frac{1}{\sqrt{2\pi\bar{x}}} e^{-(x_i-\bar{x})^2/2\bar{x}}$$

$$P_N(n) = \frac{1}{\sqrt{2\pi(15)}} e^{-(12-15)^2/2(15)}$$

$$= 0.103e^{-0.3} = 0.0764$$

Example 13-2 shows that the normal distribution yields a probability close to that calculated by the more accurate Poisson distribution in Example 13-1 for a mean of 15 events. The results for 17–20 or more are essentially the same.

A data set that is governed by the normal distribution is fully defined by two parameters, the true mean (μ) and the standard deviation (σ), which indicates the degree of spread among values of the individual observations (x_i) as illustrated in Figure 13-4 for two data sets with the same true mean but different values of σ.

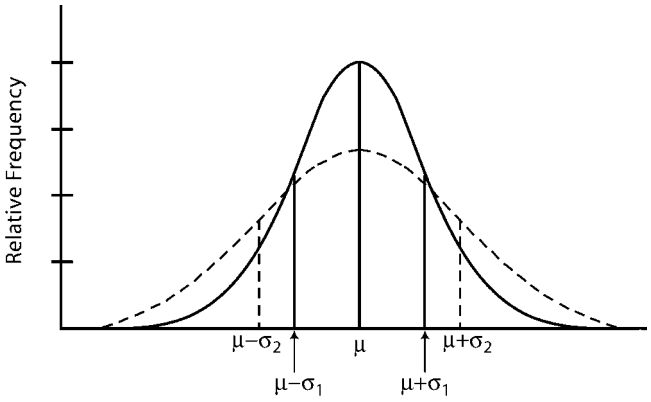

Fig. 13-4 Normal distribution curves with the same true mean but different standard deviations.

A normal distribution curve, as shown in Figures 13-4 and 13-5, has two distinct features. First, it is symmetrical about a vertical line drawn through the value for the true mean which is at the maximum of the curve; second, regardless of the relative magnitude of σ and μ, zero probability only occurs at $+\infty$ and $-\infty$.

Integration of the normal distribution function between the limits $-\infty$ to $+\infty$ yields the total area (i.e., $p = 1.0$) and all normal curves, regardless of their values of σ and μ, have the property that the area between $\mu - \sigma$ and $\mu + \sigma$ is 68.3% of the total area, as shown in Figure 13-5. Extending the interval to $\mu \pm 2\sigma$ includes 95.5% of the total area, and between $\mu \pm 3\sigma\mu$ it encompasses 99.7% of the area under the normal curve. In practical terms, when an estimated mean is assigned an uncertainty of 1σ, 2σ, or 3σ, one can be 68.3, 95.5, and 99.7% confident that the true mean lies somewhere in the assigned interval. These degrees of confi-

dence, referred to as confidence intervals, are generally stated as percent confidence or as multiples of σ; Table 13-1 summarizes and relates the two.

Table 13-1. Confidence intervals based on the normal distribution for multiples of the standard deviation (σ) of a measurement.

Interval	Confidence level (%)
$\bar{x} \pm 1\sigma$	68.3
$\bar{x} \pm 1.96\sigma$	95.0
$\bar{x} \pm 2\sigma$	95.4
$\bar{x} \pm 2.58\sigma$	99.0
$\bar{x} \pm 3\sigma$	99.7

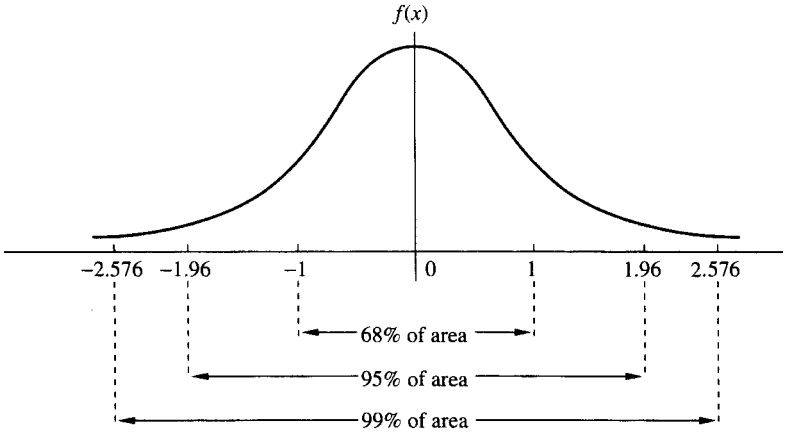

Fig. 13-5 Percent area between intervals of the standard deviation for the normal distribution curve.

A normal curve can be fitted to a data set of 17 or more events if only one parameter, the arithmetic mean $\bar{x}$, is given. This fit can be made by determining the standard deviation of the mean which is obtained by $\sqrt{\bar{x}}$. For Poisson-distributed events numbering 17 or more, all of the properties of the normal distribution can be applied to the data obtained, and the standard deviation can be readily obtained once the best estimate of the mean is made. If, however, the number of counts falls to a very small value (less than 17), the distribution no longer follows the normal curve and the statement of confidence limits must be based on the Poisson distribution. The confidence limits for small numbers of counts at the 95% confidence level are shown in Table 13-2.

Table 13-2. Poisson-distributed 95% confidence limits of the true mean for low numbers of counts.

Observed count	Lower limit	Upper limit
1	0.03	5.57
2	0.24	7.22
3	0.62	8.77
4	1.09	10.24
5	1.62	11.67
6	2.20	13.06
7	2.81	14.42
8	3.45	15.76
9	4.12	17.08
10	4.80	18.39
11	5.49	19.68
12	6.20	20.96
13	6.92	22.23
14	7.65	23.49
15	8.40	24.74
16	9.15	25.98

13.1.4
Mean and Standard Deviation of a Set of Measurements

The *Arithmetic mean value* $\bar{x}$ of a set of measurements is the best estimate of the transformation rate of the source; it is calculated as

$$\bar{x} = \frac{1}{n} \sum_{i=1}^{i=n} x_i$$

where x_i is the value of each measurement and n is the number of measurements. If only one measurement is made, $\bar{x}$ is obviously that value.

The s*tandard deviation*, which describes the degree of fluctuation of the data set about the mean, is the next most useful descriptor of a statistical data set. The standard deviation is denoted as σ and is calculated for a single radioactivity measurement as $\sqrt{N}$ where N is the number of observed counts. If several measure-

ments are made, σ is calculated from the arithmetic mean value and each measured value x_i in the data set as

$$\sigma = \left[\frac{\sum_{i=1}^{n} (x_i - \bar{x})^2}{n-1} \right]^{1/2}$$

where the term $(n - 1)$ is associated with the number of "degrees of freedom." When n independent observations of x are made, n values are obtained; however, the calculation of σ (the sample standard deviation) includes $\bar{x}$, which is computed from the data for n observations, thus there are only $(n - 1)$ independent data left. This is consistent with only one observation in which $\bar{x} = x$ and σ is indeterminate because $(n - 1)$ goes to zero.

13.1.5
Uncertainty in the Activity of a Radioactive Source

For any radioactive source the challenge is to estimate from a finite number of observations a result that can only be known exactly by making an infinite number of observations, which of course is impossible. Successive counts of a long-lived radioactive source will, as shown in Example 13-3, yield different results, which raises the question of which count represents the true activity of the source. The best estimate of the true count is the arithmetic mean (or the average value), which for the data Example 13-3 is $\bar{x} = 328$ counts. The value of $\bar{x}$ itself is only an estimate, but since it is a calculated average of 5 observations there is added confidence that it represents the true activity of the source. Having made this estimate, however, the statistical uncertainty in the estimate is determined by standard deviation of the data.

Two approaches can be taken to determine the standard deviation (i.e., uncertainty) of the mean of several measurements. If it is not known that the data are radioactivity counts, then it is common practice to determine the mean and the standard deviation in the usual way using the specific definitions of the mean and standard deviation of a set of observed counts. But this approach unnecessarily constrains the precision of the estimated mean. Since the data in Example 13-3 are radioactive transformations, which are independent random events, and each measurement was taken the same way then the individual counts can be summed and used directly to compute σ. Examples 13-3 and 13-4 show the relative features of treating observed counts as individual versus separate independent random events.

Example 13-3. A sample is counted 5 times for 10 minutes each and 315, 342, 335, 321, and 327 counts recorded. What are the mean count and the standard deviation of the data set, and the mean count rate and its uncertainty based on the data set?

Solution.

x_i	$(x_i - \bar{x})$	$(x_i - \bar{x})^2$
315	–13	169
342	+14	196
335	+7	49
321	–7	49
327	–1	1
$\sum x_i = 1640$ counts		$\sum (x_i - \bar{x})^2 = 464$

The mean is $\bar{x} = 1640/5 = 328$ counts.

The standard deviation of the data set is

$$\sigma = \sqrt{\frac{464}{4}} = 11 \text{ counts}$$

$$\text{Count rate} = \frac{328 \pm 11 \text{ counts}}{10 \text{ min}} = 32.8 \pm 1.1 \text{ c/m}$$

Example 13-4. For the data in Example 13-3, determine the mean, the count rate, and the standard deviation of each based on the fact that these are counts of radioactive events.

Solution. Since radioactivity counts are discrete independent random events, the five 10min counts can be examined as a group of 1640 counts. The mean is

$$\bar{x} = 1640/5 = 328 \text{ counts}$$

The standard deviation is

$$\sigma = \sqrt{1640} = 40.5 \text{ counts}$$

and the mean count rate and its uncertainty is

$$\bar{x} = \frac{1640 \pm 40.5}{50 \text{ min}} = 32.8 \pm 0.81 \text{ c/m}$$

It is clear from Examples 13-3 and 13-4 that a certain amount of precision is given up by the statistical treatment of the data as a group of numbers. If it is known that the detector system and source are steady over the period that the measurements are made, then the measurement can be treated as a set of cumulative counts which can be used directly to estimate the count rate and its uncertainty with a somewhat smaller value for the uncertainty of the measurement.

13.1.6 Uncertainty in a Single Measurement

A common procedure is to make a single observation of a radioactive sample. Consequently, it is the best estimate of the true transformation rate of the sample since no other value is in hand. The true mean is probably different from this measurement, but limits can be specified within which the true mean probably lies by use of the normal distribution. When a single measurement is used to estimate the mean and a standard deviation (or two or three) is assigned to it, in effect one is drawing a normal curve around the estimated mean with a data spread equal to the square root of the measured counts. This can be shown to be a reasonable practice using the data in Example 13-3. If only one count is selected randomly from the table, say 321, the standard deviation is $\sqrt{321} = 18$. This single measurement would be reported as 321 ± 18 counts, which is equivalent to stating that the "true" activity of the source has a 68.3% probability (or 1σ) of being between 303 and 339 counts in 10 minutes. The mean count for the 5 separate observations listed in Example 13-3 is 328 counts in 10 min which falls within the range.

Checkpoints

Before proceeding on to practical applications of statistics to common radiation protection circumstances, the following points need to be emphasized:

- Radioactivity measurements simply record the number of random events (transformations) that occur in a given time interval, and these events are truly random with very small probabilities of occurrence.
- Since radioactivity events are binary (they either occur or they do not), their predictability is governed by the broadly applicable binomial probability distribution function, but this is generally too cumbersome to use for more than a few counts.
- The Poisson distribution can be used instead of the binomial distribution when the probability of any given event is $\ll 1$, which is the case for radioactive transformation.
- The normal (or Gaussian) distribution is a continuous function that provide statistical results equivalent to the Poisson distribution if the number of events (counts) is greater than 17–20. It is symmetrical about the mean and is easier to use, plot, and describe than either the binomial or Poisson distributions, which is the main reason it is used to describe radioactivity measurements.
- Both the Poisson and normal distributions are characterized by the mean (estimated as $\bar{x}$ from a single measurement or from n measurements) from which the standard deviation can be calculated as $\sqrt{\bar{x}}$.

13.2 Propagation of Error

It is important to remember that the statistical model assumptions apply only to an observed number of counts. For radioactivity measurements, the standard deviation or any multiples of it cannot be associated with the square root of any quantity that is not a directly measured number of counts. Two values $A \pm \sigma_A$ and $B \pm \sigma_B$ can be combined arithmetically in such a way as to aggregate their respective uncertainties. The appropriate term for this process is propagation of error. The aggregate uncertainty for arithmetic operations involving A and B and their computed standard deviations can be propagated as follows:

- For addition or subtraction of $(A \pm \sigma_A)$ and $(B \pm \sigma_B)$, the results and the aggregate standard deviations are $(A \pm B) \pm \sqrt{\sigma_A^2 + \sigma_B^2}$
- For multiplication or division of $(A \pm \sigma_A)$ and $(B \pm \sigma_B)$, the results and the aggregate standard deviations are

  $$A/B \pm A/B\sqrt{(\sigma_A/A)^2 + (\sigma_B/B)^2}$$

  or

  $$AB \pm AB\sqrt{(\sigma_A/A)^2 + (\sigma_B/B)^2}$$

Multiplying or dividing total counts or a count rate by a constant is not propagated by a statistical operation, but is simply altered by the constant applied. A common example of this is conversion of an observed number of counts to a count rate r by dividing by the count time t, or

$$r = \frac{C_{\text{s+b}}}{t}$$

The standard deviation for a counting rate r can be calculated one of two ways:

$$\sigma = \frac{\sqrt{C_{\text{s+b}}}}{t}$$

or

$$\sigma = \sqrt{\frac{r}{t}}$$

where r = counting rate; $C_{\text{s+b}}$ = gross sample counts including background; and t = sample counting time.

Example 13-5. A long-lived sample was counted for 10 min and produced a total of 87,775 counts. What is the counting rate and its associated standard deviation?
Solution. The counting rate r is

$$r = 87{,}775/10 = 8778 \text{ c/m}$$

and the standard deviation of the count rate is

$$\sigma = \sqrt{87,775}/10 = 30 \text{ c/m}$$

Alternatively, the standard deviation can be determined from the count rate *r*:

$$\sigma = \sqrt{\frac{8778}{10}} = 30 \text{ c/m}$$

and thus there is a 68.3% probability that the true (i.e., the 1σ) counting rate is 8778 ± 30 c/m, i.e., between 8748 and 8808 c/m.

13.2.1 Statistical Subtraction of a Background Count or Count Rate

When a measurement includes a significant contribution from the radiation background, the background value must be subtracted and the total uncertainty in the net result is obtained by propagation of the error associated with each. The resulting net count has a standard deviation associated with it that is greater than that of either the sample or the background alone.

Example 13-6. What is the net count and its standard deviation for a sample if the sample count is 400 ± 20 and the background count is 64 ± 18?
Solution. Since the uncertainty of each measurement is given, the uncertainty in the net count and its uncertainty are determined by subtracting the background count from the sample count and propagating the error of each measurement:

$$\text{Sample net count} = (A - B) \pm \sqrt{\sigma_A^2 + \sigma_B^2}$$

$$= (400 - 64) \pm \sqrt{(20)^2 + (18)^2} = 336 \pm 27 \text{ counts}$$

Example 13-6 is computed with a 1σ uncertainty or a 68.3% confidence interval; if a 95% confidence interval is desired, the net count would be computed as $A - B$ with an uncertainty of 1.96σ for each value and reported as 400 ± 39 and 64 ± 35. The result and the aggregate uncertainty at the 95% confidence level would be (400 – 64) ± 53 counts or 336 ± 53 counts. The uncertainty of 1.96σ can be calculated for *A* and *B* separately and aggregated as shown in Example 13-6 or applied to the result (i.e., 1.96 × 27 = 53 counts).

The *uncertainty for a net count rate* is often determined directly from the counting data for the sample and the background associated with its measurement. The net count rate R is calculated as

$$R = \frac{C_{s+b}}{t_{s+b}} - \frac{B}{t_b}$$

where R = net count rate (c/m); C_{s+b} = gross count of sample plus background; B = background count; t_{s+b} = gross sample counting time; and t_b = background counting time. The standard deviation of the net count rate is

$$\sigma_{net} = \sqrt{\frac{C_{s+b}}{t_{s+b}^2} + \frac{B}{t_b^2}}$$

This general expression for the standard deviation of a net count rate is applicable to any circumstance when the background count (measured for a count time t_b) is subtracted from a sample count measured for a time t_{s+b} regardless of whether t_b and t_{s+b} are equal or not, as shown in Example 13-7. If the counting time for both the sample and the background is the same, this simplifies to

$$R = \frac{C_{s+b} - B}{t} \quad \text{and} \quad \sigma = \frac{\sqrt{C_{s+b} + B}}{t}$$

Example 13-7. A sample counted for 10 min yields 3300 counts. A 1 min background measurement yields 45 counts. Find the net counting rate and the standard deviation.

Solution.

$$\text{Net count rate} = \frac{3300}{10} - \frac{45}{1} = 285\ \text{c/m}$$

$$\sigma = \sqrt{\frac{3300}{10^2} + \frac{45}{1^2}} = 8.83\ \text{c/m}$$

The net count rate is thus

$$\text{Net count rate} = 285 \pm 8.83\ \text{c/m}$$

with a 1σ (or 68.3%) confidence level; for a 95% confidence level the net count rate is

$$\text{Net count rate (95\%)} = 285 \pm 1.96 \times 8.83\ \text{c/m} = 285 \pm 17.3\ \text{c/m}$$

13.2.2 Error Propagation of Several Uncertain Parameters

Laboratory results are often calculated from a number of parameters, more than one of which may have a specified uncertainty. For example, a common measured result is a sample count divided by the detector efficiency and the chemical/physical recovery of the procedure to determine the activity in a collected sample, i.e., before it is processed. Detector efficiency is determined by counting a known source and dividing the measured count rate by the disintegration rate which requires a statement of uncertainty. Similarly the chemical yield is usually determined by processing a tracer or several known spikes and taking the mean of the recorded counts divided by the known activity, calculations that combine measured values and their uncertainties. Count times can be reasonably assumed to be constant because electronic timers are very accurate, and geometry factors can also be considered constant if samples are held in a stable configuration.

The reported uncertainty in a measured value is obtained by propagating the relative standard errors (i.e., 1σ) of each of the uncertainties according to the rule for dividing or multiplying values with attendant uncertainties. The uncertainty in a calculated value u is

$$\sigma_u = u\left[\left(\frac{\sigma_a}{a}\right)^2 + \left(\frac{\sigma_b}{b}\right)^2 + \left(\frac{\sigma_c}{c}\right)^2 + \cdots\right]^{1/2}$$

where u is the calculated value and σ_a, σ_b,... are the relative standard errors of each of the parameters used to calculate u. Typical cases are shown in Examples 13-8 and 13-9.

Example 13-8. A counting standard with a transformation rate of 1000 ± 30 d/m is used to determine the efficiency of a counting system. The measured count rate is 200 ± 10 c/m. What is the efficiency of the counting system and its uncertainty?
Solution. The efficiency is

$$\varepsilon = \frac{200\,\text{min}^{-1}}{1000\,\text{min}^{-1}} = 0.2 \text{ or } 20\%$$

and the standard deviation of the efficiency is calculated as

$$\sigma_\varepsilon = 0.2\sqrt{\left(\frac{30}{1000}\right)^2 + \left(\frac{10}{200}\right)^2} = 0.058 = 5.8\%$$

and the recorded efficiency with a 1σ confidence interval would be 20 ± 5.8% (or 0.2 ± 0.058).

Example 13-9. A 1 g sample is processed in the laboratory and counted in a measurement system with a precise timer and a fixed geometry that has a counting efficiency of 20 ± 2%. The chemical yield was determined by processing several known spikes and was recorded as 70 ± 5%. The recorded count rate was 30 ± 5 c/m. What is the activity concentration and its associated uncertainty?
Solution.

$$\text{Concentration (d/m per g)} = \frac{30\,\text{c/m}}{0.2\,(\text{c/m})/(\text{d/m}) \times 0.7 \times 1\,\text{g}}$$

$$= 214\ \text{d/m per g}$$

The uncertainty for the measurement is

$$\sigma_{\text{conc}} = 214\sqrt{\left(\frac{5}{30}\right)^2 + \left(\frac{0.02}{0.2}\right)^2 + \left(\frac{0.05}{0.7}\right)^2}$$

$$= 214\sqrt{0.0278 + 0.01 + 0.0051}$$

$$= 214\sqrt{0.0429} = 44\ \text{dpm per g}$$

The result would be reported as 214 ± 44 d/m per g at a 1σ confidence interval; i.e., the true concentration has a 68.3% probability of being between 170 and 258 d/m per g. The 95% confidence interval would be 1.96 × 44 d/m per g and the result would be reported as 214 ± 86 d/m per g.

13.3 Comparison of Data Sets

A typical problem in radiation protection is whether two measured values of radioactivity differ from each other with statistical significance. Perhaps the most common example of radiation measurement is whether a measured value is significantly above that due to the surrounding background.

13.3.1 Are Two Measurements Different?

Two single measurements can be compared using Student's *t* test. The test is performed by calculating a value τ_{calc} and comparing it with a true probability value τ_{table}, obtained from the normal distribution as listed in abbreviated form in Table 13-3. The calculated value τ_{calc} is determined from the absolute value $|r_1 - r_2|$ of the difference between two counting rates r_1 and r_2:

$$\tau_{\text{calc}} = \frac{|r_1 - r_2|}{\sqrt{\frac{r_1}{t_1} + \frac{r_2}{t_2}}}$$

or since $\sigma_i^2 = r_i/t_i$

$$\tau_{\text{calc}} = \frac{|r_1 - r_2|}{\sqrt{\sigma_1^2 + \sigma_2^2}}$$

where τ_{calc} = relative error for a given confidence interval; r_1 and r_2 = count rate (c/m) for the sample and the background "blank"; t_1 and t_2 = counting time (min) for r_1 and r_2, respectively; and σ_1 and σ_2 = standard deviation of count rate r_1 and r_2, respectively.

Table 13-3. Student's t test values (or τ_{table}) for selected p values, where $(1 - p)$ corresponds to the confidence interval of the two-sided normal distribution.

τ_{table}	p	τ_{table}	p
0.0	1.000	1.5	0.134
0.1	0.920	1.6	0.110
0.2	0.841	1.7	0.090
0.3	0.764	1.8	0.072
0.4	0.689	1.9	0.060
0.5	0.617	2.0	0.046
0.6	0.548	2.1	0.036
0.7	0.483	2.2	0.028
0.8	0.423	2.3	0.022
0.9	0.368	2.4	0.016
1.0	0.317	2.5	0.0124
1.1	0.272	2.6	0.0093
1.2	0.230	2.7	0.0069
1.3	0.194	2.8	0.0051
1.4	0.162	2.9	0.0037

The most-used values of τ_{table} and the corresponding probability values for radiation measurements are

τ_{table}	p
2.580	0.010
1.960	0.050
1.645	0.100
1.000	0.317

where values of p for 0.010, 0.050, 0.100, and 0.317 correspond to confidence intervals of 99, 95, 90, and 68.3%, respectively.

Example 13-10. A sample measurement yields 735 counts in 50 min. A background measurement with the same detector system and geometry yields 1320 counts in 100 min. Can we say at the 95% confidence level that this sample contains radioactivity above the background activity?
Solution. First, the hypothesis is made that the sample contains no radioactivity with at least 95% certainty; i.e., $\tau_{calc} \leq \tau_{table} = 1.96$. The value of τ_{calc} is determined from the values of r_1 and r_2 based on the observed counts and the recorded count times t_1 and t_2:

$r_1 = 14.7$ c/m; $t_1 = 50$ min

$r_2 = 13.2$ c/m; $t_2 = 100$ min

and thus the value of τ_{calc} is

$$\tau_{calc} = \frac{|14.7 - 13.2|}{\sqrt{\frac{14.7}{50} + \frac{13.2}{100}}} = 2.3$$

From Table 13-3 for $p = 0.05$, $\tau_{table} = 1.96$, which is less then τ_{calc}; therefore, the hypothesis is rejected (τ_{calc} is not $\leq \tau_{table}$), and there is at least a 95% chance (i.e., $1 - p = 0.95 = 95\%$) that the sample contains radioactivity above background.

With the computed τ_{calc} value and values of τ_{table} from Table 13-3, it can be determined whether observed differences are caused by the random nature of radioactive transformation or whether there is a "real" difference between dissimilar samples.

Example 13-11. Two different samples from an area were counted for 1 min. The net count rate was 1524 ± 47 c/m for the first and 1601 ± 49 c/m for the second. Is the difference significant?

Solution.

$$\tau_{\text{calc}} = \frac{|x_1 - x_2|}{\sqrt{\sigma_1^2 + \sigma_2^2}}$$

$$= \frac{|1524 - 1601|}{\sqrt{(47)^2 + (49)^2}}$$

$$= 1.13$$

From Table 13-3, the probability p that corresponds to $\tau_{\text{calc}} = 1.13$ is 0.259 (or 25.9%) that measured values of two identical samples would differ due only to the random variation of the count rate; thus, the probability that the difference between the samples is significant is 1 – 0.259 = 0.741 or 74%.

13.4
Statistics for the Counting Laboratory

Statistics can be used in the counting laboratory for several circumstances, for example assigning an uncertainty to a total count or count rate, determining an optimal count time, for an optimal distribution of available counting time between sample and background, doing gamma spectroscopy, checking whether equipment is working properly, determining a weighted average of several measurements, and whether and when it is acceptable to reject data.

13.4.1
Uncertainty of a Radioactivity Measurement

Perhaps the most common radioactivity measurement is to place a prepared sample in a counter for a set count time: examples of such samples may be a routine air filter or an evaporated volume of water (e.g., 1 L of a stream sample). The size of the prepared sample, the count time, the background count time, and the sensitivity (efficiency) of the detector system are usually chosen to provide an optimal balance between sample work load, desired accuracy, and cost. For many practical reasons, samples are often counted just once for a set time, and typically the background will be counted for a different time, usually larger than the sample count time.

Sample counting data are reported as the best estimate of the true activity (based on the true count rate) with a stated level of uncertainty or confidence interval. Typical reported uncertainties are one standard deviation (known as probable error, the 1σ error, or the 68.3% confidence interval), a 90% confidence interval (1.645σ), or the 95% confidence interval (1.96σ, often rounded to 2σ) which is perhaps the value most used for low-level radioactivity measurements.

Example 13-12. An overnight background count is made for a gas-flow proportional counter and this value is used throughout the next day for 10 min measurements of routine air filters. If the background count is 7600 counts in 800 min and the sample count plus the background is 240 counts in 10 min, determine (a) the net count rate for the sample and its uncertainty with a 95% confidence level, and (b) the sample count rate and the 95% confidence interval if it were to be counted for 30 min to yield 720 counts.

Solution. (a) The sample count rate with a 1σ uncertainty is $240/10 = 24 \pm 1.55$ c/m and the background count rate is 9.5 ± 0.11 c/m. The net sample count rate at the 95% confidence level (1.96σ) is

$$\text{Net c/m} = 24 - 9.5 \pm 1.96\sqrt{(1.55)^2 + (0.11)^2}$$

$$= 14.5 \pm 1.96(1.554) \text{ c/m}$$

$$= 14.5 \pm 3.05 \text{ c/m}$$

(b) For a 30 min sample count the sample count rate remains at 24 c/m; however, the uncertainty is ±0.894 c/m. At the 95% confidence level (1.96σ), the net count rate is

$$\text{Net c/m} = 24 - 9.5 \pm 1.96\sqrt{(0.894)^2 + (0.11)^2}$$

$$= 14.5 \pm 1.96(0.812) \text{ c/m}$$

$$= 14.5 \pm 1.59 \text{ c/m}$$

As shown in Example 13-12, increasing the sample count time narrows the 95% confidence interval with a corresponding reduction in the uncertainty of the measurement. The long background count is also a significant factor in reducing the uncertainty if it can be presumed that the same conditions exist during the overnight and daytime hours, which may not always be the case. Measurement uncertainty can also be reduced by using larger samples to increase the total counts and/or reducing background radiation by shielding the detector or other means.

13.4.2 Determining a Count Time

Statistical comparisons of data can be used to optimize the time a sample is counted. Many measurements of radioactivity are simply made and the data are then used to calculate the net counting rate and its uncertainty; however, once a desired confidence level has been selected, counting the sample beyond an optimized time intervals yields no improvement in the reported result. The counting time can also be calculated by the t test by making the following *a priori* determinations:

- the confidence level to be used in reporting the data
- the background count rate and its counting time
- the minimum detectable count rate to be detected above background.

Example 13-13. A detector system in a laboratory is routinely set to accumulate a 1000 min background count overnight. If the background count rate from the 1000 min count is 11 c/m, how long must a sample be counted the next morning in order to measure 1 c/m above background with 95% confidence?
Solution. From Table 13-3, $\tau_{calc} = 1.96$ for the 95% confidence interval ($p = 0.05$). This value is used as follows:

$$1.96 = \frac{|12.0 - 11.0|}{\sqrt{\frac{12.0}{t_1} + \frac{11.0}{1000\,\text{min}}}}$$

Squaring both sides and solving for t_1 gives

$$\frac{12.0}{t_1} + 0.011 = \frac{1}{(1.96)^2}$$

$$t_1 = \frac{12}{0.26 - 0.011}$$

$$= 48.1\ \text{min}$$

Example 13-14. How long should a sample that has an approximate gross counting rate of 800 counts in 2 min be counted to obtain the net counting rate with an accuracy of 1% if the background for the counting system is 100 ± 2 c/m?
Solution. The approximate net count rate is 400 – 100 = 300 c/m and the desired uncertainty of 1% is thus 3 c/m. The general expression for the standard deviation of the difference in two count rates is

$$\sigma_r = \sqrt{\frac{R_{s+b}}{t_{s+b}} + \sigma_b^2}$$

Solving for t_{s+b} where $\sigma_r = 3$ c/m and the approximate count rate $R_{s+b} = 400$ c/m yields

$$t_{s+b} = \frac{400}{3^2 - 2^2} = 80\,\text{min}$$

13.4.3 Efficient Distribution of Counting Time

An optional distribution of available counting time can be made between the sample count and the background to reduce the estimated standard deviation of the net count rate to a minimum. The most efficient distribution of counting time between the sample count time t_{s+b} and the background count time t_b is determined when their ratio is

$$\frac{t_{s+b}}{t_b} = \sqrt{\frac{C_{s+b}}{C_b}}$$

where t_{s+b} = counting time for sample plus background; t_b = counting time for background; C_{s+b} = estimated count rate for sample plus background; and C_b = estimated count rate for background.

Example 13-15. The count rate for a radioactive sample, including background, is estimated from a quick count to be ~3500 c/m, and the background count rate to be ~50 c/m. What is the optimal allocation of 10 min of counting time between the sample and the background?
Solution. The optimal ratio for the two count rates is

$$\frac{t_{s+b}}{t_b} = \sqrt{\frac{r_{s+b}}{r_b}} = \sqrt{\frac{3500}{50}} = 8.37$$

or

$$t_{s+b} = 8.37 t_b$$

and since $t_{s+b} + t_b = 10$ min, this can be simplified as

$$8.37 t_b + t_b = 10 \text{ min}$$

Thus the optimal counting time for the background is

$$t_b = 1.07 \text{ min}$$

And since 10 min are available, the sample counting time is

$$t_{s+b} = 10.00 - 1.07 \text{ min}$$

$$= 8.93 \text{ min}$$

As a practical matter, the sample would be counted for 9 min and the background for 1 min

13.4.4
Detection and Uncertainty for Gamma Spectroscopy

Many radiation measurements are done on gamma spectrometers in which a spectrum of counts versus photon energy is obtained as illustrated in Figure 13-6. Each peak in such a spectrum will be superimposed on a background spectrum that is due to natural background radiation striking the detector, background radiation from the shield and surrounding components, and Compton scattered photons produced by interactions of gamma rays with energies above the peak energy. The net count at a given energy is used to quantitate the activity at the peak, its uncertainty or standard deviation, and whether it is considered detected or not, either through the decision tools of L_c and/or LLD (as discussed in Sections 13.5.1 and 13.5.2).

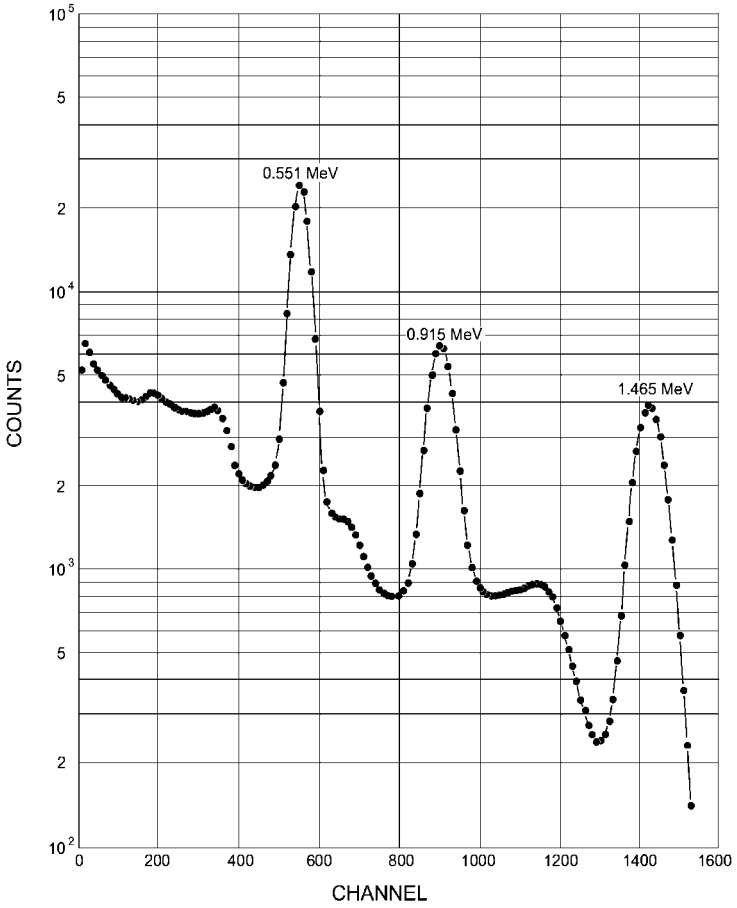

Fig. 13-6 Gamma spectrum of ^{148}Pm ($T_{1/2}$ = 5.37 d) with an energy peak of 0.910 MeV superimposed on a detector background and Compton continuum of 800 counts and a 0.551 MeV peak on a background/continuum of 1800 average counts per channel.

The net count determination for the peak is made by subtracting the background at the peak energy, which is actually incorporated in the measurement of the sample. Background subtraction involves selecting a region of interest of several channels on each side of the peak taking care to select a similar number on each side. The average number of counts per channel due to background in each channel under the peak is determined and this value is then multiplied by the number of channels covered by the peak area to obtain the total background that should by subtracted from the total peak counts. Selecting the peak region is somewhat of an art to maximize peak counts relative to background counts. Once this is done, calculations of net counts, uncertainty L_c, and LLD are performed as usual and any determinations of activity per unit volume, mass, etc., are obtained by incorporating the relevant factors of the system as shown in Example 13-16. Modern gamma spectroscopy systems usually incorporate algorithms based on this approach to perform background subtraction and report net peak values in counts or activity.

Example 13-16. For the 0.91 MeV peak in the gamma spectrum in Figure 13-6, determine (a) the net count and its uncertainty at the 95% confidence level and (b) the concentration of ^{148}Pm in the measured sample if the count time is 10 min, the detector efficiency for a 1.5 L geometry is 8 ± 1.0% at the 0.910 MeV peak, the chemical recovery of the processed sample is 90 ± 4%, and the yield for the 0.910 MeV gamma ray is 12.5%.

Solution. (a) From Figure 13-6, for the 200 channels encompassing the 0.910 MeV peak, the peak total is about 665,000 counts and the background under the peak is 200 × 800 counts/channel or 160,000 counts; therefore, the net count and its uncertainty at 95% confidence (1.96σ) is

$$\text{Net} = 665{,}000 - 160{,}000 \pm 1.96\sqrt{665,000} = 505{,}000 \pm 1600 \text{ counts}$$

(b) The sample concentration is

$$\text{Concentration} = \frac{505{,}000 \text{ counts}}{10 \text{ min} \times 0.125\gamma/\text{d} \times 0.08 \text{ c/d} \times 1.5 \text{ L} \times 0.9 \times 2.22 \times 10^{-6} \text{ d/m per } \mu\text{Ci}}$$

$$= 1.68 \ \mu\text{Ci/L}$$

The uncertainty for this measurement is determined by propagation of individual relative errors (σ/x_i) as illustrated in Example 13-9. The standard deviation of the concentration measurement is

$$\sigma_{\text{conc}} = 1.68 \ \mu\text{Ci/L} \times \sqrt{\left(\frac{1600}{505,000}\right)^2 + \left(\frac{0.010}{0.08}\right)^2 + \left(\frac{0.04}{0.90}\right)^2}$$

$$= 1.68 \ \mu\text{Ci/L} \times \sqrt{9.7 \times 10^{-6} + 0.0156 + 0.00197}$$

$$= 1.68 \ \mu\text{Ci/L} \times \sqrt{1.758 \times 10^{-2}} = 0.22 \ \mu\text{Ci/L}$$

at the 1σ level. For 95% confidence (or 1.96σ), the uncertainty is 0.44 μCi/L and the measured concentration is reported as 1.68 ± 0.44 μCi/L. It is noteworthy that the largest contribution to the uncertainty is not due to the statistics of radiation counting but to the uncertainty in the determination of detector efficiency which is likely high for this type of measurement.

13.4.5 Testing the Distribution of a Series of Counts (the Chi-square Statistic)

The operation of a counting system can be tested by comparing the distribution of a series of repeat measurements with the expected distribution. One measure of performance is the Poisson index of dispersion, or the chi-square statistic, defined as

$$\chi^2 = \frac{\sum_{i=1}^{n} (x_i - \bar{x})^2}{\bar{x}}$$

where $\bar{x}$ is the arithmetic mean of the set of measurements and x_i is the value of each measurement.

The chi-square statistic is plotted as a function of the degrees of freedom F where $F = n - 1$ (Figure 13-7). A system is expected to work normally if the probability of χ^2 lies between 0.1 and 0.9. The system performance is suspect if the p-value of χ^2 lies outside this range. If the measured value of χ^2 is <0.1 (e.g., $p = 0.01$), the replicate counts are fluctuating more than would be expected for a Poisson distribution, and a stability problem in the electronics of the system is likely. If the measured value of χ^2 is >0.9 (e.g., $p = 0.99$), the replicate counts are not fluctuating as would be expected in a Poisson distribution, and it should be suspected that a strong bias problem exists in the counting system.

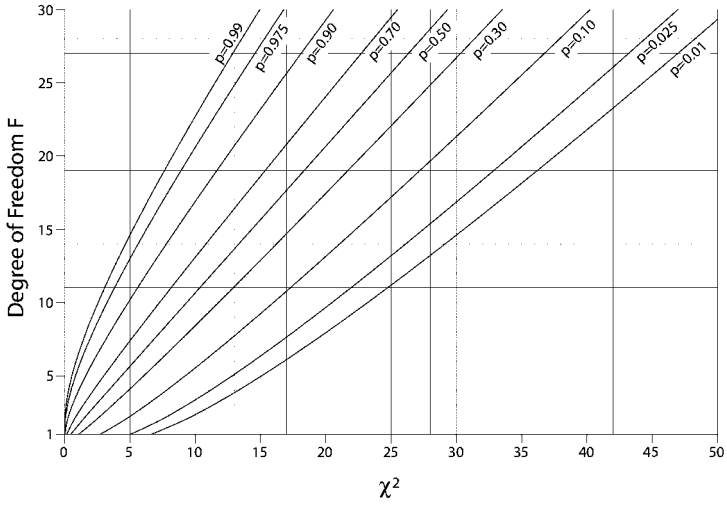

Fig. 13-7 Integrals of the chi-square distribution.

Example 13-17. Five 1 min counts of a given sample had values of 11, 9, 11, 13, and 9. Does the system follow the Poisson distribution?

Solution. The value of χ^2 for the five counts, which have an estimated mean $\bar{x} = 10.6$ is

$$\chi^2 = \frac{\sum (x_i - \bar{x})^2}{\bar{x}} = \frac{11.2}{10.6}$$

$$\chi^2 = 1.06$$

and from Figure 13-7, for $F = n - 1$ or 4 degrees of freedom, $p = 0.90$. The data look somewhat more uniform than expected, but they follow the Poisson distribution and the counting system can be judged to be functioning properly.

13.4.6 Weighted Sample Mean

When measured values are to be averaged and some have better precision than others, a weighted sample mean and a weighted sample standard deviation are desirable. The weighting factor w_i to be assigned to each measurement is

$$w_i = \frac{1}{\sigma_i^2}$$

The weighted mean is given by

$$\bar{x}_w = \frac{\sum_{i=1}^{n} w_i \bar{x}_i}{\sum_{i=1}^{n} w_i}$$

and the weighted standard deviation is

$$\sigma_w = \sqrt{\frac{n}{\sum_{i=1}^{n} w_i}}$$

where n = total number of measurements; $\bar{x}$ = sample mean of a given measurement; σ_i = standard deviation of a given measurement; w_i = weighting factor for a given measurement; $\bar{x}_w$ = weighted sample mean; and σ_w = weighted sample standard deviation.

Example 13-18. Five persons measured the radioactivity in a liquid waste sample. Each took an aliquot, prepared it for counting, and reported the mean of several 10 min counts. The mean of each person's measurements, the weighting factor w_i, and the values of $w_i \bar{x}_i$ are:

$x_i \pm \sigma_i$	w_i	$w_i\bar{x}_i$
315 ± 18 counts	0.00309	0.973
342 ± 20 counts	0.00250	0.885
335 ± 42 counts	0.00057	0.191
321 ± 12 counts	0.00695	2.232
327 ± 25 counts	0.00160	0.523
	$\sum w_i = 0.01471$	$\sum w_i\bar{x}_i = 4.774$

Determine the weighted mean and the weighted standard deviation.
Solution. The weighted mean $\bar{x}_w$ is $\bar{x}_w = 4.774/0.0147 = 324$ counts
The weighted standard deviation is

$$\sigma_w = \sqrt{\frac{5}{0.01471}} = 18 \text{ counts}$$

$$\text{The weighted count rate} = \frac{324 \pm 18 \text{ counts}}{10 \text{ min}} = 32.4 \pm 1.8 \text{ c/m}$$

13.4.7 Rejection of Data

Occasionally, a set of measurements will contain one or more values that appear to be true outliers, and the temptation is to just cast them aside. This is not scientifically correct, nor should it be a standard practice. The appropriate procedure is to first determine if the counting system is performing satisfactorily. If it is, a sample count can be rejected (or kept) based on Chauvenet's criterion, which states that any count of a series of n counts (also the number of observations) shall be rejected when the magnitude of its deviation from the experimental mean is such that the probability of occurrence of all deviations that large or larger does not exceed the value $1/2n$ (assuming that the data represent a normal distribution). Chauvenet's criterion is applied to a set of measurements by determining Chauvenet's ratio, CR, which is

$$\text{CR} = \frac{|x - \bar{x}|}{\sqrt{\bar{x}}}$$

where x is the suspect value in the data set and $\bar{x}$ is its mean.

If the calculated CR for a given value is greater than that listed in Table 13-4 for the specified number of observations, it is appropriate to reject the datum; otherwise, the datum has an acceptable value.

Table 13-4. Limiting values of Chauvenet's ratio, CR.

Number of observations	Limiting ratio	Number of observations	Limiting ratio
2	1.15	15	2.13
3	1.38	19	2.22
4	1.54	20	2.24
5	1.68	25	2.33
6	1.73	30	2.39
7	1.79	35	2.45
8	1.86	40	2.50
9	1.92	50	2.58
10	1.96	75	2.71
12	2.03	100	2.80

Chauvenet's criterion is used to reject a suspect count when it deviates so much from the statistical mean that it adversely affects the experimental mean. If counts from a data set are rejected, the experimental mean is recalculated to obtain a new value that more closely approximates the statistical mean.

Example 13-19. The following 25 observations were made on a sample. Should any of the counts be discarded?

15 19 19 28 18

24 11 20 23 19

20 13 29 23 14

17 22 22 32 30

26 17 18 20 24

Solution. First, a chi-square analysis of the data is performed to determine if the measurement system is performing satisfactorily:

$$\bar{x} = \frac{\sum x_i}{25} = 21$$

and

$$\chi^2 = \frac{\sum_{1}^{25} (x_i - \bar{x})}{21} = 32$$

which is in the satisfactory region of Figure 13-7. Since the system that recorded the counts is functioning properly, Chauvenet's ratio can be used to test the highest and lowest values, 32 and 11, for possible rejection. The CRs for 32 and 11 counts are

$$CR_{32} = \frac{32 - 21}{\sqrt{21}} = 2.4$$

and

$$CR_{11} = \frac{21 - 11}{\sqrt{21}} = 2.2$$

From Table 13-4, CR = 2.33 for 25 observations; therefore, the gross count of 32 can be rejected since $CR_{32} = 2.4 > 2.33$. However, $CR_{11} = 2.22 < 2.33$, and the gross count of 11 should be kept. The chi-square statistic and the mean for the data should then be recalculated without the value of 32.

Caution must be used when rejecting data. Even if data do not meet expectations, they may in fact be quite meaningful, i.e., the data are correct and it is the expectation that is wrong. For example, if Michelson and Morley had rejected their data, we may still be discussing the "omniferous ether," or if Geiger and Marsden (graduate students of Lord Rutherford) had rejected data from their experiments on alpha scattering, discovery of the atomic nucleus would have been missed.

13.5 Levels of Detection

The previous discussions have addressed applications of statistics to measured values in which counts, count rate, or activity levels are determined and an uncertainty is assigned to the measurement. It is often desirable to determine just how sensitive a given radioanalytical procedure, which will be influenced by statistical variations in observed counts, can be. This sensitivity is characterized as a detection level, and many regulatory programs require its determination. The detection level is also of considerable interest for measuring low-activity samples and is influenced considerably by the level of background radiation.

The sensitivity of a measurement system is specified as a detection limit at or near the background level, which at best is only an estimate; it is useful as a guidepost, not an absolute level of activity that can or cannot be detected by a counting system. Three such guideposts are the critical level (L_c), the lower limit of detection (LLD), and the minimum detectable activity (MDA), each of which has a specific definition and application which should not be interchanged in dealing with measurements of radioactivity.

13.5.1 Critical Level

The critical level (L_c) is defined as the net count rate which must be exceeded before the sample can be said, with a certain level of confidence, to contain measurable radioactivity above background. The critical level is derived from the statistical variation that is associated with a true zero net counting rate; when the background counting rate is subtracted from the gross counting rate, the result is zero and the gross counting rate is identical to the background counting rate. A net counting rate of zero has a normal distribution of counts about a mean of zero as shown in Figure 13-8 for which various probabilities exist for observing negative or positive net counting rates. A negative net counting rate occurs when the gross counting rate is less than the background counting rate, and it is understandable that the samples with negative net count rates would be considered as having no activity above background. A positive net counting rate may either be due to activity being present, or it may be due to the statistical probability of observing a net count rate above zero even though the true count rate is zero. Obviously the more positive net counting rate deviates from the zero net counting rate, the more likely it is that radioactivity is present, and, conversely, the closer the net counting rate approaches the zero net counting rate, the greater the probability that a true net zero counting rate exists. A net positive counting rate that is high enough to be concluded as positive with statistical confidence can be referred as the critical level (L_c). It is expressed as

$$L_c = k_\alpha \sigma_0$$

where k_α is the one-sided (i.e., we are interested only in values that are statistically positive) confidence factor of the normal distribution, and σ_0 is the standard deviation of a zero net count rate. If k_α is chosen so that 95% of the measurements of a true zero net count rate are less than L_c, i.e., $k_\alpha = 1.65$, then there is only a 5% chance that a true mean count of zero will be falsely recorded as a positive value.

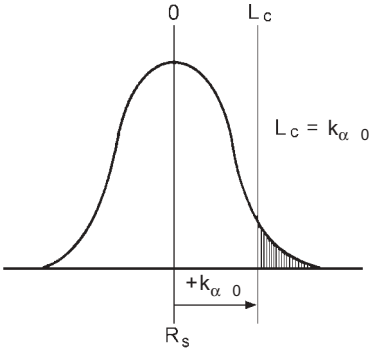

Fig. 13-8 Critical level L_c is that point on the normal distribution curve of counts for a true zero net count above which there is a specified level of confidence that a true mean count of zero would be falsely recorded as positive, i.e., activity is recorded as present when in fact it is not.

If the net count rate of a sample exceeds L_c, it is reported as positive and the two-sided confidence interval is reported in the usual way. If the net count is less than L_c, it can only be said that the total count rate R_{s+b} is not statistically different from the background at the 95% confidence level (or when the false probability = 0.05). A value of L_c based on a different confidence level can be determined from the value of k_α that corresponds to the desired one-sided confidence probability from Table 13-5. For example, if it is desired that a false positive occurs only 1% of the time, a k_α value of 2.326 would be used in determining L_c.

Table 13-5. Probability of a false positive observation of a true net count of zero and the corresponding k_α constant based on the normal distribution.

False positive probability	k_α constant
0.010	2.326
0.025	1.96
0.050	1.645
0.100	1.282

Because the standard deviation of the zero net count rate is a theoretical number it is useful to express the critical level in terms of the standard deviation σ_b of the background count rate R_b:

$$L_c = k_\alpha \sigma_b \sqrt{1 + \frac{t_b}{t_{s+b}}}$$

where k_α is a constant corresponding to a stated false positive probability, t_b is the background counting time, t_{s+b} is the counting time of the sample plus background, and

$$\sigma_b = \sqrt{\frac{R_b}{t_b}}$$

If the count times for the sample and the background are equal, then

$$L_c = k_\alpha \sigma_b \sqrt{2}$$

For a false positive probability of 0.05 (or 95 % confidence), $k_\alpha = 1.645$; therefore

$$L_c = k_\alpha \sigma_b \sqrt{2} = 2.33 \sigma_b$$

or in terms of the background count rate and the background count time

$$= 2.33\sqrt{\frac{R_b}{t_b}}$$

where R_b is the background count rate; thus, L_c is directly related to the background of the detector system and inversely related to the background count time. This relationship and equations for calculating L_c for various other conditions are shown in Table 13-6.

Table 13-6. Equations for calculating the critical level L_c, and conditions for their use.

Condition	Equation
General equation	$L_c = k_a\sigma_b\sqrt{1+\frac{t_b}{t_{s+b}}}$
Unequal count times for background and sample (k_a = 1.645 for 95% confidence)	$L_c = 1.645\left[\frac{R_b}{t_b}\left(1+\frac{t_b}{t_{s+b}}\right)\right]^{1/2}$
Equal count times for background and sample (k_a = 1.645 for 95% confidence)	$L_c = 2.33\sigma_b = 2.33\sqrt{\frac{R_b}{t_b}}$

The critical level should only be used to determine if a measurement is statistically different from background. It is an *a priori* determination and should not be reported as a "less-than" value.

13.5.2 Detection Limit (L_d) or Lower Level of Detection (LLD)

The concept of *minimum detectable activity (MDA)* for a measurement procedure is often stated in terms of the sensitivity of the technique in observing the presence of radioactivity. The MDA can be thought of as a claim of how good the laboratory is, or it may be used to judge a procedure. Some regulatory programs require that the MDA be stated for routine procedures in a radiation protection program and that action be taken for measured activity above the MDA, e.g., waste material that contains measured radioactivity above the MDA be considered as radioactive. Such a regulatory requirement can be quite different from the laboratory perspective in which the MDA is designed to answer the question "what sample count is required to be sure of detecting it on a routine basis?" It is not desirable to specify the MDA in terms of L_c because a single measurement of a true mean net count rate of L_c has an equal chance of being above or below L_c because the counts are normally distributed. This appears contradictory because the L_c itself is determined at the 95% confidence level, but it is a decision tool for ensur-

ing that a true zero net count rate is not falsely interpreted due to its statistical variability. Obviously this is too restrictive and a more reliable value is desirable.

The detection limit (L_d) is the value that should be specified for determining a minimum activity that can be reported as detected with a degree of assurance that it is in fact present; it is defined as the smallest quantity of radioactive material that can be detected with some specified degree of confidence, preferably (and often) as 95%. The detection limit (or L_d) for a measurement is commonly referred to as the lower limit of detection (LLD), and even though LLD and L_d are synonymous, LLD will be used since it connotes the most common use of the statistical concept.

The LLD should be defined above L_c, and, as shown in Figure 13-9, it is the smallest amount of sample activity that will yield a net count above background such that the probability of concluding that activity is present when in fact it is not is limited to a predetermined value, typically $p = 0.05$ (also referred to as a type II (or β) error). A value of k_β that corresponds to the accepted false positive probability (e.g., $k_\alpha = 1.645$ for $p = 0.05$) is chosen for a one-sided confidence interval since wrong determinations relative to the distribution of the net mean of zero are the only ones of interest. Defining LLD in terms of $k_\beta = 1.645$ where $p = 0.05$ states a willingness to accept being wrong only 5% of the time; i.e., when activity is measured at or above the LLD there is a 95% level of confidence that it is actually present, or similarly, a count at LLD will be erroneously concluded to contain activity only 5% of the time. Thus, the LLD is a practical detection limit that considers the statistical variation in measured counts of both sample and background; it is related to L_c as follows:

$$\text{LLD} = L_c + k_\beta \sigma_d$$

where k_β is, again, the one-sided confidence factor and σ_d is the standard deviation of a net count rate equal to LLD.

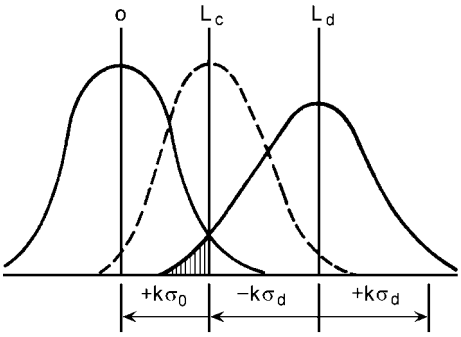

Fig. 13-9 Lower limit of detection (LLD) is the smallest amount of net activity above background that will be registered as positive with a given level of confidence, typically with a false positive level of $p = 0.05$, which corresponds to $k_\beta = 1.645$ for the one-sided normal distribution.

The LLD can be determined in terms of counts per unit time by substituting the expression for L_c and assuming that $k_\alpha = k_\beta = k$:

$$\text{LLD} = \frac{k^2}{t_{s+b}} + 2k\left[\frac{R_b}{t_b}\left(1 + \frac{t_b}{t_{s+b}}\right)\right]^{1/2}$$

This general relationship, the specific generalizations derivable from it, and the conditions for the use of each are summarized in Table 13-7. The latter two expressions, for which it is assumed that $k_\alpha = k_\beta = 1.645$, are frequently used for measurements of radioactivity when it is desirable that the LLD for the observed counts be at the 95% confidence interval. If, however, a different level of confidence is desired, then it is necessary to use the more general equation with the values of k that correspond to the confidence interval selected (Table 13-5 and Example 13-20).

Table 13-7. Equations for calculating the lower limit of detection (LLD) for various conditions and $k = k_\alpha = k_\beta$.

Prerequisites for use	Equation[a]
General equation for LLD as a count rate	$\text{LLD} = \frac{k^2}{t_{s+b}} + 2k\left[\frac{R_b}{t_b}\left(1 + \frac{t_b}{t_{s+b}}\right)\right]^{1/2}$
LLD as a count rate for equal count times for sample and background and for any value of k	$\text{LLD} = \frac{k^2}{t} + 2k\left(2\frac{R_b}{t}\right)^{1/2}$
LLD as a count rate for equal count times for background and sample where $k = 1.645$ 95% confidence level)	$\text{LLD} = \frac{2.706}{t} + 4.653\sqrt{\frac{R_b}{t}}$
LLD in counts for a total background B, equal count times for background and sample, $k = 1.645$ (95% confidence level)	$\text{LLD} = 2.706 + 4.653\sqrt{B}$
LLD in counts for a background B and $t \gg 2.706$	$\text{LLD} = 4.653\sqrt{B}$

a R_b in these equations is the background count rate in counts per unit time t and $\sqrt{B} = \sigma_b$.

The LLD is related only to the observed counts produced by the detector system; i.e., it is not dependent on other factors involved in the measurement method or on the sample characteristics. These other factors, some of which have their own uncertainty, should of course be included in the calculation of the measured activity of the sample and the individual uncertainties should be propagated through the calculation. A typical circumstance is measurement of a sample which includes detector efficiency, chemical recovery, and a measured volume or mass.

Example 13-20. What is the LLD for a detection system that records 50 background counts in 2 h (a) at a 95% confidence level and (b) at a 90% confidence level?

Solution. (a) For 95% confidence, $k = 1.645$, and

$$\text{LLD} = \frac{(1.645)^2}{120\,\text{min}} + 2(1.645)\left[2\left(\frac{0.42\,\text{c/m}}{120\,\text{min}}\right)\right]^{1/2}$$

$$= 0.02 + 0.27$$

$$= 0.29\ \text{c/m}$$

(b) For a 90% confidence level, $k = 1.282$ (Table 13-5), and

$$\text{LLD} = \frac{(1.282)^2}{120\,\text{min}} + 2(1.282)\left[2\left(\frac{0.42\,\text{c/m}}{120\,\text{min}}\right)\right]^{1/2}$$

$$= 0.014 + 0.215 = 0.23\ \text{c/m}$$

Example 13-21. A single measurement of a sample yields a gross count of 465 c/m. If the counting system has a background of 400 ± 10 c/m recorded for the same time interval and for which $t \gg 2.706$, should the measurement be reported as being radioactive?

Solution. The decision point is the critical level, and since the net count rate is 465 – 400 = 65 c/m and $\sqrt{B} = \sigma_b = 10$, then

$$L_c = k_a \sigma_b \sqrt{2} = 2.33 \times 10 = 23.3\ \text{c/m}$$

For even greater confidence, the LLD for 95% confidence can be used; it is

$$\text{LLD} = 4.653 \times 10 = 46.53\ \text{c/m}$$

Since the net count of 65 exceeds the critical level for the system, it can be concluded that the sample is radioactive; it is also above the 95% confidence LLD, a more conservative criterion.

Example 13-22. A gamma peak at 0.910 MeV has a total peak activity of 665,000 counts and the peak background is 160,000 counts (see Example 13-16). Determine the critical level, the LLD, and whether it is appropriate to quantitate the 0.910 MeV peak activity.

Solution. The critical level is

$$L_c = 2.33\sqrt{B} = 2.33\sqrt{160{,}000\,\text{counts}} = 400\ \text{counts}$$

The LLD at the 95% confidence level if $t \ll 2.706$ is

$$\text{LLD} = 4.653\sqrt{160{,}000\ \text{counts}} = 1861\ \text{counts}$$

or in terms of count rate, 186 c/m. Since the net sample count is well above L_c and LLD, the concentration can be calculated directly and the associated uncertainty assigned.

13.6 Minimum Detectable Concentration or Contamination

The LLD can be used to derive a minimum detectable concentration (MDConc.) or contamination (MDCont.) that is measurable with a given detector system and protocol. This quantity is often denoted as minimum detectable activity (or MDA), but MDConc. and MDCont. are more precise terms. The MDC is the *a priori* activity level that a measurement system can be expected to detect and report correctly 95% of the time. Once a confident activity level is determined, it is then adjusted by various conversion factors to give units of activity per unit volume, weight, area, etc. The value of MDC so determined is thus the estimated level of activity per unit volume, weight, area, etc., that can be detected using a given protocol. It should be used before any measurements are made, not after.

13.6.1 Minimum Detectable Concentration (MDConc.)

The MDConc. is a level (not a limit) derived from the LLD (also the detection level L_d). It is a concentration of radioactivity in a sample that is practically achievable by the overall method of measurement. The MDConc. considers not only the instrument characteristics (background and efficiency), but all other factors and conditions that influence the measurement. These include sample size, counting time, self-absorption and decay corrections, chemical yield, and any other factors that influence the determination of the amount of radioactivity in a sample. It cannot serve as a detection limit per se, because any change in measurement conditions or factors will influence its value. It establishes that some minimum overall measurement conditions are met, and is often used for regulatory purposes. When so used it is commonly referred to as the MDA.

The MDConc. for a measurement system is derived from the LLD and expressed as pCi per unit volume or weight of the sample:

$$\text{MDConc.}(\text{pCi/unit}) = \frac{\text{LLD}}{(EY)(\text{volume or weight})(2.22)t}$$

where MDConc. = minimum detectable concentration of activity in a sample; LLD = $2.706 + 4.653\sqrt{B}$; B = counts due to background; E = counting efficiency for a

given detector and geometry; Y = chemical recovery; 2.22 = d/m per pCi; and t = count time for B (min).

A *regulatory MDA* is one use of the LLD, such as determining whether material is a radioactive waste. For example, various plants collect floor drains in a sump to determine whether it can be disposed without regard to its radioactivity or whether it must be considered a radioactive waste that is required to be held for decay, treated, or disposed of according to radioactive waste regulations. The regulatory basis for this decision is the LLD of the detector/sampling system, as long as the activity meets other environmental and public health regulations. This situation is illustrated in Example 13-23.

Example 13-23. Floor drains are consolidated at a nuclear power plant. Two liters of water from the uncontaminated plant water supply (i.e., background) are counted in a Marinelli beaker on a germanium detector that has an efficiency of 8% for ^{137}Cs gamma rays and produces 2000 counts in 2 h. (a) What concentration of ^{137}Cs in the floor drain sump could be disposed of without regard to its radioactivity. (b) What concentration would be allowed if the background for the plant water system measured 500 counts in 30 min under the same conditions?

Solution. (a) Although the critical level for this measurement could provide a determination of positive activity above background, it is too restrictive for this purpose because the confidence level is too low; therefore, the limiting concentration, or the regulatory MDA, should be based on the LLD:

$$\text{LLD} = 2.706 + 4.653\sqrt{2000} = 211 \text{ counts}$$

Therefore, any 2 L sump sample that had a gross number of counts above 2211 (2000 + LLD) for a 2 h measurement would be declared as containing radioactivity and would require additional consideration. An activity of 2000 counts + LLD would correspond to a measured MDConc. in sump water of

$$\text{MDConc.} = \frac{(2000 + 211)\text{ counts}}{0.08\,\text{c/d} \times 120\,\text{min} \times 2\,\text{L} \times 2.22\,\text{d/m per pCi}} = 51.9\ \text{pCi/L}$$

(b) Similarly, for a 30 min measurement of the same background rate, or 500 counts in 30 min:

$$\text{MDConc.} = 56.9\ \text{pCi/L}$$

These two results indicate that a 10% greater concentration could escape regulation if the routine method of measuring sump water were based on a 30 min count of sample and background rather than 120 min. Conversely, if increased sensitivity were the main goal, the longer count would be chosen.

13.6.2 Minimum Detectable Contamination (MDCont.)

For an integrated measurement over a preset time, the MDCont. for a surface activity measurement is based first on the LLD, which is then adjusted for measurement time, detector efficiency, and the active area of the detector:

$$\text{MDCont.} = \frac{2.706 + 4.653\sqrt{B}}{t\varepsilon A}$$

where MDCont. = minimum detectable contamination (d/m per cm^2); B = background counts; t = counting time in min; ε = total detector efficiency in counts/disintegration; and A = physical probe area in cm^2. MDCont. values for other measurement conditions may be derived from this equation depending on the efficiency and area of the detector and contaminants of concern.

Example 13-24. Determine the minimum detectable contamination in units of d/m per 100 cm^2 at a 95% confidence level for a detector with a 20% detection efficiency and an active area of 15 cm^2 if the background level under identical conditions measures 40 counts in 1 min.
Solution.

$$\text{MDCont.} = \frac{2.706 + 4.653\sqrt{40}}{(1)(0.2)(15)} = 10.7\,\text{d/m per cm}^2$$

or, when adjusted to a reference area of 100 cm^2

$$\text{MDCont.} = 1070\ \text{d/m per } 100\ \text{cm}^2$$

These results should be interpreted as follows. The level of contamination that would be reported as detected 95% of the time is 1070 d/m per 100 cm^2 which takes into account all the factors of the measurement, detection efficiency, probe area, scan time, etc. It is also possible to interpret the data in terms of the critical level L_c, which is calculated from the background counts B as

$$L_c = 2.33\sqrt{B} = 15\ \text{counts}$$

This result means that any count yielding 15 counts above the background count of 40 (or 55 total counts) during a 1 min period would be regarded as greater than background. However, any net counts of 15 or more recorded in a 1 min period would represent a positive measurement of activity above background only 50% of the time due to the normal distribution of counts around L_c. Even though it appears that use of L_c increases the sensitivity of the measurement technique, it occurs with considerable loss of confidence in the result. As the net count increases above L_c, the confidence that activity is present also increases.

13.6.3 Less-than Level (L_t)

It is often desirable to record a quantity of radioactive material that could be present but is below detectable levels, or a less-than level L_t. The requirements for L_t are not met by either L_c, which is used for determining if a measured count rate is statistically greater than background, nor by the LLD, which is the true net count a sample must have above background to be sure at a stated level of confidence (e.g., 95%) that a single determination will measure the activity. L_t is, therefore, defined as the maximum true count rate that a sample could have based on the measured count rate, and the standard deviation σ_s of R_s, or

$$L_t = R_s + k\sigma_s$$

where k is the one-sided confidence factor, typically selected for a 95% confidence level, or $k = 1.645$. When so used the calculation of L_t states that there is only a 5% chance that the activity actually present exceeds the stated value of L_t.

In the special case where the sample net count rate is exactly zero, then

$$L_t = k\sigma_0 = L_c$$

and it is possible to have $R_s < 0$ due to the statistical nature of low-level counting but in practical terms calculated values of L_t lie somewhere between L_c and L_d. In terms of count rate

$$L_t = R_s + k\left(\frac{R_s}{t_s} + \frac{R_b}{t_b}\right)^{1/2}$$

and if the sample plus background count time t_{s+b} and the background count time t_b are equal

$$L_t = R_s + k\left(\frac{R_{s+b} + R_b}{t}\right)^{1/2}$$

13.6.4 Interpretations and Restrictions

Perhaps the most onerous aspect of nuclear counting determinations and their uncertainties is the meaning of the reported values. First and foremost, neither the statistically rigorous LLD nor quantities derived from it (e.g., MDA, MDCont., or MDConc.) should be used for routine counting and reporting of measured data. They can, however, be used when the minimum detectable values from a measurement system must be specified (e.g., to a regulatory agency). The LLD, MDCont., or MDConc. (commonly referred to as MDA) are only estimates for a system; they are not absolute levels of activity or activity concentration that can or

cannot be detected in any given sample. Their practical significance is to serve as guideposts or criteria for experimental design, comparison, and optimization purposes, and to serve, for regulatory purposes, as minimally acceptable levels that can be practically achieved and reported.

All measurement results should be reported directly as obtained, and any estimated MDCs should be specified separately and used only to indicate the ability of a sampling/measurement system to detect radioactivity. An MDC derived from the LLD for a detector system should not be calculated for each individual measurement. For routine low-level counting, measurements of the net count rate R_s of a source (or sample) above background should be determined and used as follows:

- If $R_s > L_c$, the result can be determined to be positive; it is reported as $R_s \pm k\sigma_s$, where k corresponds to the chosen two-sided confidence level (e.g., $k = 1.96$ at the 95% confidence ($p = 0.05$) level).
- If $R_s \leq L_c$, L_t is calculated using the one-sided confidence interval and reported as less than $R_s + k\sigma_s$, where $k = 1.645$ at the 95% confidence ($p = 0.05$) level.
- If the data are to be averaged, L_t may be reported but the *absolute* activities (whether positive, negative, or zero) should be recorded and averaged (if the L_t values are used in determining an average value, the result will be biased).

13.7 Log Normal Data Distributions

Many natural entities, when plotted versus their frequency of occurrence, exhibit a skewed distribution with large numbers of smaller entities and a small number of the largest ones. Examples are: areal coverage of vegetation (e.g., kg/m^2); particle sizes (see below); and soil concentrations of minerals such as uranium and thorium, the primordial progenitors of concentrations of radon and thoron (see Chapter 6) which results in skewed distribution of radon levels in homes, as shown in Figure 13-10a. The arithmetic average of such data will be dominated by the small number of large concentrations, which makes it a poor characterization of the data set. A better descriptor is to use the logarithm of each of the values in the set to determine the geometric mean and the geometric standard deviation (GSD). The logarithms are usually normally distributed (see Figure 13-10b) even though the values themselves are not; thus, log-normally distributed data can be characterized in terms of the features of the normal distribution as long as the logarithmic nature of the data set is recognized. For example, 68.3% (a feature of the normal distribution) of log-normally distributed values will lie within one GSD of the geometric mean.

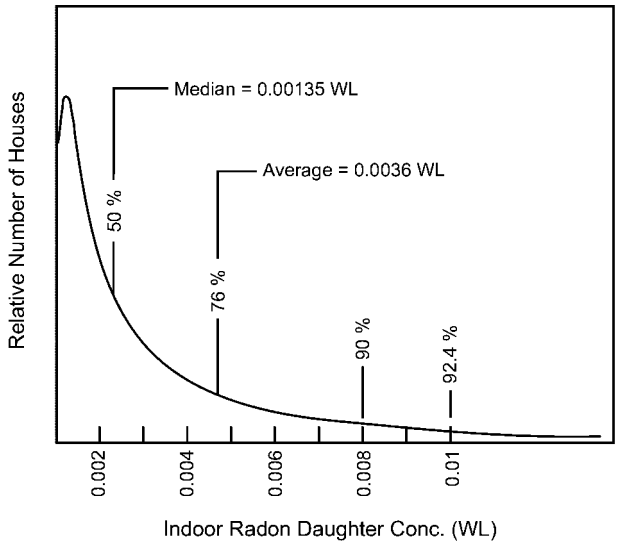

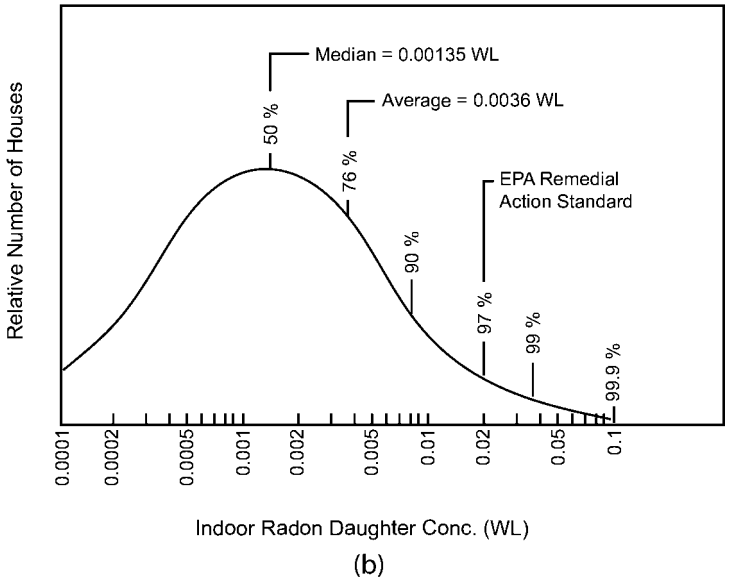

Fig. 13-10 Indoor radon progeny concentrations in 9999 houses plotted (a) as a linear cumulative distribution and (b) logarithmically.

The log normal distribution is a continuous function of the natural (or base10) logarithm of values of x, or

$$f(x) = \frac{1}{\ln(\text{GSD})\sqrt{2\pi}} \exp\left[-\frac{1}{2}\left(\frac{\ln x - \ln(\text{median})}{\ln(\text{GSD})}\right)^2\right]$$

The *geometric mean* can be calculated for n values of x_i by determining the average value of the logarithms of the value $\overline{\ln x_i}$ and finding its antilogarithm:

$$\text{Geometric mean} = \overline{\ln x_i}$$

where

$$\overline{\ln x_i} = \frac{1}{n}\left(\sum_i^n \ln x_i\right)$$

The *geometric standard deviation* (GSD) is calculated for n values of x_i as

$$\text{GSD} = \sqrt{\frac{\sum (\ln x_i - \overline{\ln x})^2}{n-1}}$$

Log normal data analysis uses the features of the normal distribution but with important distinctions. For normally distributed data the mean, median, and the mode (the most likely value) are the same and 68.3% of the data values fall within plus and minus one standard deviation from the mean. Similarly, for log-normally distributed data, 68.3% of the data will also fall between the mean and one geometric standard deviation to either side, but the logarithmic nature of the distribution requires that the mean value be multiplied by the GSD (or a multiple thereof) to obtain the upper value of the spread and divided by the same factor to obtain the lower limit of the data spread. Naturally occurring entities typically have a GSD of about 3.0 (e.g., radon progeny concentrations). This means that 68.3% of the values (a property of the normal distribution) are within the geometric mean divided by 3.0 and the geometric mean times 3.0. This is often referred to as the times-divided-by factor, or

$$\text{Geometric mean} \frac{\times}{\div} \text{GSD}$$

Also due to their logarithmic nature, 95.4% of the values will fall between the geometric mean $\frac{\times}{\div}$ GSD^2.

In practice, therefore, a statement of the geometric mean of a skewed data set indicates that half the values (50%) fall below it and half above it. The GSD represents the spread of the data about the mean; i.e., a small GSD represents a tightly spread set of data and a large GSD a much wider spread. Thus, a calculation that uses a measured data point (e.g., an environmental variable) close to or at the geo-

metric mean of a data set with a small GSD is likely to be more representative than one with a large GSD. If only one value is selected, the mode (the most frequent value) is perhaps the most representative.

Log normal data analysis can easily be done by plotting the data as a cumulative frequency distribution on log-probability graph paper (see Section 13.7.1). Three operations are important: (a) demonstration that the data yield a straight line and are thus log-normally distributed; (b) finding the geometric mean which is the 50th percentile value from the graph; and (c) determining the GSD (or the times-divided-by factor) which is just the ratio of the 84.13 and the 50th percentile values, or alternatively the 50th percentile value divided by the 15.87% value. Graphing the cumulative frequency is especially useful when the data include a substantial number of values "less than" the minimum detectable limit of the measurement system (e.g., the distribution of radiation doses received by a large number of personnel). It is useful to group the data by increasing cutoff values with the last few large values plotted individually (a 100% cumulative value cannot be plotted since the log-probability (or semi-log) scale does not go to 100%).

13.7.1 Particle Size Analysis

The sizes of particles associated with a source are usually log-normally distributed, which influences the manner in which they are measured and considered in personnel protection. The physical behavior (settling velocity, deposition, etc.) of particles in ambient air is greatly influenced by their aerodynamic diameter (d_{ae}) which is a function of both physical size d and density ρ.

Aerosols are typically sampled with a cascade impactor (Figure 13-11) which has a series of openings of successively decreasing width which produces jets of increasing velocity through each successive opening. Cascade impactors are operated at steady (by use of a critical orifice) and relatively high flow rates, which allows collection of sufficient mass for gravimetric or radioanalytical analysis.

Massive particles entering the impactor will, because of their inertia, impact on the first stage, while lighter particles can be carried by the airstream to successive stages, where they are collected by impaction as a function of their velocity. Each stage consists of a medium (a filter or a glass slide coated with adhesive) which collects the particles, and these can be measured gravimetrically, or for radioactive particles radiometrically. This process is repeated several times, before passing through a membrane filter that removes those particles small enough to have escaped impaction on the last stage.

With careful analysis the mass of material collected at each stage can be associated with a certain mass median aerodynamic diameter (MMAD), or if measured radiometrically (since radioactivity is directly proportional to mass) the activity median aerodynamic diameter (AMAD), i.e., the particle size that is collected with 50% efficiency by that stage.

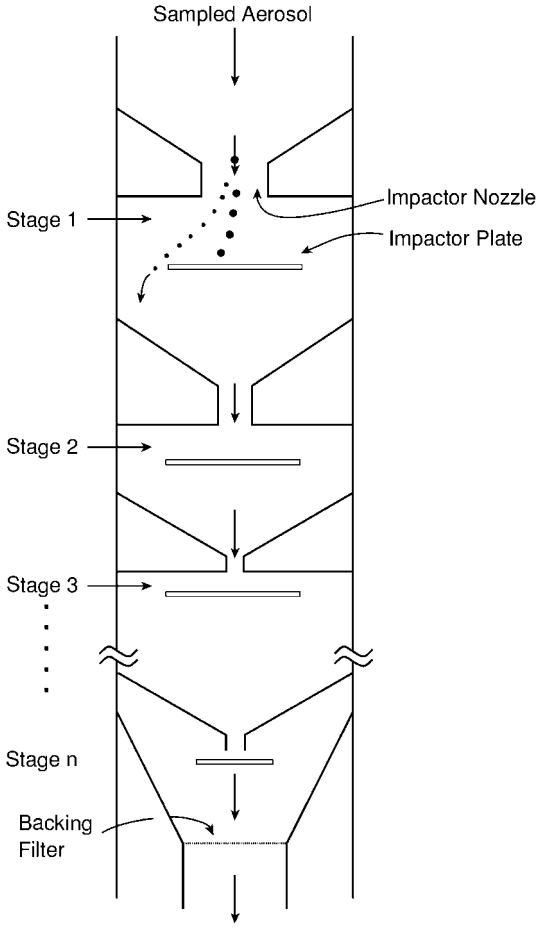

Fig. 13-11 Schematic of a cascade impactor of *n* stages and approximate flow of the sampled aerosol.

Determination of the particle size distribution of a sampled aerosol requires a series of calibration curves, as shown in Figure 13-12 for a four-stage cascade impactor. All particles above a prescribed diameter should theoretically be removed, and all those below the cutoff diameter should penetrate through to succeeding stages. In reality, however, the collection characteristics of impactors yield S-shaped calibration curves of percent deposition of unit density particles versus particle size. As shown in Example 13-25, the mass (or radioactivity) collected on each stage is measured and the aerodynamic diameter d_{ae} is calculated for each collection stage based on the density of the sampled particles (ρ_2):

$$d_{ae} = d_1 \sqrt{\frac{\rho_1}{\rho_2}}$$

where d_1 and ρ_1 are the aerodynamic equivalent diameter and density of particles used to obtain the calibration curves. The adjusted cumulative mass on each collection stage is then plotted as a function of the 50th percentile collection obtained from the calibration curves for each stage usually as a cumulative log normal function (see Figure 13-13).

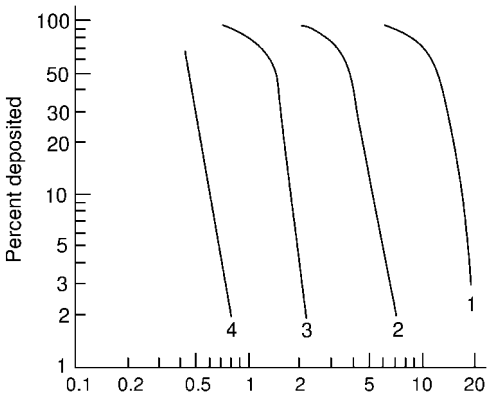

Fig. 13-12 Calibration curves of percent deposition of unit-density (1 g/cm³) aerosols for a four-stage cascade impactor. (Adapted from Cember.)

Example 13-25. Determine the median particle size of a U_3O_8 aerosol of density $\rho = 8.3$ g/cm³ that was sampled with a cascade impactor calibrated for unit-density aerosols (Figure 13-12) in which the percent of the total mass was 11.2, 12.4, 49.6, and 12.2% for stages 1 to 4 and 3.0% for the stage 5 (filter).

Solution. Since the sampled particles have a density different from the unit density particles used in obtaining the calibration curves (1 g/cm³), it is first necessary to calculate their mean aerodynamic equivalent size. For example, for stage 3 the calibration curves (Figure 13-12) show that 1.5 μm particles of unit density are collected with 50% efficiency; thus, the MMAD is

$$d_{ae} = 1.5\,\mu\text{m}\sqrt{\frac{1.0\,\text{g/cm}^3}{8.3\,\text{g/cm}^3}} = 0.52\,\mu\text{mMMAD}$$

which is also the AMAD. This value and the cumulative percentage up to the respective stage (i.e., all the weight (or activity) on the preceding stages plus one-half the weight on the stage in question) is tabulated and plotted. Data for each stage (obtained from the calibration curves and corrected for density) are listed in Table 13-8. These values are plotted on log probability paper in Figure 13-13 and the mass median diameter is found to be 0.7 μm; i.e., 50% of the mass (or activity) of the sampled aerosol is in particles less than this diameter. The GSD = 3.0 is

obtained as the ratio of the 84th and 50th percentiles. Greater emphasis is given to the weights on stages 2, 3, and 4, since the upper limit on stage 1 can be very large and the lower limit on stage 5 (the membrane filter) can be very small.

Table 13-8. Mass and size distributions of U_3O_8 aerosols.

Stage	% Total mass	Cumulative percent[a]	MMAD
1	11.2	94.4	4.26
2	12.4	71.0	1.35
3	49.6	40.0	0.52
4	12.2	9.1	0.16
Filter	3.0	1.5	–

a 50% of mass on each stage plus that on preceding stages.

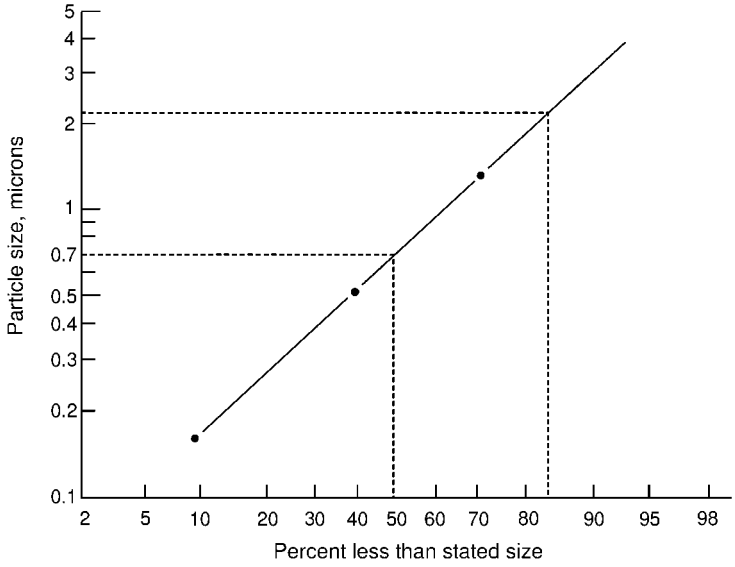

Fig. 13-13 Data from Example 13-25 plotted on log probability paper, yielding a geometric mean particle size of 0.7 μm (with a geometric standard deviation of 3.0, i.e., the ratio of the 84% (2.1 μm) and 50% (0.7 μm) sizes).

Particle size analysis is important to radiation because calculated doses ($H_{50,T}$) due to inhaled aerosols are dependent on particle size. Committed dose equivalents (CDE) can be adjusted (see Chapter 9) to reflect the aerosol size distribution present using tissue-specific CDEs provided by ICRP for 1 μm AMAD particles

for each clearance class. ICRP has listed the percentage of each tissue-specific CDE due to deposition in the NP, TB, and P regions of the lung; thus, adjusted values of $H_{50,T}$ are obtained as the ratio of the deposition fraction and those for 1 μm AMAD (Figure 9-5 or Table 9-9) particles for the size of the inhaled radioactive aerosol.

Acknowledgment

Much of the information on statistical tests and examples were assembled by Ihab R. Kamel MD, PhD and Chul Lee MS, both graduates of the University of Michigan Radiological Health Program. The presentation of detection levels relied considerably on the paper by J. C. Lochamy who brought clarity to an otherwise complex concept. The information on log normal data was suggested by Dr. Keith Schiager who has served the profession of radiation protection with distinction.

Other Suggested Sources

Altshuler, B., Pasternak, B. **1963**, Statistical measurements of the lower limit of detection of a radioactivity counter, *Health Physics* 9, 293–298.
Cember, H. **1996**, Introduction to Health Physics, 3rd ed. (McGraw Hill: New York).
Currie, L. A. **1968**, Limits for qualitative detection and quantitative determination, *Anal. Chem.* 40 (3), 586–693.
Currie, L. A. **1984**, Lower limit of detection: definition and elaboration of a proposed position for radiological effluent and environmental measurements, NUREG/CR 4007, US Nuclear Regulatory Commission.
Lochamy, J. C. **1981**, *The Minimum Detectable Activity Concept*, PSD No. 17, EG&G ORTEC, Oak Ridge, TN.
US NRC **1997**, *Multi-Agency Radiation Survey and Site Investigation Manual* (MARSSIM), NUREG-1575, US Nuclear Regulatory Commission, Washington, DC.
Watson, J. E. **1980**, *Upgrading Environmental Radiation Data*, report HPSR-1, Health Physics Society Committee.

Chapter 13 – Problems

13–1. A single count of a radioactive sample yields 100 counts in 2 min. What is the uncertainty in the count and the count rate for a 1σ confidence interval and a 95% confidence interval.
13–2. Compare the 95% uncertainties of a 2 min measurement yielding 100 counts (see Problem 13-1) and another 2 min count that gives 1000 counts.

13–3. A counter registers 400 counts in 2 min. What is the count rate and its standard deviation? How long would the sample have to be counted to show a percent error of 5% with 90% confidence?

13–4. Calculate the total number of counts that would have to be recorded in a single counting measurement in order for the 1σ uncertainty to equal exactly 1%.

13–5. A single 1 min count of a radioactive ^{137}Cs source is 2000 counts. What is the expected range of values within which another count could be expected to appear with the same counting conditions (a) at a 68.3% confidence level and (b) at 95% confidence?

13–6. If the counter setup in Problem 13-5 has a measured background rate of 100 c/m (measured during a counting time of 1 min), calculate the net count rate and its uncertainty (a) at a 68% confidence level and (b) at 95% confidence. What percent errors do these results have?

13–7. A bench model GM counter records 200,000 c/m on a wipe test sample. The counter has a dead time of 125 μs. (a) What is the true count rate? (b) If the counter efficiency is 16%, what is the actual activity in the sample?

13–8. A beta-sensitive probe with an area of 20 cm^2 is used with a scaler readout to measure total surface contamination. The readout test time is 1 min, and the background was measured for 10 min. If the efficiency is 32%, what is the MDCont. level in d/m per 100 cm^2 for the detector?

13–9. A long-lived radioactive sample produces 1100 counts in 20 min on a detector system with measured background of 900 counts in 30 min. What is the net sample count rate and its standard deviation?

13–10. A sample was measured and reported at the 95% confidence level as 65.2 ± 3.5 c/m. The background was measured at 14.7 ± 4.2 c/m. Determine the net count rate for the sample and its uncertainty at the 95% confidence level.

13–11. The gross count rate of a weak ^{60}Co source is estimated to be 65 c/m in a system with a 10 c/m background. If 1 h is allocated for counting the background and the source, calculate the optimum counting times for each.

13–12. A 10 min sample count yields 1000 counts on a GM detector system that registers 2340 background counts in 1 h. If both sample and background are to be recounted in the next 2 h, what is the optimum division of counting time between the two?

13–13. Four aliquots of a sample were measured with count rates and respective standard deviations of 95 ± 3, 105 ± 10, 94 ± 6, and 118 ± 12. Determine the weighted sample mean and the 1σ uncertainty of the weighted mean.

13–14. An environmental sample yielded 530 counts in 10 min and a 30 min background for the detector registered 50 c/m. (a) Determine the probability that the sample count is different from background and (b) whether this difference is significant at the 95% confidence level.

14
Neutrons

"The possible existence of an atom of mass 1 (and zero) charge…(with) novel properties…to move freely through matter…unite with the nucleus or be disintegrated by its intense field… How (else) on earth (are you) to build up a big nucleus with a large positive charge."
Lord Ernest Rutherford (1920)

The neutron, which was discovered by Chadwick in 1932 after about three weeks of tireless experimentation and calculation (following which he wished "to be chloroformed and put to bed for a fortnight"), had actually been predicted by Rutherford some 10 years earlier (see Chapter 2). Neutrons interact with matter by various scattering reactions and can be absorbed to yield new products some of which may be radioactive. In light materials such as water or tissue they interact by elastic scattering reactions with considerable energy transfer which rapidly slows them to thermal energies. These processes affect neutron dosimetry, neutron shielding, and detection of neutrons.

14.1
Neutron Sources

Nuclear reactors and accelerators produce neutrons with a wide range of energies; these are immediate sources, and the production of neutrons terminates when they are shut down. Various neutron generators depend on irradiation of a target material, and neutrons from these sources are also terminated when the source of irradiation is removed. Alpha-neutron sources contain beryllium or ^{2}H mixed with an alpha-emitting material which of course persists and changes according to the radioactivity of the alpha source used. Similarly, beryllium and ^{2}H can also be used with a high-energy gamma emitter as a photoneutron, or (γ,n) source of neutrons. Neutrons from accelerators or nuclear reactors typically emanate as a beam and these are readily characterized in terms of a fluence of neutrons per unit area (n/cm^2) or a fluence rate or flux (n/cm^2 s); point sources, disk sources,

Physics for Radiation Protection, Third Edition. James E. Martin

and volume sources can be similarly characterized. Table 14-1 lists common sources of neutrons, their energy range, and the average energy obtained.

Table 14-1. Neutron sources by production mode and energy.

Source	Reaction	Energy range	Average energy (MeV)
^{124}Sb–Be	(γ,n)	[a]	0.024
^{88}Y–Be	(γ,n)	[a]	0.16
^{24}Na–D_2O	(γ,n)	[a]	0.22
^{88}Y–Be	(γ,n)	[a]	0.31
^{24}Na–Be	(γ,n)	[a]	0.83
Fission	(n,n)	0–8 MeV	2
^{2}H–^{2}H (D-D)	(d,n)	[a]	3.27
^{226}Ra–Be	(α,n)	0–8 MeV	5
^{239}Pu–Be	(α,n)	0–8 MeV	4.5
^{252}Cf	Spontaneous fission	0–10 MeV	2.3
^{2}H–^{3}H (D-T)	(d,n)	[a]	14.1

a Essentially monoenergetic depending on self-absorption in the source.

The deuterium–tritium (D-T) generator is a straightforward source of high-energy neutrons in which a tritium target is bombarded by deuterons that have been accelerated to about 200 keV. The reaction is exoergic and releases 17.6 MeV, of which 14.1 MeV is given to the ejected neutron. The neutrons so produced are monoenergetic and are ejected isotropically which causes the flux to fall off as the square of the distance.

Cyclotron-produced neutrons are of high energy and are produced by accelerating high-energy deuterons onto a beryllium target. Neutrons released in the ^{9}Be(d,n)^{10}B reaction are peaked in the direction of the deuteron beam and, depending on the number of deuterons in the incident beam, can produce intense focused beams of neutrons. The neutrons are not, however, monoenergetic but are distributed around a peak energy.

Photoneutron sources yield monoenergetic neutrons which can be quite useful for many research purposes, calibration of instruments, and neutron dosimetry.

Alpha-neutron sources consist of radium, polonium, and plutonium intermixed with beryllium which, because of the *Q*-value of the reaction yields specific-energy neutrons; however, self-absorption of the alpha particles in the source causes the neutrons to be distributed about an average value that is usually several MeV (see

Table 14-1). Such sources are always a compromise between a desired source lifetime and the amount of alpha-emitting material that must be mixed with beryllium to obtain the desired source strength and energy range.

Spontaneous fission neutron sources are also available with ^{252}Cf being the most common and practical source because of its yield of 2.3×10^{12} n/s per g (4.3×10^{9} per Ci). The neutrons are emitted with a spectrum of energies from thermal up to several MeV with an average energy of about 2.3 MeV. The half-life of ^{252}Cf is 2.638 y, and transformation occurs by fission about 3% of the time and by alpha particle emission about 97% of the time (see Figures 3-21 and 3-26).

Most neutron sources produce energetic neutrons (see Table 14-1) that are termed "fast" neutrons because of their velocities at these energies. Although neutrons are born fast, they quickly undergo various interactions with media and their energy is degraded. Neutrons are best classified in terms of their energies into the following broad groups:

- cold ($T < 20\,°C$): <0.0253 eV;
- thermal: 0.0253 eV;
- epithermal: 0.0253 to ~1 eV (energies corresponding to room temperature and extending up to the sharp absorption cutoff by a cadmium absorber);
- epicadmium (neutrons that are transparent to a cadmium absorber (strong resonance capture of about 20,000 b at about 0.4 eV)): >1 eV;
- slow: 0.0253–100 eV;
- intermediate: 0.5–10^4 eV;
- fast: 0.01–10 MeV;
- high energy: >10 MeV.

The slow and intermediate classes are often used interchangeably and/or without distinction.

14.2 Neutron Parameters

The two most important properties of neutrons relative to radiation protection are the probability of interaction in a medium, denoted by the cross-section (see Chapter 4) and the energy transferred to or deposited in the medium. Cross-sections are directly related to neutron energy and the absorbing medium as illustrated in Figure 14-1 for boron and cadmium. A distinguishing characteristic of the cross-section for some absorbers (e.g., cadmium in Figure 14-1) is the presence of resonance peaks while others (e.g., boron in Figure 14-1) have large regions in which the cross-section decreases uniformly with neutron energy even though resonances may exist at higher energy ranges. Such decreases are governed by the $1/v$ law, where v is the neutron velocity which, in turn, is proportional to $\sqrt{E}$. Because of the $1/v$ dependence of many materials, it has been standard

practice to specify all neutron absorption cross-sections, whether absorbers are $1/v$ or not, at 0.0253 eV, which corresponds to the velocity a neutron has at standard room temperature, or 2200 m/s. For $1/v$ absorbers, it is straightforward to determine the absorption cross-section $\sigma_a(E)$ at any other energy, as long as it is in the $1/v$ region, by

$$\sigma_a(E) = \sigma_a(E_0)\sqrt{\frac{E_0}{E}}$$

where E and E_0 are any two known energies and $\sigma_a(E_0)$ corresponds to the lower one; $\sigma_a(E_0)$ is typically at thermal energy because precise values have been determined for many elements.

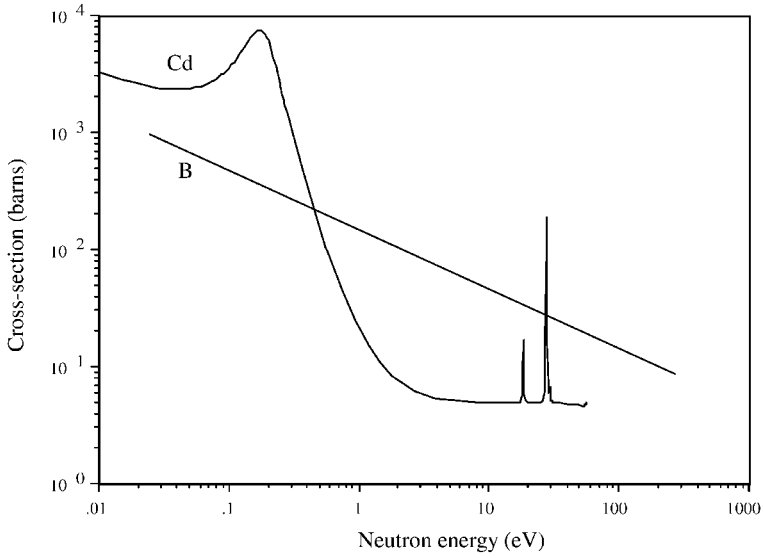

Fig. 14-1 Neutron absorption cross-section versus neutron energy for boron and cadmium.

Example 14-1. Determine σ_a for neutrons of 10 eV in hydrogen (σ_a at thermal energy = 0.333 b).

Solution. The absorption cross-section for hydrogen is $1/v$, therefore

$$\sigma_a(10\,\text{eV}) = \sigma_{a,th}\sqrt{\frac{E_0}{E}}$$

$$= 0.333\text{b}\sqrt{\frac{0.0253\,\text{eV}}{10\,\text{eV}}} = 0.0167\,\text{b}$$

14.3 Neutron Interactions

Radiation protection for neutrons involves three types of interactions: elastic scattering, inelastic scattering, and capture. Each of these occurs between the neutron and the nuclei of target atoms; electrons of atoms are rarely involved in the primary interaction. *Elastic scattering interactions* are quite effective in slowing down neutrons in light materials, especially hydrogen. The energy spectrum will of course change significantly as these scattering reactions moderate the original neutrons in the beam. A free neutron will eventually be captured; however, since free neutrons are unstable, some may undergo radioactive transformation ($T_{1/2}$ = 10.25 m) to create a hydrogen ion and a beta particle before capture can occur. Both will be absorbed nearby. *Inelastic scattering* interactions are also effective in slowing neutrons. These produce excitation of nuclei in the absorbing medium, and this energy is almost immediately released by the emission of photons. Inelastic scattering is most prominent for fast neutrons and heavy nuclei; consequently fast-neutron interactions often produce an associated source of gamma rays, especially if the neutron energy is above 1 or 2 MeV and the absorbing medium contains high-Z atoms. Neutron shields will usually absorb the photons released in inelastic scattering reactions because the thickness required to absorb most of the neutrons is also sufficient to attenuate any gamma rays released by the excited nuclei.

Capture reactions are likely to occur after elastic and inelastic interactions slow neutrons down (or moderate them) to resonance or thermal energies so they can be readily absorbed in target nuclei of the absorbing medium. Capture gamma rays can be quite energetic at several MeV and, depending on the shield material, may require additional consideration because of their very high energy.

The amount of energy transferred to a target atom during elastic and inelastic interactions is most useful for radiation dose determinations because the recoiling target atoms will deposit all of the energy transferred to them within a few micrometers of the sites of interactions. For elastic collisions the average energy $\bar{E}'$ transferred to recoiling target atoms by neutrons of initial energy E is

$$E - \bar{E}' = \tfrac{1}{2}(1 - \alpha)E$$

where

$$\alpha = \left(\frac{A-1}{A+1}\right)^2$$

and A is the mass number of the target nucleus.

Scattering interactions in hydrogen, a large component of tissue, are unique. Inelastic scattering cannot occur in either hydrogen or deuterium since these nuclei have no excited states. Resonance scattering or absorption also does not occur (see Figure 14-3 below) and σ_s is constant up to above 10^4 eV and σ_a follows

the $1/v$ law. For elastic scattering interactions $E'_{\min}$ is zero, and the average energy transferred is

$$E - \bar{E}' = \frac{1}{2}(1 - a)E = \frac{1}{2}E$$

since a for ^{1}H is zero. Hydrogen is thus important for neutron dosimetry because one-half of the energy of intermediate and fast neutrons is transferred to the recoiling hydrogen atoms. This energy transfer relationship also explains why hydrogenous materials are so effective in slowing down (or moderating) high-energy neutrons.

For heavier media, the amount of energy transferred by elastic scattering interactions decreases appreciably and is less than 1% for lead and uranium absorbers. Consequently, the principal mechanism of energy loss by high-energy neutrons in heavy materials is by inelastic scattering interactions. Under these conditions, σ_{is} is generally quite a bit less (of the order of 2–3 b) than elastic scattering cross-sections for fast neutrons ($E > 1$MeV), but it is still the most effective mechanism for slowing neutrons in heavy materials because of the large energy decrease that occurs with these interactions. Neutrons of energy E will have an average energy $\bar{E}'_{is}$ after inelastic scattering in a medium of atomic mass A of approximately

$$\bar{E}'_{is} \cong 6.4\sqrt{\frac{E}{A}}$$

For example, if iron is used to shield 14.1 MeV neutrons from a D-T generator, the average energy after an inelastic collision with an iron atom ($A = 56$) will be about 3.2 MeV. Elastic scattering of 14.1 MeV neutrons in water or paraffin only reduces their energy by about half, or to 7 MeV. On the other hand, neutron energy deposition in tissue, made up of light elements, is due almost solely to elastic scattering since inelastic scattering interactions are very small in light elements.

Cross-section data for inelastic scattering are sparse. Most of the available data are for uranium, plutonium, etc., and mainly because of the need to describe neutron energy spectra related to fission. Inelastic cross-sections for neutron interactions in these media are also relatively small (of the order of 1–3 b).

14.3.1
Neutron Attenuation and Absorption

It is practical, useful, and convenient to represent neutron intensity in terms of the number per unit area, either as a fluence (n/cm^2) or as a fluence rate or flux (n/cm^2 s). The interactions that slow neutrons down and cause their eventual removal from a beam are probabilistic: they either occur or they do not. Consequently, a flux of neutrons of intensity I will be diminished in a thickness x of absorber proportional to the intensity of the neutron source and the neutron removal coefficient Σ_{nr} of the absorbing material:

$$-\frac{dI}{dx} = \Sigma_{nr} I$$

which, like photon attenuation, has the solution

$$I(x) = I_0 e^{-\Sigma_{nr} x}$$

where I_0 is the initial intensity and $I(x)$ refers to those neutrons that penetrate a distance x in an absorber without a collision; therefore, $e^{-\Sigma_{nr} x}$ represents the probability that a given neutron travels a distance x without an interaction. Conceptually, Σ_{nr} can be thought of as the probability per unit path length that a neutron will undergo an interaction as it moves through an absorber and be removed from the beam either by absorption or scattering. In this context then it very much resembles the attenuation coefficient for photons in "good (or narrow-beam) geometry," and can be similarity developed and used for neutron shielding and dosimetry.

The features of neutron beams, including the concept of "narrow-beam" effects, are shown schematically in Figure 14-2. The various interactions serve to remove a neutron from the beam such that it does not reach the receptor of interest, e.g., a detector or a person. In this respect, elastic and inelastic scattering interactions deflect neutrons out of the beam and Σ_{nr} accounts for all of the processes that do so. However, neutrons scattered from the narrow beam are likely to undergo other scattering interactions and be deflected back into the beam and reach the receptor. These more realistic, or "poor geometry" conditions, are accounted for with a "neutron buildup" factor.

When no hydrogenous materials are present the neutron removal coefficient Σ_{nr} is determined by the macroscopic cross-section, $\Sigma = N\sigma_t$ where N is the number of target atoms/cm^3 in an absorber and σ_t is the total cross-section in barns (10^{-24} cm^2/atom) for each atom in a unit volume of absorber. Therefore Σ_{nr} has units of cm^{-1} and is closely related physically to the attenuation coefficient for photons (and the beta absorption coefficient for electrons), and is in fact used in a

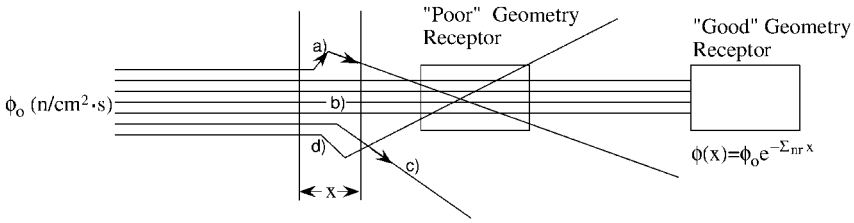

Fig. 14-2 Schematic of interactions in an absorber of thickness x that deplete a beam of neutrons by (a) inelastic scattering followed by photon emission and another scattering reaction back into the beam, (b) absorption or capture, (c) elastic scattering out of the beam, or (d) elastic scattering with additional scattering back into the beam. However, in poor geometry conditions some of the scattered neutrons are scattered back into the beam which must be accounted for with a neutron buildup factor.

similar way; it can be converted to a neutron mass coefficient (cm^2/g) by dividing by the density of the absorber:

$$\text{Neutron mass coefficient } (cm^2/g) = \Sigma_{nr}/\rho$$

Another related concept is the mean free path which is the average distance a neutron of a given energy will travel before it undergoes an interaction. The mean free path can also be thought of as the average thickness of a medium in which an interaction is likely to occur and is similar to the mean life of a radioactive atom. It has the value

$$\text{Mean free path} = 1/\Sigma_{nr}$$

Example 14-2. What is the neutron removal coefficient and mean free path of 100 keV neutrons in liquid sodium which has a total cross-section of 3.4 b at 100 keV?

Solution. Sodium at STP contains 0.0254×10^{24} atoms/cm^3; therefore, the neutron removal coefficient in this case is the macroscopic cross-section

$$\Sigma_{nr} = 0.0254 \times 10^{24} \text{ atoms/cm}^3 \times 3.4 \times 10^{-24} \text{ cm}^2/\text{atom} = 0.0864 \text{ cm}^{-1}$$

The mean free path (i.e., the average travel distance without an interaction) is

$$\text{Mean free path} = \frac{1}{\Sigma} = \frac{1}{0.0864} = 11.6 \text{ cm}$$

Note that in these types of calculations it is somewhat convenient to express the atom density in units of 10^{-24} since it cancels with the 10^{-24} unit for the barn.

14.4 Neutron Dosimetry

The composition of tissue, which is the primary medium of interest in neutron dosimetry, is shown in Table 14-2. The macroscopic cross-section, $\Sigma = N_i\sigma_i$, is used to determine energy deposition in tissue due to interactions with its various components. It is important to recognize that it is different from the total neutron removal coefficient used for shielding calculations (see below); i.e., the approach for energy deposition in tissue uses specific values for the interaction processes involved, whereas shielding calculations use values of Σ_{nr} specifically measured for shielding materials.

Table 14-2. Atom density in tissue.

Element	Atoms/cm^3 or g
Hydrogen	5.98×10^{22}
Oxygen	2.45×10^{22}
Carbon	9.03×10^{21}
Nitrogen	1.29×10^{21}
Sodium	3.93×10^{19}
Chlorine	1.70×10^{19}

Source: Adapted from ICRP-23, Standard Man.

Fast neutrons lose energy in tissue primarily by elastic scattering, and slow and thermal neutrons undergo capture reactions primarily by $^1H(n,\gamma)^2H$ and $^{14}N(n,p)^{14}C$ reactions. The (n,γ) reaction in hydrogen releases a capture photon of 2.225 MeV which may also deposit some of its energy in the body. The (n,p) reaction with nitrogen produces a 0.626 MeV proton and all of this energy will be deposited near the site of the interaction. Neutron interactions may also occur with carbon and oxygen in tissue. Since hydrogen, nitrogen, carbon, and oxygen are important to neutron energy deposition in tissue, their cross-sections versus neutron energy are plotted in Figures 14-3, 14-4, 14-5, and 14-6, respectively.

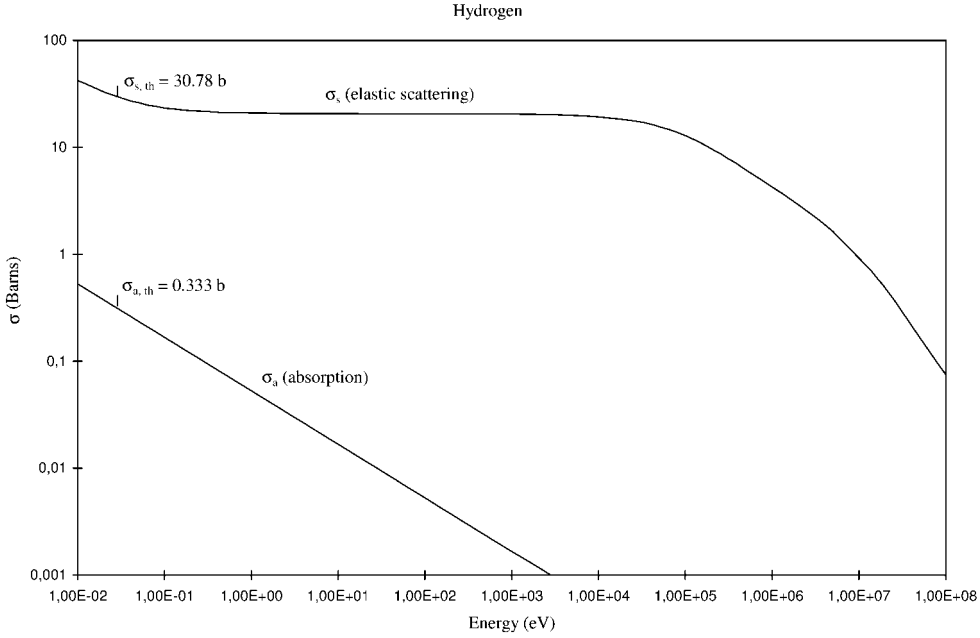

Fig. 14-3 Neutron absorption (capture) and elastic scattering cross-sections (in barns) in hydrogen. The curve for elastic scattering is effectively the total neutron interaction in hydrogen since σ_a is small.

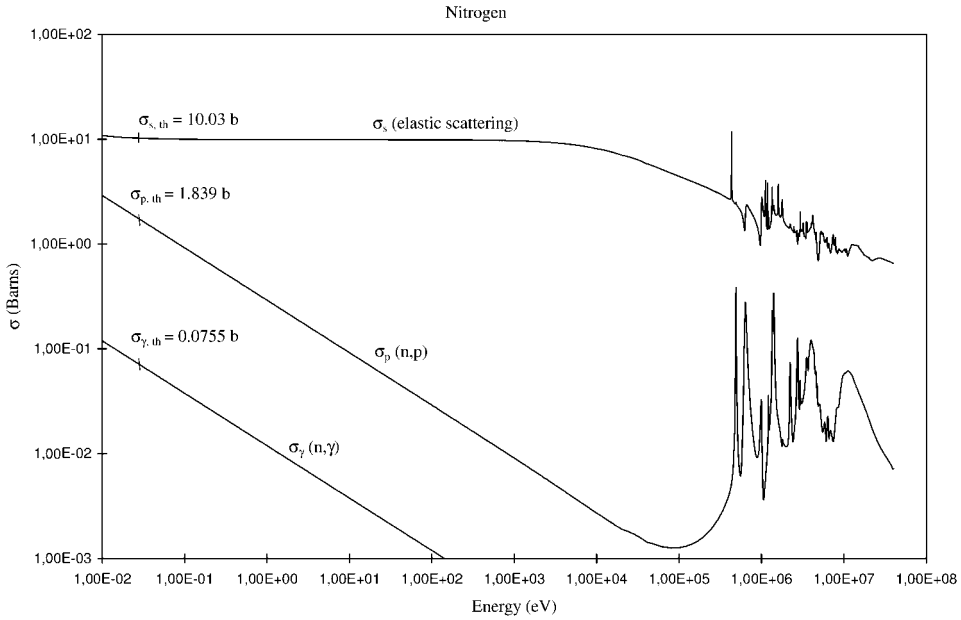

Fig. 14-4 Neutron absorption (capture) and elastic scattering cross-sections (in barns) for nitrogen.

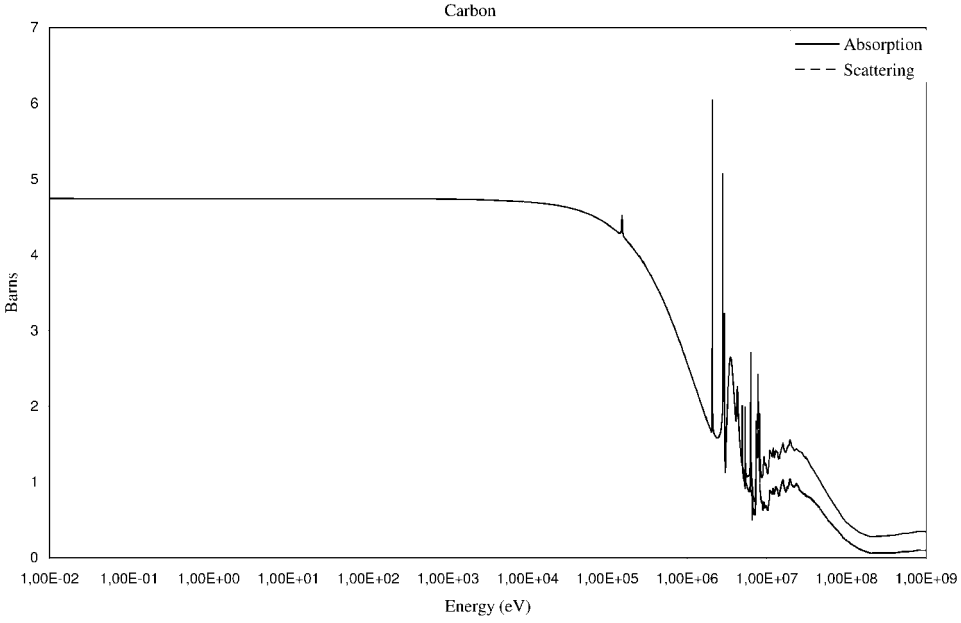

Fig. 14-5 Total neutron (absorption + scattering) and elastic scattering cross-sections (in barns) for carbon.

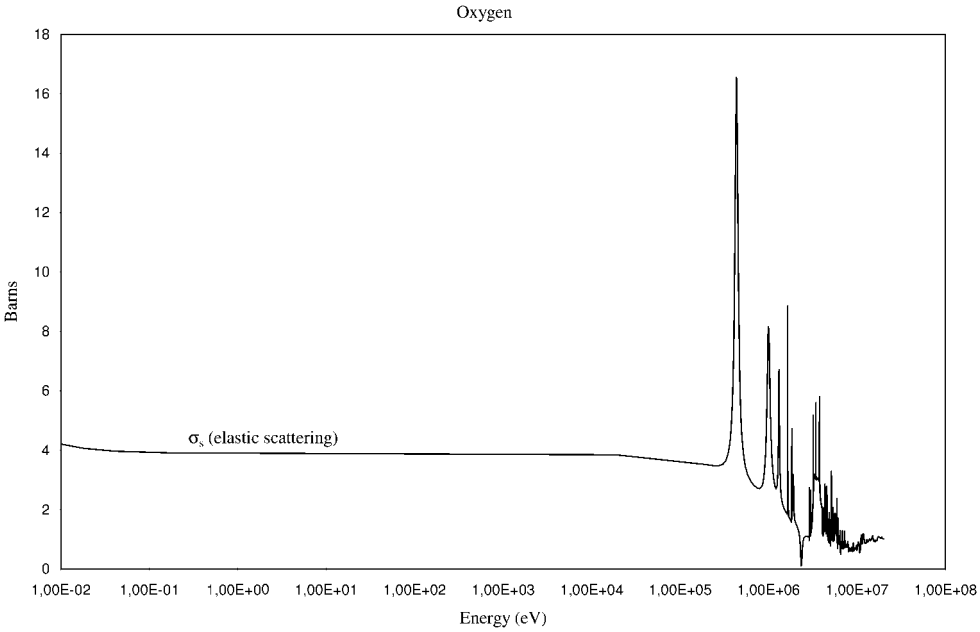

Fig. 14-6 Elastic scattering cross-section (in barns) for oxygen; the total cross-section is also equal to the elastic scattering cross-section.

14.4.1 Dosimetry for Fast Neutrons

For fast neutrons up to about 20 MeV, the main mechanism of energy transfer in tissue is by elastic collisions with light elements. These interactions occur mostly in hydrogen for two reasons: it represents the largest number of tissue atoms, and since one-half the energy is transferred it represents the largest fractional transfer of energy. The concept of *first collision dose* is used to describe this energy deposition which is due to the recoiling hydrogen atom; the scattered neutron is likely to leave the body of a person before it undergoes another scattering interaction, and even if it does the energy deposited will be only 25% of the initial energy. The first collision dose concept for fast neutrons does not, however, account for energy deposition due to absorption reactions or those neutrons that undergo additional scattering before exiting the body. These processes will obviously occur, but since a person is not very thick the energy deposited in humans will be relatively small compared to the first collision interactions. A 5 MeV neutron, for example, has a macroscopic cross-section in soft tissue of 0.051 cm^{-1}, and so its mean free path is 1/0.051 = 20 cm which suggests that a 5 MeV neutron will only have one interaction (a first collision dose) before it penetrates through the total body.

Example 14-3. Calculate the first collision dose in tissue due to scattering interactions in hydrogen for a fluence of 5 MeV neutrons.
Solution. The density of hydrogen atoms in tissue is 5.98×10^{22}/g and the cross-section for elastic scattering of 5 MeV neutrons is about 1.5 b (Figure 14-3). The mean energy loss per collision is about one-half the incident neutron energy or $E = 2.5$ MeV per collision; thus, the dose for each neutron per cm^2 due to hydrogen collisions is

$$D = (\text{n/cm}^2) \times 5.98 \times 10^{22}\ \text{atoms/g} \times 1.5 \times 10^{-24}\ \text{cm}^2/\text{atom} \times \frac{2.5\ \text{MeV} \times 1.6022 \times 10^{-6}\ \text{erg/MeV}}{100\ \text{erg/g rad}} = 3.6 \times 10^{-9}\ \text{rad per neutron/cm}^2$$

The first collision dose is due entirely to the fraction of the energy transferred to the recoiling nucleus; the scattered neutron is not considered after the primary interaction.

Scattering interactions are obviously possible with all of the constituents of tissue; therefore, a more accurate procedure, as illustrated in Example 14-4, is to consider them in determining the absorbed dose.

Example 14-4. What is the absorbed dose rate to soft tissue for a fluence of 5 MeV neutrons?
Solution. It is convenient in calculating the first collision dose rate from neutrons of energy E to first determine a neutron energy mass absorption coefficient for all the constituents or

$$\sum f_i N_i \sigma_i$$

where f_i is the fraction of the neutron energy transferred in an elastic collision with a nucleus. It is determined from the mass of the neutron (mass = 1) and the mass M_i of the recoiling atom as

$$f_i = \frac{2M_i}{(M+1)^2}$$

which can be combined, as shown in Table 14-3, with the neutron removal cross-section σ_i for each of the elements in tissue to yield a mass absorption coefficient in tissue for 5 MeV neutrons of 0.0512 cm^2/g. The neutron dose to tissue for a unit flux of 5 MeV neutrons is

$$D_n = \frac{1\ \text{n/cm}^2 \times 5\ \text{MeV/n} \times 1.6022 \times 10^{-6}\ \text{erg/MeV} \times 0.0512\ \text{cm}^2/\text{g}}{100\ \text{erg/g rad}}$$

$$= 4.1 \times 10^{-9}\ \text{rad/n cm}^2$$

which is about 12% higher than the dose calculated in Example 14-3 due to interactions with hydrogen only; i.e., 88% of the dose due to elastic interactions is due to hydrogen interactions.

Table 14-3. Neutron absorption factors for 5 MeV neutrons in tissue.

Element	N_i (atoms/g)	f_i	σ_s (cm^2)	$N_i\sigma_s f_i$
Hydrogen	5.98×10^{22}	0.500	1.50×10^{-24}	4.485×10^{-2}
Oxygen	2.69×10^{22}	0.111	1.55×10^{-24}	4.628×10^{-3}
Carbon	6.41×10^{21}	0.142	1.65×10^{-24}	1.502×10^{-3}
Nitrogen	1.49×10^{21}	0.124	1.00×10^{-24}	1.848×10^{-4}
Sodium	3.93×10^{19}	0.080	2.3×10^{-24}	7.231×10^{-6}
Chlorine	1.70×10^{19}	0.053	2.8×10^{-24}	2.523×10^{-6}
				$\sum_i N_i\sigma_s f_i = 0.0512$ cm^2/g

Example 14-4 considered only monoenergetic neutrons of 5 MeV. If a beam contains neutrons of several energies, then a similar calculation must be carried out separately for each energy group.

14.4.2 Dose from Thermal Neutrons

Thermal neutrons incident on tissue transfer energy only if they are absorbed because they are already at thermal energies; i.e., all elastic and inelastic reactions that could occur have already done so. Only two reactions need be considered: the (n,p) reaction with nitrogen which produces recoil protons of 0.626 MeV (the Q-value of the ^{14}N(n,p)^{14}C reaction) and the (n,γ) reaction with hydrogen which yields 2.225 MeV gamma rays (the Q-value of the ^{1}H(n,γ)^{2}H reaction). All of the recoil protons from the (n,p) reaction will almost assuredly be absorbed; however, only part of the capture gamma rays from the (n,γ) reactions can be assumed to be absorbed to deposit energy.

The radiation dose rate for a thermal neutron fluence rate (or flux of ϕ) due to 0.626 MeV protons from (n,p) interactions with nitrogen in tissue is

$$\dot{D}_{np} = \frac{\phi N_N \sigma_N E_p \times 1.6022 \times 10^{-6}\,\text{erg/MeV} \times 3600\,\text{s/h}}{100\,\text{erg/g rad}}$$

$$= 9.846 \times 10^{-8}\phi$$

since there are 1.49×10^{21} nitrogen atoms per gram of tissue and the neutron absorption cross-section for nitrogen is 1.83×10^{-24} cm^2.

Radiation dose from the gamma rays produced by the ^{1}H(n,γ)^{2}H reaction can be significant if the whole body is exposed. In these reactions, the "neutron dose" is actually delivered by the 2.225 MeV gamma rays released in the reaction. Since hydrogen is uniformly distributed in the body, the total body is both the source organ that produces the dose and the target organ that receives the dose. The gamma emission source term in gamma rays per second per gram is determined by the thermal neutron flux ϕ that produces (n,γ) reactions with 5.98×10^{22} hydrogen atoms per gram of tissue with a cross-section of 0.333 b, and is

$$\gamma/\text{s g} = \phi\, N_H \sigma_H = 1.99 \times 10^{-2} \phi$$

where ϕ is the thermal neutron flux (n/cm^2 s). The radiation absorbed dose due to thermal neutrons is thus produced by a combination of proton recoils and gamma radiation from neutron absorption reactions, each of which has a different damage factor. These damage functions have been weighted to provide an overall quality factor for thermal neutrons of 2.0.

Example 14-5. Determine the dose rate to the total body uniformly exposed to a thermal flux of 10,000 neutrons/cm^2 per second from (a) the (n,p) reactions in nitrogen, (b) the gamma rays released by (n,γ) reactions in hydrogen, and (c) the total absorbed dose and dose equivalent.

Solution. (a) The energy deposition from recoil protons due to (n,p) reactions in nitrogen in tissue (σ = 1.83 b) is due to the protons ejected by (n,p) reactions. These protons are charged particles and will deposit their energy within a few micrometers of the sites of interaction. Therefore

$$\dot{D}_{np} = 10^4 \text{ n/cm}^2 \text{ s} \times 1.49 \times 10^{21} \text{ atoms/g} \times 1.83 \times 10^{-24} \text{ cm}^2\text{/atom} \times 0.626 \text{ MeV} \times 1.6022 \times 10^{-6} \text{ erg/MeV} \times 3600 \text{ s/h}$$

$$= 9.846 \times 10^{-2} \text{ erg/g h} = 0.98 \text{ mrad/h}$$

(b) The flux of 2.225 MeV prompt gamma rays released by (n,γ) reactions in hydrogen is determined by the number of (n,γ) reactions, or

$$\gamma/\text{s g} = 10^4 \text{ n/cm}^2 \text{ s} \times 5.98 \times 10^{22} \text{ atoms/g} \times 0.333 \times 10^{-24} \text{ cm}^2\text{/atom}$$

$$= 199.1\ \gamma/\text{s g}$$

These gamma rays occur uniformly throughout the body so the total body is both the source of the energy flux and the target organ in which the energy is absorbed. For such high-energy gamma rays, only a fraction of the energy emitted will be absorbed since many of the photons will escape the body without interacting. This "absorbed fraction" AF (Total body ← Total body) for 2.225 MeV gamma rays is

0.278. Therefore, the dose rate for the total body as a source organ irradiating the total body as a target organ is

$$\dot{D}_\gamma = \frac{199.1\gamma/\text{s} \times 2.225\ \text{MeV} \times 1.6022 \times 10^{-6}\ \text{erg/MeV} \times 0.278 \times 3600\ \text{s/h}}{100\ \text{erg/g rad}}$$

$$= 7.1 \times 10^{-3}\ \text{rad/h or } 7.1\ \text{mrad/h}$$

(c) The absorbed dose rates from proton recoils and gamma rays are then added together to yield the absorbed dose rate in rad/h, or

$$\dot{D}_{\text{np}} + \dot{D}_\gamma = 0.98\ \text{mrad/h} + 7.1\ \text{mrad/h} = 8.08\ \text{mrad/h}$$

To convert absorbed dose to an effective dose equivalent in millirems, the absorbed dose is multiplied by the quality factor 2.0 for thermal neutrons:

$$D\ (\text{mrem/h}) = 8.08\ \text{mrad/h} \times 2.0 = 16.16\ \text{mrem/h}$$

As demonstrated in Example 14-5, about 88% of the absorbed dose from thermal neutrons is due to gamma rays produced by neutron capture in hydrogen. Auxier et al. (in Attix and Roesch 1968) have shown that the gamma component is about 86% for neutrons up to about 0.01 MeV (10^4 eV) and then declines rapidly as elastic scattering with hydrogen in tissue and associated energy deposition by recoil protons becomes more dominant than the (n,γ) reaction. For neutrons above about 1 MeV the absorbed dose due to gamma rays from (n,γ) reactions in hydrogen becomes negligible.

14.4.3 Monte Carlo Calculations of Neutron Dose

The most accurate representation of dose equivalent for neutrons of different energies is based on Monte Carlo calculations of multiple neutron scattering and energy deposition as neutrons are transmitted through tissue. In these calculations neutron transport through a target is based on a statistical distribution of neutron events, and the dose equivalent is determined not only by the energy deposited by each interacting event but also by the quality factor for each neutron energy; therefore, the dose equivalent constantly changes as a fast neutron undergoes repeated collisions and produces recoiling nuclei of various energies. Monte Carlo techniques, which are possible with modern computers, allow the deposited energy from each neutron to be followed through multiple neutron histories and the appropriate quality factor to be assigned for each energy sequence to obtain the distribution of dose equivalent in the absorbing medium. When done for a large number of neutron histories, the variance in the calculated quantities can be reduced considerably.

The results of Monte Carlo calculations for 5 MeV neutrons and for thermal neutrons (0.025 MeV) incident on a slab of tissue 30 cm thick (about the thickness of the body) are shown in Figure 14-7. The total dose for 5 MeV neutrons (Figure 14-7b) builds up somewhat in the first few centimeters of tissue depth and then decreases by a factor of about 10 at 30 cm as the neutrons in the beam become degraded in energy and are eventually absorbed, primarily by (n,γ) reactions in hydrogen.

When 5 MeV neutrons penetrate into tissue, they are moderated to thermal energies which increases their absorption by (n,γ) reactions in hydrogen as reflected in the rise of the gamma dose curve E_γ between 6 and 14 cm. The first

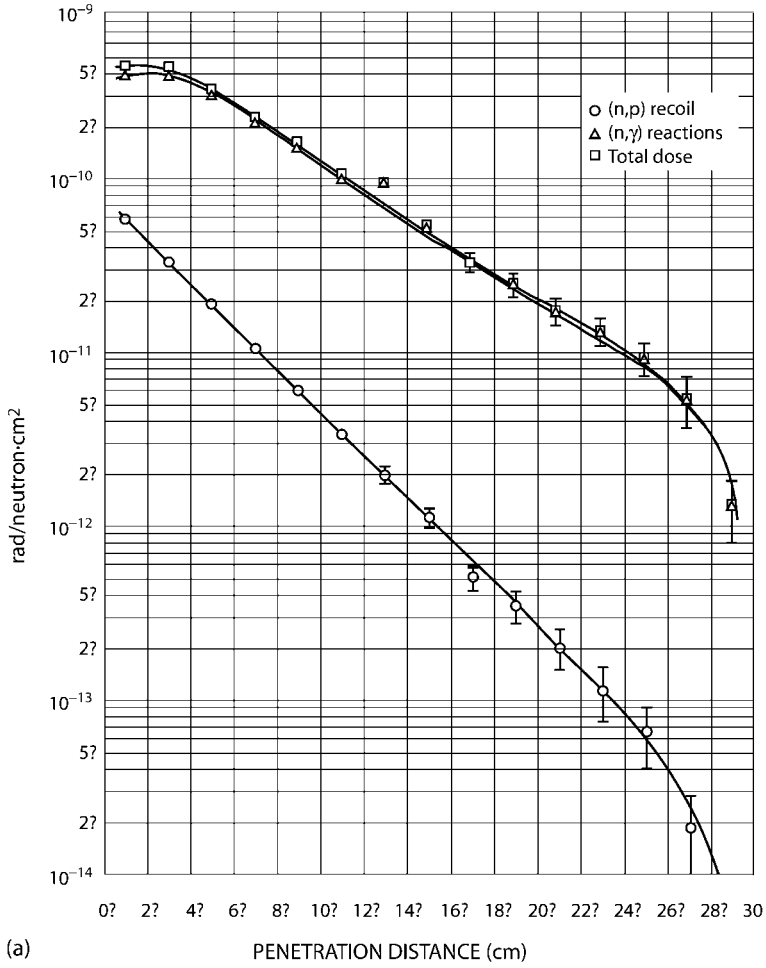

Fig. 14-7 Dose equivalent (rem) per unit neutron fluence (n/cm^2) versus depth in tissue due to protons, photons, and recoil nuclei for (a) thermal neutrons. (From NBS Handbook 63, 1957.)

collision dose of 3.6×10^{-9} rad per n/cm^2 in Example 14-3 is less than the entrance dose (4.8×10^{-9} rad per n/cm^2) shown in Figure 14-7a because the Monte Carlo calculation accounts for increases in the first collision dose due to backscatter within the tissue slab. Most of the dose from 5 MeV neutrons is due to recoiling hydrogen nuclei caused by elastic scattering collisions with hydrogen atoms, and very little is due to capture gammas.

The dose due to thermal neutrons in Figure 14-7a is quite different from 5 MeV neutrons in that the dose due to hydrogen recoil nuclei only exceeds the gamma dose over the first 3 cm. The thermal neutron density reaches a maximum at about 10 cm and then decreases due to absorption. Thermal neutrons are not energetic enough to produce recoiling hydrogen nuclei protons in collisions with hydrogen; however, protons are produced by absorption of thermal neutrons in nitrogen by $^{14}N(n,p)^{14}C$ reactions ($\sigma = 1.83$ b and $Q = 0.626$MeV).

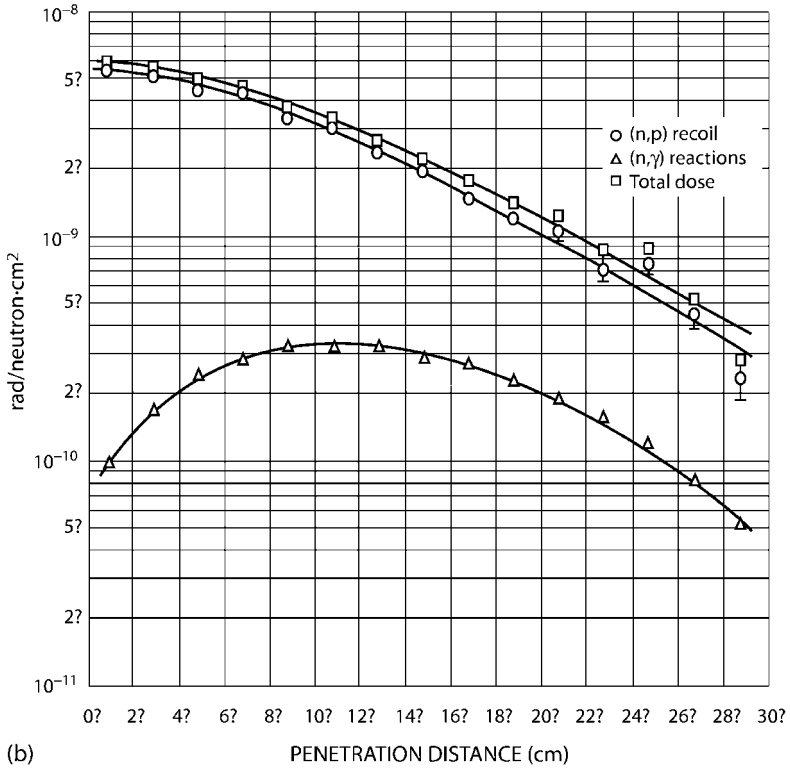

Fig. 14-7 Dose equivalent (rem) per unit neutron fluence (n/cm^2) versus depth in tissue due to protons, photons, and recoil nuclei for (b) 5 MeV neutrons. (From NBS Handbook 63, 1957.)

14.4.4 Kerma for Neutrons

Kerma and absorbed dose are essentially equal for (n,p) interactions with nitrogen in tissue because the energies of the recoil products are deposited within a few micrometers of the sites of interaction. Charged particle equilibrium is thus quickly established and bremsstrahlung production, which could carry energy away, is highly unlikely for these heavier recoil nuclei. Since elastic scattering is the dominant interaction for intermediate and fast neutrons, kerma is equal to deposited dose; the same is true for (n,p) interactions with tissue nitrogen at thermal energies. In contrast, kerma and absorbed dose are significantly different for (n,γ) absorption in hydrogen because a significant distance is required for equilibrium to be established for each 2.225 MeV gamma ray emitted. Kerma from the indirect (n,γ) reaction with hydrogen will dominate in a tissue mass the size of an adult human because of its uniform distribution in tissue and its larger proportion of tissue (about 40 times more hydrogen than nitrogen). For thermal neutrons, kerma from the $^{1}H(n,\gamma)^{2}H$ reaction is about 25 times larger than the (n,p) reaction in nitrogen, which is also true for intermediate neutrons because they become thermalized in passing through body tissue.

14.4.5 Dose Equivalent Versus Neutron Flux

As shown in Example 14-5 it is straightforward to calculate a neutron dose rate once the incident flux is known. This relationship between dose rate and neutron flux is presented in Table 14-4 and Figure 14-8 in terms of the neutron flux at various energies required to produce a dose equivalent rate of 1 mrem/h (the total dose equivalent for a given neutron fluence can be obtained by multiplying the dose rate by the exposure time). The two sets of data contained in Table 14-4 and Figure 14-8 are different because of differing interpretations in the value of the quality factor for neutrons of different energies. The upper curve in Figure 14-8 reflects current regulations; however, the NCRP has recently recommended increasing the neutron quality factor by a factor of about 2.0–2.5, and the effects of these changes are reflected in the lower curve. Whether and/or when these recommendations will be incorporated into regulations is not known, but as shown in Figure 14-8, the dose equivalent for a given flux will be higher if the NCRP recommendations are considered. The curves in Figure 14-8 also demonstrate that a unit flux of high-energy neutrons will yield a higher dose than the same flux of neutrons at lower energy primarily because of the increase in the quality factor at higher energies.

Table 14-4. Fluence rates for monoenergetic neutrons that correspond to a dose equivalent rate of 1 mrem/h.

Neutron energy (eV)	Fluence rate (n/cm^2 s) for 1 mrem/h	
	10 CFR 20[a]	NCRP-112[b]
0.025 (thermal)	272	112
0.1	272	112
1	224	112
10	224	112
10^2	232	116
10^3	272	112
10^4	280	120
10^5	46.0	16.0
5×10^5	10.8	6.40
10^6	7.6	3.88
5×10^6	6.4	3.88
10^7	6.8	3.20
1.4×10^7	4.8	2.72
6×10^7	4.4	–
10^8	5.6	–

a Adapted from Title 10, Code of Federal Regulations, Part 20 (1993) by the US Nuclear Regulatory Commission (the rates incorporate neutron quality factors of 2.0 for thermal and low-energy neutrons and 2.5–11 for higher energy neutrons).

b These fluence rates are based on NCRP Report 112 (1987) which recommends increasing Q for neutrons by a factor of 2.5 for thermal neutrons and 2.0 for all other energies.

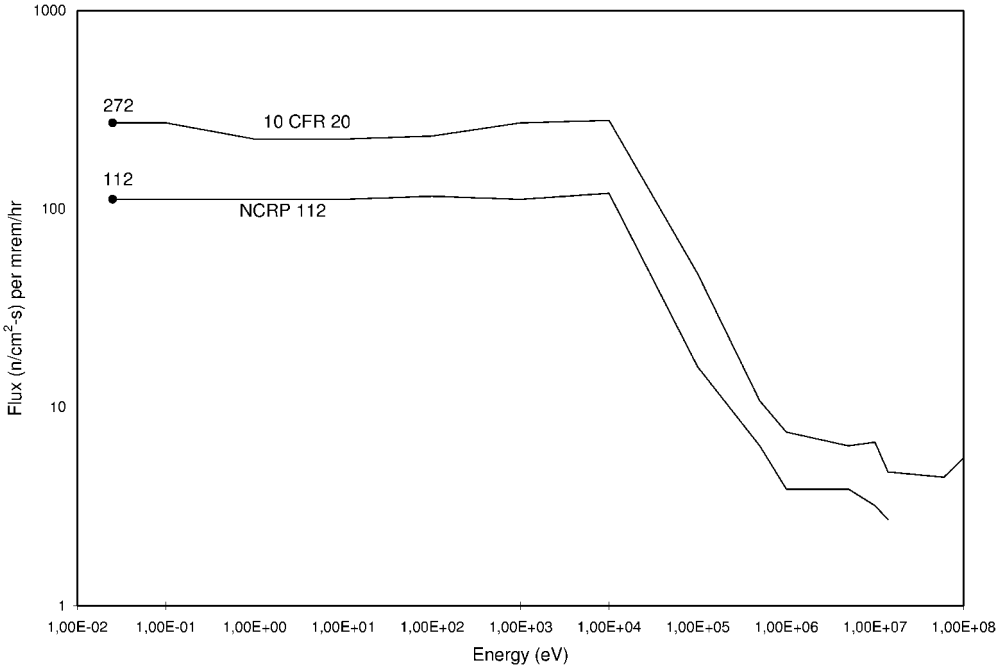

Fig. 14-8 Fluence rates for neutrons of energy E that produce 1 mrem/h as stated in Federal Regulations (10CFR20) and as recommended by NCRP (1987) based on a re-evaluation of neutron quality factors.

Example 14-6. Estimate the dose equivalent rate 1 m from an unshielded ^{239}Pu–Be source that emits 3×10^7 neutrons/s with an average energy of 4.5 MeV.

Solution. Point sources that emit S neutrons/s can be specified at a distance r (cm) in terms of a neutron flux ϕ:

$$\phi(\text{n/cm}^2\ \text{s}) = \frac{S(\text{n/s})}{4\pi r^2}$$

Figure 14-8 indicates that the flux corresponding to a dose equivalent rate of 1.0 mrem/h due to 4.5 MeV neutrons is about 6.4 neutrons/cm^2 s or 0.156 mrem/h per neutron/cm^2 s. The dose equivalent rate at 100 cm from the unshielded neutron source is

$$\dot{D}_0 = \frac{3 \times 10^7 \times 0.156}{4\pi(100)^2} = 37.2\,\text{mrem/h}$$

14.4.6
Boron Neutron Capture Therapy (BNCT)

BNCT is an experimental radiation therapy that takes advantage of the neutron absorption properties of boron for the treatment of malignant tumors, especially those in the brain. Boron-10 (^{10}B), a constituent of natural boron, has a large cross-section for thermal neutron absorption (3840 b), and the ^{10}B(n,α)^{7}Li reaction yields

$$
{}^{10}_{5}\mathrm{B} + {}^{1}_{0}\mathrm{n} \;\begin{cases} \nearrow\ 4\% & {}^{7}_{3}\mathrm{Li} + {}^{4}_{2}\mathrm{He} + 2.79\,\mathrm{MeV} \quad (\sigma_{\mathrm{th}} = 3840\mathrm{b}) \\ \searrow\ 96\% & {}^{7}_{3}\mathrm{Li}^{*} + {}^{4}_{2}\mathrm{He} + 2.31\ \mathrm{MeV} \end{cases}
$$

where * indicates excitation energy emitted as a 0.48 MeV photon.

The ^{7}Li nucleus and the alpha particle have energies of 0.83 and 1.47 MeV, respectively, which is deposited within a distance of about 10 μm in tissue. This energy is deposited in a single cell and/or its immediate neighbor to cause cell death. The success of the BCNT technique depends on selectively concentrating ^{10}B in the tumor mass so that irradiation of the area with thermal neutrons will produce high-energy deposition in tumor cells with minimal damage to normal tissue.

14.5
Neutron Shielding

Neutron shields incorporate materials that enhance interactions that deplete neutrons from the primary beam. For fast neutrons, materials that slow neutrons down through elastic and inelastic scattering are used in combination with materials that enhance capture of neutrons when they reach thermal energies. Hydrogen is very effective in removing neutrons, especially energetic ones, from a beam because collisions with hydrogen, the dominant interaction, diminish the energy by about one-half. The cross-section for the scattered neutrons is considerably greater because of the lower energy and the mean free path length is reduced considerably; therefore, a collision with hydrogen effectively removes a fast neutron from the beam.

14.5.1
Neutron Shielding Materials

Many shielding materials produce capture gamma rays or photons from inelastic scattering interactions. These can be minimized by adding lithium or boron to the shield. Lithium-6 which has a large ($n_{thermal}$,α) cross-section of 941 b does not yield capture gamma rays by neutron absorption, and the helium and tritium atoms that are formed are easily absorbed. Natural boron contains 20% ^{10}B, and is

a very effective shielding material for thermal neutrons through $^{10}B(n,\alpha)^{7}Li$ reactions. About 96% of the ^{7}Li atoms created in these reactions are in an excited state which is relieved promptly by emission of a 0.48 MeV gamma ray, but these are easier to shield than the 2.225 MeV gamma rays from hydrogen capture and boron is commonly used in neutron shields.

Hydrogenous materials such as paraffin and water make efficient neutron shields because of the effectiveness of elastic scattering with hydrogen atoms, but not without potential problems. Paraffin is flammable, water can leak and evaporate, and thermal neutron capture produces 2.225 MeV gamma rays. When H_2O is used as a neutron shield, it is necessary to prevent leakage, minimize corrosion, and keep contaminants out, which is generally done by demineralization.

Metals such as lead, iron, tungsten, and depleted uranium are relatively poor shield materials for neutrons; however, they are often used as a gamma shield, especially around nuclear reactors, and their neutron shielding properties are important because of such uses. Lead and iron can produce capture gamma rays of 7.4 and 7.6 MeV, respectively, although with low probability and (n,γ) interactions in ^{58}Fe produce radioactive ^{59}Fe ($T_{1/2}$ = 44.51 d) which emits 1.1 and 1.29 MeV gamma rays. *Tungsten* is dense and is almost as effective as lead as a gamma shield. It is much better than lead for neutron attenuation, although secondary gamma radiation is produced due to capture reactions. *Depleted uranium*, which is readily available from nuclear fuel enrichment processes, is very dense (ρ = 19) and is the best attenuator available on a volume basis for gamma rays. Neutron attenuation in uranium is about the same as in lead, and even though it does not produce significant capture gamma rays, fast fission reactions may yield gamma-emitting fission products.

Boron is often incorporated into neutron shields because of its absorption cross-section (760 b) and the large (n,γ) cross-section of ^{10}B (3840 b). The alpha particles from ^{10}B reactions are easily absorbed and the 0.48 MeV gamma rays from the excited ^{7}Li product, which occur in 96% of the interactions, are not too difficult to shield. Borax (sodium borate) is a crystalline powdery material that can be easily shaped into various shield configurations is not subject to leakage, and is cheap and effective. Borated water and borated polyethylene are useful, as are boron oxide, boric acid, and boron carbide (B_4C). A sandwich material called boral is available that consists of an Al–B_4C mixture clad in aluminum. Boron has also been added to various steels to absorb preferentially thermal neutrons and reduce activation products and associated gamma rays.

Concrete and earth are often the shield materials of choice for neutron sources, especially around nuclear reactors and accelerators since they are dense, contain hydrogen and other light materials that promote neutron capture, and can be easily shaped. Barytes, iron-portland, and colemanite aggregate are some of the many varieties of concrete that are used in neutron shields. Barytes concrete contains boron for neutron absorption and hydrogen for moderation of fast neutrons; it also is a good gamma shield. Colemanite is used as an aggregate and contains hydrated calcium borate which enhances neutron capture because of the boron it contains. Additives that promote neutron capture can be incorporated into con-

crete; however, care must be taken to ensure that cracks, access ports, ducts, or other penetrations do not permit the escape of neutrons.

Polyethylene is a pure hydrocarbon which contains 18% more hydrogen per unit volume than water (about 8×10^{22} atoms of H/cm^3 versus 5.98×10^{22} atoms of H/cm^3 for H_2O). Unfortunately, it softens at about 110 °C and will burn; a more dense ($\rho = 0.96$) variety is available that softens at about 200 °C but with slightly diminished neutron removal properties. Boron can also be added to polyethylene to absorb thermal neutrons from hydrogen interactions. *Water extended polyethylene* (WEP) is a special formulation of polyethylene that is an especially effective neutron shield.

Lithium hydride contains about 12.6% hydrogen by weight and is a very effective material for neutron attenuation. It is, however, difficult to fabricate into solid shields. It also actively combines with water, and because of this property needs to be protected from water by encapsulation or other means. Lithium hydroxide is often mixed with water to absorb thermal neutrons and has been used as a burnable reactivity shim in nuclear reactors or added to water shields to absorb thermal neutrons after they are slowed down. Capture reactions in lithium do not produce gamma rays, but absorption of neutrons by ^{6}Li in natural lithium produces tritium which can be minimized by using lithium depleted in ^{6}Li.

Cadmium has a high (n,γ) neutron capture cross-section (2450 b) and is frequently used as a neutron absorber, but like hydrogen has the disadvantage of emitting energetic 9.05 MeV capture gamma rays, which themselves require shielding.

14.5.2 Neutron Shielding Calculations

In concept, neutron attenuation and absorption in a shielding material is similar to "good geometry" photon attenuation and can be represented by an exponential function based on absorber thickness and the neutron removal cross-section Σ_{nr} (cm^{-1}):

$$I(x) = I_0 e^{-\Sigma_{nr} x}$$

where, for radiation protection considerations, neutron intensity is expressed as a flux (or fluence rate) of n/cm^2 s. The flux at a distance r from a point source of neutrons is straightforward, but may be more difficult to establish for other sources.

The data in Table 14-4 and Figure 14-8 can be used as a starting point to determine the dose equivalent rate of $\dot{D}(x)$ outside a shield of thickness x if the neutron flux is known. The shielded value $\dot{D}(x)$ can then be obtained by

$$\dot{D}(x) = \dot{D}_0 B e^{-\Sigma_{nr} x}$$

where Σ_{nr} is the neutron removal cross-section and $\dot{D}_0$ is the dose equivalent rate per unit neutron fluence rate; i.e., mrem/h per neutron/cm^2 s for neutrons of the

source energy. The buildup factor B is necessary to account for neutrons that are scattered back into the beam after they undergo an elastic or inelastic collision in the absorber. Scattered neutrons can contribute significantly to the dose outside a shield, and since Σ_{nr} is basically an attenuation coefficient (somewhat similar to photons), it is necessary to adjust calculated neutron intensities by a buildup factor. Buildup factors for neutrons are sparse; however, a neutron buildup factor of about 5.0 is appropriate for most calculations in which water or paraffin shields of 20 cm or more are used.

14.5.3 Neutron Removal Coefficients

Whereas photon attenuation and absorption coefficients vary smoothly with atomic number and energy, neutron removal coefficients can change irregularly from element to element because neutron cross-sections have complicated resonance structures as their energies change. Neutron removal coefficients are further complicated by the amount of hydrogenous material incorporated in the shield to take advantage of its slowing down properties; therefore, Σ_{nr} is determined experimentally for each shield material as a combined removal coefficient. These are included in Table 14-5 for shields with a thickness of less than mean free paths and at least 6 g/cm^2 of hydrogenous material; also included are values for shielding materials: those for the substance alone (i.e., no hydrogen absorber).

Table 14-5. Neutron removal coefficients Σ_{nr} for fission neutrons in several common materials surrounded by sufficient hydrogenous material to absorb neutrons that are degraded in energy due to scattering interactions.

Medium	Σ_{nr} (cm^{-1})
Sodium	0.032
Graphite	0.078
Carbon	0.084
Concrete (6% H_2O)	0.089
D_2O	0.092
Zirconium	0.101
H_2O	0.103
Paraffin	0.106
Polyethylene	0.111
Lead	0.118
Beryllium	0.132
Iron	0.156
Copper	0.167
Uranium	0.182
Tungsten	0.212

Source: Report TID-25951, 1973.

The *macroscopic cross-section* Σ is the neutron removal coefficient for materials or elements used without a layer of hydrogenous material. It is calculated as

$$\Sigma = N_i \sigma_i$$

where $N = N_A/\rho$ atoms (or molecules) per gram and σ_i is the microscopic cross-section which is obtained from the chart of nuclides for thermal neutrons or plots of cross-section versus energy for higher energy neutrons (e.g., Figure 14-1 or Figures 14-3 to 14-6). If a material such as lead, iron, or concrete is used by itself the macroscopic cross-section Σ should be used for determining the change in neutron intensity; if, however, the material is used with a sufficient amount of hydrogenous material, the neutron removal coefficients Σ_{nr} listed in Table 14-5 should be used.

The effectiveness of a neutron shield is dependent on Σ_{nr}; therefore, considerable care must be exercised in determining Σ_{nr} for shielding calculations. When shield materials meet the conditions for the values in Table 14-5, these should be used in shielding calculations. If, however, the shield material is used alone, the macroscopic cross-section calculated from the total microscopic cross-section for the particular neutron energy should be used.

Empirical relationships for mass neutron removal coefficients Σ_{nr}/ρ (cm^2/g) have been derived:

$$\Sigma_{nr}/\rho \ (cm^2/g) = 0.190 Z^{-0.43} \text{ for } Z \leq 8$$

$$\Sigma_{nr}/\rho \ (cm^2/g) = 0.125 Z^{-0.565} \text{ for } Z > 8$$

or more generically

$$\Sigma_{nr}/\rho \ (cm^2/g) = 0.206 A^{-1/3} Z^{-0.294}$$

where A is the atomic mass number and Z is the atomic number of the element. The neutron removal coefficient is obtained by multiplying the neutron mass removal coefficient by the density of the absorber.

Lead plus polyethylene is a convenient shield that can be constructed in layers to use the mass attenuation of lead for photons followed by the neutron removal properties of hydrogen-rich polyethylene. Neutron removal coefficients for lead plus a thickness t of polyethylene have been determined experimentally and can be represented by the fit equation

$$\Sigma_{nr}(t) = 0.1106 \ (1 - 0.9836 e^{-0.109t})$$

where t is the thickness (in cm) of polyethylene. This relationship is good for up to 40 cm of polyethylene, irrespective of the thickness of lead.

Example 14-7. Determine the neutron removal cross-section for a lead shield with a 20 cm thick layer of polyethylene enclosing it.
Solution.

$$\Sigma_{nr}\,(t = 20\text{ cm}) = 0.1106\,(1 - 0.9836e^{-0.109 \times 20})$$

$$= 0.098\text{ cm}^{-1}$$

Mixtures of nuclei may include natural or enriched abundances of isotopes of an element, or chemical mixtures such as boron in H_2O. Neutron removal cross-sections for such mixtures and compounds can also be obtained by first determining the effective microscopic cross-section σ for the compound as shown in Examples 14-8 and 14-9.

Example 14-8. Determine Σ_{nr} for paraffin ($C_{22}H_{46}$; $\rho = 0.87$ g/cm^3) if Σ_{nr} for carbon ($\rho = 12.0$) is 0.6 cm^{-1} and 0.61 cm^{-1} for hydrogen ($\rho = 1.0$).
Solution. The molecular weight for paraffin is $(46 \times 1) + (22 \times 12) = 310$. The neutron removal coefficient is

$$\Sigma_{nr} = \left(\frac{46 \times 1}{310} \times 0.87 \times 0.61\right) + \left(\frac{22 \times 12}{310} \times 0.87 \times 0.6\right)$$

$$= 0.52\text{ cm}^{-1}$$

Example 14-9. The scattering cross-section for 1 MeV neutrons in hydrogen is 3 b and 8 b for oxygen. Determine the scattering cross-section for H_2O and the macroscopic scattering cross-section.
Solution. Since each water molecule contains two atoms of hydrogen and one of oxygen

$$\sigma_{s,H_2O} = (2)3\text{b} + (1)8\text{b} = 14\text{b}$$

and the macroscopic scattering cross-section is

$$\Sigma_{s,H_2O} = N\sigma_t$$

$$= \frac{6.022 \times 10^{24}\text{ mol/mol}}{18\text{ g/mol}} \times 14 \times 10^{-24}\text{ cm}^2/\text{molecule}$$

$$= 0.468\text{ cm}^2/\text{g} \times 1\text{ g/cm}^3$$

and since the density of H_2O is 1.0

$$\Sigma_{s,H_2O} = 0.468\,\text{cm}^2/\text{g} \times 1\,\text{g/cm}^3$$

These approaches assume that the different nuclei in a mixture act independently of each other such that the atoms of each represent independent targets for interactions. This is a valid assumption for all neutron interactions except elastic scattering of low-energy neutrons by molecules and solids; these must be obtained by experiment. Consequently, the results of Example 14-9 for H_2O would not be applicable for thermal neutrons since it yields a value of 46 b; the experimental, and correct, value is 103 b.

Example 14-10. Determine the dose rate for the Pu–Be source in Example 14-6 if shielded by 25 cm of water.
Solution. A 25 cm water shield obviously contains sufficient hydrogen to ensure absorption of scattered neutrons. The dose equivalent, including a buildup factor of 5, is determined with Σ_{nr} from Table 14-5 of 0.103 cm^{-1}, or

$$\dot{D}(25\,\text{cm}\,H_2O) = \dot{D}_0 B e^{-\Sigma_{nr} x} = 5 \times 37.2 e^{-0.103 \times 25\,\text{cm}}$$

$$= 14.2\ \text{mrem/h}$$

14.5.4 Neutron Attenuation in Concrete

Since concrete is a widely used neutron shield, Clark et al. (1966) at ORNL performed Monte Carlo calculations of the dose rate outside concrete slabs of various thicknesses. Figure 14-9 shows the dose rate versus slab thickness for 2 MeV neutrons (typical of fission reactors) and 14 MeV neutrons (as produced in D-T interactions). These may be used for the design of neutron shields for these common sources; dose rates for other energies can be approximated by interpolation of these values, or from the original reference.

Example 14-11. A flux of 10^3 fission neutrons/cm^2 s with $\bar{E} \cong 2$ MeV impinges on a concrete slab 60 cm thick. What is the dose equivalent rate on the exit side of the slab?
Solution. From Figure 14-9, the dose rate after penetration of <60 cm slab of concrete is 2×10^{-4} mrem/h per unit flux. Therefore

$$\dot{D} = 103\ \text{n/cm}^2\,\text{s} \times 2 \times 10^{-4}\ \text{mrem/h per n/cm}^2\,\text{s} = 0.2\ \text{mrem/h}$$

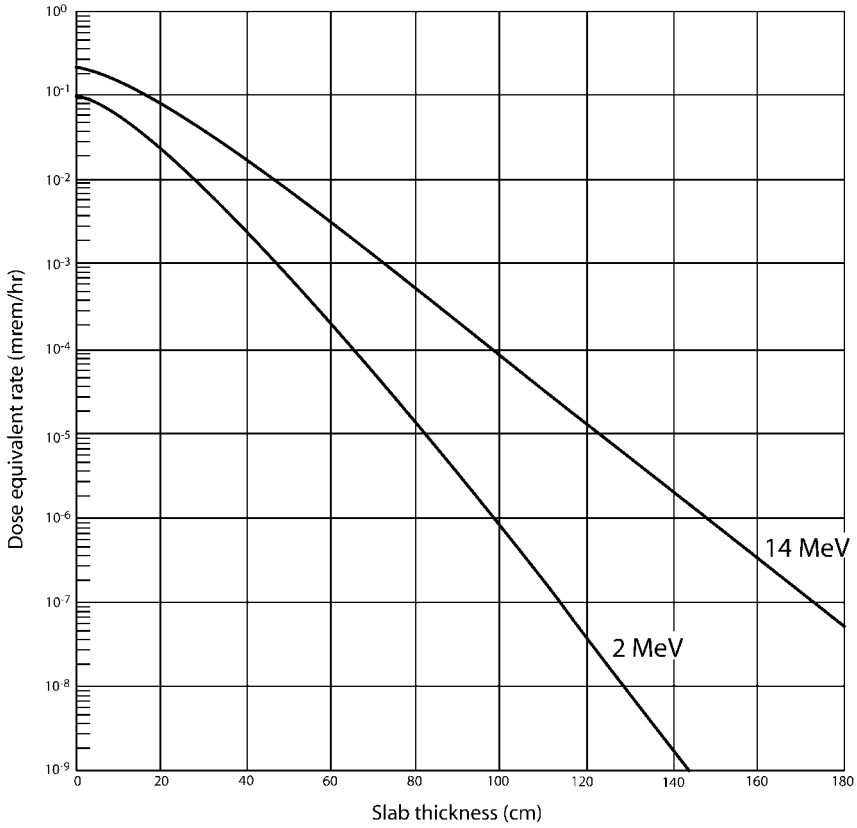

Fig. 14-9 Dose equivalent rate (mrem/h) for unit intensity (n/cm^2 s) for 2 MeV neutrons (lower curve) and 14 MeV neutrons (upper curve) versus thickness of concrete shielding. (Adapted from Clark et al. (1966), based on a quality factor of 10.)

14.6 Neutron Detection

Since neutrons are not ionizing particles, their detection depends on the ionizing properties of the products of neutron capture reactions, the three most important of which are:

$$
\begin{aligned}
&\qquad\quad 4\% \quad {}^{7}_{3}\mathrm{Li} + {}^{4}_{2}\mathrm{He} + 2.79\,\mathrm{MeV} \quad (\sigma_{\mathrm{th}} = 3840\,\mathrm{b})\\
&{}^{10}_{5}\mathrm{B} + {}^{1}_{0}\mathrm{n} \quad \nearrow \\
&\qquad\quad 96\% \quad {}^{7}_{3}\mathrm{Li}^{*} + {}^{4}_{2}\mathrm{He} + 2.31\,\mathrm{MeV}\\
&{}^{6}_{3}\mathrm{Li} + {}^{1}_{0}\mathrm{n} \rightarrow {}^{3}_{1}\mathrm{H} + {}^{4}_{2}\mathrm{He} + 4.78\,\mathrm{MeV} \quad (\sigma_{\mathrm{th}} = 941\,\mathrm{b})\\
&{}^{3}_{2}\mathrm{He} + {}^{1}_{0}\mathrm{n} \rightarrow {}^{3}_{1}\mathrm{H} + {}^{1}_{1}\mathrm{H} + 0.76\,\mathrm{MeV} \quad (\sigma_{\mathrm{th}} = 5330\,\mathrm{b})
\end{aligned}
$$

where * indicates excitation energy emitted as a 0.48 MeV photon.

The alpha particles, protons, and recoil atoms produced by these reactions are energetic (moderate to high *Q*-values) and highly ionizing. These properties as well as the large capture cross-sections for thermal neutrons in ^{10}B, ^{6}Li, and ^{3}He are used in the design of neutron detectors.

14.6.1 Measurement of Thermal Neutrons

Various measurement techniques can be used for thermal neutrons. Most of these depend on the thermal neutron cross-section of selected materials from which one can deduce the total fluence rate of thermal neutrons striking an absorber.

Boron-type detectors are used to detect thermal neutrons because of the high cross-section for (n,*a*) reactions in ^{10}B. Boron trifluoride (BF_3) gas, often enriched in ^{10}B, can be used as a detector gas in a proportional counter to detect thermal neutrons. The pulse heights produced in the BF_3 counter are large due to the *Q*-value of 2.31 MeV (and 2.79 MeV in 4% of reactions that produce ground-state ^{7}Li). These large pulses allow discrimination against gamma rays, which are usually present with neutrons, which also may ionize the BF_3 gas, but with much smaller pulses (multiple pulses from photon interactions in the BF_3 counter can become a problem if the gamma fields are intense).

Other neutron detectors are designed by lining the interior walls of the detector with a boron compound and filling it with a gas that may be more suitable for proportional counting than BF_3. Boron can also be impregnated in scintillators (e.g., ZnS) for slow-neutron detection. Each of these methods also relies on the high cross-section of boron and the ionization produced by the recoil products.

Lithium detectors incorporate lithium (σ_a = 941 b for ^{6}Li) to detect slow neutrons. The $^{6}Li(n,a)^{3}H$ reaction has a higher *Q*-value than the (n,*a*) reaction in boron which provides potentially better gamma ray discrimination, but at reduced sensitivity due to the lower cross-section. The isotope ^{6}Li is only 7.5% abundant in nature, but lithium enriched in ^{6}Li is available. Lithium-6 fabricated into crystals of LiI(Eu) is similar to NaI(Tl) for photon detection, but gamma ray discrimination in such crystal detectors is poor compared to BF_3 gas. Lithium compounds can also be mixed with ZnS to make small detectors which have good gamma ray discrimination because secondary electrons produced by gamma rays easily escape the crystal without interacting to produce a detector pulse.

Helium-filled detectors take advantage of the high cross-section for (n,p) reactions in ^{3}He at 5330 b. A ^{3}He proportional counter will lose pulses because of the low energies supplied to the products by the low *Q*-value; however, ^{3}He is a better counter gas and can be operated at high pressures with good detection efficiency. Gamma discrimination is poor because the lower energy protons produce smaller pulses due to the low *Q*-value.

Fission counters use fissile material coated onto the inner surface of an ionization chamber. Isotopes of ^{233}U, ^{235}U, or ^{239}Pu fission readily when exposed to thermal neutrons and produce very energetic fission fragments since they share about 165 MeV of kinetic energy. The fission "explosion" literally tears the fragments

away from their orbital electron fields and each fragment has charge of about +20 which produces extremely large pulses; thus, slow-neutron counting can be done at low levels, even in a high background. Since fissile materials are also alpha emitters, alpha particle pulses will also be produced, but these are considerably smaller and can be easily discriminated against. Since the fission fragments are highly charged and very energetic, sufficient ionization occurs for fission counters to be operated as ion chambers containing standard air.

14.6.2 Measurement of Intermediate and Fast Neutrons

Two general methods of measuring intermediate and fast neutrons are to first moderate them to thermal energies so they can be detected with a thermal neutron detector and to use an assortment of activation foils to detect them directly. The two principal measurement systems that moderate fast neutrons are the long counter and Bonner spheres.

The long counter (Figure 14-10) contains a BF_3 tube surrounded by an inner paraffin moderator; it responds uniformly to neutron energies from about 10 keV to 5 MeV. Neutrons incident on the front cause a direct response after being thermalized in the inner paraffin layer. Those from other directions are either reflected or thermalized by the outer paraffin jacket and then absorbed in a layer of boron oxide. With this arrangement, the probability that a moderated neutron will enter the BF_3 tube and be counted is not dependent on the initial energy; therefore, no information on the spectral distribution of neutron energies is obtained.

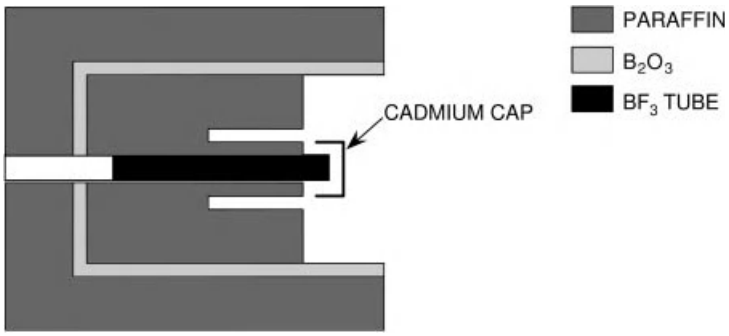

Fig. 14-10 Schematic of the long counter in which a BF_3 tube is surrounded by layers of parrafin and metal to reflect and thermalize fast neutrons so they will be absorbed by (n,α) reactions in the boron trifluoride (BF_3) gas.

Bonner sphere detectors consist of a series of polyethylene moderating spheres of different diameters that enclose small lithium iodide scintillators at their centers. Bonner spheres can be used to obtain neutron spectral information. The spheres range in diameter from 2 to 12 in, and each provides varying degrees of

moderation for neutrons of different energies. Each sphere is calibrated with monoenergetic neutrons ranging in energy from thermal neutrons to 10 MeV or so. An unfolding procedure is used to infer information about the neutron spectrum based on the calibration curves and the measured count rates, but the unfolding procedure is not very precise.

A Bonner sphere detector is very useful for neutron dose measurements because, as shown in Figure 14-11, the detector response inside a 10–12 in polyethylene sphere is very close to the dose equivalent delivered by neutrons at any given energy. The detector is also totally insensitive to gamma radiation which is a distinct advantage. Since the energy response is similar to the dose equivalent per neutron, the instrument is often called a "rem ball" and is often used as a neutron rem meter. The correspondence between dose equivalent and neutron energy for the rem ball appears to be a coincidence rather than a distinct physical correlation, but a fortunate one nevertheless for neutron fields of unknown energy. As shown in Figure 14-11 the response of the 10 cm Bonner sphere with a LiI scintillation detector is high for high-energy neutrons (with a high quality factor) and lower

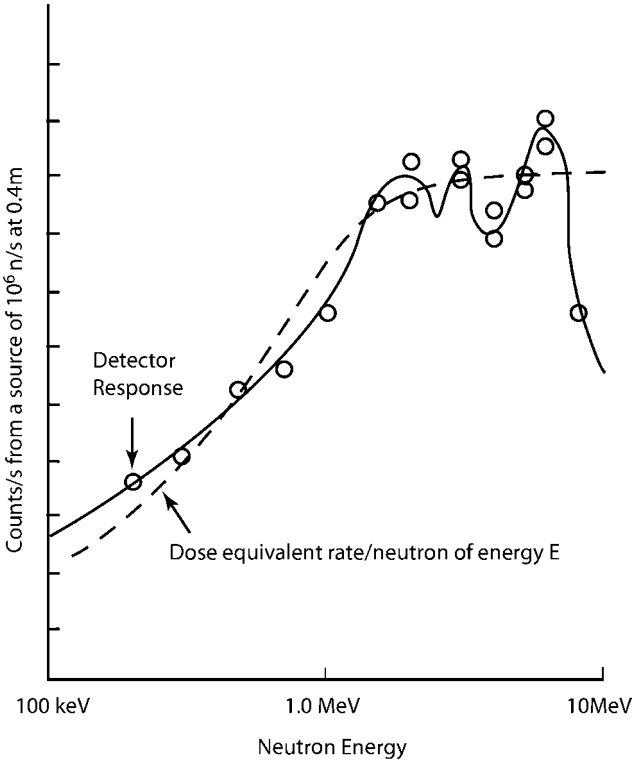

Fig. 14-11 Response (arbitrary units of c/s at 40 cm) of a 10 cm Bonner Sphere "rem-ball" Detector to fast neutrons and the corresponding dose equivalent per neutron versus neutron energy showing a relatively close relationship for neutron energies up to about 5 MeV and substantial underresponse 8 MeV.

for the lower energy neutrons (with corresponding lower quality factor) which causes the counts to be automatically weighted as neutron energy changes. The detector overresponds up to a factor of about 2 (greatest for 10 keV neutrons) for neutron energies below about 100 keV which is conservative for radiation protection decisions. In contrast, for neutrons above 8 MeV or so it underresponds sometimes by a considerable amount, and caution must be exercised when using Bonner spheres for high-energy neutrons. Larger spheres and unfolding procedures to determine neutron fluence and energy spectra are needed if accurate dose determinations are to be made for neutrons above 5 MeV or so.

14.6.3 Neutron Foils

Neutron foil activation is one of the best methods for determining neutron spectral information because different foils have differing threshold energies for activation, as shown in Table 14-6. For example, if an exposed indium foil shows induced activity from ^{115m}In and a ^{58}Ni foil exposed simultaneously shows no ^{58}Co activity, then the neutron energies are likely to be between 0.5 and 1.9 MeV. They can also be used to capture neutrons and induce radioactivity for analysis after an actual exposure or if one is suspected. These form the basis of personal neutron dosimeters or stationary monitors for areas where neutron exposure or nuclear criticality could occur. The amount of induced activity will depend on a number of factors: the element chosen, the mass of the foil, the neutron energy spectrum, the capture cross-section, and the time of irradiation. Manganese, cobalt, copper, silver, indium, dysprosium, and gold are examples of foils used to detect thermal neutrons.

Table 14-6. Threshold activation energies for neutron foils.

Reaction	$T_{1/2}$	Threshold energy (MeV)
^{115}In(n,n,γ)^{115m}In	4.49 h	0.5
^{54}Fe(n,p)^{56}Mn	312 d	2.2
^{58}Ni(n,p)^{58}Co	70.9 d	2.9
^{27}Al(n,p)^{27}Mg	9.45 m	3.8
^{64}Zn(n,p)^{64}Cu	12.8 h	4.0
^{56}Fe(n,p)^{56}Mn	2.58 d	4.9
^{59}Co(n,α)^{56}Mn	2.58 d	5.2
^{24}Mg(n,p)^{24}Na	15 h	6.0
^{27}Al(n,α)^{27}Mg	15 h	8.1
^{197}Au(n,2n)^{196}Au	6.18 d	8.6
^{19}F(n,2n)^{18}F	110 m	11.6
^{58}Ni(n,2n)^{57}Ni	36 h	13

An effective, and somewhat clever, method of determining the fraction of thermal neutrons in a beam is to take advantage of the high neutron absorption property of cadmium. As shown in Figure 14-1, cadmium effectively removes all neutrons of energy below about 0.4 eV and is completely transparent to neutrons above about 1 eV. If a foil such as indium or gold is irradiated bare and an identical one is wrapped in a cadmium foil 0.1–0.2 in thick and irradiated under the same conditions, the activity of each is a measure of the number of thermal and fast neutrons in the beam. The activity of the bare foil is due to thermal plus fast neutrons while the activity of the cadmium-covered foil is due only to fast neutrons since essentially all the thermal neutrons will be absorbed by the cadmium. The ratio of thermal to fast neutrons is given by the cadmium ratio:

$$\text{Cd ratio} = \frac{A\,(\text{bare})}{A\,(\text{with Cd})}$$

This technique provides a rough division between thermal and fast neutrons since σ_a falls off as $1/v$ for most foils; i.e., the induced activity from fast neutrons, which is a function of σ_a, will decrease as the neutron energy increases. For gold, σ_a = 98 b for thermal neutrons and the $1/v$ relation holds up to about 0.1 eV, but due to strong resonance absorption of about 40,000 b at 5eV, a non-$1/v$ correction factor needs to be applied when gold foils are used.

Fission foils can also be used for fission neutron fields such as may be encountered around nuclear reactors. The basic techniques for use of these foils were developed by Hurst et al. (1956) in the early 1950s. Foils of ^{237}Np, ^{238}U, and ^{239}Pu are generally used. ^{237}Np has a fission threshold at about 0.4 MeV and ^{238}U at about 1.4 MeV; a ^{239}Pu foil encased in a spherical shell of boron with density thickness of 1–2 g/cm^2 has a pseudo-threshold of about 0.01 MeV even though it is fissionable at all energies and especially so at thermal energies ($\sigma_f \sim 740$ b). Selective counting of a gamma-emitting fission product such as ^{140}Ba–La or ^{65}Zn for each foil provides measurements that can be used to determine the relative distribution of neutron fluences between 0.01–0.4 MeV, 0.4–1.4 MeV, and above 1.4 MeV. Unfortunately, gram quantities of strictly regulated fissionable material are required, and if used as a personal dosimeter to measure low neutron exposures, fission foil dosimeters can be somewhat heavy.

Carbon activation can also be used as a threshold detector for neutrons with energies above 20 MeV. The ^{12}C(n,2n)^{11}C reaction has a threshold at about 20 MeV and the cross-section for the reaction is essentially constant from 20 to 40 MeV at 20 mb. The carbon detector can be shaped around a NaI(Tl) detector to provide good geometry for counting (e.g., in the form of a cylinder) or constructed in a disc shape that can be placed on the detector to measure the ^{11}C activation produced. Since ^{11}C transforms by positron emission, the 0.511 MeV annihilation photons are easily measured. The geometry/efficiency can be determined by calibrating the system with a standard of a positron emitter such as ^{22}Na or, if an accelerator is available, the positron emitter can be produced locally, e.g., ^{18}F or ^{11}C itself.

14.6.4 Albedo Dosimeters

Thermoluminescent crystals made of lithium fluoride (LiF) can be used to measure fast neutrons indirectly by using the body to moderate and reflect them to the LiF crystal which is sensitive to thermal neutrons. Fast neutrons that strike the human body (or a phantom can be used) undergo a series of elastic collisions until they reach thermal energies. A fraction of these are in turn diffused out of the body and are captured by ^{6}Li in the LiF dosimeter crystal with a (n,α) cross-section of 941 b. It is known as an albedo (the Greek word for reflection) dosimeter because it depends on the body to "reflect" neutrons back to the LiF crystal; therefore, the dosimeter must be worn on the surface of the body and it must be calibrated on a slab of tissue-equivalent material. The albedo factor is the fraction of incident neutrons reflected back to the dosimeter; it decreases gradually from about 0.8 for thermal neutrons to about 0.1 for 5 MeV neutrons. Intermediate values of the albedo factor are 0.5 at 1 eV, 0.4 at 10 eV, 0.3 at 1 keV, and 0.2 at 100 keV.

14.6.5 Flux Depression of Neutrons

It is often important to determine if a neutron flux is significantly altered as it passes through an absorber, be it a sample, a detector, or perhaps a person. Such alteration constitutes flux depression. It is calculated as a ratio of the attenuated neutron flux to that before attenuation occurs, ϕ_0, via the relationship

$$\phi(x) = \phi_0 e^{-\Sigma x}$$

where Σ is the macroscopic cross-section for a medium and x is its thickness.

Example 14-12. Determine the flux depression for thermal neutrons in a BF_3 long counter that is 30 cm long and 5 cm in diameter if the boron content is essentially all ^{10}B.

Solution. The macroscopic cross-section Σ for the BF_3 gas is, neglecting the minor contribution of F,

$$\Sigma = \frac{0.6022 \times 10^{24}\ \text{atoms/mol}}{22{,}400\ \text{cm}^3/\text{mol}} \times 3840 \times 10^{-24}\ \text{cm}^2/\text{atom}$$

$$= 0.1032\ \text{cm}^{-1}$$

The fractional flux depression for the diameter of the counter is

$$\frac{\phi(5\ \text{cm})}{\phi_0} = e^{-0.1032\text{cm}^{-1} \times 5\ \text{cm}} = 0.597$$

and for the length of the counter

$$\frac{\phi(30\,\text{cm})}{\phi_0} = e^{-0.1032\,\text{cm}^{-1} \times 30\,\text{cm}} = 0.045$$

Therefore, only 59.7% of the flux penetrates across the detector and only 4.5% the length of the detector, and flux depression is significant.

14.7 Summary

The two most important properties of neutrons relative to radiation protection are the probability of interaction in a medium (denoted by the cross-section) and the energy transferred to or deposited in the medium. Most neutron sources produce energetic neutrons that are classified as "fast" because of their velocities at these energies; however, they quickly undergo various interactions with media and their energy is degraded to intermediate and thermal energies, the other two major classifications. Such sources are readily characterized in terms of a fluence of neutrons per unit area (n/cm^2) or a fluence rate or flux (n/cm^2 s).

The intensity of a neutron beam will be diminished when it strikes a receptor of interest, which may be an absorber to change or attenuate the beam, a shielding material, a detector, or a person that may receive a proportionate dose. Three types of interactions are important: elastic scattering, inelastic scattering, and capture. Scattering interactions, whether elastic or inelastic, reduce the neutron energy and transfer the energy lost to the absorbing medium where it is deposited by recoiling nuclei. Capture interactions yield new products that may emit capture gamma rays, eject a charged particle from the compound nucleus formed, or produce radioactive atoms that emit various forms of radiation as they undergo radioactive transformation after formation. All of these processes require consideration in determinations of neutron dose, design of shields, and methods of detection.

Acknowledgment

This chapter came about because of the patient and skillful work of Chul Lee MS, a graduate of the University of Michigan Radiological Health Program.

Other Suggested Sources

Attix, F. H. **1986**, *Introduction to Radiological Physics and Radiation Dosimetry*, Wiley, New York, Chapter 16.
Attix, F. H., Roesch, W. C. (eds) **1968**, *Radiation Dosimetry*, Vol. 1, Academic Press, San Diego, CA, Chapter 6.
Clark, F. H., Betz, N. A., Brown, J. **1966**, *Monte Carlo Calculations of the Penetration of Normally Incident Neutron Beams through Concrete*, Report. ORNL-3926, Oak Ridge National Laboratory, TN.

Hurst, G. A. et al. **1956**, The neutron long counter, *Rev. Sci. Instrum.* 27, 153.
International Commission on Radiological Protection **1975**, Publ 23, Report of the Task Group on Reference Man, Pergamon, Oxford.
Lamarsh, J. R. **1983**, *Introduction to Nuclear Engineering*, 2nd edn, Addison Wesley, Reading, MA.
NCRP **1987**, Reports 38 and 112, National Council on Radiation Protection, Washington, DC.

Problems – Chapter 14

14–1. Estimate the dose equivalent rate at a distance of 120 cm from a ^{210}Po–B (average energy of 2.5 MeV) point source that emits 2×10^7 neutrons/s and is shielded by 30 cm of water.
14–2. What is the maximum number of neutrons/s that a ^{210}Po–Be (average energy of 4 MeV) point source can emit if it is to be stored behind 65 cm of paraffin and the dose equivalent rate is not to exceed 2 mrem/h at a distance of 1 m?
14–3. The cross-section for the ^{6}Li(n,α)^{3}H reaction is 941 b for thermal neutrons and ^{6}Li is a $1/v$ absorber. If the average neutron energy in a zone of the K reactor is 5 eV what is the absorption cross-section for ^{6}Li targets placed in the zone?
14–4. Calculate the amount of energy transferred to carbon atoms in a graphite moderator due to elastic scattering of neutrons which have an average energy of about 2 MeV and the fraction of the initial energy transferred.
14–5. If 5 cm of lead is added to the inside of a concrete shield, what fractional increase in removal of fast-fission neutrons will occur?
14–6. Determine the tissue dose to a person exposed to a fluence of 10^7 thermal neutrons due to (n,p) absorption reactions in nitrogen.
14–7. Determine the dose equivalent rate for neutrons emitted from a point source of ^{252}Cf if the source strength is 10 mCi, the fraction of transformations that occur by spontaneous fission is 0.029, 2.45 neutrons are emitted per fission, and the receptor is positioned at 80 cm from the source.
14–8. A neutron source of intermediate energy produces an intensity of 10^7 n/cm^2 s. If a lead shield 2 cm thick is placed in the beam followed by 30 cm of water, what would the intensity be just outside the water barrier?
14–9. Calculate the dose equivalent rate for the unshielded and shielded conditions in Problem 14-8.
14–10. The fluence rate of 14.1 MeV neutrons several feet from a D-T generator is 10^3 n/cm^2 s. If a 60 cm slab of concrete is used to shield the beam, what would be the dose equivalent rate just outside the slab?
14–11. A carbon disk is exposed to a flux of neutrons around a high-energy accelerator for 20 min. It is counted immediately after exposure and 1000 gammas of 0.511 MeV are recorded. If the system geometry/efficiency is 4%, what is the flux of neutrons with energies above 20 MeV?

Answers to Selected Problems

Corrected answers (if advisable) are available at: www-personal.umich.edu/~jemartin

Chapter 1

1-1. (a) 6p, 8n; (c) 54p, 79n
1-2. (b) 3.9 fermi
1-3. 1.98 eV; 1.98 eV; 4.784×10^{14}/s
1-5. (a) 1.226×10^{-9} m; (b) 1.4×10^{-12} m (relativistic); (c) 1.798×10^{-10} m; (d) 1.59×10^{-38} m

Chapter 2

2-1. 2.254 MeV
2-2. $6{,}507 \times 10^{21}$ atoms
2-4. 5.9737×10^{23} atoms
2-5. 3.3407×10^{-24} g
2-7. (c) 700 keV or 1.1215×10^{-13} J
2-8. $v = 0.866c$
2.9. (a) 37.6 MeV or 5.37 MeV/nucleon; (c) 1801.72 MeV or 7.7 MeV/nucleon

Chapter 3

3-1. 2403 Ci
3-3. 1.81 h
3-4. 209 y
3-5. (a) 276 d; (b) 8.88×10^{-4} g
3-6. (a) 1.23×10^{6} Ci; (b) 7.3×10^{-11} g
3-9. 11.5 μCi of ^{40}K
3-10. 304 mCi
3-11. (a) 352 mCi; (b) 14.93 d
3-13. (b) 0.637 od original
3-16. (a) 8.3 μg; (b) 1.33 μg of ^{3}H
3-17. 5.28 min

Physics for Radiation Protection, Third Edition. James E. Martin

3-19. (a) 1.94 mCi; (b) 9.97 mCi
3-20. 9.98 mCi at 766 h
3-21. (b) 146.9 mCi at 5.6533 d
3-23. 5.4 mg for 4.732 L.

Chapter 4

4-2. (a) 17.35 MeV; (c) 2.1257 MeV; (e) –0.2813 MeV; (g) 4.9658 MeV
4-3. (a) –1.853 MeV; (b) –3.005 MeV; (c) –2.454 MeV
4-4. (b) 2.575 MeV
4-5. 12C + n; $E = 10 + 4.9458$ MeV
4-6. (a) 13.125, 18.7213, and 4.9463 MeV
4-7. (a) 8.691 MeV; (b) 15.9566 MeV; (c) 17.5337 MeV
4-9. 9.049 MeV
4-10. 8.665 MeV
4-11. 205 MeV
4-12. 14.1 MeV
4-13. (b) 34.7 MeV
4-14. 2.73 MeV
4-16. 0.1565 MeV
4-17. 3.58×10^9 t/s
4-20. (a) 11,600 Ci ^{60m}Co; (b) 11,154 Ci ^{60}Co
4-21. 7668 Ci ^{60}Co
4-22. 1.74×10^{-9} g of Mn
4-24. 0.152 Ci ^{203}Hg
4-25. (b) 3.16×10^{10} t/s of ^{192}Ir per mg of iridium
4-26. 5.94×10^{10} t/s of ^{204}Tl (minus target depletion)
4-27. 298 MBq of ^{11}C

Chapter 5

5-1. 3.57%
5-2. (b) 1.765×10^8 Ci at equilibrium (~53 d)
5-3. 1.4×10^6 Ci
5-5. (a) 9.6 μCi
5-6. (a) 1.06×10^5 Ci; (b) 5574 + 1723 Ci
5-7. 9.3×10^6 Ci (thermal fission)
5-8. 1.4×10^6 Ci
5-9. (a) 1.09×10^8 Ci; (b) 1.05×10^8 Ci
5-10. (a) 1.54×10^4 Ci; (b) same

Chapter 6

6-1. ~97%
6-2. 36.5 d
6-5. 1.794×10^6 erg
6-7. 3520 y
6-9. 2.6×10^6 y
6-10. 16.3 y
6-12. 43 pCi/g
6-17. 0.096 WL

Chapter 7

7-1. (a) 6.5 MeV
7-3. 1.728 MeV for positron; 0.249 MeV for electron
7-5. 37.7 rad/h for betas plus conversion electrons in 0.2 cm tissue
7-7. (a) 12 keV
7-9. (a) 0.463 R/h Ci at 1 m; (b) 1.7 rad/h in tissue at 50 cm
7-11. (a) $\phi = 2.62\ \beta/\text{cm}^2$ s; (b) $\phi_{\beta,\text{E}} = 183$ MeV/cm^2 s; (c) $D_{\beta,\text{Sh}} = 97$ mrad/h
7-13. (a) 1.77 rad/h; (b) 0.996 rad/h

Chapter 8

8-1. 42 μm
8-3. (a) $x = 0.42$ cm
8-4. 8.42 cm
8-7. 0.7176
8-9. 5.4 cm
8-10. 2.1 mR/h
8-11. 11.6 cm (includes buildup)
8-12. 0.367 mR/h
8-13. ~20 cm (includes buildup)
8-16. 0.04 mrem/h
8-19. 32.3 rem/h
8-22. 12.5 μR/h

Chapter 9

9-1. (a) 7.29 d
9-3. (a) 30.53 rad/h; (b) 7.7×10^3 rad
9-5. (a) 466 mrad to lung and 48.3 mrad total body due to photons
9-7. (a) 4.95×10^{12} t; (b) 0.5 rad
9-9. 6220 DAC h (nonstochastic)

9-11. (a) ALI = 1.4×10^8 Bq, DAC = 5.82×10^4 Bq/m^3; (b) ALI = 7.66×10^6 Bq, DAC = 3.2×10^3 Bq/m^3
9-13. 1.2×10^{-4} Sv
9-15. 34.3 Sv
9-17. 1.8×10^6 Bq

Chapter 10

10-1. (a) 2.24×10^{-4} Ci/m^3; (b) 4.38×10^{-4} Ci/m^3
10-3. 71 m
10-4. (a) 2.7×10^{-2} g/m^3 (or 2.0×10^{-2} g/m^3 by virtual source); (b) 1.57×10^{-2} g/m^3 by selection rule
10-7. 5.29×10^{-7} Ci/m^3
10-9. 0.62 Bq/m^2

Chapter 11

11-4. 9.3×10^6 Ci (assuming thermal neutron fission)
11-6. 6.58×10^7 Ci
11-8. (a) 1.06×10^7 Ci; (b) 5574 + 1723 Ci
11-9. 800–2000 rad
11-10. 1.222 mCi (thermal fission)

Chapter 12

12-1. ce-K = 12 keV; ce-L = 35 eV
12-3. 0.796 MeV
12-4. 166.8 keV
12-8. 26 c/m
12-11. (a) Extrapolated range ~760 mg/cm^2; (b) ~1.7 MeV; (c) 1.68 MeV

Chapter 13

13-1. 100 ± 10 c or 50 ± 5 c/m at 68.3% confidence; 100 ± 19.6 c or 50 ± 9.8 c/m at 95% confidence
13-3. (a) 200 ± 10 c/m; (b) 5.41 min (90% confidence)
13-5. (a) 1955 to 2045 c; (b) 1912 to 2088 c
13-7. (a) 342,860 c/m; (b) $2.143 \times 10^6 \pm 472$ d/m
13-9. 25 ± 1.94 c/m
13-11. (a) t(s + b) = 43 min; t(b) = 17 min
13-14. 74.3% probability that sample contains activity above background; at 95% confidence it does not

Chapter 14

14-1. 0.72 mrem/h
14-3. 66.94 b
14-6. 0.273 mrad or 0.684 mrem (for $Q = 2.5$)
14-8. 3.6×10^5 n/cm^2 s
14-10. 3.5 mrem/h
14-11. 5×10^7 n/cm^2 s

Appendix A

Constants of Nature and Selected Particle Masses

Speed of light	c	2.99792458×108 m/s
Charge of electron	e	$1.60217733 \times 10^{-19}$ C
Boltzmann constant	k	1.380658×10^{-23} J/K
		8.617385×10^{-5} eV/K
Faraday's constant		96485.309 C/mol
Planck's constant	h	$6.6260755 \times 10^{-34}$ J s
		$4.1356692 \times 10^{-15}$ eV s
Gravitational constant	G	6.67259×10^{-11} m^3 kg^{-2} s^{-2}
Avogadro's number	N_A	6.0221367×10^{23} per mole
Universal gas constant	R	8.314510 J/mol K
Stefan–Boltzmann constant	k	5.6705×10^{-8} W/m^2 K^4
Rydberg constant	R	10973731.534 m^{-1}
Bohr radius	a_0	$0.529177249 \times 10^{-10}$ m
Fine structure constant	a	1/137.0359895
Electron volt	eV	$1.60217733 \times 10^{-19}$ J
Joule	J	6.2415×10^{18} eV
		10^7 erg
erg		10^{-7} J

Physics for Radiation Protection, Third Edition. James E. Martin

Unified mass unit		1.66054×10^{-27} kg	1.00000 u	931.502 MeV
Electron	e	$9.1093897 \times 10^{-31}$ kg	5.4857990×10^{-4} u	0.5109990 MeV
Proton	p	$1.6726231 \times 10^{-27}$ kg	1.00727647 u	938.27231 MeV
Neutron	n	$1.6749286 \times 10^{-27}$ kg	1.00866490 u	939.56563 MeV
Deuteron	d	$3.3435856 \times 10^{-27}$ kg	2.01355320 u	1875.62883 MeV
Tritium (^{3}H)	T	$5.0073595 \times 10^{-27}$ kg	3.015500688 u	2808.94492 MeV
Alpha	α	$6.6446618 \times 10^{-27}$ kg	4.001506178 u	3727.38025 MeV
Helium	He	$6.6464828 \times 10^{-27}$ kg	4.002603250 u	3728.43293 MeV

Source: National Institute of Technology (NIST) 1986 CODATA Recommended Values of the Fundamental Physical Constants (Internet address: physics.nist.gov/PhysRefData/codata86/codata86.html).

Appendix B

Atomic Masses and Binding Energies for Selected Isotopes of the Elements

Physics for Radiation Protection, Third Edition. James E. Martin

Z		A	Binding energy (MeV)	Atomic mass (umu)	Z		A	Binding energy (MeV)	Atomic mass (umu)	Z		A	Binding energy (MeV)	Atomic mass (umu)
0	n	1	0	1.0086649	8	O	14	98.733	14.0085953	13	Al	25	200.528	24.9904286
							15	111.956	15.0030654			26	211.894	25.9868917
1	H	1	0	1.0078250			16	127.619	15.9949146			27	224.952	26.9815384
		2	2.225	2.0141018			17	131.763	16.9991315			28	232.677	27.9819102
		3	8.482	3.0160493			18	139.807	17.9991604			29	242.113	28.9804448
							19	143.763	19.0035787					
2	He	3	7.718	3.0160293			20	151.371	20.0040762	14	Si	26	206.046	25.9923299
		4	28.296	4.0026033								27	219.357	26.9867048
					9	F	17	128.22	17.0020952			28	236.537	27.9769265
3	Li	6	31.995	6.0151223			18	137.369	18.0009377			29	245.01	28.9764947
		7	39.245	7.0160040			19	147.801	18.9984032			30	255.62	29.9737702
		8	41.277	8.0224867			20	154.403	19.9999813			31	262.207	30.9753633
							21	162.504	20.9999489			32	271.41	31.9741481
4	Be	7	37.6	7.0169292										
		8	56.5	8.0053051	10	Ne	18	132.153	18.0056971	15	P	29	239.285	28.9818014
		9	58.165	9.0121821			19	143.781	19.0018798			30	250.605	29.9783138
		10	64.977	10.0135337			20	160.645	19.9924402			31	262.917	30.9737615
		11	65.481	11.0216577			21	167.406	20.9938467			32	270.852	31.9739072
							22	177.77	21.9913855			33	280.956	32.9717253
5	B	8	37.738	8.0246067			23	182.971	22.9944673					
		9	56.314	9.0133288			24	191.836	23.9936151	16	S	30	243.685	29.9849030
		10	64.751	10.0129370								31	256.738	30.9795544
		11	76.205	11.0093055	11	Na	21	163.076	20.9976551			32	271.781	31.9720707
		12	79.575	12.0143521			22	174.145	21.9944368			33	280.422	32.9714585
							23	186.564	22.9897697			34	291.839	33.9678668
6	C	10	60.321	10.0168531			24	193.523	23.9909633			35	298.825	34.9690321
		11	73.44	11.0114338			25	202.535	24.9899544			36	308.714	35.9670809
		12	92.162	12.0000000			26	208.151	25.9925899			37	313.018	36.9711257
		13	97.108	13.0033548										
		14	105.285	14.0032420	12	Mg	22	168.578	21.9995741	17	Cl	33	274.057	32.9774518
		15	106.503	15.0105993			23	181.725	22.9941249			34	285.566	33.9737620
							24	198.257	23.9850419			35	298.21	34.9688527
7	N	13	94.105	13.0057386			25	205.588	24.9858370			36	306.789	35.9683069
		14	104.659	14.0030740			26	216.681	25.9825930			37	317.1	36.9659026
		15	115.492	15.0001089			27	223.124	26.9843407			38	323.208	37.9680106
		16	117.981	16.0061014			28	231.628	27.9838767			39	331.282	38.9680077
		17	123.865	17.0084497										

Z		A	Binding energy (MeV)	Atomic mass (umu)	Z		A	Binding energy (MeV)	Atomic mass (umu)	Z		A	Binding energy (MeV)	Atomic mass (umu)
18	Ar	34	278.721	33.9802701	22	Ti	44	375.475	43.9596902	26	Fe	52	447.697	51.9481165
		35	291.462	34.9752567			45	385.005	44.9581243			53	458.38	52.9453123
		36	306.716	35.9675463			46	398.194	45.9526295			54	471.759	53.9396148
		37	315.505	36.9667759			47	407.072	46.9517638			55	481.057	54.9382980
		38	327.343	37.9627322			48	418.699	47.9479471			56	492.254	55.9349421
		39	333.941	38.9643134			49	426.841	48.9478708			57	499.9	56.9353987
		40	343.81	39.9623831			50	437.78	49.9447921			58	509.944	57.9332805
		41	349.909	40.9645008			51	444.153	50.9466160			59	516.525	58.9348805
		42	359.335	41.9630464			52	451.961	51.9468982			60	525.345	59.9340769
												61	530.927	60.9367495
19	K	37	308.573	36.9733769	23	V	48	413.904	47.9522545					
		38	320.647	37.9690801			49	425.457	48.9485169	27	Co	57	498.282	56.9362962
		39	333.724	38.9637069			50	434.79	49.9471628			58	506.855	57.9357576
		40	341.523	39.9639987			51	445.841	50.9439637			59	517.308	58.9332002
		41	351.618	40.9618260			52	453.152	51.9447797			60	524.8	59.9338222
		42	359.152	41.9624031			53	461.631	52.9443425			61	534.122	60.9324794
		43	368.795	42.9607157										
					24	Cr	48	411.462	47.9540359	28	Ni	56	483.988	55.9421363
20	Ca	38	313.122	37.9763186			49	422.044	48.9513411			57	494.235	56.9398005
		39	326.411	38.9707177			50	435.044	49.9460496			58	506.454	57.9353479
		40	342.052	39.9625912			51	444.306	50.9447718			59	515.453	58.9343516
		41	350.415	40.9622783			52	456.345	51.9405119			60	526.842	59.9307906
		42	361.895	41.9586183			53	464.284	52.9406538			61	534.662	60.9310604
		43	369.828	42.9587668			54	474.003	53.9388849			62	545.259	61.9283488
		44	380.96	43.9554811			55	480.25	54.9408442			63	552.097	62.9296729
		45	388.375	44.9561859			56	488.506	55.9406452			64	561.755	63.9279696
		46	398.769	45.9536928								65	567.853	64.9300880
		47	406.045	46.9545465	25	Mn	52	450.851	51.9455701					
		48	415.991	47.9525335			53	462.905	52.9412947	29	Cu	61	531.642	60.9334622
		49	421.138	48.9556733			54	471.844	53.9403632			62	540.528	61.9325873
							55	482.07	54.9380496			63	551.381	62.9296011
21	Sc	43	366.825	42.9611510			56	489.341	55.9389094			64	559.297	63.9297679
		44	376.525	43.9594030			57	497.991	56.9382875			65	569.207	64.9277937
		45	387.849	44.9559102								66	576.273	65.9288730
		46	396.61	45.9551703								67	585.391	66.9277503
		47	407.254	46.9524080										
		48	415.487	47.9522350										

Z		A	Binding energy (MeV)	Atomic mass (umu)	Z		A	Binding energy (MeV)	Atomic mass (umu)	Z		A	Binding energy (MeV)	Atomic mass (umu)
30	Zn	62	538.119	61.9343341	34	Se	72	622.43	71.9271123	38	Sr	82	708.128	81.9184013
		63	547.232	62.9332156			73	630.823	72.9267668			83	716.987	82.9175550
		64	559.094	63.9291466			74	642.89	73.9224766			84	728.906	83.9134248
		65	567.073	64.9292451			75	650.918	74.9225236			85	737.436	84.9129327
		66	578.133	65.9260368			76	662.072	75.9192141			86	748.926	85.9092624
		67	585.185	66.9271309			77	669.491	76.9199146			87	757.354	86.9088793
		68	595.383	67.9248476			78	679.989	77.9173095			88	768.467	87.9056143
		69	601.866	68.9265535			79	686.951	78.9184998			89	774.825	88.9074529
		70	611.081	69.9253249			80	696.865	79.9165218			90	782.631	89.9077376
		71	616.915	70.9277272			81	703.566	80.9179929					
							82	712.842	81.9167000	39	Y	87	754.71	86.9108778
31	Ga	67	583.402	66.9282049			83	718.66	82.9191191			88	764.062	87.9095034
		68	591.68	67.9279835								89	775.538	88.9058479
		69	601.989	68.9255809	35	Br	77	667.343	76.9213801			90	782.395	89.9071514
		70	609.644	69.9260277			78	675.633	77.9211461			91	790.325	90.9073034
		71	618.948	70.9247050			79	686.32	78.9183376					
		72	625.469	71.9263694			80	694.212	79.9185300	40	Zr	88	762.606	87.9102262
		73	634.657	72.9251698			81	704.369	80.9162911			89	771.923	88.9088889
							82	711.962	81.9168047			90	783.893	89.9047037
32	Ge	68	590.792	67.9280973			83	721.547	82.9151802			91	791.087	90.9056450
		69	598.98	68.9279720								92	799.722	91.9050401
		70	610.518	69.9242504	36	Kr	76	654.235	75.9259483			93	806.456	92.9064756
		71	617.934	70.9249540			77	663.499	76.9246679			94	814.676	93.9063158
		72	628.685	71.9220762			78	675.558	77.9203863			95	821.139	94.9080427
		73	635.468	72.9234594			79	683.912	78.9200830			96	828.993	95.9082757
		74	645.665	73.9211782			80	695.434	79.9163780			97	834.573	96.9109507
		75	652.17	74.9228595			81	703.306	80.9165924					
		76	661.598	75.9214027			82	714.272	81.9134846	41	Nb	91	789.052	90.9069905
		77	667.671	76.9235485			83	721.737	82.9141360			92	796.934	91.9071932
							84	732.257	83.9115066			93	805.765	92.9063775
33	As	73	634.345	72.9238253			85	739.378	84.9125270			94	812.993	93.9072835
		74	642.32	73.9239291			86	749.235	85.9106103			95	821.482	94.9068352
		75	652.564	74.9215964			87	754.75	86.9133543					
		76	659.892	75.9223939										
		77	669.59	76.9206477	37	Rb	83	720.045	82.9151120					
							84	728.794	83.9143847					
							85	739.283	84.9117893					
							86	747.934	85.9111671					
							87	757.853	86.9091835					
							88	763.936	87.9113186					

Z		A	Binding energy (MeV)	Atomic mass (umu)	Z		A	Binding energy (MeV)	Atomic mass (umu)	Z		A	Binding energy (MeV)	Atomic mass (umu)
42	Mo	90	773.728	89.9139362	46	Pd	100	856.371	99.9085046	50	Sn	110	934.562	109.9078527
		91	783.835	90.9117508			101	864.643	100.9082891			111	942.743	110.9077354
		92	796.508	91.9068105			102	875.213	101.9056077			112	953.529	111.9048208
		93	804.578	92.9068122			103	882.837	102.9060872			113	961.272	112.9051734
		94	814.256	93.9050876			104	892.82	103.9040349			114	971.571	113.9027818
		95	821.625	94.9058415			105	899.914	104.9050840			115	979.117	114.9033460
		96	830.779	95.9046789			106	909.477	105.9034831			116	988.68	115.9017441
		97	837.6	96.9060210			107	916.016	106.9051285			117	995.625	116.9029538
		98	846.243	97.9054078			108	925.236	107.9038945			118	1004.952	117.9016063
		99	852.168	98.9077116			109	931.39	108.9059535			119	1011.437	118.9033089
		100	860.458	99.9074771			110	940.207	109.9051524			120	1020.544	119.9021966
		101	865.856	100.9103465			111	945.958	110.9076440			121	1026.715	120.9042369
												122	1035.529	121.9034401
43	Tc	95	819.152	94.9076565	47	Ag	105	897.787	104.9065282			123	1041.475	122.9057219
		96	827.024	95.9078708			106	905.729	105.9066664			124	1049.962	123.9052746
		97	836.498	96.9063648			107	915.266	106.9050930			125	1055.695	124.9077849
		98	843.776	97.9072157			108	922.536	107.9059537			126	1063.889	125.9076540
		99	852.743	98.9062546			109	931.723	108.9047555					
		100	859.507	99.9076576			110	938.532	109.9061105	51	Sb	119	1010.061	118.9039465
												120	1017.081	119.9050743
44	Ru	94	806.849	93.9113596	48	Cd	104	885.841	103.9098481			121	1026.323	120.9038180
		95	815.802	94.9104127			105	894.266	104.9094678			122	1033.13	121.9051754
		96	826.496	95.9075977			106	905.141	105.9064580			123	1042.095	122.9042157
		97	834.607	96.9075545			107	913.067	106.9066142			124	1048.563	123.9059375
		98	844.791	97.9052871			108	923.402	107.9041834			125	1057.276	124.9052478
		99	852.254	98.9059393			109	930.727	108.9049856					
		100	861.928	99.9042197			110	940.642	109.9030056	52	Te	118	999.457	117.9058252
		101	868.73	100.9055822			111	947.618	110.9041816			119	1006.985	118.9064081
		102	877.949	101.9043495			112	957.016	111.9027572			120	1017.281	119.9040199
		103	884.182	102.9063237			113	963.556	112.9044009			121	1024.505	120.9049298
		104	893.085	103.9054301			114	972.599	113.9033581			122	1034.33	121.9030471
		105	898.995	104.9077503			115	978.74	114.9054306			123	1041.259	122.9042730
							116	987.44	115.9047554			124	1050.685	123.9028195
45	Rh	101	867.406	100.9061635			117	993.217	116.9072182			125	1057.261	124.9044247
		102	874.844	101.9068428								126	1066.375	125.9033055
		103	884.163	102.9055042	49	In	111	945.97	110.9051107			127	1072.665	126.9052173
		104	891.162	103.9066553			112	953.648	111.9055333			128	1081.441	127.9044614
		105	900.13	104.9056924			113	963.091	112.9040612			129	1087.524	128.9065956
							114	970.365	113.9049168			130	1095.943	129.9062228
							115	979.404	114.9038783			131	1101.872	130.9085219
							116	986.188	115.9052600					

Z		A	Binding energy (MeV)	Atomic mass (umu)	Z		A	Binding energy (MeV)	Atomic mass (umu)	Z		A	Binding energy (MeV)	Atomic mass (umu)
53	I	125	1056.293	124.9046242	56	Ba	128	1074.727	127.9083089	60	Nd	140	1167.521	139.9093098
		126	1063.437	125.9056194			129	1082.459	128.9086737			141	1175.318	140.9096048
		127	1072.58	126.9044684			130	1092.731	129.9063105			142	1185.146	141.9077186
		128	1079.406	127.9058053			131	1100.225	130.9069308			143	1191.27	142.9098096
		129	1088.239	128.9049875			132	1110.042	131.9050562			144	1199.087	143.9100826
		130	1094.74	129.9066740			133	1117.232	132.9060024			145	1204.842	144.9125688
							134	1126.7	133.9045033			146	1212.407	145.9131121
54	Xe	122	1027.641	121.9085484			135	1133.673	134.9056827			147	1217.7	146.9160958
		123	1035.785	122.9084707			136	1142.78	135.9045701			148	1225.032	147.9168885
		124	1046.254	123.9058958			137	1149.686	136.9058214			149	1230.071	148.9201442
		125	1053.858	124.9063982			138	1158.298	137.9052413			150	1237.451	149.9208866
		126	1063.913	125.9042689			139	1163.021	138.9088354			151	1242.785	150.9238247
		127	1071.136	126.9051796										
		128	1080.743	127.9035304	57	La	136	1139.128	135.9076512	61	Pm	143	1189.446	142.9109276
		129	1087.651	128.9047795			137	1148.304	136.9064657			144	1195.973	143.9125858
		130	1096.907	129.9035079			138	1155.778	137.9071068			145	1203.897	144.9127439
		131	1103.512	130.9050819			139	1164.556	138.9063482			146	1210.153	145.9146922
		132	1112.447	131.9041545			140	1169.717	139.9094726			147	1217.813	146.9151339
		133	1118.887	132.9059057			141	1176.405	140.9109570			148	1223.71	147.9174678
		134	1127.435	133.9053945								149	1230.979	148.9183292
		135	1133.817	134.9072075	58	Ce	134	1120.922	133.9090264					
		136	1141.877	135.9072195			135	1128.882	134.9091456	62	Sm	142	1176.619	141.9151933
		137	1145.903	136.9115629			136	1138.819	135.9071436			143	1185.221	142.9146236
							137	1146.299	136.9077776			144	1195.741	143.9119947
55	Cs	131	1102.377	130.9054602			138	1156.04	137.9059856			145	1202.498	144.9134056
		132	1109.545	131.9064298			139	1163.495	138.9066466			146	1210.913	145.9130368
		133	1118.532	132.9054469			140	1172.696	139.9054340			147	1217.255	146.9148933
		134	1125.424	133.9067134			141	1178.125	140.9082711			148	1225.396	147.9148179
		135	1134.186	134.9059719			142	1185.294	141.9092397			149	1231.268	148.9171795
		136	1141.015	135.9073057			143	1190.439	142.9123812			150	1239.254	149.9172715
		137	1149.293	136.9070835			144	1197.335	143.9136427			151	1244.85	150.9199284
												152	1253.108	151.9197282
					59	Pr	139	1160.584	138.9089322			153	1258.976	152.9220939
							140	1168.526	139.9090712			154	1266.943	153.9222053
							141	1177.923	140.9076477			155	1272.75	154.9246359
							142	1183.766	141.9100399					
							143	1191.118	142.9108122					

Z		A	Binding energy (MeV)	Atomic mass (umu)	Z		A	Binding energy (MeV)	Atomic mass (umu)	Z		A	Binding energy (MeV)	Atomic mass (umu)
63	Eu	149	1229.79	148.9179259	67	Ho	163	1329.595	162.9287303	71	Lu	173	1397.681	172.9389269
		150	1236.211	149.9196983			164	1336.269	163.9302306			174	1404.442	173.9403335
		151	1244.144	150.9198460			165	1344.258	164.9303192			175	1412.109	174.9407679
		152	1250.451	151.9217404			166	1350.501	165.9322813			176	1418.397	175.9426824
		153	1259.001	152.9212262			167	1357.786	166.9331262			177	1425.469	176.9437550
		154	1265.443	153.9229754										
		155	1273.595	154.9228894	68	Er	161	1311.486	160.9300013	72	Hf	172	1388.333	171.9394580
							162	1320.7	161.9287749			173	13952.94	181.4065000
64	Gd	150	1236.4	149.9186555			163	1327.603	162.9300293			174	1403.933	173.9400402
		151	1242.898	150.9203443			164	1336.449	163.9291970			175	1410.642	174.9415030
		152	1251.488	151.9197879			165	1343.1	164.9307228			176	1418.807	175.9414018
		153	1257.735	152.9217463			166	1351.574	165.9302900			177	1425.185	176.9432200
		154	1266.629	153.9208623			167	1358.01	166.9320454			178	1432.811	177.9436977
		155	1273.065	154.9226188			168	1365.781	167.9323678			179	1438.91	178.9458151
		156	1281.601	155.9221196			169	1371.784	168.9345881			180	1446.298	179.9465488
		157	1287.961	156.9239567			170	1379.043	169.9354603			181	1451.994	180.9490991
		158	1295.898	157.9241005			171	1384.725	170.9380259					
		159	1301.842	158.9263851						73	Ta	179	1438.017	178.9459341
		160	1309.293	159.9270506	69	Tm	167	1356.479	166.9328488			180	1444.662	179.9474657
		161	1314.928	160.9296657			168	1363.32	167.9341704			181	1452.239	180.9479963
							169	1371.353	168.9342111			182	1458.302	181.9501524
65	Tb	157	1287.119	156.9240212			170	1377.946	169.9357979					
		158	1293.896	157.9254103			171	1385.433	170.9364258	74	W	178	1429.243	177.9458484
		159	1302.03	158.9253431								179	1436.175	178.9470717
		160	1308.405	159.9271640	70	Yb	166	1346.666	165.9338796			180	1444.587	179.9467057
		161	1316.102	160.9275663			167	1353.743	166.9349469			181	1451.268	180.9481981
							168	1362.794	167.9338945			182	1459.333	181.9482055
66	Dy	154	1261.749	153.9244220			169	1369.662	168.9351871			183	1465.524	182.9502245
		155	1268.584	154.9257490			170	1378.132	169.9347587			184	1472.935	183.9509326
		156	1278.025	155.9242783			171	1384.747	170.9363223			185	1478.689	184.9534206
		157	1284.995	156.9254613			172	1392.767	171.9363777			186	1485.883	185.9543622
		158	1294.05	157.9244046			173	1399.134	172.9382068			187	1491.35	186.9571584
		159	1300.882	158.9257357			174	1406.599	173.9388581					
		160	1309.458	159.9251937			175	1412.421	174.9412725	75	Re	183	1464.185	182.9508213
		161	1315.912	160.9269296			176	1419.285	175.9425684			184	1470.67	183.9525243
		162	1324.109	161.9267947			177	1424.852	176.9452571			185	1478.34	184.9529557
		163	1330.38	162.9287275								186	1484.519	185.9549865
		164	1338.038	163.9291712								187	1491.879	186.9557508
		165	1343.754	164.9316998								188	1497.75	187.9581123

Z		A	Binding energy (MeV)	Atomic mass (umu)	Z		A	Binding energy (MeV)	Atomic mass (umu)	Z		A	Binding energy (MeV)	Atomic mass (umu)
76	Os	182	1454.06	181.9521862	80	Hg	194	1535.495	193.9653818	85	At	209	1633.3	208.9861587
		183	14612.71	191.5311000			195	1542.395	194.9666390			210	1640.465	209.9871313
		184	1469.919	183.9524908			196	1551.234	195.9658148			211	1648.211	210.9874808
		185	1476.545	184.9540430			197	1558.02	196.9671953					
		186	1484.806	185.9538384			198	1566.504	197.9667518	86	Rn	211	1644.536	210.9905854
		187	1491.099	186.9557479			199	1573.168	198.9682625			222	1708.184	222.0175705
		188	1499.088	187.9558360			200	1581.197	199.9683087					
		189	1505.009	188.9581449			201	1587.427	200.9702853	87	Fr	212	1646.6	211.9961950
		190	1512.801	189.9584452			202	1595.181	201.9706256			223	1713.461	223.0197307
		191	1518.559	190.9609280			203	1601.174	202.9728571					
		192	1526.117	191.9614790			204	1608.669	203.9734756	88	Ra	223	1713.828	223.0184971
		193	1531.702	192.9641481			205	1614.336	204.9760561			224	1720.311	224.0202020
												225	1725.213	225.0236045
77	Ir	189	1503.694	188.9587165	81	Tl	201	1586.161	200.9708038			226	1731.61	226.0254026
		190	1510.018	189.9605923			202	1593.034	201.9720906					
		191	1518.091	190.9605912			203	1600.883	202.9723291	89	Ac	225	1724.788	225.0232206
		192	1524.289	191.9626022			204	1607.539	203.9738486			226	1730.187	226.0260898
		193	1532.06	192.9629237			205	1615.085	204.9744123			227	1736.715	227.0277470
		194	1538.127	193.9650756			206	1621.589	205.9760953					
										90	Th	229	1748.341	229.0317553
78	Pt	188	1494.208	187.9593957	82	Pb	202	1592.202	201.9721438			230	1755.135	230.0331266
		189	1500.941	188.9608319			203	1599.126	202.9733755			231	1760.253	231.0362971
		190	1509.853	189.9599301			204	1607.52	203.9730288			232	1766.691	232.0380504
		191	1516.29	190.9616847			205	1614.252	204.9744671			233	1771.478	233.0415769
		192	1524.966	191.9610352			206	1622.34	205.9744490					
		193	1531.221	192.9629845			207	1629.078	206.9758806	91	Pa	230	1753.043	230.0345326
		194	1539.592	193.9626636			208	1636.446	207.9766359			231	1759.86	231.0358789
		195	1545.697	194.9647744			209	1640.382	208.9810748			232	1765.414	232.0385817
		196	1553.619	195.9649349			210	1645.567	209.9841731					
		197	1559.465	196.9673234						92	U	233	1771.728	233.0396282
		198	1567.022	197.9678760	83	Bi	207	1625.897	206.9784552			234	1778.572	234.0409456
		199	1572.578	198.9705762			208	1632.784	207.9797267			235	1783.87	235.0439231
							209	1640.244	208.9803832			236	1790.415	236.0455619
79	Au	195	1544.688	194.9650179			210	1644.849	209.9841049			237	1795.541	237.0487240
		196	1551.331	195.9665513			211	1649.983	210.9872581			238	1801.695	238.0507826
		197	1559.402	196.9665516								239	1806.501	239.0542878
		198	1565.914	197.9682252	84	Po	207	1622.206	206.9815782					
		199	1573.498	198.9687480			208	1630.601	207.9812311	93	Np	236	1788.703	236.0465597
							209	1637.568	208.9824158			237	1795.277	237.0481673
							210	1645.228	209.9828574			238	1800.765	238.0509405

Z		A	Binding energy (MeV)	Atomic mass (umu)	Z		A	Binding energy (MeV)	Atomic mass (umu)
94	Pu	238	1801.275	238.0495534	107	Bh	260	19013.73	261.2180300
		239	1806.921	239.0521565			261	19094.47	262.2180000
		240	1813.455	240.0538075			262	19163.93	263.2300900
		241	1818.697	241.0568453			263	19243.36	264.2314600
		242	1825.006	242.0587368			264	19309.32	265.2473000
							265	19385.68	266.2519800
95	Am	241	1817.935	241.0568229			266	19449.52	267.2700900
		242	1823.473	242.0595430			267	19523.42	268.2774000
		243	1829.84	243.0613727					
					108	Hn	263	19183.71	264.2871000
96	Cm	246	1847.827	246.0672176			264	1926.724	264.1284083
		247	1852.983	247.0703468			265	19333.11	266.3000100
		248	1859.196	248.0723422			266	19413.45	267.3004200
							267	19478.03	268.3177400
97	Bk	247	1852.246	247.0702985			268	19555.18	269.3215600
							269	19617.65	270.3411400
98	Cf	251	1875.103	251.0795801					
					109	Mt	265	19264.13	266.3656700
99	Es	252	1879.232	252.0829722			266	19332.05	267.3794000
							267	19416.62	268.3752600
100	Fm	257	1907.511	257.0950986			268	19485.32	269.3881600
							269	19563.33	270.3910600
101	Md	258	1911.701	258.0984253			270	19628.98	271.4072300
							271	19704.98	272.4122900
102	No	259	19165.69	260.0102400					
					110	Xa	267	19348.9	268.4395600
103	Lr	260	19196.21	261.0557200			268	19433.59	269.4352900
							269	19499.27	270.4514400
104	Db	261	19239.49	262.0875200			270	19584.8	271.4462600
							271	19651.99	272.4607800
105	Jl	262	19262.06	263.1415300			272	19730.54	273.4631000
							273	19783.92	274.4924500
106	Rf	258	18940.73	259.1315100					
		259	19007.45	260.1465200	111	Xb	272	19655.96	273.5347700
		260	1909.019	260.1144354					
		261	19154.47	262.1619900					
		262	19232.59	263.1647700					
		263	19296.2	264.1831300					
		264	19371.23	265.1892400					
		265	19431.99	266.2106600					
		266	19504.68	267.2192800					

Appendix C

Fission Product Chains

Thermal neutron fission product chains for selected mass numbers 85 through 149 showing cumulative fission product yields for U-235 and (Pu-239), half-lives, and branching ratios. (Fission Product Yields: England, T.R., and Rider, B.F., Evaluation and Compilation of Fission Product Yields, LA-UR-94-3106, ENDF-349, Los Alamos National Laboratory, October, 1994)

Physics for Radiation Protection, Third Edition. James E. Martin

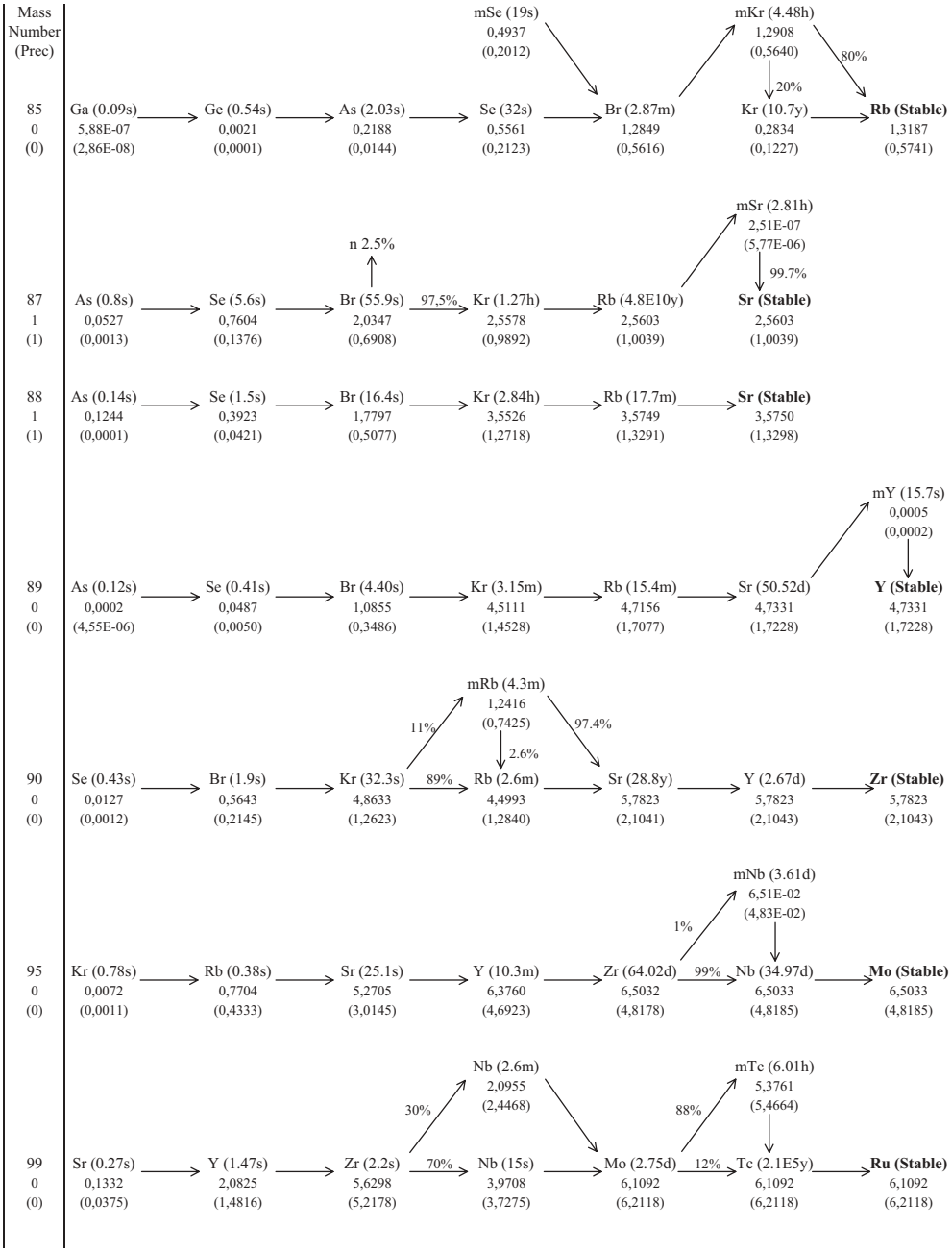
Mass Number (Prec)
85 0 (0)
Ga (0.09s) 5,88E-07 (2,86E-08)
Ge (0.54s) 0,0021 (0,0001)
As (2.03s) 0,2188 (0,0144)
Se (32s) 0,5561 (0,2123)
mSe (19s) 0,4937 (0,2012)
Br (2.87m) 1,2849 (0,5616)
mKr (4.48h) 1,2908 (0,5640)
80%
20%
Kr (10.7y) 0,2834 (0,1227)
Rb (Stable) 1,3187 (0,5741)
87 1 (1)
As (0.8s) 0,0527 (0,0013)
Se (5.6s) 0,7604 (0,1376)
Br (55.9s) 2,0347 (0,6908)
n 2.5%
97,5%
Kr (1.27h) 2,5578 (0,9892)
Rb (4.8E10y) 2,5603 (1,0039)
mSr (2.81h) 2,51E-07 (5,77E-06)
99.7%
Sr (Stable) 2,5603 (1,0039)
88 1 (1)
As (0.14s) 0,1244 (0,0001)
Se (1.5s) 0,3923 (0,0421)
Br (16.4s) 1,7797 (0,5077)
Kr (2.84h) 3,5526 (1,2718)
Rb (17.7m) 3,5749 (1,3291)
Sr (Stable) 3,5750 (1,3298)
89 0 (0)
As (0.12s) 0,0002 (4,55E-06)
Se (0.41s) 0,0487 (0,0050)
Br (4.40s) 1,0855 (0,3486)
Kr (3.15m) 4,5111 (1,4528)
Rb (15.4m) 4,7156 (1,7077)
Sr (50.52d) 4,7331 (1,7228)
mY (15.7s) 0,0005 (0,0002)
Y (Stable) 4,7331 (1,7228)
90 0 (0)
Se (0.43s) 0,0127 (0,0012)
Br (1.9s) 0,5643 (0,2145)
Kr (32.3s) 4,8633 (1,2623)
11%
89%
mRb (4.3m) 1,2416 (0,7425)
2.6%
97.4%
Rb (2.6m) 4,4993 (1,2840)
Sr (28.8y) 5,7823 (2,1041)
Y (2.67d) 5,7823 (2,1043)
Zr (Stable) 5,7823 (2,1043)
95 0 (0)
Kr (0.78s) 0,0072 (0,0011)
Rb (0.38s) 0,7704 (0,4333)
Sr (25.1s) 5,2705 (3,0145)
Y (10.3m) 6,3760 (4,6923)
Zr (64.02d) 6,5032 (4,8178)
1%
mNb (3.61d) 6,51E-02 (4,83E-02)
99%
Nb (34.97d) 6,5033 (4,8185)
Mo (Stable) 6,5033 (4,8185)
99 0 (0)
Sr (0.27s) 0,1332 (0,0375)
Y (1.47s) 2,0825 (1,4816)
Zr (2.2s) 5,6298 (5,2178)
30%
70%
Nb (2.6m) 2,0955 (2,4468)
Nb (15s) 3,9708 (3,7275)
Mo (2.75d) 6,1092 (6,2118)
88%
12%
mTc (6.01h) 5,3761 (5,4664)
Tc (2.1E5y) 6,1092 (6,2118)
Ru (Stable) 6,1092 (6,2118)

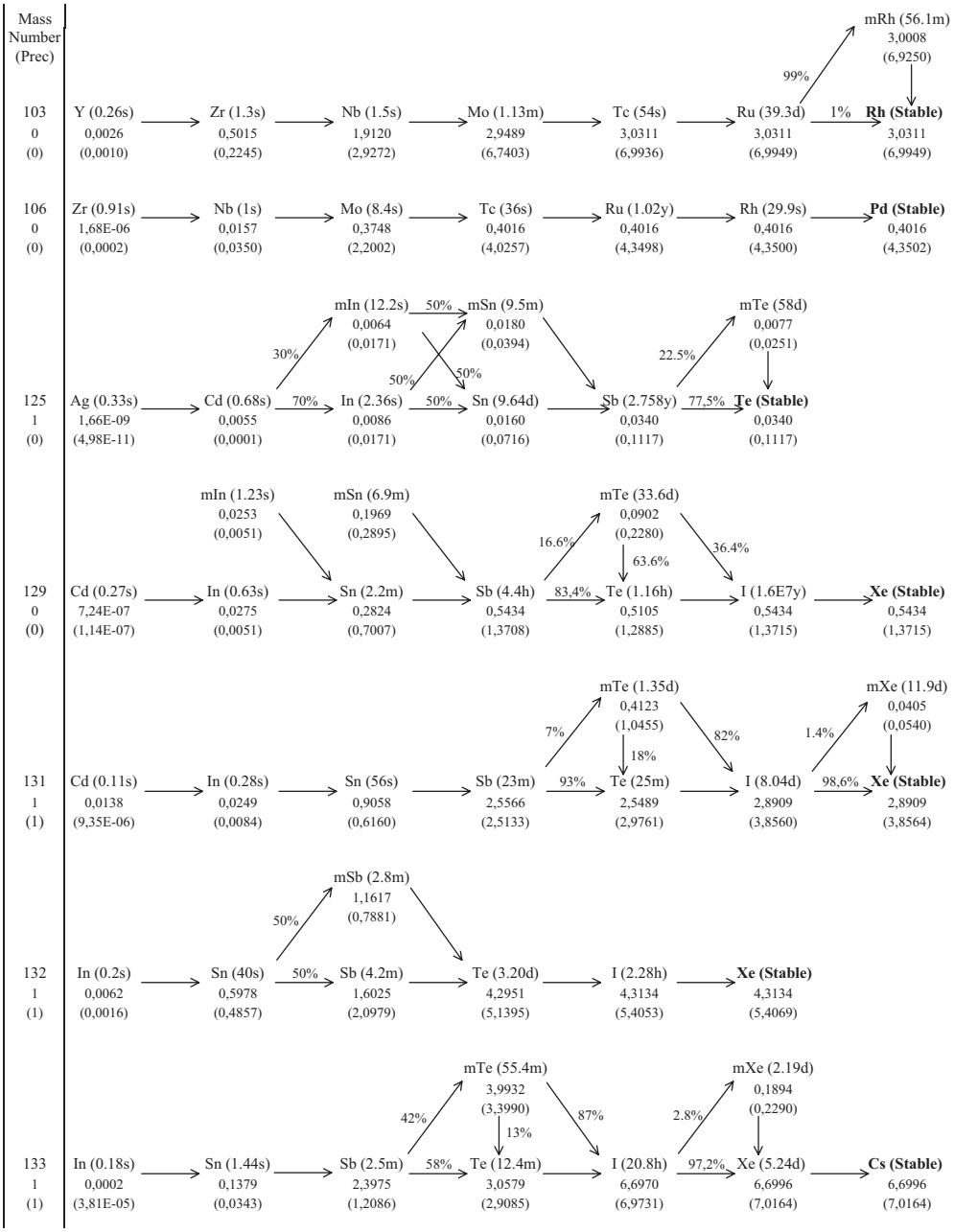
Mass Number (Prec)
103 0 (0)
Y (0.26s) 0,0026 (0,0010)
Zr (1.3s) 0,5015 (0,2245)
Nb (1.5s) 1,9120 (2,9272)
Mo (1.13m) 2,9489 (6,7403)
Tc (54s) 3,0311 (6,9936)
Ru (39.3d) 3,0311 (6,9949)
99%
1%
mRh (56.1m) 3,0008 (6,9250)
Rh (Stable) 3,0311 (6,9949)
106 0 (0)
Zr (0.91s) 1,68E-06 (0,0002)
Nb (1s) 0,0157 (0,0350)
Mo (8.4s) 0,3748 (2,2002)
Tc (36s) 0,4016 (4,0257)
Ru (1.02y) 0,4016 (4,3498)
Rh (29.9s) 0,4016 (4,3500)
Pd (Stable) 0,4016 (4,3502)
125 1 (0)
Ag (0.33s) 1,66E-09 (4,98E-11)
Cd (0.68s) 0,0055 (0,0001)
70%
30%
mIn (12.2s) 0,0064 (0,0171)
In (2.36s) 0,0086 (0,0171)
50%
50%
50%
50%
mSn (9.5m) 0,0180 (0,0394)
Sn (9.64d) 0,0160 (0,0716)
Sb (2.758y) 0,0340 (0,1117)
22.5%
77,5%
mTe (58d) 0,0077 (0,0251)
Te (Stable) 0,0340 (0,1117)
129 0 (0)
Cd (0.27s) 7,24E-07 (1,14E-07)
In (0.63s) 0,0275 (0,0051)
mIn (1.23s) 0,0253 (0,0051)
Sn (2.2m) 0,2824 (0,7007)
mSn (6.9m) 0,1969 (0,2895)
Sb (4.4h) 0,5434 (1,3708)
16.6%
83,4%
mTe (33.6d) 0,0902 (0,2280)
63.6%
Te (1.16h) 0,5105 (1,2885)
36.4%
I (1.6E7y) 0,5434 (1,3715)
Xe (Stable) 0,5434 (1,3715)
131 1 (1)
Cd (0.11s) 0,0138 (9,35E-06)
In (0.28s) 0,0249 (0,0084)
Sn (56s) 0,9058 (0,6160)
Sb (23m) 2,5566 (2,5133)
7%
93%
mTe (1.35d) 0,4123 (1,0455)
18%
Te (25m) 2,5489 (2,9761)
82%
I (8.04d) 2,8909 (3,8560)
1.4%
98,6%
mXe (11.9d) 0,0405 (0,0540)
Xe (Stable) 2,8909 (3,8564)
132 1 (1)
In (0.2s) 0,0062 (0,0016)
Sn (40s) 0,5978 (0,4857)
50%
50%
mSb (2.8m) 1,1617 (0,7881)
Sb (4.2m) 1,6025 (2,0979)
Te (3.20d) 4,2951 (5,1395)
I (2.28h) 4,3134 (5,4053)
Xe (Stable) 4,3134 (5,4069)
133 1 (1)
In (0.18s) 0,0002 (3,81E-05)
Sn (1.44s) 0,1379 (0,0343)
Sb (2.5m) 2,3975 (1,2086)
42%
58%
mTe (55.4m) 3,9932 (3,3990)
13%
Te (12.4m) 3,0579 (2,9085)
87%
I (20.8h) 6,6970 (6,9731)
2.8%
97,2%
mXe (2.19d) 0,1894 (0,2290)
Xe (5.24d) 6,6996 (7,0164)
Cs (Stable) 6,6996 (7,0164)

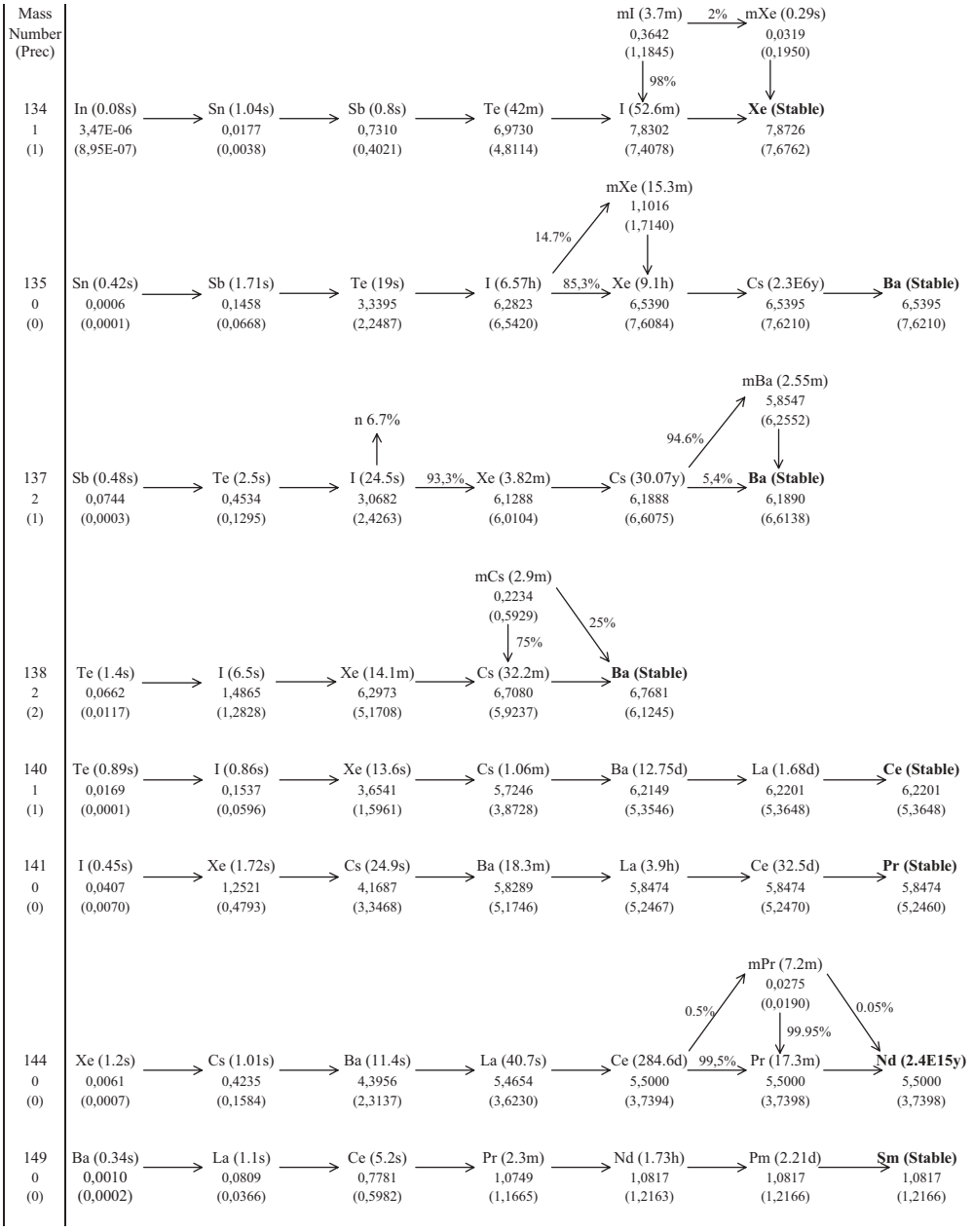
Mass Number (Prec)
mI (3.7m) 0,3642 (1,1845)
2%
mXe (0.29s) 0,0319 (0,1950)
98%
134 1 (1)
In (0.08s) 3,47E-06 (8,95E-07)
Sn (1.04s) 0,0177 (0,0038)
Sb (0.8s) 0,7310 (0,4021)
Te (42m) 6,9730 (4,8114)
I (52.6m) 7,8302 (7,4078)
Xe (Stable) 7,8726 (7,6762)
mXe (15.3m) 1,1016 (1,7140)
14.7%
135 0 (0)
Sn (0.42s) 0,0006 (0,0001)
Sb (1.71s) 0,1458 (0,0668)
Te (19s) 3,3395 (2,2487)
I (6.57h) 6,2823 (6,5420)
85,3%
Xe (9.1h) 6,5390 (7,6084)
Cs (2.3E6y) 6,5395 (7,6210)
Ba (Stable) 6,5395 (7,6210)
mBa (2.55m) 5,8547 (6,2552)
n 6.7%
94.6%
137 2 (1)
Sb (0.48s) 0,0744 (0,0003)
Te (2.5s) 0,4534 (0,1295)
I (24.5s) 3,0682 (2,4263)
93,3%
Xe (3.82m) 6,1288 (6,0104)
Cs (30.07y) 6,1888 (6,6075)
5,4%
Ba (Stable) 6,1890 (6,6138)
mCs (2.9m) 0,2234 (0,5929)
25%
75%
138 2 (2)
Te (1.4s) 0,0662 (0,0117)
I (6.5s) 1,4865 (1,2828)
Xe (14.1m) 6,2973 (5,1708)
Cs (32.2m) 6,7080 (5,9237)
Ba (Stable) 6,7681 (6,1245)
140 1 (1)
Te (0.89s) 0,0169 (0,0001)
I (0.86s) 0,1537 (0,0596)
Xe (13.6s) 3,6541 (1,5961)
Cs (1.06m) 5,7246 (3,8728)
Ba (12.75d) 6,2149 (5,3546)
La (1.68d) 6,2201 (5,3648)
Ce (Stable) 6,2201 (5,3648)
141 0 (0)
I (0.45s) 0,0407 (0,0070)
Xe (1.72s) 1,2521 (0,4793)
Cs (24.9s) 4,1687 (3,3468)
Ba (18.3m) 5,8289 (5,1746)
La (3.9h) 5,8474 (5,2467)
Ce (32.5d) 5,8474 (5,2470)
Pr (Stable) 5,8474 (5,2460)
mPr (7.2m) 0,0275 (0,0190)
0.5%
0.05%
99.95%
144 0 (0)
Xe (1.2s) 0,0061 (0,0007)
Cs (1.01s) 0,4235 (0,1584)
Ba (11.4s) 4,3956 (2,3137)
La (40.7s) 5,4654 (3,6230)
Ce (284.6d) 5,5000 (3,7394)
99,5%
Pr (17.3m) 5,5000 (3,7398)
Nd (2.4E15y) 5,5000 (3,7398)
149 0 (0)
Ba (0.34s) 0,0010 (0,0002)
La (1.1s) 0,0809 (0,0366)
Ce (5.2s) 0,7781 (0,5982)
Pr (2.3m) 1,0749 (1,1665)
Nd (1.73h) 1,0817 (1,2163)
Pm (2.21d) 1,0817 (1,2166)
Sm (Stable) 1,0817 (1,2166)

Appendix D

Radioactive Transformation Data

Radioactive transformation diagrams (decay schemes) herein were compiled from resources at the National Nuclear Data Center (NNDC) and were current as of March 2003 (the date listed on the decay scheme is usually different because it is the last date the experimental data for the radionuclide were evaluated). For those circumstances where the most recent authoritative data are desirable, it is prudent to access the NNDC database at www.nndc.bnl.gov, a website maintained by Brookhaven National Laboratory for the US Department of Energy.

Each decay-scheme drawing shows: the radionuclide, its mass number and atomic number in conventional notation, and the half-life in parentheses to the right (e.g., $^{14}_{6}$C (5700 y)); the predominant transformation mode(s) and the energy change associated with each; the energy of the emitted particle or radiation; the percentage of transformations of the parent, unless noted otherwise, that produce the emission; and the product nuclide and whether it is stable or radioactive (if a half-life is shown). Since radioactive transformation produces an energy change, the various energy levels associated with each transformation are shown including those for particle emissions and subsequent emissions of gamma rays and/or conversion electrons (ce) above the ground state of the product nuclide.

As helpful at it is to have a pictorial decay scheme, it is difficult to obtain complete information on the emissions from a given radionuclide; therefore, listings of the average energy of each significant particle emission and/or radiation are provided along with the yield (%) of each. Since many of the decay schemes and associated data listings can be quite complex, these have been simplified for radiation protection purposes by eliminating radiations that contribute less than 1% (and in some noted cases, 2%) of the energy emitted per transformation of the parent unless they are necessary to understand the mode(s) of transformation. The primary particle emissions are β^-, β^+, and $\alpha_i + \alpha_i$ recoils, which designate negatron, positron, and alpha particle emissions, respectively. The average energy associated with each emission is listed in increasing order (the listing only shows average β^- and β^+ energies; their maxima are shown in the decay scheme). Radiations are listed by the same designators used by NNDC: e.g., characteristic x-rays are

Physics for Radiation Protection, Third Edition. James E. Martin

designated as $K_{\alpha 1}$, $K_{\alpha 2}$, $K_{\beta 1}$, $K_{\beta 2}$, L_{α}, L_{β}, etc.; conversion electrons as ce-K γ_i, ce-L γ_i, etc. to designate the specific electron shell that is vacated and the particular gamma ray involved. Gamma ray emissions are listed as γ_i by increasing energy and $\gamma\pm$ denotes annihilation photons of 0.511 MeV. Auger electrons are listed as Auger-K, Auger-L, etc. to designate the shell vacancy that gives rise to the Auger electron.

The mode of production of each radionuclide is shown at the upper left of the table of radiations, and the date (at the upper right) the data were last reviewed by the NNDC. For example, for ^{32}P there are three primary modes of production: an (n,γ) reaction with ^{31}P; irradiation of stable ^{34}S with deuterons to produce ^{32}P by a (d,α) reaction; and an (n,p) reaction with stable ^{32}S. The data were last reviewed by the National Nuclear Data Center in March 2001 (as shown at the far right). The listing shows one beta particle, emitted with a yield, Y_i, of 100% with an average energy per transformation of 0.6949 MeV; the maximum beta energy is listed in the decay scheme as 1.7106 MeV.

Decay schemes are shown in this appendix roughly by increasing mass number, or in the text on the page number listed; the following radionuclides are included:

^{3}H	^{68}Ge–Ga	^{134m}Cs–^{134}Cs
^{7}Be	^{85}Sr	^{137}Cs
^{14}C	^{85}Kr	^{141}Ce
^{18}F	^{87}Kr (p 51)	^{133}Ba
^{22}Na	^{86}Rb	^{140}Ba
^{24}Na	^{76}As	^{140}La
^{32}P	^{75}Se	^{144}Ce
^{33}P	^{82}Br	^{144}Pr
^{35}S	^{87}Br (p 51)	^{148}Gd
^{36}Cl	^{95}Zr–^{95m}Nb–^{95}Nb	^{154}Eu
^{38}Cl	^{90}Sr–^{90}Y	^{192}Ir
^{41}Ar	^{88}Y	^{195}Au
^{40}K	^{99}Mo	^{198}Au
^{45}Ca	^{99m}Tc	^{197}Hg
^{46}Sc	^{99}Tc	^{203}Hg
^{51}Cr (p 55)	^{103}Ru–Rh	^{201}Tl
^{54}Mn	^{106}Ru–Rh	^{204}Tl
^{55}Fe (p 34)	^{110m}Ag–^{110}Ag	^{226}Ra (p 38)
^{59}Fe	^{124}Sb	^{228}Ra
^{57}Co	^{125}Sb	^{222}Rn
^{58}Co	^{123}I	^{230}Th
^{60}Co	^{125}I	^{238}Pu
^{59}Ni	^{129}I	^{239}Pu
^{63}Ni	^{131}I	^{240}Pu (p 41)
^{65}Ni	^{133m}Xe–^{133}Xe	^{241}Am
^{64}Cu (p 50)	^{113}Sn (p 48)	^{252}Cf (p 52)
^{65}Zn	^{113m}In (p 48)	

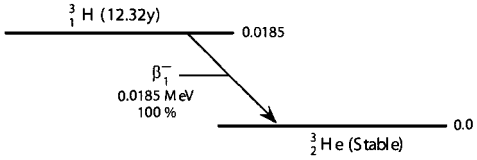

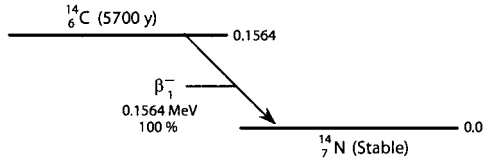

^{6}Li(n,α); Natural [^{14}N(n,t); ^{16}O(n,t)] July, 2000

Radiation	Y_i (%)	E_i (MeV)
β^-1	100.0	0.0057*

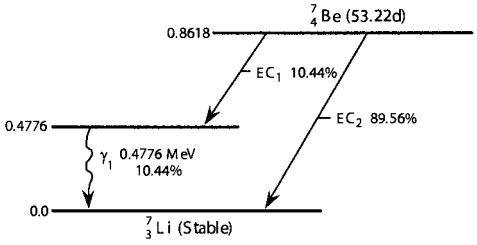

^{6}Li(d,n); ^{10}B(p,α); ^{12}C(^{3}He,2α); Natural May, 2001

Radiation	Y_i (%)	E_i (MeV)
γ_1	10.44	0.4776
ce-K, γ_1	8.04E-06	0.4776
ce-L1, γ_1	1.18E-07	0.4776[a]
Kα1 X-ray	0.0163	0.0001

^{14}N(n,p); Natural [^{14}N(n,p)] October, 2001

Radiation	Y_i (%)	E_i (MeV)
β^-1	100.0	0.0495*

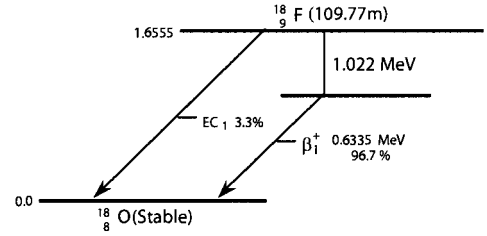

^{18}O(p,n);^{16}O(t,n); ^{16}O(^{3}He,p); ^{19}F(n,2n); ^{19}F(d,t); Ne(d,α) November, 1996

Radiation	Y_i (%)	E_i (MeV)
β^+1	96.73	0.2498*
$\gamma\pm$	193.46	0.5110
K X-ray	0.018	0.0005*
Auger-K	3.07	0.0005*

* Average Energy
[a] Maximum Energy for Subshell

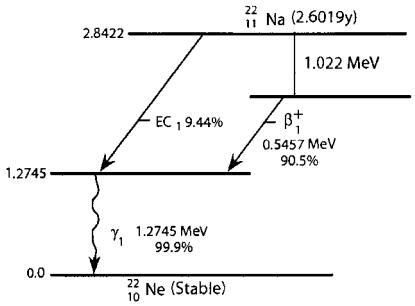

$^{19}F(\alpha,n)$; $^{24}Mg(d,\alpha)$ April, 2000

Radiation	Yi (%)	Ei (MeV)
β^+1	90.5	0.2155*
$\gamma\pm$	181	0.5110
γ_1	99.9	1.2745
K X-ray	0.125	0.0008*
Auger-K	9.18	0.0008*

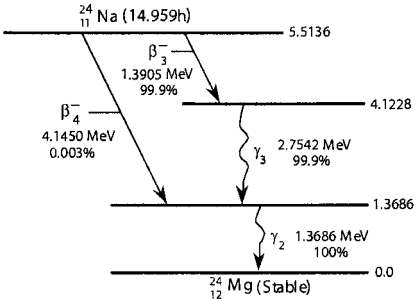

$^{23}Na(n,\gamma)$ April, 2000

Radiation	Yi (%)	Ei (MeV)
β^-3	99.9	0.5541*
β^-4	0.0030	1.8650*
$\gamma2$	100.0	1.3686
$\gamma3$	99.9	2.7542

* Average Energy

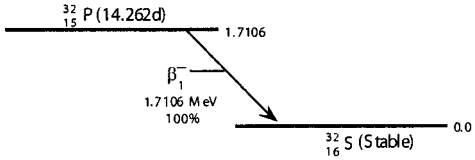

$^{31}P(n,\gamma)$; $^{34}S(d,\alpha)$; $^{32}S(n,p)$ March, 2001

Radiation	Yi (%)	Ei (MeV)
β^-1	100.0	0.6949*

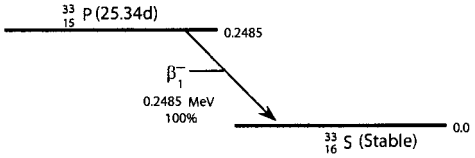

$^{33}S(n,p)$; $^{37}Cl(\gamma,\alpha)$ March, 2001

Radiation	Yi (%)	Ei (MeV)
β^-1	100.0	0.0764*

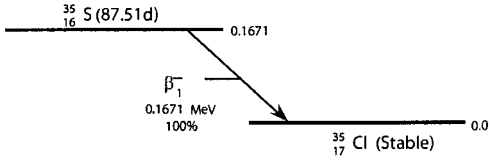

$^{34}S(n,\gamma)$; $^{37}Cl(d,\alpha)$ March, 2001

Radiation	Yi (%)	Ei (MeV)
β^-1	100.0	0.0486*

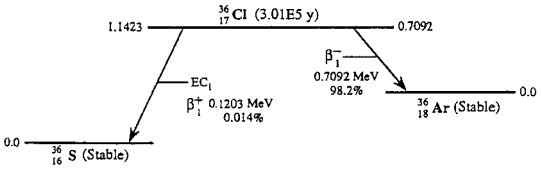

^{35}Cl(n,γ) (June 24, 1993)

Radiation	Y_i (%)	E_i (MeV)
β_1^+	0.014	0.0502[a]
$\gamma^{\pm}$	0.028	0.5110
β_1^-	98.2	0.2512[a]
K x ray	0.130	0.0023[a]
Auger-K	1.57	0.0021[a]

[a]Average energy.

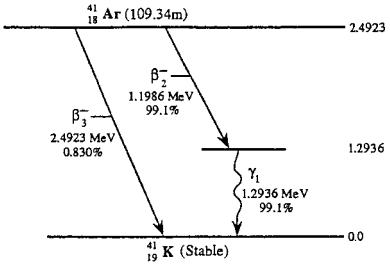

^{40}Ar(n,γ) (Oct. 6, 1994)

Radiation	Y_i (%)	E_i (MeV)
β_2^-	99.1	0.4595[a]
β_3^-	0.83	1.0770[a]
γ_1	99.1	1.2940

[a]Average energy.

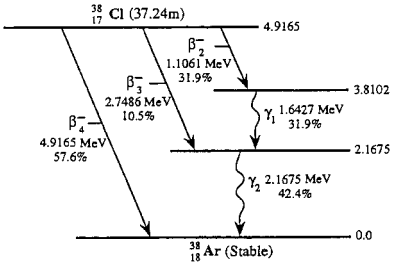

^{37}Cl(n,γ) (June 24, 1993)

Radiation	Y_i (%)	E_i (MeV)
β_2^-	31.9	0.4200[a]
β_3^-	10.5	1.1810[a]
β_4^-	57.6	2.2440[a]
γ_1	31.9	1.6427
γ_2	42.4	2.1675

[a]Average energy.

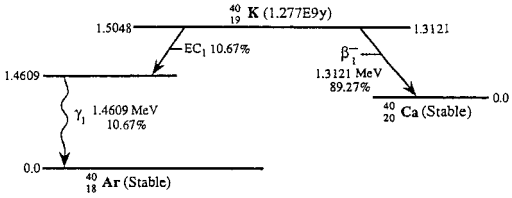

Natural (June 24, 1993)

Radiation	Y_i (%)	E_i (MeV)
γ_1	10.67	1.4609
β_1^-	89.27	0.5606[a]
K x ray	0.938	0.0030[a]
Auger-K	7.22	0.0027[a]

[a]Average energy.

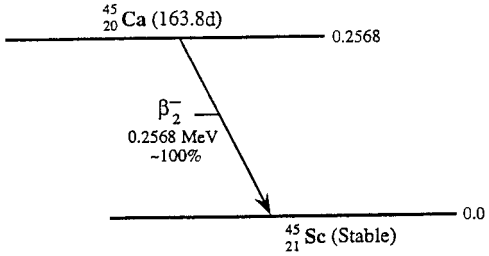

^{44}Ca(n,γ) (June 22, 1995)

Radiation	Y_i (%)	E_i (MeV)
β_2^-	100.0	0.0772[a]
Auger-K	0.0012	0.0036[a]

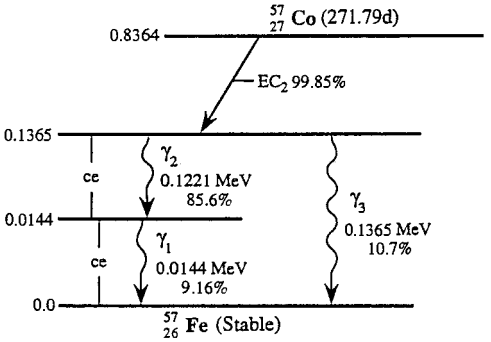

^{58}Ni(γ,p); ^{56}Fe(d,n); ^{56}Fe(p,γ); ^{55}Mn(α,2n) (Dec. 3, 1998)

Radiation	Y_i (%)	E_i (MeV)
γ_1	9.16	0.0144
ce-K, γ_1	71.1	0.0073
ce-L, γ_1	7.36	0.0136[a]
γ_2	85.6	0.1221
ce-K, γ_2	1.83	0.1149
ce-L, γ_2	0.192	0.1212[a]
ce-M$^+$, γ_2	0.0317	0.1220[a]
γ_3	10.7	0.1365
ce-K, γ_3	1.3	0.1294
$K_{\alpha 1}$ x ray	33.7	0.0064
$K_{\alpha 2}$ x ray	17.2	0.0064
K_β x ray	6.97	0.0071[b]
L x ray	1.52	0.0007[b]
Auger-K	105.0	0.0056[b]

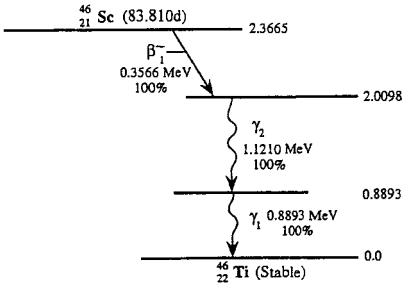

^{45}Sc(n,γ) (Apr. 28, 1993)

Radiation	Y_i (%)	E_i (MeV)
β_1^-	100.0	0.1118[a]
γ_1	100.0	0.8893
γ_2	100.0	1.1210

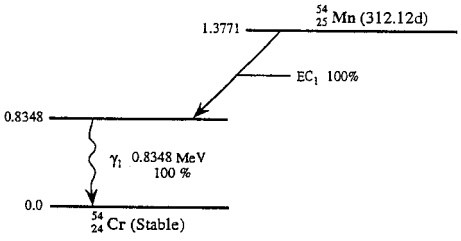

^{56}Fe(d,α); ^{51}V(α,n); ^{53}Cr(d,n); ^{54}Cr(p,n) (Nov. 9, 1995)

Radiation	Y_i (%)	E_i (MeV)
γ_1	100.0	0.8348
ce-K, γ_1	0.022	0.8289
$K_{\alpha 1}$ x ray	14.7	0.0054
$K_{\alpha 2}$ x ray	7.43	0.0054
K_β x ray	2.95	0.0060[a]
L x ray	0.37	0.0006[a]
Auger-K	63.9	0.0048[a]

[a]Average energy.

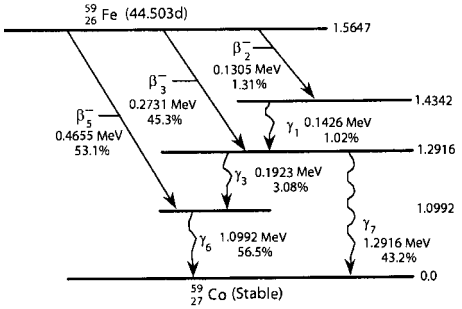

^{58}Fe(n,γ) November, 1993

Radiation	Yi (%)	Ei (MeV)
β-2	1.31	0.0356*
β-3	45.3	0.0808*
β-5	53.1	0.1491*
γ1	1.02	0.1426
γ3	3.08	0.1923
γ6	56.5	1.0992
γ7	43.2	1.2920

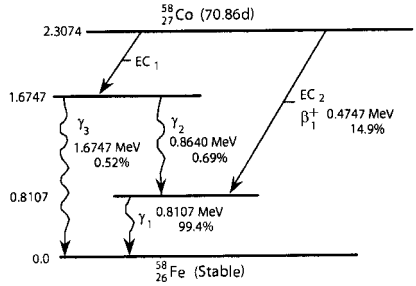

^{55}Mn(α,n); ^{58}Ni(n,p) September, 2000

Radiation	Yi (%)	Ei (MeV)
β+1	14.9	0.2011*
γ±	29.8	0.5110
γ1	99.4	0.8107
γ2	0.69	0.8640
γ3	0.52	1.6750
Kα1, X-ray	15.7	0.0064
Kα2, X-ray	8.0	0.0064
K, X-ray	3.24	0.0071*
Auger-K	48.8	0.0056*

* Average Energy

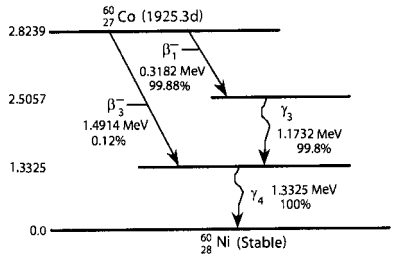

^{59}Co(n,γ) September, 2000

Radiation	Yi (%)	Ei (MeV)
β−1	99.88	0.0958*
β−3	0.12	0.6259*
γ3	99.8	1.1732
γ4	100.0	25

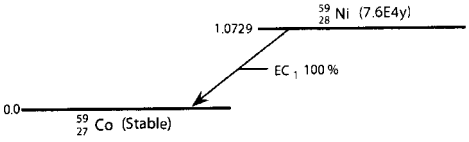

^{58}Ni(n,γ); ^{59}Co(d,2n) November, 1993

Radiation	Yi (%)	Ei (MeV)
Kα1 X-ray	20.0	0.0069
Kα2 X-ray	10.3	0.0069
Kβ, X-ray	4.16	0.0077*
L X-ray	0.975	0.0008*
Auger-K	54.3	0.0061*

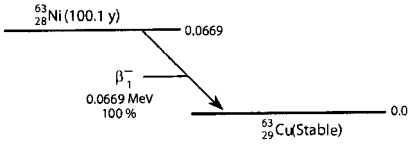

^{62}Ni (n,γ) December. 1991

Radiation	Yi (%)	Ei (MeV)
β−1	100.0	0.0174*

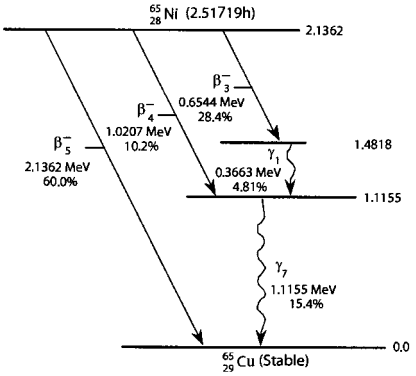

^{64}Ni(n,γ) August, 1993

Radiation	Yi (%)	Ei (MeV)
β−3	28.4	0.2205*
β−4	10.2	0.3717*
β−5	60.0	0.8754*
γ1	4.81	0.3663
γ7	15.4	1.1155
γ8	23.6	1.4818

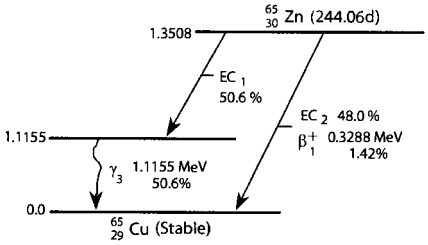

^{64}Zn(n,γ) September, 2000

Radiation	Yi (%)	Ei (MeV)
β+1	1.42	0.1430*
γ±	2.84	0.5110
γ3	50.6	1.1160
Kα1 X-ray	22.9	0.0080
Kα2 X-ray	11.8	0.0080
Kβ X-ray	4.83	0.0089*
L X-ray	1.24	0.0009*
Auger-K	47.5	0.0070*

* Average Energy
[a] Maximum Energy for Subshell

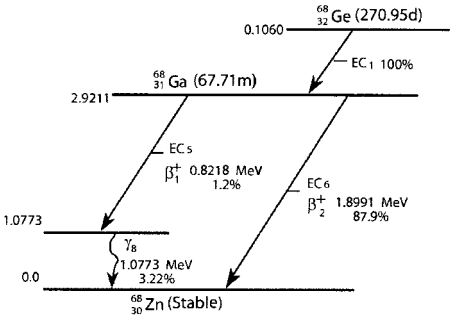

^{68}Ge: ^{66}Zn(α,2n) ^{68}Ga: Daughter of ^{68}Ge; August, 2000
^{68}Ga: From ^{68}Ge; ^{65}Cu(α,n); ^{68}Zn(p,n); ^{67}Zn(d,n)

Radiation	Yi (%)	Ei (MeV)
^{68}Ge		
Kα1 X-ray	25.8	0.0093
Kα2 X-ray	13.3	0.0092
Kβ X-ray	5.68	0.0103*
L X-ray	1.52	0.0011*
Auger-K	41.7	0.0080*
^{68}Ga		
β+1	1.2	0.3526*
β+2	87.9	0.8360*
γ±	178	0.5110
γ8	3.22	1.0770

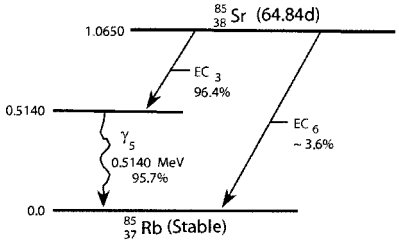

^{84}Sr (n,γ); ^{85}Rb (p,n); ^{85}Rb (d,2n) April, 1991

Radiation	Yi (%)	Ei (MeV)
γ5	95.70	0.5140
ce-K, γ5	0.603	0.4988
ce-L, γ5	0.068	0.5119[a]
Kα1 X-ray	33.1	0.0134
Kα2 X-ray	17.2	0.0133
Kβ X-ray	8.98	0.0150*
L X-ray	2.59	0.0017*
Auger-K	28.6	0.0114*

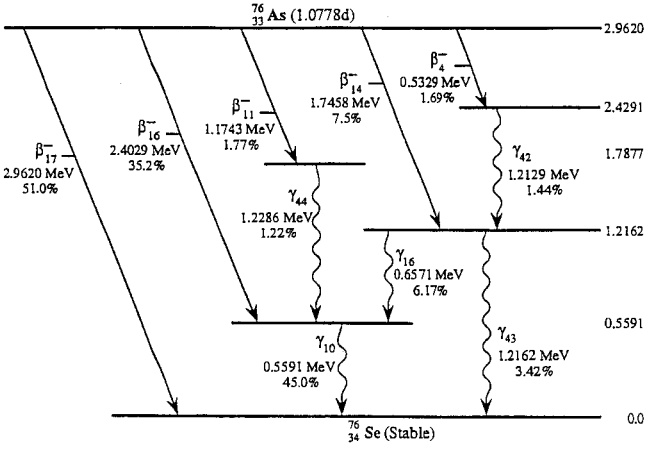

^{75}As(n,γ) (Mar. 15, 1995)

Radiation	Y_i (%)	E_i (MeV)
β^-_4	1.69	0.1736[a]
β^-_{11}	1.77	0.4363[a]
β^-_{14}	7.50	0.6915[a]
β^-_{16}	35.2	0.9963[a]
β^-_{17}	51.0	1.2670[a]
γ_{10}	45.0	0.5591
γ_{11}	1.20	0.5632
γ_{16}	6.17	0.6571
γ_{42}	1.44	1.2129
γ_{43}	3.42	1.2162
γ_{44}	1.22	1.2286

[a]Average energy.

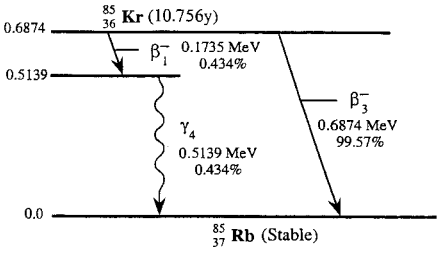

FP; ^{84}Kr (n,γ) ^{85m}Kr; ^{84}Kr (n,γ) ^{85}Kr April, 1991

Radiation	Y_i (%)	E_i (MeV)
^{85}Kr (β⁻)		
β^-_1	0.434	0.0477*
β^-_3	99.57	0.2516*
γ_4	0.434	0.5139

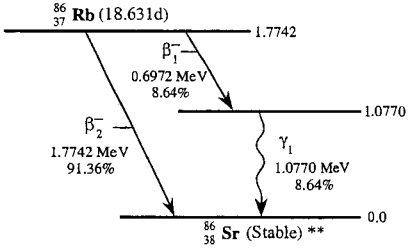

^{85}Rb(n,γ); FP December, 2001

Radiation	Y_i (%)	E_i (MeV)
β^-_1	8.64	0.2325*
β^-_2	91.4	0.7094*
γ_1	8.64	1.0770

*Average Energy
** EC to ^{86}Kr (stable) also occurs <0.01%

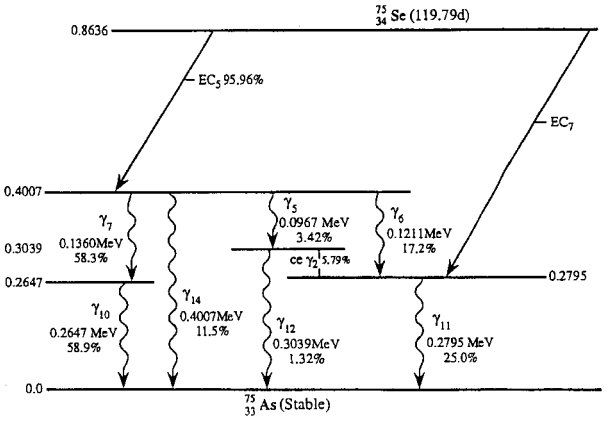

^{74}Se(n,γ); ^{75}As(d,n); ^{75}As(p,n) (Aug. 15, 1996)

Radiation	Y_i (%)	E_i (MeV)
ce-K, γ_2	4.57	0.0125
ce-L, γ_2	1.22	0.0229[a]
γ_3	1.11	0.0661
γ_5	3.42	0.0967
γ_6	17.2	0.1211
γ_7	58.3	0.1360
γ_{10}	58.9	0.2647
γ_{11}	25.0	0.2795
γ_{12}	1.32	0.3039
γ_{14}	11.5	0.4007
$K_{\alpha 1}$ x ray	46.2	0.0105
$K_{\alpha 2}$ x ray	23.8	0.0105
K_β x ray	11.0	0.0117[b]
Auger-K	59.8	0.0091[b]

[a]Maximum energy for subshell.
[b]Average energy.

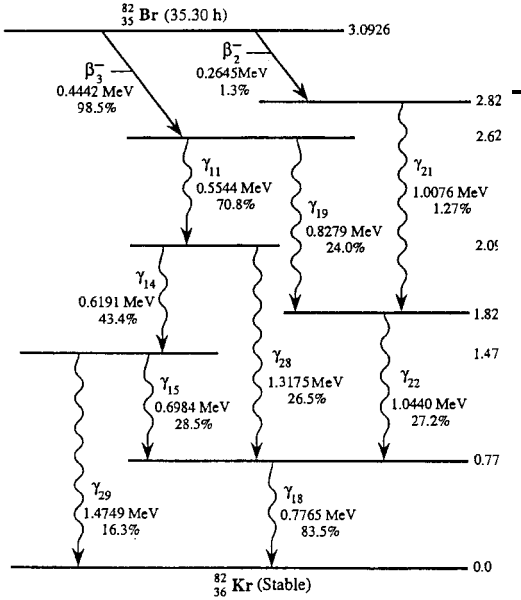

^{81}Br(n,γ); Independent Yield FP Shielded from β^- Decay (Dec. 12, 1995)

Radiation	Y_i (%)	E_i (MeV)
β_2^-	1.3	0.0762[a]
β_3^-	98.5	0.1377[a]
γ_{11}	70.8	0.5544
γ_{14}	43.4	0.6191
γ_{15}	28.5	0.6984
γ_{18}	83.5	0.7765
ce-K, γ_{18}	0.0685	0.7622
γ_{19}	24.0	0.8279
γ_{21}	1.27	1.0076
γ_{22}	27.2	1.0440
γ_{28}	26.5	1.3175
γ_{29}	16.3	1.4749

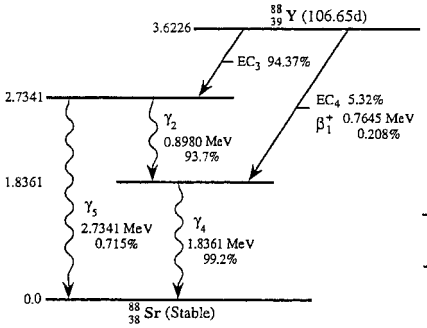

^{88}Sr(p,n); ^{88}Sr(d,2n) (Aug. 25, 1988)

Radiation	Y_i (%)	E_i (MeV)
β_1^+	0.208	0.3595[a]
$\gamma^{\pm}$	0.416	0.5110
γ_2	93.7	0.8980
ce-K, γ_2	0.0253	0.8819
γ_4	99.2	1.8361
ce-K, γ_4	0.0129	1.8200
γ_5	0.715	2.7341
$K_{\alpha 1}$ x ray	33.7	0.0142
$K_{\alpha 2}$ x ray	17.5	0.0141
K_β x ray	9.40	0.0158[a]
L x ray	2.79	0.0018[a]
Auger-K	26.4	0.0121[a]

[a]Average energy.

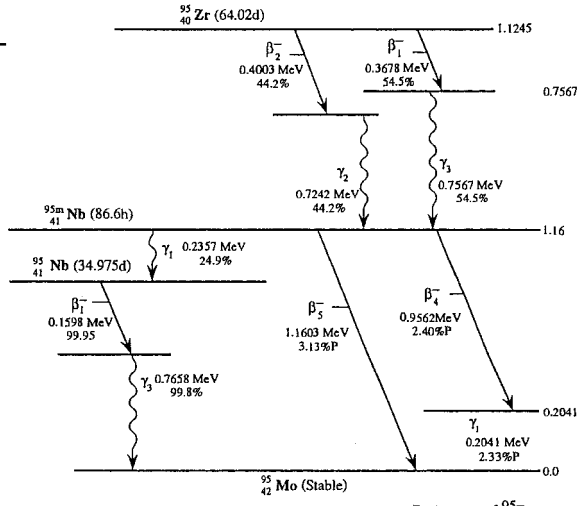

P = Percent of ^{95}Zr parent

FP (Apr. 5, 1994)

Radiation	Y_i (%)	E_i (MeV)
^{95}Zr		
β_1^-	54.5	0.1097[a]
β_2^-	44.2	0.1209[a]
β_3^-	1.13	0.3276[a]
γ_2	44.2	0.7242
γ_3	54.5	0.7567
^{95m}Nb-IT		
γ_1	24.9	0.2357
^{95m}Nb(β^-)		
β_4^-	2.4	0.3346[a]
β_5^-	3.13	0.4374[a]
γ_1	2.33	0.2041
$K_{\alpha 1}$ x ray	23.1	0.0165
$K_{\alpha 2}$ x ray	12.1	0.0165
K_β x ray	6.87	0.0186[a]
L x ray	2.42	0.0022[a]
Auger-K	13.9	0.0140[a]
^{95}Nb		
β_1^-	99.95	0.0434[a]
γ_3	99.8	0.7658

[a]Average energy.

^{98}Mo(n,γ); FP July, 2001

Radiation	Y_i (%)	E_i (MeV)
^{99}Mo		
β−6	16.4	0.1331*
β−9	1.14	0.2897*
β−10	82.4	0.4428*
γ2	1.05	0.0405
ce-K, γ2	3.44	0.0195
γ4	4.52	0.1405
γ8	5.99	0.1810
γ11	1.19	0.3664
γ28	12.1	0.7395
γ30	4.26	0.7779
Kα1 X-ray	2.00	0.0184 a
Kα2 X-ray	1.04	0.0183 a
^{99m}Tc		
ce-M, γ1	74.6	0.0016*
γ2	89.1	0.1405
ce-K, γ2	8.84	0.1195
ce-L, γ2	1.07	0.1375*
ce-M, γ2	0.194	0.1400*
Kα1 X-ray	4.01	0.0184
Kα2 X-ray	2.1	0.0183
Auger-K	2.04	0.0155 a
^{99}Tc		
β−1	0.0016	0.0817 *

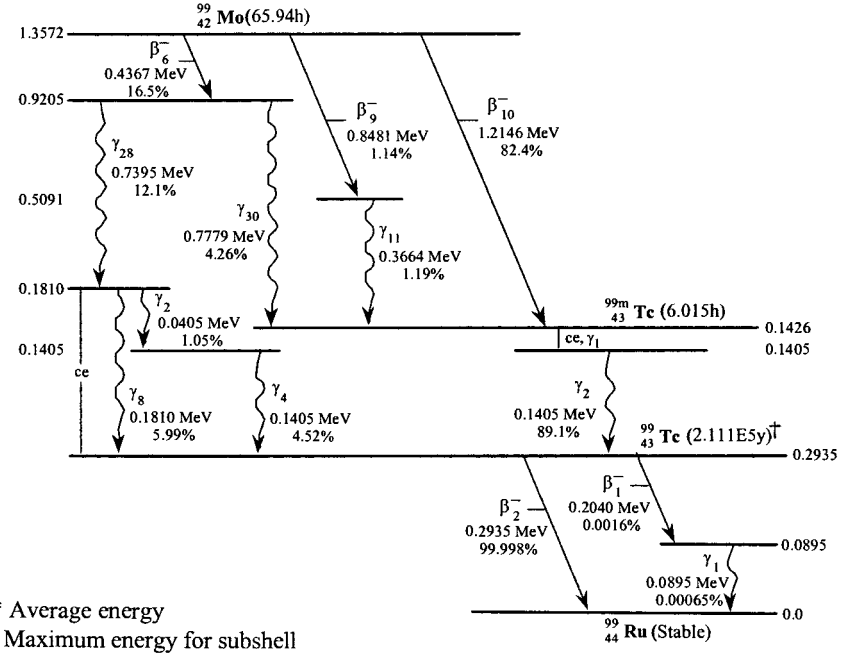

* Average energy

[a] Maximum energy for subshell

† NOTE: 87.907% of transitions of ^{99}Mo produce the 0.1427 and in turn the 0.1405 level of ^{99m}Tc. Metastable ^{99m}Tc is relieved in 89.1% of its transitions by a 0.1405 MeV gamma ray; therefore, the 0.1405 MeV γ is produced in 78.32% of the transformations of ^{99}Mo. However, if the ^{99}Mo parent and the ^{99m}Tc product are together and in equilibrium, the 0.1405 MeV gamma is produced in 82.84 % of transformations of ^{99}Mo (this accounts for the 4.52% contribution through β^-_6 and γ_4).

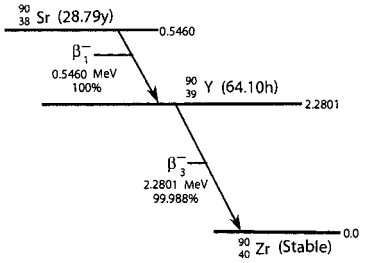

FP; $^{89}Sr(n,\gamma)^{90}Sr$; $^{89}Sr(n,\gamma)^{90}Y$ January, 1998

Radiation	Yi (%)	Ei (MeV)
90Sr		
β−1	100.0	0.1958*
90Y		
β−3	99.988	0.9337*

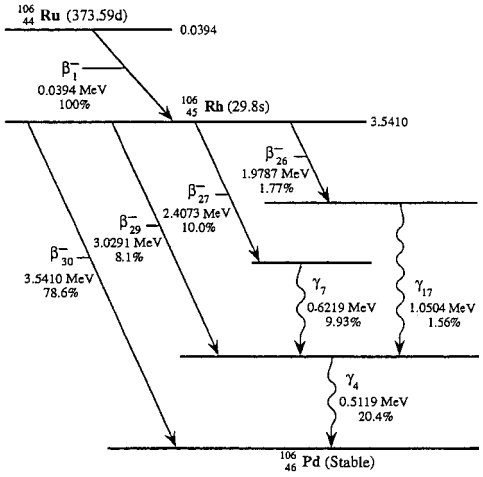

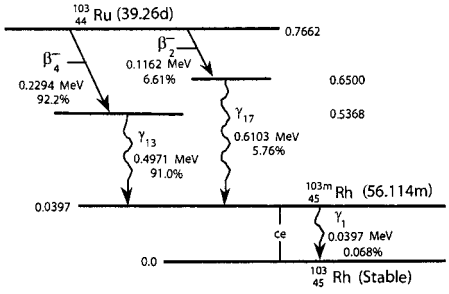

$^{102}Ru(n,\gamma)$; FP August, 2001

Radiation	Yi (%)	Ei (MeV)
β−2	6.61	0.0307*
β−4	92.2	0.0641*
γ1 b	0.068	0.0398
ce-K, γ1	9.89	0.0165
ce-L, γ1	73.3	0.0364[a]
ce-M, γ1	14.5	0.0391[a]
γ14	91.0	0.4971
γ18	5.76	0.6103
Kα1 X-ray	4.88	0.0202
Kα2 X-ray	2.58	0.0201
Auger-K	2.12	0.0170*

FP (Aug. 16, 1994)

Radiation	Y_i (%)	E_i (MeV)
^{106}Ru		
β_1^-	100.0	0.0100[a]
^{106}Rh		
β_{26}^-	1.77	0.7790[a]
β_{27}^-	10.0	0.9760[a]
β_{29}^-	8.1	1.2670[a]
β_{30}^-	78.6	1.5080[a]
γ_4	20.4	0.5119
γ_7	9.93	0.6219
γ_{17}	1.56	1.0504

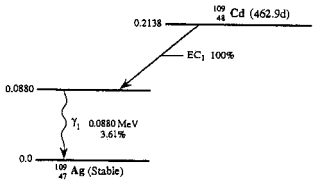

$^{108}Cd(n,\gamma)$; $^{109}Ag(d,2n)$ (Feb. 14, 1994)

Radiation	Y_i (%)	E_i (MeV)
γ_1	3.61	0.0880
ce-K, γ_1	41.7	0.0625
ce-L, γ_1	44.0	0.0842[a]
ce-M, γ_1	8.95	0.0873[a]
ce-N+, γ_1	1.59	0.0879[a]
$K_{\alpha 1}$ x ray	55.2	0.0222
$K_{\alpha 2}$ x ray	29.1	0.0220
K_{β} x ray	17.8	0.0249[b]
L x ray	11.2	0.0030[b]
Auger-K	20.9	0.0185[b]

[a] Maximum energy for subshell.
[b] Average energy.

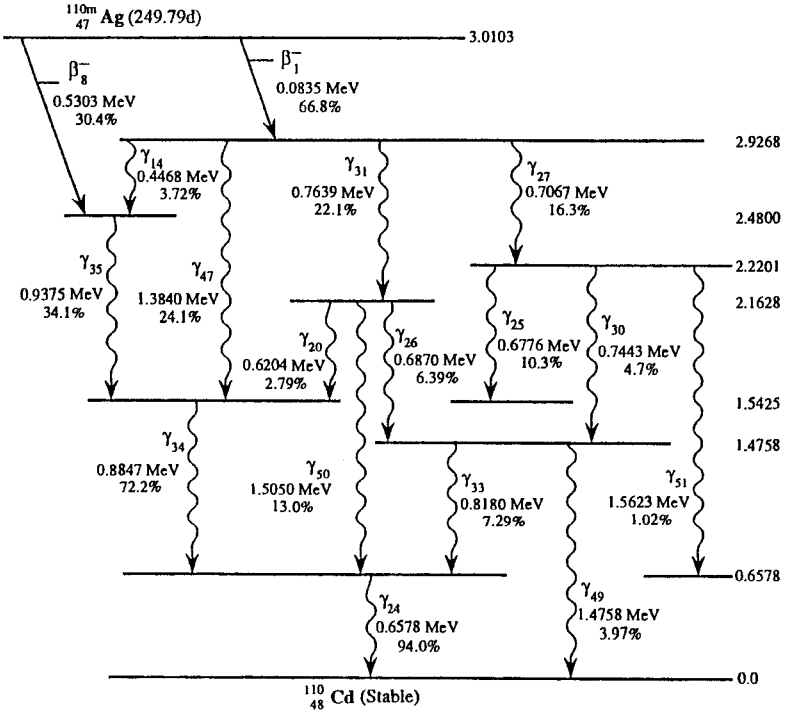

^{109}Ag(n,γ) (Jan. 14, 1993)

Radiation[a]	Y_i (%)	E_i (MeV)
ce-K, γ_2	0.794	0.0910
β_1^-	66.8	0.0218[b]
β_8^-	30.4	0.1655[b]
γ_{14}	3.72	0.4468
γ_{20}	2.79	0.6204
γ_{24}	94.0	0.6578
γ_{25}	10.3	0.6776
γ_{26}	6.39	0.6870
γ_{27}	16.3	0.7067
γ_{30}	4.7	0.7443
γ_{31}	22.1	0.7639
γ_{33}	7.29	0.8180
γ_{34}	72.2	0.8847
γ_{35}	34.1	0.9375
ce-K, γ_{35}	0.0403	0.9108
γ_{47}	24.1	1.3840
γ_{49}	3.97	1.4758
γ_{50}	13.0	1.5050
γ_{51}	1.02	1.5623

[a]Radiations from ^{110m}Ag only; transformations through ^{110}Ag ($T_{1/2}$ = 24.6 s) are negligible.
[b]Average energy.

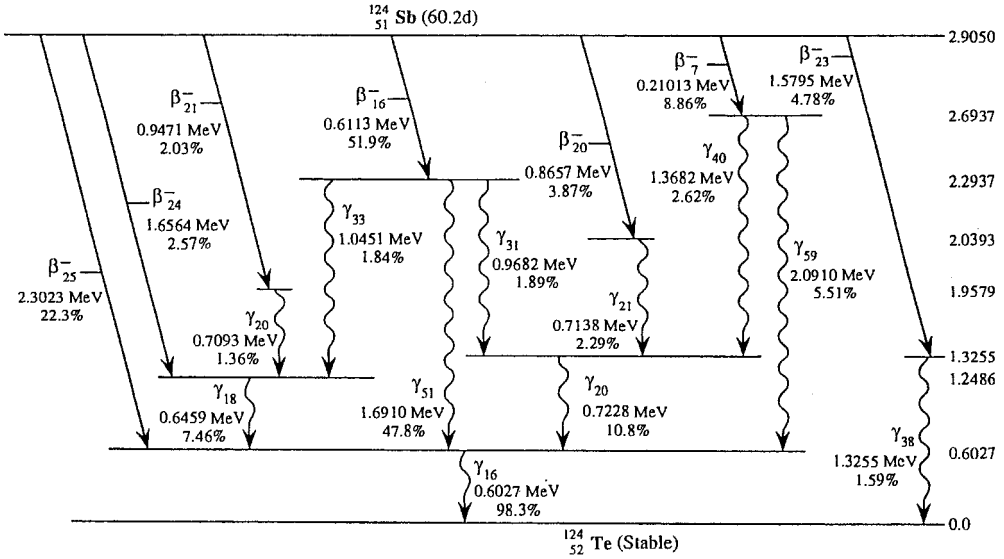

^{123}Sb(n,γ) (May 8, 1997)

Radiation[a]	Y_i (%)	E_i (MeV)
β^-_7	8.86	0.0581[b]
β^-_{16}	51.9	0.1938[b]
β^-_{20}	3.87	0.2918[b]
β^-_{21}	2.03	0.3245[b]
β^-_{23}	4.78	0.5932[b]
β^-_{24}	2.57	0.6271[b]
β^-_{25}	22.3	0.9184[b]
γ_{16}	98.3	0.6027
ce-K, γ_{16}	0.413	0.5709
γ_{18}	7.46	0.6459
γ_{20}	1.36	0.7093
γ_{21}	2.29	0.7138
γ_{22}	10.8	0.7228
γ_{31}	1.89	0.9682
γ_{33}	1.84	1.0450
γ_{38}	1.59	1.3255
γ_{40}	2.62	1.3682
γ_{51}	47.8	1.6910
γ_{59}	5.51	2.0910

[a]Several other βs and γs with yields less than 1%. ^{124}Sb is also formed with metastable ^{124m}Sb, which undergoes isomeric transition 75% of the time with a half-life of 93 s and is dominated by internal conversion; 25% of ^{124m}Sb transforms to ^{124}Te (stable) by β^- emission.
[b]Average energy.

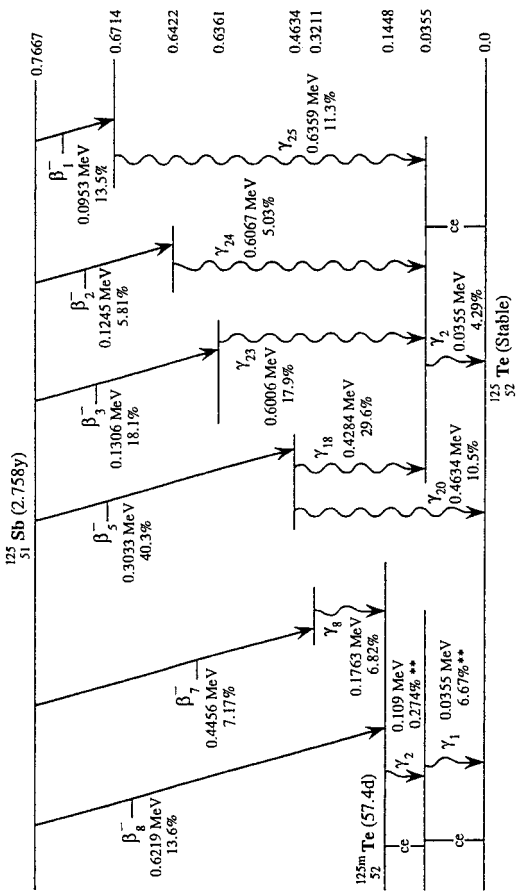

^{124}Sn(n,γ); ^{125}Sn(β^-) (Feb. 10, 1994)

Radiation	Y_i (%)	E_i (MeV)
^{125}Sb		
β_1^-	13.5	0.0249[a]
β_2^-	5.8	0.0330[a]
β_3^-	18.1	0.0348[a]
β_4^-	1.59	0.0675[a]
β_5^-	40.3	0.0870[a]
β_7^-	7.17	0.1345[a]
β_8^-	13.6	0.2155[a]
γ_2	4.29	0.0355
ce-K, γ_2	51.5	0.0037
ce-L, γ_2	6.91	0.0306[b]
ce-M, γ_2	1.38	0.0345[b]
γ_7	6.82	0.1763
γ_{18}	29.6	0.4279
γ_{20}	10.4	0.4634
γ_{23}	17.9	0.6006
γ_{24}	5.03	0.6067
γ_{25}	11.3	0.6359
γ_{27}	1.79	0.6714
$K_{\alpha 1}$ x ray	24.7	0.0275
$K_{\alpha 2}$ x ray	13.3	0.0272
K_β x ray	8.58	0.0310[a]
Auger-K	6.64	0.0227[a]
^{125m}Te		
γ_1	6.67[c]	0.0355
ce-K, γ_1	80.0	0.0037
ce-L, γ_1	10.7	0.0306[b]
ce-M, γ_1	2.15	0.0345[b]
γ_2	0.274[c]	0.1093
ce-K, γ_2	51.8	0.0775
ce-L, γ_2	37.3	0.1043[b]
ce-M, γ_2	8.55	0.1083[b]
ce-N$^+$, γ_2	2.24	0.1091[b]
$K_{\alpha 1}$ x ray	61.3	0.0275
$K_{\alpha 2}$ x ray	32.8	0.0272
K_β x ray	21.3	0.0310[a]
L x ray	15.2	0.0038[a]
Auger-K	16.5	0.0227[a]

[a] Average energy.
[b] Maximum energy for subshell.
[c] Yield from ^{125m}Te only.

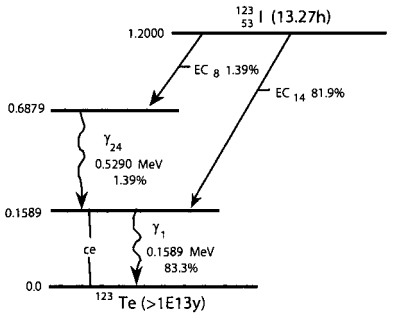

$^{121}Sb(\alpha,n)$ February, 1994

Radiation	Y_i (%)	E_i (MeV)
γ_1	83.3	0.1589
ce-K, γ_1	13.6	0.1272
ce-L, γ_1	1.77	0.1540[a]
γ_{24}	1.39	0.5290
Kα1 X-ray	45.9	0.0275
Kα2 X-ray	24.2	0.0272
Kβ X-ray	16.0	0.0310*
L X-ray	8.98	0.0038*
Auger-K	12.3	0.0227*

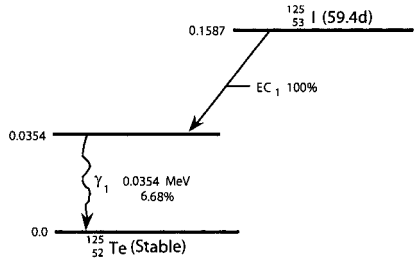

$^{123}Sb(\alpha,2n)$; ^{125}Xe product; $^{125}Te(d,n)$ July, 1999

Radiation	Y_i (%)	E_i (MeV)
γ_1	6.68	0.0354
ce-K, γ_1	80.2	0.0037
ce-L, γ_1	10.8	0.0306[a]
ce-M, γ_1	2.15	0.0345[a]
Kα1 X-ray	74.4	0.0275
Kα2 X-ray	40.0	0.0272
Kβ X-ray	25.9	0.0310*
L X-ray	14.9	0.0038*
Auger-K	20.0	0.0227*

* Average Energy
[a] Maximum Energy for Subshell

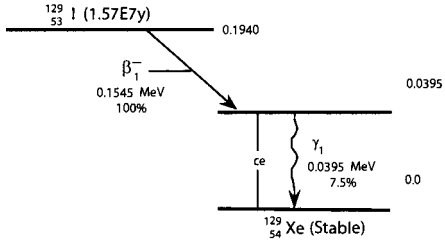

FP; $^{128}Te(n,\gamma)$; $^{129}Te(\beta^-)$ May, 1996

Radiation	Y_i (%)	E_i (MeV)
β^-_1	100.0	0.0409*
γ_1	7.5	0.0395
ce-K, γ_1	78.8	0.0050
ce-L, γ_1	10.7	0.0341
ce-M, γ_1	2.16	0.0384
Kα1 X-ray	36.9	0.0298
Kα2 X-ray	19.9	0.0295
Kβ X-ray	13.2	0.0336
L X-ray	7.98	0.0041
Auger-K	8.79	0.0246
Auger-L	73.9	0.0034

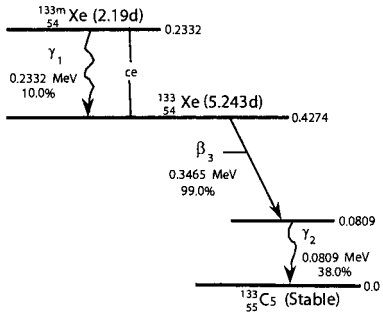

FP; $^{132}Xe(n,\gamma)$ October, 1995

Radiation	Y_i (%)	E_i (MeV)
β^-_3	99.0	0.1005*
γ_2	38.0	0.0809
ce-K, γ_2	55.1	0.0450
ce-L, γ_2	8.21	0.0753[a]
ce-M, γ_2	1.69	0.0798[a]
Kα1 X-ray	26.1	0.0310
Kα2 X-ray	14.1	0.0306
Kβ X-ray	9.47	0.0350*
L X-ray	6.06	0.0043*
Auger-K	5.86	0.0255*

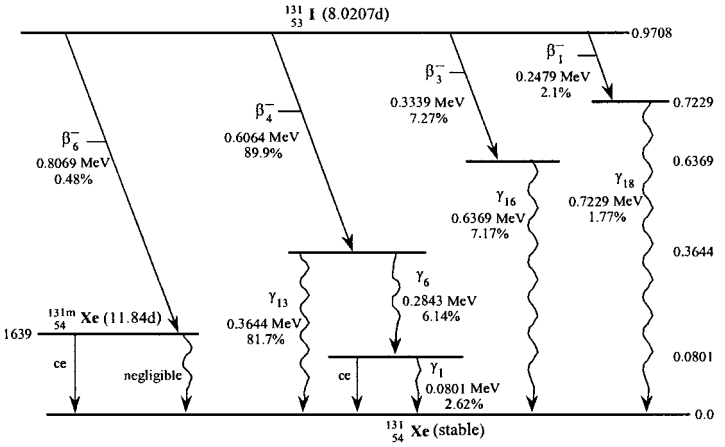

FP December, 1994

Radiation	Yi (%)	Ei (MeV)
β−1	2.10	0.0694*
β−3	7.27	0.0966*
β−4	89.9	0.1916*
β−6	0.48	0.2832*
γ1	2.62	0.0801
ce-K, γ1	3.54	0.0456
γ6	6.14	0.2842
γ13	81.7	0.3644
ce-K, γ13	1.55	0.3299
ce-L, γ13	0.246	0.3590a
γ16	7.17	0.6370
γ18	1.77	0.7229
Kα1 X-ray	2.56	0.0298
Kα2 X-ray	1.38	0.0295

*Average Energy
a Maximum Energy For Subshell
131mXe product, yield 1.18%; 131Xe yield 98.8%

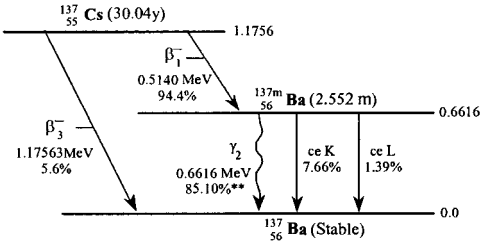

FP August, 1997

Radiation	Yi (%)	Ei (MeV)
β−1	94.40	0.1734*
β−3	5.60	0.4163*
γ2	85.10**	0.6617
ce-K, γ1	7.66	0.6242
ce-L, γ1	1.39	0.6557
Kα1 X-ray	3.61	0.0322
Kα2 X-ray	1.96	0.0318
Kβ X-ray	1.33	0.0364*
L X-ray	0.91	0.0045*
Auger-K	0.76	0.0264*
Auger-L	7.20	0.0367*

* Average Energy
** Photon yield per transformation of 137Cs; photon yield from each transformation of 137mBa is 90.11%

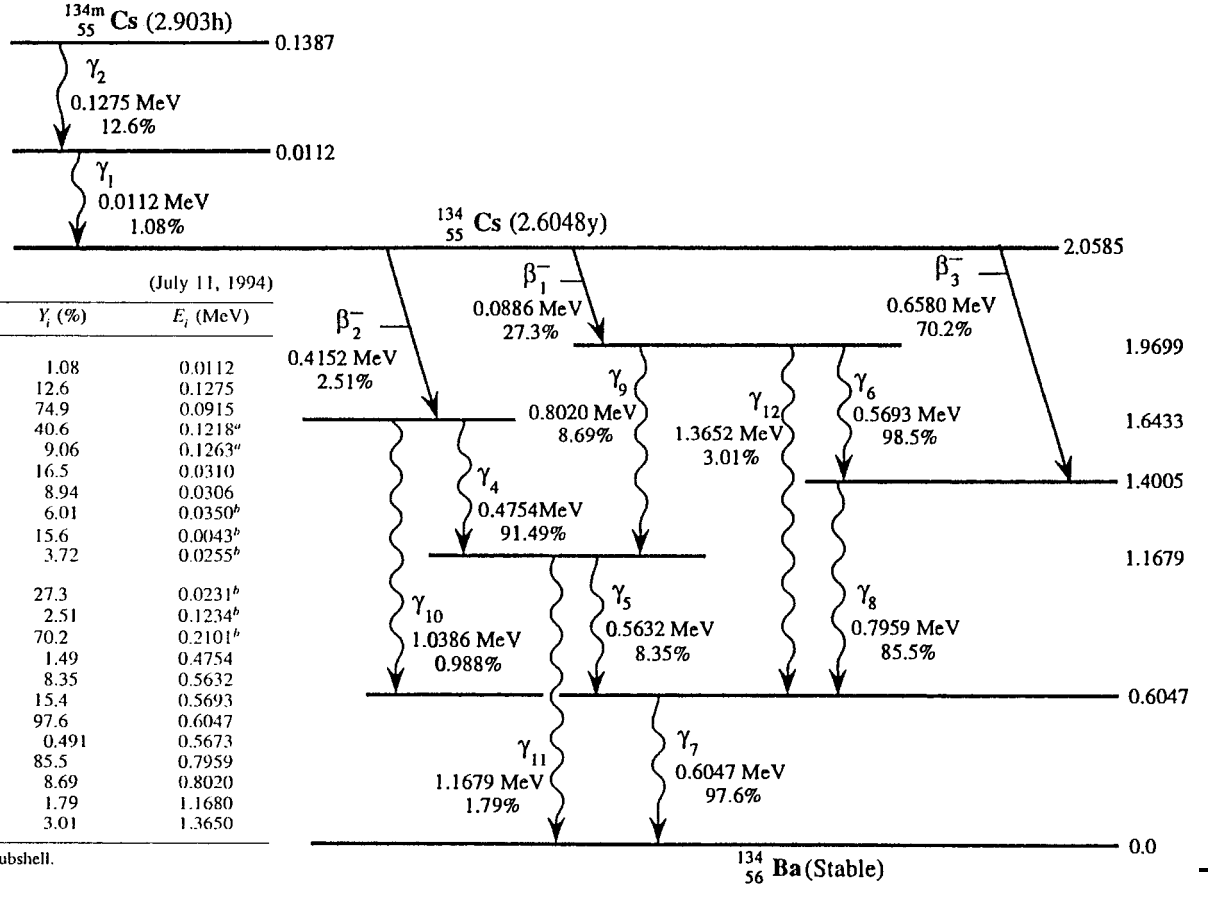

FP; ^{133}Cs(n,γ) (July 11, 1994)

Radiation	Y_i (%)	E_i (MeV)
^{134m}Cs		
γ_1	1.08	0.0112
γ_2	12.6	0.1275
ce-K, γ_2	74.9	0.0915
ce-L, γ_2	40.6	0.1218[a]
ce-M, γ_2	9.06	0.1263[a]
$K_{\alpha 1}$ x ray	16.5	0.0310
$K_{\alpha 2}$ x ray	8.94	0.0306
K_{β} x ray	6.01	0.0350[b]
L x ray	15.6	0.0043[b]
Auger-K	3.72	0.0255[b]
^{134}Cs		
$\beta_1^{-(1)}$	27.3	0.0231[b]
$\beta_2^{-(1)}$	2.51	0.1234[b]
$\beta_3^{-(1)}$	70.2	0.2101[b]
γ_4	1.49	0.4754
γ_5	8.35	0.5632
γ_6	15.4	0.5693
γ_7	97.6	0.6047
ce-K, γ_7	0.491	0.5673
γ_8	85.5	0.7959
γ_9	8.69	0.8020
γ_{11}	1.79	1.1680
γ_{12}	3.01	1.3650

[a]Maximum energy for subshell.
[b]Average energy.

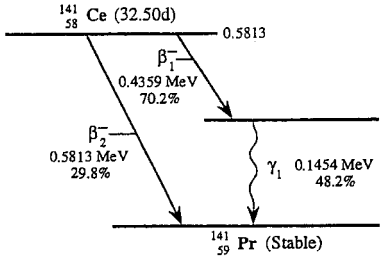

(Nov. 13, 1991)

^{140}Ce(n,γ); Decay Product of ^{141}La; ^{141}Pr(n,p); FP

Radiation	Y_i (%)	E_i (MeV)
β_1^-	70.2	0.1300[a]
β_2^-	29.8	0.1811[a]
γ_1	48.2	0.1454
ce-K, γ_1	18.7	0.1034
ce-L, γ_1	2.58	0.1386[b]
ce-M, γ_1	0.542	0.1439[b]
ce-N$^+$, γ_1	0.148	0.1451[b]
$K_{\alpha 1}$ x ray	8.91	0.0360
$K_{\alpha 2}$ x ray	4.86	0.0356
K_β x ray	3.35	0.0407[a]
L x ray	2.64	0.0050[a]
Auger-K	1.59	0.0294[a]

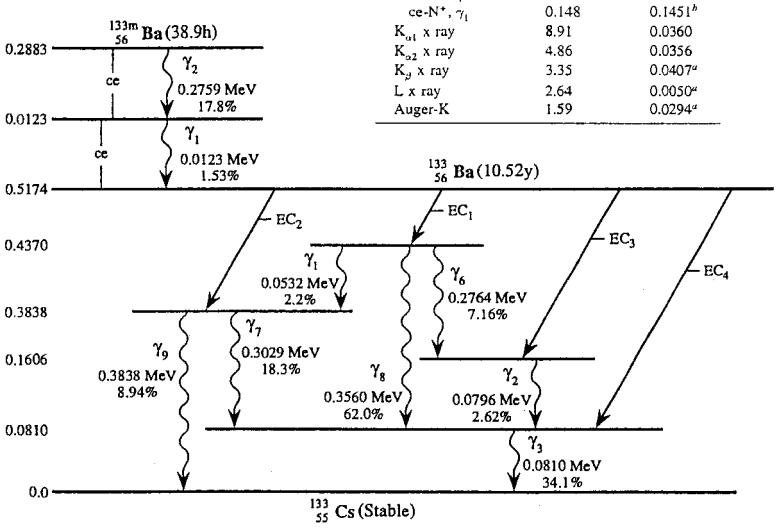

^{132}Ba(n,γ); ^{133}Cs(p,n) (Oct. 6, 1995)

Radiation	Y_i (%)	E_i (MeV)
^{133m}Ba		
γ_1	1.53	0.0123
ce-L, γ_1	84.5	0.0063[a]
ce-M, γ_1	17.3	0.0110[a]
γ_2	17.8	0.2759
ce-K, γ_2	60.3	0.2385
ce-L, γ_2	18.4	0.2699[a]
ce-M, γ_2	4.12	0.2746[a]
ce-N$^+$, γ_2	1.17	0.2757[a]
$K_{\alpha 1}$ x ray	28.0	0.0322
$K_{\alpha 2}$ x ray	15.2	0.0318
K_β x ray	10.2	0.0364[b]
L x ray	18.5	0.0045[b]
^{133}Ba		
γ_1	2.2	0.0532
ce-K, γ_1	11.0	0.0172
ce-L, γ_1	1.87	0.0475[a]
γ_2	2.62	0.0796
ce-K, γ_2	3.97	0.0436
ce-L, γ_2	0.574	0.0739[a]
γ_3	34.1	0.0810
ce-K, γ_3	43.9	0.0450
ce-L, γ_3	7.36	0.0753[a]
ce-M, γ_3	1.51	0.0798[a]
ce-N$^+$, γ_3	0.392	0.0808[a]
γ_6	7.16	0.2764
γ_7	18.3	0.3029
ce-K, γ_7	0.69	0.2669
γ_8	62.0	0.3560
ce-K, γ_8	1.31	0.3200
ce-L, γ_8	0.216	0.3503[a]
γ_9	8.94	0.3838
$K_{\alpha 1}$ x ray	62.5	0.0310
$K_{\alpha 2}$ x ray	33.7	0.0306
K_β x ray	22.4	0.0350[b]
L x ray	15.7	0.0043[b]
Auger-K	13.9	0.0255[b]

[a] Maximum energy for subshell.
[b] Average energy.

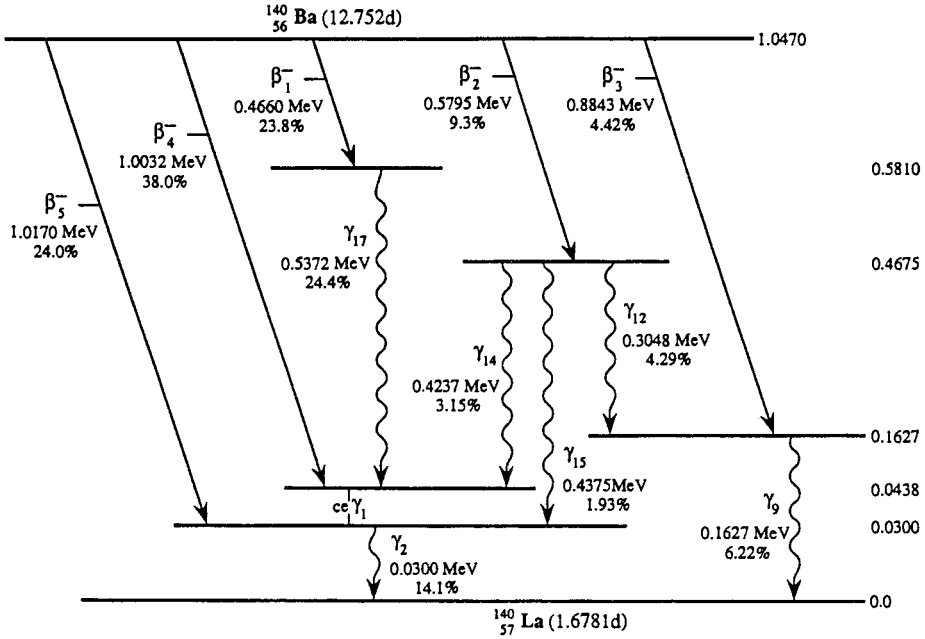

FP (Jan. 26, 1995)

Radiation	Y_i (%)	E_i (MeV)
β_1^-	23.8	0.1360[a]
β_2^-	9.3	0.1760[a]
β_3^-	4.42	0.3050[a]
β_4^-	38.0	0.3390[a]
β_5^-	24.0	0.3570[a]
ce-L, γ_1	53.7	0.0076[b]
ce-M, γ_1	11.1	0.0125[b]
γ_2	14.1	0.0300
ce-L, γ_2	61.2	0.0237[b]
ce-M, γ_2	12.6	0.0286[b]
γ_9	6.22	0.1627
ce-K, γ_9	1.48	0.1237
γ_{12}	4.29	0.3048
γ_{14}	3.15	0.4237
γ_{15}	1.93	0.4375
γ_{17}	24.4	0.5372
$K_{\alpha 1}$ x ray	0.813	0.0334
L x ray	15.2	0.0047[a]

[a]Average energy.
[b]Maximum energy for subshell.

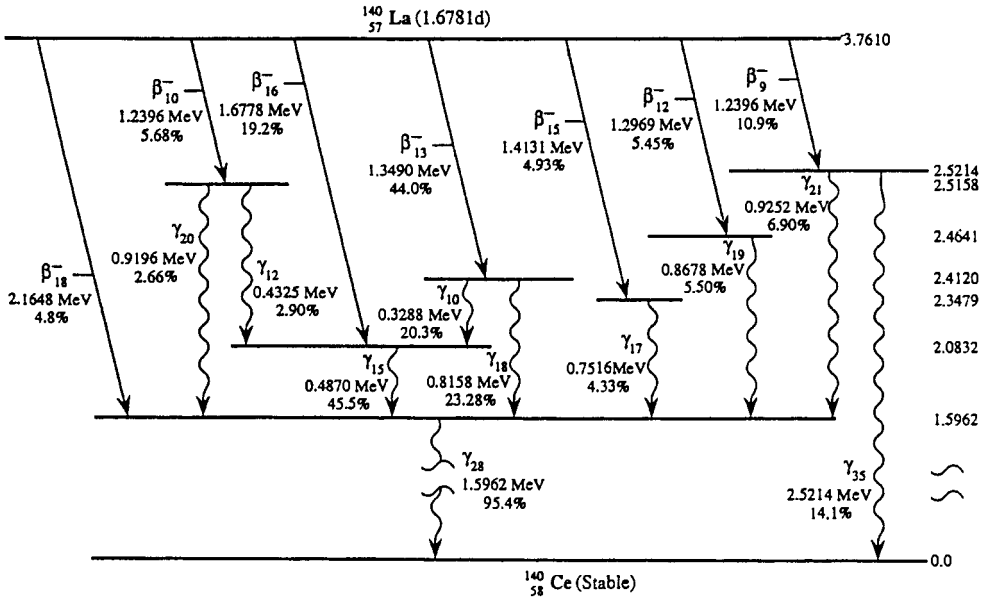

^{139}La(n,γ); FP (Nov. 13, 1991)

Radiation	Y_i (%)	E_i (MeV)
β^-_9	10.9	0.4415[a]
β^-_{10}	5.68	0.4439[a]
β^-_{12}	5.45	0.4656[a]
β^-_{13}	44.0	0.4877[a]
β^-_{15}	4.93	0.5151[a]
β^-_{16}	19.2	0.6298[a]
β^-_{18}	4.8	0.8465[a]
γ_{10}	20.3	0.3288
ce-K, γ_{10}	0.804	0.2883
γ_{12}	2.90	0.4325
γ_{15}	45.5	0.4870
γ_{17}	4.33	0.7516
γ_{18}	23.28	0.8158
γ_{19}	5.5	0.8678
γ_{20}	2.66	0.9196
γ_{21}	6.90	0.9252
γ_{28}	95.4	1.5962
γ_{35}	3.46	2.5214

[a]Average energy.

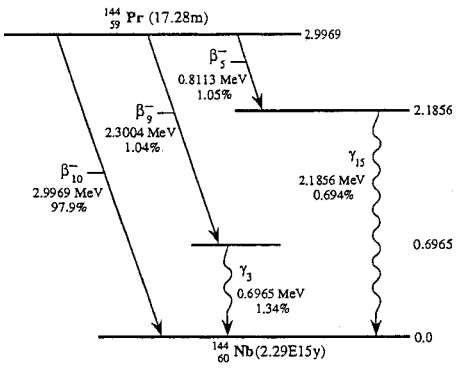

FP (Aug. 22, 1989)

Radiation	Y_i (%)	E_i (MeV)
β_5^-	1.05	0.2666[a]
β_9^-	1.04	0.9040[a]
β_{10}^-	97.9	1.2210[a]
γ_3	1.34	0.6965
γ_{15}	0.694	2.1860

[a]Average energy.

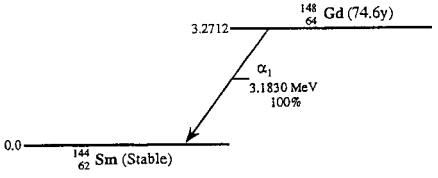

^{147}Sm(α,3n); ^{151}Eu(p,4n) (May 7, 1998)

Radiation	Y_i (%)	E_i (MeV)
α_1	100.0	3.1830
α recoil	100.0	0.0862

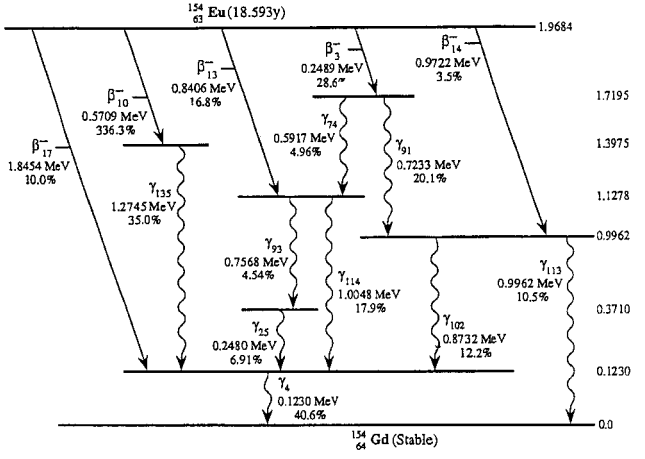

^{153}Eu(n,γ); FP (Independent Yield) (Dec. 3, 1998)

Radiation	Y_i (%)	E_i (MeV)
β_3^-	28.6	0.0693[a]
β_6^-	1.64	0.1014[a]
β_{10}^-	36.3	0.1762[a]
β_{13}^-	16.8	0.2766[a]
β_{14}^-	3.5	0.3281[a]
β_{17}^-	10.0	0.6956[a]
γ_4	40.6	0.1230
ce-K, γ_4	26.8	0.0728
ce-L, γ_4	16.8	0.1147[b]
ce-M, γ_4	3.91	0.1212[b]
ce-N$^+$, γ_4	1.1	0.1227[b]
γ_{25}	6.91	0.2480
γ_{74}	4.96	0.5917
γ_{89}	1.79	0.6924
γ_{91}	20.1	0.7233
γ_{93}	4.54	0.7568
γ_{102}	12.2	0.8732
γ_{113}	10.5	0.9962
γ_{114}	17.9	1.0048
γ_{135}	35.0	1.2745
γ_{154}	1.79	1.5965

[a]Average energy.
[b]Maximum energy for subshell.

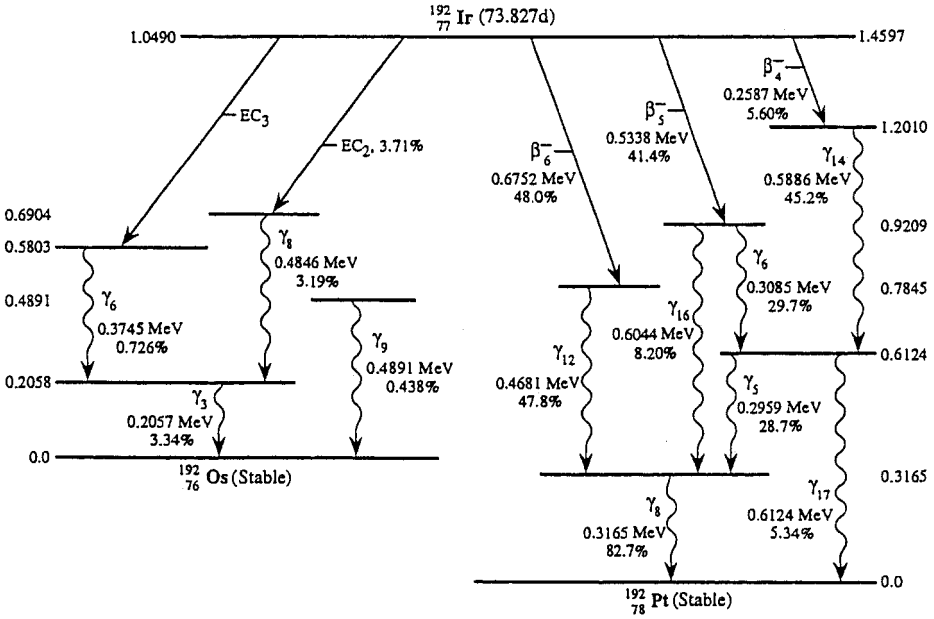

^{191}Ir(n,γ); ^{192}Os(d,2n) (Sept. 4, 1996)

Radiation	Y_i (%)	E_i (MeV)
Via EC		
γ_2	0.473	0.2013
γ_3	3.3	0.2057
γ_8	3.18	0.4846
$K_{\alpha 1}$ x ray	2.09	0.0630
Via beta minus		
β_4^-	5.61	0.0717[a]
β_5^-	41.4	0.1622[a]
β_6^-	48.0	0.2099[a]
γ_5	28.7	0.2960
ce-K, γ_5	1.88	0.2176
γ_6	29.7	0.3085
ce-K, γ_6	1.80	0.2301
γ_8	82.7	0.3165
ce-K, γ_8	4.44	0.2381
ce-L, γ_8	1.95	0.3026[b]
γ_{12}	47.8	0.4681
ce-K, γ_{12}	1.02	0.3897
γ_{14}	4.52	0.5886
γ_{17}	8.20	0.6044
γ_{18}	5.34	0.6124
$K_{\alpha 1}$ x ray	4.55	0.0668
$K_{\alpha 2}$ x ray	2.66	0.0651
$K\beta$ x ray	1.97	0.0757[a]

[a] Average energy.
[b] Maximum energy for subshell.

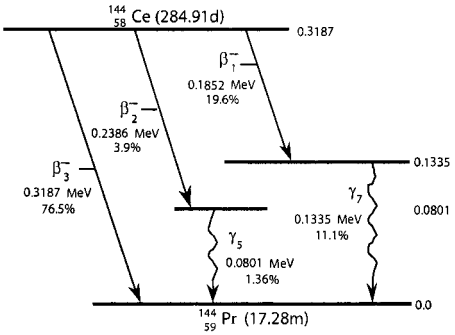

FP August, 2001

Radiation	Yi (%)	Ei (MeV)
β−1	19.6	0.0502*
β−2	3.9	0.0661*
β−3	76.5	0.0911*
γ5	1.36	0.0801
γ7	11.1	0.1335
ce-K, γ7	5.47	0.0915
Kα1 X-ray	4.5	0.0360
Kα2 X-ray	2.47	0.0356

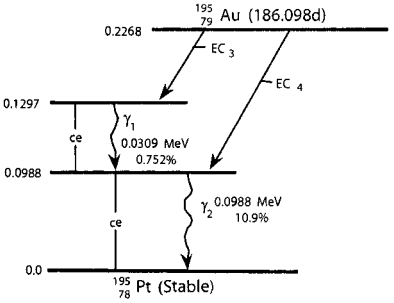

Deuterons on Pt; ^{193}Ir(α,2n); ^{195}Pt(p,n) May, 1999

Radiation	Yi (%)	Ei (MeV)
ce-L, γ1	22.7	0.0170[a]
ce-M, γ1	5.23	0.0276[a]
γ2	10.9	0.0988
ce-K, γ2	63.1	0.0205
ce-L, γ2	11.1	0.0850[a]
ce-M, γ2	2.57	0.0956[a]
Kα1 X-ray	49.2	0.0668
Kα2 X-ray	28.7	0.0651
Kβ X-ray	21.2	0.0757*
L X-ray	53.8	0.0094*
Auger-K	4.19	0.0510*

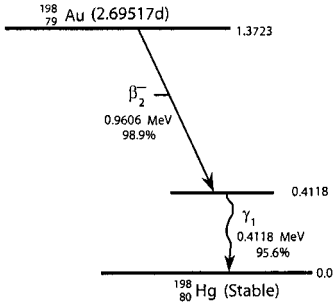

^{197}Au(n,γ); ^{198}Pt(p,n) March, 1995

Radiation	Yi (%)	Ei (MeV)
β−2	99.0	0.3147*
γ1	95.6	0.4118
ce-K, γ1	2.88	0.3287
ce-L, γ1	1.02	0.3970[a]
Kα1 X-ray	1.38	0.0708

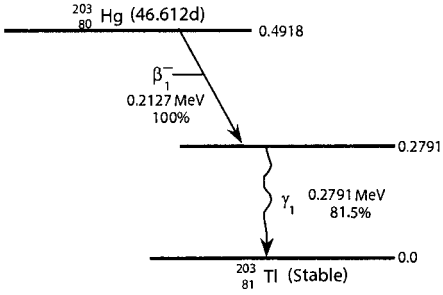

^{202}Hg(n,γ) November, 1993

Radiation	Yi (%)	Ei (MeV)
β−1	100.0	0.0577*
γ1	81.5	0.2791
ce-K, γ1	13.4	0.1937
ce-L, γ1	3.91	0.2638[a]
ce-M+, γ1	1.3	0.2769[a]
Kα1 X-ray	6.33	0.0729
Kα2 X-ray	3.75	0.0708
Kβ X-ray	2.79	0.0826*
L X-ray	5.42	0.0103*

* Average Energy
[a] Maximum Energy for Subshell

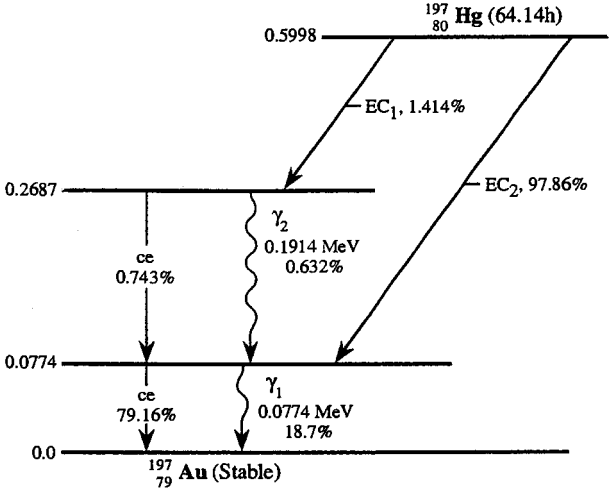

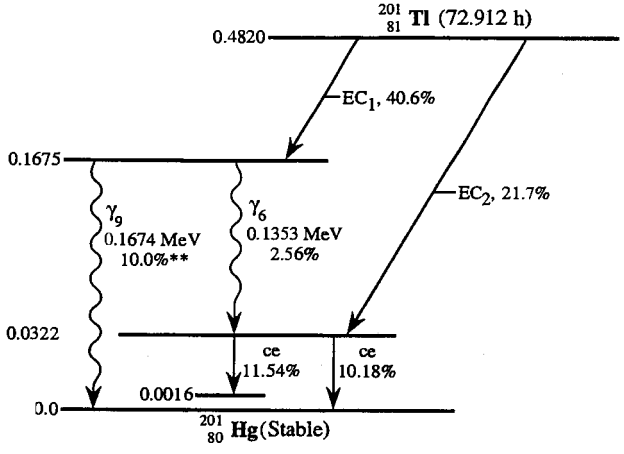

^{196}Hg(n,γ); ^{197m}Hg[a] (Jan. 4, 1996)

Radiation	Y_i (%)	E_i (MeV)
γ_1	18.7	0.0774
ce-L, γ_1	60.0	0.0630[b]
ce-M, γ_1	14.6	0.0739[b]
ce-N$^+$, γ_1	4.56	0.0766[b]
γ_2	0.632	0.1914
$K_{\alpha 1}$ x ray	54.6	0.0688
$K_{\alpha 2}$ x ray	31.9	0.0670
K_β x ray	23.9	0.0780[c]
L x ray	64.8	0.0097[c]
Auger-K	4.11	0.0524[c]

[a]Contribution of ^{197m}Hg ($T_{1/2}$ = 23.8 h) to the activity of a ^{197}Hg source may be significant.
[b]Maximum energy for subshell.
[c]Average energy.

^{201}Pb(EC); ^{201m}Tl; ^{199}Hg(d,γ); ^{200}Hg(d,n) (July 8, 1994)

Radiation	Y_i (%)	E_i (MeV)
ce-L, γ_4	9.36	0.0158[a]
ce-M, γ_4	2.18	0.0270[a]
ce-L, γ_5	8.26	0.0174[a]
ce-M, γ_5	1.92	0.0286[a]
γ_6	2.56	0.1353
ce-K, γ_6	7.23	0.0522
ce-L, γ_6	1.23	0.1205[a]
γ_9	10.0	0.1674
ce-K, γ_9	15.4	0.0843
ce-L, γ_9	2.62	0.1526[a]
$K_{\alpha 1}$ x ray	46.4	0.0708
$K_{\alpha 2}$ x ray	27.3	0.0689
K_β x ray	20.4	0.0803[b]
L x ray	45.6	0.0100[b]
Auger-K	3.29	0.0538[b]

[a]Maximum energy for subshell.
[b]Ayerage energy.

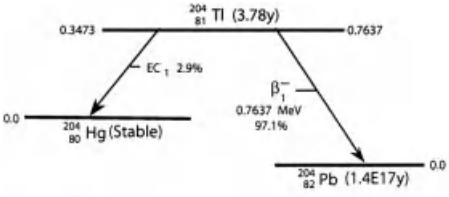

203Tl(n,γ) November, 1994

Radiation	Yi (%)	Ei (MeV)
Kα1 X-ray	0.817	0.0708
Kα2 X-ray	0.476	0.0689
Kβ X-ray	0.355	0.0803*
L X-ray	0.802	0.0100*
β−1	97.1	0.2440*

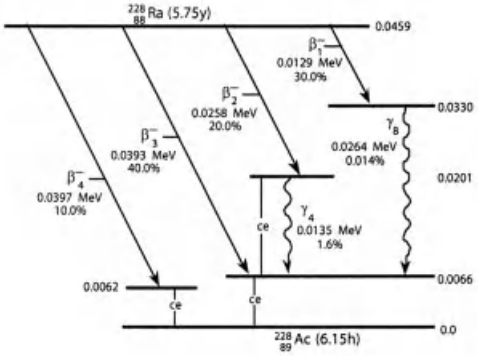

232Th series April 1997

Radiation	Yi (%)	Ei (MeV)
β−1	30.0	0.0032*
β−2	20.0	0.0065*
β−3	40.0	0.0099*
β−4	10.0	0.0100*
ce-M, γ1	7.5	0.0013[a]
ce-M, γ2	37.5	0.0017[a]
γ4	1.60	0.0135
ce-M, γ4	7.31	0.0085[a]
ce-L, γ5	2.21	0.0066[a]
L X-ray	1.03	0.0127*
Auger-K	1.18	0.0093*

* Average Energy
[a] Maximum Energy for Subshell

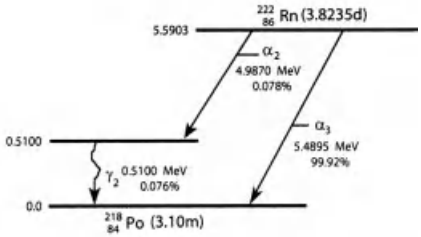

238U series January, 1996

Radiation	Yi (%)	Ei (MeV)
α2	0.078	4.9870
α recoil	0.078	0.0900
α3	99.9	5.4895
recoil	99.9	0.0991
γ1	0.076	0.5100

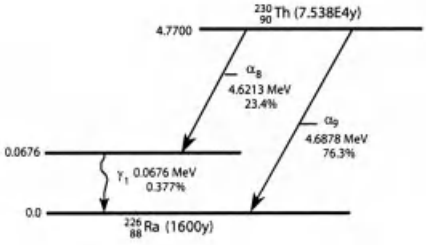

238U series April 1996

Radiation	Yi (%)	Ei (MeV)
α8	23.4	4.6213
α recoil	23.4	0.0811
α9	76.3	4.6878
α recoil	76.3	0.0822
γ1	0.377	0.0676
ce-L, γ1	17.0	0.0484[a]
ce-M, γ1	4.6	0.0629[a]
ce-N+, γ1	1.66	0.0665[a]
L X-ray	7.73	0.0123*

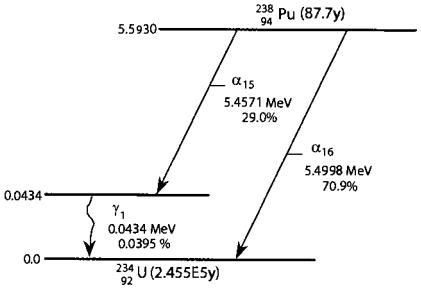

β⁻ transformation from $^{237}Np(n,\gamma)^{238}Np$; product of ^{242}Cm April 1994

Radiation	Yi (%)	Ei (MeV)
α15	29.0	5.4571
α recoil	29.0	0.0925
α16	70.9	5.4998
α recoil	70.9	0.0932
γ1	0.0395	0.0434
ce-L, γ1	20.9	0.0217[a]
ce-M, γ1	5.76	0.0380[a]
L X-ray	10.5	0.0136*

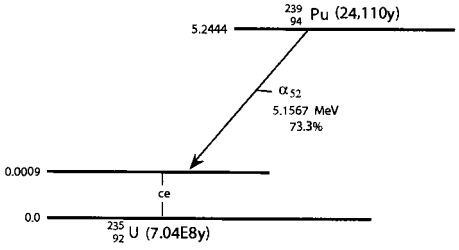

β⁻ transformation from $^{238}U(n,\gamma)^{239}U$ August 1993

Radiation	Yi (%)	Ei (MeV)
α52	73.3	5.1567
α recoil	73.3	0.0868
ce-M, γ2	12.9	0.0074[a]
ce-N+, γ2	5.52	0.0115[a]
ce-L, γ4	2.36	0.0169[a]
ce-L, γ10	6.24	0.0299[a]
ce-M, γ10	1.72	0.0461[a]
L X-ray	4.39	0.0136*
Auger-K	4.38	0.0099*

Note: Greatly simplified; 52 separate α energies, very closely spread; numerous conversion electrons from 168 γ-energy states.

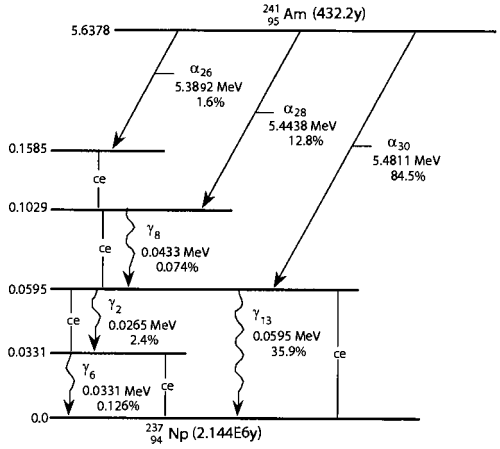

Transformation Product of ^{241}Pu May 1995

Radiation	Yi (%)	Ei (MeV)
α26	1.6	5.3892
α recoil	1.6	0.0902
α28	13.0	5.4438
α recoil	13.0	0.0911
α30	84.5	5.4811
α recoil	84.5	0.0972
γ2	2.40	0.0265
ce-L, γ2	14.4	0.0039[a]
ce-M, γ2	3.84	0.0206[a]
γ5	0.126	0.0331
ce-L, γ5	17.4	0.0108[a]
ce-M, γ5	4.41	0.0275[a]
γ8	0.073	0.0433
ce-L, γ8	9.05	0.0210[a]
ce-M, γ8	2.39	0.0377[a]
γ13	35.9	0.0595
ce-L, γ13	30.2	0.0371[a]
ce-M, γ13	8.11	0.0538[a]
ce-N+, γ13	3.37	0.0580[a]
Auger-L	35.3	0.0101*

* Average Energy
[a] Maximum Energy for Subshell

Index

Physics for Radiation Protection, Third Edition. James E. Martin